

Illinois State Water Survey Division

ATMOSPHERIC CHEMISTRY SECTION

AT THE
UNIVERSITY OF ILLINOIS



SWS Contract Report 426

STUDY OF ATMOSPHERIC POLLUTION SCAVENGING

Twenty-First Progress Report
Contract Number DE -AC02 - 76EV01199

July 1987

Authors

Richard G. Semonin
Van C. Bowersox
Gary J. Stensland
Mark E. Peden
Kevin G. Doty
Donald F. Gatz
Jacqueline M. Lockard
Susan R. Bachman
Loretta M. Skowron
Jack Su
Scott R. Dossett

Sponsored by
United States Department of Energy
Office of Health and Environmental Research
Washington, DC

Richard G Semonin
Principal Investigator



Illinois Department of Energy and Natural Resources

SWS Contract Report 426

**STUDY OF ATMOSPHERIC POLLUTION
SCAVENGING**

*Twenty-First Progress Report
Contract Number DE-AC02-76EV01199*

July 1987

Authors:

Richard G. Semonin
Van C. Bowersox
Gary J. Stensland
Mark E. Peden
Kevin G. Doty
Donald F. Gatz
Jacqueline M. Lockard
Susan R. Bachman
Loretta M. Skowron
Jack Su
Scott R. Dossett

*Sponsored by:
United States Department of Energy
Office of Health and Environmental Research
Washington, D.C.*

*Richard G. Semonin
Principal Investigator*

TABLE OF CONTENTS

	Page
CHAPTER 1. WET DEPOSITION CHEMISTRY <i>Richard G. Semonin</i>	1
CHAPTER 2. INTRA-ANNUAL VARIATIONS IN THE CONCENTRATIONS OF MAJOR INORGANIC IONS IN THE PRECIPITATION OF THE UNITED STATES <i>Van C. Bowersox and Gary J. Stensland</i>	21
CHAPTER 3. ESTIMATION OF BIAS IN THE AVERAGE WET DEPOSITION OF CALCIUM, SULFATE, AND SODIUM FROM NATIONAL ATMOSPHERIC DEPOSITION PROGRAM/NATIONAL TRENDS NETWORK (NADP/NTN) DATA <i>Van C. Bowersox, Gary J. Stensland and Mark E. Peden</i>	39
CHAPTER 4. SPATIAL RELATIONSHIPS BETWEEN ACID RAIN, AIR QUALITY, AND VISIBILITY DATA <i>Gary J. Stensland</i>	53
CHAPTER 5. VARIATIONS IN PRECIPITATION COMPOSITION AND DEPOSITION WITH SYNOPTIC WEATHER TYPE <i>Kevin G. Doty and Donald F. Gatz</i>	69
CHAPTER 6. BACK TRAJECTORY CLIMATOLOGIES FOR SULFATE AND NITRATE WET DEPOSITION FLUXES AT A CENTRAL ILLINOIS SITE <i>Kevin G. Doty and Van C. Bowersox</i>	81
CHAPTER 7. INTERLABORATORY COMPARISONS OF REFERENCE PRECIPITATION SAMPLES <i>Mark E. Peden and Jacqueline M. Lockard</i>	159
CHAPTER 8. QUALITY ASSURANCE OF PRECIPITATION CHEMISTRY ANALYSES USING ION BALANCE CALCULATIONS <i>Jacqueline M. Lockard</i>	169
CHAPTER 9. A COMPARISON OF ION CHROMATOGRAPHY AND AUTOMATED COLORIMETRY FOR THE DETERMINATION OF MAJOR ANIONS IN PRECIPITATION <i>Susan R. Bachman</i>	193

CHAPTER 10.	LONG-TERM IONIC STABILITY OF PRECIPITATION SAMPLES <i>Mark E. Peden and Loretta M. Skowron</i> —————	203
CHAPTER 11.	SYNTHETIC RAINWATER REFERENCE SAMPLES <i>Loretta M. Skowron and Mark E. Peden</i> —————	215
CHAPTER 12.	PRELIMINARY DATA FOR DAILY AMBIENT AEROSOL MEASUREMENTS AT THE BONDVILLE RESEARCH SITE <i>Gary J. Stensland</i> —————	231
CHAPTER 13.	RATIOS OF ION CONCENTRATIONS IN PRECIPITATION TO AEROSOLS AT THE BONDVILLE SITE <i>Gary J. Stensland and Van C. Bowersox</i> —————	251
CHAPTER 14.	A COMPUTER PROGRAM FOR CALCULATING STATE AVERAGES FROM POINT VALUES <i>Jack Su and Gary J. Stensland</i> —————	261
CHAPTER 15.	THE DESCRIPTION AND COMPARISON OF A PROTOTYPE TRAJECTORY MODEL WITH THE ARL-ATAD MODEL <i>Kevin G. Doty</i> —————	279
CHAPTER 16.	SCREENING CRITERIA FOR NADP DRY BUCKET DATA <i>Donald F. Gatz, Van C. Bowersox, and Jack Su</i> —————	309
CHAPTER 17.	AN ANNOTATED DESCRIPTION OF THE ATMOSPHERIC CHEMISTRY SAMPLING STATION AT BONDVILLE, ILLINOIS <i>Scotty R. Dossett</i> —————	329

CHAPTER 1

WET DEPOSITION CHEMISTRY¹

Richard G. Semonin

ABSTRACT

Interest in precipitation chemistry dates back to the 18th century, but only since 1977 has the U.S. established a national network for monitoring at a level sufficient to describe the chemical climate. The siting criteria, quality assurance, and standardized equipment and analytical methodology are addressed to insure the highest quality data for interpretive research. The national distribution of concentration and deposition for calcium, ammonium, chloride, nitrate, sulfate, and pH are shown in a series of maps. The maps show high concentrations of calcium and ammonium in the Great Plains, high concentrations of nitrate, sulfate, and hydrogen ion in the eastern states, and high concentrations of chloride along the coastal states. The primary conclusions are 1) the greatest deposition is directly associated with the largest emission regions, and 2) dry deposits are largely unknown but clearly must be measured before the biochemical and geochemical cycles will be fully understood.

INTRODUCTION

We have often heard the saying, "What goes up must come down", but all too frequently have not given the concept too much thought. It now has become a very important issue not only in this country, but everywhere on the planet earth and is the center focus of the acid rain debate. The debate today does not question the statement given above, but rather addresses the tougher problem of "When something goes up how, when and where does it come down?". A related question might be "When it comes down, is it beneficial or harmful to its final resting place?". A further important question is "Is the acidity of precipitation increasing and is it spreading to larger areas in the U.S. and beyond its borders?". The answers to these questions are central to the establishment of policy regarding how to deal with the national and international concerns about acidic deposition.

To begin to address these and other questions, it is appropriate to very briefly examine what little is known about previous studies of the chemistry of precipitation. It must be borne in mind, however, that while there are some indications of great interest in atmospheric chemistry over

¹ Published in ACS Symposium Series 318, Materials Degradation Caused by Acid Rain, 1986.

many years, the technology for providing analyses of both the atmosphere and its precipitation is still improving. An implication of this is that it is most difficult to compare more recently acquired data with those of the relatively distant past to determine the extent and trend of changing precipitation chemistry.

It seems central to the on-going debates, both scientific and political, that the local and regional trend of important chemical ions in precipitation be determined in order that their contribution to the chemical cycle of local ecosystems can be more accurately assessed. Equally important to such an assessment is the quantification of the magnitude of the wet and dry deposition from the atmosphere and their ultimate disposition in the identified cycles.

In this brief paper, we will not attempt to address all of the complex biochemical and geochemical sciences, but we will attempt to describe the chemistry of precipitation as a single, and frequently minor, input to those chemical budgets of importance to the environment. We will also not attempt a comprehensive description of dry deposition as there is no single agreed-upon method for its measurement. Experience tells us that it does not precipitate all of the time, and in the eastern mid-latitude of the U.S. no precipitation is observed about 90% of the time during any given year. However, experience also tells us that material from the atmosphere is continuously returning to the earth in dry form. Some preliminary data obtained from exposed bucket collections will be discussed as a "poor man's" estimate of a portion of the dry deposition.

PRECIPITATION CHEMISTRY BACKGROUND

There is early documentation of interest in the chemical composition of rain dating back to 1727, followed by a fairly thorough study of the subject in the mid-1800's (Cowling, 1982). These early efforts focused on sulfur in rain, snow, and dew, and some of the perceived impacts on health and agriculture. The modern interest began in the post-World War II years when some monitoring of precipitation chemistry was initiated in the Scandinavian countries (Rossby and Egner, 1955). A particular effort was put forth in Sweden with agriculturalists and meteorologists expressing equal interest in the chemistry of precipitation, but for entirely different reasons. The agricultural interests focused on the quantity of nutrients being deposited by precipitation as an aid to plant growth while the atmospheric scientists were attempting to use the chemistry to further their knowledge of the origin of precipitation water and to trace atmospheric motions. The national commitment of Sweden to continue the network operation placed them in the forefront of the emerging issues related to acid rain.

U.S. Sampling Activities

During the early quarter of this century, agriculturalists in the U.S. showed interest in the amount of nutrient falling on productive soils

as evidenced by the literature in the 1920's (MacIntire and Young, 1923, Stewart, 1920). Following the lead of Sweden, some interest in the chemistry of precipitation was expressed by meteorologists in the U.S. which culminated in the establishment of a national network in 1955 (Junge and Gustafson, 1956; Junge and Werby, 1958). This network was operated for a single year (1955-1956) and the data have been used by some as the baseline data for demonstrating that acid rain is worsening and spreading in the eastern U.S. (Cogbill and Likens, 1974; Cogbill, 1976; Likens and Butler, 1981).

A short time after the demise of this initial network a similar one was begun by the U.S. Public Health Service (PHS) in 1960. This network was maintained until 1966 with management responsibilities eventually falling upon the National Center for Atmospheric Research (NCAR) (Lodge, et al, 1968). No national network was operated after the closing of the PHS/NCAR stations in the 1960's although several isolated measurement programs were carried out in various parts of the country (e.g., Semonin, 1976). An excellent summary of sampling activities in North America is available for additional information (Wisniewski and Kinsman, 1982).

The First International Symposium on Acid Precipitation and the Forest Ecosystem in 1975 concluded with workshops addressing various needs to properly research the topic of acidic deposition in the U.S. (Dochinger and Seliga, 1976). Among the recommendations from one of the workshops was that a network be established for the purpose of long-term monitoring of the precipitation chemistry across the U.S. and its territories. This currently operating network extends from Alaska to Puerto Rico, and from Maine to American Samoa with 190 sampling sites. Many of the stations have been identified as National Trends Network (NTN) sites - the monitoring network of the National Acid Precipitation Assessment Program (NAPAP) (NAPAP, 1982).

PRECIPITATION CHEMISTRY CHARACTER

The chemistry of precipitation is characterized by trace quantities of most substances found in the atmosphere. Concentrations are typically measured in parts per million, parts per billion, and even parts per trillion. When considered as an ionic solution, about 95% of the total ionic strength is accounted for by the analysis of calcium, magnesium, ammonium, sodium, potassium, hydrogen, chloride, nitrate, and sulfate. The hydrogen ion is usually determined from measurements of the sample pH.

The acidity of precipitation is commonly presented as pH although more and more evidence is becoming available to show that organic acids also contribute to the total acidity of a sample (Peden and Lockard, 1984; Bachman et al, 1984; Galloway and Likens, 1978). However, it is important to also examine all of the other ions in a sample to understand the effects on the environment. There has been a suggestion put forth to limit the sulfate deposition without regard to the precipitation acidity. It is presumed that a sulfate reduction will automatically result in higher pH values, and, thus, a double environmental benefit will result.

But without better quantification of all sources of sulfate and their relation to acidity, any reduction strategy may not bring about the desired result.

PRECIPITATION COLLECTION FOR CHEMICAL ANALYSIS

A discussion of the quality of precipitation chemistry must include the analytical methods used as well as a description of the device used to collect samples. Most importantly, the quality of the data must be assured when assessing the impacts on the precipitation-receiving environmental system. Students of precipitation chemistry have used everything from glass bottles to baby bottle plastic liners to collect samples for analysis. Laundry baskets, staked to the ground, as well as fence-post mounted plastic bottles have also been used in network operations (Semonin, 1983). One of the most interesting collectors was the entire roof of a wood frame building covered with polyethylene sheeting and special guttering. A very large sample could be collected in a very short period of time even during the lightest rainfalls.

A number of other devices have been built directed toward acquiring one sample after another during a single rain event to obtain fine detail of the chemical structure of precipitation (Semonin, 1977, Miller et al, 1984). There are various means used to control the sample collection by either the volume per sample or time interval between sample collections. Owing to the rapid collection of numbers of samples in a very short period of time, none of these sequential collection devices have been used in a regional network.

The most widely used sampler in the United States networks today is comprised of two buckets, and a rain-activated switch to operate a movable cover. During non-precipitating periods, the cover remains tightly sealed on one bucket. Precipitation falling on the sensitive switch completes an electrical circuit activating a motor which lifts the cover from one side and places it on the opposite bucket. The sampler thus provides a dry sample as well as a wet sample. This is the standard instrument used throughout the NADP/NTN network.

Anyone wishing to collect rain or snow for chemical analysis is cautioned to first check the collection vessel for the chemicals of interest to see if, in fact, the analysis will be contaminated. For example, it would be unwise to collect samples in a weighing-bucket rain gauge for zinc analysis when the bucket is zinc-coated and leaches into the sample.

A second serious consideration is whether one wishes to collect a bulk sample as opposed to a wet-only sample. A bulk sample is one which is directly exposed to the atmosphere and remains open throughout a prescribed interval of time. This is not a very satisfactory way of collecting precipitation samples because of the natural tendency of birds to perch on the rim of the collector always facing outward contributing to the debris deposited inside the container. Equally important, dust,

leaves, and other natural wind-blown materials are likely to enter the sampler and contaminate the precipitation in an unpredictable manner.

The interval between the collection of samples is largely determined by the goals for the sampling program. If one wants to study the effects of precipitation chemistry on the forest, for example, it is highly unlikely that it is necessary to collect samples on intervals of anything less than a one-week period and perhaps even one month may suffice for the majority of biological effects studies. On the other hand, if one wants to study the variability of precipitation chemistry in convective storms during the warm season, a sequential sampler may be necessary to obtain samples as frequently as one or more per minute (Semonin, 1977). So in establishing a sampling program, it is most important to carefully consider the goal of that program and then determine the need for event sampling, as opposed to less costly, longer periods, to achieve that goal. The NADP/NTN weekly collection network is an arbitration between event samples and monthly samples, but was chosen to address the program goals of determining 1) the long-term trend of precipitation chemistry and 2) atmospheric deposition effects on the environment.

PRECIPITATION CHEMISTRY QUALITY ASSURANCE

Once a sample has been confined within the collecting vessel, the safest thing is to immediately seal that vessel and carry it or ship it to the analytical laboratory. However, it is a practice in some operations to allow prior handling of the sample such as withdrawal of aliquots for the local determination of a particular parameter. For example, the NADP/NTN allows extraction of a few milliliters for the field determination of pH and conductivity. Immediately after the aliquot has been withdrawn, the sample is sealed and then shipped to a central laboratory for further chemical analysis. Shipment of the sample is an important consideration for any type of sampling program since one must be sure that the collecting vessel does not leak in transit.

Written documentation of everything concerning the sample up to this point should be provided for the laboratory staff as the analysis of precipitation chemistry proceeds. Certainly, any laboratory, whether it is adjacent to the sampling site or several thousands of kilometers distant, should have certain analytical capabilities for the determination of trace materials in precipitation. The analysts must be trained to recognize the expected concentrations in precipitation and detect contamination in a sample. Contamination can originate from either natural causes or handling of the sample.

Finally, one must be alert that even though a determination may be perfectly accurate and within statistically allowable errors of the instrumentation, the value may, in fact, be excluded from a data set for other reasons. For example, a loose covering over the collection vessel can allow crustal dust to enter into the collector during non-precipitating intervals and can artificially raise the concentrations of those materials. A "leaky" seal results in values that are not representative

of precipitation but are more representative of a bulk sample. The major point is that the sample quality control does not begin or end in the laboratory, but must be extended to include everything from the sample collection in the field to the point of preparing the data for dissemination or further interpretation and archiving (NADP, 1984)

Concern has been expressed about the chemical integrity of samples collected less frequently than the duration of a single storm. There is reason for some scientific inquiry on this matter, but the available data suggest that any chemical changes in a sample will occur in a relatively brief period after the precipitation has ended (Peden and Skowron, 1978). However, event samples may not be any more stable than weekly samples if the delay between collection of the sample and its analysis is of the order of one or more days. Consequently, until real-time chemical analysis can be performed in the field, all currently available data contain largely unknown errors from chemical changes that occur between the end of an event and the analysis.

SELECTED INTERPRETIVE ANALYSES

There are at least two obvious ways of viewing the chemistry data from precipitation samples. The first is the concentration of samples and the second is the deposition (or loading) of ions of interest to the surface. From a simple perspective, the concentration is of interest to atmospheric chemists while the deposition is of interest to effects research scientists. It should be kept in mind that the concentration and precipitation are the observables and the deposition is a derived quantity. The deposition is calculated by multiplying the observed concentration by the amount of precipitation associated with the sample thereby obtaining a value of the mass deposited per unit area. In the following discussion, both the concentration and deposition will be shown and described. Only the major ions calcium, ammonium, chloride, nitrate, sulfate, and hydrogen ion will be shown. There are many ways that the data can be displayed, but for this discussion median values from the entire data set were selected for each site and maps were hand-drawn to illustrate national patterns for each ion.

Calcium

The calcium contribution to the ionic strength of a sample is thought to be mainly due to the incorporation of soil aerosol into the precipitation before it is collected. Owing to agricultural practices and the semi-aridness of the Great Plains, it is not surprising to find the highest concentrations in that region (Figure 1). A large area of relatively high concentration is seen extending from Montana-North Dakota south through central and western Texas. A secondary area is seen extending northwest into southern Idaho from the Four Corners area where Utah, Colorado, New Mexico, and Arizona join. The coast lines of the U.S. are areas of relatively low concentration with values 3 to 6 times less than in the interior continent.

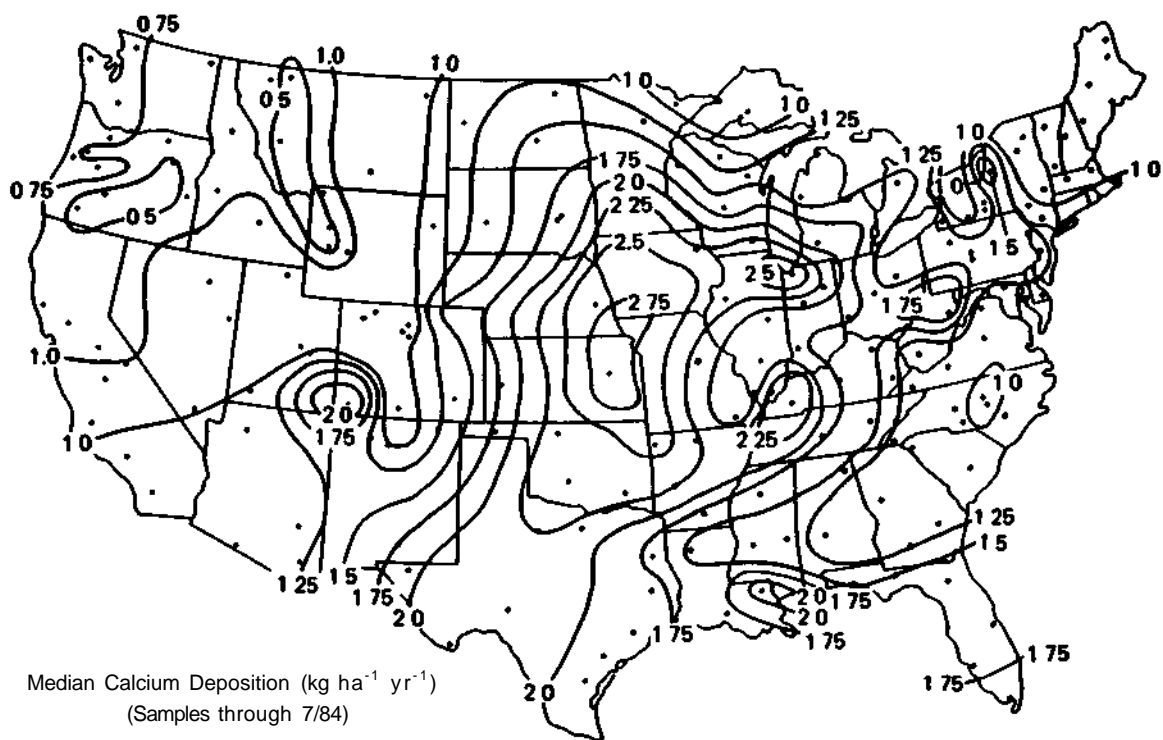
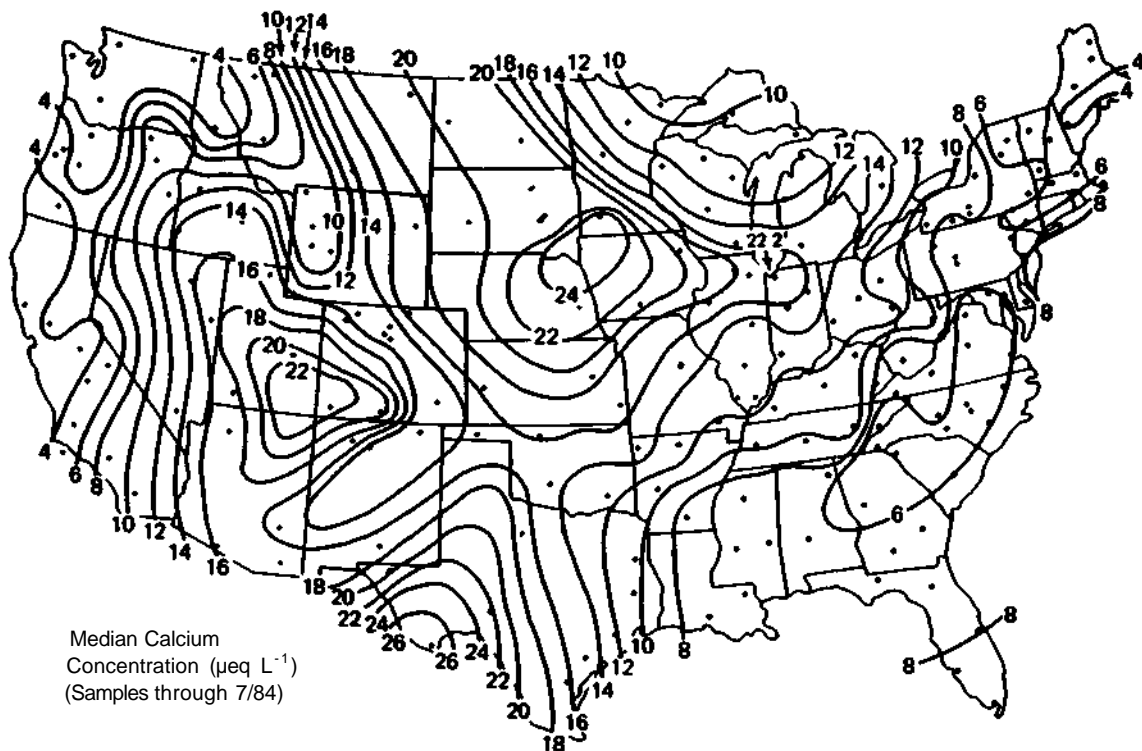


Figure 1. The median calcium concentration (top) and deposition year (bottom).

The deposition, expressed in kilograms per hectare per year, also shown in Figure 1, maximizes slightly to the southeast from the center of maximum concentration and is found over the southeast South Dakota, southwest Minnesota, northwest Iowa, and northeast Nebraska area. This slight shift is due to the somewhat greater precipitation toward the southeast while maintaining high concentrations. The isolated maximum in the Four Corners area is a direct result of an isolated maximum in precipitation and the maximum concentration. The same is true of the maximum in southeastern Louisiana. Note the excursions of high deposition into northern Illinois, western Kentucky, and even a small maximum in northern West Virginia. During periods of drought and attendant dust storms, such excursions can be more severe and cover much larger areas leading to misinterpretation of the meaning of the chemistry regarding trends (Stensland and Semonin, 1982)

Ammonium

The calcium likely appears in precipitation as the result of natural causes. It is in relative abundance in the natural sources of the oceans and the earth's crust. The source strength has not been quantified although some have attempted adjustments for seawater contributions to observed concentrations (Granat, 1972)

The ammonium ion source is also largely undetermined. The concentration pattern shown in Figure 2 suggests a relationship to the large feed lots associated with the cattle industry of the central Plains region. However, this possible source has not been measured, but only surmised from the geographical relationship between the maximum concentration and the known feed lot distribution. In one sense, the distribution of ammonium in precipitation has a natural source, but somewhat controlled by man

Unlike the calcium ion, the ammonium maximum is over the center of the interior U S decreasing outward in all directions with a few small, isolated high values scattered in other areas. For the most part, the coastline precipitation contains the lowest observed ammonium concentrations.

The deposition of ammonium is dominated by the concentration pattern as modulated slightly by the precipitation (Figure 2). The maximum deposition of greater than 4 kilograms per hectare per year is centered over the identical area of the maximum concentration. Since the deposition is influenced greatly by the regional weather (winds, storm systems and movement), it is interesting to observe the close relationship between the presumed source, the concentration, and the deposition. This distributional relationship certainly suggests a region for the testing of long-range transport and transformation models or it suggests something about the atmospheric chemistry of ammonium

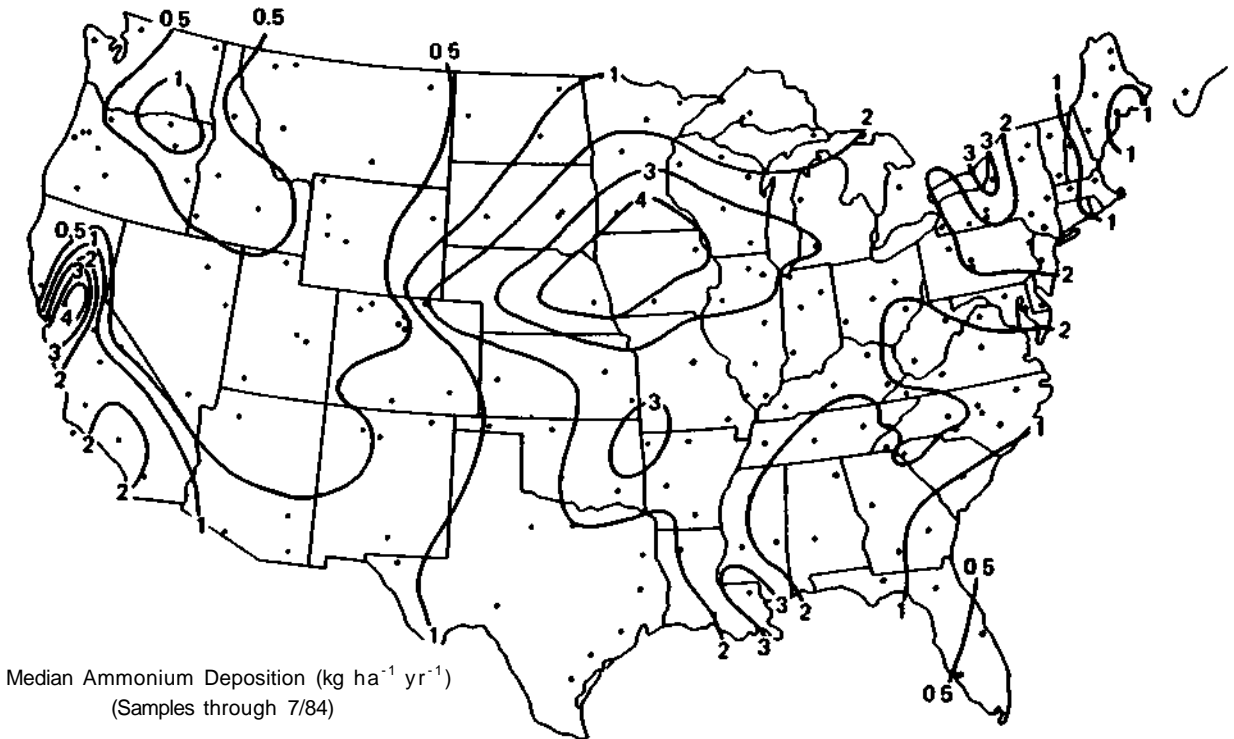
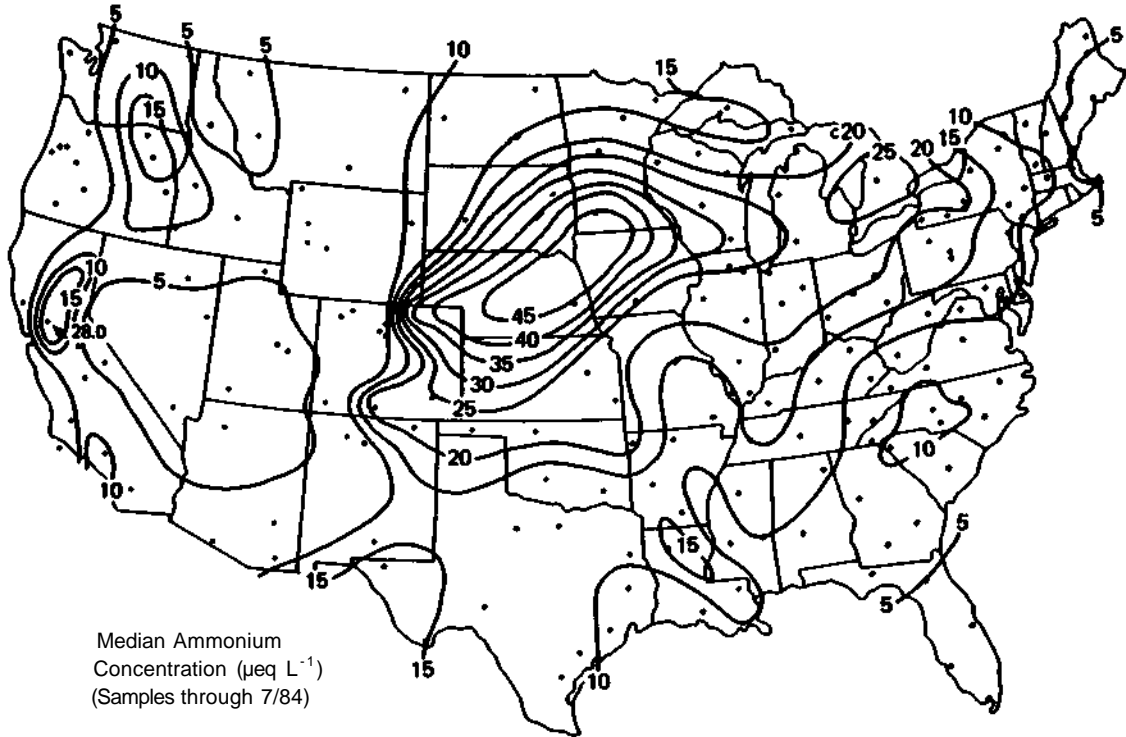


Figure 2. The median ammonium concentration (top) and deposition (bottom).

Chloride

The distribution of this ion is acknowledged to be controlled by the proximity of a sampling site to the oceans. This is borne out by the concentration pattern shown in Figure 3. The ratio of sodium to chloride at many of the coastal sites is very close to that for seawater of 0.86. There are two features of the concentration pattern that is interesting and cause for some speculation. Chloride shows a relative maximum extending from the Gulf coast northward across Texas into the upper Great Plains states. The seawater ratio, however, does not hold beyond northern Texas and the ratio becomes one or greater further north. This observation suggests either an inland source of sodium (soil?) or a selective decrease of chloride during the precipitation process. There is also a low concentration area observed over the Smokey Mountains, but the seawater ratio seems to be sustained. One could interpret this observation as due to the simple reduction of the seasalt component in the atmosphere with increased altitude and distance from the coast. There is also a tongue of high concentration extending from the central Gulf coast northeastward to Ohio with a strong possibility of a seawater influence as evidenced by the nearness to that ratio. This may reflect the meteorologists notion that the source of atmospheric water vapor for precipitation in the Midwest originates in the Gulf of Mexico, particularly during the warm season.

The deposition of chloride, obviously, is a mirror image of the precipitation pattern showing decreasing values with distance from the U.S. coastline (lower half of Figure 3). This ion, along with sodium, are worthy of additional study because of their domination by natural sources, and their obvious relationship to coastal influences.

Nitrate

The nitrate concentration in Figure 4 shows the highest values over central New York and Pennsylvania and an equal maximum over southwestern Michigan. The extension of these isolated maxima to the west as far as South Dakota and Nebraska appears to be associated with the ammonium concentration maximum in the same area indicating the possible presence of ammonium nitrate.

The major source for atmospheric nitrate is attributed to vehicular traffic and certainly the small center of high concentration over southwest California seems to confirm that relationship. It is not so easy to relate the other areas of high concentration to such high density mobile sources. This pattern is not easily traceable to the currently identified sources and considerable research is needed to explain the distribution of nitrate in precipitation.

The deposition pattern in Figure 4 is almost identical to the concentrations. The one exception to the simple correlation between concentration and deposition is in the southeast Louisiana. The heavy precipitation in that area explains the relative maximum in deposition extending from the Delta region northward into central Arkansas.

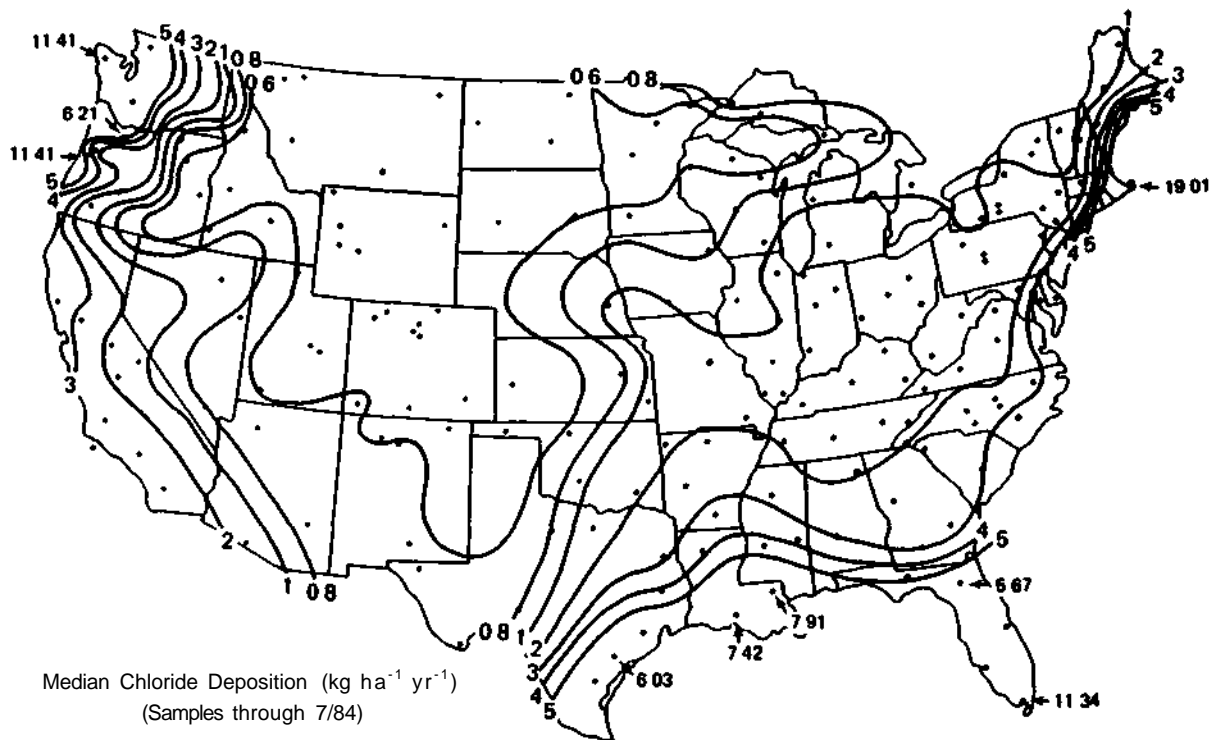
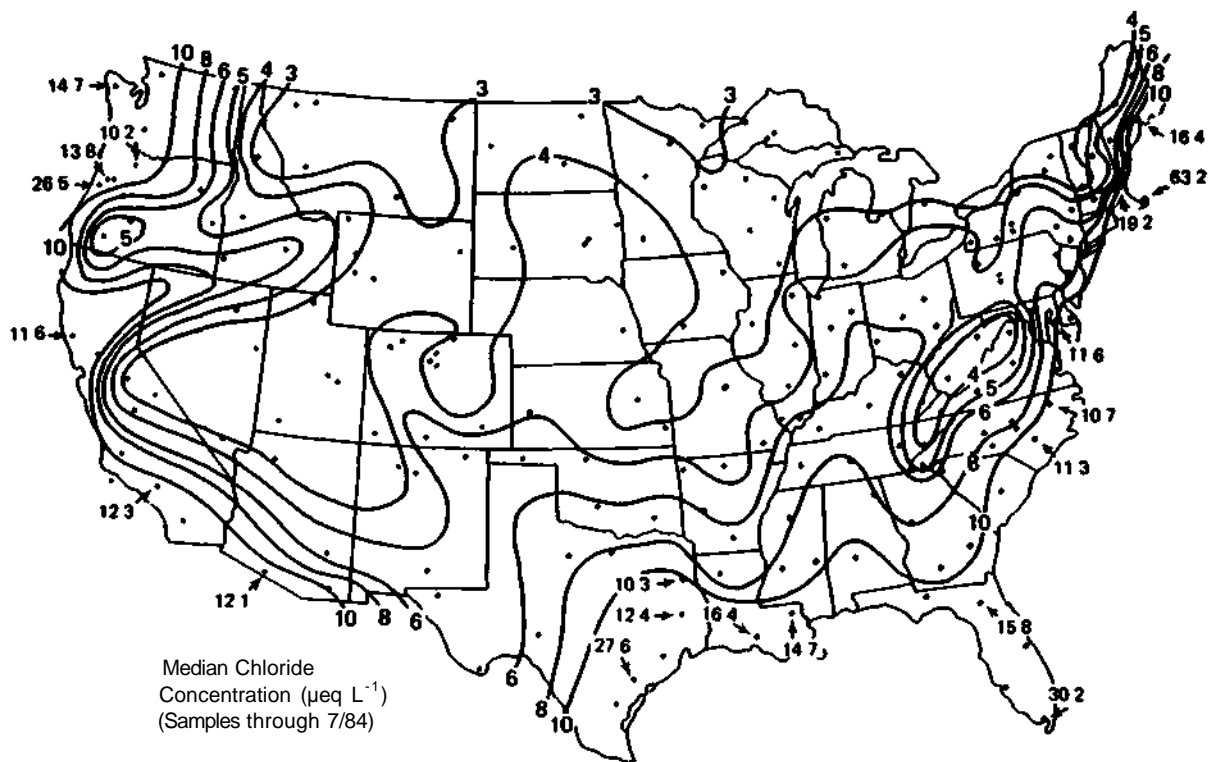


Figure 3. The median chloride concentration (top) and deposition (bottom).

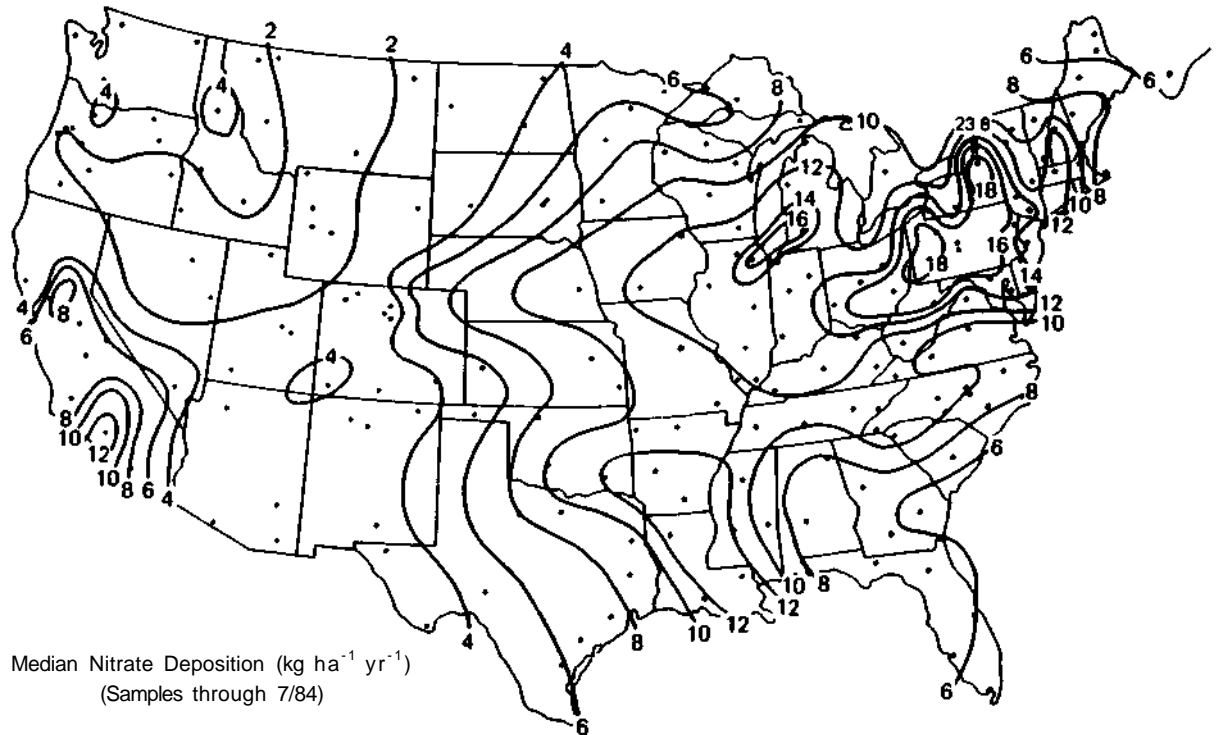
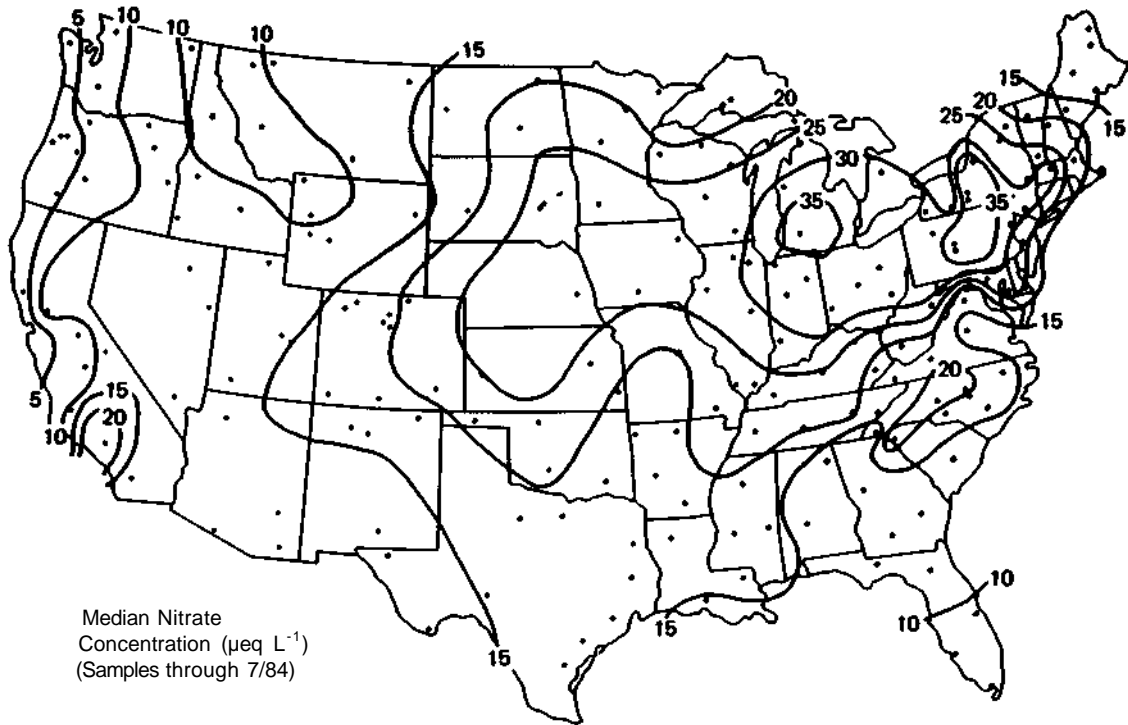


Figure 4. The median nitrate concentration (top) and deposition (bottom).

Sulfate

The sulfate concentration is shown in Figure 5. The most obvious feature in this figure is the large area of high concentration in the eastern U.S.. The values decrease outward from maxima over southwestern Pennsylvania and south-central New York. It is interesting to note that the east-west axis of the maximum lies to the north of the Ohio River frequently presumed to be the major source region for sulfur dioxide in the east.

The west coast population centers of San Francisco and Los Angeles appear with minor maxima associated with them. The other two small maxima over the central Washington and Oregon border and over the southern Arizona and New Mexico border are difficult to explain. Equally noticeable is the lack of high concentrations in the Four Corners region.

The deposition shown in Figure 5 is a good visual representation of the product of the concentration and precipitation. The axis of the major high deposition area is shifted to the south and oriented northeast-southwest. This slightly shifted pattern from the concentration maximum is due to the gradual increase of precipitation from Illinois southeastward. The pattern, then, gives the appearance of little long-range transport from the primary source region, that is, the heaviest deposition occurs directly over the highest sulfur dioxide emission area.

pH and Hydrogen Ion

The mean pH distribution shown in Figure 6 reveals values less than 5.0 over almost the entire eastern half of the U.S.. It has been argued that this pattern has not changed significantly since prior to the early 1950's (Stensland and Semonin, 1982). The major features to be noted are the low pH values in the east, the high values in the Great Plains from the Canadian border south to the Texas border, and the more variable pattern in the mountainous west.

The hydrogen ion deposition, also shown in Figure 6, exceeds 20 grams per hectare per year over most of Michigan, Illinois, eastern Missouri and Arkansas, Mississippi, Alabama, and the northern half of Georgia. The greatest deposition of over 60 grams per hectare per year is observed over western Pennsylvania.

SUMMARY AND DISCUSSION

The author has briefly recounted the history of scientific interest in precipitation chemistry and focused attention on some of the important problems dealing with the quality assurance of analyzed samples. These considerations lead the author to conclude that comparisons between data collected prior to the late 1970's and those more recently acquired should not be used to establish trends. The variety of sampling methods used, frequently unknown analytical procedures used, and the absence of measured

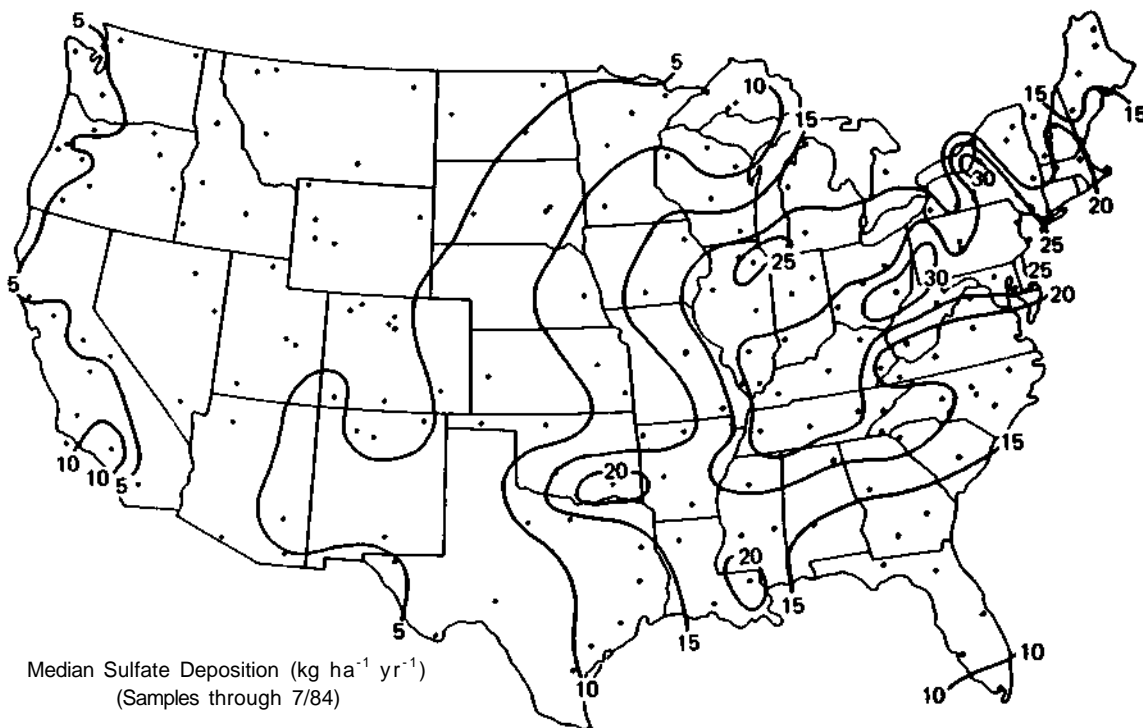
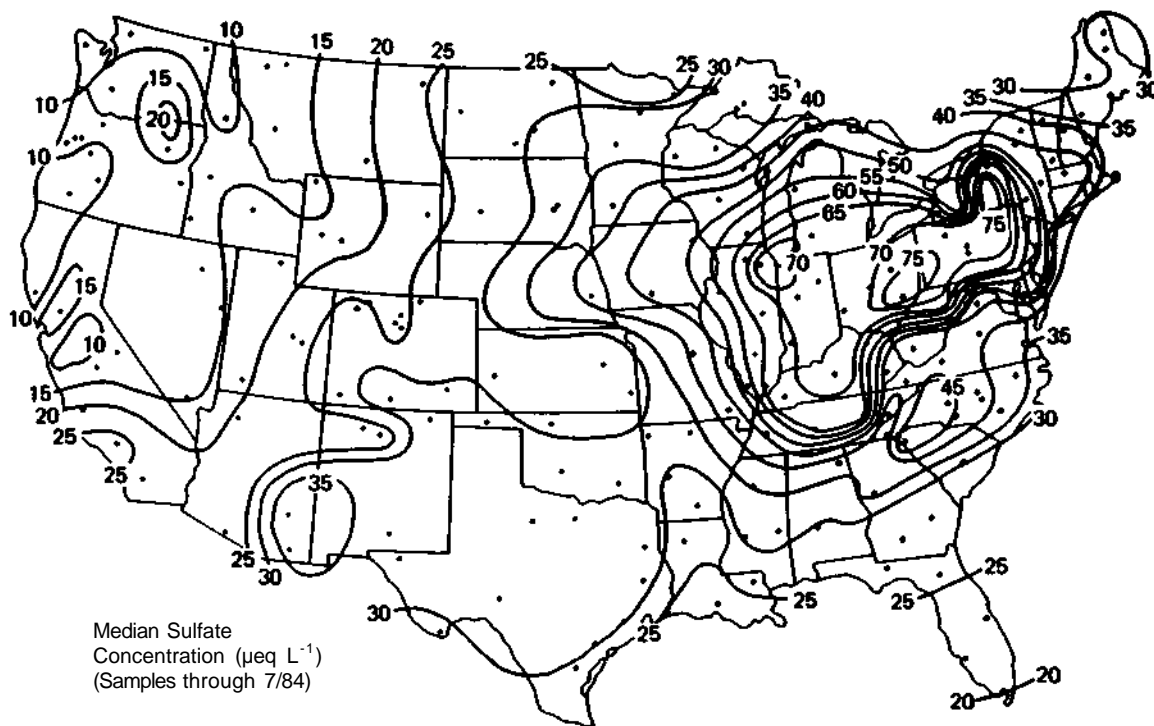


Figure 5. The median sulfate concentration (top) and deposition (bottom).

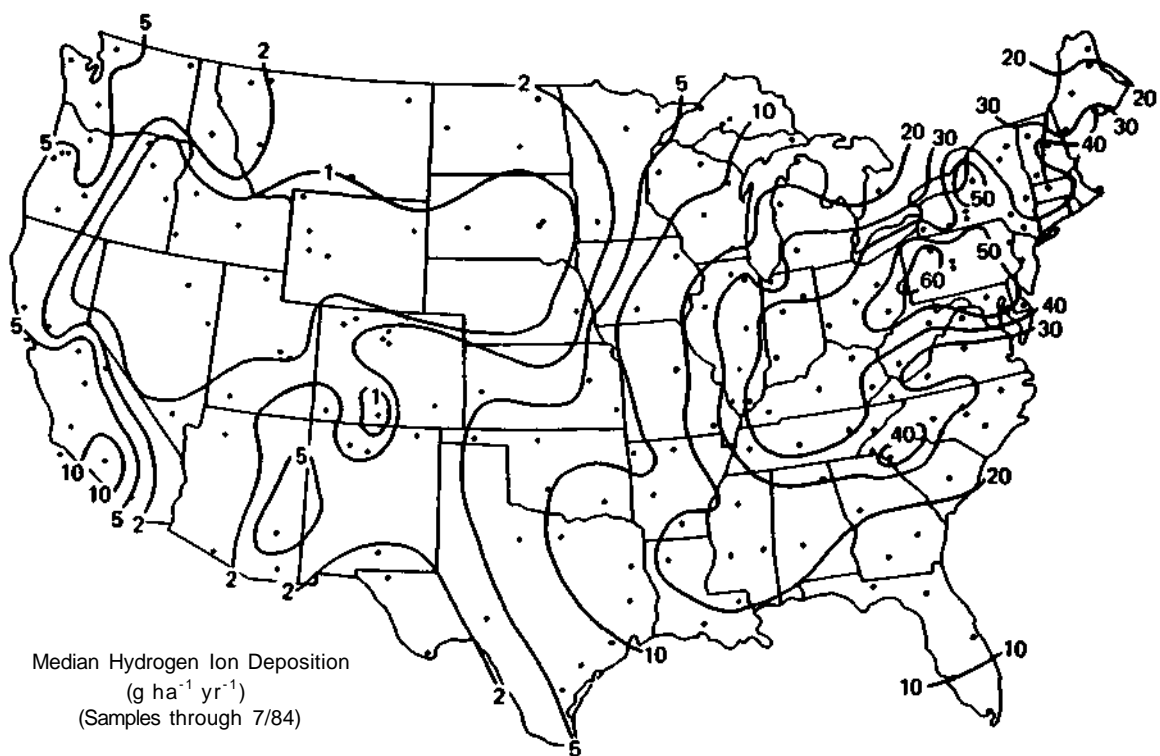
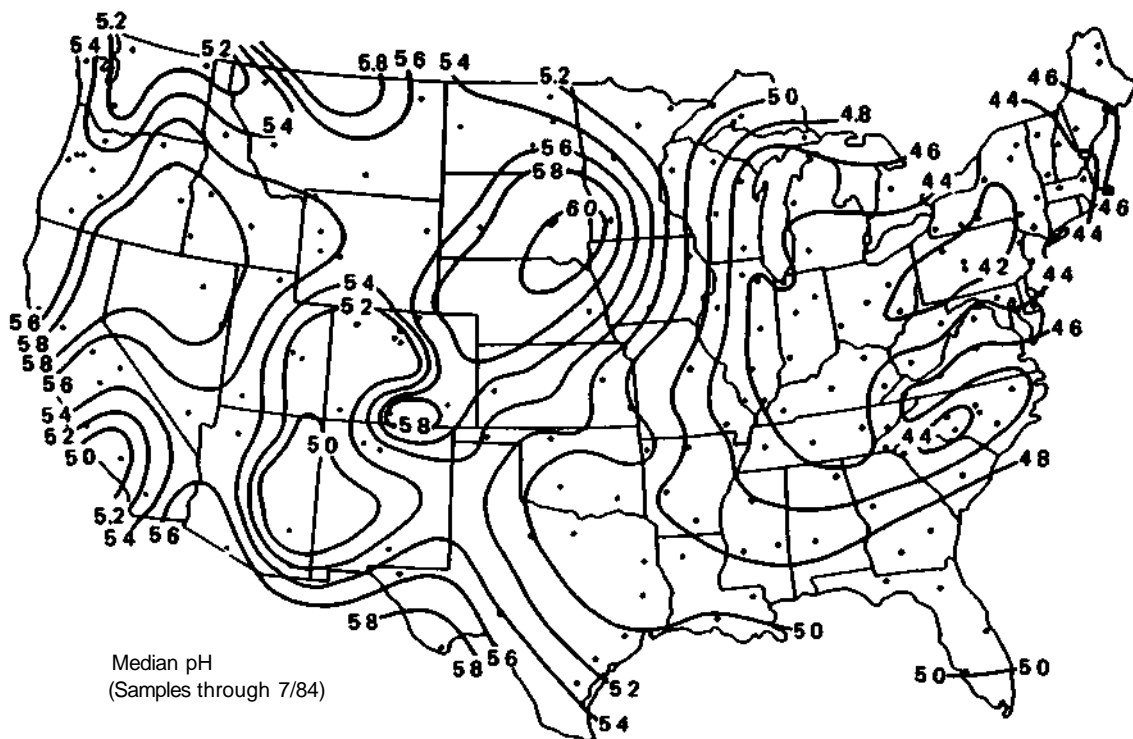


Figure 6. The median pH (top) and the hydrogen ion deposition (bottom).

key chemistry variables do not permit objective interpretation of the older data. These inadequacies of the available data prior to the establishment of the NADP/NTN network gave rise to controversy concerning the reality of a presumed trend toward greater precipitation acidity in the Northeast U.S. and areal spreading to the Midwest and Southeast (Likens and Butler, 1981; Stensland and Semonin, 1982). The trend issue is of importance as national policy is gradually emerging from the work of the National Acid Precipitation Assessment Program.

An example of the variability of pH and sulfate is shown in Figure 7. The data shown are from a site in rural, east-central Illinois. The individual weekly samples were used to generate 12 week moving averages which emphasizes the seasonality of the sulfate in precipitation. A linear fit to the concentration data shows a marked decline of sulfate over the period of record (not shown on the figure). The peak in concentration during the summer months is readily seen in this figure although there are year-to-year differences in the maximum value. The middle part of Figure 7 depicts the precipitation moving average. The seasonality of the Illinois precipitation is also quite noticeable with summertime peaks. The next curve, moving up on the figure, is the sulfate deposition. The seasonal peaks are emphasized for the deposition because the concentration and the precipitation are in phase. Note that the deposition, however, is dominated by the precipitation. For example, the greatest concentration was observed in the 1980 summer, but the greatest deposition was observed in the 1981 summer due to the higher summer rainfall in that year. Finally, the pH moving average, short-term trend is shown at the top of Figure 7. While there appears to be a direct correlation between the sulfate concentration and the pH, it is by no means perfect. One of the most obvious discrepancies appears in 1984 where the sulfate peak concentration occurs with a relative maximum pH although there is a decline noticeable shortly thereafter.

One final point can be made from the data in Figure 7. If we assume that a reduction by 50 percent of the peak concentration (90 micro-equivalents per liter) in the 1983 summer, the resulting concentration would be approximately that observed in the previous winter. Yet, the pH change over those two seasons was observed to be from about 4.3 to 4.5 or 0.2 pH units. Clearly, the acid rain issue is a complex one with no easy solutions.

It was stated at the outset that no dry deposition monitoring method has been decided and approved, but the dry bucket data from the precipitation network are available and, perhaps, are a source of some information. The total deposition was calculated at five sites in the NADP/NTN network and the percentage that was observed wet and dry was determined. The sites are located in east-central Illinois, northeast Ohio, southeast New York, central North Carolina, and extreme southwest North Carolina. All sites are rural in character with the southwest North Carolina site standing in a forest clearcut area. The data are shown in Figure 8. Recall the point made earlier that the first three ions shown in the figure are related to crustal dust. At all but one of the sites, these ions are deposited primarily dry while those associated with the oceans and anthropogenic sources are deposited wet. The one exception is the

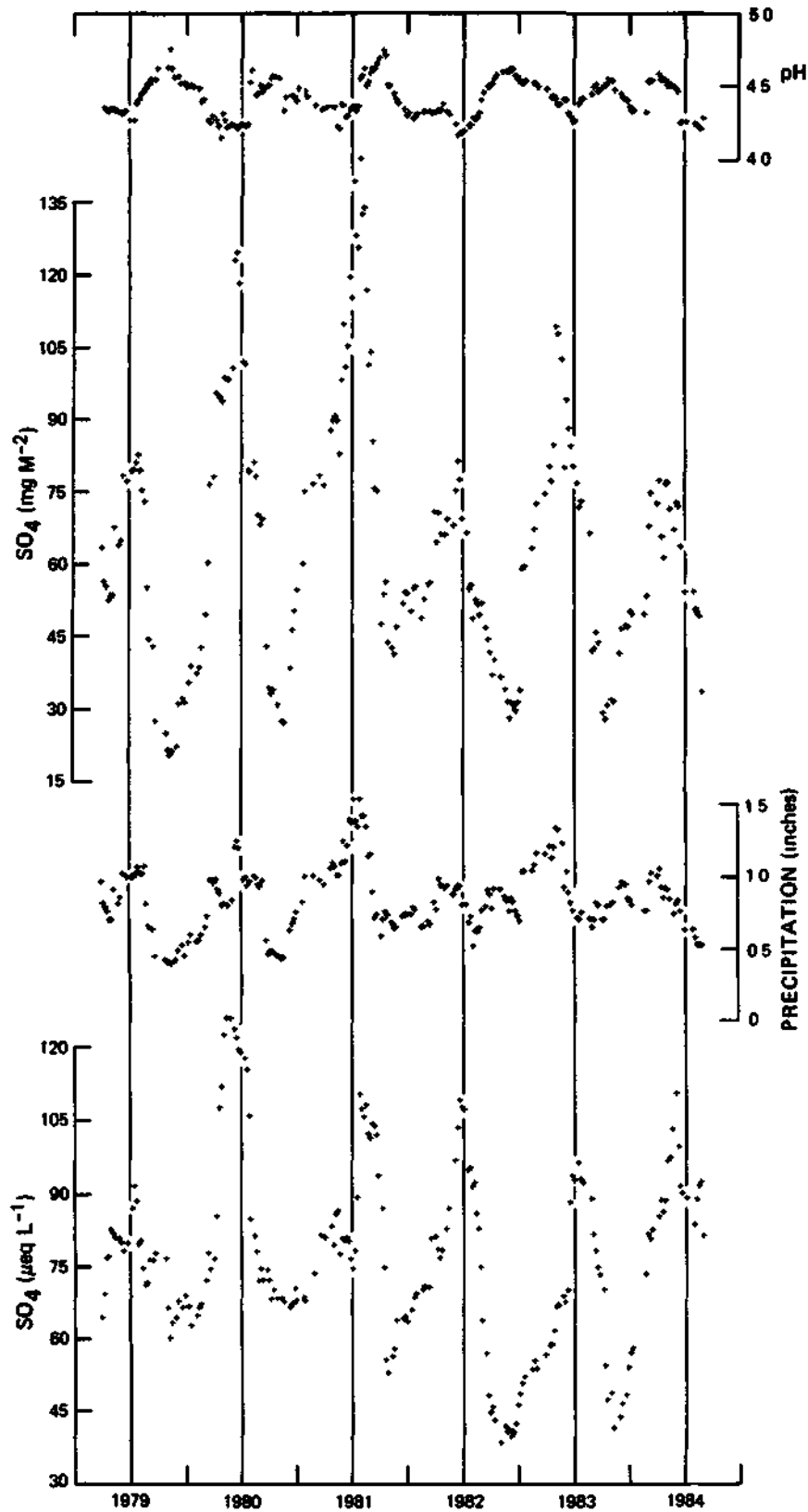


Figure 7. The pH (top), sulfate deposition (first down from the top), precipitation (first up from the bottom), and the sulfate concentration (bottom) from the Bondville, Illinois NADP/NTN site.

TOTAL DEPOSITION AT SELECTED NADP SITES
(mg M⁻²)

		Ca	Mg	K	Na	NH ₄	NO ₃	Cl	SO ₄	Total
IL 11 (17)	T	11.2	1.7	1.3	1.0	6.6	35.2	2.5	62.4	121.8
	%D	69.2	70.5	74.2	25.4	17.7	26.0	24.0	27.9	31.6
	%W	30.8	29.5	25.8	74.6	82.3	74.0	76.0	72.1	68.4
OH 71 (14)	T	13.1	1.9	1.4	1.6	5.2	32.0	3.5	71.0	129.7
	%D	78.5	67.5	77.7	31.5	10.9	20.7	31.5	30.9	33.4
	%W	21.5	32.5	22.3	68.5	89.1	79.3	68.5	69.1	66.6
NY 51 (13)	T	4.8	1.9	0.6	3.7	3.0	31.4	4.4	69.5	109.4
	%D	55.5	58.9	38.8	36.5	11.0	10.3	16.7	17.2	18.3
	%W	44.5	41.1	61.2	63.5	89.0	89.7	83.3	82.8	81.7
NC 41 (12)	T	3.8	1.2	1.4	3.8	6.7	22.8	5.5	44.8	89.9
	%D	58.6	53.9	73.1	40.4	53.0	23.0	32.1	30.8	33.1
	%W	41.4	46.1	26.9	59.6	47.0	77.0	67.9	69.2	66.9
NC 25 (10)	T	2.5	0.7	0.9	2.6	3.2	22.1	3.6	45.6	81.1
	%D	18.7	16.0	52.5	12.7	9.3	1.7	3.2	7.5	6.9
	%W	81.3	84.0	47.5	87.3	90.7	98.3	96.8	92.5	93.1

Figure 8. The total and percent wet and dry deposition at selected NADP/NTN network sites.

forest clearcut site in North Carolina where wet deposition accounts for almost all of the deposition for all ions but potassium.

In conclusion, as the data base for precipitation chemistry grows so does our knowledge of its variability and trend. It seems rather clear, that there is not a rapidly declining quality of precipitation and any changes in recent years are going to be difficult to quantify in the presence of the observed great variability (Semonin and Stensland, 1984). It is equally clear, that to try to estimate a trend using data prior to the implementation of the NADP/NTN network opens the door to controversy since those data were not collected for trend analysis and did not include some of the important ions necessary to address the precipitation acidity issue. The total deposition must be measured if the insult to the biosphere is to be fully assessed. In the absence of a dry deposition monitoring network, the bucket estimates suggest that for some ions dry deposition is most important while for others wet deposition dominates. In any event, there does not appear to be a 50-50 split between the two forms. Damage mitigation strategies must consider this imbalance between wet and dry deposition and its regionality. It must be obvious, from the foregoing data and discussion, that additional work needs to be accomplished before answers to many key questions will be forthcoming

ACKNOWLEDGEMENT

This work was supported by the National Acid Precipitation Assessment Program under USDOE Office of Health and Environmental Research Contract DE-AC02-76EV01199.

REFERENCES

- Bachman, S. R. , J. M. Lockard, and M. E. Peden, 1984: In "Study of Atmospheric Pollution Scavenging". 20th Progress Report", Illinois State Water Survey, Champaign, IL, 233-250.
- Cogbill, C. V., 1976: Water, Air, and Soil Pollution. 6, 407, 413.
- Cogbill, C. V., and G. E. Likens, 1974: Water Resources Res. 10, 1133-1137.
- Cowling, E. B., 1982: Environ. Sci. Technol., 16, 110A-123A.
- Dochinger, L. S., and T. A. Seliga, 1976: First Intern. Symp. on Acid Precip. and Forest Ecosystems. 1009 pp.
- Galloway, J. N., and G. E. Likens, 1978: Tellus. 30, 71-82.
- Granat, L., 1972: Tellus. 24, 550-560.

- Junge, C. E., and P. E. Gustafson, 1956: Bull Am Meteor. Soc., 37, 344.
- Junge, C E., and R. J. Werby, 1958: J. Meteorol., 15, 417-425.
- Likens, G. E., and T. J. Butler, 1981: Atmos. Environ., 15, 1103-1109.
- Lodge, J. P., Jr., J. B. Pate, W. Basbergill, S. G. Swanson, K. C. Hill, E. Lorange, and A. L. Lazrus, 1968: "Chemistry of United States Precipitation. Final Report on the National Precipitation Sampling Network", National Center for Atmospheric Research, Boulder, CO, 66 pp.
- MacIntire, W. H , and J. B Young, 1923 Soil Sci., 15, 205-227
- Miller, J. M. , G. J. Stensland, and R. G. Semonin, 1984. "The Chemistry of Precipitation for the Island of Hawaii During the HAMEC Project", NOAA/ARL, Boulder, CO, 3-9.
- NADP, 1984: "NADP Quality Assurance Plan for Deposition Monitoring", National Atmospheric Deposition Program, Ft Collins, CO, 39 pp.
- NAPAP, 1982: "National Acid Precipitation Assessment Plan", Interagency Task Force on Acid Precipitation, 92 pp.
- Peden, M. E., and L M. Skowron, 1978. Atmos. Environ. 12, 2343-2349
- Peden, M. E., and J. M. Lockard, 1984: In "Study of Atmospheric Pollution Scavenging. 20th Progress Report". Illinois State Water Survey, Champaign, IL, 75-84.
- Rossby, C G , and H. Egner, 1955 Tellus, 7, 118-133.
- Semonin, R. G., 1976 Water. Air, and Soil Pollution. 6, 395-406
- Semonin, R. G. , 1977 Proc of the Conf. on Metropolitan Physical Environ., 53-61.
- Semonin, R. G., 1983: Proc. of the 12th Annual ENR Conference, 182-217.
- Semonin, R. G., and G J. Stensland, 1984. Weatherwise. 37, 250-251
- Stensland, G J., and R. G. Semonin, 1982: Bull. Am Meteor. Soc., 63, 1277-1284.
- Stewart, R. , 1920. Univ of Illinois Ag. Exp. Station Bulletin 227, 99-108.
- Wisniewski, J , and J D. Kinsman, 1982: Bull. Am Meteor Soc. 63, 598-618.

CHAPTER 2

INTRA-ANNUAL VARIATIONS IN THE CONCENTRATIONS OF MAJOR INORGANIC IONS IN THE PRECIPITATION OF THE UNITED STATES

Van C Bowersox and Gary J. Stensland

INTRODUCTION

It has been shown that the concentrations of the major inorganic ions in precipitation exhibit seasonal (3-month average) excursions at eastern U.S. sampling locations. Summertime minima and wintertime maxima in the record of precipitation pH were reported in New York and New Hampshire (Likens and Borman, 1974). Examination of the data from the MAP3S network (Pack, 1978) at Whiteface and Ithaca, NY, State College, PA, and Charlottesville, VA suggested that precipitation sulfate maximized throughout most of the northeastern U.S. in summer, as did hydrogen ion (Bowersox and de Pena, 1980). A comparison of aerosol and precipitation sulfate throughout much of the eastern U.S. showed that May through September concentrations were more than 20% higher than November through March concentrations, and that seasonal (3-month) differences could be as much as 60% higher in the warm, compared to the cold, seasons (Bowersox and Stensland, 1981). In addition, National Atmospheric Deposition Program/National Trends Network (NADP/NTN) precipitation chemistry data exhibited a north to south increase in the warm versus cold period ratio of nitrate concentrations. In the south, the May through September nitrate concentrations were 30% to 60% higher than November through March values, but at northern latitudes the differences were insignificant.

The purpose of this study was to extend previous work by examining intra-annual variations in concentrations for all of the major inorganic ions in both the western and eastern U.S. NADP/NTN data from October 1978 to March 1984 were used. Concentration ratios were calculated, where the ratio was either warm season concentration/cold season concentration or warm period concentration/cold period concentration. Seasons were 3-month intervals while periods were 5-month intervals. The summer (warm) season was June, July, and August while the winter (cold) season was December, January, and February. The summer (warm) period covered the 5-month interval from May through September while the winter (cold) period covered the interval from November through March. For most of the U.S., the warm and cold periods approximated the growing seasons and dormant seasons, respectively.

METHODS

Data from the NADP/NTN (1984) were used for this study, because it included sites from across the continental United States. This network began operations in 1978 with about 20 sites and grew to about 140 sites

by the end of 1983. During the early years of the project, the sites were located primarily in the eastern U S.

All sites were equipped with the same automatic wet/dry deposition sampler. At each site the daily precipitation and the volume of sample caught in the wet deposition bucket during the sampling period were reported. Most sites employed a recording (weighing bucket) raingage, which had been modified to include an "event marker" to record periods when the wet-side bucket was exposed to precipitation. This record was evaluated to ascertain that the sampler had operated correctly to collect a wet-only sample. Even when no precipitation occurred, the wet-side bucket was sent to the CAL. The contents of these dry wet-side buckets were analyzed as (quality assurance) system blank samples (Stensland, et al., 1983).

Every Tuesday the sample bucket on the wet side of the sampler was removed and sent to a single laboratory at the Illinois State Water Survey, the Central Analytical Laboratory (CAL) of NADP. At the CAL, the sample volume, pH, and solution conductance were measured, along with chloride, ammonium, calcium, magnesium, sodium, potassium, sulfate, nitrate, and phosphate (see Peden, 1986, for laboratory methods). Since phosphate was usually below the analytical limit of detection, it was not considered here. Samples of about 35 mL or more liquid precipitation were analyzed at the concentration received. Normalized by the collection cross section (bucket radius = 14.7 cm), this volume was equivalent to a liquid precipitation depth of 0.02 inches or 0.52 mm. Volumes smaller than 35 mL required dilution in order to satisfy the liquid volume requirement of each analytical method. To avoid the added uncertainties due to the extra handling and due to the propagation of errors from the calculation of a dilution factor, only data for undiluted samples were used in this study.

Data for each sample, along with pertinent information from communications with site operators, were reviewed by CAL data management staff to assess a) whether the proper collection, handling, and measurement protocols were followed, and b) whether visible organic contamination in the sample had produced a sample unrepresentative of the site. Along with the various physical and chemical measurements of each sample, a record was generated in a computerized database to document the results of this data validation process (Bowersox, 1985). Only valid data were used in this study.

In selecting sites for this study, it was necessary that sampling had been initiated before the end of 1982, thus at least a year of data was available. It was also required that the (3-month) seasonal or (5-month) period concentrations be derived from >10 values. Either median concentrations or sample volume weighted concentrations were calculated from the 10 or more values to represent seasonal and period "averages." Finally data for some sites (about 15) were not considered because a) the site had discontinued operation, or b) the site had a history of irregular operation.

Computer generated isopleth maps are presented in this study. Through an objective analysis, based on a successive correction scheme developed

by Barnes (1964; 1973) and modified by Achtemeier et al. (1977), the irregularly spaced site data were interpolated to a regular grid. Isoleths were then drawn on this grid-point field. These maps describe the general or synoptic features of the ratios of seasonal or period concentrations.

RESULTS AND DISCUSSION

Figure 1 depicts the sites for which data were used in this study and the total number of valid samples for the warm period. Four regions are outlined in this figure, the Northeast (NE), Southeast (SE), Midwest (MW), and Rocky Mountains (RM). A summary of these regions is presented in Table 1, discussed later. The site in Oregon with 16 samples, had the least amount of data. For the cold period, the minimum number of samples available at any site was 20.

To indicate the direction and size of intra-annual variations, the dimensionless ratio of the warm period median concentration divided by the cold period median concentration was computed at each site. Figure 2 shows the spatial variations of the ratios for ammonium ion. To generate this map, the distribution of station ratios was objectively analyzed and the resulting grid point field of ratios was contoured. Throughout much of the country, values were above 1. This indicates that NH_4^+ was generally higher in the warm (growing season) than in the cold period. In New England and Rocky Mountain states, the warm period medians were more than twice the cold period medians, suggesting an even stronger growing season high. At coastal sites in Oregon and Texas and in Florida, the ratios were less than 1, as they were at two mid-continental sites in Nebraska and Minnesota.

In a study of the spatial distribution of inorganic ions in precipitation of the U.S. and Canada, Semonin and Bowersox (1983) found that ammonium ion contributed over 10% of the total inorganic ion concentrations throughout much of the mid-continental U.S. and lower Canadian provinces. Average concentrations maximized over the same Nebraska and southern Minnesota sites where warm/cold period ratios were less than 1. Over much of the U.S., emissions of ammonia are dominated by land-use practices. Chief among the anthropogenically related emissions is animal waste from domestic livestock production (Harriss and Michaels, 1982). Because of the size and number of feedlot operations near the Mead site in eastern Nebraska, there is likely to be a strong link between emissions from animal waste, NH_3 in the air, and NH_4^+ in precipitation. Since NH_4^+ was higher in the cold than the warm period at the Mead site, several hypotheses can be posed: (1) emissions from feedlots are higher in the cold period than the warm period; or (2) NH_3 from feedlot and other sources is oxidized to NO_x in the atmosphere and much as for SO_2 , cyclic photochemical processes, which maximize during the warm period, dominate the oxidation; or (3) meteorological factors related to storm type, storm size, storm track, etc., control the intra-annual variations of NH_4^+ in precipitation; or (4) NH_4^+ in weekly precipitation samples is decomposed chemically during the warm period of the year, resulting in an artifact

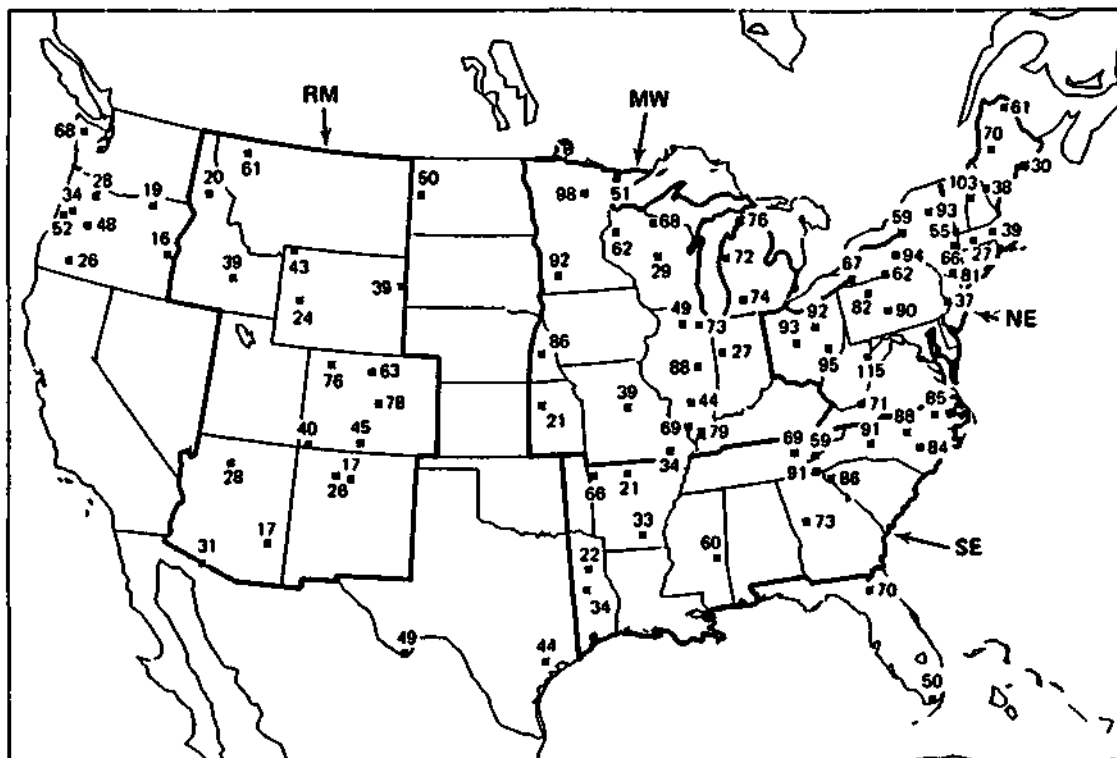


Figure 1. Precipitation chemistry sites and the number of samples used to calculate warm period medians and averages. Also shown are the four regions used for Table I.

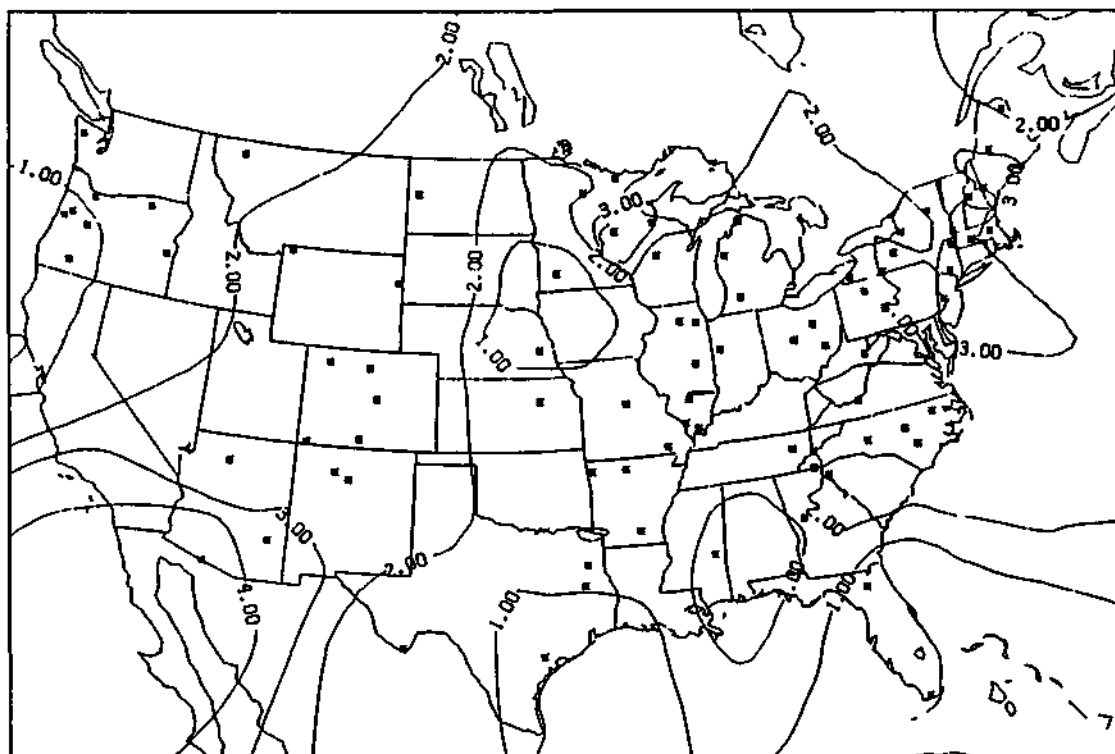


Figure 2. Warm period/cold period ratios of the median concentrations of ammonium ion in precipitation.

due to NADP/NTN protocols. To assess the strengths and weaknesses of these hypotheses, the spatial patterns of the intra-annual variations of NH_4^+ were compared with the patterns of other ions.

Warm period/cold period concentration ratios of nitrate are plotted in Figures 3 and 4. Weighted average concentrations were used to calculate the ratios in Figure 3 and medians in Figure 4. Though the spatial patterns of the two ratios were similar in the eastern half of the country, ratios in the Rocky Mountain states in Figure 4 were somewhat larger than in Figure 3. For nitrate the magnitudes of the ratios were sensitive to the choice of a median or weighted average, while the positions of relative highs and lows were not so sensitive. Additional comparisons are shown in Table 1, which is discussed later.

The results in Figure 4 support the earlier conclusion by Bowersox and Stensland (1981) that there is the suggestion of a south-to-north gradient in the seasonality of nitrate in precipitation. In general, ratios were largest in the southern states and decreased toward the north. Median nitrate concentrations were two or more times higher in the warm period than the cold period at southern sites. Throughout the northeastern U S , warm and cold period median concentrations were nearly equal; and in the Upper Midwest, the cold period medians were larger than warm period medians at every site. Only at sites in the Northwest were warm period/cold period ratios consistently above one at latitudes north of about 40° . That the nitrate concentrations at Nebraska and Minnesota sites with high NH_4^+ were not higher in the warm than the cold period weakens the hypothesis that photochemical conversion of NH_3 to NO_x results in lower NH_4^+ concentrations in the warm period. Though NH_3 may be oxidized to NO_x in the atmosphere, there is no strong evidence to support that hypothesis in the intra-annual variations of NH_4^+ and NO_3^- in precipitation

This study of intra-annual variations was based on both 5-month warm and cold periods and on 3-month warm and cold seasons. Comparisons of ratios for these two averaging times are presented in Figures 5 through 10 for $\text{SO}_4^{=}$, H^+ , and Mg^{++} . Although seasonal ratios tended to be larger than period ratios, areas where both ratios 1.5 for $\text{SO}_4^{=}$ and Mg^{++} or 2.0 for H^+ were spatially similar. For example, seasonal ratios in Figure 5 exceeded 3 in much of New England, where period ratios in (Figure 6) were between 2.5 and 3. Both figures showed a 1,000-2,000 km wide area, beginning in North Dakota and Minnesota and extending south to Texas and Louisiana, where ratios for $\text{SO}_4^{=}$ were <1.5 . In this area cold season (or period) concentrations were similar to or greater than warm season (or period) concentrations. East and west of this mid-continental area were areas where warm season or period concentrations were distinctly higher than cold season or period concentrations. For H^+ in Figure 7, there were a few sites with seasonal ratios greater than 5 in the Rocky Mountain region, while in Figure 8 the highest period ratios in the same region were less than 5. General features of the season and period maps are similar in pattern but different in degree of variation. In comparing intra-annual variations between different studies or among different ions, it is important that the averaging times be the same. It is important that the statistical "averages" (median or weighted average) be the same, as well.

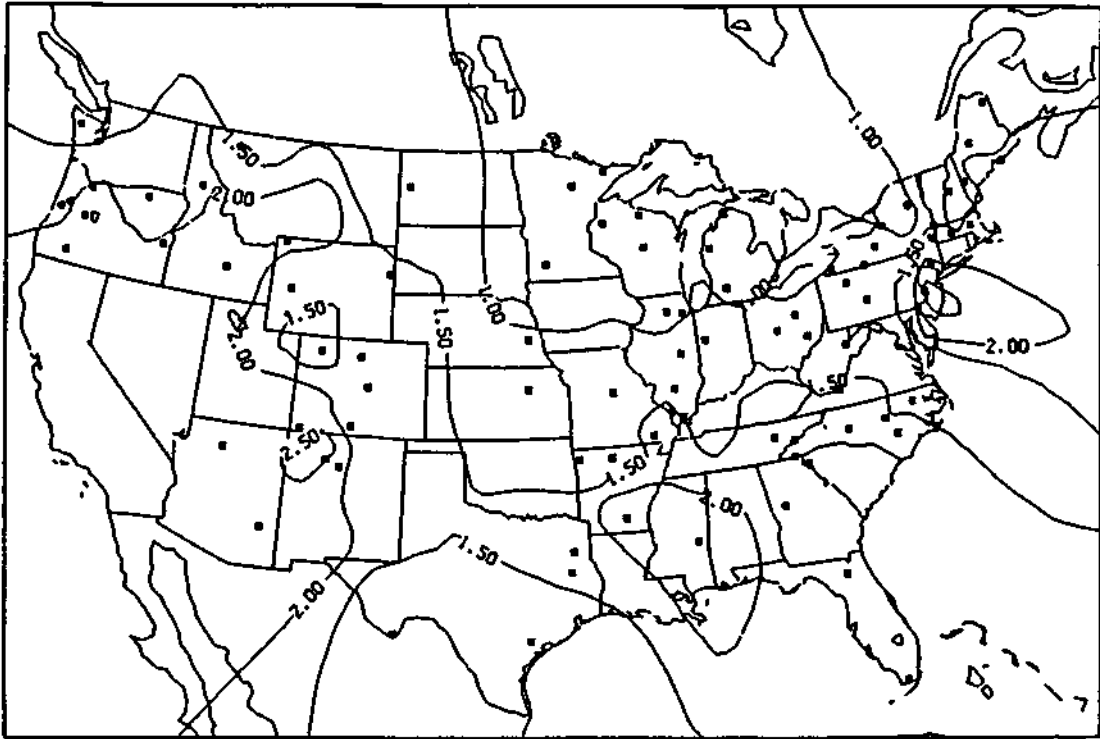


Figure 3. Warm period/cold period ratios of weighted average nitrate concentrations in precipitation.

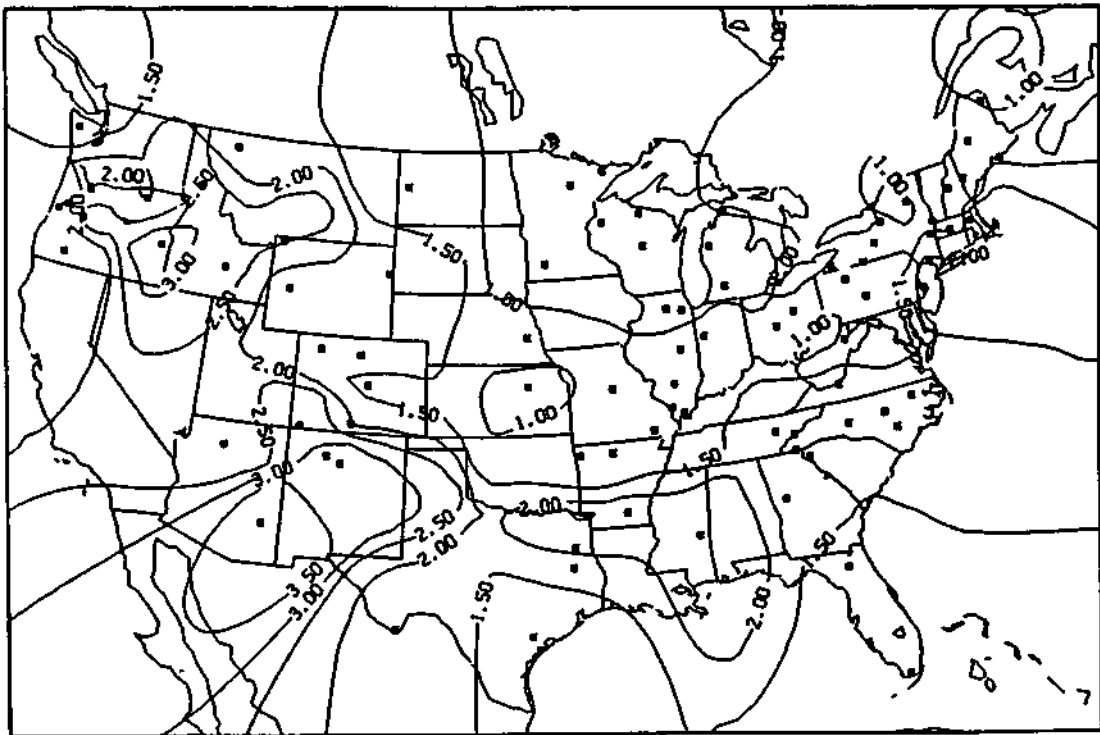


Figure 4. Warm period/cold period ratios of median nitrate concentrations in precipitation.

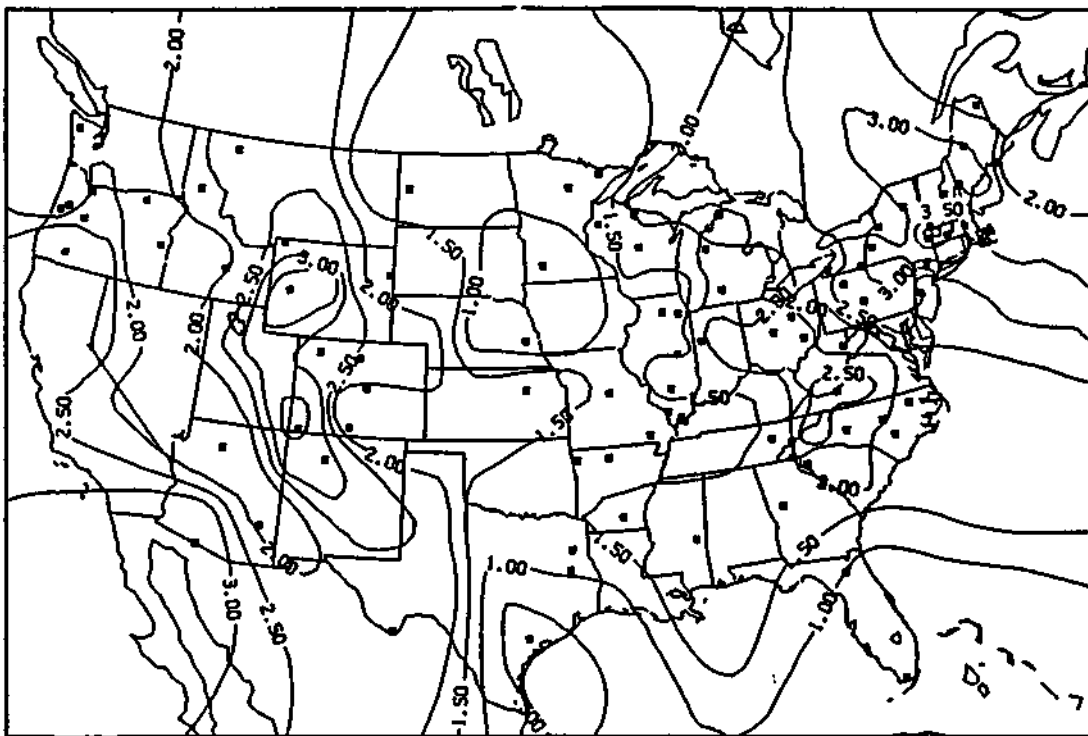


Figure 5. Warm season/cold season ratios of median sulfate concentrations in precipitation.

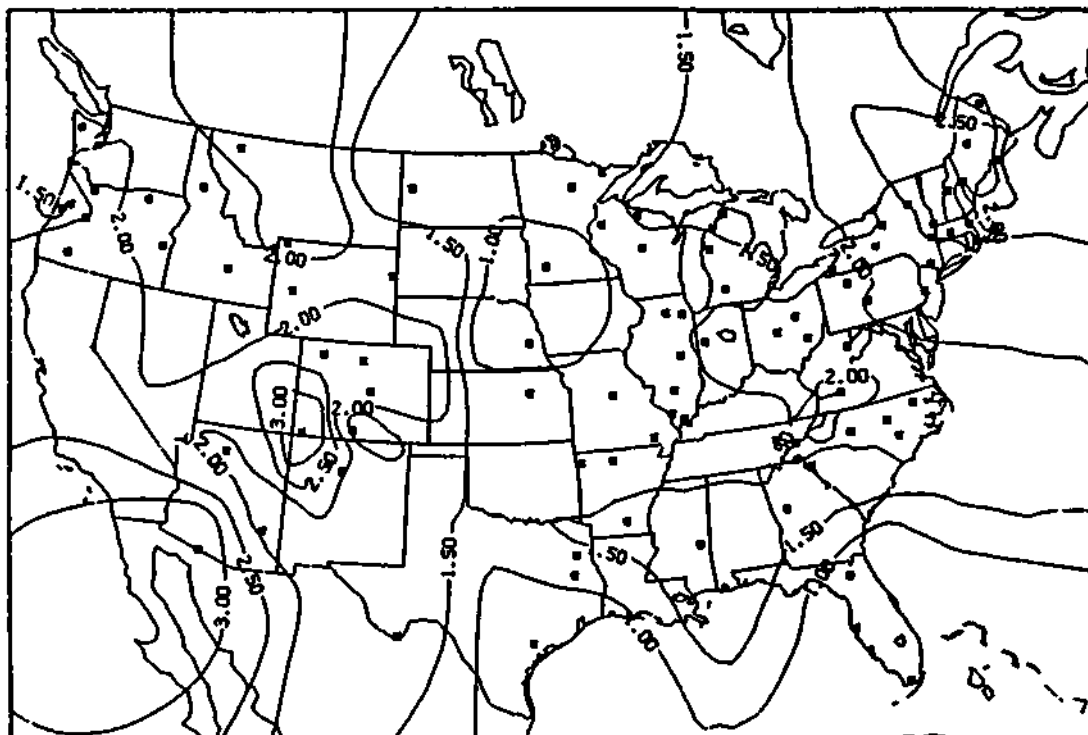


Figure 6. Warm period/cold period ratios of median sulfate concentrations in precipitation.

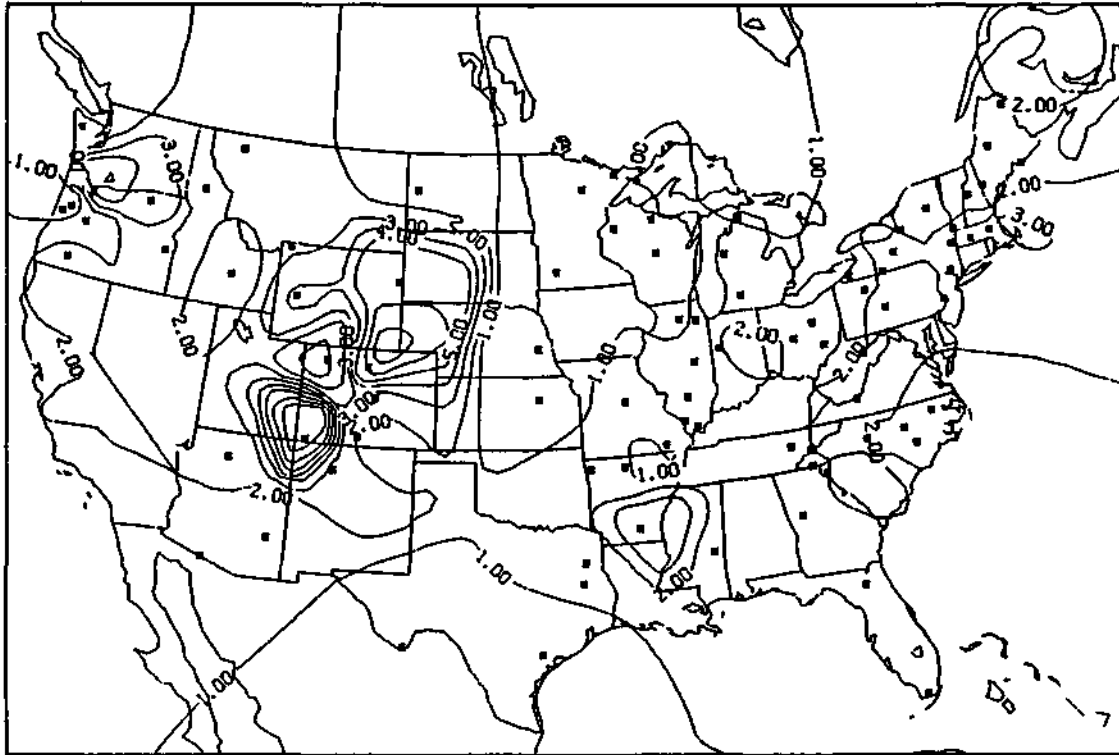


Figure 7. Warm season/cold season ratios of median hydrogen ion concentrations in precipitation.

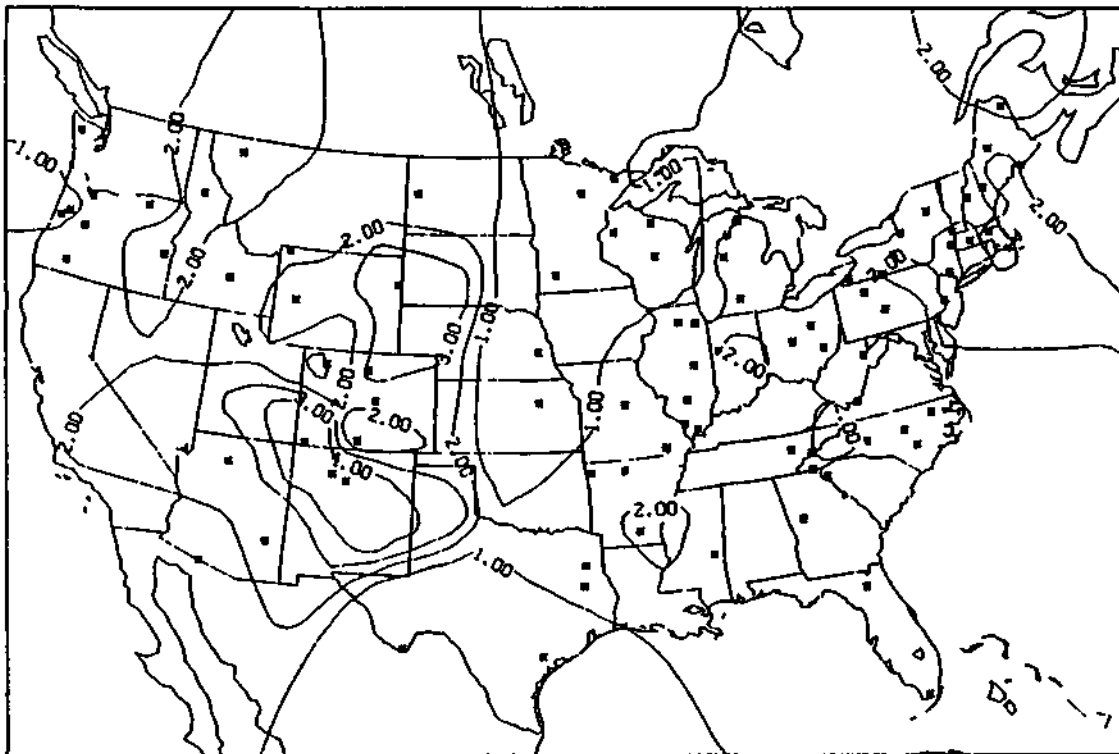


Figure 8. Warm period/cold period ratios of median hydrogen ion concentrations in precipitation.

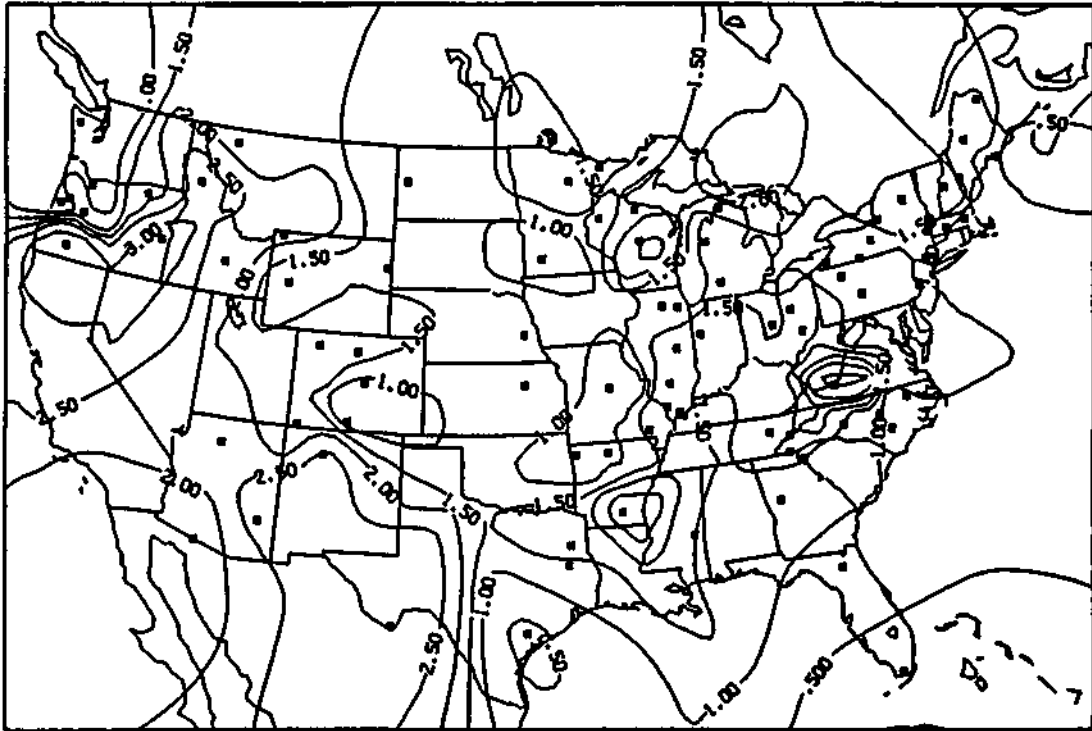


Figure 9. Warm season/cold season ratios of median magnesium concentrations in precipitation.

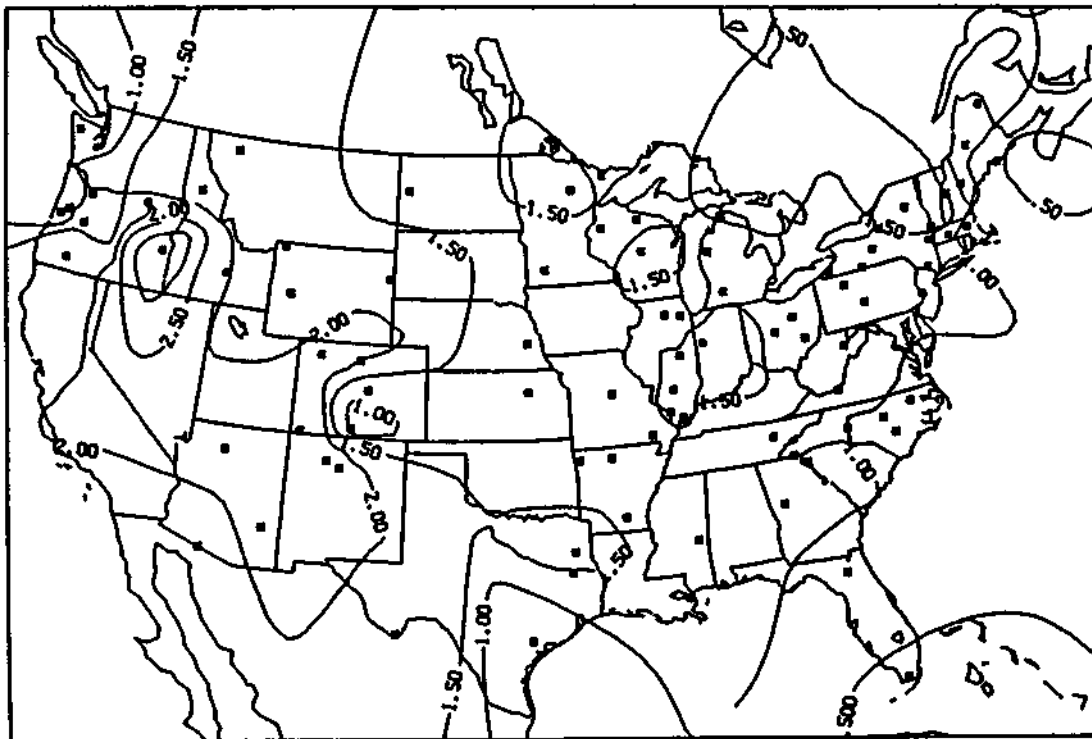


Figure 10. Warm period/cold period ratios of median magnesium concentrations in precipitation.

By contrasting the spatial patterns of ion concentration ratios, one can infer something about seasonal variations in scavenging efficiency or in air quality. Isopleth maps of concentration data have been presented elsewhere (Semonin, 1986) and are not included here. A key feature of these maps is the relatively high values of sulfate and nitrate in the northeastern quadrant of the United States. In the eastern U.S. where these acidic anions are highest, there were some important differences in their warm period/cold period variations. For sulfate (in Figure 6) the highest warm to cold ratios were in the New England states and values tended to decrease toward the south and west. As previously discussed, nitrate (in Figure 4) in the eastern U.S. exhibited an opposite north/south pattern. This reversal in the patterns of intra-annual variations in the eastern U.S. suggests a link between the oxidation and scavenging of SO_x and NO_x in the warm versus the cold period. Sulfate and nitrate attained the highest warm period/cold period ratios in the Rocky Mountain states. In the more arid climate of these western sites, distant from a large combustion-related source region, the putative link between SO_x and NO_x was not apparent. It is worth adding that the pattern for NH_4^+ in the eastern U.S. was similar to SO_4^{2-} . Together, variations in SO_4^{2-} , NO_3^- , and NH_4^+ support the hypothesis that transport (meteorological) and transformation (chemical) factors have a strong influence on intra-annual variations.

Hydrogen ion ratios in Figure 8 exhibited spatial variations similar to the combined features of sulfate and nitrate. For example, the pattern in Figure 8 of higher values in the Northeast and lower values in the southeast was like that for sulfate, while the large area of values <1.0 from Kansas toward the north was more like that for nitrate. West from the Plains states toward the Rocky Mountain states the ratios increased for H^+ as they did for all the other ions.

Figures 10 through 12 showed the spatial distributions of ratios for three ions that are derived primarily from surficial sources, such as dust from wind erosion and tilling and dust from unpaved roads (Gatz *et al.*, 1985). The major cation from these sources, calcium, had ratios for the eastern U.S. that were generally greater than 1 but less than 2. Just as for sulfate in the East, the warm period concentrations for all three ions were greater than the cold period concentrations. For all three ions, ratios in the Rocky Mountain states were larger than 1 and were larger than values in the East. For these crustal cations in general, warm (growing) period concentrations averaged higher than cold (dormant) period concentrations, except in the Pacific Northwest and coastal areas of Texas, Florida, and the East.

Figures 13 and 14 present the ratios for sodium and chloride. A principal source of these ions in air and precipitation is marine salts, though sodium is also found in soils and chloride in combustion sources. Compared to the crustal ions, sodium and chloride ratios were smaller. Notice that values even less than .5 occurred for some sites near the coast. These low values probably resulted from higher airborne sea-salt concentrations during the cold period. Airborne sea salt increases as ocean wave activity increases and the stronger average winds of the cold period give rise to greater wave activity, hence higher sea-salt concentrations. In obvious contrast to the behavior of all of the other

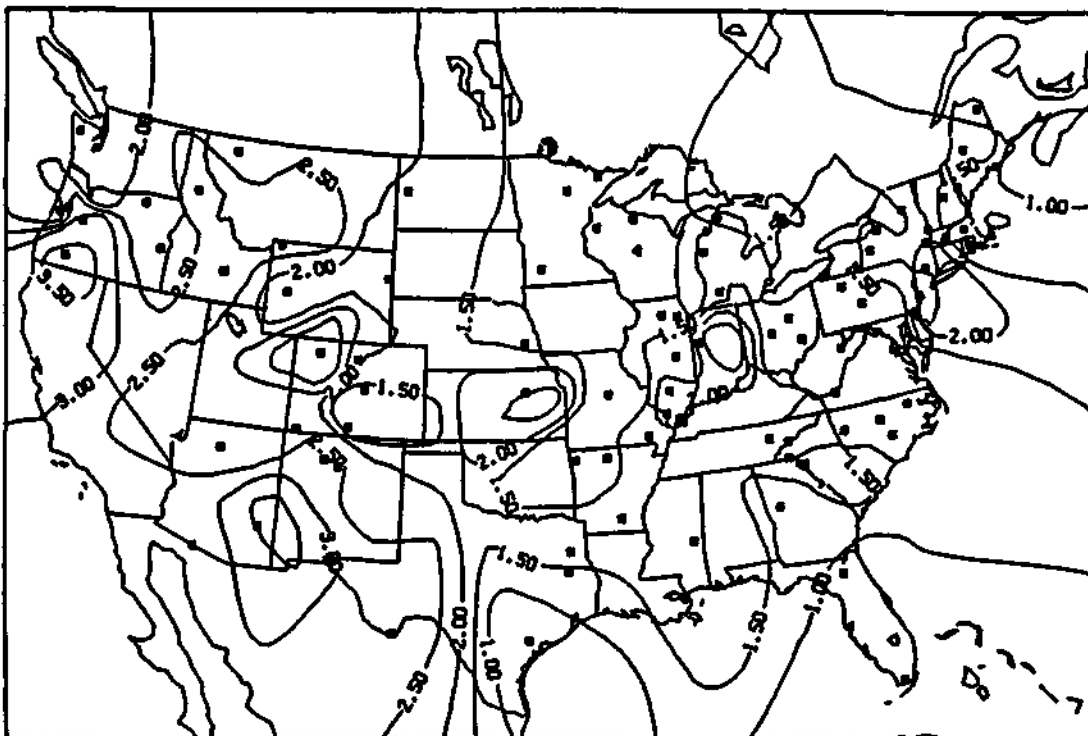


Figure 11. Warm period/cold period ratios of median calcium concentrations in precipitation.

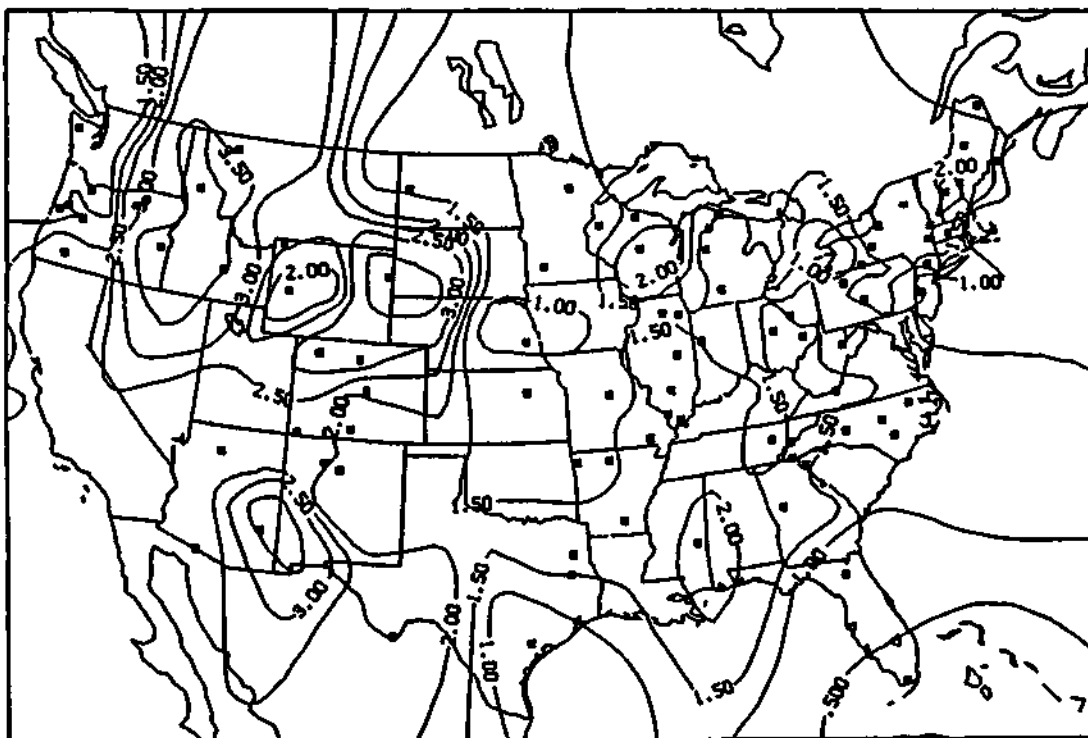


Figure 12. Warm period/cold period ratios of median potassium concentrations in precipitation.

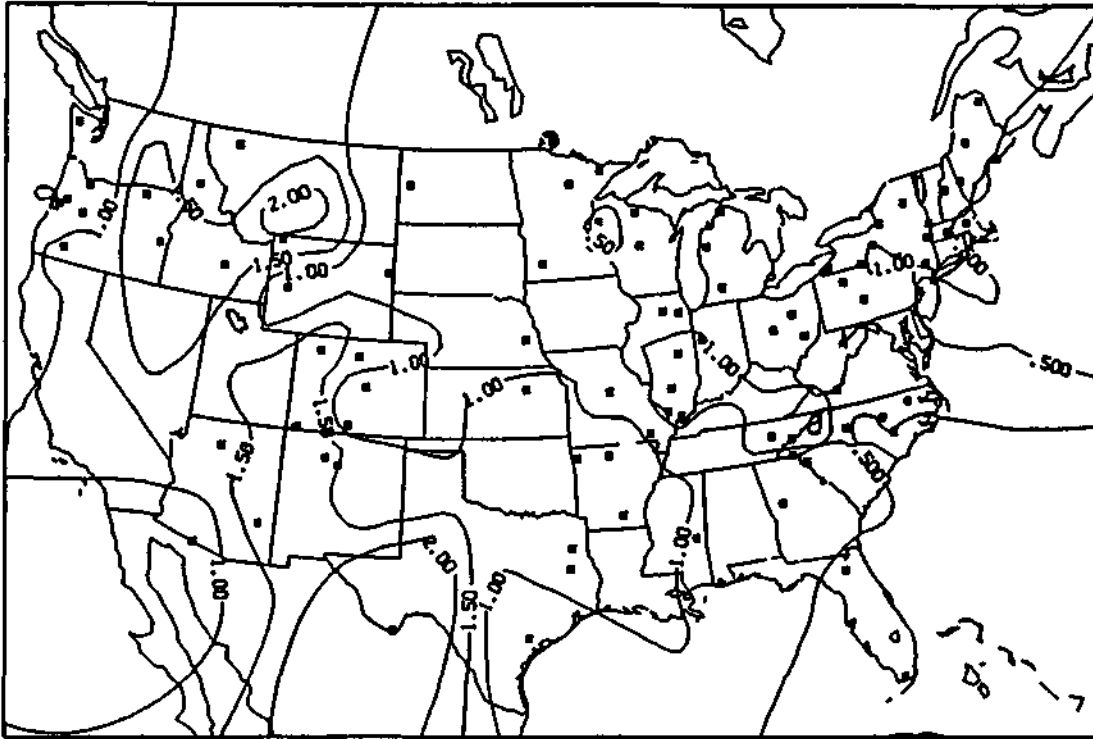


Figure 13. Warm period/cold period ratios of median sodium concentrations in precipitation.

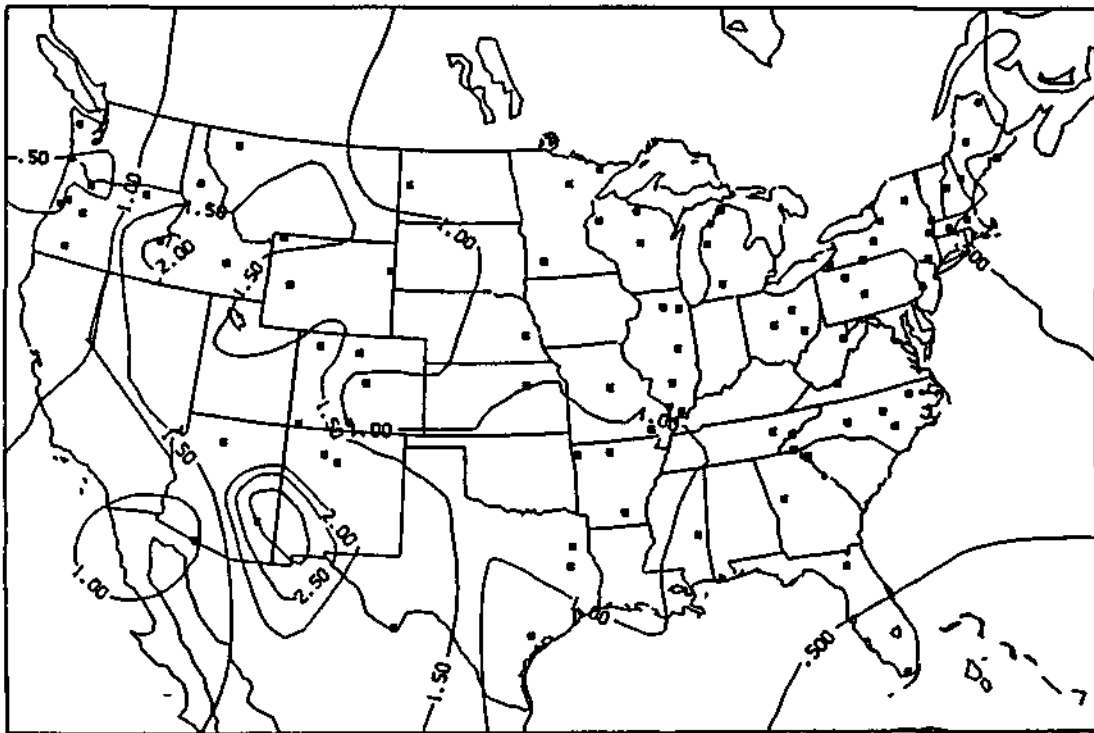


Figure 14. Warm period/cold period ratios of median chloride concentrations in precipitation.

ions, sodium and chloride were higher in the cold period than in the warm period over large areas of the eastern U.S. and the Northern Plains. At Rocky Mountain sites the warm to cold period ratios for sodium and chloride had a pattern similar to other ions. This suggests that the crustal sources there dominated the sea-salt and other influences, affecting the pattern elsewhere.

Figure 15 shows the ratios for pH. This is another way of displaying the hydrogen ion ratios in Figure 8, however, the more frequently used units of pH were entered in the calculations. Recall that where values were greater than 1, warm period hydrogen ion concentrations were less than cold period concentrations. The mid-continental area from Minnesota to Texas, where this occurred, is a distinctive feature of this map. This feature was also noted for the spatial pattern of sulfate.

The last figure, Figure 16, shows the ratio of the median precipitation sample volumes for the warm versus the cold period. For the Plains, much of the Rocky Mountain region, and the Northeast, sample volumes were larger for the warm period. The sample volume is of course an indication of the precipitation that fell at a site. Higher ion concentrations in precipitation samples were often, at least in part, attributed to smaller precipitation events and thus smaller sample volumes. Figure 16 demonstrates that on average this notion is not appropriate to explain the seasonal or period concentration patterns shown in the previous figures for weekly samples. For most of the ions, higher warm period concentrations were occasioned by heavier rains.

A final summary of the data by the regions illustrated in Figure 1 is presented in Table 1. Warm to cold period ratios were averaged for the sites in each region to provide this quantitative summary. Means and medians in Table 1 were similar, which is evidence that the mean values were not strongly influenced by a few outliers. Four features should be noted from these data. First, the highest mean and median ratios for all ions except SO_4^{2-} were observed in the Rocky Mountain region. Second, the lowest median ratios for the 4 major ions associated with acidic deposition (H^+ , SO_4^{2-} , NO_3^- , and NH_4^+) were in the Midwest region. Third, the largest differences between the lowest and highest mean or median ratios occurred for nitrate and hydrogen ions. Fourth, the sulfate ratio was higher in the Northeast than in the Southeast, while the opposite was true for nitrate.

CONCLUSIONS

This study examines the intra-annual variations of inorganic ion concentrations in precipitation across the U.S. These variations were summarized on contour maps showing the spatial distribution of ratios of warm period to cold period weighted average and median ion concentrations. Comparison of the magnitudes of ratios of weighted averages to medians suggested that there were differences; however, the location of relative high and low ratios was about the same. Comparisons of 3-month warm season to cold season ratios with 5-month warm period to cold period

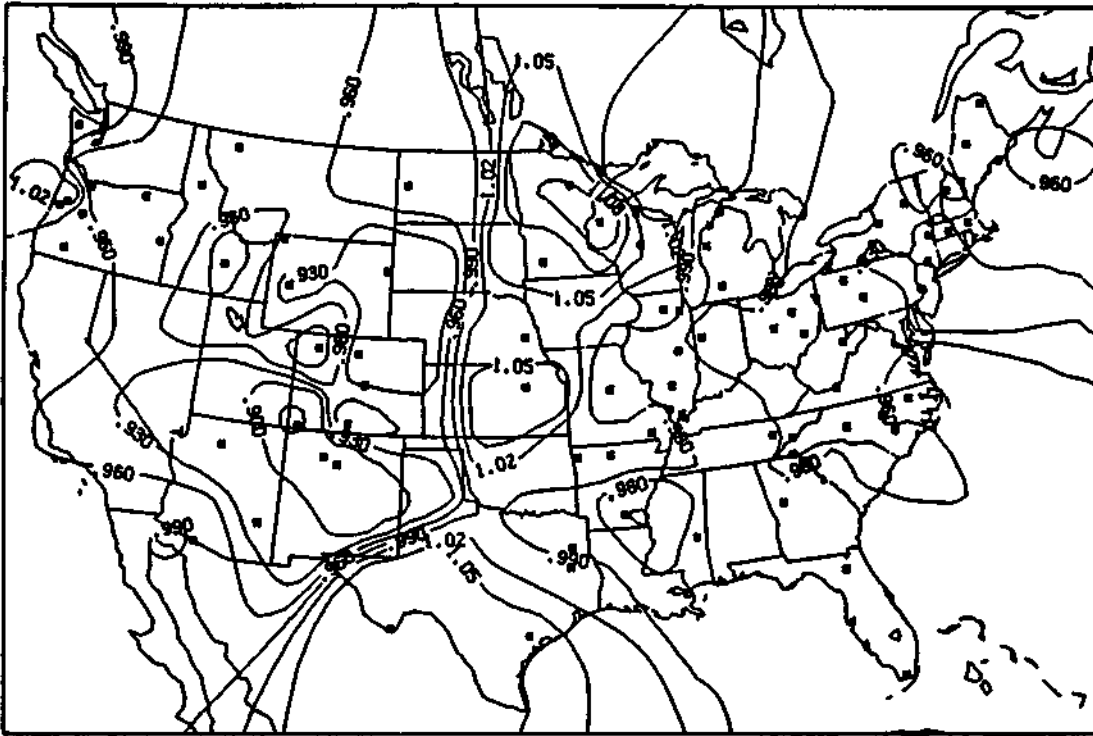


Figure 15. Warm period/cold period ratios of the median pH of precipitation.

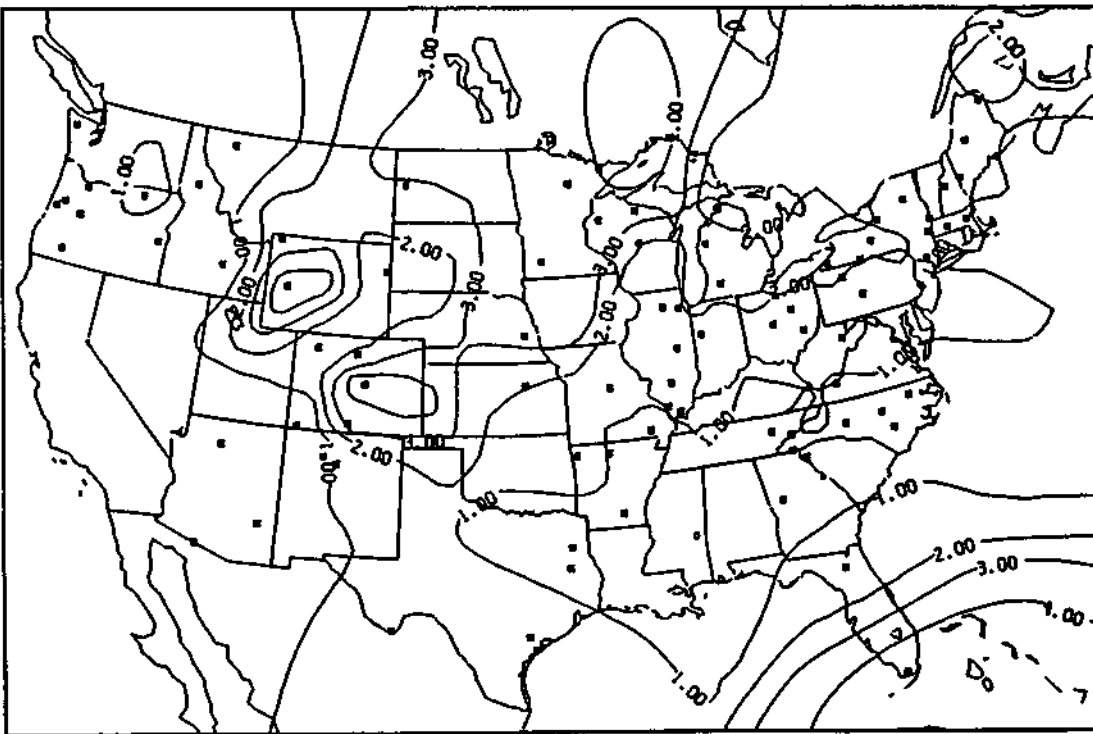


Figure 16. Warm period/cold period ratios of median precipitation sample volumes.

Table 1. Summary of ratio values (warm period/cold period precipitation concentrations) for all sites in the four regions outlined in Figure 1.

Region ^a		***** Mean ± 2 Std. Dev. of Period Ratios *****					
N		SO ₄ ²⁻	NO ₃ ⁻	NH ₄ ⁺	Ca ²⁺	H ⁺	
MW	20	1.35 ± .64	1.00 ± .47	1.67 ± 1.45	1.63 ± 1.02	1.03 ± .88	
SE	15	1.52 ± .60	1.73 ± .92	1.87 ± .92	1.57 ± .62	1.52 ± .87	
NE	23	2.19 ± .80	1.36 ± .88	2.45 ± 1.48	1.44 ± .72	1.89 ± .64	
RM	16	2.15 ± 1.11	2.63 ± 2.87	2.65 ± 1.54	2.39 ± 1.30	2.58 ± 2.37	

Region ^a		***** Mean ± 2 Std. Dev. of Period Ratios *****				
N		Mg ²⁺	K ⁺	Na ⁺	Cl ⁻	
MW	20	1.40 ± .67	1.55 ± .68	.79 ± .58	.92 ± 1.21	
SE	15	1.23 ± .69	1.53 ± .54	.95 ± .73	.87 ± .51	
NE	23	1.17 ± .65	1.43 ± .67	.67 ± .53	.64 ± .36	
RM	16	1.82 ± .90	2.67 ± 1.58	1.30 ± .84	1.51 ± 1.05	

Region ^a		***** Median of Period Ratios *****				
N		SO ₄ ²⁻	NO ₃ ⁻	NH ₄ ⁺	Ca ²⁺	H ⁺
MW	20	1.32	.92	1.38	1.46	1.08
SE	15	1.56	1.72	2.00	1.58	1.48
NE	23	2.20	1.20	2.21	1.47	1.86
RM	16	2.10	2.33	2.54	2.40	2.53

Region ^a		***** Median of Period Ratios *****				
N		Mg ²⁺	K ⁺	Na ⁺	Cl ⁻	
MW	20	1.34	1.48	.68	.78	
SE	15	1.28	1.41	.93	.83	
NE	23	1.14	1.50	.70	.67	
RM	16	1.96	2.52	1.39	1.50	

^aNE is Northeast; SE is Southeast; MW is Midwest; and RM is Rocky Mountain as illustrated in Figure 1. N is the number of sites in the region.

ratios were also shown for three ions. The results of this comparison were qualitatively similar to the weighted average versus median comparison spatial patterns of highs and lows were about the same but magnitudes were different. For this comparison, though, seasonal ratios were almost always more extreme in the highs and lows. This suggests that precipitation concentrations followed a rather well defined pattern of intra-annual variations with summer and winter extremes

The highest warm/cold period ratios for all ions but sulfate were observed in the Rocky Mountain region. Median ratios in this region varied from 1.39 for sodium to 2.54 for ammonium. Growing season concentrations averaged higher than dormant season concentrations for crustal and non-crustal elements alike in that region of the country. The lowest ratios for the 4 major ions associated with acidic deposition were observed in the Midwestern region. In the eastern U.S., sulfate ratios were larger in the Northeast than in the Southeast, while the opposite was true for nitrate ratios. This observation bears closer inspection with respect to the SO_x/NO_x interactions giving rise to acidic sulfates and nitrates in eastern U.S. precipitation. For sodium and chloride, the Northern Plains and nearly all of the East had warm/cold period ratios <1.0 . Some east coast sites even had ratios <0.5 , probably owing to higher wintertime airborne sea-salt concentrations.

For ions other than sodium and chloride there were generally higher average warm (growing) season than cold (dormant) season concentrations over much of the country. Frequent exceptions to this were coastal sites in Texas and Florida and sites in an area from eastern Kansas north to Minnesota and western Wisconsin. In addition, except for the Southeast and areas west of the Rocky Mountain region, growing period precipitation was higher than dormant period precipitation, therefore, the higher precipitation amounts and higher concentrations result in higher depositions during the growing period.

REFERENCES

- Achtemeier, G. L., P. H. Hildebrand, P. T. Schickedanz, B. Ackerman, S. A. Changnon, Jr., and R. G. Semonin, "Illinois Precipitation Enhancement Program Design and Evaluation Techniques for High Plains Cooperative Program," Ill. State Water Survey Final Report on Contract 14-06-D-7197, Appendix B.
- Barnes, S. L., 1964: "A technique for maximizing details in numerical weather map analysis," J. Appl. Meteorol., 3: 396-409.
- Barnes, S. L., 1973. "Mesoscale objective map analysis using weighted time-series observations," NOAA Tech. Memo. 62, NSSL, 60 pp.
- Bowersox, V. C. and R. G. de Pena, 1980. "Analysis of precipitation chemistry at a central Pennsylvania site," J. Geophys. Res., 85:5614-5620.

- Bowersox, V. C. and G. J. Stensland, 1981: "Seasonal patterns of sulfate and nitrate in precipitation in the United States," Paper 81-6.1, 74th Annual APCA Meeting, Philadelphia, PA, 16 pp.
- Bowersox, V. C., 1985: "Data validation procedures for wet deposition samples at the Central Analytical Laboratory of the National Atmospheric Deposition Program," In: Transactions, APCA International Specialty Conference on Quality Assurance in Air Pollution Measurements, Boulder, CO (October 1984), T. R. Johnson and S. J. Penkala [Eds.], APCA, Pittsburgh, PA, p 500-524.
- Gatz, D. F. , W. R. Barnard and G. J. Stensland, 1985: "Dust from unpaved roads as a source of cations in precipitation," Paper 85-6B.6, 78th Annual APCA Meeting, Detroit, MI, 16 pp.
- Harriss, R. G. and J. T. Michaels, 1982: "Sources of atmospheric ammonia," In: Proceedings Second Symposium, Composition of the Non-Urban Troposphere, American Meteorological Society, Boston, MA, pp 33-35.
- Likens, G. E. and F. H. Borman, 1974: "Acid rain: a serious regional environmental problem," Science. 184. 1176-1179.
- National Atmospheric Deposition Program/National Trends Network, NADP/NTN Data Tape for 1978-March 1984, available from NADP/NTN Coordinator's Office, Natural Resource Ecology Laboratory, CSU, Fort Collins, CO.
- Pack, D. W. , 1978: "Sulfate behavior in eastern U.S. precipitation," Geophys. Res. Letters, 5:673-674.
- Peden, M. E. , S. R. Bachman, C. J. Brennan, B. Demir, K. O. James, B. W. Kaiser, J. M. Lockard, J. E. Rothart, J. Sauer, L. M. Skowron, and M. J. Slater, 1986: "Methods for Collection and Analysis of Precipitation," Illinois State Water Survey, 2204 Griffith Dr., Champaign, IL, 276 pp.
- Semonin, R. G., 1986: "Wet deposition chemistry," In Materials Degradation Caused by Acid Rain, Robert Baboian [Ed.], Am. Chem. Soc. Symposium Series No. 318, Washington, DC, 41 pp.
- Semonin, R. G. and V. C. Bowersox, 1983: "Characterization of the inorganic chemistry of the precipitation of North America," In: Precipitation Scavenging, Dry Deposition, and Resuspension, Pruppacher, Semonin and Slinn [Eds.], Elsevier Science Publishing Co., Inc., pp. 191-202.
- Stensland, G. J., M. E. Peden and V. C. Bowersox, 1983: "NADP quality control procedures for wet deposition sample collection and field measurements," Paper 83-32.2, 76th Annual APCA Meeting, Atlanta, GA, 20 pp.

CHAPTER 3

ESTIMATION OF BIAS IN THE AVERAGE WET DEPOSITION
OF CALCIUM, SULFATE, AND SODIUM FROM NATIONAL ATMOSPHERIC DEPOSITION
PROGRAM/NATIONAL TRENDS NETWORK (NADP/NTN) DATA

Van C. Bowersox, Gary J. Stensland and Mark E. Peden

INTRODUCTION

In 1978 a network to measure the atmospheric deposition of chemicals across the United States began operations as part of the National Atmospheric Deposition Program (NADP). This program was created by the Association of State Agricultural Experiment Stations in the North Central Region (Project No. NC-141). The primary objective of the network was to identify the geographic patterns and temporal trends in atmospheric deposition, so that its potential benefits and detriments to terrestrial and aquatic ecosystems could be assessed. Since data from all across the country were sought, the focus was on the synoptic scale. Influences from local sources were to be minimized by siting the collection stations so as to be representative of entire regions (Bigelow, 1984). To complement the network design, standard equipment and standard operating procedures were defined for field site operations (National Atmospheric Deposition Program, 1982). One-week, precipitation-only samples were collected and sent to a single Central Analytical Laboratory (CAL) for analysis. Standard methods were employed at this CAL (Peden *et al.*, 1986). In addition to analytical services, the CAL also coordinated site operations (Stensland *et al.*, 1983) and screened and reported the data to site personnel (Bowersox, 1984). To demonstrate the growth in this network, listed below are the number of sites active at the end of each calendar year.

	1978	1979	1980	1981	1982	1983*	1984	1985	1986
Number of Sites	22	39	81	96	110	143	176	193	201

*Note that in 1983, NADP and the National Trends Network (NTN) combined to form a single network, which led to the addition of new sites in areas where previous coverage had been sparse.

Wet deposition data from 1978 to 1986 are available from the NADP/NTN Coordinator's Office (National Atmospheric Deposition Program/National Trends Network, 1986). Quality assurance summaries that report on various measurements of bias and precision are now becoming available, also (Lockard, 1987). Important sources of possible bias in the NADP/NTN system include (1) analytical measurements, (2) laboratory handling, (3) the sampling container, a plastic (LPE) bucket, (4) dust that enters the collection bucket while it is in the collector but covered during dry weather (i.e., infiltration), and (5) field handling. By combining

measurements of bias from these sources, estimates were made of the percent bias in the average deposition of Ca^{++} , Na^+ , and SO_4^- . (Note: in the text that follows all ionic charges have been eliminated, thus Ca^{++} is Ca.) Each of these ions has a characteristically different source in precipitation. For example, Ca is present in aerosols derived from surficial sources such as soils or road dust, whereas Na is largely from sea salt, road salt, and soils. The source of bias in each of these ions is characteristically different, as well. Just as there are patterns which reflect the effect of geographic differences in sources and airborne concentrations on the chemistry of precipitation, there are also spatial patterns in the amount of bias. These geographic differences result from the effects of dust and/or field handling. In principle other sources of bias are uniform over the network.

In this study, estimates were made of the bias in Ca, Na, and SO_4 that resulted from the collection and handling of wet deposition samples in the NADP/NTN. The geographic patterns and relative importance of this bias to deposition from precipitation are demonstrated.

METHODS

A major part of the quality assurance monitoring program of the NADP/NTN addresses the bias, precision, and comparability of the data (NADP Quality Assurance Steering Committee, 1984). An assessment of each of these is not possible via a single measurement. The one set of measurements that most nearly encompasses the potential bias from the 5 sources listed earlier, however, is the data from dry blank samples. These samples result when the wet-only collection bucket was never exposed to precipitation. The collection bucket was installed in the collector and remained there for an entire sampling period (nominally 1 week). At the end of the sampling period it was removed, sealed, and sent to the CAL. Deionized water was added and after approximately 8 hours this leachate was removed and treated as a rain sample. Stensland *et al.* (1983), have described the details of the laboratory handling of these samples (designated in that paper as 'DA' samples, after the laboratory code assigned to identify dry wet-side samples).

One possible source of bias, listed in the introduction, comes from the accumulation of dust particles and other aerosols that infiltrate the lid-to-bucket seal. The underside of the lid of the collector in use in the NADP/NTN is fitted with a foam pad covered with a thin plastic film. During dry weather this pad covers the collection bucket and is slightly compressed against its rim. This design retards both evaporation of the collected sample and the infiltration of wind-borne particles. Neither are arrested, however. With the foam pad removed, there is evidence that contamination from infiltration is significantly increased (Stensland *et al.*, 1983). Data from the dry blank samples can be used to assess the importance of bias from infiltration.

Another source of bias, listed earlier, is the sampling container itself, a plastic (LPE) bucket. Buckets are cleaned at the CAL according to a standard set of procedures (Lockard, 1987). Bucket blanks are measured by the addition of de-ionized water to buckets taken randomly from the clean supply ready for shipment to field sites. After addition of the water, the samples are allowed to equilibrate, just as dry blank samples. One difference between the handling of dry blanks and bucket blanks is that the buckets are all left upright for dry blank samples, while some are inverted for bucket blank samples. Inverted bucket blanks were first measured in 1981, after concern was raised that a gasket in the bucket lid could contribute a significant amount of contaminant mass to precipitation samples (Lockard, 1987). It was thought that inverted bucket blanks would better simulate the contact of a sample with the bucket and lid during transport from the site to the CAL. what's important is that data from the dry blank samples includes a component due to infiltration and a component due to the bucket but not the lid (gasket).

Handling the sample at the field site can also result in bias from (a) logistical movements of the bucket from its shipping case, to and from the sampler, back to its shipping case, and (b) removal of a liquid aliquot for field pH and conductance measurements. Because the dry blank samples do not contain liquid, only the former element (a) is captured. Further the dry buckets might be handled somewhat differently than if they contained precipitation, though the standard procedures are not different (National Atmospheric Deposition Program, 1982). The analysis of data in this study does not address the element (b) of bias resulting from aliquot removal. Tests at the CAL of the syringe used to withdraw the aliquot have not uncovered a significant mass of contaminant. Future tests of the entire procedure are needed to verify that element (b) is not an important source of error.

Finally, elements of bias can accrue from laboratory handling and analytical measurements. Lockard (1987) describes the procedures and summarizes the data for CAL operations. Standard samples are submitted for analysis. These samples originate as a result of internal QA procedures and from people outside of the analytical operations group. Results from measurements of these internal and external QA samples and from interlaboratory comparisons form the basis for the assessment of CAL bias. From 1978 through 1986, 20 separate interlaboratory comparisons were performed between the CAL of NADP/NTN and other laboratories around the world. These comparisons were sponsored by the World Meteorological Organization, the Norwegian Institute for Air Research, and the Canadian government. Samples tested were either synthetic or natural precipitation. An overall analytical bias for Ca, SO₄ and Na was calculated from data for the 20 comparisons. Results, below, show that one cannot reject the (null) hypothesis that the bias is 0 for all three ions. On the whole, analytical bias is insignificant and can be discounted.

	Ca (mg/L)	SO ₄ (mg/L)	Na (mg/L)
Mean	.017	.08	-.010
Standard Error	.024	.08	.006
t-test*	not significant	not significant	not significant

*Test for mean not equal to zero.

Dry blank samples capture all or part of 5 possible sources of possible bias in the NADP/NTN system. Of the elements missed: (1) evaporation, (2) handling during the removal of the field aliquot, and (3) contamination from the lid (gasket), only (2) cannot be addressed because of a lack of data. Though evaporation of the sample results in a loss of water, it does not change the mass of conservative ions. (Even though this paper deals with SO₄, Ca, and Na, it's worth noting that free hydrogen ion is not conservative and would be affected by evaporation.) The mass of calcium, sulfate, and sodium would not be changed by sample evaporation, though concentrations of all 3 would rise. Contamination from the lid can be estimated by calculating the difference between the inverted and upright bucket blanks. Addition of this bias to the bias from dry blank samples would result in the current best estimate of bias in the measurement system.

RESULTS AND DISCUSSION

Figure 1 shows the areas of the country where the median contaminant mass of Ca in the dry blank samples exceeded the median mass from the upright bucket blanks. Dry blank data from mid-1978, when the NADP monitoring network began, through 1986 were used. Only data for dry blank samples that contained no organic or other extrinsic contaminants or that were not invalid for other reasons (see Bowersox, 1984) were used. Sampling sites appear as squares in the figure. Where a site appears, there were 7 or more valid dry blank samples in the 1978-1986 time period. Seven was set as the minimum number of data points necessary to be included in the analysis; because with 7 or more points, the calculation of the 25th and 75th percentiles was independent of the extremes, hence the middle half of the distribution was unaffected by the minimum and maximum values. Seventy-two sites did not meet this criterion. Nearly 2/3 of those were east of the Mississippi River, where whole weeks without any precipitation were infrequent. As a result, data in the East were sparse. Isolines (equal to 2.2) were located after the data were objectively analyzed using a scheme developed by Barnes (1964; 1973) and modified by Achtemeier (1977). The diagonal cross-hatch pattern in the figure depicts the areas where the median dry blank mass exceeded 2.2 μg , the median upright bucket blank mass. Dry blank data from areas not hatched could have resulted from contaminant from the bucket alone, since values were at or below 2.2 μg .

Although the median mass of dry blank samples across most of the country was greater than the mass from the buckets alone, there were some large spatially contiguous areas where that was not the case; for example, see data from California, parts of Oregon, Washington, and other western states (Figure 1). This suggests two things. First, there were large areas where infiltration by dust bearing soluble Ca was unimportant. Second, the bias due to field handling of the dry buckets was also unimportant in these same areas. That field handling was unimportant has a broader implication. Because procedures for handling samples were standard throughout the network, one can infer that the Ca bias from field handling in general was small. In the (cross-hatched) areas where the bucket blank mass was exceeded, infiltration thus had a positive net input to the overall bias. Some sites are in areas where tillage, soil erosion by wind, and/or dust from unpaved roads (Gatz *et al* , 1985) result in elevated concentrations of airborne particles that carry soluble Ca (and other elements). On occasions when winds support high soil particle counts, these same conditions promote infiltration of the lid-to-bucket seal by these particles. Reports of soil particles in dry blank samples from eastern Nebraska, southern Minnesota, and central Illinois stand as direct visible evidence of this phenomenon.

In Figure 1 notice too that the median mass at some sites has been especially labeled. Calcium values were more than 3 times the bucket blank values at these sites. Exceptionally high values, such as these, have prompted the CAL to request that extra checks of the sampler be made to assure an adequate seal (Gatz *et al* . . 1983). Corrective action was warranted where the lid-to-bucket seal was substandard. Of the sites labeled, only the one in southern Illinois required some adjustment to the foam pad, following an on-site check. The other exceptional values may indeed have reflected sites with high air concentrations and winds sufficient to have invaded the lid seal. That values at nearly all sites in the Great Plains were well above $2.2 \mu\text{g}$ is consistent with this hypothesis. The overall maximum of $12 \mu\text{g}$ in southwestern Minnesota is in this area.

To put the Ca bias in Figure 1 into perspective, the values of the median dry blank mass were compared to the values of the median precipitation sample mass. These were plotted as the estimated percent bias in Figure 2. Placement of the contours was again done objectively (as for all of the maps). These percentages were calculated from the set of valid dry blank data of record, as in Figure 1, and on the set of valid precipitation chemistry data of record. Based on the overall data of record, these percentages represent a typical or average bias, rather than the possible bias in a single value. Individual or monthly or seasonal values may be larger or smaller than the values in Figure 2. Outside of an area in eastern Montana and a second area covering parts of Oregon, Nevada, and California, the estimated bias was less than 5% throughout the country. Even at sites labeled as exceptional in Figure 1, the values were less than 5%, but for the site in southern Alberta, Canada. Both areas where the percentages peaked were defined by a group of 3 or more stations. In the Oregon/Nevada/California area the percentages were relatively high, because the mass of Ca in precipitation was so low (less than 1 mg/M^2). The wet deposition loading of Ca minimized in this part of the country. In eastern Montana the wet loading of Ca was often well above 1 mg/M^2 , and

the dry blank loadings were high, as well. Through much of this area infiltration was the major contributor to the relative maximum. Though the number of data points was too small to examine the bias over shorter periods of time at all sites, variations that reflect air quality and wind speed changes across the seasons no doubt occur. Differences from year-to-year may also exist but were not investigated.

The estimated percent bias in the median sample mass of SO_4 was plotted in Figure 3. Criteria used to define the data to be presented were the same as for Ca in Figure 2. Concentrations of upright bucket blank measurements over the 8-year period were mostly at or below the analytical limit of detection (0.10 mg/L). Consequently, a dry blank mass $>5 \mu\text{g}$ /sample was necessary to exceed the contribution from the bucket alone. Only east of the Mississippi River did this occur with regularity. A noticeable exception was sites in central and eastern North Carolina. In the west, a median dry blank mass greater than $5 \mu\text{g}$ /sample occurred at only a few widely scattered sites. As for Ca, one can infer from this that SO_4 bias from handling dry blank samples was negligible, in general. In contrast to the Ca data, the effects of infiltration were confined almost entirely to the east. This is the region where the air and precipitation concentrations of sulfate maximize, as well. In Figure 3 it is obvious that despite the higher dry blank masses in the east, the overall percent bias was less than 1%. Indeed the percentages were less than 5% everywhere. The only area defined by 3 or more sites where the bias was above 1% was centered in southern and eastern Oregon. This is the area where wet sulfate deposition in the contiguous U.S. minimizes.

Although the percent bias in SO_4 from Figure 3 are of little consequence, it is important to note that the potential for infiltration even exists. For infiltration to occur, recall that aerosol particles bearing SO_4 must have sufficient momentum to invade the compressible lid seal of the NADP/NTN collector. Except in coastal areas where supermicron particles of ocean salts occur and in areas where gypsum salts may become airborne, sulfate exists primarily as submicron aerosols. Throughout the eastern U.S. sulfate aerosols form in the atmosphere as the result of gas and aqueous (haze, cloud drops, precipitation) phase oxidation of S (IV) to S (VI). These tiny particles have little momentum, yet they apparently can penetrate the lid to bucket seal. What is important is that collection devices with an incomplete seal or with no compressible seal at all may permit a significant bias in measurements of wet sulfate loading, due to a high dry blank mass. Stensland *et al.*, 1983 cited data from an NADP site in New York, where the compressible pad had been temporarily removed. Dry blank data during that period showed masses of 38 to 343 μg per sample, from 10 to 100 times the values with the pad installed. The importance of monitoring dry blank data to detect such anomalies and initiate corrective action is clear.

Unlike Ca and SO_4 , a likely potential source of Na bias was human handling of the samples. Data from dry blank samples, however, did not support this notion. The median mass of Na in upright bucket blanks was 2.0 μg . As for the two other elements, there were large contiguous areas (in the upper Midwest - OH, IN, IL, MI, WI - and much of the West) where the median dry blank mass did not exceed this number. Apparently operator handling of the dry blank samples was careful and consistent and conducive

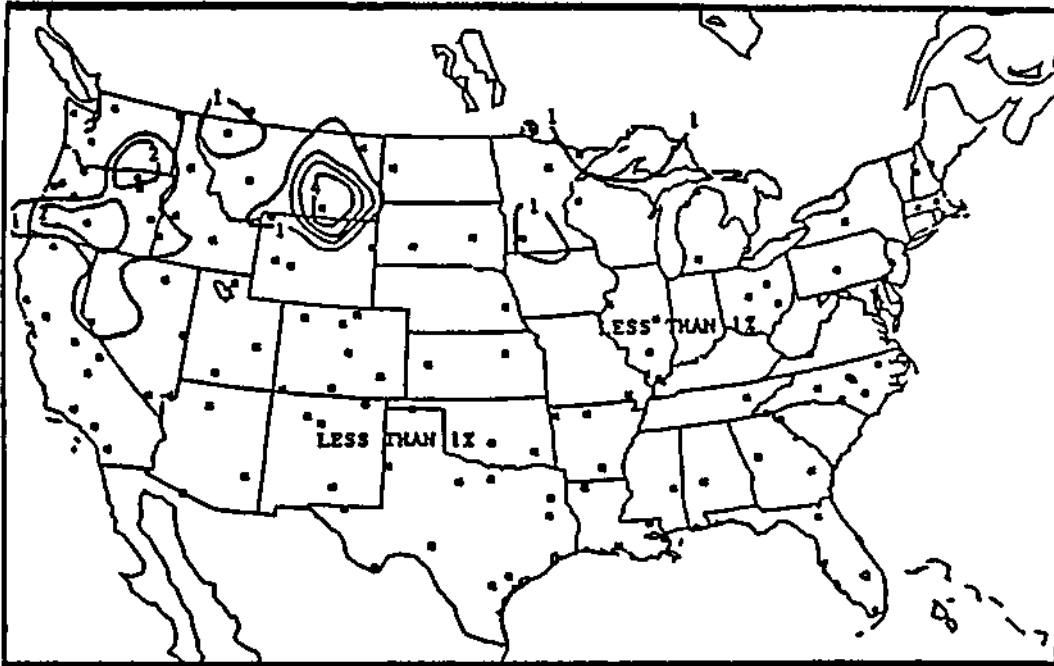


Figure 3. Estimated percent bias in median sample mass of SO_4 resulting from dry blank loading. Calculated as in Figure 2.

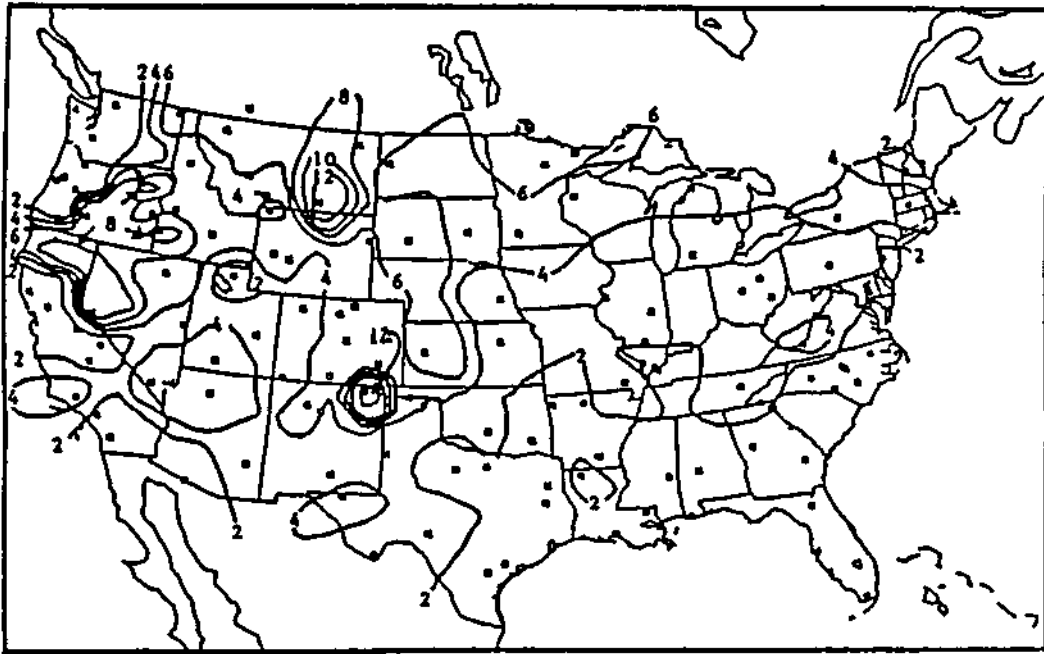


Figure 4. Estimated percent bias in median sample mass of Na resulting from dry blank loading. Calculated as in Figure 2.

to preservation of the chemical integrity of these samples. Where 20 μg was exceeded, infiltration must have played an important role. Highest values occurred in Florida and along the east coast. Airborne ocean salts rich in Na and soil aerosols carrying Na are the presumed cause of this feature.

When the Na bias was plotted as a percentage of the wet loading in Figure 4, a much different pattern emerged. Percentages generally decreased from inland areas toward the coast. This pattern was consistent with and dominated by the wet loading of Na, which exhibited a coastal maximum resulting from scavenged sea salt. Values of the percent bias ranged from 2% or less near the coast to inland maxima of 8% and 12%. Typical values in the eastern U.S. were less than 5%. The 12% maximum in eastern Montana and the 8% maxima in the Oregon/Nevada/California area were analogous to the pattern for Ca (see Figure 2). The 12% maximum in the northeastern corner of New Mexico resulted from a single site. It was unique to the region, not because of a high Na blank but because of an especially low median sample mass of 0.28 $\mu\text{g}/\text{M}^2$ of Na. This flux resulted from the low weekly sample volumes at a site where the Na concentrations were also low.

Finally to provide a current estimate of the overall bias in the NADP/NTN system for Ca, SO_4 , and Na, the contribution from the bucket lid must be added to the dry blank mass. As explained in the methods, contamination from the lid was largely from the gasket. This contribution was derived from the difference of the inverted and upright bucket blanks. Below are the values based on all data of record through the end of 1986:

	Ca ($\mu\text{g}/\text{sample}$)	SO_4 ($\mu\text{g}/\text{sample}$)	Na ($\mu\text{g}/\text{sample}$)
Lid (gasket)	6.7	4.0	5.0
Upright bucket	2.2	<5.0	2.0

For comparison, the median mass from the upright bucket alone was included. Notice that the lid contribution was about 3 times the upright blank for Ca. Recall that there were just 5 sites (especially labeled) in Figure 1 where the dry blank mass was more than 3 times the upright bucket blank, hence the Ca bias from the lid (gasket) was greater than the typical bias from dust infiltration. A key distinction is that the lid (gasket) contribution was uniform over the entire network. For SO_4 the lid contribution was comparable to the upright bucket. As for Ca, the lid contribution for SO_4 was larger than the typical bias from infiltration, even at most eastern sites, where the infiltration of SO_4 was greatest. For Na, the contribution from the dry blank data exceeded the combined contribution of the bucket plus lid at only one site, located in the Everglades near the southern coastline of Florida. Figures 5, 6, and 7 show the current best estimate of the percent bias in Ca, SO_4 , and Na, respectively. Calculation of the percent bias was analogous to Figures 2, 3, and 4, with the lid (gasket) contribution added to the median dry blank mass. Using 10% as a reference, the bias in Ca in Figure 5 exceeded that value in Maine and north and west of a line roughly running from central California to the northeastern corner of Montana. Percent bias in this

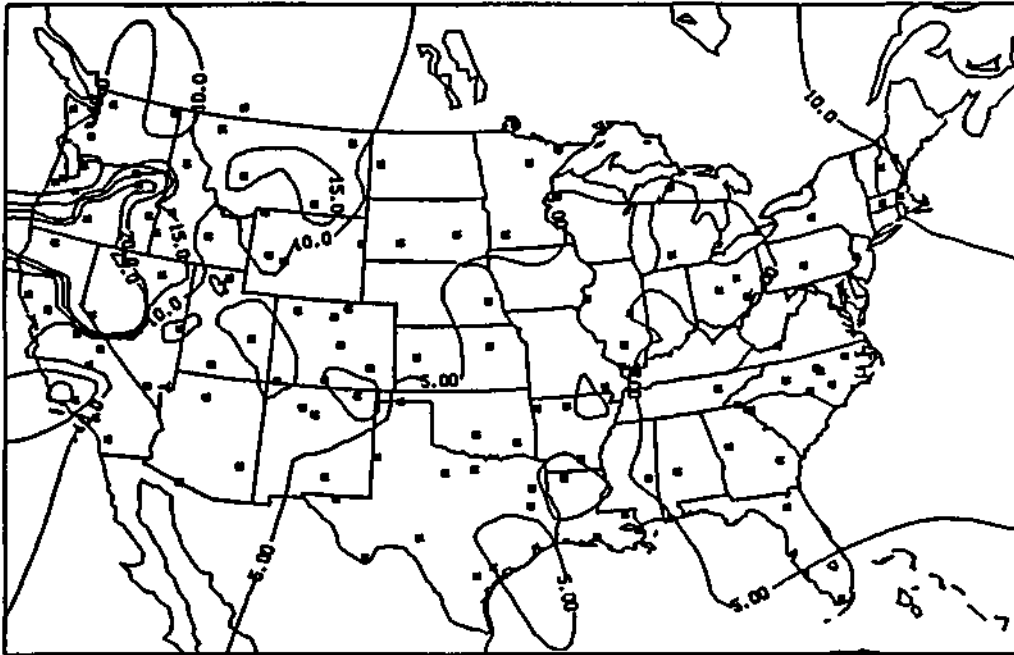


Figure 5. Estimated percent bias in median sample mass of Ca resulting from overall blank loading.

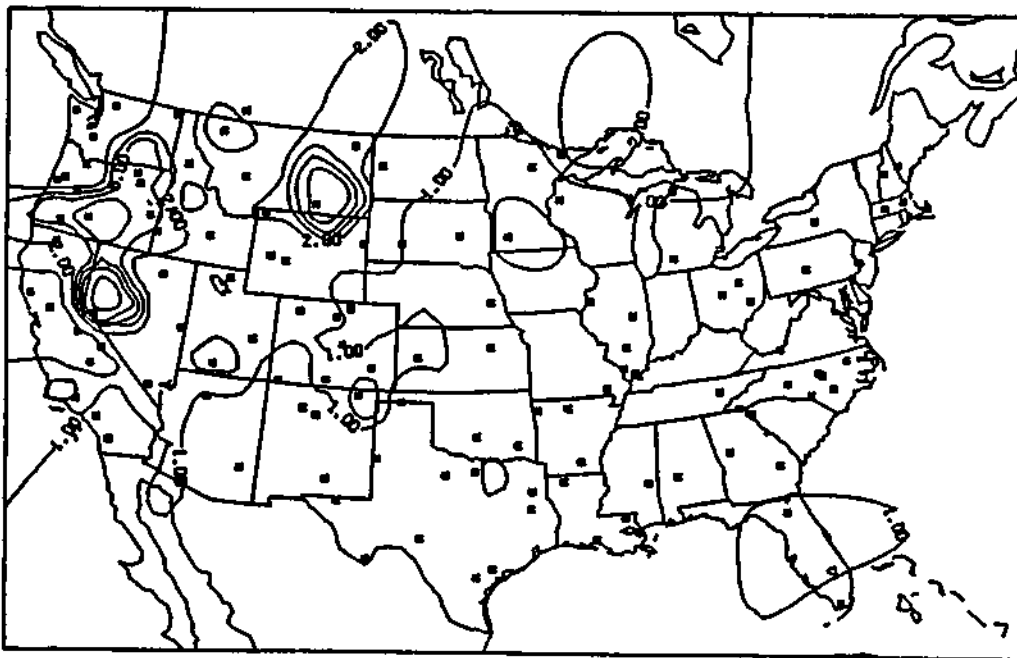


Figure 6. Estimated percent bias in median sample mass of SO₄ resulting from overall blank loading.

area was even greater than 25% in the Oregon/Nevada/California area discussed earlier. The bias in SO_4 in Figure 6 was everywhere less than 10% and was less than 5% except at a few isolated sites. Finally in Figure 7 the percent bias in Na generally exceeded 10% north and west of a line running from west Texas to the southeastern corner of New York. There were values above 25% at a few scattered sites in this area.

CONCLUSIONS

Estimates were made of the percent bias in the wet deposition loading of Ca, SO_4 , and Na from the NADP/NTN data set. These estimates were based on the data of record from mid-1978 through 1986 and are thus applicable to long-term averages, not seasonal, monthly, or individual values. The calculations of an overall bias were based on data for the contamination from field handling of dry buckets, laboratory handling and analysis, and the buckets themselves. Sources of possible contamination that were not addressed included (a) field handling to remove a liquid aliquot of sample for field chemistry measurements and (b) chemical degradation of the liquid sample from time of collection to time of analysis. No attempt was made to address the bias due to sampler undercatch or overcatch of precipitation either.

Significant findings include:

- (1) Analytical bias was not significant for any of the ions.
- (2) When standard operating procedures were followed, the contribution to bias from field handling of dry buckets was not significant for any of the ions.
- (3) Infiltration of the lid to bucket seal by aerosol Ca, SO_4 , and Na occurred over large spatially contiguous areas. These areas were distinctly different for each of the ions and they reflected conditions where airborne concentrations and winds combined to cause the aerosol particles to violate the seal.
- (4) Contamination from the lid (gasket) was typically the largest single source of bias. Only at a few sites did infiltration exceed the lid bias
- (5) The percent bias in Ca was greater than 10% north and west of a line from central CA to eastern MT.
- (6) The overall estimate of bias in SO_4 was less than 10% throughout the continental U.S. and it was less than 5% except at a few scattered sites.
- (7) The percent bias in Na exceeded 10% over large areas of the country, with values of above 25% at a few sites.

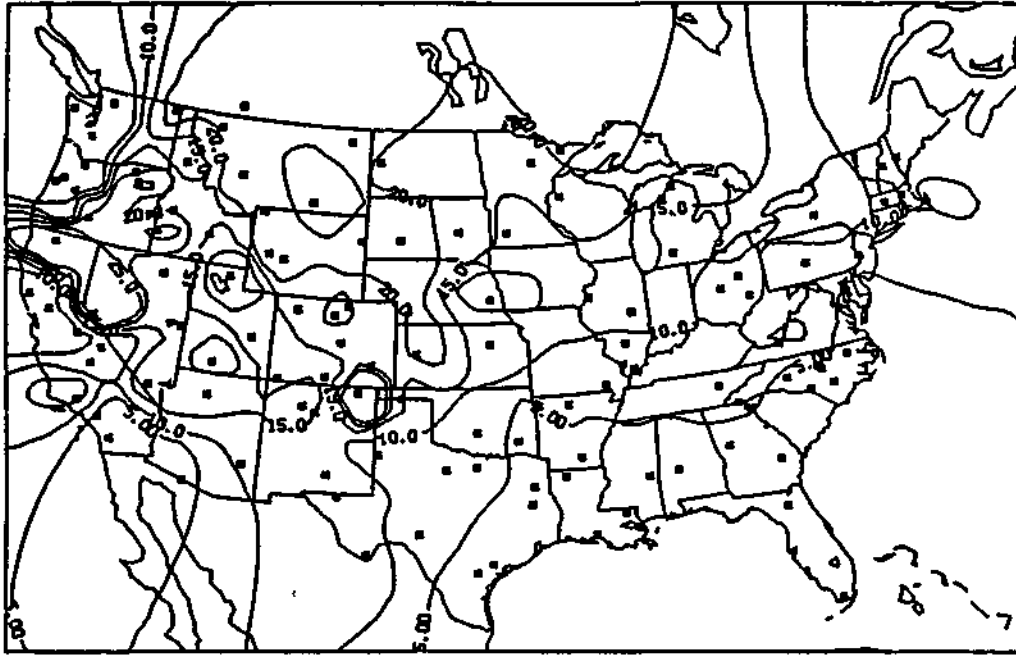


Figure 7. Estimated percent bias in median sample mass of Na resulting from overall blank loading.

REFERENCES

- Achtemeier, G. L., P. H. Hildebrand, P. T. Schickedanz, B. Ackerman, S. A. Changnon, Jr., and R. G. Semonin, 1977: "Illinois Precipitation Enhancement Program Design and Evaluation Techniques for High Plains Cooperative Program," Ill. State Water Survey Final Report on Contract 14-06-D-7197, Appendix B.
- Barnes, S. L. 1964: "A technique for maximizing details in numerical weather map analysis," J. Appl. Meteorol. 3: 396-409.
- Barnes, S. L. , 1973: "Mesoscale objective map analysis using weighted time-series observations," NOAA Tech. Memo. 62, NSSL, 60 pp.
- Bigelow, D. S., 1984: "Instruction manual for NADP/NTN site selection and installation," Natural Resource Ecology Laboratory, Ft. Collins, CO, 43 p.
- Bowersox, V. C, 1984: "Data validation procedures for wet deposition samples at the Central Analytical Laboratory of the National Atmospheric Deposition Program, In: Transactions, APCA Specialty Conference on Quality Assurance in Air Pollution Measurements, T. R. Johnson and S. J. Penkala, editors, p. 500-524.
- Gatz, D. F., W. R. Barnard, and G. J. Stensland, 1985: "Dust from unpaved roads as a source of cations in precipitation," paper 85-6B.6, 78th Annual APCA Meeting, Detroit, MI, 16 p.
- Lockard, J. M. , 1987: "Quality assurance report-NADP/NTN deposition monitoring: laboratory operations-Central Analytical Laboratory-July 1978 through December 1983," NREL, Ft. Collins, CO., 180 p.
- National Atmospheric Deposition Program, 1982: "NADP instruction manual for site operation," Natural Resource Ecology Laboratory, Ft. Collins, CO, 37 p
- National Atmospheric Deposition Program/National Trends Network, 1986: NADP/NTN data tape for 1978 to 1986, NADP/NTN Coordinator's Office, Natural Resource Ecology Laboratory, Ft. Collins, CO.
- NADP Quality Assurance Steering Committee, 1984: "NADP quality assurance plan - deposition monitoring," Natural Resource Ecology Laboratory, Fort Collins, CO, 39 p.
- Peden M. E., S. R. Bachman, C. J. Brennan, B. Demir, K. O. James, B. W. Kaiser, J. M. Lockard, J. E. Rothart, J. Sauer, L. M. Skowron, and M. J. Slater, 1986: "Methods for collection and analysis of precipitation," Illinois State Water Survey, 2204 Griffith Dr., Champaign, IL, 276 p.
- Stensland, G. J., M. E. Peden, and V. C. Bowersox, 1983: "NADP quality control procedures for wet deposition sample collection and field measurements," paper 83-32.2, 76th Annual APCA Meeting, Atlanta, GA, 20 p.

CHAPTER 4

SPATIAL RELATIONSHIPS BETWEEN ACID RAIN,
AIR QUALITY, AND VISIBILITY DATA

Gary J. Stensland

ABSTRACT

Visibility and acid rain are two different phenomena which both have direct relationships to air quality. The objective of this paper is to explore the relationships between all three data sets, with emphasis on the situations for the eastern U.S. This paper presents interpretation of the most current precipitation chemistry data from the National Atmospheric Deposition Program/National Trends Network (NADP/NTN), which started in the eastern U.S. in 1978 with less than 20 sites and continues today with over 200 sites spread across the entire U.S. The high site density and relatively long data record make the precipitation sulfate data particularly important. Spatial and seasonal maps and tables of sulfate in precipitation are compared to literature and unpublished values for visibility and air quality sulfate. Reasonable spatial and seasonal correspondence is found between precipitation sulfate and air quality sulfate. For visibility, the spatial pattern for coastal areas is not consistent with the precipitation sulfate pattern, presumably due to the effect of relative humidity. The seasonality pattern of visibility is not consistent with that for precipitation sulfate in Illinois, but is consistent for areas to the east.

INTRODUCTION

A precipitation chemistry network, the National Atmospheric Deposition Program/National Trends Network (NADP/NTN) began operations in 1978 and continues today. There is a rather good density of sites in the eastern U.S. that have data for several years. The primary purpose of this paper is to describe this network, present results for sulfate, and comment on how the spatial and temporal features of these sulfate data compare with a) air quality data for sulfate, and b) visibility data. The main idea is to consider if the "acid rain" data are of substantial use to the community of visibility scientists.

There exists a large number of papers demonstrating the importance of aerosol sulfate to visibility degradation. If precipitation sulfate were only due to scavenging of aerosol sulfate, then it too would be firmly related to visibility degradation. However, the relative importance of SO₂ scavenging versus aerosol sulfate scavenging in accounting for the sulfate measured in precipitation is an unresolved question in the midst of intense research. We would simply comment that the atmospheric aerosol

sulfate burden is sufficiently large to account for the sulfate deposited by precipitation

Even with the role of gaseous versus particulate sulfate scavenging being unresolved, it is of interest to compare patterns of precipitation and aerosol sulfate concentrations to those of prevailing visibility.

METHODS

General Description of the Precipitation Chemistry Data Base

Data from the NADP/NTN were used for this study (National Atmospheric Deposition Program/National Trends Network, 1986). This data set was chosen because it includes sites from across the United States, and thus a broad range of ion concentrations is encountered. The first sites in this network began operation in 1978. By the end of 1978, about 20 sites were in operation; almost 100 were in operation by the end of 1981, and about 140 were in operation by the end of 1983. As of early 1987, 203 sites were in operation. During the early years of the project, the sites were concentrated in the eastern U.S.

All sites are equipped with the same automatic wet/dry precipitation chemistry sampler. Each week, on Tuesday, the sample bucket on the wet deposition side of the sampler is removed and sent to the laboratory at the Illinois State Water Survey. At the laboratory, the sample volume, pH, and solution conductance are measured along with chloride, ammonium, calcium, magnesium, sodium, potassium, sulfate, nitrate, and phosphate (which is usually below the analytical detection limit and is not considered in this paper).

At each site the daily precipitation values and the volume of sample caught in the wet deposition bucket during the entire sampling period are reported. Most sites employ a recording (weighing bucket) raingage, which has been modified to include an "event marker" to record periods when the wet-side bucket was exposed to precipitation. This record is evaluated to ascertain that the wet/dry sampler operated correctly to collect a wet-only deposition sample. Even when no precipitation occurs, the wet-side bucket is sent to the laboratory. The contents of these dry wet-side buckets are analyzed as (quality assurance) system blank samples.

Data for each wet deposition sample, along with pertinent information from communications with site operators, are reviewed by the laboratory data management staff to assess a) whether the proper collection, handling, and measurement protocols were followed, and b) whether visible organic contamination in the sample had produced a sample unrepresentative of the site. Along with the various physical and chemical measurements of each sample, a record is generated in a computerized data base to document the results of this data validation process.

Details of the sample collection, analytical, QA, and data screening procedures are described in detail elsewhere (Stensland et al., 1980; Bigelow, 1982; 1986; Peden et al., 1986; Lockard, 1987; Bowersox, 1985).

Data Selection Procedures

Since the NADP/NTN computerized data base contains wet deposition chemical data as well as other supplemental and qualifying information for each sample, the user community is afforded the opportunity of selecting data appropriate to its research activities. For example, if the volume of water in the bucket received at the CAL was 10 mL, then only pH or pH and conductance measurements are available. A user must decide whether or not to include samples with this limited data in his/her study, especially since a check of the cation/anion balance is not possible.

At the analytical laboratory, samples of nominally 35 mL or more liquid precipitation are analyzed at the concentration received, that is, without further dilution. This volume of 35 mL, normalized by the collection cross section (bucket radius =14.7 cm), translates to a liquid precipitation depth of 0.02 inches or 0.76 mm. Smaller volumes require an initial dilution step in order to satisfy the liquid volume requirement of each analytical procedure. This dilution step adds uncertainties to the reported data due to the extra handling and due to the propagation of errors from the calculation of a dilution factor. For the present study we have used only data corresponding to undiluted samples, i.e., samples with a volume equivalent 0.76 mm of liquid precipitation. In addition, it was necessary that each sample pass the data validation review at the CAL with no problems related to protocol or contamination.

Computer generated isopleth maps are presented in this paper. The site data were gridded through the use of an objective analysis algorithm based on a successive correction scheme developed by Barnes (1964; 1973), and modified by Achtemeier (1977). Sites with adequate data are explicitly shown on each map. The computer generated contours which are extrapolated to areas far from sites should obviously be considered with due caution.

RESULTS AND DISCUSSION

Precipitation Sulfate Pattern

The NADP/NTN precipitation sulfate concentration maps are shown in Figures 1-4. The asterisks indicate the location of each sampling site used in the analysis. For Figures 1-3 the data for the 24-month period from October 1984 to September 1986 were used. For Figure 4 all data since the beginning in summer 1978 through the end of 1986 were used. The medians of the valid concentration values for each site were calculated, objectively analyzed, and then contoured.

The objective analysis procedure, developed for meteorological mapping applications, considers the five nearest sites, with each site value being

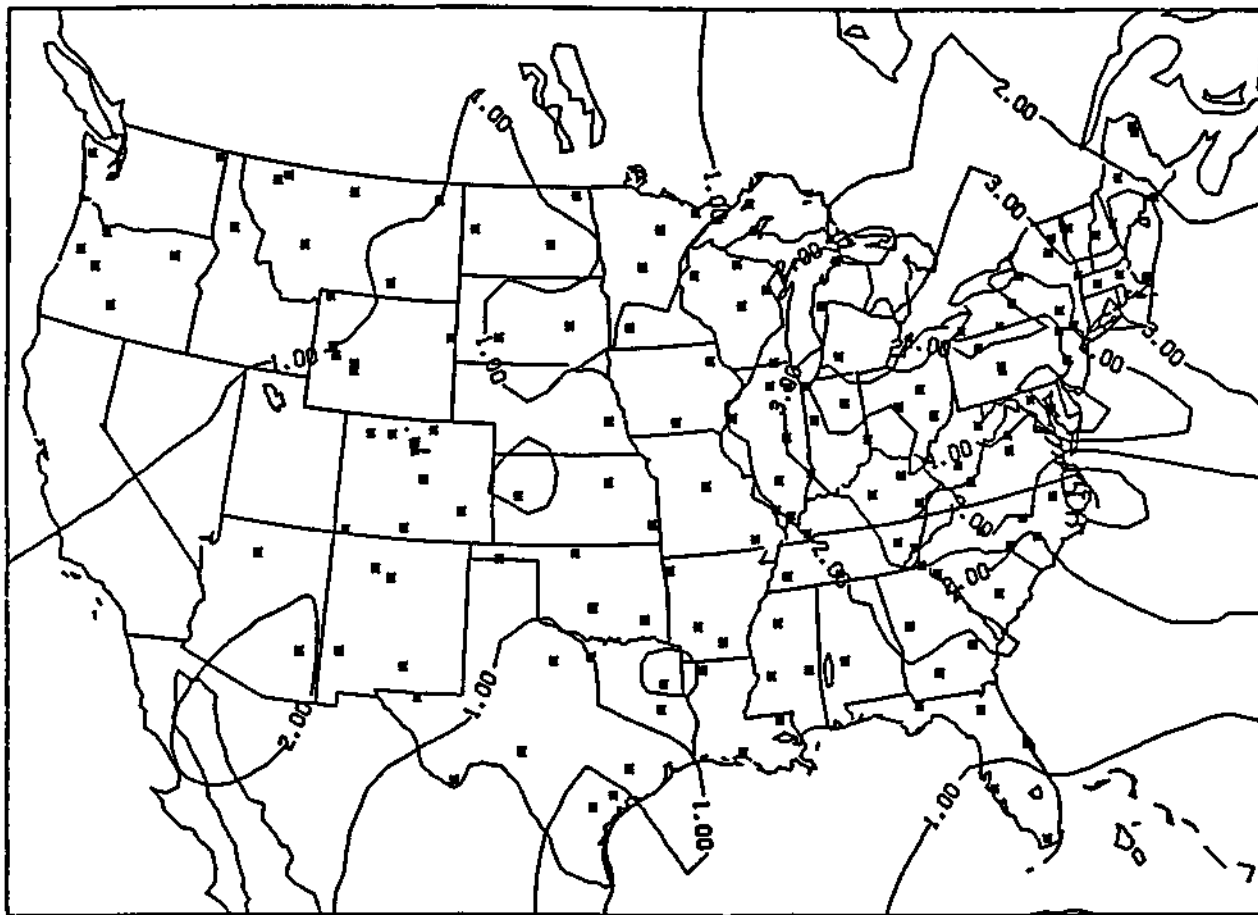


Figure 1. Median precipitation sulfate concentration (mg/L) for summer months (June-August) during the 1984-1986 period.

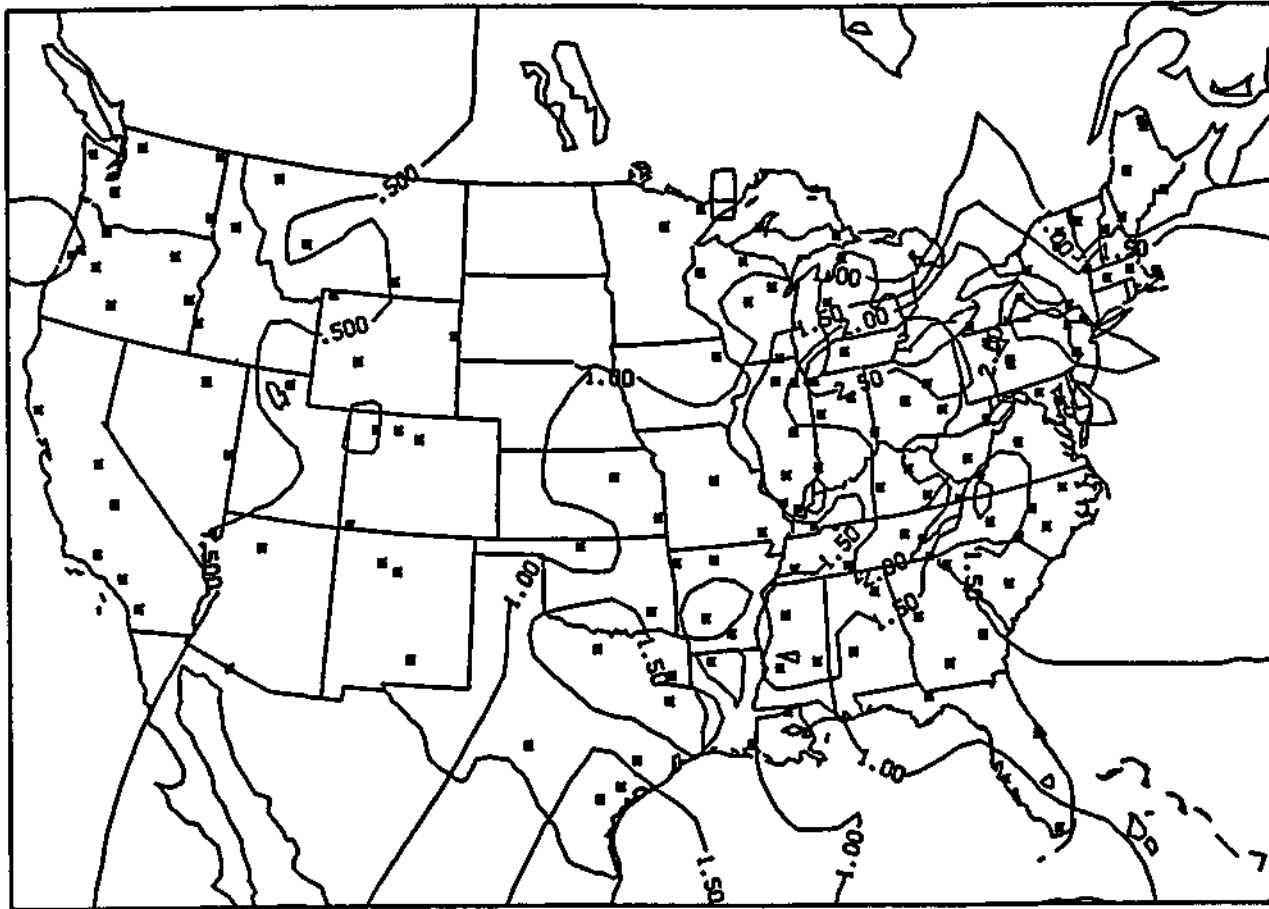


Figure 2. Median precipitation sulfate concentration (mg/L) for winter months (December-February) during the 1984-1986 period.

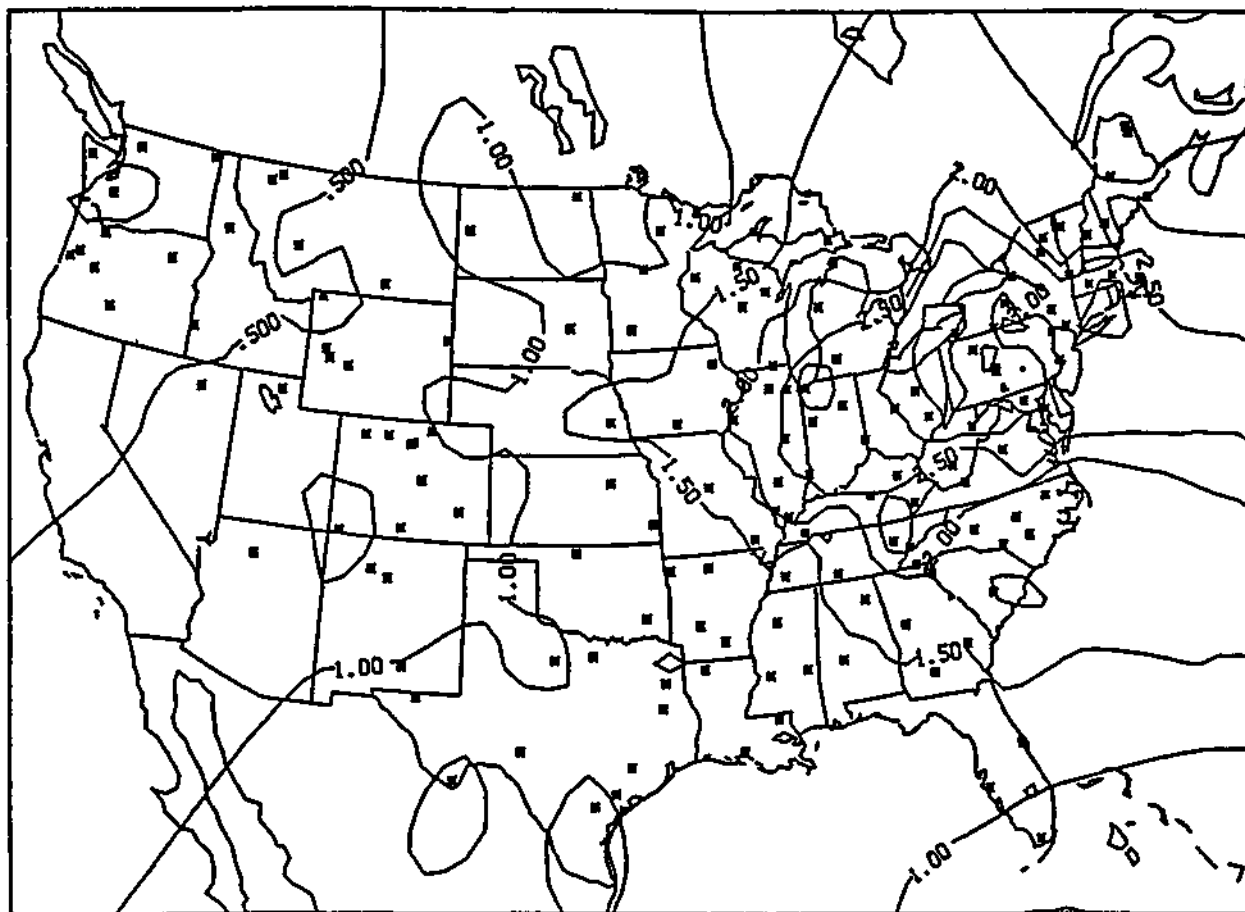


Figure 3. Median precipitation sulfate concentration (mg/L) for the 1984-1986 period.

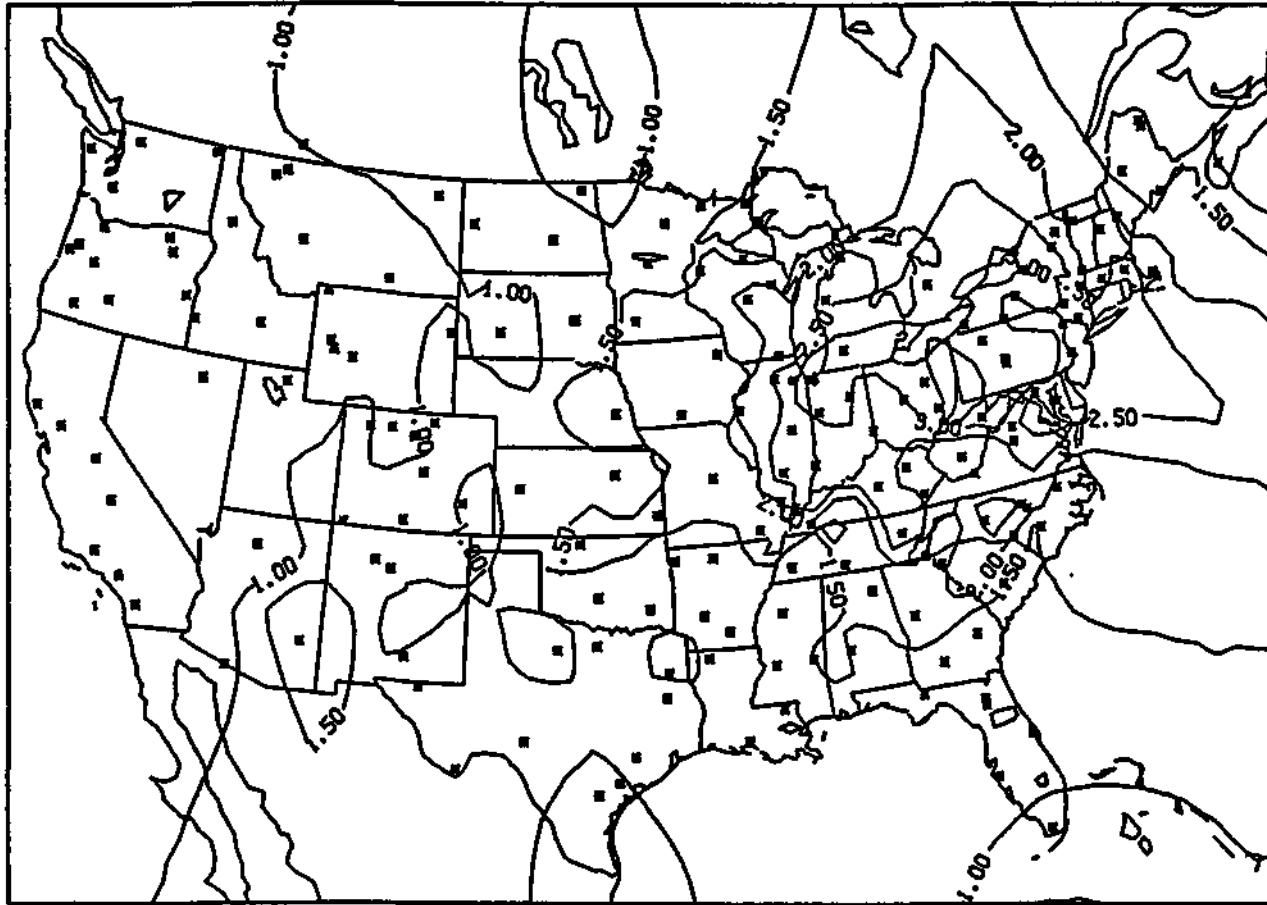


Figure 4. Median precipitation sulfate concentration (mg/L) for the 1978-1986 period.

weighted by the negative exponential of the distance from the site to the vertex in determining values for each vertex of a rectangular grid. The gridded values are then contoured by computer software. We elected to apply the objective procedure in such a way that the final contour pattern agrees well with the pattern that results from a careful manual analysis. That is, we chose to accept rather irregular contour lines instead of setting the adjustable constants to produce relatively more smoothing

We arbitrarily deleted sites that did not have 10 valid values for the seasonal maps and 50 valid values for Figures 3 and 4. Notice in Figure 2 that sites in Nebraska and the Dakotas were deleted because of the n 10 criterion. We calculated and compared the median maps to maps of volume weighted concentration. There was no major difference between the two presentations and we chose to present the median maps to reduce the influence of extreme values.

For each map the highest sulfate concentration is in the northeastern quadrant of the U.S. In the summer the maximum was about 4.5 mg/L for a Maryland site. In the winter the maximum was about 2.5 mg/L for sites in northern Indiana and Ohio and southern Michigan. In the winter relatively high values extend southwest into Texas. The sulfate values drop off sharply toward Maine, Florida, and the West with the lowest values being along the West coast.

The 24-month median sulfate map in Figure 3 is very similar in the East to the 78-86 map in Figure 4. For both maps a maximum contour with a value of 3.5 mg/L is placed to include eastern Ohio, northern West Virginia and western Pennsylvania. The 2.5 and 3.0 contours support the conclusion that the larger sulfate values are displaced to the north and east of the Ohio River Valley. A difference in the West is that with the shorter record the California sites are excluded in Figure 3 and this apparently explains the 0.5 mg/L line in the Northwest being present in Figure 3 but not Figure 4.

The advantages of Figure 4 compared to Figure 3 is that more sites are available for the analysis. The disadvantage is that for Figure 4 the different sites operated for different lengths of time while in Figure 3 essentially all the sites were in operation during the entire 24-month period. Overall Figure 3 and Figure 4 are very similar.

Over the years we have noted certain sites with values that are abnormal compared to their neighbors. For Figure 3 the extreme south central New York site has a value of 2.58 mg/L; the northwest Indiana site at Indiana Dunes National Park has a value of 3.25; the west central North Carolina site has a value of 2.54; and the east central Tennessee site has a value of 2.81. These are examples of sites that produce persistent irregularities in the contour lines.

Aerosol Sulfate and Sulfur Dioxide Pattern

There is no air quality sulfur data record with space and time extent similar to that for precipitation. Perhaps the most useful comparison is

with the data from the 1977-78 SURE study in the Northeast (Mueller and Hidy, 1983). For 5 intensive sampling months, in the period from August 1977 to July 1978, the SO₂ was maximum in a strip from southern Illinois to western Connecticut. For aerosol sulfate the maximum was similar except that the very highest values were to the south of the Ohio River. These air quality records are too short to permit an exact spatial comparison with Figure 3. In general, the different data sets are consistent. With an extensive air quality data set perhaps a careful spatial comparison would be useful in quantifying the relative roles of SO₂ and aerosol SO₄ in producing the precipitation sulfate patterns.

Average Visibility Pattern

The median annual and summer visibility maps by Trijonis (1982) and the 60th percentile map by Sloane (1983) are useful for comparison to the precipitation sulfate map. Sloane analyzed data for 1948-1978 for 15 sites for the area from IL to PA to SC. The lowest visibility (8 miles) site was Dayton. The second lowest visibility (9 miles) was for the four sites: Cleveland and Columbus (OH); Louisville (KY); and Richmond (VA). These sites are all within the >2.50 mg/L area on Figure 3. The 14 mile visibilities for Williamsport, PA and Washington, DC do not fit well with Figure 3. Also the 10 mile visibility for Charlotte, NC and Greensboro, NC are lower than might be expected from the sulfate pattern in Figure 3.

Trijonis presented median annual visibility for 1974-76 for sites across the entire U.S. His low visibility area (10 mile median values) which included four sites in IN, OH, and WV is consistent with Figure 3 while his values of 12, 17, and 19 in PA are larger than expected from Figure 3. His values of 10 at a southeastern NC site and 9 at sites in LA and AL are certainly lower than expected from the sulfate in Figure 3. In the west the maximum visibility values of >70 miles in NV, UT, and CO and <45 in much of OR and WA is counter to the gradient of the data in Figure 3.

The Trijonis disagreement between the pattern in Figure 3 compared to the annual coastal visibility data for coastal areas in the Southeast is most likely due to the effect of relative humidity on visibility.

The Trijonis median summer visibility map for 1974-76 has low visibility for most of the region from LA to IN to PA to GA. Again this pattern is not entirely consistent with the precipitation sulfate map for summer in Figure 1.

The precipitation data in Figure 3 are for a different time period than the visibility maps of Trijonis or Sloane. Spatial shifts in locations of sulfur emission sources and the spatial shifts in weather variables patterns (such as for relative humidity) should be examined in future studies.

Precipitation Sulfate Seasonality

In an earlier paper seasonal (3-month) and period (5-month) variations in the concentrations of the major anions and cations in the precipitation

of the United States were examined by Bowersox and Stensland using data from the NADP/NTN for 1978 through 1983 (Bowersox and Stensland, 1985). For most ions, concentrations during the warm (growing) period were higher than during the cold (dormant) period throughout much of the country. Previous investigators had often focused their time variation studies on hydrogen, sulfate, and nitrate ion behavior for the eastern U.S. Results of the Bowersox and Stensland study indicated that seasonal variations are neither confined to the East nor limited to the ions most frequently associated with acidic deposition. Median values by region of the warm/cold period ratio are shown in Table 1. The Northeast region included states from OH to VA to ME. The Southeast region included AR and extreme eastern TX to NC and GA, excluding FL. The Midwest region included states from MN to eastern KS to IN and KY. The Rocky Mountain region included states from ID and MT to AZ and NM. Seasonal (3-month) ratios for sulfate were found to be somewhat larger than the period (5-month) ratios.

Seasonal ratios for 1984-86 can be deduced from Figures 1 and 2. The seasonality remains largest for the NE region, especially for the New England states. For two coastal states, FL and TX, the winter season sulfate concentrations are equal to or exceed the summer values. Because it will be referred to later, notice that the warm/cold season ratio for the east central IL site (known as the Bondville site) is about 1.5.

Aerosol Sulfate Seasonality

At the Bondville, IL site daily medium volume aerosol samples have been collected. From February 1983 to June 1986 the filters used have been 37 mm 1 μm teflon. To protect the samples from rain the filter holders are mounted face down under inverted polyethylene funnels. After exposure the filters are extracted by placing them in a 50 mL linear polyethylene (LPE) bottle containing 25 mL of pH = 4.3 hydrochloric acid solution. The bottles are agitated for 24-48 hours on a horizontal action shaker. This solution is filtered through a Millipore HA 0 45 μm filter and collected in another 50 mL LPE bottle. Sulfate is then determined by ion chromatography and calcium, magnesium, and potassium are measured by flame atomic absorption.

The seasonal concentrations for these constituents are shown in Table II. The summer concentrations exceed the winter concentrations for sulfate as well as the dust type constituents. These results agree with the time variations for precipitation shown in Table I. From Figures 1 and 2, the seasonal precipitation ratio is 1.5 for Bondville while the aerosol ratio in Table II is 2.1. One possible explanation for the difference in these ratio values is that higher winter ambient SO_2 provides the extra winter sulfate in precipitation to lower the ratio to 1.5.

Many other studies have reported on the higher summer compared to winter ambient aerosol sulfate. Mathai and Tombach (1987) summarized much of the recent ambient aerosol sulfate data for the East. Summer to winter sulfate ratios of the order of two result from their data summary.

Table I. Summary of ratio values (warm period/cold period precipitation concentration) for all sites in four regions (from ref. 14).

<u>Region^a</u>	<u>N^b</u>	<u>SO₄²⁻</u>	<u>NO₃⁻</u>	<u>NH₄⁺</u>	<u>Ca²⁺</u>	<u>H⁺</u>
MW	20	1.32	.92	1.38	1.46	1.08
SE	15	1.56	1.72	2.00	1.58	1.48
NE	23	2.20	1.20	2.21	1.47	1.86
RM	16	2.10	2.33	2.54	2.40	2.53

<u>Region^a</u>	<u>N^b</u>	<u>Mg²⁺</u>	<u>K⁺</u>	<u>Na⁺</u>	<u>Ca⁻</u>
MW	20	1.34	1.48	.68	.78
SE	15	1.28	1.41	.93	.83
NE	23	1.14	1.50	.70	.67
RM	16	1.96	2.52	1.39	1.50

^aMW is Midwest; SE is Southeast; NE is Northeast; and RM is Rocky Mountain.

N is number of sites in each region.

Table II. February 1983 - June 1986 aerosol median concentrations ($\mu\text{g}/\text{m}^3$) for Bondville, IL.

	<u>W</u>	<u>Sp</u>	<u>Su</u>	<u>F</u>	<u>All Seasons</u>
Sulfate	2.91	3.22	5.98	3.29	3.56
Calcium	.19	.35	.61	.45	.37
Magnesium	.031	.058	.093	.068	.060
Potassium	.058	.056	.078	.090	.068

Note: W = Dec., Jan., and Feb.;
 Sp = Mar., Apr., and May;
 Su = June, July, and Aug.;
 F = Sept., Oct., and Nov.

Number of samples by season was 273 for W; 322 for Sp; 281 for Su; and 288 for F.

Visibility Seasonality

Sloane (1983) reported the quarterly 60th percentile visibility for the 1947-78 period for 15 sites in the northeastern quadrant of the U.S. The summer and winter values listed in the upper portion of Table III are averages of the 1975 and 1977 quarterly values reported by Sloane. The Vinzani and Lamb (1985) data in Table III are similar except that they reported data through 1980, considered only sites near or in Illinois, and used meteorological definitions of seasons (Dec -Feb. for winter and June-Aug. for summer) instead of the quarterly intervals used by Sloane. In the ratio column in Table III we note that winter visibility exceeds summer visibility at almost all sites considered by Sloane. This is consistent with the higher summer sulfate in both the precipitation and air quality data discussed earlier. The exception was Chicago. The Moline, Peoria, and Springfield sites at the bottom of Table III indicate that the feature of summer visibility equal to or exceeding winter visibility is not due to one anomalous urban site (Chicago) but instead covers a larger region. The Evansville site with a ratio value exceeding 1.0 is on the east edge of the Vinzani and Lamb study area. The seasonal visibility pattern for Illinois is not consistent with the precipitation sulfate data nor the rather comprehensive aerosol sulfate record for Bondville, IL. The primary winter landscape in the general area near the Illinois sites is relatively bare tilled fields or snow cover. One might then suggest that airborne dust leads to decreased winter visibility. The precipitation quality calcium and magnesium data (Semonin, 1986) indicate that the concentrations increase steadily from the eastern states toward the plains states, with values of about 0.1 mg/L along the East Coast and 0.5 mg/L in the Plains. The Bondville, IL aerosol data for Ca^{++} and Mg^{++} indicate that the concentrations are very low compared to SO_4^{++} and are lower in the winter than in the summer. Therefore dust does not seem to explain the visibility at Illinois sites is lower in the winter. Perhaps studies should be done to see if meteorological gradients combined with the exposed soil surfaces might produce relative humidity gradients that can explain the seasonal visibility patterns for Illinois.

CONCLUSIONS

1. There is reasonable agreement between the spatial patterns of sulfate in precipitation, ambient aerosol sulfate, and visibility. Evidently, a meteorological (relative humidity) adjustment would be necessary to make visibility and precipitation sulfate data even more consistent with each other. The NADP/NTN precipitation quality data base, having a rather good site density and length of record, may be useful in interpreting and extrapolating air quality data and to a lesser extent, visibility data.
2. The seasonal pattern of sulfate concentration in precipitation is consistent with aerosol sulfate data in the eastern U.S. The same is true for visibility at most eastern locations; the Illinois stations are inconsistent with precipitation quality data.

Table III. The 60th percentile visibility (miles) and winter/summer ratios.

<u>From Sloane (1982):^a</u>	<u>Summer^a</u>	<u>Winter^a</u>	<u>Winter Summer</u>
Dayton, OH	6.4	9.0	
1.4			
Columbus, OH	7.2	9.8	
1.4			
Cleveland, OH	7.8	9.7	
1.2			
Louisville, KY	8.0	10.7	
1.3			
Lexington, KY	7.2	11.6	
1.6			
Williamsport, PA	9.0	17.7	
2.0			
Washington, DC	10.2	11.9	
1.2			
Richmond, VA	6.2	10.9	
1.8			
Roanoke, VA	12.8	38.4	
3.0			
Lynchburg, VA	10.9	30.4	
2.8			
Knoxville, TN	7.8	9.1	
1.2			
Greensboro, NC	6.6	12.6	
1.9			
Charlotte, NC	6.8	15.4	
2.3			
Columbia, SC	8.6	10.4	
1.2			
Chicago, IL	9.6	9.9	
1.0			
<u>From Vinzani and Lamb (1985):</u>			
Chicago, IL	10.1 ^b	8.7 ^b	
.9			
Moline, IL	10.6	7.9	
.7			
Peoria, IL	12.5	10.0	
.8			
Springfield, IL	8.9	8.7	
1.0			
Evansville, IN	7.2	7.7	
1.1			

^aAverage of 1975 and 1977 values.

^bAverage of 1976, 1977, 1978, 1979, and 1980 values. For Springfield 1976 was missing and for Chicago 1979 and 1980 were missing.

3. A dense aerosol sulfate and SO₂ network might help quantify the relative importance of the gaseous versus particulate scavenging mechanisms for wet deposition for different regions.

REFERENCES

- Achtemeier, G. L., P. H Hildebrand, P T. Schickedanz, B. Ackerman, S A. Changnon, Jr., and R G. Semonin, 1977: "Illinois precipitation enhancement program design and evaluation techniques for high plains cooperative program," Ill. State Water Survey Final Report on Contract 14-06-D-7197, Appendix B.
- Barnes, S. L. , 1964: "A technique for maximizing details in numerical weather map analysis," J. Appl Meteorol., 3, 396-409.
- Barnes, S. L. , 1973: "Mesoscale objective map analysis using weighted time-series observations," NOAA Tech. Memo. 62, NSSL, 60 pp.
- Bigelow, D. S., 1982: "NADP instruction manual - site operation," NREL, CSU, Ft. Collins, CO.
- Bigelow, D.S., 1986. "Quality assurance report, NADP/NTN deposition monitoring, field operations," NREL, CSU, Ft. Collins, CO.
- Bowersox, V C, 1985: "Data validation procedures for wet deposition samples at the Central Analytical Laboratory of the National Atmospheric Deposition Program," In: Transactions, APCA International Specialty Conference on Quality Assurance in Air Pollution Measurements, Boulder, CO, (October 1984), T. R. Johnson and S. J. Penkala, Eds., APCA, Pittsburgh, PA, p. 500-524.
- Bowersox, V C. and G. J. Stensland, 1985: "Seasonal variations in the chemistry of precipitation of the United States," paper 85-6A.2 at the 78th Annual APCA Mtg., Detroit, MI
- Lockard, J. M. , 1987: "Quality assurance report, NADP/NTN deposition monitoring, CAL laboratory operations," NREL, CSU, Ft. Collins, CO.
- Mathai, C. V. and I. H Tombach, 1987: "A critical assessment of atmospheric visibility and aerosol measurements in the eastern United States," in press, J. Air Pollut. Control Assoc.
- Mueller, P. K. and G. M. Hidy, 1983: "The sulfate regional experiment report of findings," EPRI EA-1901, Vol. 1, 2, 3. Electric Power Research Institute, Palo Alto, CA.
- National Atmospheric Deposition Program/National Trends Network, 1986. NADP/NTN Data Tape for 1978-December, 1986, available from NADP/NTN Coordinator's Office, NREL, CSU, Ft. Collins, CO.

- Peden, M.E. , S. R. Bachman, C. J. Brennan, B. Demir, K. O. James, B. W. Kaiser, J. M. Lockard, J. E. Rothert, J. Sauer, L. M. Skowron, and M. J. Slater, 1986: "Development of standard methods for the collection and analysis of precipitation," ISWS Contract Report 381, Champaign, IL.
- Semonin, R. G. , 1986: "Wet deposition chemistry," in the ACS Symposium Series 318 Materials Degradation Caused by Acid Rain, R. Baboian, Ed. , ACS, Arlington, VA, 23-41.
- Sloane, C. S., 1983: "Visibility trends: II. midwestern United States," Atmos. Environ., 17. 763.
- Stensland, G. J., R. G. Semonin, M. E. Peden, V. C. Bowersox, F. F. McGurk, L. M. Skowron, M. J. Slater and R. K. Stahlhut, 1980: "NADP Quality Assurance Report, Central Analytical Laboratory, 1 January 1979 to 31 December 1979," NREL, CSU, Ft. Collins, CO.
- Trijonis, J, 1982: "Existing and natural background levels of visibility and fine particles in the rural east," Atmos. Environ... 16. 2431.
- Vinzani, P. G. and P. J. Lamb, 1985: "Temporal and spatial visibility variations in Illinois vicinity during 1949-80," J. Climate and Appl. Meteorol., 24, 435-451.

CHAPTER 5

VARIATIONS IN PRECIPITATION COMPOSITION AND DEPOSITION WITH SYNOPTIC WEATHER TYPE

Kevin G. Doty and Donald F. Gatz

INTRODUCTION

As one portion of a broader analysis of five years of event precipitation chemistry data for central Illinois, we examined variations in ion composition and deposition with synoptic weather type. The purpose of this effort was to improve our scientific understanding of the chemical and physical mechanisms of scavenging and deposition of pollutants by precipitation. The ultimate goal is to improve our ability to predict the locations and magnitudes of atmospheric wet deposition.

METHODS

The event precipitation chemistry data set is described in the Chapter by K.G. Doty on back trajectory climatology, elsewhere in this report. The same chapter describes the synoptic classifications and the methods and criteria used to classify samples. The classifications and their associated abbreviations are: pre-cold front (PCF), cold front (CF), pre-warm front (PWF), warm front (WF), pre-occluded front (POF), occluded front (OF), stationary front (SF), low pressure center (L), trough of low pressure (T), squall line (SL), squall zone (SZ), and air mass (AM).

The cited chapter also describes the calculation of deposition frequencies for the various synoptic types. In this chapter we describe the results of examining both deposition frequencies and the usual volume-weighted mean concentrations for differences between the various classes of synoptic weather conditions. Separate analyses were carried out for each of the four seasons, where winter is defined as the months of December-February, spring as March-May, and so forth. For each season, two frequency distributions were prepared, one for deposition and one for concentration. For convenience of comparison, both diagrams show the same plots of seasonal frequency of synoptic types and the distribution of sample volume by synoptic type.

RESULTS

Winter results are shown in Figures 1-2, spring in Figures 3-4, summer in Figures 5-6, and fall in Figures 7-8. For each season, the first figure of the pair presents the deposition results and the second the concentra-

tion results As just mentioned, both figures show the seasonal data on distribution of sample volume and frequency of synoptic types.

Seasonal Variations in Frequencies of Synoptic Type

Seasonal differences in relative frequencies of the various synoptic types may be seen in Figures 1-8, and are summarized in Table 1 Cold fronts and warm fronts are among the four highest-frequency classes in all four seasons, and low pressure centers and stationary fronts appear in three of the four seasons Low pressure centers occurred with the highest frequency of any class in winter and spring, and cold fronts were the highest frequency class in summer and fall. In each season the four highest frequency classes accounted for about 65-75% of all precipitation events.

Table 1. Summary of highest synoptic frequencies by season.

<u>Season</u>	<u>Synoptic class of highest frequency</u>	<u>Classes with next highest frequencies</u>	<u>Total frequency of these 4 classes (%)</u>
Winter	L	CF, WF, T	70.6
Spring	L	CF, WF, SF	64.1
Summer	CF	SF, T, WF	73.4
Fall	CF	L, SF, WF	73.2

Sample Volume as a Function of Synoptic Type

Even a brief inspection of the lowest two panels of one of the figures for each season is enough to notice that the distribution of sample volumes over the various synoptic types is strongly influenced by the frequencies with which the synoptic classes occur. In each season, the four synoptic types that occurred with the highest frequency also had the four highest sample volume fractions. In most seasons the order of the synoptic classes is the same for both frequencies as well, although there are some minor differences.

Variations of Deposition and Concentration with Synoptic Type

Results for winter are shown in Figures 1-2 Comparison of deposition frequencies (Table 1) with the distribution of sample volumes shows that deposition frequencies of all three ions were largely determined by the distribution of sample volume over the various synoptic classes Warm fronts, stationary fronts, low pressure centers, and troughs produced the highest deposition frequencies for all three ions, and also accounted for the highest frequencies of sample volume. Figure 2 shows that ion concentrations were relatively constant, at least by comparison with depositions, over the various synoptic types in winter The highest volume-weighted mean concentrations of all three ions were observed for air mass precipitation, but this synoptic type accounted for only a very small

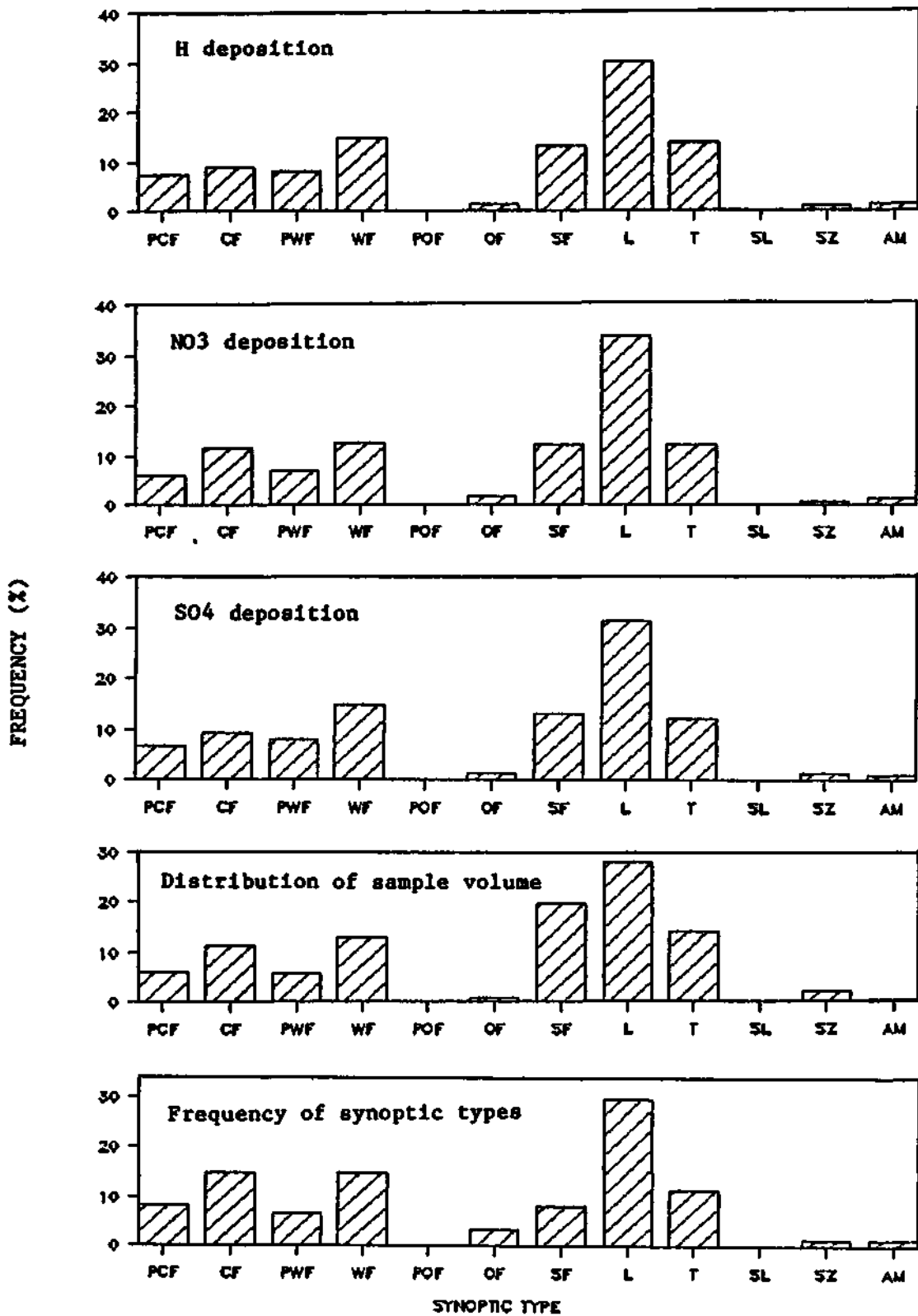


Figure 1. Winter season variations of percent frequency of ion deposition in precipitation with synoptic class. The frequency distributions of sample volume and synoptic type are also shown.

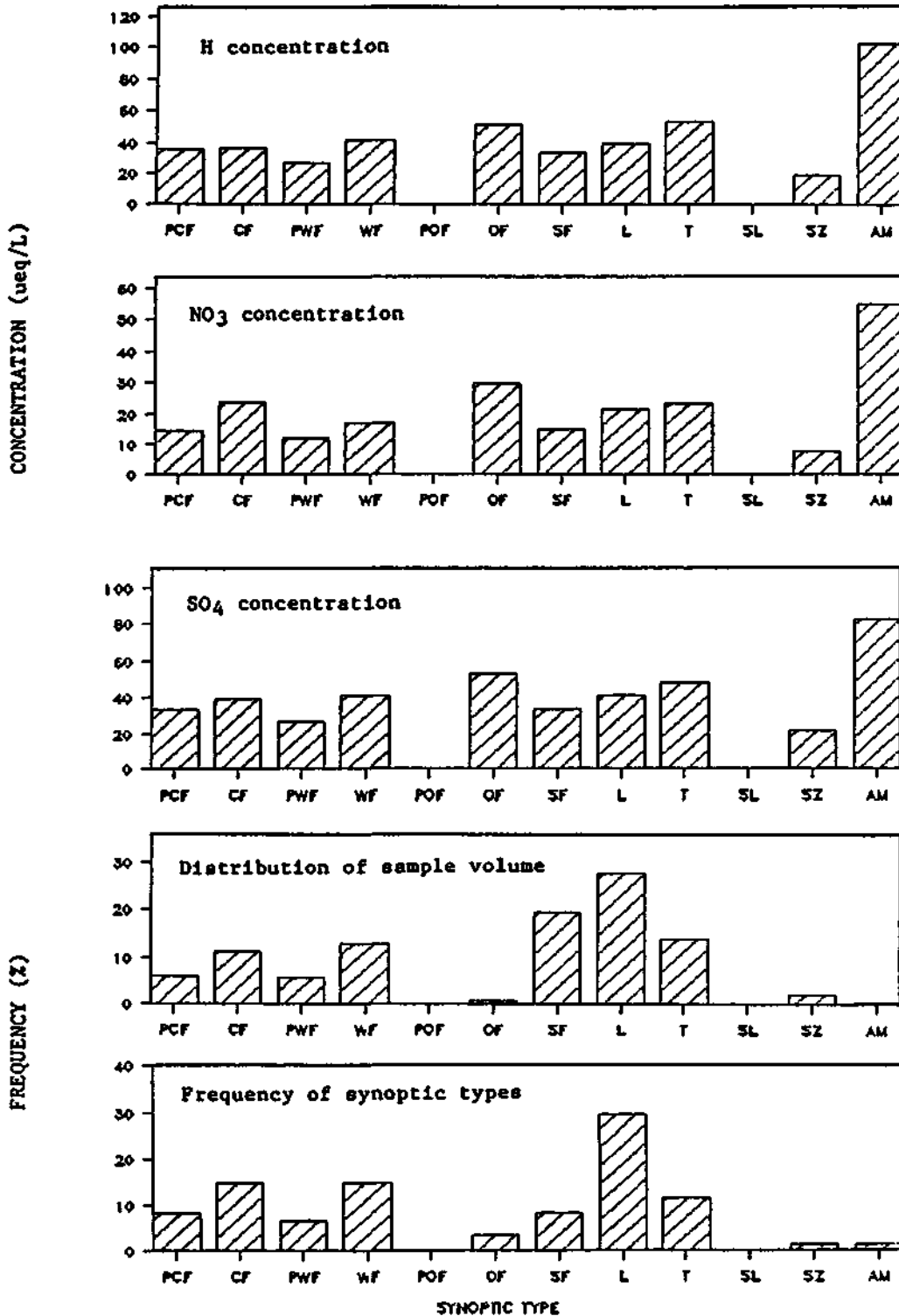


Figure 2. Winter season variations in volume-weighted mean concentrations in precipitation with synoptic class. The frequency distributions of sample volume and synoptic type are also shown.

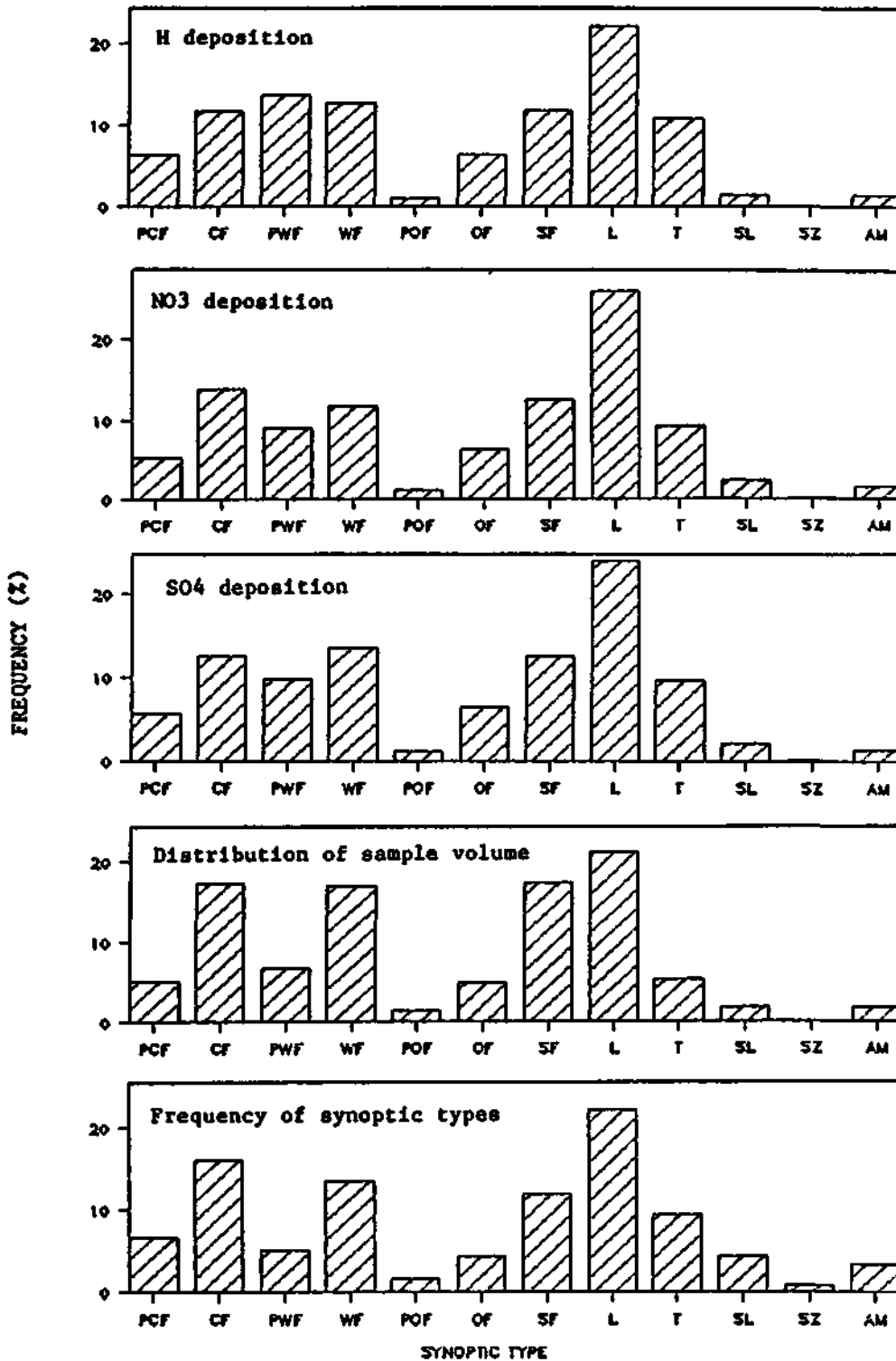


Figure 3. Spring season variations of percent frequency of ion deposition in precipitation with synoptic class. The frequency distributions of sample volume and synoptic type are also shown.

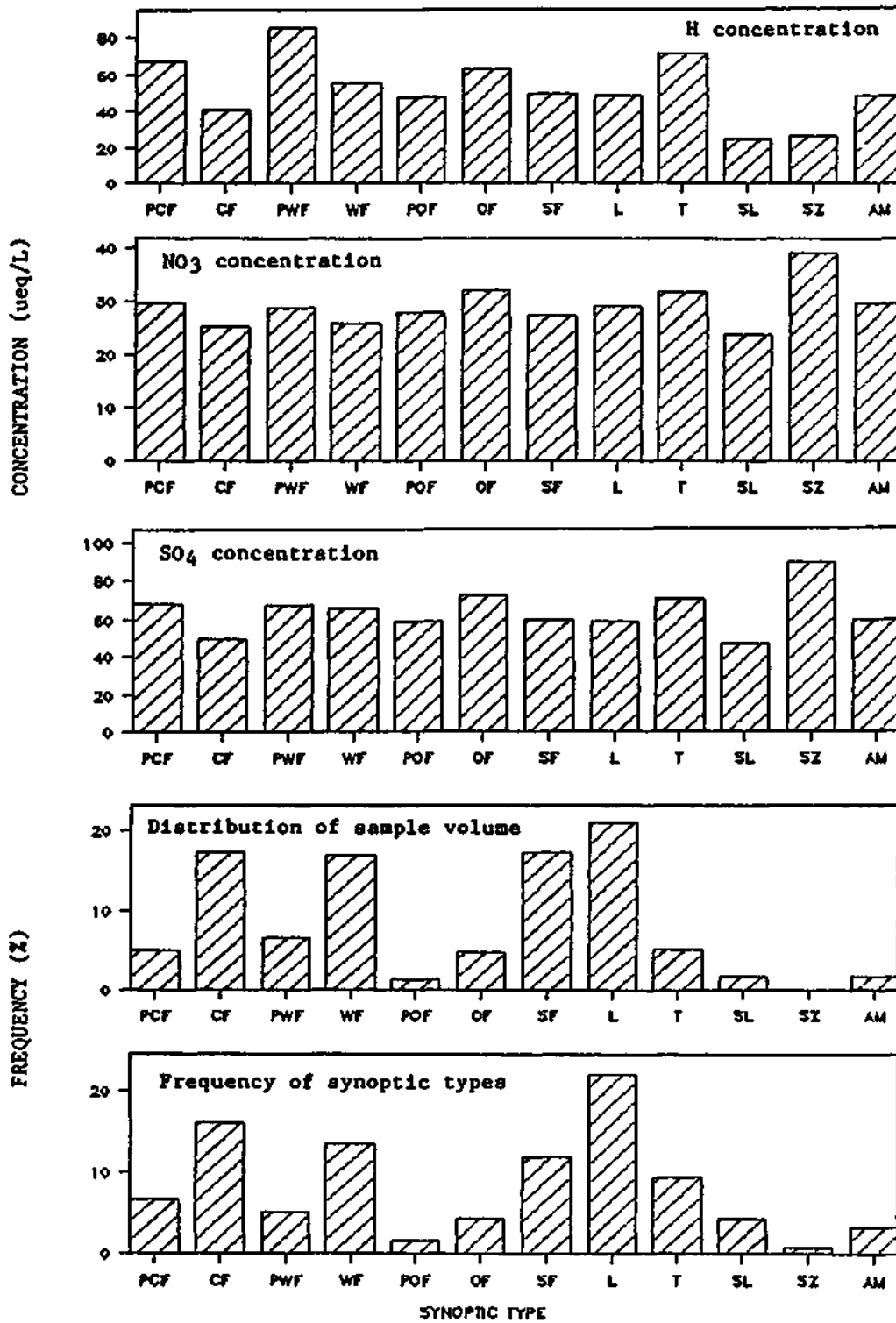


Figure 4. Spring season variations in volume-weighted mean concentrations in precipitation with synoptic class. The frequency distributions of sample volume and synoptic type are also shown.

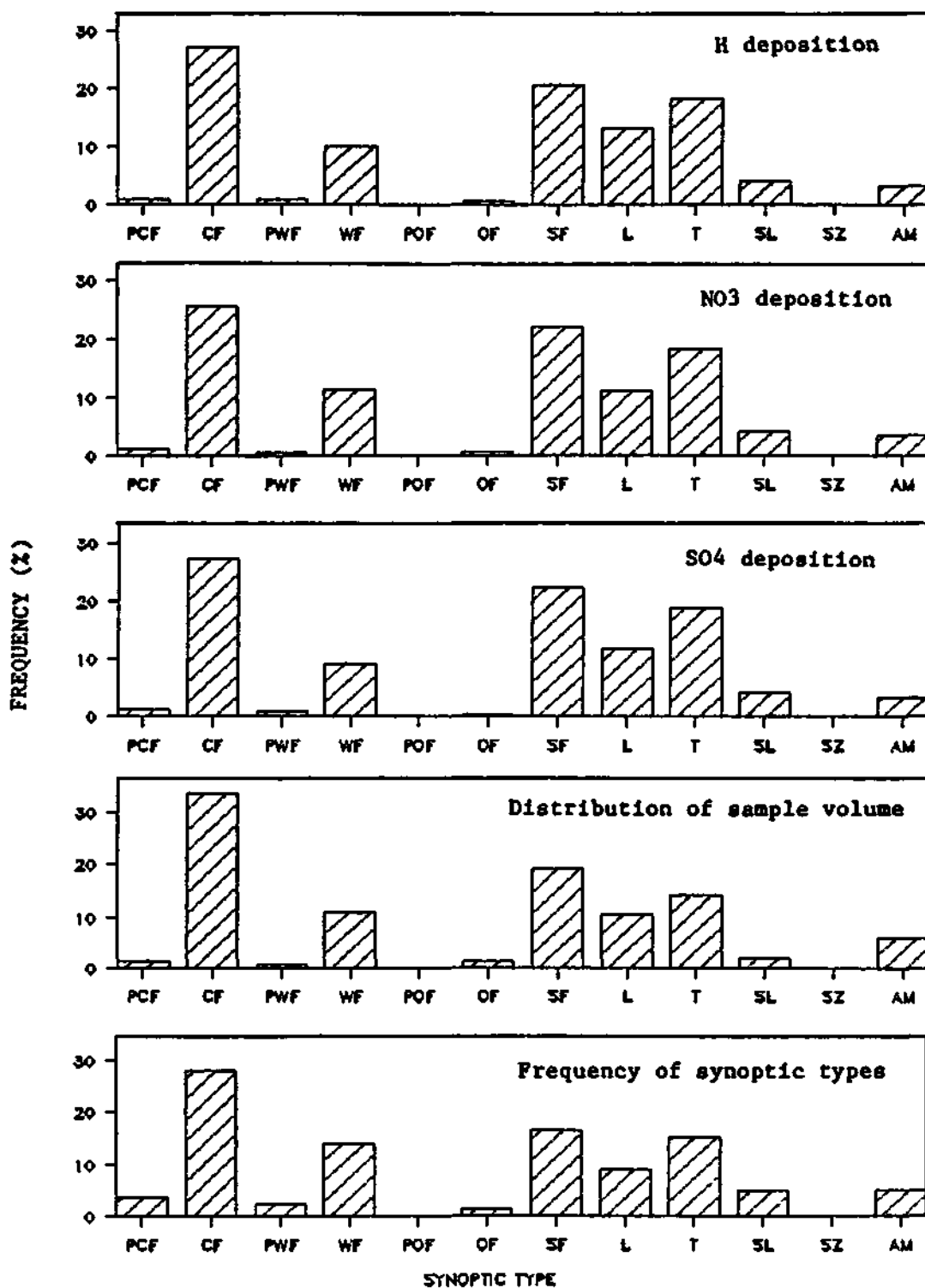


Figure 5. Summer season variations of percent frequency of ion deposition in precipitation with synoptic class. The frequency distributions of sample volume and synoptic type are also shown.

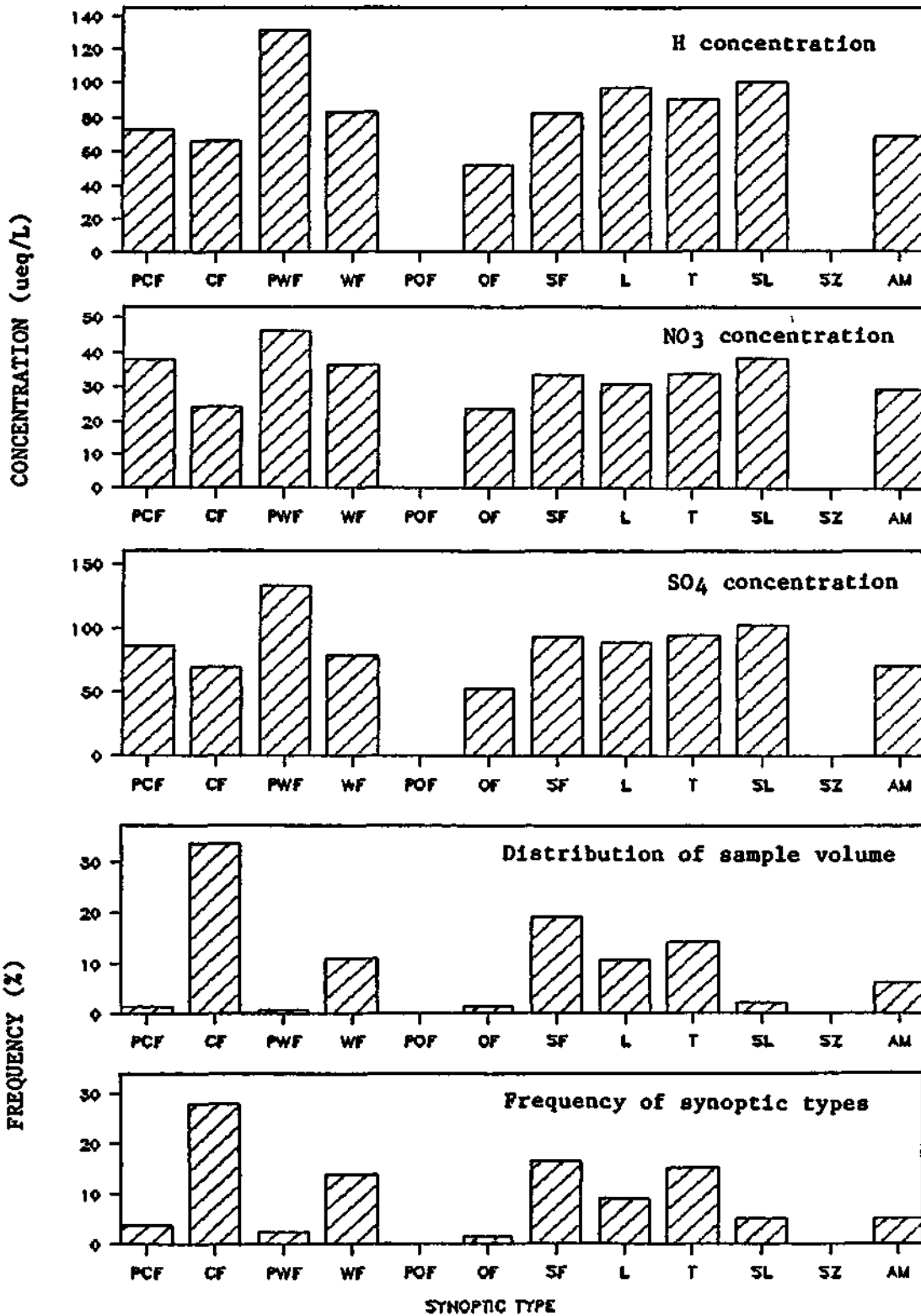


Figure 6. Summer season variations in volume-weighted mean concentrations in precipitation with synoptic class. The frequency distributions of sample volume and synoptic type are also shown.

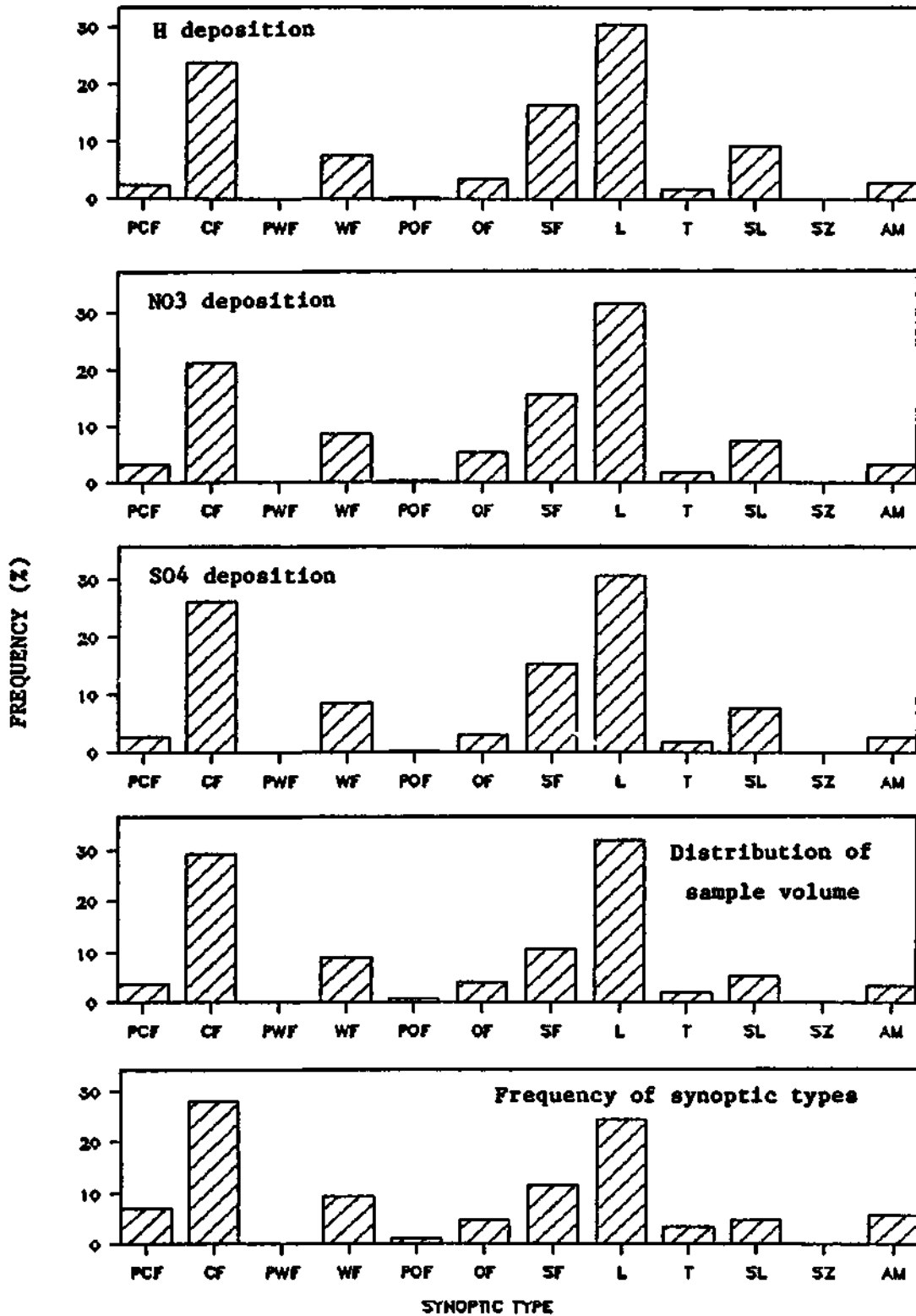


Figure 7. Fall season variations of percent frequency of ion deposition in precipitation with synoptic class. The frequency distributions of sample volume and synoptic type are also shown.

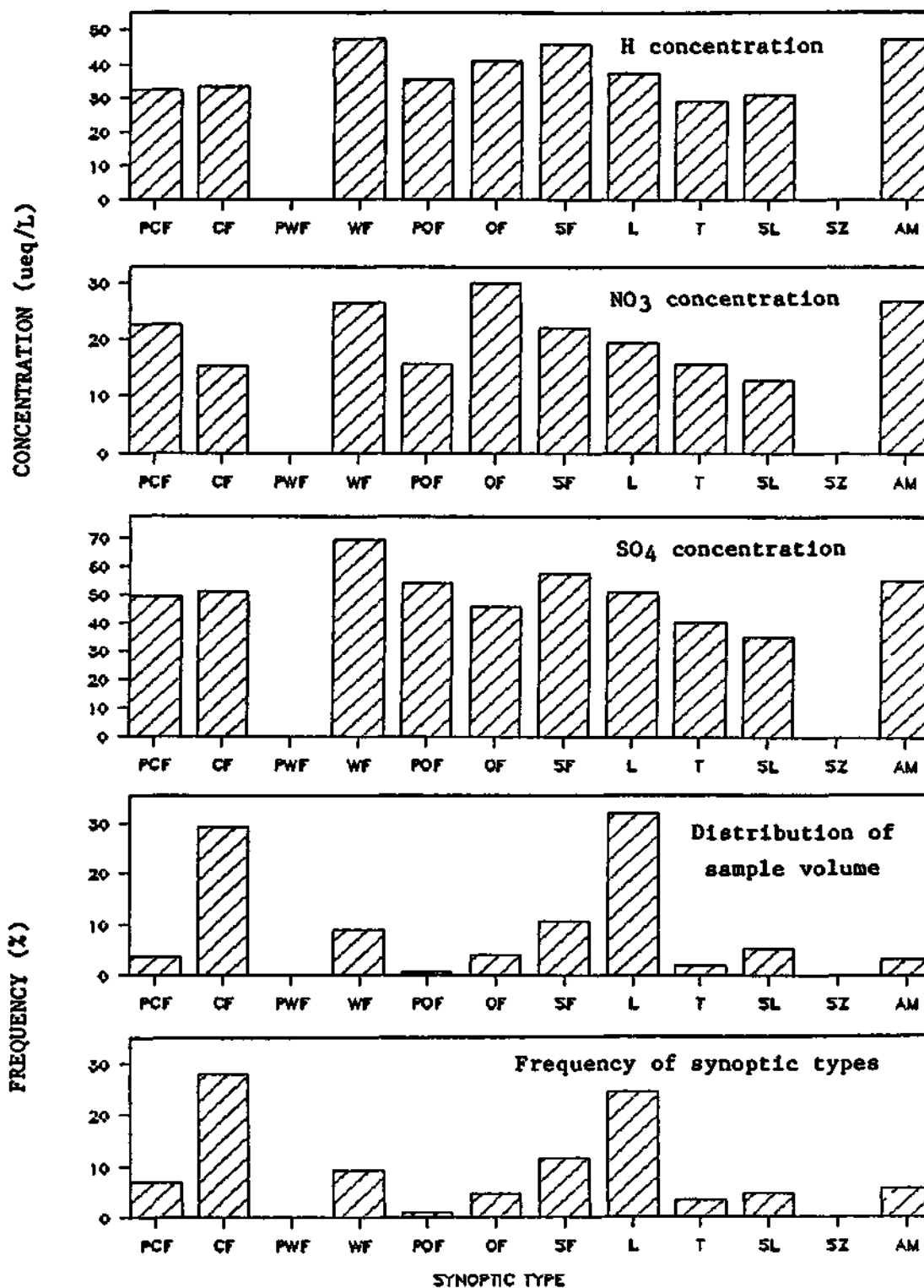


Figure 8. Fall season variations in volume-weighted mean concentrations in precipitation with synoptic class. The frequency distributions of sample volume and synoptic type are also shown.

fraction of the total, and these concentrations were based on very few samples.

Results for spring appear in Figures 3-4. Again, the strong influence of the sample volume distribution on the deposition frequencies (Figure 3) is apparent. Cold fronts, warm fronts, stationary fronts, and low pressure centers produced the highest frequencies of sample volume, and the highest frequencies of deposition for all three ions as well. However, the deposition frequencies for precipitation from low pressure centers were disproportionately high, and this also occurred for all three ions. As was the case for winter, Figure 4 shows that concentrations of all three ions were relatively constant over the various synoptic classes, and somewhat higher than those of winter.

Results for summer are given in Figures 5-6. The strong influence of sample volume on deposition (Figure 5) is clear here also. Cold fronts, stationary fronts, and troughs produced the highest deposition frequencies of all three ions and also dominated the sample volume distribution. Once again, concentrations (Figure 6) were relatively more constant over synoptic type, although differences between classes in the range of factors of 2-3 occurred. Summer concentrations of H and SO_4 were somewhat higher than those of spring, while those of NO_3 were about the same.

Results for fall in Figures 7-8 tell much the same story. Deposition (Figure 7) followed sample volume, with cold fronts, stationary fronts, and low pressure centers dominant. Concentrations (Figure 8) were again relatively constant over the various synoptic types; they were also generally lower than those of summer, but still above those of winter.

DISCUSSION AND CONCLUSIONS

Variations of H, NO_3 , and SO_4 deposition and concentration with synoptic weather type were very consistent in all four seasons. Deposition frequencies were strongly a function of the sample volume distribution, which was in turn largely determined by the frequency of the various synoptic types during which the precipitation occurred. Concentrations, in contrast, were relatively constant over all synoptic types. Season variations in concentrations were much as expected. The highest concentrations occurred in spring and summer, and the lowest in fall and winter. The amplitudes of these annual cycles were greatest for SO_4 and H and least for NO_3 .

These results emphasize that our ability to predict the deposition of acidity in precipitation is to a large extent controlled by our ability to predict precipitation. Synoptic type does not appear to be an important consideration in specifying the concentrations of H, SO_4 , or NO_3 in precipitation, although the relative frequencies of the various synoptic types may, of course, help to determine total annual precipitation.

The results also suggest that historical depositions of certain ions in precipitation might be estimated from precipitation records, combined with appropriate annual mean concentrations of the major ions. The appropriate concentrations might be inferred from airborne concentration measurements, if available, or relevant emissions data.

CHAPTER 6

BACK TRAJECTORY CLIMATOLOGIES FOR SULFATE AND NITRATE WET DEPOSITION FLUXES AT A CENTRAL ILLINOIS SITE

Kevin G. Doty and Van C. Bowersox

INTRODUCTION

Precipitation samples have been collected routinely since September 1979 at a field site, operated under this contract, in rural east-central Illinois. Samples were collected with automated wet-only collectors of the HASL design (Volchok and Graveson, 1975). To monitor operations, a rain gage tandem to the collectors was installed to record the precipitation amount, time of occurrence, and the open/close status (i.e., "event record") of the sample collection buckets on the collectors. Data from the gage were combined with the chemical concentration measurements of samples from the collectors to compute wet-only fluxes of sulfate and nitrate. The fluxes were divided into high, middle, and low classes. The goal of this chapter is to summarize the results of the back trajectory calculations for these flux classes utilizing the trajectory model (the ISWS model) described in chapter 15, where it was compared with the ARL-ATAD model of Heffter (1980). This analysis involved approximately 250 precipitation chemistry samples and the calculation of about 1100 back trajectories 72 hours in length.

DESCRIPTION OF DATA SET

Methods

Field Site. The field site where samples were collected for this study is located in rural east-central Illinois, about 13 kilometers southwest of Champaign near Bondville, Illinois. Relatively flat homogeneous terrain surrounds the site in all directions. Collection equipment is installed on a 2.5 hectare grass-covered plot, which is surrounded by agricultural fields. Corn and soybeans are planted in these fields on a rotational basis. These crops are typically planted in April and May, and after emergence, they offer a nearly continuous ground cover until harvest in September and October. During the dormant season, the soils are often tilled and lie bare. This pattern of intensive cash crop farming is characteristic of an area of at least 150 km in diameter and it is interrupted only by river valleys and towns. A more complete description of the location of the site, soil types, etc., can be found in chapter 17.

The agricultural activities in east-central Illinois are a major regional source of soil particles in the boundary layer. Planting and

harvesting in the spring and fall result in airborne concentrations of total suspended particles (TSP) that are higher than during the dormant season, when the soil is bare (Hopke, 1986). Another important source of aerosols is road dust from traffic on unpaved roads (Gatz *et al.* 1985). Together the large particle sources tend to maximize during the warm period, from April to October, resulting in monthly average TSP concentrations of 30-50 $\mu\text{g m}^{-3}$. Analogous concentrations during the dormant period are in the range of 15-25 $\mu\text{g m}^{-3}$ (Hopke, 1986). Since these aerosols are rich in alkali and alkaline earth metals, such as Ca^{++} , Mg^{++} , Na^+ , and K^+ , they tend to offset the acidity of the sulfates and nitrates when incorporated into precipitation

Robertson (1987) has located the significant point sources of SO_2 , NO_x , and other criteria pollutants within 50 km of the field site. Within this area, combined annual emissions of SO_2 and NO_x were around 23,000 and 7,000 metric tonnes, respectively. Almost 2/3 of the local point sources were in the southwest and the northeast quadrants (See Figure 1 of chapter 17 for detailed locations). Seven of the 12 significant point sources in the northeast quadrant were in Urbana-Champaign, a city ("100,000 people) that is 10-15 km northeast of the site. Predominant wind directions at the surface are southerly to southwesterly in every month of the year except February, when they are from the northwest (Changnon, 1959). Because the prevailing winds often have a southerly component, the nearby influence of sources in Urbana-Champaign are minimized. Regional point sources of SO_2 and NO_x within 50 km, however, may be important contributors to the SO_x and NO_x in the air and precipitation at the site.

Field Procedures. A wet deposition collector and raingage were operated in tandem to collect data on the chemistry and the amount of precipitation occurring at the site. Data from January 1981 through December 1985 were used in this study. Throughout this period, criteria for the collection of samples were as follows:

- (1) The sample bucket was changed on Tuesday, whether or not precipitation had been collected since the last bucket change. Sample buckets that did not contain precipitation were rinsed with 50 mL of de-ionized water and the aqueous leachate from this rinse was treated like a rain sample. Results from analyses of these rinse water samples were used to assess the potential bias from sample handling and the collection process. (See Stensland *et al.*, 1983 for a more thorough description of this procedure.)
- (2) On Monday, Wednesday, Thursday, and Friday the sample bucket was changed if precipitation had accumulated since the last bucket change and when the precipitation was not ongoing. This often resulted in collection of a sample representing precipitation from the passage of an entire system (e.g., an extratropical cyclone). Precipitation associated with both warm and cold frontal mechanisms was frequently in a single (composite) sample. Only when there was a clear break in the precipitation during "regular working hours" was a sample collected that represented a single thunderstorm or line of storms, or a cold or warm frontal passage.

- (3) On weekends, the sample bucket was changed on occasions when the site was visited by a staff member. Those occasions were infrequent and unscheduled, therefore, few samples were collected on weekends. During weekend site visits, the criterion used to decide whether the bucket should be changed was the same as in (2).

With each visit to the site, tests of the automated collector and the raingage were made to assure correct operation. When the criteria for sample collection were met, the sample bucket was removed and replaced with another pre-cleaned bucket. The contents of the bucket were inspected and a log was completed to describe any evidence of sample contamination, improper collector operation, or other unusual circumstances during the sampling period. The collected sample was covered and sealed in the polyethylene (LPE) collection bucket for delivery to the laboratory. No special preservation steps, such as refrigeration or the addition of a biocide, were taken before the samples were returned for analysis. To mitigate the potential for contamination, nothing was removed from or introduced into the sample, so no in situ field measurements of the sample were taken. With each collected sample, the raingage chart for the corresponding sampling period was replaced and the chart was returned to the laboratory with the sample bucket.

Laboratory Procedures. At the lab, the sample volume was determined from the difference of the gross and the tare weights of the collection bucket. Within a working day, the pH and solution conductance (corrected to 25° C) were measured and recorded; and the sample was filtered to separate the dissolved from the undissolved fractions. Filtration was shown by Peden and Skowron (1978) to effectively retard degradation of the major inorganic ions in precipitation samples. Following filtration the samples were put in a queue for later analyses of Ca^{++} , Mg^{++} , Na^+ , K^+ , SO_4^- , NO_3^- , Cl^- , and NH_4^+ . Techniques for the measurement of these ions have been described in detail by Peden et al. (1987). Sulfate and nitrate are the focus of this study and they were both determined by colorimetric, wet chemical techniques prior to May 1985, and by ion chromatography subsequently. Limits of detection (LOD) and the precision and accuracy of measurements have been reported by Lockard (1987). In general, the precision was better than 10% for all measurements, except those very near the LOD. Bias was virtually zero. For convenience, sulfate and nitrate will be referred to without their ionic charge as SO_4 and NO_3 .

The volume necessary to complete the full suite of ion measurements was 35 mL. Samples of less than that volume required the addition of diluting water to satisfy this constraint. To correct the concentration measurements in the diluted samples to their original values, it was necessary to calculate a dilution factor. This entails added uncertainties that result in estimates of imprecision that are larger than those for undiluted samples. To avoid these added uncertainties, only data for samples with a laboratory volume of 35 mL or more were used in this study. In addition, any sample that contained a visible contaminant other than soil particles was excluded from this study.

Also in the laboratory, the raingage charts were manually read and then digitized to obtain a file of precipitation amounts as a function of time.

Any evidence that the collection bucket was exposed to atmospheric deposition during dry weather resulted in the exclusion of data. Data for precipitation-only samples were used in this study. The operational definition of a precipitation-only sample was the one described by Bowersox (1984) for "wet-deposition-only" samples. Since the efficiency with which the automated collector sensed precipitation was less than 100%, the sample catch by the collector was frequently less than the catch of the raingage. This was especially true for snow, because the wind often prevented the snowflakes from exciting the precipitation sensor.

RESEARCH METHODOLOGY

Storm Definition

To classify the temporal scale of the raingage data, the terminology and techniques of Thorp (1986) were utilized. Thorp (1986) used hourly precipitation data from first-order National Weather Service (NWS) sites to study, among other things, the length of wet and dry periods for the northeastern United States. Thorp (1986) defined a storm as one or more precipitation events, where a precipitation event was defined as a period of successive hours of measurable precipitation. Consecutive events may be separated by one or more hours when no measurable precipitation was observed. Thorp (1986) referred to these intervening intervals as the number of dry hours (NDHR). Selection of NDHR then determines the number of events which will be included in a storm. For this study the length of a precipitation event was based on the number of consecutive non-zero five minute precipitation rates calculated from the raingage data. For the warm season (March-August) NDHR was set to 2 hours and for the cool season (September-February) NDHR was set to 3 hours. These values were within the range suggested by Thorp (1986). The smaller value for the warm season was a reflection of convective type precipitation which typically has storm durations which are shorter than those of synoptic scale systems in the cool season. With storms defined in this manner, half of the acceptable chemistry samples had 2 storms or less, with the maximum being 7 storms. Average storm duration ranged from a minimum of about 2 hours for summer months to a maximum of about 7 hours for winter months.

Calculation of SO₄ and NO₃ Fluxes

SO₄ and NO₃ sample depositions were calculated in the usual manner by taking the product of the concentration, sample volume, and a constant accounting for bucket area. Precipitation chemistry data from a network such as the National Atmospheric Deposition Program (NADP), which are collected on a weekly basis, allow for consideration of weekly deposition values at a site after a sufficient amount of data have been collected. However, for this data set no standard sampling period was followed, and therefore no comparison of sample depositions by themselves was possible. They were therefore normalized by dividing by the total time that measurable precipitation was observed during the chemistry sampling period. This total precipitation time was the sum of all five minute periods with

non-zero precipitation rates. The total of all precipitation times for all chemistry samples and storms was averaged to obtain the "mean precipitation time" in Tables 1-12. The precipitation time rather than the storm duration was used as several dry hours could be within a given storm as mentioned above. The resultant SO_4 and NO_3 fluxes then had the units of $\mu\text{eq}/\text{m}^2/\text{hour}$, which were ranked from smallest to largest for the warm and cool seasonal divisions. The 5th, 35th, 65th and 95th percentiles were then calculated from the ranked data by a commonly used algorithm (SAS, 1982). Data within the 5th-35th, 35th-65th, and 65th-95th percentile ranges will subsequently be referred to as lower, middle, and upper categories (or percentiles), respectively. With three percentile ranges, two fluxes, and two seasonal periods (spring-summer and fall-winter), there were a total of 12 data classifications to be considered.

Classification by Precipitation and Synoptic Type

The daily observations from the local climatological data (LCD) of the Morrow Plots site in Urbana-Champaign were used to characterize the precipitation types which contributed to each chemistry sample. Given the daily nature of the precipitation type data, the same precipitation types could be assigned to two consecutive chemistry samples when significant changes occurred during the day. For example, rain in the morning could turn to snow by afternoon resulting in both types being recorded in the LCD. If the sampling bucket was changed at noon, assigning the rain-snow mix to both the morning and afternoon samples would not be correct. Unfortunately, the latter procedure was followed in this study due to time limitations. In practice, examination of the data reveals that such conflicts were rare. Typically, the hypothetical example above would involve only one chemistry sample and the rain-snow mix would be an accurate description of the precipitation types encountered. For precipitation type data, the following abbreviations will be used: L, drizzle; R, rain; RW, rain showers; TRW, thunderstorms; A, hail; ZL, freezing drizzle; ZR, freezing rain; IP, ice pellets; S, snow; SW, snow showers; TSW, thunderstorms with snow; and T, thunder with no precipitation at the time.

Each storm (as defined above) for a chemistry sample was classified by one or more synoptic types as based on inspection of 3-hour surface maps from the National Climatic Center (NCC) of the National Atmospheric and Oceanic Administration (NOAA). Ideally, synoptic classification should involve not only surface maps but upper-air and radar charts as well. This was not possible for this analysis given the time limitations and the volume of data. The synoptic classification scheme used in this analysis was adapted from Changnon and Huff (1987). Precipitation occurring within 150 statute miles of the surface position of a cold, stationary, or occluded front was classified accordingly. Precipitation occurring more than 150 miles ahead of cold or occluded fronts was called pre-cold or pre-occluded. Warm frontal precipitation was classified as such when occurring within 75 miles on the warm side and within 150 miles on the cool side of the front. Precipitation in advance of a warm front by more than 150 miles was called pre-warm front. Precipitation was assigned to a low pressure center category in three situations: when the site was influenced by both a cold and a warm front within a short period of time,

when a low pressure system was present with no well defined frontal systems, and when precipitation occurred within a well defined warm sector which could not be assigned to a cold or warm front. As opposed to a low pressure center, precipitation was assigned to troughs if within 150 miles of such a synoptic feature. An additional category of squall line was used when analyzed as such on a surface chart. Squall lines can have durations much less than 3 hours so the technique followed in this study definitely underestimated their number. The category of a squall zone was used for precipitation which was close to an analyzed squall line on a surface map. Finally, an air mass category was used for precipitation which did not meet any of the criteria above and seemed to be the result of instability within warm or cold air. For synoptic types, the following abbreviations will be used: PCF, pre-cold front; CF, cold front, PWF, pre-warm front, WF, warm front; POF, pre-occluded front; OF, occluded front; SF, stationary front; L, low pressure center; T, trough of low pressure; SL, squall line; SZ, squall zone; and AM, air mass. In many cases more than one synoptic type was assigned to a given storm because of the proximity of the site to several synoptic features or the rapid movement of synoptic systems across the site.

The statistical summaries in Tables 1-12 of this chapter were calculated in the following manner. For a given chemistry sample, the storm with the largest precipitation amount from the raingage data was assumed to represent the entire chemistry sample with respect to the precipitation and synoptic types. If the largest storm was assigned more than one synoptic type, each type received a count of one. For example, for a given precipitation chemistry data category (such as the middle 30% of NO₃ fluxes for the warm season) the total of all counts in each of the 12 synoptic classifications was recorded for these largest storms. These frequency statistics are labeled as column "F₂" in Tables 1-12. The F₂ values for each synoptic classification were then expressed as a percentage of the grand total of all synoptic classifications in the columns labeled "P₂". The grand total of synoptic counts for the largest storms in a given data category will be larger than the total number of chemistry samples because several storms will have more than one synoptic type. The precipitation amount of the largest storm was divided equally among the assigned synoptic type(s). These amounts in inches of liquid precipitation were then summed for a given synoptic classification to give the totals in the columns labeled "SVOLMAX." The SVOLMAX values were then expressed as a percentage of the sum of the SVOLMAX values across all synoptic types in the column "SVOL (%)" To give an indication of the validity of using the largest storm approach, the sum of the SVOLMAX column was divided by the grand total of all storms for all chemistry samples within a data category. This percentage is the "largest storm/all storms (LA/AS)" ratio in Tables 1-12. This ratio was typically around 80-85% for the warm season categories and around 75% for the cool season categories. While the SO₄ and NO₃ fluxes were used to establish the percentile groupings for trajectory analyses, they were converted back to depositions by multiplication by their respective precipitation times to give deposition values ($\mu\text{eq}/\text{m}^2$) which were used in the calculations for the columns labeled "DEP. %" For each of the largest storms, the total sample deposition for SO₄ or NO₃ was assigned to each of the synoptic

type(s) These depositions were then summed for each synoptic classification. The totals in each synoptic type were then expressed as a percentage of the grand deposition total across all synoptic types for a synoptic category in the column "DEP. %." Future work will require a more refined treatment of the situations where more than one synoptic type and/or storms per chemistry sample were involved.

The statistics discussed thus far have been based on using the storm with the largest precipitation amount for a given chemistry sample. For the precipitation type statistics, all storms for each chemistry sample were considered. Each precipitation type for each day of a given storm received a count of one. The sum of these counts by precipitation type comprise the frequency values labeled "F₁." These values were then expressed as percentages of the grand total across all precipitation types for a given data category in the column "P₁."

Trajectory Calculations

One or more trajectories were calculated for each storm of each chemistry sample using the ISWS model described in chapter 15. The trajectories were calculated backward in time for a period of 72 hours from the Bondville site. Determination of the starting times for the trajectories was handled in one of two ways. If the storm duration was 3 hours or less, only one trajectory was calculated for the storm, with the starting time being the 15 minute period with the highest precipitation rate. For storms greater than 3 hours in length, the starting times were every 3 hours, spaced from the end of the storm backwards in time.

The locus of trajectory locations can be analyzed in at least two ways. These are illustrated by the schematic in Figure 1, where three hypothetical trajectories and their respective starting times have been illustrated. One way to examine the locus of trajectory points is to examine all points which have the same time interval between their current and starting times. This would correspond to the group of points labeled "MODE 1" in Figure 1 with points t-6, t-3, and t, which are all 6 hours back in time from their respective starting times. Another way is to examine all points which have the same time but vary in their interval of time from the origin. An example of this would be the group of points labeled "MODE 2" in Figure 1 with points t-6 for trajectories I, II, and III. The latter technique was the one chosen for use in this study.

Figure 2 shows the 100 km square grid mesh used in determining the trajectory patterns at a given time. The total count of trajectory endpoints within a grid square was then expressed as a percentage of the total number of trajectories within the grid domain. This was similar to the technique used by Ashbaugh (1983) The grid square percentages were then assigned to the center of each square and contoured by the CONREC routine in the National Center for Atmospheric Research (NCAR) graphics package. The trajectory plots therefore represent contoured fields of spatial percentages. The contours have been labeled where space allows in the following figures. For major groups of trajectories, the relative grid maxima in percentages are given by underlined values as close as possible to the actual location. In the discussion of major groupings of

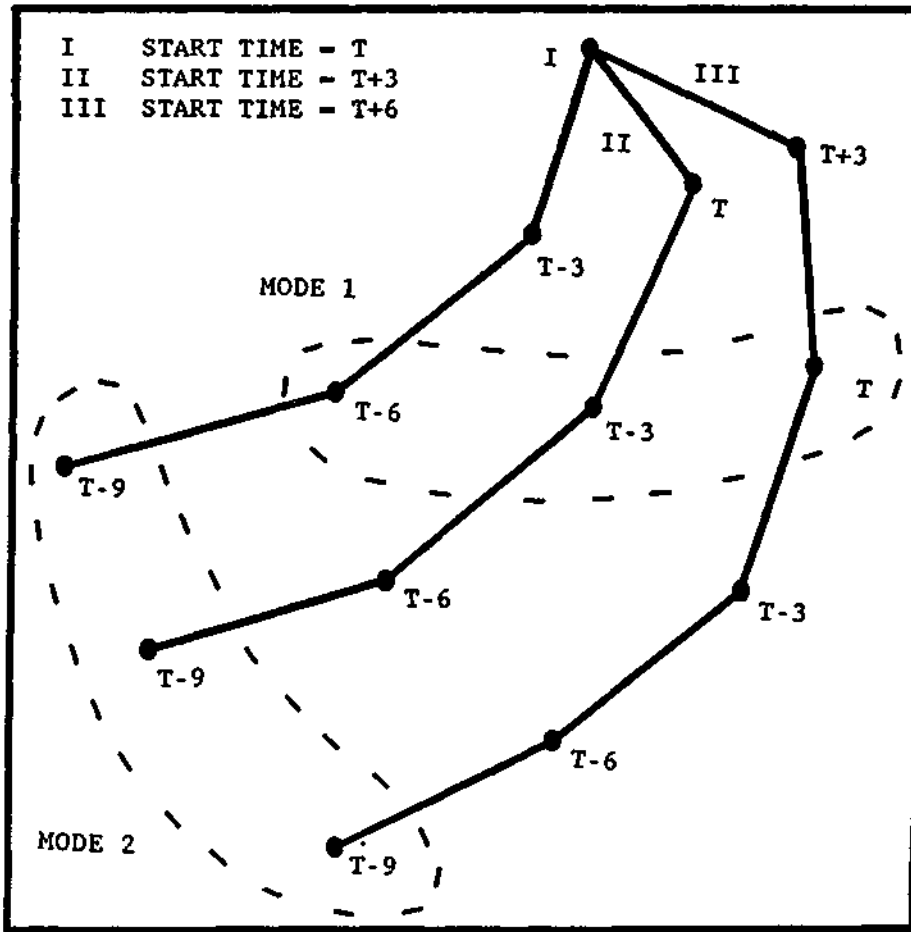


Figure 1. Three hypothetical back trajectories labeled I, II, and III with the same origin and with starting times of T, T+3, and T+6 hours, respectively. Positions of each trajectory at 3 hour intervals are marked. "MODE 1" and "MODE 2" are discussed in the text.

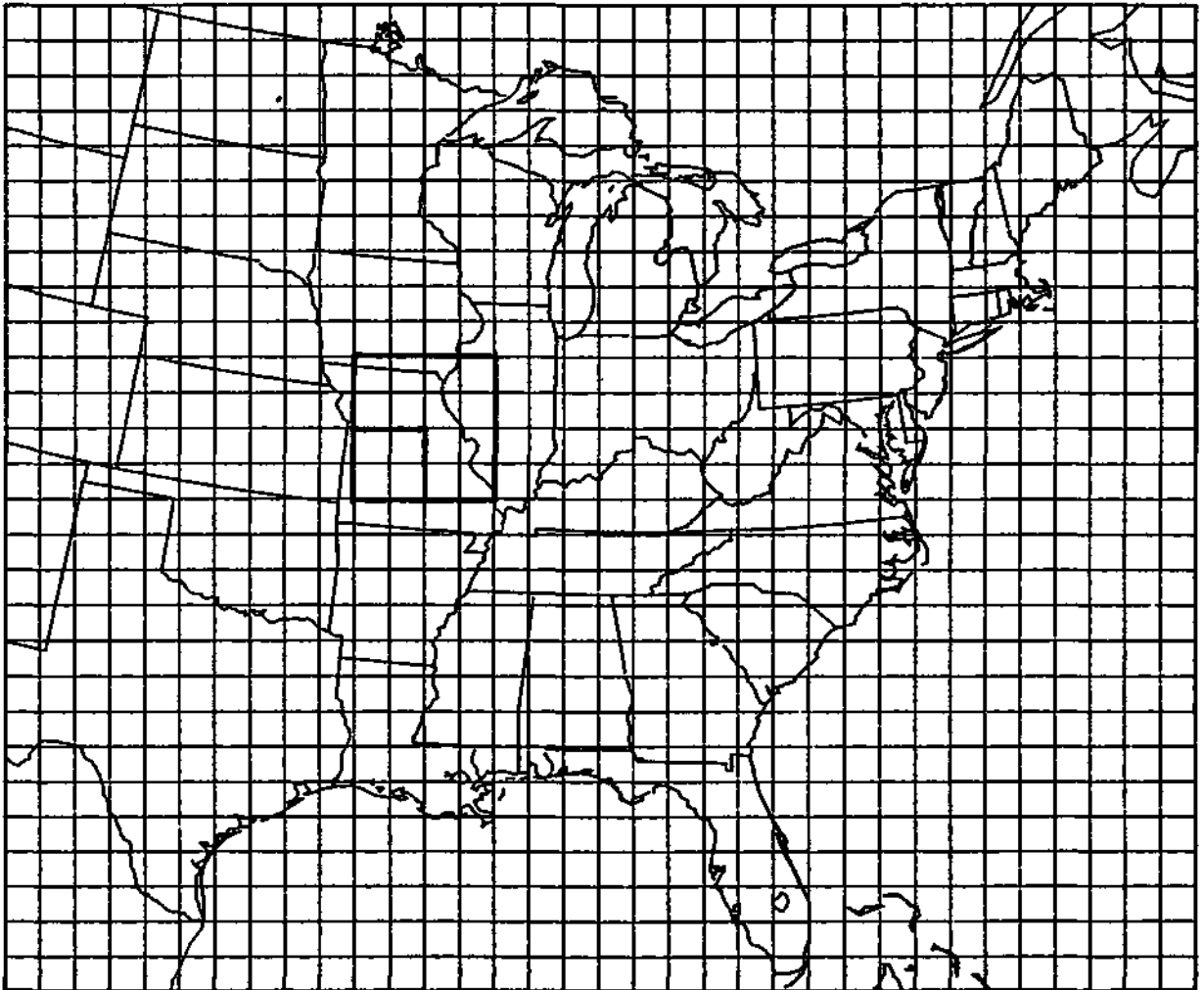


Figure 2. Grid of 100 km squares used to tally locations of back trajectories at a specified time. Squares of dimensions 400 km and 200 km are in bold.

Table 1. Synoptic and precipitation type statistics for spring and summer months for the lower SO₄ flux category as based on 48 chemistry samples. Column headings described in text. LS/AS represents the ratio of the volumes of the largest storms to all storms.

SYNOPTIC TYPE STATISTICS
 A. mean SO₄ flux - 98.4 µeq/L/hour
 spring percentage - 77.1 LS/AS - 82.8%
 summer percentage - 22.9
 mean precipitation time - 7.5 hours
 mean chemistry sample volume - 413 mL

Synoptic Type	F ₂	P ₂	SVOLMAX	SVOL (%)	DEP %
PCF	2	3.2	1.5	5.5	5.3
CF	10	15.9	3.6	13.5	9.5
PWF	2	3.2	1.8	6.9	7.3
WF	7	11.1	3.9	14.6	9.9
POF	1	1.6	0.5	1.8	1.2
OF	5	7.9	1.8	6.7	11.5
SF	10	15.9	5.8	21.9	15.4
L	17	27.0	6.3	23.9	34.3
T	6	9.5	0.9	3.5	4.7
SL	1	1.6	0.0	0.1	0.3
SZ	0	0.0	0.0	0.0	0.0
AM	2	3.2	0.4	1.6	0.8

PRECIPITATION TYPE STATISTICS
 B

Precip Type	F ₁	P ₁
L	25	9.4
R	64	24.1
RW	80	30.1
TRW	58	21.8
A	13	4.9
ZL	1	0.4
ZR	3	1.1
IP	8	3.0
S	2	0.8
SW	12	4.5
TSW	0	0.0
T	0	0.0

Table 2. Synoptic and precipitation type statistics for spring and summer months for the middle SO₄ flux category as based on 49 chemistry samples. Column headings described in text. LS/AS represents the ratio of the volumes of the largest storms to all storms.

SYNOPTIC TYPE STATISTICS

mean SO₄ flux - 188 0 µeq/L/hour
 spring percentage - 65.3 LS/AS - 83 8%
 summer percentage - 34.7
 mean precipitation time - 3.5 hours
 mean chemistry sample volume - 307 mL

Synoptic

Type	F ₂	P ₂	SVOLMAX	SVOL (%)	DEP. %
PCF	6	10.0	0.7	3.9	6.1
CF	16	26.7	6.1	35.1	21.5
PWF	3	5.0	0.7	4.2	9.3
WF	11	18.3	3.8	21.7	20.0
POF	1	1.7	0.1	0.7	1.3
OF	1	1.7	0.7	4.2	2.1
SF	5	8.3	1.3	7.3	7.8
L	4	6.7	1.4	8.2	8.8
T	8	13.3	1.9	11.0	18.2
SL	3	5.0	0.5	2.9	3.1
SZ	1	1.7	0.1	0.3	0.5
AM	1	1.7	0.1	0.5	1.3

PRECIPITATION TYPE STATISTICS

B.

Preclp. Type	F ₁	P ₁
L	21	13.4
R	28	17.8
RW	50	31.8
TRW	46	29.3
A	5	3.2
ZL	0	0.0
ZR	3	1.9
IP	1	0.6
S	1	0.6
SW	1	0.6
TSW	0	0.0
T	1	0.6

Table 3 Synoptic and precipitation type statistics for spring and summer months for the upper SO₄ flux category as based on 48 chemistry samples. Column headings described in text. LS/AS represents the ratio of the volumes of the largest storms to all storms.

SYNOPTIC TYPE STATISTICS
A

mean SO₄ flux - 414 0 µeq/L/hour
 spring percentage - 35 4 LS/AS - 82 5%
 summer percentage - 64.6
 mean precipitation time - 2.3 hours
 mean chemistry sample volume - 350 mL

Synoptic Type	F ₂	P ₂	SVOLMAX	SVOL (%)	DEP. %
PGF	3	5.5	0.4	2.2	2.0
CF	10	18.2	2.8	15.4	16.4
PWF	3	5.5	0.6	3.1	4.2
WF	9	16.4	2.7	14.8	13.1
POF	0	0.0	0.0	0.0	0.0
OF	0	0.0	0.0	0.0	0.0
SF	10	18.2	5.0	27.2	27.3
L	7	12.7	2.6	14.3	13.3
T	3	5.5	1.3	7.2	9.4
SL	5	9.1	0.8	4.6	8.0
SZ	0	0.0	0.0	0.0	0.0
AM	5	9.1	2.0	11.2	6.3

PRECIPITATION TYPE STATISTICS
B

Precip Type	F ₁	P ₁
L	5	3.5
R	20	14.0
RW	39	27.3
TRW	72	50.3
A	6	4.2
ZL	0	0.0
ZR	0	0.0
IP	0	0.0
S	0	0.0
SW	0	0.0
TSW	0	0.0
T	1	0.7

trajectories, when it is mentioned that a certain group contains a specified number of trajectory endpoints, it is referring to the number of endpoints that are enclosed by the lowest contour (usually 1.0%).

In chapter 15, the estimated average horizontal errors in trajectory calculations resulting from the nature of upper-air data and model type were around 200 km after 24 hours of transport and 200-400 km after 48 hours of transport (Kuo *et al.*, 1985, and Kahl and Samson, 1986). Square boxes of 400 and 200 km are indicated in Figure 2 to give an indication of these dimensions. When considering the details of spatial trajectory patterns in conjunction with the SO_x and NO_x emission patterns in Figures 3 and 28 these limitations should be kept in mind.

Emission Maps

The trajectory patterns for a given data category and for a given time will be compared with emission maps for SO_x and NO_x to investigate any apparent relationships. The emission maps in Figures 3 and 28 are derived from those of Wilson and Mohnen (1982) and give the estimated total annual mass of pollutant emitted per degree latitude and longitude.

Discussion Sequence

The discussion will focus on four large groupings of the 12 possible data categories: warm and cool season SO₄ fluxes, and warm and cool NO₃ fluxes. Each of these four groups will be discussed in the following manner. First the synoptic and precipitation statistics will be investigated for each of the three percentile groupings. This will be followed by a comparison of the trajectory locations for a given time between the percentile groupings for each of the series of trajectory times chosen. While trajectories were calculated three days back in time, because of the insufficient number of trajectories at that time the spatial patterns were very scattered. Discussion therefore will start at 48 and 18 hours for warm and cool season SO₄ fluxes, respectively, and 24 and 18 hours for warm and cool season NO₃ fluxes, respectively. These times were chosen which demonstrated the earliest visual differences between the flux categories in the trajectory patterns.

WARM SEASON SO₄ FLUXES

Precipitation and Synoptic Statistics

Tables 1-3 give the precipitation and synoptic statistics for the precipitation chemistry data collected during the spring and summer months for the lower, middle, and upper percentiles of SO₄ fluxes. Each of the percentile groupings was based on 48-49 chemistry samples. The three percentile groupings had a definite seasonal bias, with a trend towards summer samples from the lower to the upper percentiles of 23, 35, and 65%, respectively. The synoptic categories contributing to the top four SO₄

deposition percentages for the lower percentile group in Table 1 were L, SF, WF, and CF with 34.3, 15.4, 9.9, and 9.5%. In a similar manner for the middle percentiles in Table 2 the synoptic categories were CF, WF, T, and L with 21.5, 20.0, 18.2, and 8.8% of the depositions. The same ranking for the upper group in Table 3 gave SF, CF, L, and WF with 27.3, 16.4, 13.3, and 13.1% of the depositions. Although with different ranks, CF, WF, and L were in the top four synoptic groups in each of the percentiles, while SF appeared in the lower and upper percentiles and T for the middle percentile. The shift from the dominant L category in the lower percentile to the dominant SF category in the upper category was the result of the synoptic pattern changes with season, with cyclonic systems being more numerous and more intense in spring than in summer. Although it is discussed in detail in chapter 5, one observes a fairly consistent relationship between the sample volume and deposition percentages for the top four synoptic categories in each percentile grouping. This suggests that if one knows the precipitation amounts for a given synoptic type, one can estimate the resultant seasonal SO_4 depositions to a fair degree. In looking at the precipitation statistics, it was observed that with the seasonal shift across the percentiles there was also a shift from stratiform precipitation in the lower percentile to convective activity (thunderstorms) in the upper percentile. This was also reflected in the reduction of the mean precipitation times of 7.5, 3.5, and 2.3 hours for the respective percentile groupings. These synoptic and precipitation summaries indicate that large SO_4 wet deposition fluxes for the warm season were dominated by summer thunderstorms associated with stationary and cold frontal activity.

Back Trajectory Patterns

SO_x Emission Patterns. Figure 3 gives the annual SO_x emissions pattern for much of the eastern United States. Much of the upcoming discussion of trajectory results will refer to high emission areas in or close to Illinois, and these are described here. One main area is roughly a north-south line from Peoria to an area just east of St. Louis, and then westward over the St. Louis area itself. This area in central and southwestern Illinois covered one degree latitude-longitude grids having 200×10^6 to over $600 \times 10^6 \text{ kg yr}^{-1}$ of SO_x emissions. The other major area was over extreme southern Illinois and parts of west central Kentucky and Tennessee. This area had grid squares of SO_x emissions of again 100×10^6 to $600 \times 10^6 \text{ kg yr}^{-1}$.

Pattern for 48 hours. Figures 4-6 give the trajectory locations 48 hours back in time from the storms of the related chemistry samples for the lower, middle, and upper percentile SO_4 flux groups. Two major concentrations of trajectories were noted for the lower percentile group in Figure 4. One was over the eastern portions of southern Michigan, while the other extended from southern Missouri southeast across Arkansas to northern Mississippi. The northern group contained 16 trajectories and the southern group contained 24 trajectories. Neither of the two major groups enclosed high emission areas when compared to Figure 3.

The trajectory pattern in Figure 5 for the middle flux category shows only one major group, which was over southern Illinois and then extended

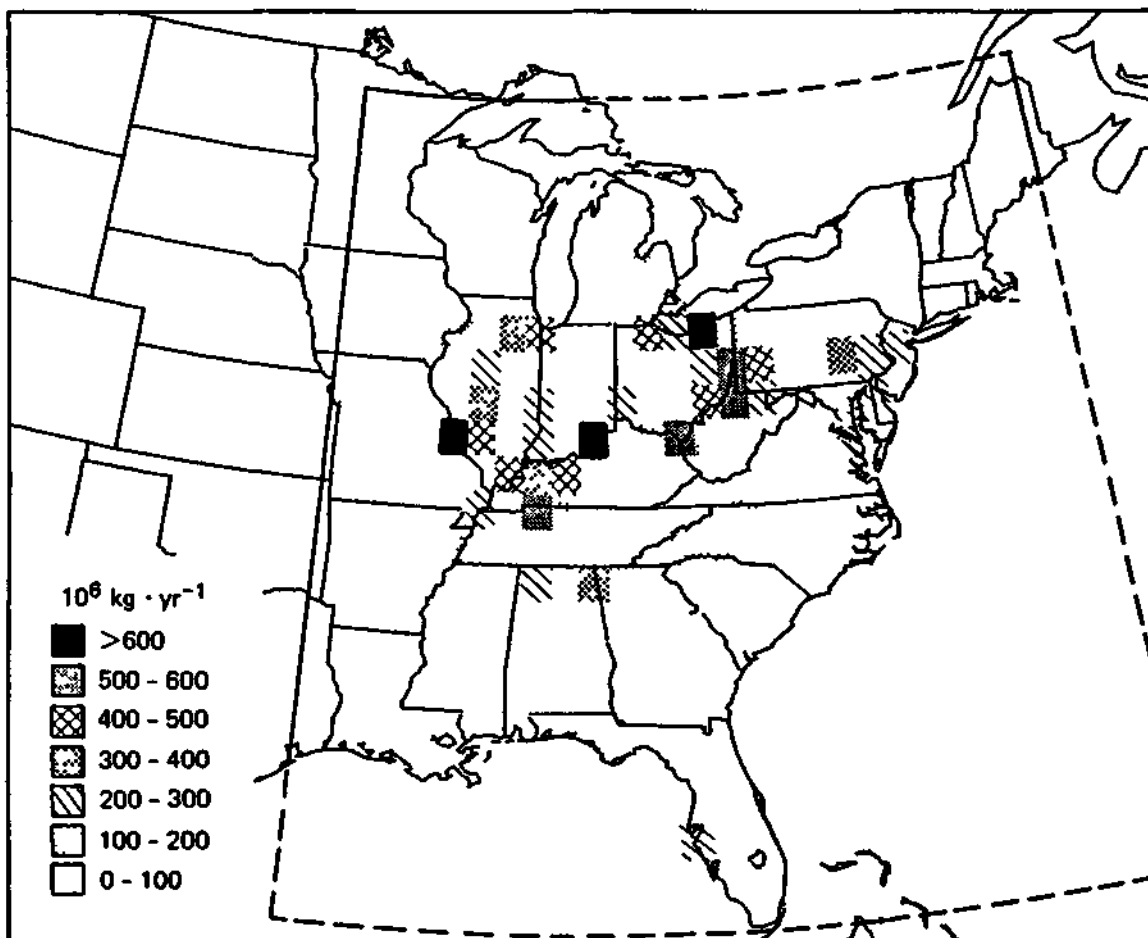


Figure 3. Total annual SO_x emissions (10⁶ kg yr⁻¹) per degree latitude and longitude for the continental eastern United States. Map adapted from Wilson and Mohnen (1982).

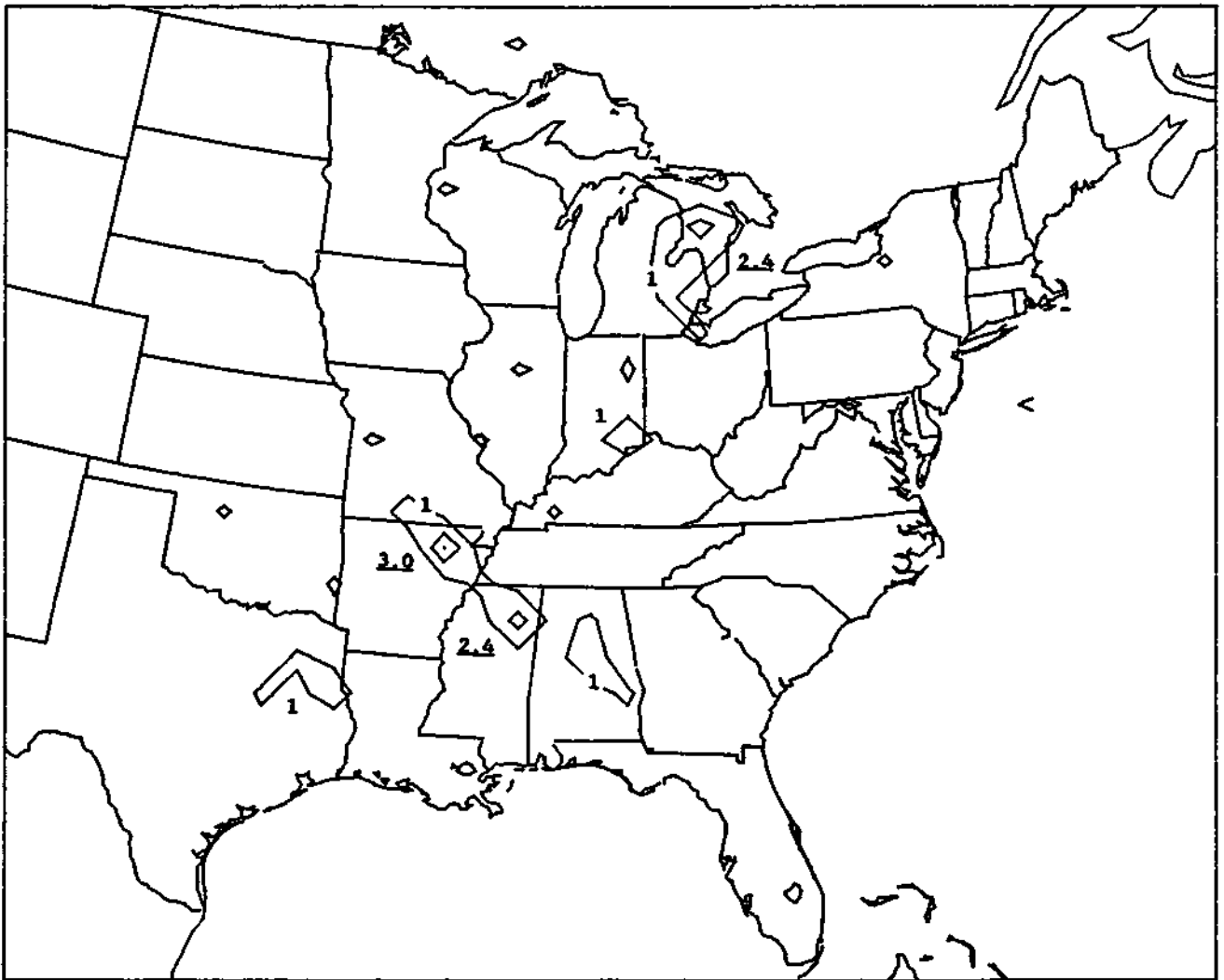


Figure 4. Percentage contours of back trajectory locations for endpoints 48 hours back in time for all storms related to chemistry samples having SO_4 fluxes in the 5th to 35th percentile range for spring and summer. Contour interval is 1.0% with grid square maxima values underlined. Total number of trajectories in domain is 165.

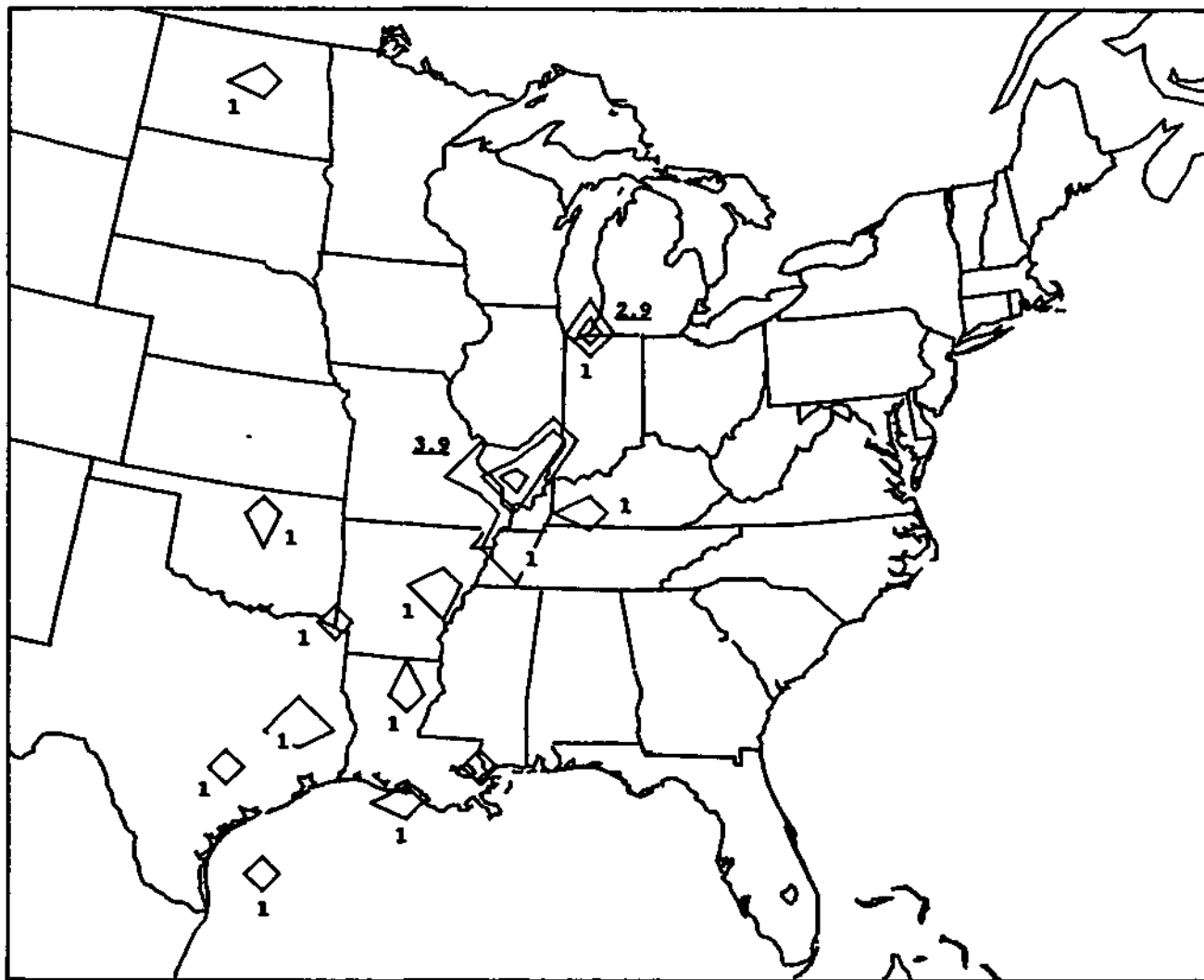


Figure 5. Percentage contours of back trajectory locations for endpoints 48 hours back in time for all storms related to chemistry samples having SO_4 fluxes in the 35th to 65th percentile range for spring and summer. Contour interval is 1.0% with grid square maxima values underlined. Total number of trajectories in domain is 104.

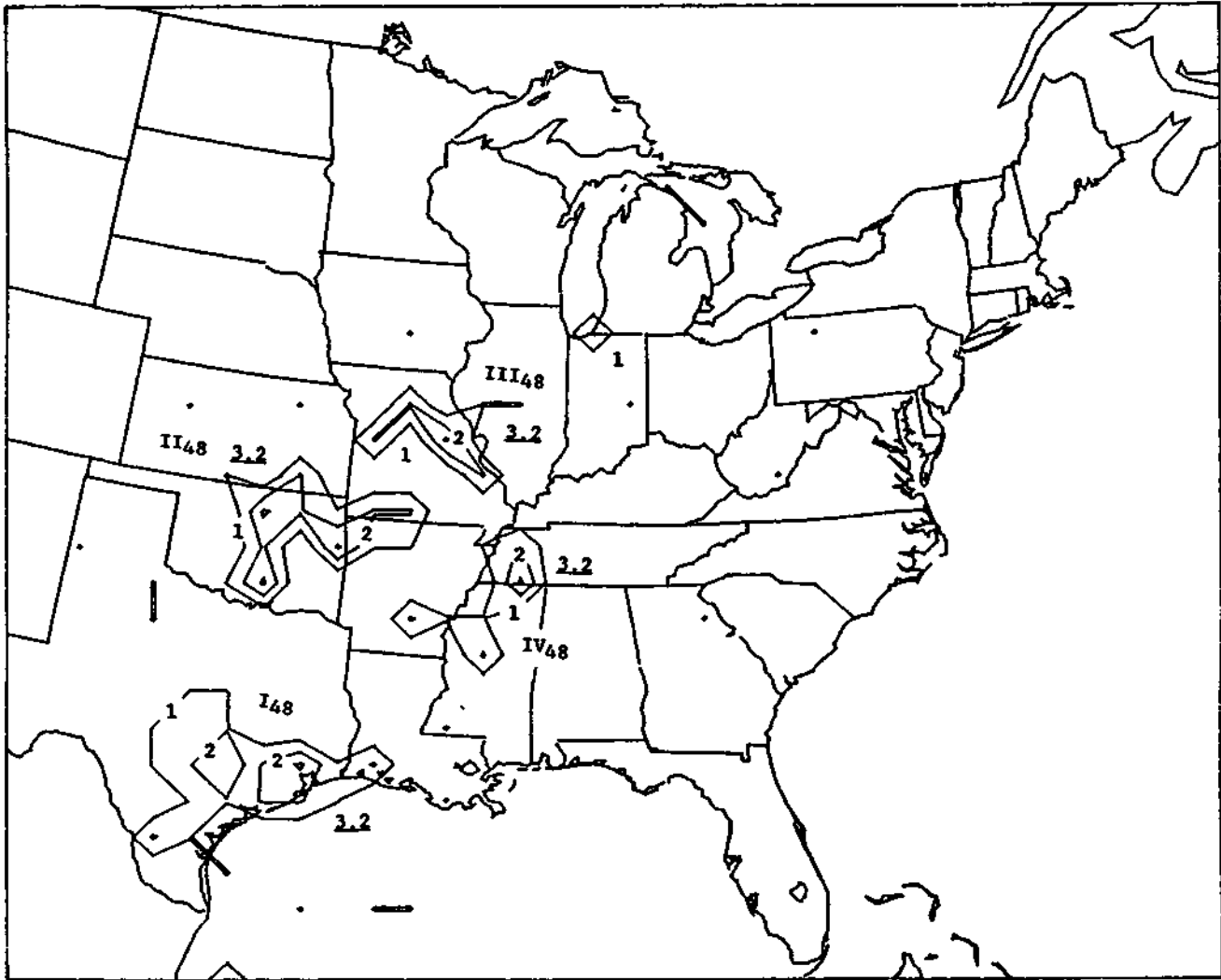


Figure 6. Percentage contours of back trajectory locations for endpoints 48 hours back in time for all storms related to chemistry samples having SO_4 fluxes in the 65th to 95th percentile range for spring and summer. Contour interval is 1.0% with grid square maxima values underlined. Total number of trajectories in domain is 95.

southward over the extreme western portions of Kentucky and Tennessee. Thirteen trajectories were in this group. Unlike the groups for the lower flux category, this group was over or near high SO_x emission areas.

The pattern in Figure 6 indicates four major groups which are labeled as I₄₈, II₄₈, III₄₈, and IV₄₈. Groups I-IV contained 26, 23, 11, and 13 trajectories, respectively. Not including possible trajectory error, groups III and IV were near but were not over high emission areas.

In summary, the patterns of the trajectories for the three flux groups 48 hours back in time indicated a consolidation into larger groups with less scatter and a predominance of major groups south and southwest of the Bondville site from the lower to upper percentiles. The major trajectory group for the middle flux category was over high emission areas, while two major groups of the upper flux category were near high emission areas.

Pattern for 36 hours. Figure 7 reveals the pattern for trajectories at the 36 hour mark for the lower flux category. Very little continuity was seen when compared to the 48 hour map in Figure 4, with the dominant structure being groups scattered in all directions with few trajectories in each group.

The pattern for the middle flux category at 36 hours in Figure 8 shows one major group over Tennessee of 15 trajectories with other smaller groups with considerable scatter. When compared with Figure 5, it appears the locus of points over southern Illinois at 48 hours had drifted south to a position centered over western Tennessee in Figure 8. This southward drift was over high emission areas.

The 36 hour pattern for the upper flux category in Figure 9 once again shows four major groupings which are labeled I₃₆, II₃₆, III₃₆, and IV₃₆ to distinguish them from the groups at the 48 hour period. It appears that I₄₈ had dispersed somewhat with the remnants forming I₃₆ over southeastern Texas. Group II₄₈ had also apparently split, with a portion moving southwestward to help create group II₃₆ over Oklahoma and another portion merging with III₄₈ to create II₃₆ over Missouri and adjacent parts of Kansas, Arkansas, and Illinois. Group IV₄₈ had also apparently dispersed with the remnants forming group IV₃₆ over western Tennessee. Of these four groups, III₃₆ and IV₃₆ showed the least amount of movement as compared to the 48 hour positions. Groups I-IV at 36 hours contained 8, 13, 22, and 6 trajectories, respectively. Group III₃₆ contained air which had drifted southwestward across the high emission areas of west-central Illinois, while group IV₃₆ was very close to the high emission areas in Kentucky and Tennessee.

The following comments can be made about the general patterns at 36 hours. Very little structure was seen for the lower flux category, whereas the one major group at 48 hours for the middle flux category continued to move southward over high emission areas. The upper flux category revealed two major groups which either moved very little or drifted southwestward and merged with others. These two latter groups either had a history of moving over or were near high emission areas in the 48 to the 36 hour travel interval.



Figure 7. Percentage contours of back trajectory locations for endpoints 36 hours back in time for all storms related to chemistry samples having SO_4 fluxes in the 5th to 35th percentile range for spring and summer. Contour interval is 1.0% with grid square maxima values underlined. Total number of trajectories in domain is 202.



Figure 8. Percentage contours of back trajectory locations for endpoints 36 hours back in time for all storms related to chemistry samples having SO_4 fluxes in the 35th to 65th percentile range for spring and summer. Contour interval is 1.0% with grid square maxima values underlined. Total number of trajectories in domain is 119.

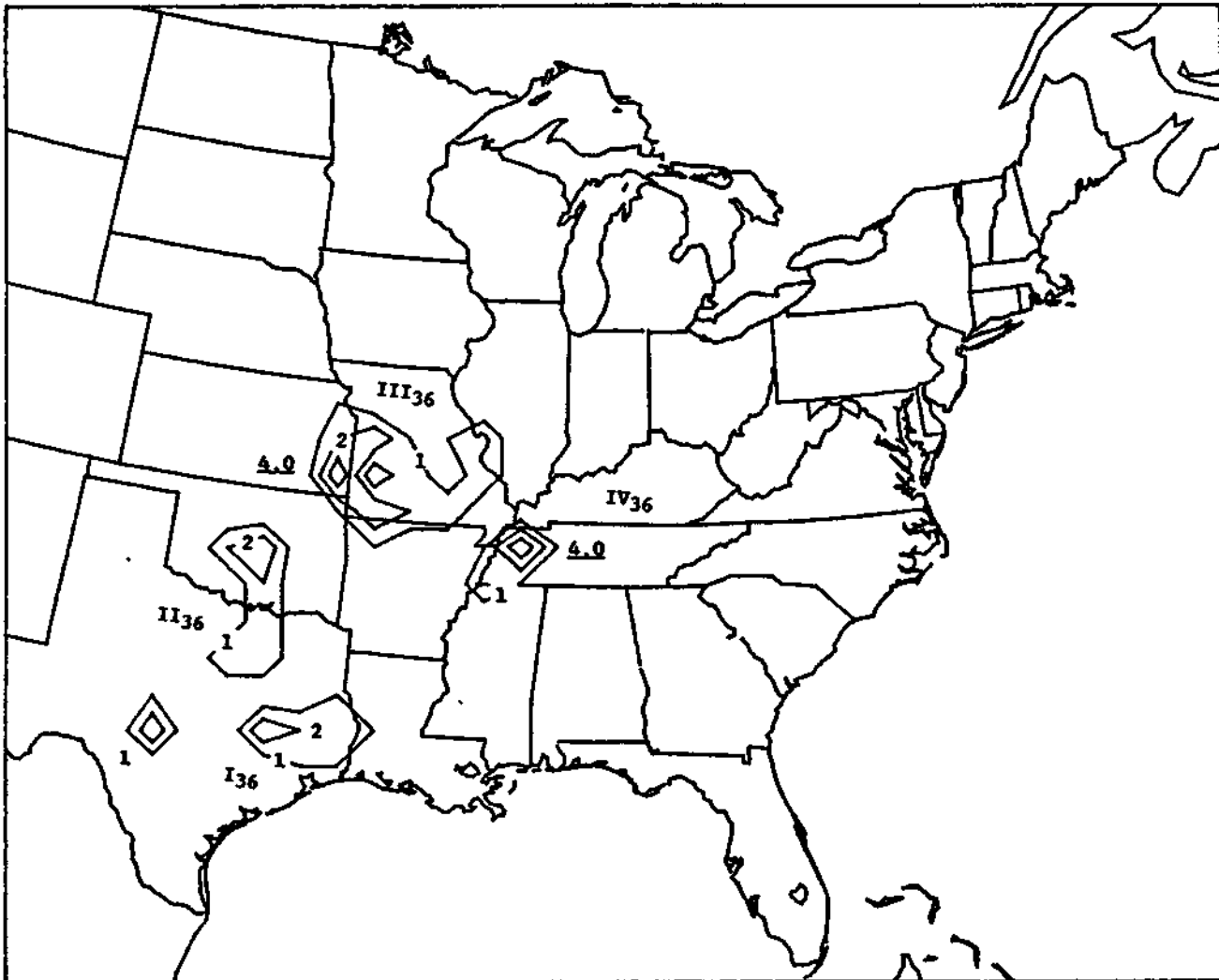


Figure 9. Percentage contours of back trajectory locations for endpoints 36 hours back in time for all storms related to chemistry samples having SO_4 fluxes in the 65th to 95th percentile range for spring and summer. Contour interval is 1.0% with grid square maxima values underlined. Total number of trajectories in domain is 101.

Pattern for 24 hours. Figure 10 shows the trajectory pattern at 24 hours for the lower flux category. It shows the most structure for the lower flux category when compared to the maps for 36 and 48 hours. Two main groups existed: a rather large one extending across parts of Ohio, Indiana, Illinois, Kentucky, and Tennessee consisting of 48 trajectories; and the other much smaller one over Missouri and Arkansas consisting of 14 trajectories. The large group encompasses high emission areas, but this was the first time for the low flux category, whereas one or more trajectory groups for the middle and upper categories had been over or near high emission areas during the 36 and 48 hour periods.

The trajectory pattern at 24 hours for the middle flux category in Figure 11 shows six major groups labeled I_{24} through VI_{24} with each group having 7, 10, 5, 7, 6, and 13 trajectories, respectively. Group VI, which had the largest number of trajectories, was the same group which had moved very slowly from the southern Illinois area at the 48 hour mark to western Tennessee and adjacent areas at the 36 hour period. During this entire period this group was over high SO_x emission areas.

The 24 hour pattern for the upper flux category in Figure 12 shows that the I_{36} - IV_{36} groups had essentially evolved into one large group with 43 trajectories over southern Illinois and Missouri and adjacent parts of Arkansas, Kentucky, and Missouri. Within this large group relative maxima were observed over northern Missouri, central Illinois, south central Missouri, extreme western Kentucky, and extreme northeastern Arkansas. The latter three maxima were all over or near high emission areas. It is also noticed that at the 24 hour mark a considerable number of trajectories were very close to the Bondville site, indicating generally slow transport wind speeds for many of the storms.

The 24 hour patterns for the lower, middle, and upper SO_4 wet deposition fluxes showed distinct differences in their trajectory groupings. One major group for the lower flux category moved over high emission areas for the first time, whereas one major group for the middle flux category continued to be over high emission areas. The upper flux category was dominated by one large group over several states which contained several relative maxima over or near high emission areas.

Pattern for 18 hours. Figure 13 shows one major group consisting of 93 trajectories for the lower flux category at the 18 hour mark, stretching across parts of Ohio, Indiana, Kentucky, Illinois, and Missouri. The maximum within this group was located in east central Illinois and then southeastward across Indiana and west central Kentucky. This maximum continued to be over high emission areas.

Most of the six major groups at the 24 hour mark for the middle flux category have merged into one group of 58 trajectories at the 18 hour time period in Figure 14. This group was composed of four arm-like structures extending from a central position over eastern Missouri. The persistent maximum over Tennessee over high emission areas remained but with an extension northwestward across Missouri.

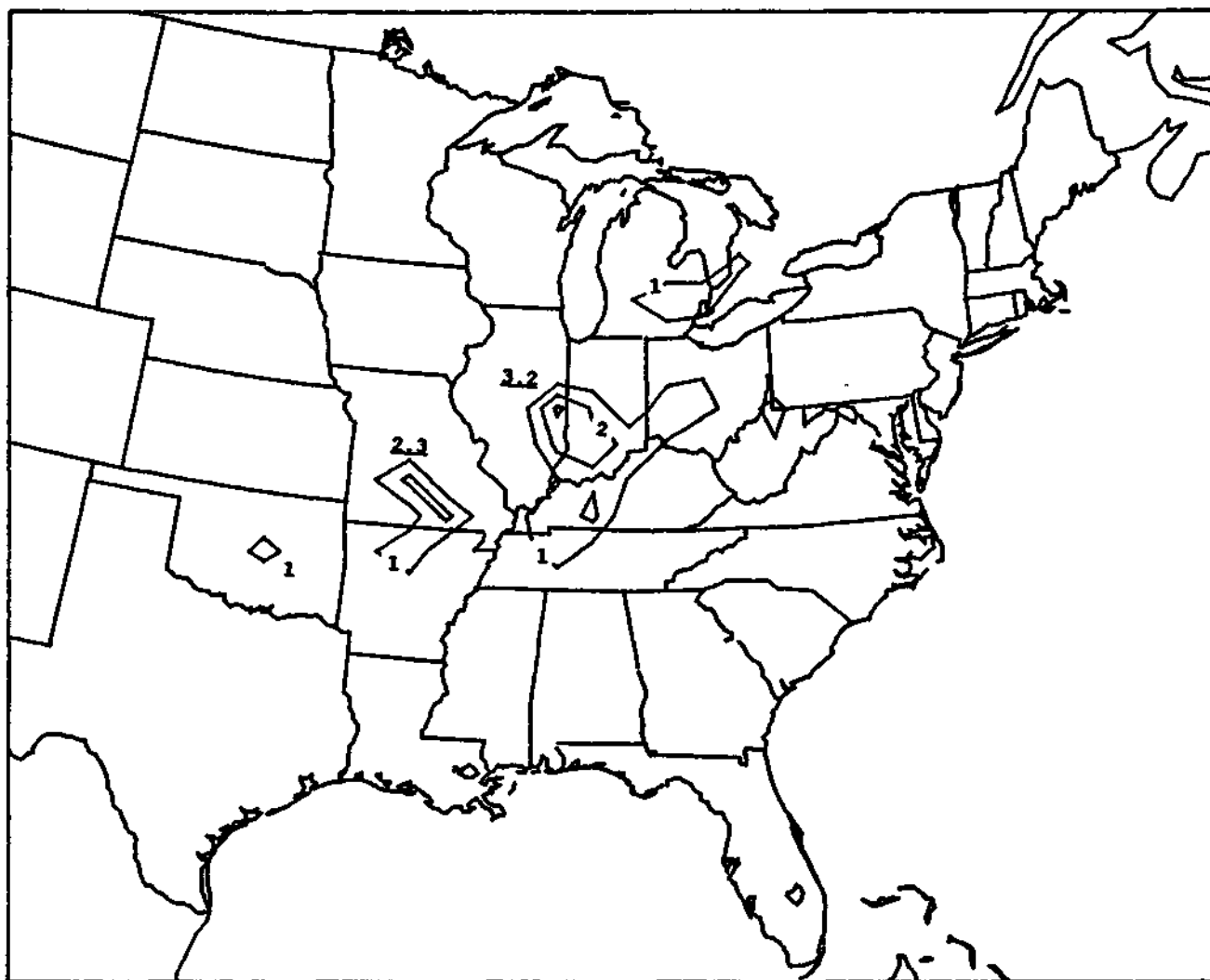


Figure 10. Percentage contours of back trajectory locations for endpoints 24 hours back in time for all storms related to chemistry samples having SO_4 fluxes in the 5th to 35th percentile range for spring and summer. Contour interval is 1.0% with grid square maxima values underlined. Total number of trajectories in domain is 217.

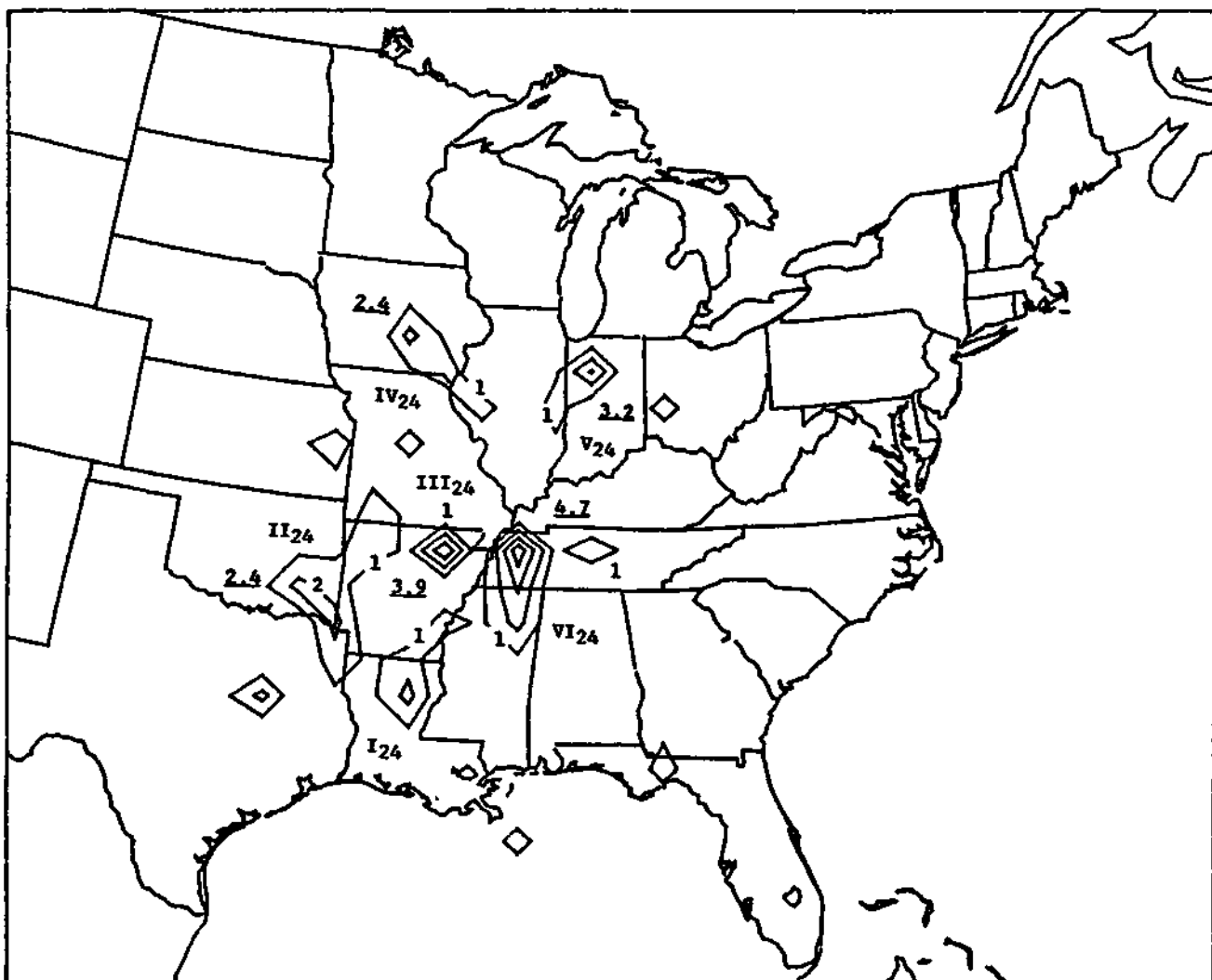


Figure 11. Percentage contours of back trajectory locations for endpoints 24 hours back in time for all storms related to chemistry samples having SO_4 fluxes in the 35th to 65th percentile range for spring and summer. Contour interval is 1.0% with grid square maxima values underlined. Total number of trajectories in domain is 127.

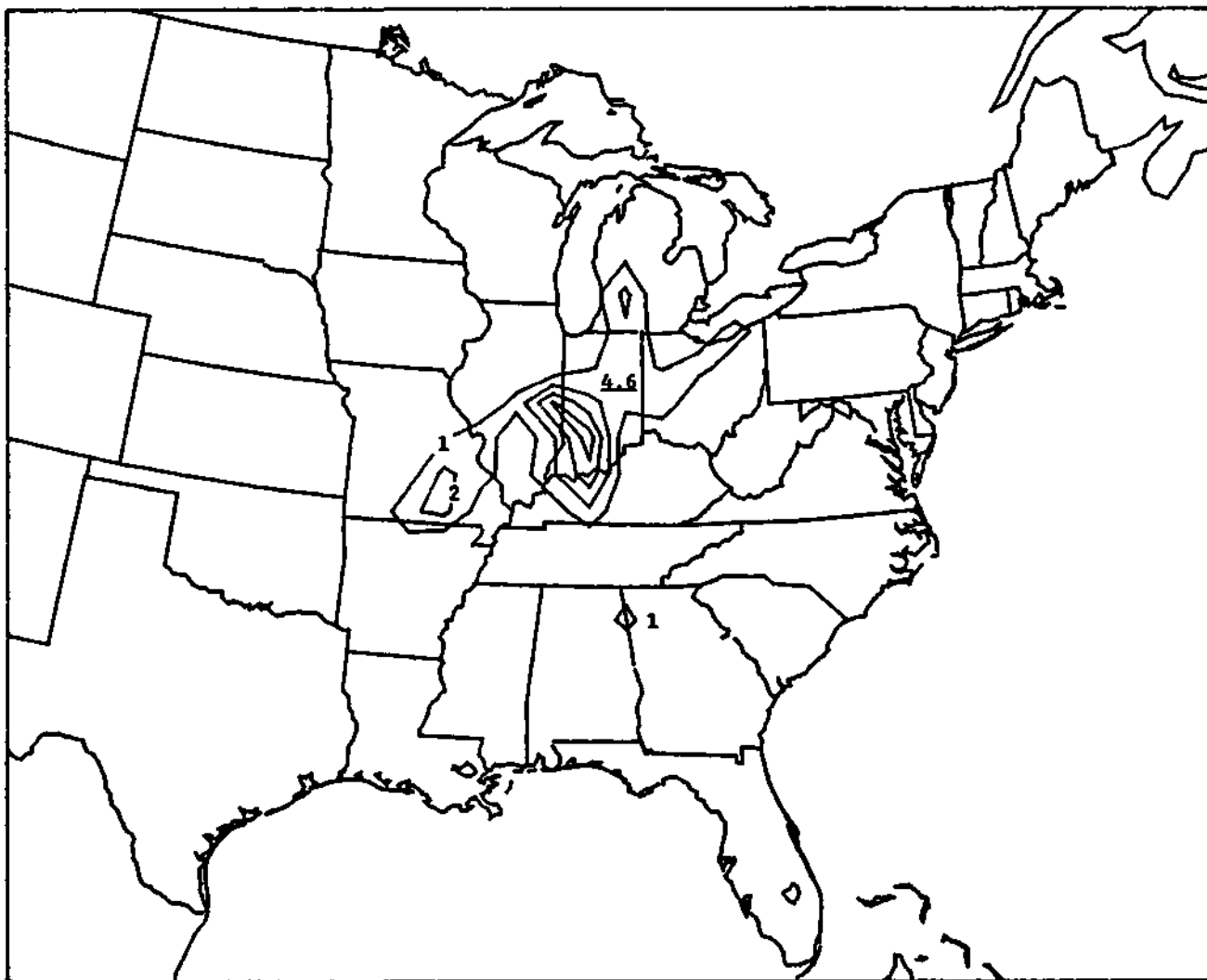


Figure 13. Percentage contours of back trajectory locations for endpoints 18 hours back in time for all storms related to chemistry samples having SO_4 fluxes in the 5th to 35th percentile range for spring and summer. Contour interval is 1.0% with grid square maxima values underlined. Total number of trajectories in domain is 219.

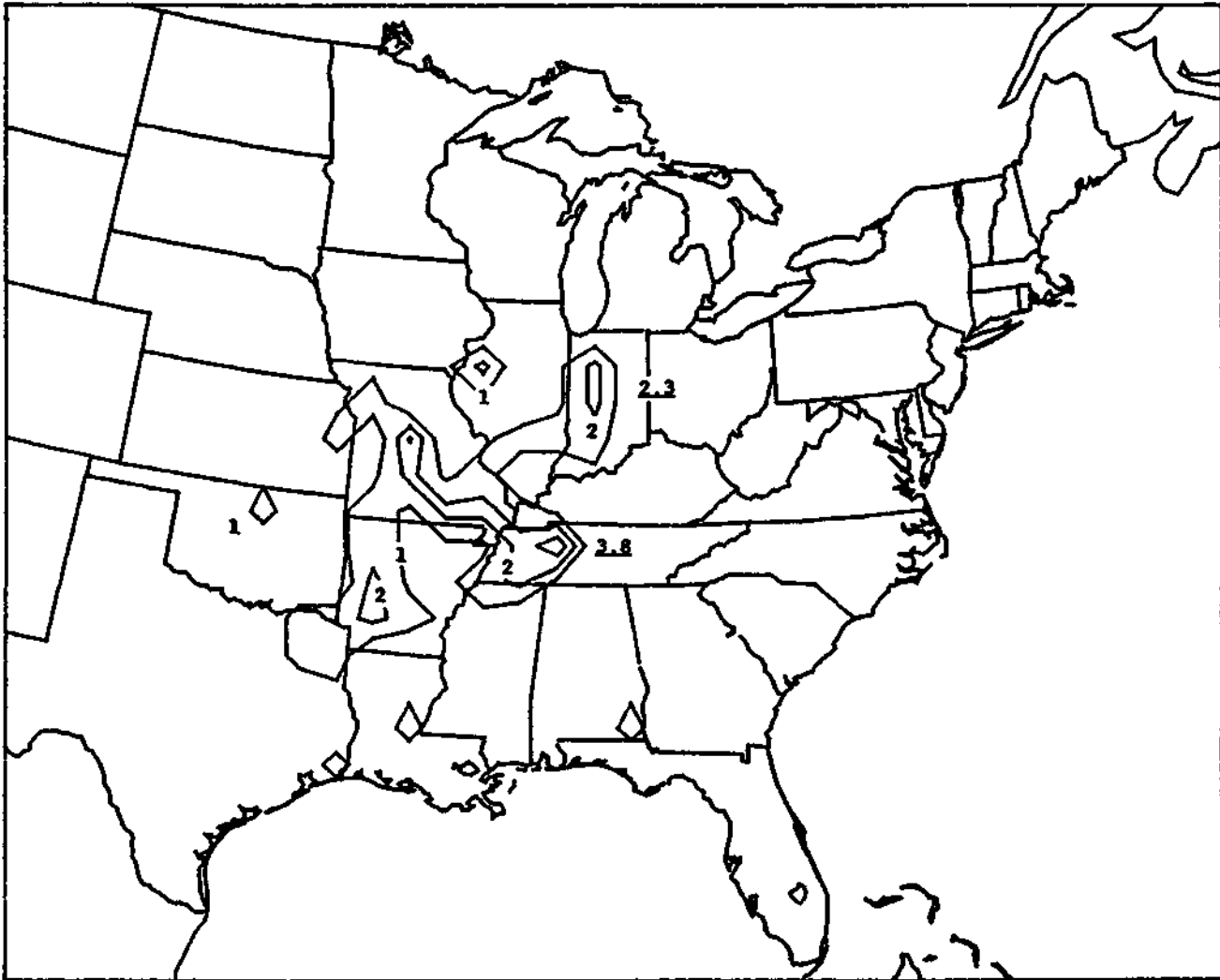


Figure 14. Percentage contours of back trajectory locations for endpoints 18 hours back in time for all storms related to chemistry samples having SO_4 fluxes in the 35th to 65th percentile range for spring and summer. Contour interval is 1.0% with grid square maxima values underlined. Total number of trajectories in domain is 130.

The trajectory pattern at 18 hours for the upper flux category in Figure 15 shows a pattern of one major group of 65 trajectories. The maximum within this group was defined by a very sharp gradient across western Illinois, eastern Missouri, and northeastern Arkansas. Based on the behavior of the groups from 48 hours until 18 hours for the high flux category, this maximum seemed to be composed of air parcels with at least three different histories. One configuration was composed of air parcels which moved across Illinois from the northeast, stalled somewhere over Missouri, and now at this time period were under westerly or southwesterly flow ahead of the next frontal system. This type of feature allowed parcels to move over the high emission areas of southwestern Illinois at least twice. Another configuration was composed of parcels which were moving across western Illinois for the first time and which in part had origins over Kansas, Oklahoma, and Texas as observed in the major groups at the 48 hour time. The final configuration was composed of parcels which were over the Tennessee Valley at the 48 hour mark and have moved slowly northwestward to help compose the southern end of the linear maximum from Iowa to Arkansas. The latter pattern also gave the opportunity for double exposure to high emission areas - once over portions of western Kentucky and Tennessee and then later over western and southwestern Illinois. This feature will become more apparent when the results for the 12 hour period are examined for the high flux category.

All the SO₄ flux categories at the 18 hour mark demonstrated one major trajectory group. All covered several states but with explicit differences in directional orientation and air parcel histories. The low flux category showed a maximum mainly over Indiana associated with southeasterly flow, while the middle flux category had nodes in several directions but with a longstanding maximum over western Tennessee. The upper flux category had a sharply defined maximum along the Mississippi River from Iowa to Arkansas with air parcels having a predominant history of multiple passes over high emission areas. The average transport winds were also explicitly slower for this category given the proximity of the maximum to the Bondville site.

Pattern for 12 hours. The major group of the lower flux category in Figure 16 contained 83 trajectories at the 12 hour mark. The group extended primarily across Ohio, Indiana, and Illinois with a maximum very close to the Bondville site and with a strong node to the southeast across Indiana.

The trajectory pattern at 12 hours for the middle flux category in Figure 17 showed a major group mainly over Illinois and Missouri which had 94 trajectories. The maximum within this group consisted of two linear, perpendicular protrusions from an areal maximum over southeastern Illinois. The one linear ridge extended from northwestern Illinois to the southeastern portion of the state, while the other extended from southern Missouri to the same location. Examination of the results at the 15 hour mark for this category (not shown) revealed that the maximum over western Tennessee at 18 hours had moved northward to help create the areal maximum over southeastern Illinois. This type of motion repeats the exposure of such parcels to the high emission areas over western Tennessee and Kentucky and southern Illinois which were experienced during the southward movement of these parcels previously at the 48 and 36 hour time periods.

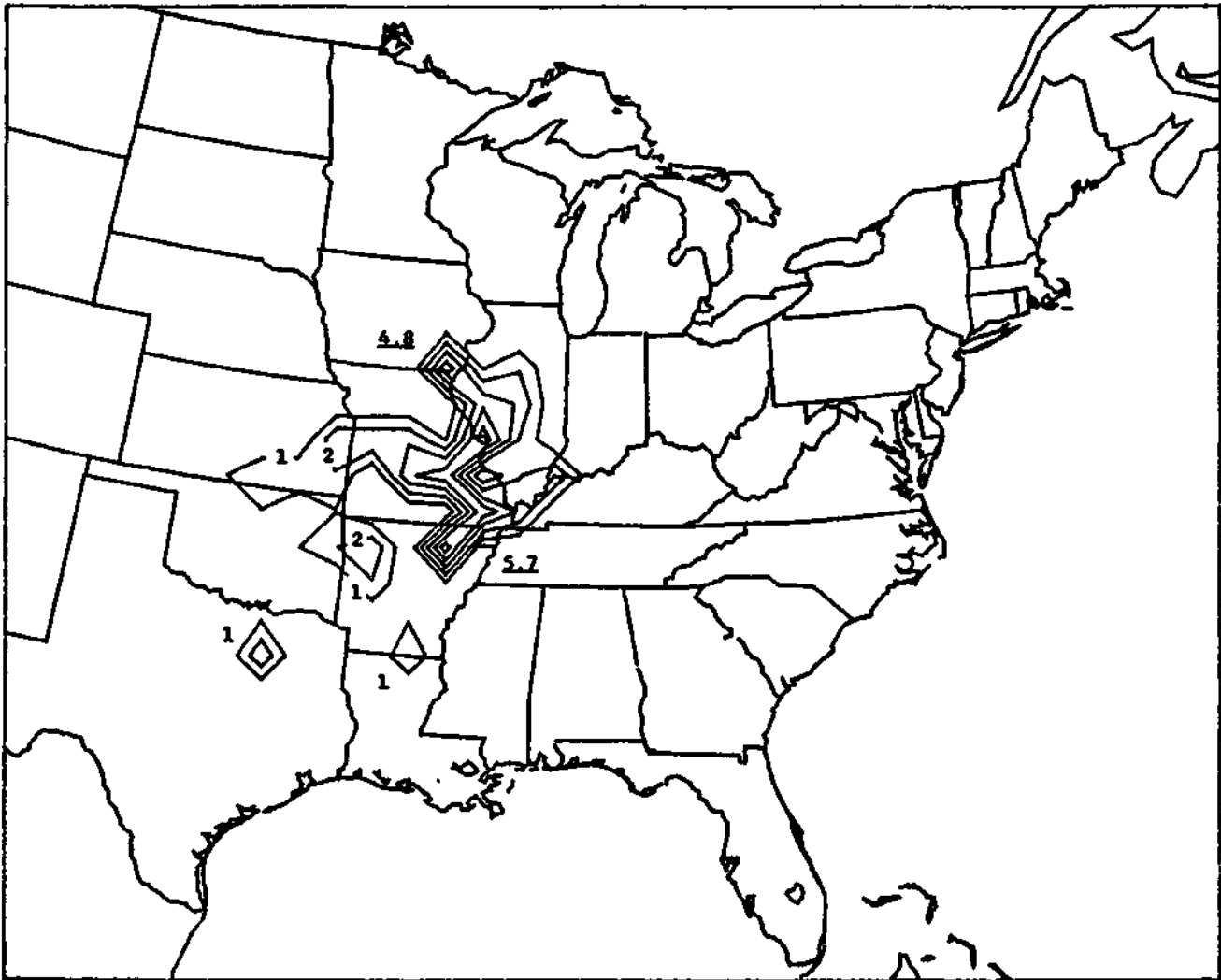


Figure 15. Percentage contours of back trajectory locations for endpoints 18 hours back in time for all storms related to chemistry samples having SO_4 fluxes in the 65th to 95th percentile range for spring and summer. Contour interval is 1.0% with grid square maxima values underlined. Total number of trajectories in domain is 105.

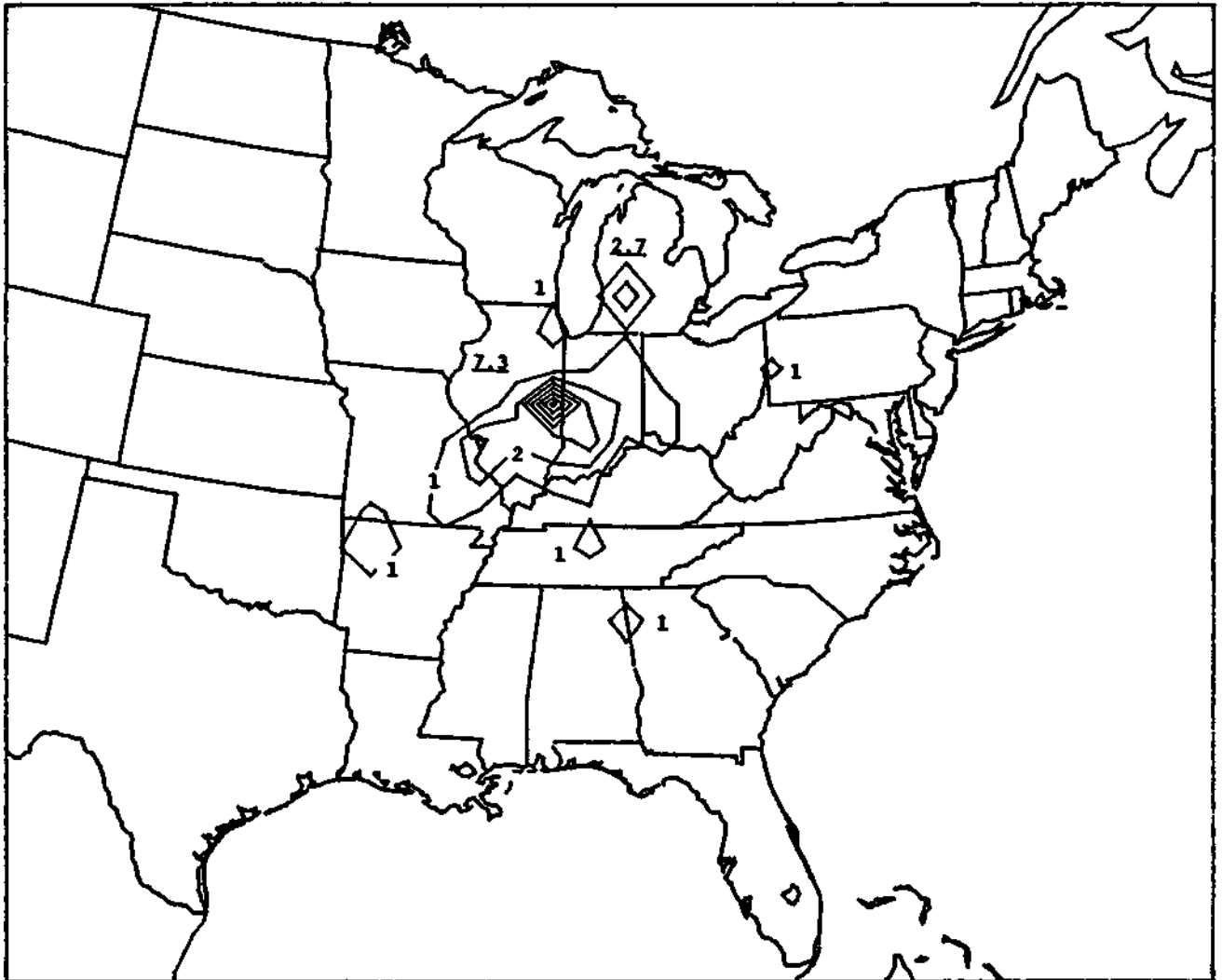


Figure 16. Percentage contours of back trajectory locations for endpoints 12 hours back in time for all storms related to chemistry samples having SO_4 fluxes in the 5th to 35th percentile range for spring and summer. Contour interval is 1.0% with grid square maxima values underlined. Total number of trajectories in domain is 219.

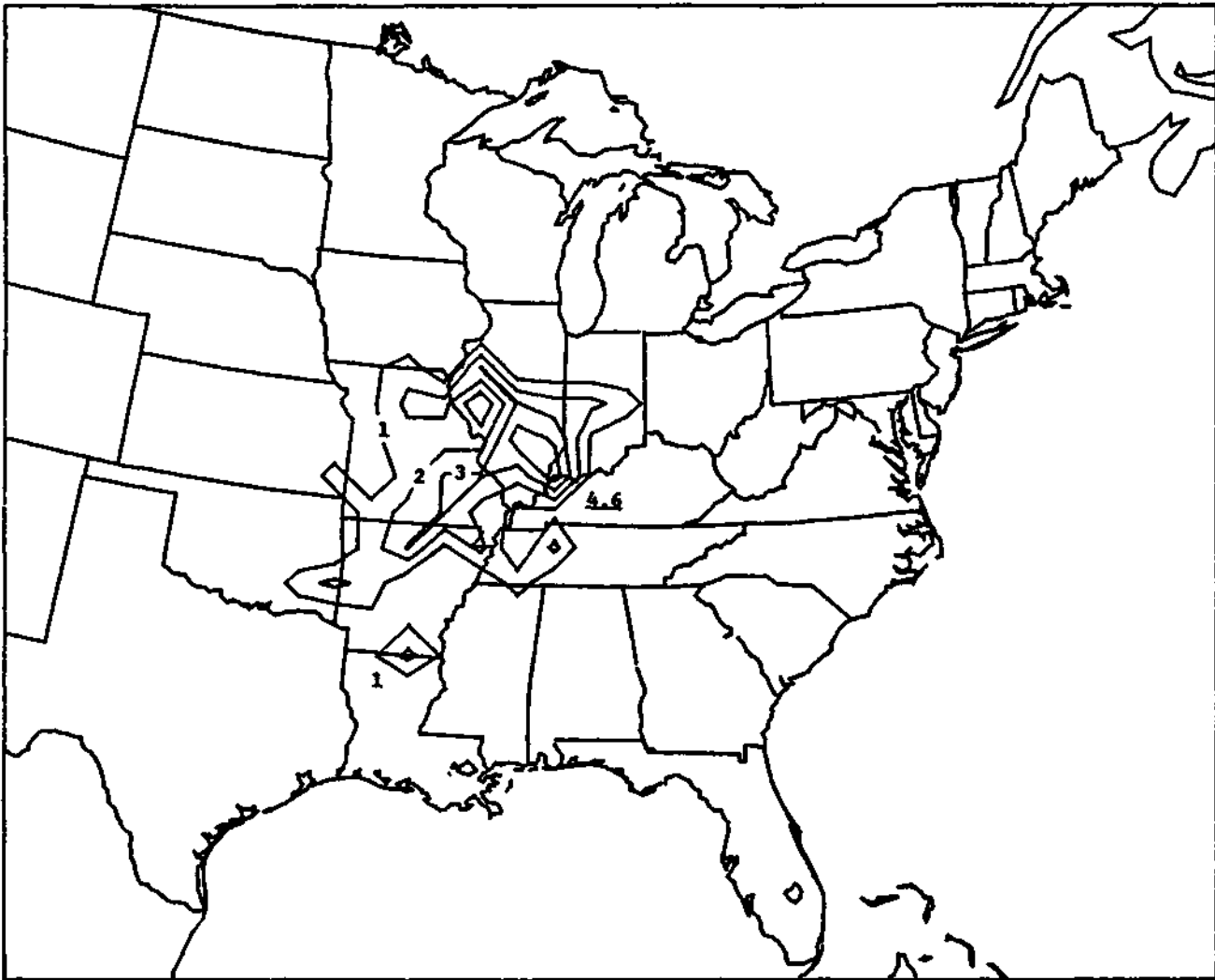


Figure 17. Percentage contours of back trajectory locations for endpoints 12 hours back in time for all storms related to chemistry samples having SO_4 fluxes in the 35th to 65th percentile range for spring and summer. Contour interval is 1.0% with grid square maxima values underlined. Total number of trajectories in domain is 130.

Parcels moving along the linear maximum to the southwest were moving over the high emission areas of southwestern Illinois.

The major group for the upper flux category at 12 hours in Figure 18 was composed of 67 trajectories and was the simplest of the three categories at this time period, being limited almost entirely to Illinois and Missouri and with a strong southwesterly orientation. Of the three categories, the upper flux category had far more trajectories at a closer distance to the Bondville site, which implied slower transport wind speeds over the high emission areas across southwestern Illinois. With no maximum protruding directly southward from Illinois, it also implied the air parcels formerly over the high emission areas of western Kentucky and Tennessee had moved anticyclonically into southwesterly flow over high emission areas again in Illinois. Thus, the air parcels of this flux category were exemplified by slow movement over high emission areas multiple times.

Conclusions. Examination of the back trajectory locations at 48, 36, 24, 18, and 12 hour periods for the lower, middle, and upper SO₄ flux categories for spring and summer has provided evidence for very different flow characteristics between the three categories. The lower flux category was dominated by spring conditions with a dominance of southeasterly flow which passed over high emission areas in Indiana and Kentucky but for a relatively short period of time. The middle flux category was dominated by two major pathways. One consisted of a group of parcels at the 48 hour mark which moved across southern Illinois to western Tennessee at 36 hours, followed by little movement until 18 hours when they began to retrace their path northward. The other major pathway was composed of parcels moving from the southwest across the high emission areas of southwestern Illinois but at a relatively fast rate. The upper flux category was strongly dominated by southwesterly flow which consisted of air parcels that had multiple passes or long residence time over the high emission areas of western and southwestern Illinois, and parcels originally over western Tennessee and adjacent areas with subsequent movement over the high emission areas of southwestern Illinois.

COOL SEASON SO₄ FLUXES

Precipitation and Synoptic Statistics

The statistics for the cool season SO₄ fluxes are given in Tables 4-6. Once again there was a definite seasonal bias between the lower, middle, and upper flux categories, each having 34-35 chemistry samples. The lower category consisted of 43% fall samples and 57% winter samples, while the middle category consisted of an even split between fall and winter samples. The upper category was heavily dominated by fall with 94% of the samples from that season. Because of the seasonal patterns between the categories there was a trend from stratiform and frozen precipitation in the lower category to rain showers and thunderstorms in the upper category. This was also reflected in the mean precipitation times, which were 10.3, 7.4, and 5.4 hours for the lower, middle, and upper categories,



Figure 18. Percentage contours of back trajectory locations for endpoints 12 hours back in time for all storms related to chemistry samples having SO_4 fluxes in the 65th to 95th percentile range for spring and summer. Contour interval is 1.0% with grid square maxima values underlined. Total number of trajectories in domain is 105.

Table 4. Synoptic and precipitation type statistics for fall and winter months for the lower SO₄ flux category as based on 35 chemistry samples. Column headings described in text. LS/AS represents the ratio of the volumes of the largest storms to all storms.

SYNOPTIC TYPE STATISTICS
A

mean SO₄ flux - 43.7 µeq/L/hour
fall percentage - 42.9 LS/AS - 75.1%
winter percentage - 57.1
mean precipitation time - 10.3 hours
mean chemistry sample volume - 445 mL

Synoptic Type	F ₂	P ₂	SVOLMAX	SVOL (%)	DEP. %
PCF	6	13.3	1.6	10.6	11.4
CF	9	20.0	1.9	12.6	9.4
PWF	3	6.7	1.0	6.7	11.0
WF	5	11.1	1.4	8.9	9.4
POF	1	2.2	0.3	1.8	1.4
OF	2	4.4	0.8	5.2	3.7
SF	3	6.7	2.5	16.5	11.0
L	12	26.7	4.9	32.0	36.3
T	1	2.2	0.3	1.8	2.1
SL	0	0.0	0.0	0.0	0.0
SZ	1	2.2	0.4	2.8	1.9
AM	2	4.4	0.2	1.0	2.5

PRECIPITATION TYPE STATISTICS
B.

Precip. Type	F ₁	P ₁
L	21	13.3
R	60	38.0
RW	25	15.8
TRW	11	7.0
A	0	0.0
ZL	0	0.0
ZR	8	5.1
IP	9	5.7
S	21	13.3
SW	3	1.9
TSW	0	0.0
T	0	0.0

Table S. Synoptic and precipitation type statistics for fall and winter months for the middle SO₄ flux category as based on 34 chemistry samples. Column headings described in text. LS/AS represents the ratio of the volumes of the largest storms to all storms.

SYNOPTIC TYPE STATISTICS mean SO₄ flux - 83.2 µeq/L/hour
 A. fall percentage - 50.0 LS/AS - 77.7%
 winter percentage - 50.0
 mean precipitation time - 7.4 hours
 mean chemistry sample volume - 443 mL

Synoptic Type	F ₂	P ₂	SVOLMAX	SVOL (%)	DEP. %
PCF	4	8.7	0.7	4.6	5.2
CF	10	21.7	3.1	19.9	22.2
PWF	0	0.0	0.0	0.0	0.0
WF	5	10.9	1.4	8.9	12.2
POF	0	0.0	0.0	0.0	0.0
OF	2	4.3	0.3	2.2	3.3
SF	4	8.7	1.9	12.3	9.4
L	12	26.1	3.8	24.0	22.6
T	5	10.9	2.8	17.5	14.1
SL	1	2.2	0.8	4.9	7.8
SZ	0	0.0	0.0	0.0	0.0
AM	3	6.5	0.9	5.7	3.3

PRECIPITATION TYPE STATISTICS
 B

Precip Type	F ₁	P ₁
L	18	12.4
R	46	31.7
RW	43	29.7
TRW	9	6.2
A	0	0.0
ZL	0	0.0
ZR	6	4.1
IP	7	4.8
S	13	9.0
SW	2	1.4
TSW	1	0.7
T	0	0.0

Table 6 Synoptic and precipitation type statistics for fall and winter months for the upper SO₄ flux category as based on 35 chemistry samples. Column headings described in text. LS/AS represents the ratio of the volumes of the largest storms to all storms.

SYNOPTIC TYPE STATISTICS
 A. mean SO₄ flux - 207.6 µeq/L/hour
 fall percentage - 94.3 LS/AS - 77.6%
 winter percentage - 5.7
 mean precipitation time - 5.4 hours
 mean chemistry sample volume - 522 mL

Synoptic Type	F ₂	P ₂	SVOLMAX	SVOL (%)	DEP. %
PCF	1	2.3	0.1	.3	0.3
CF	10	22.7	3.9	21.8	14.1
PWF	0	0.0	0.0	0.0	0.0
WF	5	11.4	2.7	15.0	11.5
POF	0	0.0	0.0	0.0	0.0
OF	2	4.5	0.3	2.0	2.3
SF	6	13.6	2.0	11.3	19.0
L	14	31.8	7.4	41.5	41.7
T	2	4.5	0.2	1.0	1.5
SL	3	6.8	1.1	5.9	7.9
SZ	0	0.0	0.0	0.0	0.0
AM	1	2.3	0.2	1.1	1.8

PRECIPITATION TYPE STATISTICS
 B.

Precip. Type	F ₁	P ₁
L	12	8.8
R	33	24.1
RW	53	38.7
TRW	28	20.4
A	0	0.0
ZL	3	2.2
ZR	3	2.2
IP	0	0.0
S	4	2.9
SW	1	0.7
TSW	0	0.0
T	0	0.0

respectively. In terms of the dominant synoptic types, more synoptic classes contributed substantially to the respective depositions than in the warm season cases. For the lower category, the top six deposition contributors were: L, 36.3%; PCF, 11.4%; SF, 11.0%, PWF, 11.0%; CF, 9.4%; and WF, 9.4%. The top five classes for the middle category were: L, 22.6%; CF, 22.2%; T, 14.1%; WF, 12.2%; and SF, 9.4%. The top four groups for the upper flux category were: L, 41.7%; SF, 19.0%; CF, 14.1%; and WF, 11.5%. The low pressure center class was the largest contributor for all the flux categories, while the stationary, cold, and warm frontal groups were also held in common between the groups but at different ranks.

Back Trajectory Patterns

Pattern for 18 hours. The trajectory patterns 18 hours back in time in Figures 19-21 for the lower, middle, and upper flux categories, respectively, will be discussed together given their similarity. The lower and middle categories each had one major group, while the upper flux category had three major groups. The major group for the lower flux category extended across Illinois and Missouri, with relative maxima over the Chicago and St. Louis areas which are also high SO_x emission areas. The one major group for the middle category extended from the Chicago area southward across eastern Illinois and then into portions of western Kentucky and Tennessee. Relative maxima were observed near the Bondville site and western Tennessee. The latter maximum was over high emission areas in Tennessee and Kentucky. The three major groups for the upper flux category were over western Illinois, Indiana and western Kentucky, and the third mainly over Arkansas. The first two groups were over high emission areas. Unlike the warm season case, the spatial trajectory patterns were not differentiated by their relative positions to high emission areas. The proximity of the major groups for the lower and middle flux categories to the Bondville site suggested lower transport wind speeds than for the upper flux case, which is the opposite of the expected stagnation conditions for the upper flux category.

Pattern for 12 hours. Although still very similar, the patterns for the 12 hour period in Figures 22-24 showed more differences than those at 18 hours. All the categories had only one major group, but with each having different directional tendencies. Both the lower and the middle flux categories had large numbers of trajectories close to the Bondville site as indicated by the maxima in that area. This maximum in the lower flux category protruded to the west indicating a predominance of westerly flow at this time period, while the same maximum for the middle flux category showed little prevailing direction. Considering the major group for the middle flux category in general, its main thrust was southward across Illinois, Kentucky, and Tennessee. The major group for the upper flux category had two major pathways: one from southeasterly flow across Indiana, and the other from southwesterly flow as exhibited by maxima over southern Missouri and Arkansas.

Pattern for 6 hours. The relatively similarity between the flux categories continued for the 6 hour results in Figures 25-27. The predominance of westerly flow for the lower flux category continued for the 6 hour period in Figure 25. The patterns for the middle and upper flux

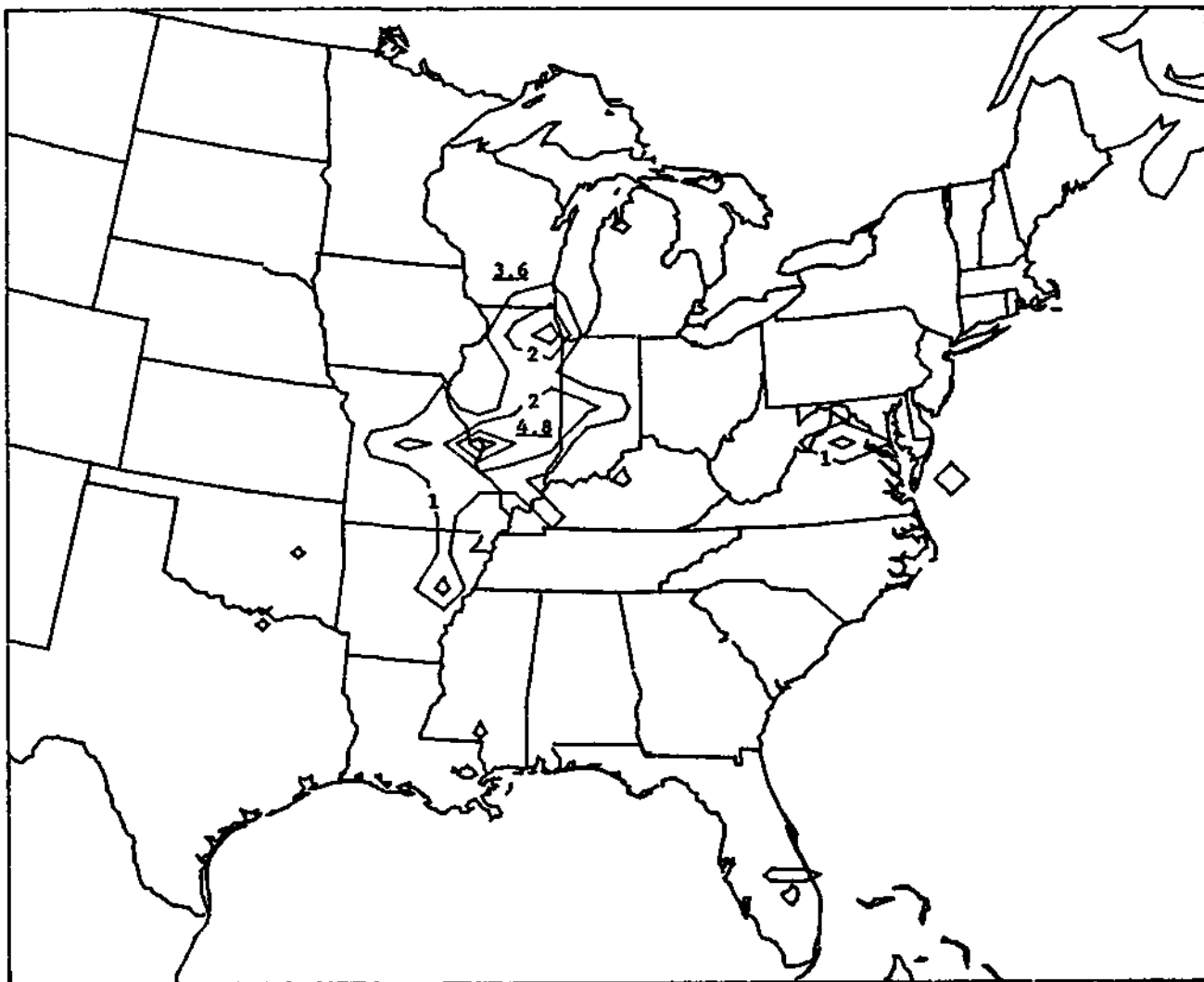


Figure 19. Percentage contours of back trajectory locations for endpoints 18 hours back in time for all storms related to chemistry samples having SO_4 fluxes in the 5th to 35th percentile range for fall and winter. Contour interval is 1.0% with grid square maxima values underlined. Total number of trajectories in domain is 167.

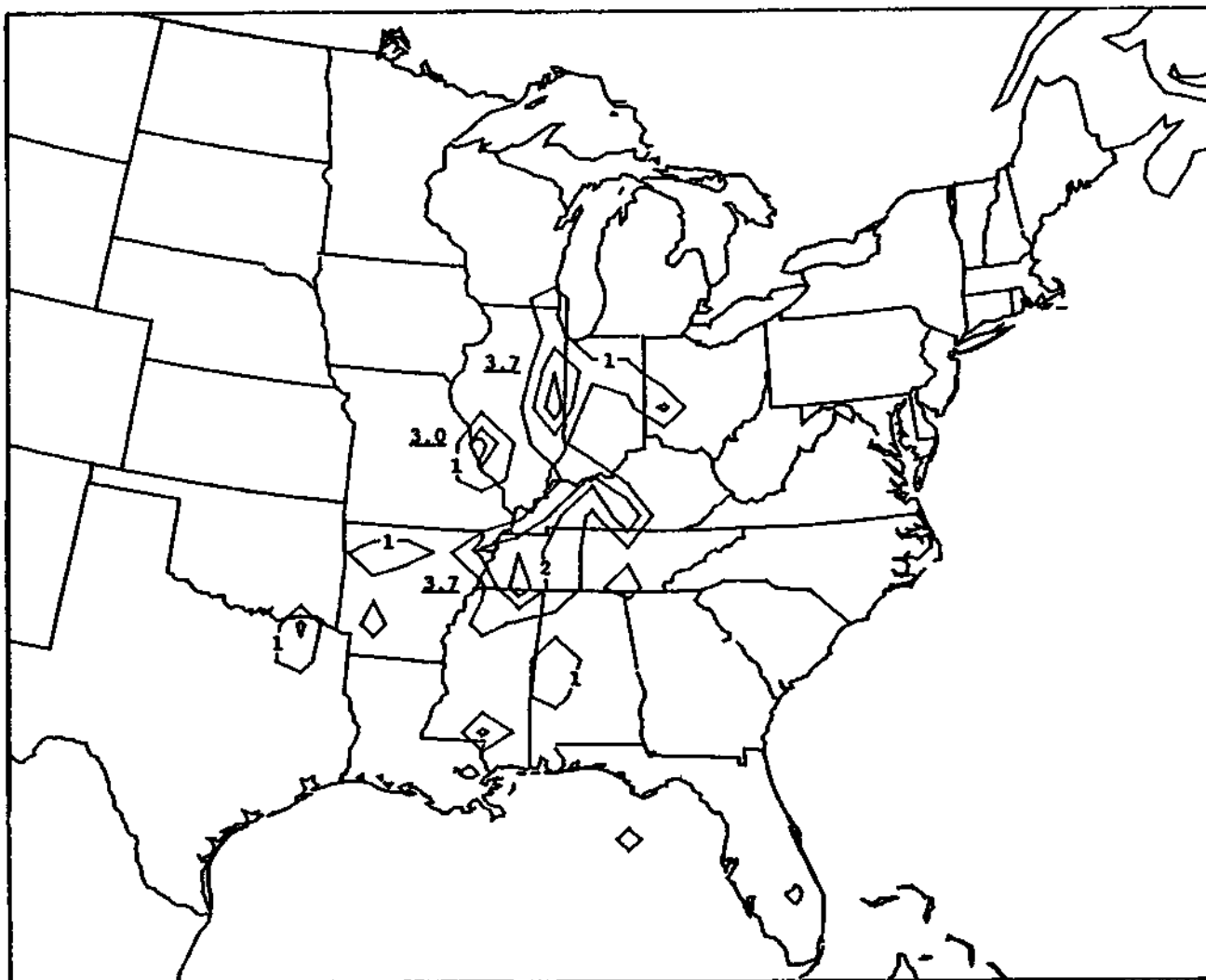


Figure 20. Percentage contours of back trajectory locations for endpoints 18 hours back in time for all storms related to chemistry samples having SO_4 fluxes in the 35th to 65th percentile range for fall and winter. Contour interval is 1.0% with grid square maxima values underlined. Total number of trajectories in domain is 134.

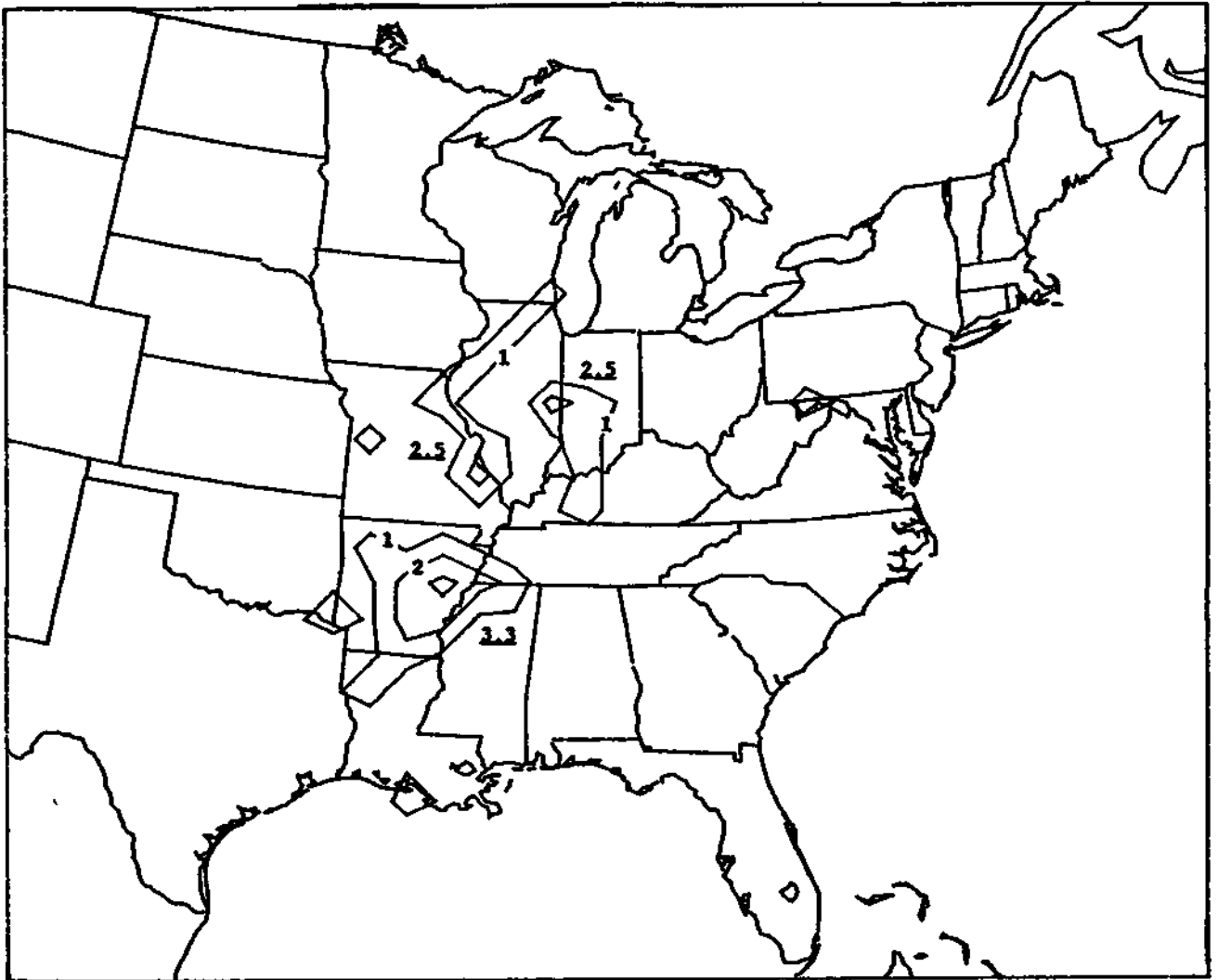


Figure 21. Percentage contours of back trajectory locations for endpoints 18 hours back in time for all storms related to chemistry samples having SO_4 fluxes in the 65th to 95th percentile range for fall and winter. Contour interval is 1.0% with grid square maxima values underlined. Total number of trajectories in domain is 121.



Figure 22. Percentage contours of back trajectory locations for endpoints 12 hours back in time for all storms related to chemistry samples having SO_4 fluxes in the 5th to 35th percentile range for fall and winter. Contour interval is 1.0% with grid square maxima values underlined. Total number of trajectories in domain is 169.



Figure 23. Percentage contours of back trajectory locations for endpoints 12 hours back in time for all storms related to chemistry samples having SO_4 fluxes in the 35th to 65th percentile range for fall and winter. Contour interval is 1.0% with grid square maxima values underlined. Total number of trajectories in domain is 136.

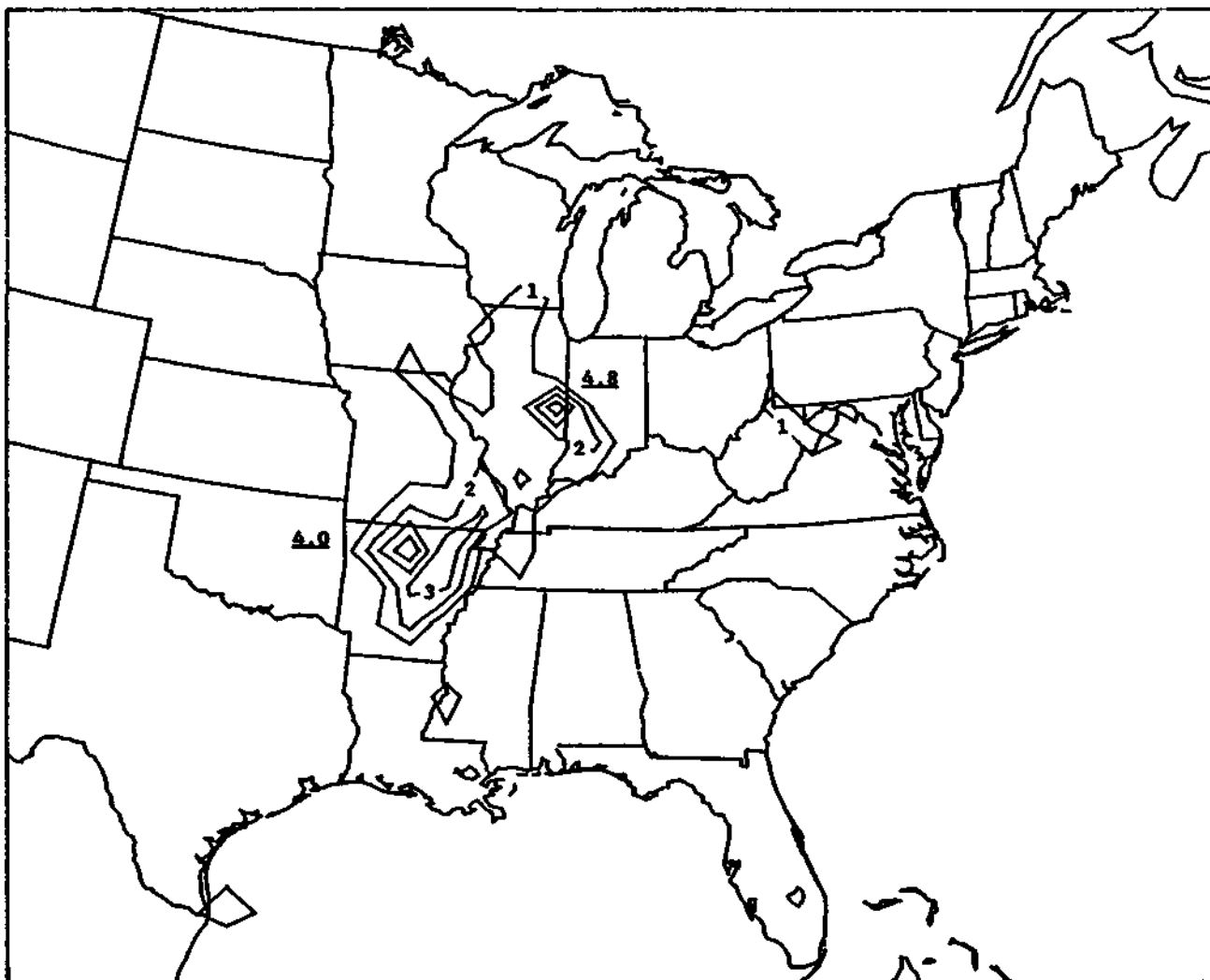


Figure 24. Percentage contours of back trajectory locations for endpoints 12 hours back in time for all storms related to chemistry samples having SO_4 fluxes in the 65th to 95th percentile range for fall and winter. Contour interval is 1.0% with grid square maxima values underlined. Total number of trajectories in domain is 125.

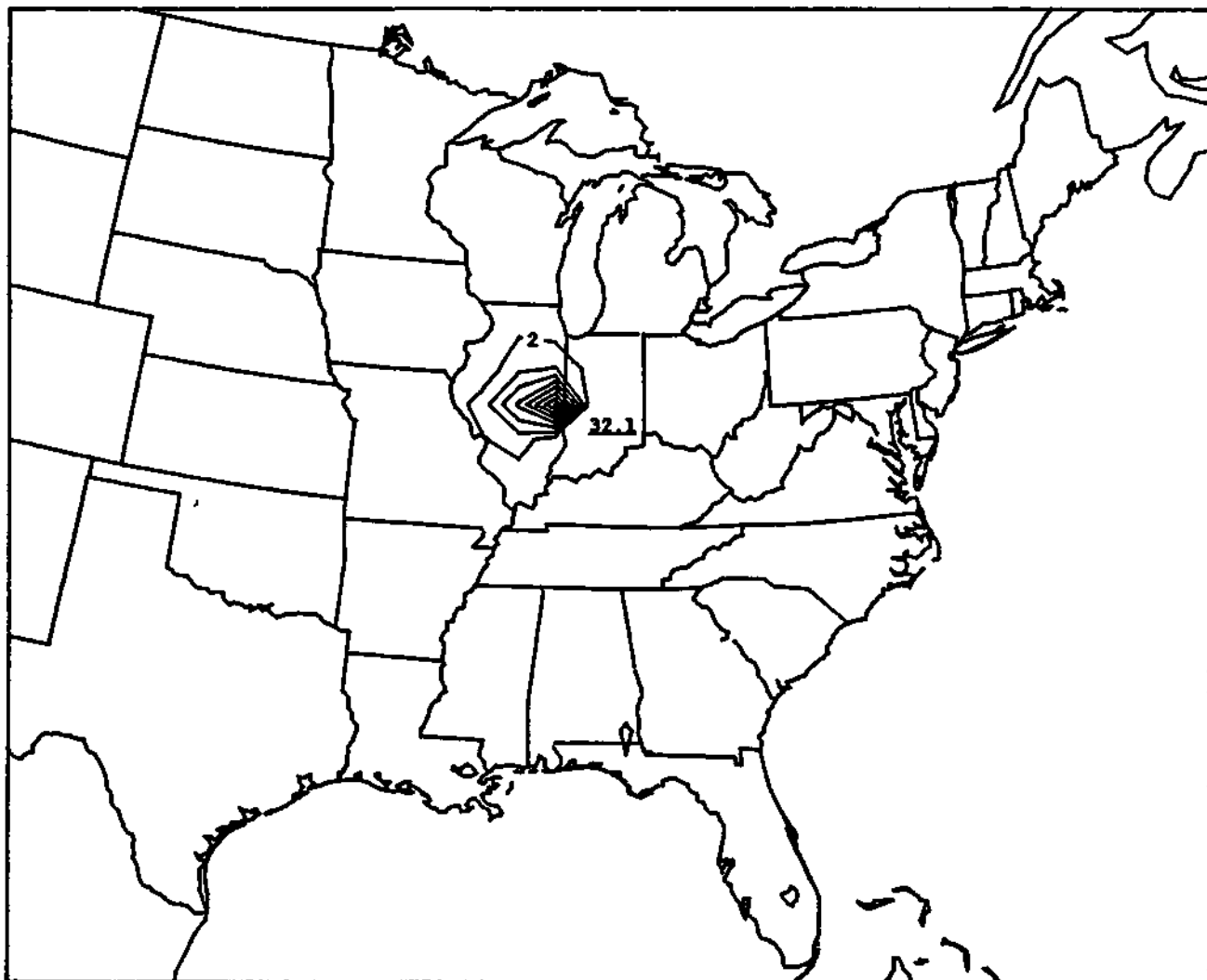


Figure 25. Percentage contours of back trajectory locations for endpoints 6 hours back in time for all storms related to chemistry samples having SO_4 fluxes in the 5th to 35th percentile range for fall and winter. Contour interval is 2.0% with grid square maxima values underlined. Total number of trajectories in domain is 168.

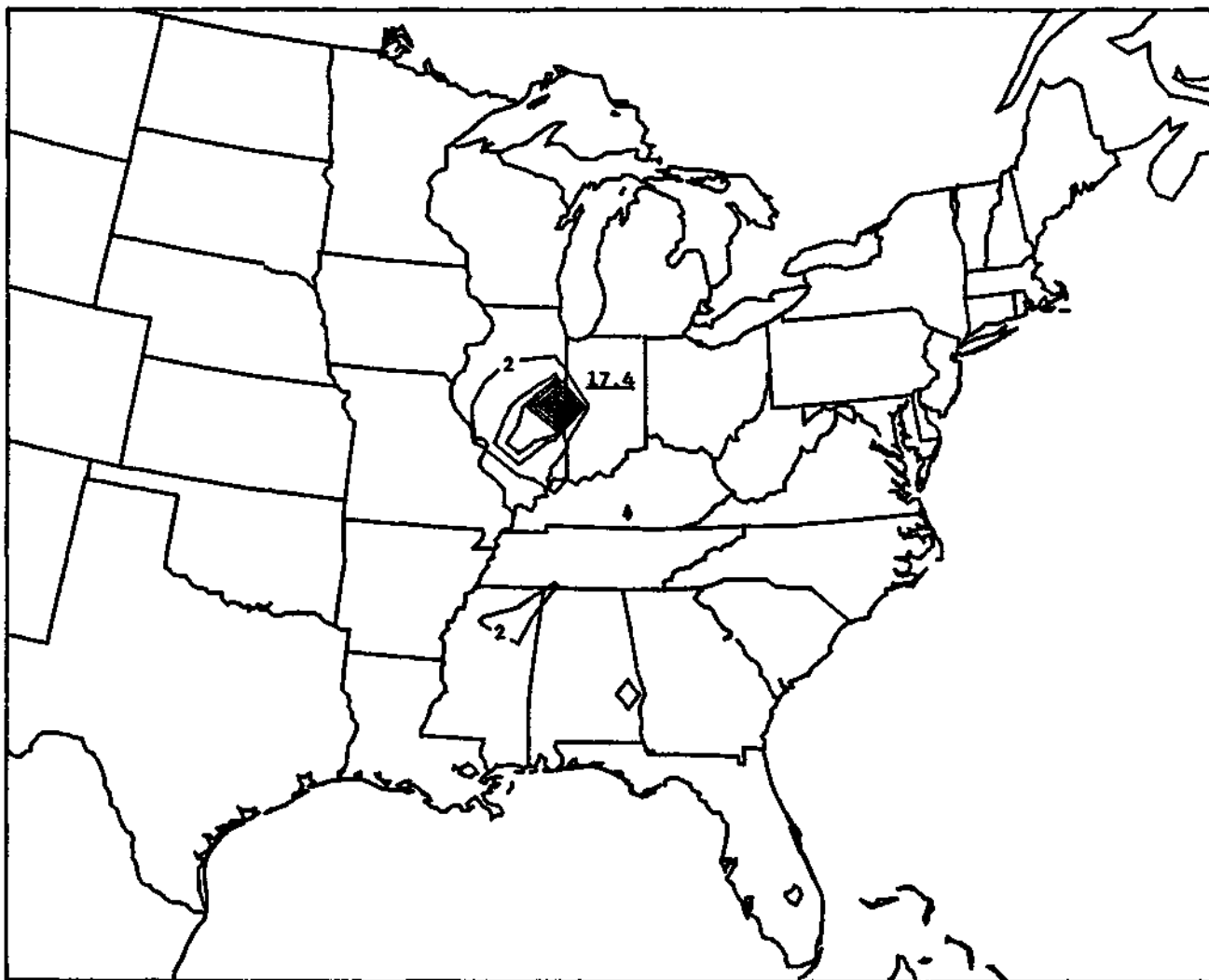


Figure 26. Percentage contours of back trajectory locations for endpoints 6 hours back in time for all storms related to chemistry samples having SO_4 fluxes in the 35th to 65th percentile range for fall and winter. Contour interval is 2.0% with grid square maxima values underlined. Total number of trajectories in domain is 138.

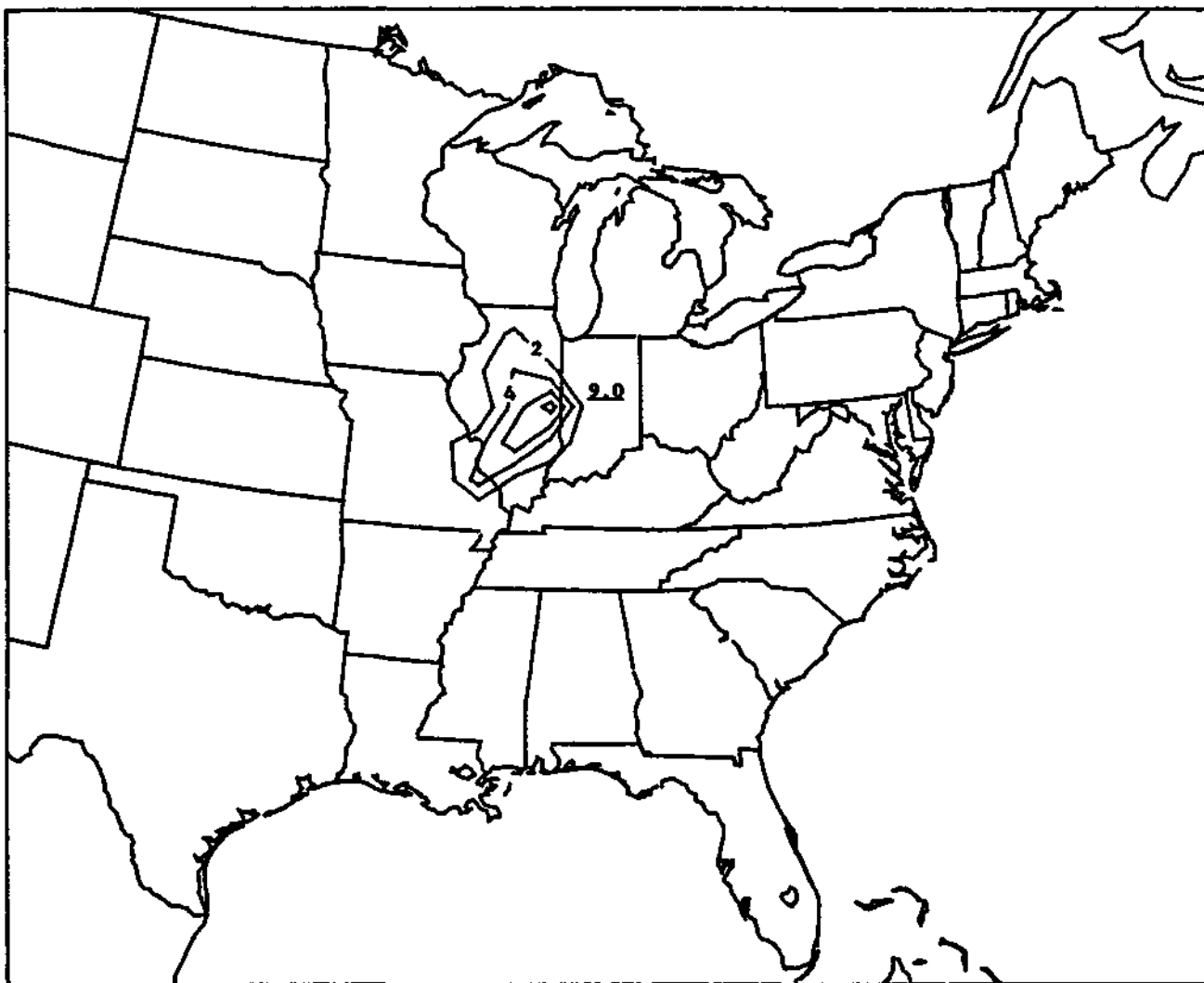


Figure 27. Percentage contours of back trajectory locations for endpoints 6 hours back in time for all storms related to chemistry samples having SO_4 fluxes in the 65th to 95th percentile range for fall and winter. Contour interval is 2.0% with grid square maxima values underlined. Total number of trajectories in domain is 122.

categories were similar in their directional characteristics but with the middle flux category having much slower transport wind speeds than those in the upper category given the large number of trajectory locations near the site.

Conclusions. The visual differences between the three flux categories in their trajectory patterns were much smaller than the corresponding comparisons for the warm season case. There was also the unexpected characteristic of higher transport wind speeds for the upper flux category as compared to the lower and middle categories. The seeming lack of a relationship between the trajectory and emission patterns and the high transport wind speeds for the high flux category may have at least three causes. As mentioned in the description of the trajectory model in chapter 15, a mistake was found in the program code after completion of these trajectory runs, which may have affected the determination of the transport layer depth in strong wind conditions. Another possibility is the rather poor collection efficiencies for both the sampling device and the rain gauge during high wind speeds, which is especially true for snow conditions. Since the SO_4 fluxes depend on the sample volume from the sampling bucket and storm duration from the rain gauge data, inaccurate estimates of these quantities could place chemistry samples in the wrong flux category. Additional weight for this hypothesis is seen in the slow transport wind speeds for the lower and middle flux categories which had most of the frozen precipitation, while the upper flux category was predominately shower and thunderstorm activity for the fall season. Finally, and most importantly, the lack of any consideration of vertical motion in the trajectory model may seriously flaw the trajectory calculations during the cool season when baroclinic systems have substantial synoptic scale vertical motion fields.

WARM SEASON NO_3 FLUXES

Precipitation and Synoptic Statistics

The precipitation and synoptic type statistics for the lower, middle, and upper NO_3 flux categories for the warm season are given in Tables 7-9. As in the case for the warm and cool season SO_4 flux statistics, there was a seasonal bias across the three categories. The spring/summer percentages were 79/21, 59/41, and 40/60 for the lower, middle, and upper categories, respectively. The shift towards summer data for the upper flux category was also reflected in increased thunderstorm activity, shorter precipitation times, and no frozen precipitation. The dominant synoptic types which contributed to deposition percentages for the lower flux category were: L, 30.9%; SF, 17.4%; FWF, 9.9%, CF, 9.8%; OF, 9.2%; and WF, 9.1%. For the middle flux category the dominant types and accompanying percentages of depositions were: CF, 24.3%; L, 16.4%; T, 14.3%; and WF, 13.9%. The main synoptic types for the upper category were: CF, 23.4%; SF, 23.0%; T, 17.0%; L, 14.2%; and WF, 11.8%. As in the case of the warm season SO_4 fluxes, the upper flux category for warm season NO_3 was dominated by thunderstorm activity associated with cold and stationary fronts.

Table 7. Synoptic and precipitation type statistics for spring and summer months for the lower NO₃ flux category as based on 48 chemistry samples. Column headings described in text LS/AS represents the ratio of the volumes of the largest storms to all storms.

SYNOPTIC TYPE STATISTICS
A.

mean NO₃ flux - 47.6 µeq/L/hour
 spring percentage - 79.2 LS/AS - 85.0%
 summer percentage - 20.8
 mean precipitation time - 7.5 hours
 mean chemistry sample volume - 431 mL

Synoptic Type	F ₂	P ₂	SVOLMAX	SVOL (%)	DEP. %
PGF	1	1.7	1.3	4.6	5.1
GF	12	20.0	4.8	17.1	9.8
FWF	4	6.7	2.3	8.3	9.9
WF	6	10.0	3.8	13.7	9.1
POF	1	1.7	0.5	1.8	1.3
OF	4	6.7	1.8	6.5	9.2
SF	10	16.7	6.4	23.0	17.4
L	16	26.7	5.7	20.2	30.9
T	5	8.3	1.3	4.5	6.3
SL	0	0.0	0.0	0.0	0.0
SZ	0	0.0	0.0	0.0	0.0
AM	1	1.7	0.1	0.3	1.0

PRECIPITATION TYPE STATISTICS
B.

Precip. Type	F ₁	P ₁
L	25	9.7
R	55	21.2
RW	87	33.6
TRW	53	20.5
A	13	5.0
ZL	1	0.4
ZR	2	0.8
IP	7	2.7
S	2	0.8
SW	14	5.4
TSW	0	0.0
T	0	0.0

Table 8. Synoptic and precipitation type statistics for spring and summer months for the middle NO₃ flux category as based on 49 chemistry samples. Column headings described in text. LS/AS represents the ratio of the volumes of the largest storms to all storms.

SYNOPTIC TYPE STATISTICS
 A. mean NO₃ flux - 86.8 µeq/L/hour
 spring percentage - 59.2 LS/AS - 80.3%
 summer percentage - 40.8
 mean precipitation time - 3.6 hours
 mean chemistry sample volume - 323 mL

Synoptic Type	F ₂	P ₂	SVOLMAX	SVOL (%)	DEP. %
PGF	5	8.1	0.8	4.4	5.1
CF	14	22.6	5.3	30.8	24.3
PWF	3	4.8	0.6	3.6	7.9
WF	9	14.5	3.2	18.7	13.9
POF	1	1.6	0.1	0.7	1.1
OF	1	1.6	0.3	1.6	2.4
SF	6	9.7	1.1	6.3	6.0
L	8	12.9	3.1	18.0	16.4
T	8	12.9	1.3	7.3	14.3
SL	5	8.1	0.9	5.0	6.9
SZ	0	0.0	0.0	0.0	0.0
AM	2	3.2	0.6	3.5	1.6

PRECIPITATION TYPE STATISTICS
 B.

Precip. Type	F ₁	P ₁
L	17	9.6
R	41	23.0
RW	48	27.0
TRW	56	31.5
A	6	3.4
ZL	0	0.0
ZR	3	1.7
IP	1	0.6
S	3	1.7
SW	2	1.1
TSW	0	0.0
T	1	0.6

Table 9. Synoptic and precipitation type statistics for spring and summer months for the upper NO₃ flux category as based on 48 chemistry samples. Column headings described in text. LS/AS represents the ratio of the volumes of the largest storms to all storms.

SYNOPTIC TYPE STATISTICS
A.

mean NO₃ flux - 172.7 µeq/L/hour
 spring percentage - 39.6 LS/AS - 83.6%
 summer percentage - 60.4
 mean precipitation time - 2.3 hours
 mean chemistry sample volume - 355 mL

Synoptic Type	F ₂	P ₂	SVOLMAX	SVOL (%)	DEP. %
PCF	3	5.6	0.3	1.5	1.8
CF	12	22.2	4.2	22.6	23.4
PWF	1	1.9	0.2	0.9	0.8
WF	9	16.7	2.3	12.4	11.8
POF	0	0.0	0.0	0.0	0.0
OF	0	0.0	0.0	0.0	0.0
SF	9	16.7	4.5	24.1	23.0
L	6	11.1	2.3	12.0	14.2
T	6	11.1	3.0	16.2	17.0
SL	3	5.6	0.3	1.8	2.7
SZ	1	1.9	0.1	0.3	0.4
AM	4	7.4	1.5	8.2	4.9

PRECIPITATION TYPE STATISTICS
B.

Precip. Type	F ₁	P ₁
L	6	4.7
R	15	11.6
RW	39	30.2
TRW	63	48.8
A	4	3.1
ZL	0	0.0
ZR	0	0.0
IP	0	0.0
S	0	0.0
SW	0	0.0
TSW	0	0.0
I	2	1.6

Back Trajectory Patterns

NO_x Emission Patterns. As in the case of SO_x emissions, the following discussion will focus on high emission areas in or close to Illinois. Three major areas are seen in Figure 28. One is basically the Chicago area, the second covers extreme southeastern Iowa and extreme northwestern Illinois, and the third covers portions of central Illinois and southward, encompassing the St. Louis area at the southern extreme.

Pattern for 24 hours. Figure 29 shows the trajectory pattern for the lower flux category at the 24 hour mark. Five relatively small major groups scattered in all directions were seen, with the one located in eastern Illinois and western Indiana having the largest number of trajectories at 23. The middle flux category in Figure 30 shows several major groups as well with considerable scatter, but with the majority being southwest of the Bondville site. The main group, consisting of 27 trajectories, covered adjacent parts of Arkansas, Missouri, Kentucky, Tennessee, and Mississippi, with relative maxima over northeastern Missouri and western Tennessee. The 24 hour pattern for the upper flux category in Figure 31 exhibited a much more coherent pattern with one major group consisting of 54 trajectories located mainly over Illinois, Missouri, and Oklahoma. Relative maxima were located over central Illinois and central Missouri. The proximity of much of this group to the site at 24 hours revealed slower transport winds compared to most of the main groups in Figures 29 and 30 which were scattered and were farther away from the site. Between the three categories, only the major group in the upper flux category had considerable exposure to high emission areas, which included the St. Louis and central Illinois vicinities.

Pattern for 18 hours. All the flux categories had only one major group by the 18 hour mark. For the lower flux category in Figure 32 this group of 72 trajectories extended across Ohio, Indiana, Illinois, and Missouri with the main relative maximum still in the eastern Illinois and western Indiana area. Although exhibiting rather slow wind speeds this maximum was over relatively low emission areas in Indiana and Illinois. For the middle flux category in Figure 33 considerable consolidation of the scattered groups had occurred since the 24 hour period, with a main group of 60 trajectories extending from Indiana southward to Tennessee and then northwest across Arkansas and Missouri. The main relative maximum was over southern Missouri. In general the main group was not exposed to high emission areas. The main group for the upper flux category in Figure 34 was even better defined than at the 24 hour mark, consisting of 57 trajectories over Illinois and Missouri. Three sharply defined maxima were in the main group one over the intersection of the state boundaries of Illinois, Iowa, and Missouri; one over the St. Louis area; and one over extreme southwestern Indiana. The first of these maxima was in or very close to the very high emission areas seen in the NO_x emissions pattern in Figure 28. The second maxima was over the high emission area over St. Louis, while the third maxima was over relatively low emission areas. A portion of the main group remained over central Illinois as in the 24 hour period, which covered moderate areas of emissions.

Pattern for 12 hours. The major group at 12 hours for the low flux category in Figure 35 consisted of 95 trajectories, located mainly over

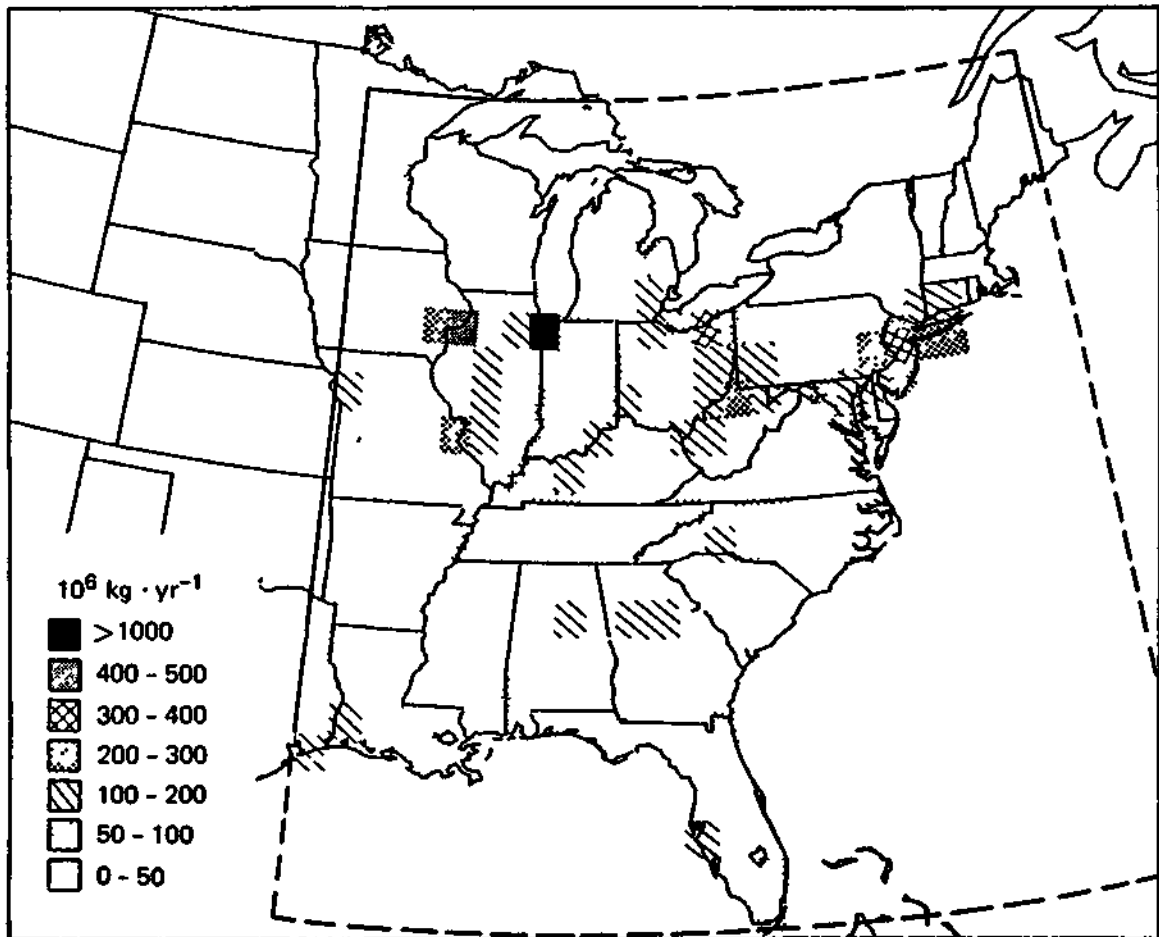


Figure 28. Total annual NO_x emissions (10⁶ kg yr⁻¹) per degree latitude and longitude for the continental eastern United States. Map adapted from Wilson and Mohnen (1982).

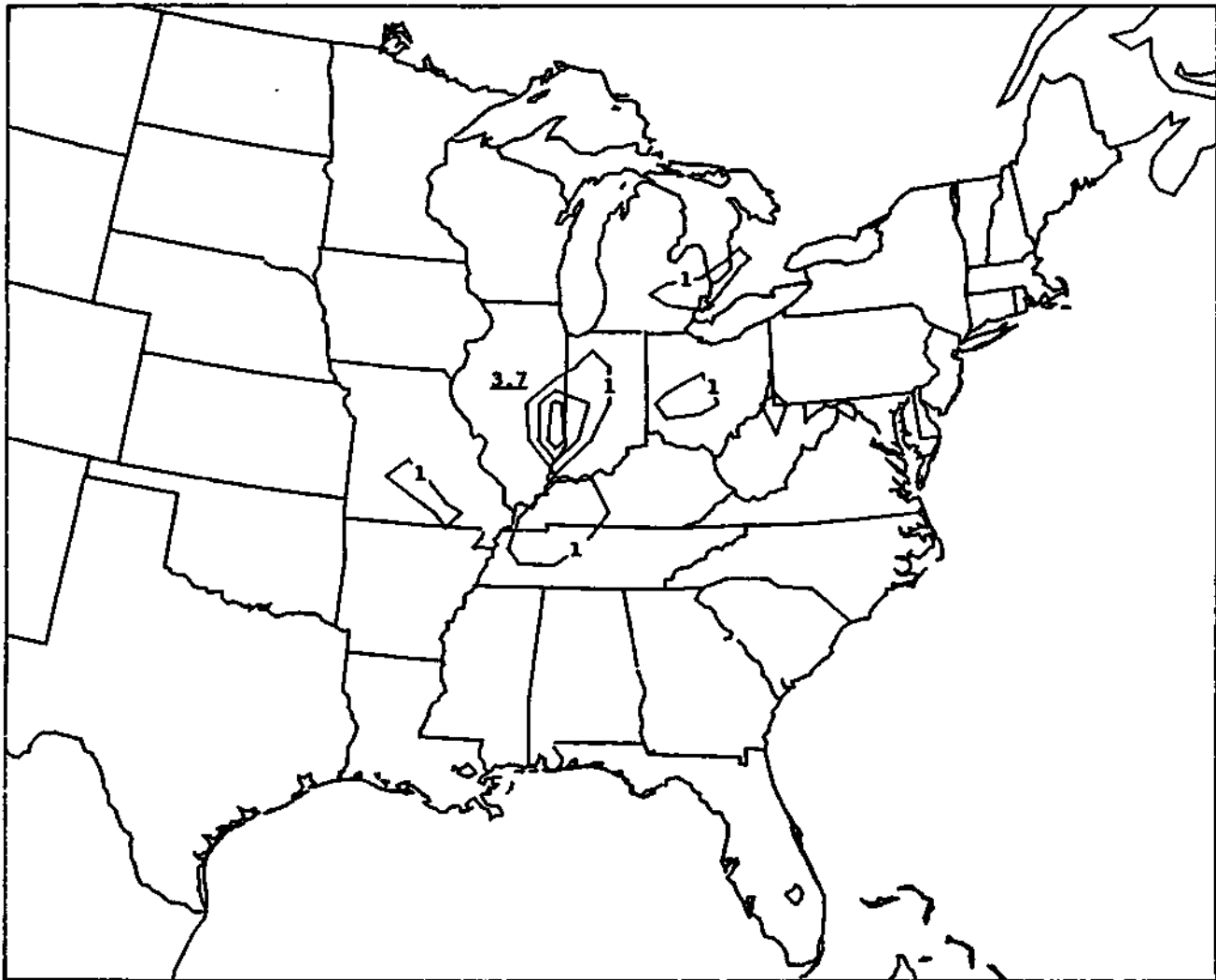


Figure 29. Percentage contours of back trajectory locations for endpoints 24 hours back in time for all storms related to chemistry samples having NO₃ fluxes in the 5th to 35th percentile range for spring and summer. Contour interval is 1.0% with grid square maxima values underlined. Total number of trajectories in domain is 215.



Figure 30. Percentage contours of back trajectory locations for endpoints 24 hours back in time for all storms related to chemistry samples having NO_3 fluxes in the 35th to 65th percentile range for spring and summer. Contour interval is 1.0% with grid square maxima values underlined. Total number of trajectories in domain is 132.



Figure 31. Percentage contours of back trajectory locations for endpoints 24 hours back in time for all storms related to chemistry samples having NO_3 fluxes in the 65th to 95th percentile range for spring and summer. Contour interval is 1.0% with grid square maxima values underlined. Total number of trajectories in domain is 103.

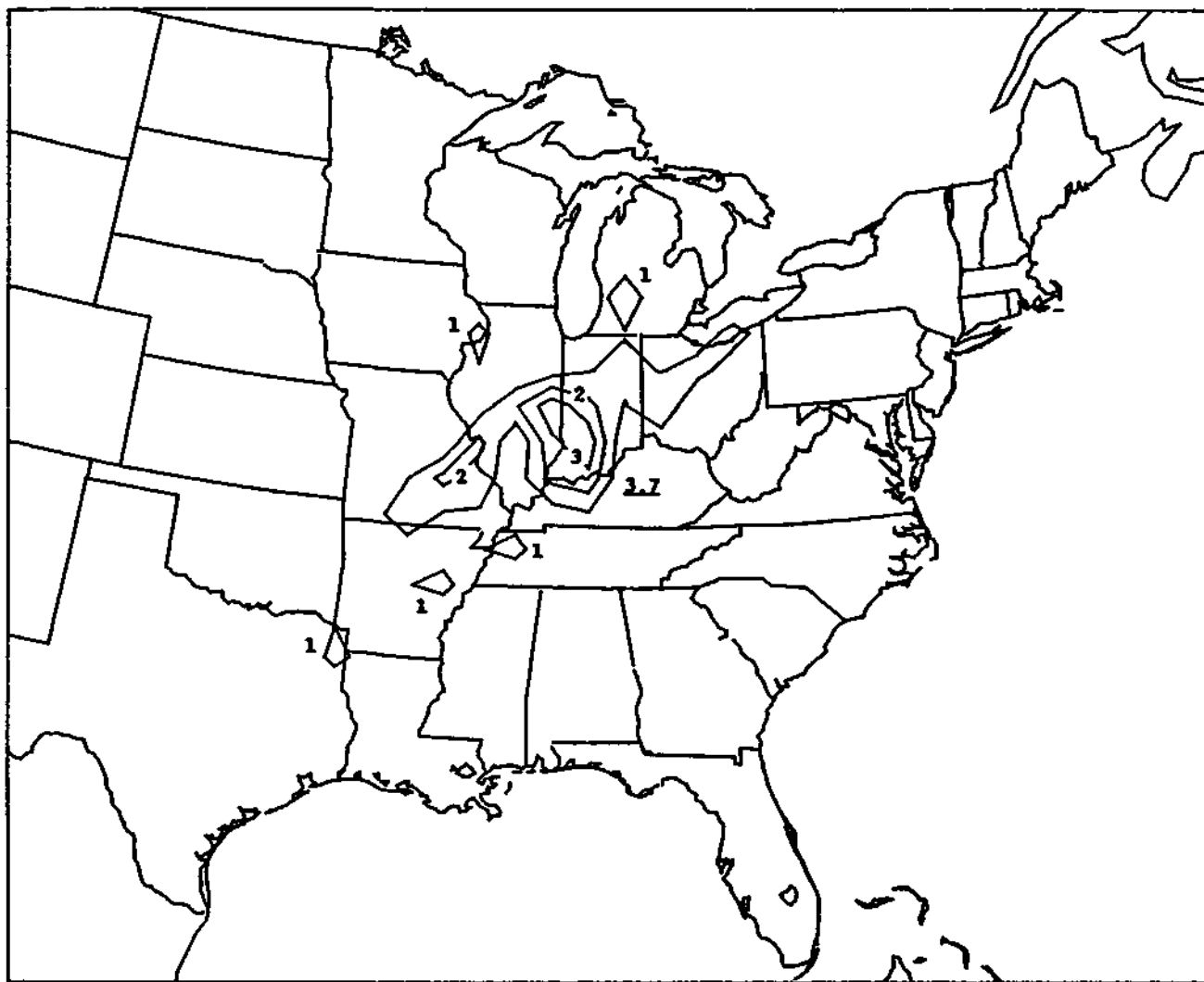


Figure 32. Percentage contours of back trajectory locations for endpoints 18 hours back in time for all storms related to chemistry samples having NO_3 fluxes in the 5th to 35th percentile range for spring and summer. Contour interval is 1.0% with grid square maxima values underlined. Total number of trajectories in domain is 216.

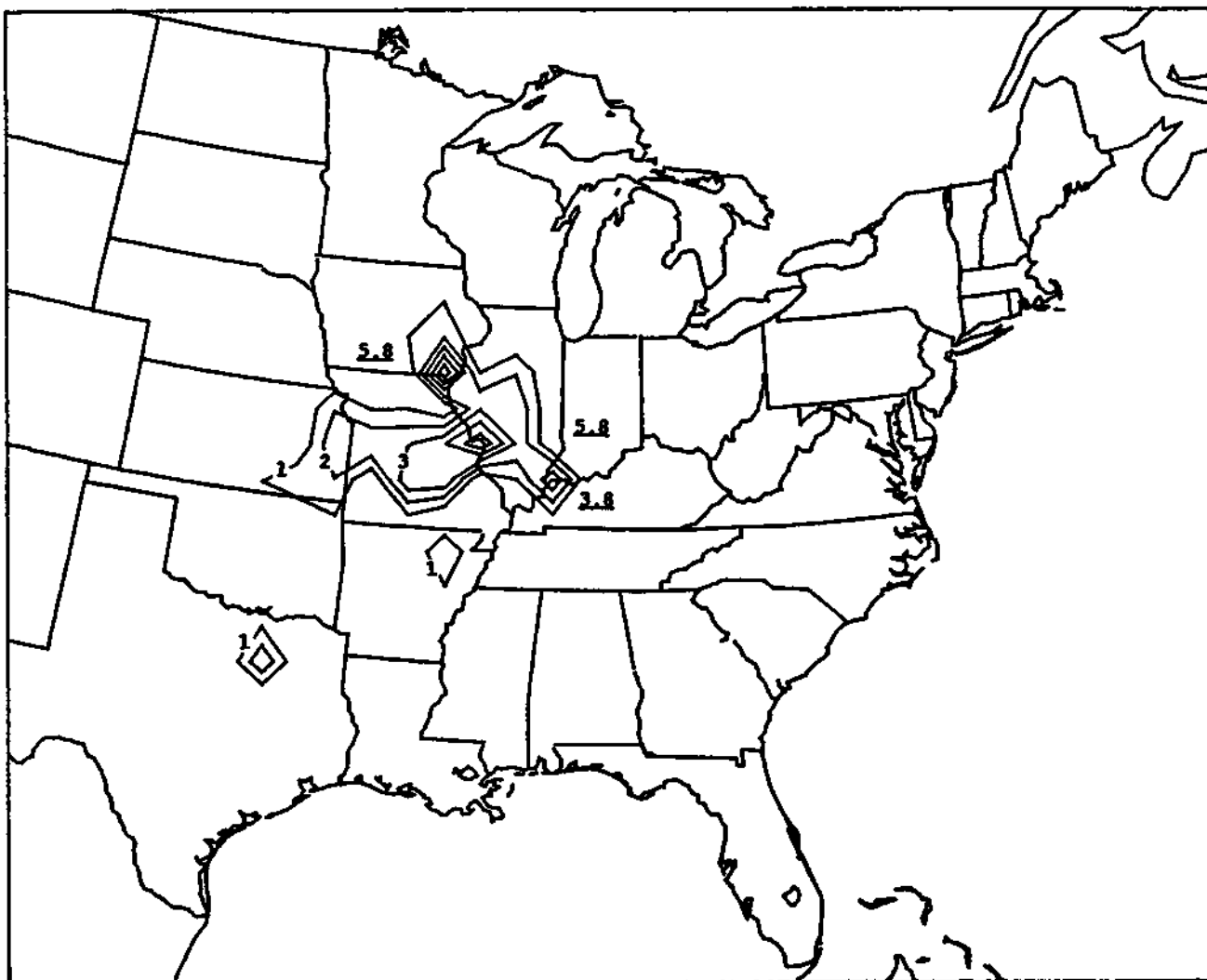


Figure 34. Percentage contours of back trajectory locations for endpoints 18 hours back in time for all storms related to chemistry samples having NO_3 fluxes in the 65th to 95th percentile range for spring and summer. Contour interval is 1.0% with grid square maxima values underlined. Total number of trajectories in domain is 103.

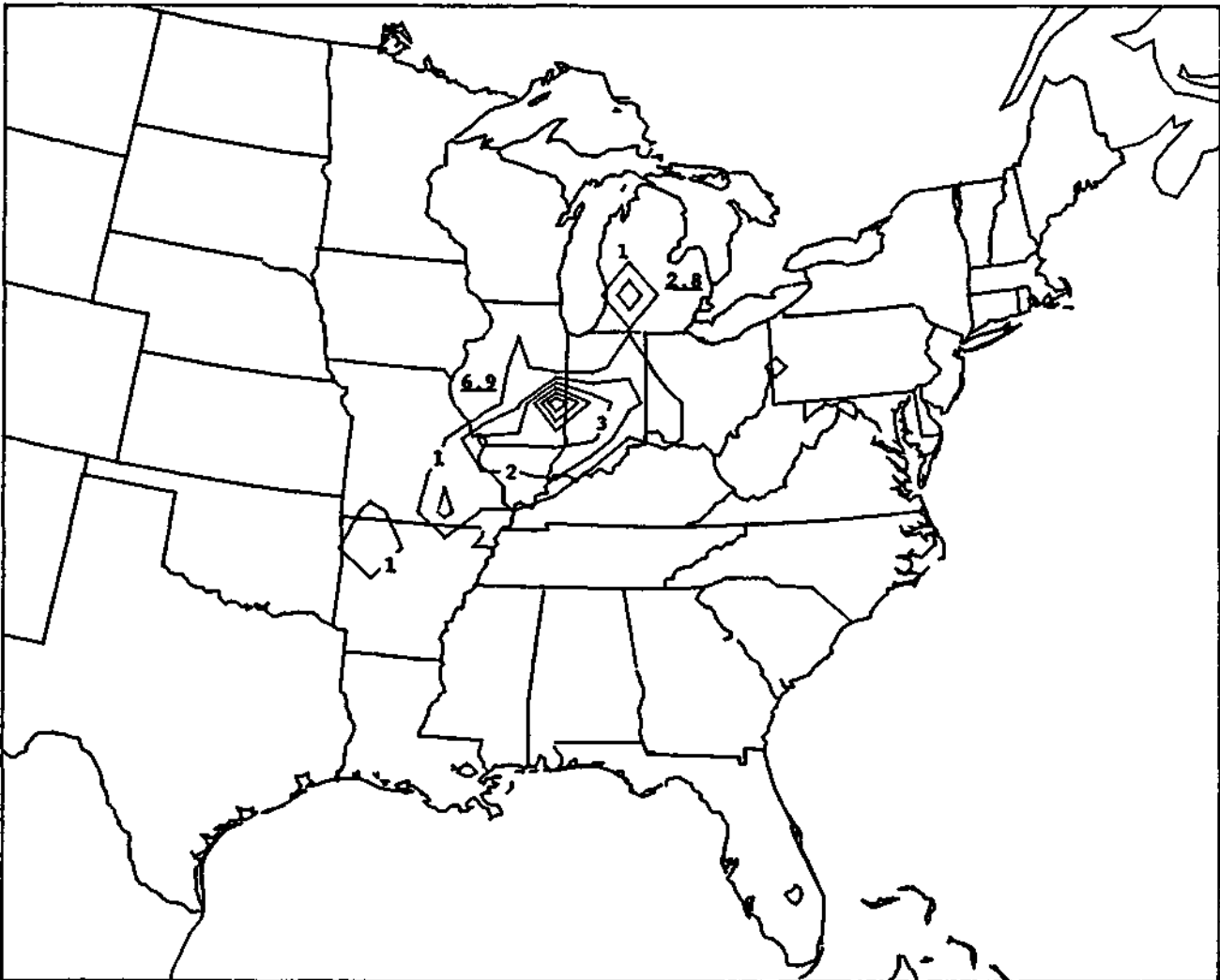


Figure 35. Percentage contours of back trajectory locations for endpoints 12 hours back in time for all storms related to chemistry samples having NO_3 fluxes in the 5th to 35th percentile range for spring and summer. Contour interval is 1.0% with grid square maxima values underlined. Total number of trajectories in domain is 216.

Indiana and Illinois, with the relative maximum over the Bondville site. This continued the trend for low transport winds for much of this group, but over only low to moderate emission areas. The main group for the middle flux category in Figure 36 of 81 trajectories was mainly over Illinois and Missouri. The maximum within this group extended from central Illinois southwestward to approximately the St. Louis area. This maximum was over moderate to high emission areas for the first time. The major group for the upper flux category in Figure 37 again showed a sharply defined pattern, having 63 trajectories over Illinois and Missouri. The maximum within this group was located over west central Illinois, with extensions southwestward across St. Louis and also southeastward to extreme southern Indiana. This maximum continued to be over moderate to high emission areas.

Conclusions. As in the case of the warm season SO_4 fluxes, the three NO_3 flux categories demonstrated very different back trajectory histories. The low flux category had slow transport winds in general but over relatively low emission areas. The middle flux category was dominated by relatively rapid southwesterly flow over the moderate to high emission areas of central and southwestern Illinois. The high flux group consisted of relatively slow transport in westerly and southwesterly flow across the moderate to high emission areas over the western half of Illinois.

COOL SEASON NO_3 FLUXES

Precipitation and Synoptic Statistics

The statistics for the cool season NO_3 fluxes are given in Tables 10-12. The respective fall/winter percentages for the three categories were-40/60, 68/32, and 77/23. The shift towards fall samples in the middle and upper categories was also reflected in the increase in thunderstorm activity and the decrease in mean precipitation times. The largest percentage of frozen precipitation was in the lower category, but the upper category had a slightly larger percentage of frozen precipitation than the middle category. This may be related to the hypothesis that frozen precipitation (snow in particular) is more efficient in scavenging nitric acid vapor than liquid precipitation. The top four synoptic classes in the lower flux category contributing to NO_3 deposition were: L, 30.0%; CF, 16.5%; SF, 11.9%; and WF, 9.7%. For the middle flux category these were: L, 45.0%; CF, 19%; PCF, 9.4%; and SF, 8.9% and for the upper flux category these were: L, 28.3%; SF, 19.8%; WF, 13.6%, and CF, 12.0%. Thus, the L class had the maximum contribution to deposition in each category and CF and SF being in common between the groups as well but at different ranks.

Back Trajectory Patterns

Pattern for 18 hours. Figures 38-40 show the trajectory patterns at the 18 hour mark for the lower, middle, and upper flux categories, respectively. The lower flux pattern had one major group of 43

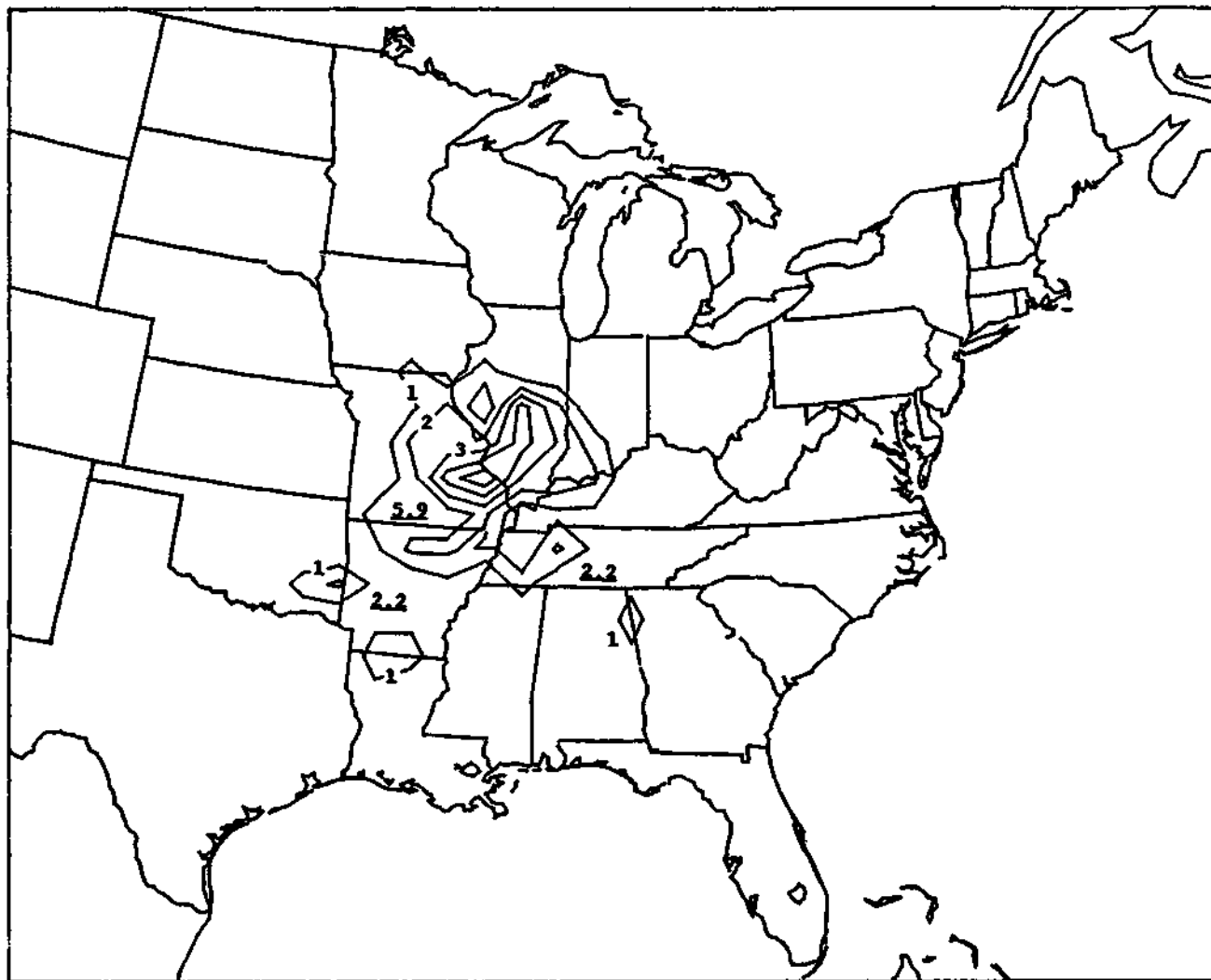


Figure 36. Percentage contours of back trajectory locations for endpoints 12 hours back in time for all storms related to chemistry samples having NO_3 fluxes in the 35th to 65th percentile range for spring and summer. Contour interval is 1.0% with grid square maxima values underlined. Total number of trajectories in domain is 135.

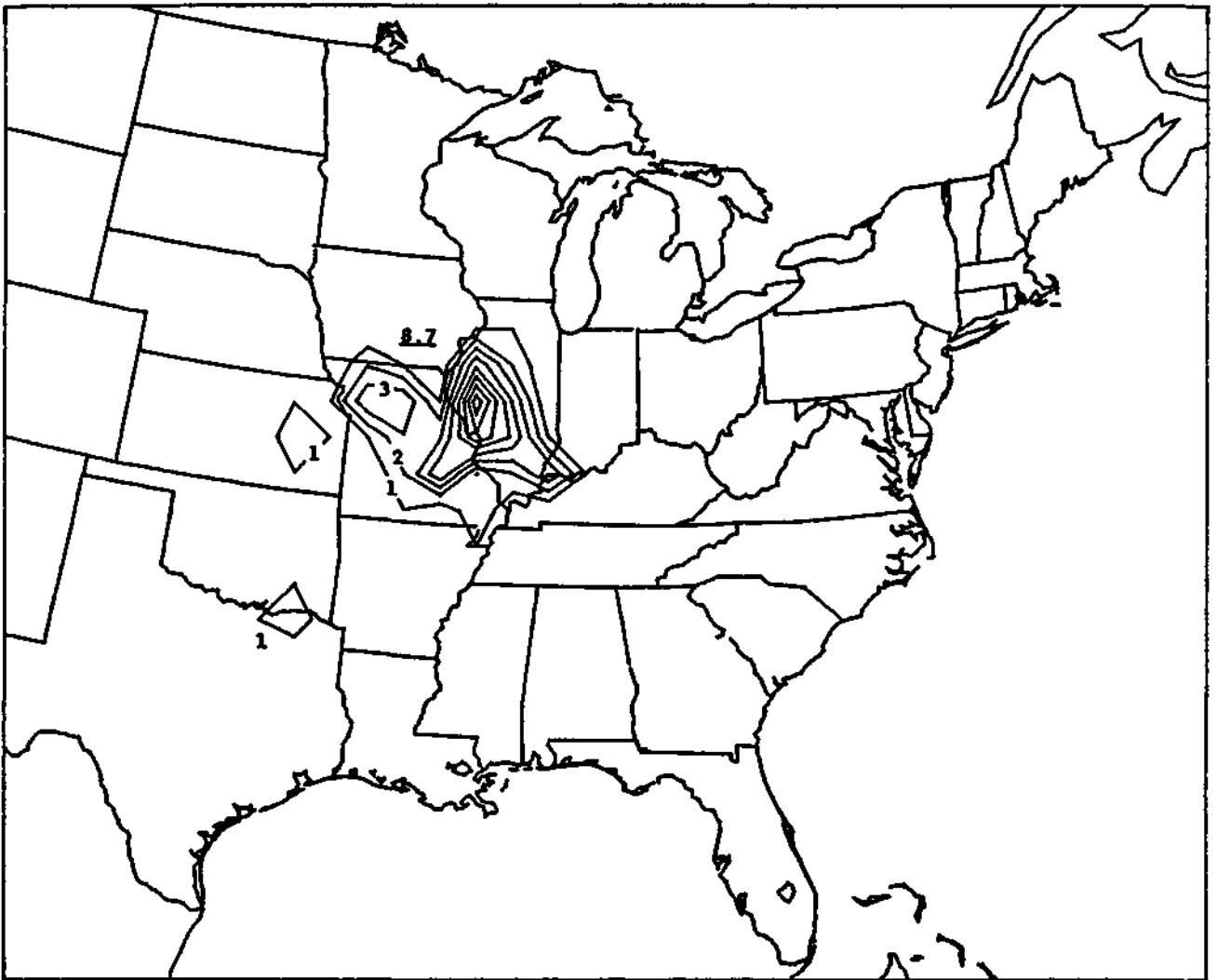


Figure 37. Percentage contours of back trajectory locations for endpoints 12 hours back in time for all storms related to chemistry samples having NO_3 fluxes in the 65th to 95th percentile range for spring and summer. Contour interval is 1.0% with grid square maxima values underlined. Total number of trajectories in domain is 103.

Table 10. Synoptic and precipitation type statistics for fall and winter months for the lower NO₃ flux category as based on 35 chemistry samples
 Column headings described in text. LS/AS represents the ratio of the volumes of the largest storms to all storms.

SYNOPTIC TYPE STATISTICS
 A. mean NO₃ flux - 21.6 µeq/L/hour
 fall percentage - 40.0 LS/AS - 74.1%
 winter percentage - 60.0
 mean precipitation time - 11.0 hours
 mean chemistry sample volume - 573 mL

Synoptic Type	F ₂	P ₂	SVOLMAX	SVOL (%)	DEP. %
PCF	4	8.5	0.8	4.0	4.9
CF	10	21.3	3.2	16.3	16.5
PCF	2	4.3	0.8	4.0	6.7
WF	5	10.6	1.8	9.2	9.7
POF	1	2.1	0.3	1.4	0.8
OF	2	4.3	0.8	4.1	2.9
SF	4	8.5	3.6	18.1	11.9
L	12	25.5	5.6	28.5	30.0
T	3	6.4	0.9	4.6	5.6
SL	1	2.1	0.8	3.9	5.8
SZ	1	2.1	0.4	2.2	1.3
AM	2	4.3	0.7	3.7	4.2

PRECIPITATION TYPE STATISTICS
 B.

Precip. Type	F ₁	P ₁
L	24	13.5
R	59	33.1
RW	37	20.8
TRW	16	9.0
A	0	0.0
ZL	0	0.0
ZR	7	3.9
IP	9	5.1
S	22	12.4
SW	4	2.2
TSW	0	0.0
T	0	0.0

Table 11. Synoptic and precipitation type statistics for fall and winter months for the middle NO₃ flux category as based on 34 chemistry samples. Column headings described in text. LS/AS represents the ratio of the volumes of the largest storms to all storms.

SYNOPTIC TYPE STATISTICS

A.

mean NO₃ flux - 38.1 µeq/L/hour
 fall percentage - 67.6 LS/AS - 77.2%
 winter percentage - 32.4
 mean precipitation time - 8.6 hours
 mean chemistry sample volume - 518 mL

Synoptic

Type	F ₂	P ₂	SVOLMAX	SVOL (%)	DEP %
PCE	6	14.3	1.6	8.7	9.4
CF	10	23.8	3.6	20.4	19.0
PWF	1	2.4	0.1	0.4	1.8
WF	3	7.1	0.7	3.8	6.4
POF	0	0.0	0.0	0.0	0.0
OF	0	0.0	0.0	0.0	0.0
SF	4	9.5	1.3	7.1	8.9
L	14	33.3	8.3	46.3	45.0
T	1	2.4	1.9	10.9	6.3
SL	1	2.4	0.2	1.1	0.8
SZ	0	0.0	0.0	0.0	0.0
AM	2	4.8	0.2	1.3	2.4

PRECIPITATION TYPE STATISTICS

B.

Preclp. Type	F ₁	P ₁
L	14	9.9
R	46	32.4
RW	51	35.9
TRW	11	7.7
A	0	0.0
ZL	0	0.0
ZR	1	0.7
IP	5	3.5
S	11	7.7
SW	2	1.4
TSW	1	0.7
T	0	0.0

Table 12. Synoptic and precipitation type statistics for fall and winter months for the upper NO₃ flux category as based on 35 chemistry samples. Column headings described in text. LS/AS represents the ratio of the volumes of the largest storms to all storms.

SYNOPTIC TYPE STATISTICS
 A. mean NO₃ flux - 93.6 µeq/L/hour
 fall percentage - 77.1 LS/AS - 82.3%
 winter percentage - 22.9
 mean precipitation time - 3.6 hours
 mean chemistry sample volume - 333 mL

Synoptic Type	F ₂	P ₂	SVOLMAX	SVOL (%)	DEP. %
PCF	1	2.1	0.1	0.4	0.5
CF	9	19.1	3.1	25.7	12.0
PWF	0	0.0	0.0	0.0	0.0
WF	6	12.8	2.6	21.5	13.6
POF	0	0.0	0.0	0.0	0.0
OF	4	8.5	0.7	5.8	9.2
SF	6	12.8	1.7	14.5	19.8
L	13	27.7	2.3	19.2	28.3
T	4	8.5	0.4	3.2	6.1
SL	2	4.3	0.9	7.2	8.0
SZ	0	0.0	0.0	0.0	0.0
AM	2	4.3	0.3	2.4	2.4

PRECIPITATION TYPE STATISTICS
 B.

Precip Type	F ₁	P ₁
L	14	11.5
R	31	25.4
RW	35	28.7
TRW	20	16.4
A	0	0.0
ZL	3	2.5
ZR	8	6.6
IP	2	1.6
S	9	7.4
SW	0	0.0
TSW	0	0.0
T	0	0.0



Figure 38. Percentage contours of back trajectory locations for endpoints 18 hours back in time for all storms related to chemistry samples having NO_3 fluxes in the 5th to 35th percentile range for fall and winter. Contour interval is 1.5% with grid square maxima values underlined. Total number of trajectories in domain is 173.

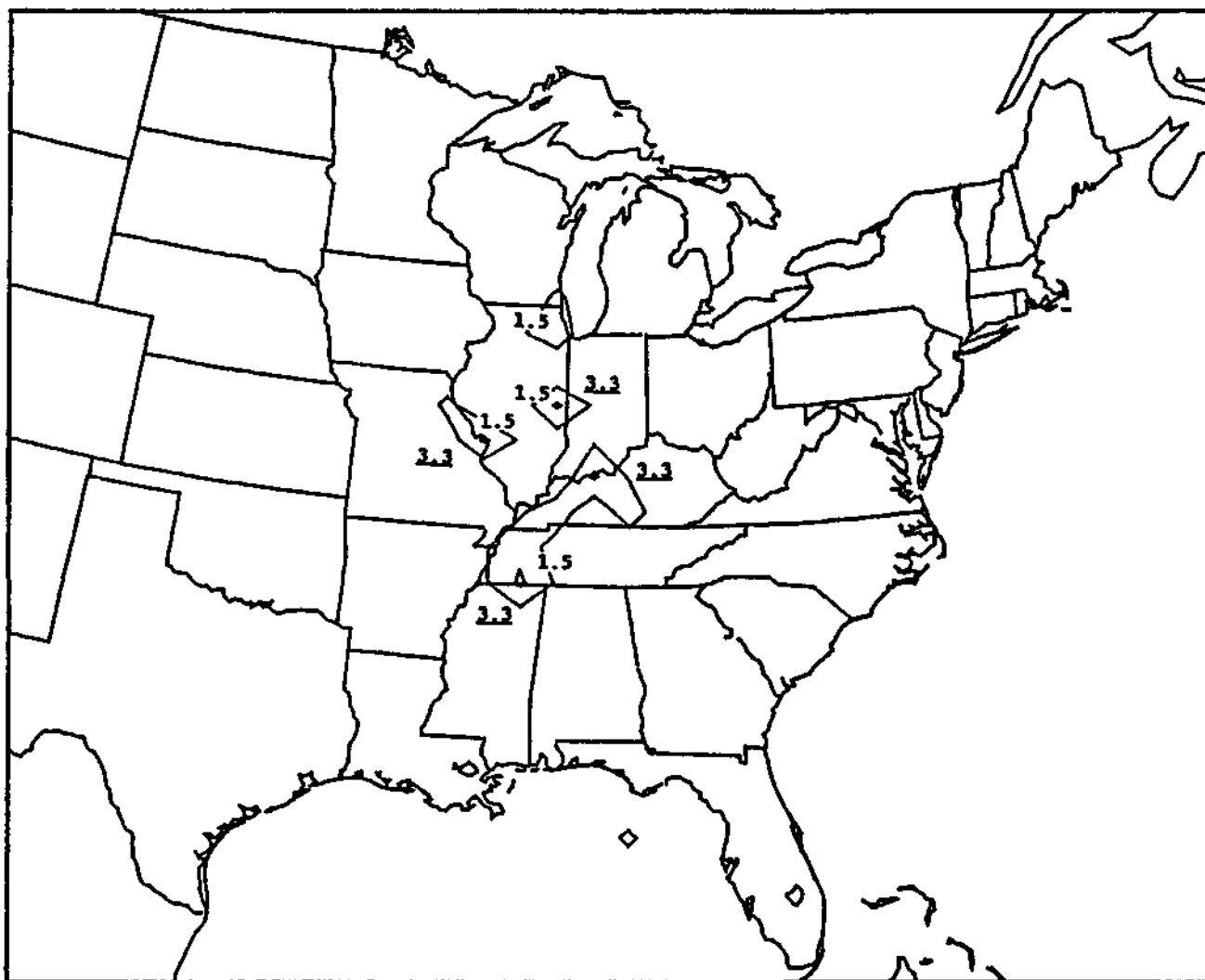


Figure 39. Percentage contours of back trajectory locations for endpoints 18 hours back in time for all storms related to chemistry samples having NO_3 fluxes in the 35th to 65th percentile range for fall and winter. Contour interval is 1.5% with grid square maxima values underlined. Total number of trajectories in domain is 154.

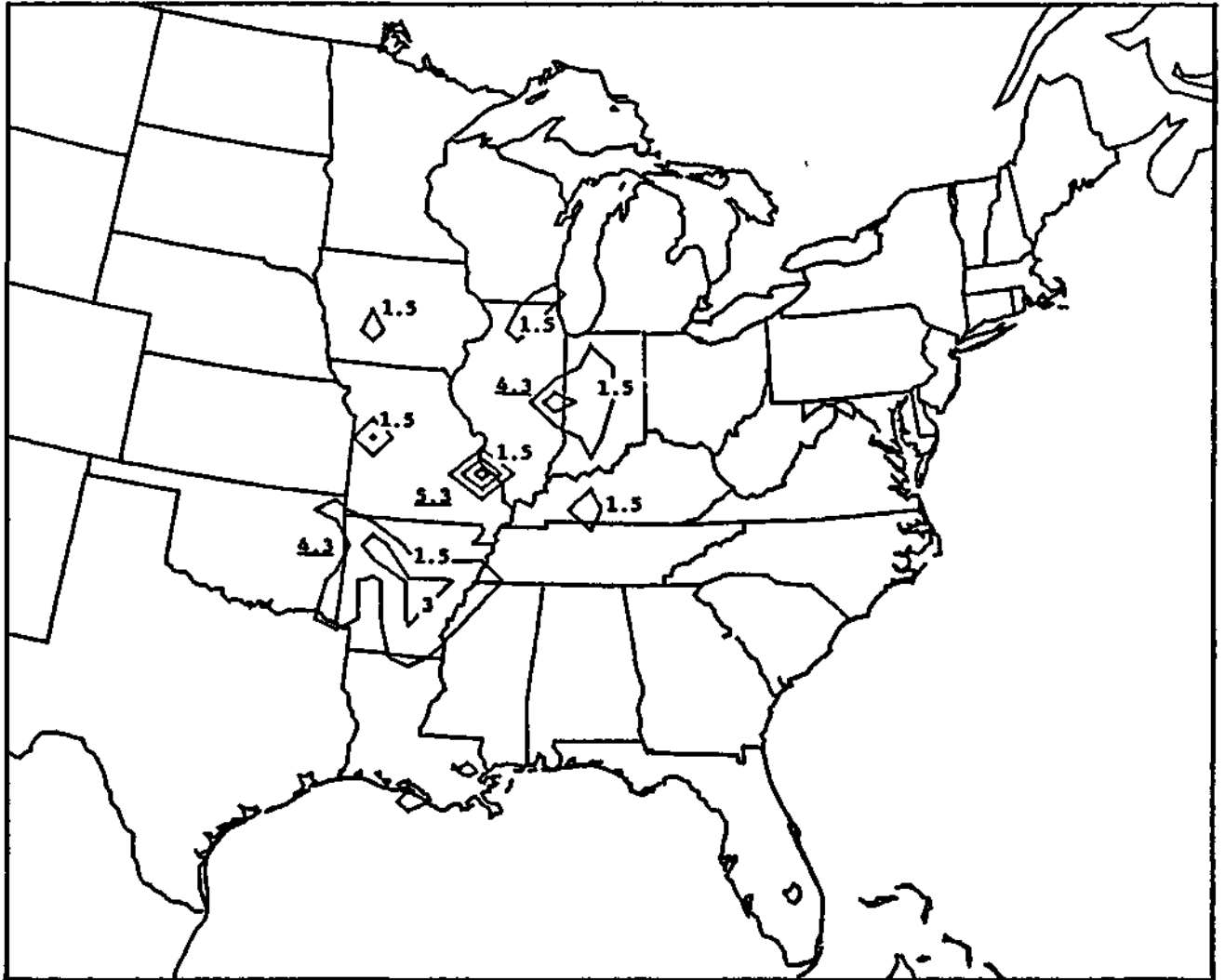


Figure 40. Percentage contours of back trajectory locations for endpoints 18 hours back in time for all storms related to chemistry samples having NO_3 fluxes in the 65th to 95th percentile range for fall and winter. Contour interval is 1.5% with grid square maxima values underlined. Total number of trajectories in domain is 94.

trajectories over Illinois and Missouri with a maximum over the St. Louis area. The middle flux pattern had four scattered groups, the largest of which was located over Kentucky and Tennessee and had 22 trajectories. The upper flux category had even more scatter in the groups, with the largest located primarily over Arkansas with 25 trajectories. The distance from the major groups to the Bondville site indicated faster transport winds for the middle and upper flux categories than the lower category. Only the major group over Illinois for the lower flux category was over high emission areas.

Pattern for 12 hours. The patterns for the lower and middle flux categories at the 12 hour mark were very similar, both having one major group with maxima over the Bondville site and extending to the south or southwest across Illinois as observed in Figures 41-42. The pattern for the same time period for the upper flux category in Figure 43 shows basically one major group of 67 trajectories but disjointed into three areas: one in northern Illinois, one over adjacent parts of Illinois and Indiana, and one over Missouri and Arkansas. No striking difference was seen between the three categories in terms of the major groups and their relationship to emission areas.

Pattern for 6 hours. The 6 hour patterns for the lower, middle, and upper flux categories in Figures 44-46 were again very similar. With the groups defined as those enclosed by the 2.5% contour, all were over Illinois with a predominant westerly flow for the lower flux category and a predominant southwesterly flow for the middle and upper flux categories. The larger surface area of the main group in the upper flux category indicated relatively higher transport wind speeds for that flux classification. Compared to the groups at 12 hours, it appeared that air parcels for the lower and upper categories were exposed to high emission areas in southwestern Illinois more than the middle flux case.

Conclusions. As in the cool SO₄ flux analysis, little correspondence was seen between the back trajectory and emission patterns with respect to the three flux categories. The same three possible explanations also apply in the apparent discrepancies: model error, poor collection efficiencies, and lack of vertical motion in the trajectory calculations.

SUMMARY

Back trajectory analyses were performed on precipitation chemistry data collected near Bondville, Illinois for the period 1981-1985. The data were divided into warm season (March-August) and cool season (September-February) groups. Sample SO₄ and NO₃ depositions ($\mu\text{eq}/\text{m}^2$) were converted to fluxes ($\mu\text{eq}/\text{m}^2/\text{hour}$) by dividing by the total precipitation time during the sample. The SO₄ and NO₃ fluxes for each season were then divided into lower, middle, and upper percentile categories.

The upper percentile flux categories for both SO₄ and NO₃ for the warm season had back trajectory histories with long residence and /or multiple exposure to high emission areas of SO_x and NO_x in Illinois or in locations

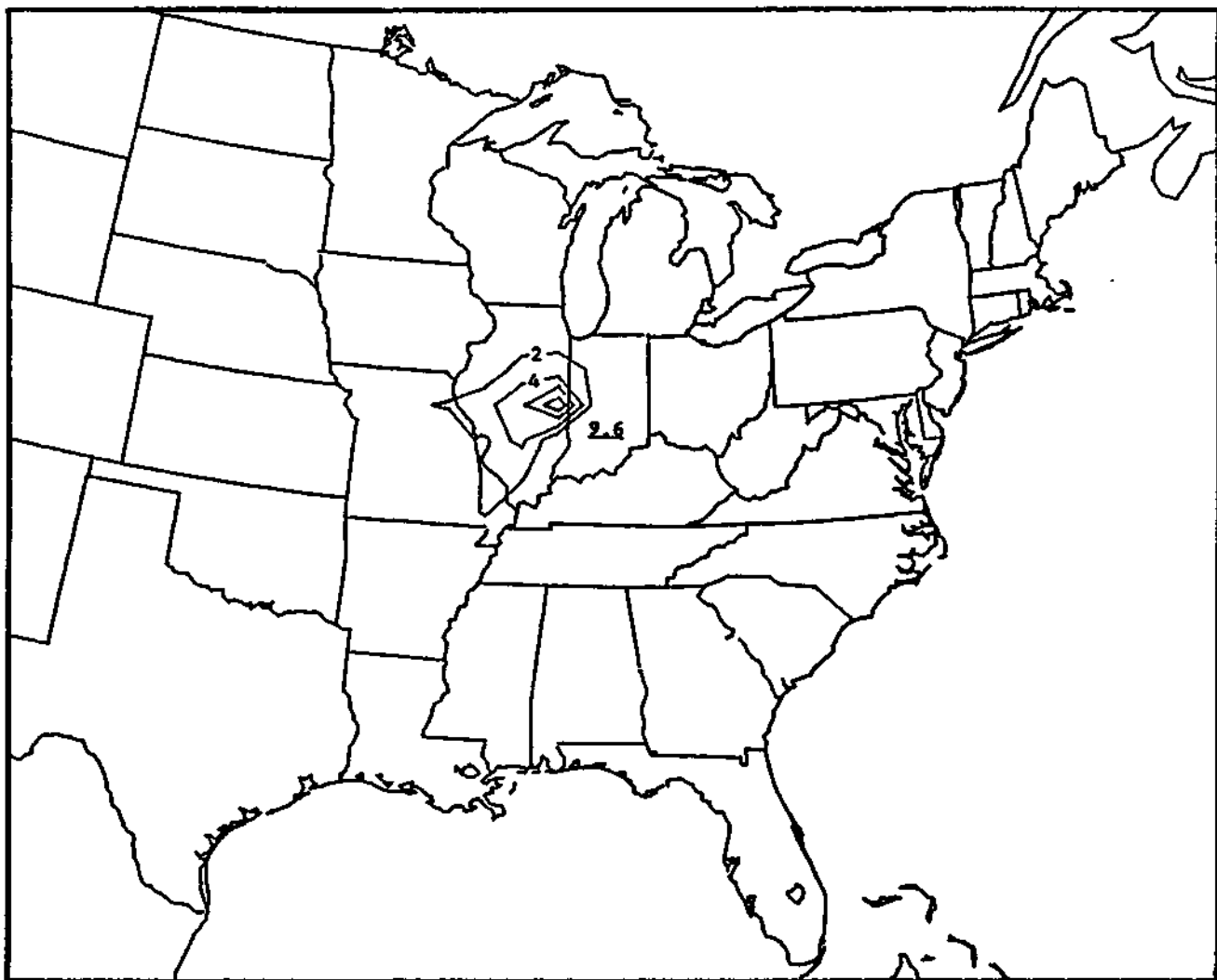


Figure 41. Percentage contours of back trajectory locations for endpoints 12 hours back in time for all storms related to chemistry samples having NO_3 fluxes in the 5th to 35th percentile range for fall and winter. Contour interval is 2.0% with grid square maxima values underlined. Total number of trajectories in domain is 177.



Figure 42. Percentage contours of back trajectory locations for endpoints 12 hours back in time for all storms related to chemistry samples having NO_3 fluxes in the 35th to 65th percentile range for fall and winter. Contour interval is 2.0% with grid square maxima values underlined. Total number of trajectories in domain is 153.



Figure 43. Percentage contours of back trajectory locations for endpoints 12 hours back in time for all storms related to chemistry samples having NO_3 fluxes in the 65th to 95th percentile range for fall and winter. Contour interval is 2.0% with grid square maxima values underlined. Total number of trajectories in domain is 99.



Figure 44. Percentage contours of back trajectory locations for endpoints 6 hours back in time for all storms related to chemistry samples having NO_3 fluxes in the 5th to 35th percentile range for fall and winter. Contour interval is 2.5% with grid square maxima values underlined. Total number of trajectories in domain is 177.



Figure 45. Percentage contours of back trajectory locations for endpoints 6 hours back in time for all storms related to chemistry samples having NO_3 fluxes in the 35th to 65th percentile range for fall and winter. Contour interval is 2.5% with grid square maxima values underlined. Total number of trajectories in domain is 151.



Figure 46. Percentage contours of back trajectory locations for endpoints 6 hours back in time for all storms related to chemistry samples having NO_3 fluxes in the 65th to 95th percentile range for fall and winter. Contour interval is 2.5% with grid square maxima values underlined. Total number of trajectories in domain is 99.

in nearby states. In addition, the upper percentile flux categories for SO_4 and NO_3 for the warm season were dominated by shower and thunderstorm activity associated with cold and stationary fronts.

The three percentile categories for both ions during the cool season did not show such a clear relationship between trajectory and emission patterns. Among other reasons, the most important is likely the lack of vertical motion in the trajectory calculations, which can be a serious omission for baroclinic systems.

A thorough statistical analysis needs to be done on this data set to quantify the extent to which transport wind speed and location downwind determine the variance of flux or deposition as opposed to other factors such as precipitation rate, sample volume, and number of dry hours between storms. Visual inspection of the results in this chapter seems to indicate that the meteorology of transport from emission areas plays a key role.

ACKNOWLEDGEMENTS

This research has been funded as part of the National Acid Precipitation Assessment Program by the U.S. Department of Energy under Contract Number DE-AC02-76EV01199. Linda Riggin developed the emission maps, while Lois Staggs performed the laborious tasks of synoptic typing and the checking of raingage charts.

REFERENCES

- Ashbaugh, L. L., 1983: A statistical trajectory technique for determining air pollution source regions. J. Air Pollut. Control Assoc., 33, 1096-1098.
- Bowersox, V. C, 1984: Data validation procedures for wet deposition samples at the Central Analytical Laboratory of the National Atmospheric Deposition Program. In: Johnson, T. R. and S. J. Penkala, Editors, Transactions-APCA International Specialty Conference on Quality Assurance in Air Pollution Measurements. APCA, Pittsburgh, PA, pp 500-524.
- Changnon, S. A. Jr., 1959: Summary of weather conditions at Champaign-Urbana, Illinois. Bulletin No. 47, Illinois State Water Survey, 2204 Griffith Drive, Champaign, IL.
- Changnon, S. A. Jr. and F. A. Huff, 1987: Design of the 1986 Illinois Weather Modification Experiment. J. Weather Modification. 19.

- Gatz, D. F., W. R. Barnard, and G. J. Stensland, 1985: Dust from unpaved roads as a source of cations in precipitation. Paper 85-6B.6, 78th Annual APCA Meeting, Detroit, MI, 16 pp.
- Heffter, J. L., 1980: Air Resources Laboratories Atmospheric Transport and Dispersion Model (ARL_ATAD). NOAA Tech. Memo. ERL ARL-81; Air Resources Laboratories, Silver Springs, Maryland.
- Hopke, P. K., 1986: Ambient air monitoring to assess the impact of the Abbott Power Plant reconversion project. Contract report to the Illinois Department of Energy and Natural Resources, ENR Contract No. ER-3.
- Kahl, J. D. and P. J. Samson, 1986: Uncertainty in trajectory calculations due to low resolution meteorological data. J. Climate Appl. Meteor. 25, 1816-1831.
- Kuo, Y. H., M. Skumanich, P. L. Haagenson and J. S. Chang, 1985: The accuracy of trajectory models as revealed by the Observing System Simulation Experiments. Mon. Wea. Rev., 113, 1852-1867.
- Lockard, J. M., 1987. Quality assurance report, NADP/NTN deposition monitoring: laboratory operations, Central Analytical Laboratory, July 1978-December 1983. NADP/NTN Coordinator's Office, Natural Resource Ecology Laboratory, Colorado State University, Ft. Collins, CO, 186 pp.
- Peden, M. E. and L. M. Skowron, 1978: Ionic stability of precipitation samples. Atmos Environ., 12, 2343-2349.
- Peden, M. E., S. R. Bachman, C. J. Brennan, B. Demir, K. O. James, B. W. Kaiser, J. M. Lockard, J. E. Rothert, J. Sauer, L. M. Skowron, and M. J. Slater, 1986: Methods for collection and analysis of precipitation. Illinois State Water Survey, 2204 Griffith Drive, Champaign, IL, 276 PP
- Robertson, J. R., 1987: NADP/NTN Site Directory (In Press).
- SAS (Statistical Analysis System), 1982: SAS User's Guide: Statistics. SAS Institute Inc., North Carolina, 584 pp.
- Stensland, G. J., M. E. Peden, and V. C. Bowersox, 1983: NADP quality control procedures for wet deposition sample collection and field measurements. Paper 83-32.2, 76th Annual APCA Meeting, Atlanta, GA, 20 pp.
- Thorp, J. M., 1986: Mesoscale storm and dry period parameters from hourly precipitation data. Atmos. Environ., 20, 1683-1689.
- Volchok, H. L. and R. T. Graveson, 1975: Wet/dry fallout collection. In: Proc. 2nd Federal Conf. on the Great Lakes, pp 259-264.
- Wilson, J. W. and V. A. Mohnen, 1982: An analysis of spatial variability of the dominant ions in precipitation in the eastern United States. Water. Air Soil Pollut., 18, 199-213.

CHAPTER 7

INTERLABORATORY COMPARISONS OF REFERENCE PRECIPITATION SAMPLES

Mark E. Peden and Jacqueline M. Lockard

INTRODUCTION

The analytical chemistry laboratory has continued its participation in the interlaboratory comparisons of precipitation chemical analyses sponsored by the World Meteorological Organization (WMO). In the past three years our involvement in international precipitation chemistry intercomparisons has expanded to include participation in studies conducted by the Canadian Long Range Transport of Atmospheric Pollutants (LRTAP) Program and the European Monitoring and Evaluation Program (EMEP) carried out by the Norwegian Institute for Air Research. These programs provide valuable data on the comparability of chemical determinations made at geographically disperse laboratories as well as documentation of the analytical procedures that are being utilized for precipitation chemistry measurements. This data base is an important source of information when comparing chemical results from different monitoring programs. Summaries of these programs and results from our laboratory are presented below.

WORLD METEOROLOGICAL ORGANIZATION (WMO) PROGRAM

Since 1977, the Illinois State Water Survey (ISWS) laboratory has been receiving synthetic precipitation samples from the U.S. Environmental Protection Agency - Precipitation Reference Laboratory (PRL) at Research Triangle Park, North Carolina. This facility is operated within the framework of the WMO Background Air Pollution Monitoring Network. These samples contain nineteen chemical constituents at levels normally found in precipitation samples. Included in these nineteen constituents are seven trace metals that are commonly found in precipitation. Laboratories receiving the samples are asked to perform chemical analyses for all parameters for which they routinely report results. The methods used are left to the discretion of each laboratory. The chemical results are forwarded to the PRL with methods documentation for each parameter measured.

Samples are distributed on a semiannual basis with analytical results due to the PRL office four to six weeks after receipt. A summary of the Water Survey results from the past five intercomparison studies are presented in Table 1. Included in this table are the mean percent deviations from the recommended values reported by the Water Survey laboratory compared to the performance of all laboratories. Outliers were removed from the combined laboratory data set prior to tabulating the percent deviations shown in the table. The following protocols (Lampe and Puzak, 1981) were used to select outlier data values:

Table 1. Summary of results from the World Meteorological Organization (WMO) Interlaboratory Comparison of Reference Precipitation Samples.^a

Laboratory Intercomparison #	Date	Number of Participating Labs (N)	Mean % Deviation From Expected Value ^b	
			All Laos	ISWS Lao
Nine	10/84	25	43.82	6.49
Ten	04/85	27	33.04	3.61
Eleven	10/85	23	19.19	3.57
Twelve	04/86	26	25.94	3.16
Thirteen	10/86	23	25.93	2.32

a
Chemical parameters used in tabulations: Ca, Mg, Na, K, NH₄, NO₃,
Cl, SO₄, pH, specific
conductance

b
Mean % Deviation =
$$\sum \left[\frac{|\text{Expected Value} - \text{Reported Value}|}{\text{Expected Value}} \times 100 \right]$$

10 (Constituents)

1. A mean and standard deviation were determined for all available data.
2. All data more than one standard deviation away from the first mean were rejected and a new mean and standard deviation determined.
3. If less than 67% of the data remained after step 2, the limits of acceptance were increased by 0.1 standard deviation until 67% of the data were included.

Most of the laboratories involved with this program do not routinely include trace metals in their analytical results. Consequently, only the 10 major chemical and physical parameters that are routinely measured by a large percentage of laboratories are included in the Table 1 summary. For each intercomparison, the data presented include pooled results for the three samples containing each of the measured ions at varying concentrations.

Examination of Table 1 indicates that our laboratory has continued to provide high quality analytical determinations as an integral part of our overall research effort. Throughout the past three years, the ISWS results have consistently yielded mean percent deviations of 2-6%. At the same time, however, the performance of the laboratories as a group, as indicated by the average percent deviation values listed in Table 1, has varied from 19-44%. If outlier values had not been removed from the overall laboratory data set, the percentage deviations for the laboratories as a whole would have been considerably larger (28-52%).

LONG RANGE TRANSPORT OF ATMOSPHERIC POLLUTANTS (LRTAP) PROGRAM

The Canadian Long Range Transport of Atmospheric Pollutants (LRTAP) Program involves many different federal and provincial laboratories producing data for various national and regional programs within that country (Aspila, et al., 1985). To assess the comparability of the data being produced, interlaboratory studies were initiated in December 1982. Under the direction of the Quality Assurance and Methods Division of the National Water Research Institute, samples were prepared and distributed to 20 laboratories in Canada for analysis. The first set of sixteen samples was primarily lake water with one composite precipitation and three synthetic preparations. As the program developed, the number of laboratories participating grew to include several from the United States, and the frequency of the studies expanded to three times per year. Two of the annual studies focus on the routine analysis of both hard (lakes, rivers, etc.) and soft (precipitation) waters and the third, on less routine analyses (trace metals, metal speciation, pH).

In August 1983, the ISWS laboratory was first asked to participate in these interlaboratory comparability studies because of our long-standing involvement in precipitation chemistry measurements. Since this first

request, the ISWS has regularly participated in the semiannual inter-comparisons of "Major Ions, Nutrients and Physical Properties in Water." The parameters included in each study are: specific conductance, pH, nitrate/nitrite, ammonia, sodium, magnesium, sulfate, chloride, potassium, and calcium. The methods employed for these analyses include electrometric analysis, conductimetric analysis, atomic absorption spectroscopy, ion chromatography, and automated wet chemistry.

A summary of the results of five performance studies (Studies 6, 8, 9, 10, and 11) was issued in May 1986. It ranked the 51 participating laboratories according to the accuracy of the data submitted. Of these 51 labs, only 25 (including the ISWS) had participated in all five inter-comparisons. The Water Survey results were ranked first among the 51 participating labs with an average score of 2.0%. This score reflects the average percentage of results that had been flagged from all five studies for either high or low bias. For comparison purposes, the mean five year score for all 51 laboratories was 34.6%. The ISWS has continued its participation in this program and has recently completed the analyses for Study 14. A summary of the performance of our laboratory relative to the other participating laboratories is presented in Table 2. As Table 2 indicates, our results have consistently been characterized by a lack of any significant bias for the ten major constituents measured in atmospheric deposition samples.

EUROPEAN MONITORING AND EVALUATION PROGRAM (EMEP)

The third international program that our laboratory is participating in is sponsored by the Norwegian Institute for Air Research in Lillestrom, Norway. Designated the EMEP, this project is designed to assess the comparability of analytical methods in use by European laboratories conducting research in the area of acidic deposition. This program is a cooperative effort of the United Nations Economic Committee for Europe as a part of the monitoring and evaluation of the long range transport of air pollutants in that region.

Four synthetic precipitation samples containing known amounts of sulfate, nitrate, ammonium, strong acid, magnesium, sodium, chloride, calcium, and potassium are provided to each laboratory participating in this study with the results forwarded to the Norwegian Institute for compilation and data reporting. Supporting methods documentation and quality assurance protocols in use at each facility are also provided. The ISWS laboratory was first invited to participate in this program in 1984 and has subsequently provided analytical results and methods documentation for two inter-comparisons. Data summaries of the ISWS measured results compared with the calculated concentrations are presented in Tables 3 and 4. No data on the performance of our laboratory relative to the rest of the EMEP participants is available, however, the mean percent deviation of the ISWS results for both studies was approximately 4%. This value is consistent with the mean percent deviations reported from the WMO and LRTAP inter-comparisons.

Table 2. Summary of results from the Long Range Transport of Atmospheric Pollutants (LRTAP) Program laboratory intercomparison studies.

Laboratory Study #	Date	Number of Participating Labs (N)	Average Score (%) ^a	
			All Labs	ISWS Lao
L-6	04/84	39	31.68	0.00
L-8	11/84	44	33.14	0.00
L-9	04/85	32	27.44	0.00
L-10	08/85	42	26.98	0.00
L-11	12/85	40	31.92	10.00
L-12	04/86	45	32.07	4.10
L-14	12/86	46	28.04	0.00

^a Average score equals the combined percent of results that were either flagged or biased. If all results were flagged and determined to be biased, a maximum score of 200% is possible.

Table 3. Summary of results from the European Monitoring and Evaluation Program (EMEP).

STUDY NUMBER EIGHT - 1984

Constituent	Units	Sample No.	Calculated Value	ISWS Value	Bias, mg/L ISWS - Calc.	Bias, % ^a
SO ₄	mg S/L	G1	1.70	1.56	-0.14	-8.2
		G2	2.61	2.57	-0.04	-1.5
		G3	2.84	2.80	-0.04	-1.4
		G4	1.83	1.73	-0.10	-5.5
NO ₃	mg N/L	G1	0.96	0.958	-0.002	-0.2
		G2	0.55	0.551	0.001	0.2
		G3	0.47	0.468	-0.002	-0.4
		G4	1.09	1.09	0.00	0.0
NH ₄	mg N/L	G1	0.24	0.210	-0.030	-12.5
		G2	0.20	0.171	-0.029	-14.5
		G3	0.87	0.863	-0.007	-0.8
		G4	1.09	1.06	-0.03	-2.8
pH	pH units	G1	4.24	4.28	0.04 ^b	-8.8 ^c
		G2	4.78	4.78	0.00 ^b	-0.0 ^c
		G3	4.88	4.85	-0.03 ^b	7.2 ^c
		G4	4.16	4.18	0.02 ^b	-4.5 ^c
Mg	mg/L	G1	0.46	0.444	-0.016	-3.5
		G2	0.40	0.386	-0.014	-3.5
		G3	0.10	0.097	-0.003	-3.0
		G4	0.08	0.077	-0.003	-3.8

^a Percent Bias = Bias/Calculated Value X 100

^b Bias values in pH units

^c Percent bias in microequivalents per liter

^d Bias values in uS/cm

Table 3. (Continued)

STUDY NUMBER EIGHT - 1984

Constituent	Units	Sample No.	Calculated Value	ISWS Value	Bias, mg/L ISWS - Calc.	Bias, %
Na	mg/L	G1	1.57	1.54	-0.03	-1.9
		G2	3.59	3.44	-0.15	-4.2
		G3	3.99	3.84	-0.15	-3.8
		G4	1.80	1.76	-0.04	-2.2
Cl	mg/L	G1	2.33	2.32	-0.01	-0.4
		G2	2.13	2.13	0.00	0.0
		G3	2.69	2.69	0.00	0.0
		G4	3.14	3.15	0.01	0.3
Ca	mg/L	G1	0.97	0.962	-0.008	-0.8
		G2	0.58	0.577	-0.003	-0.5
		G3	0.46	0.461	0.001	0.2
		G4	0.89	0.884	-0.006	-0.7
K	mg/L	G1	0.43	0.429	-0.001	-0.2
		G2	0.52	0.505	-0.015	-2.9
		G3	0.22	0.213	-0.007	-3.2
		G4	0.17	0.172	0.002	1.2
Conductivity	uS/cm	G1	44.0	46.6	2.6 ^d	5.9
		G2	35.6	38.3	2.7 ^d	7.6
		G3	38.3	41.0	2.7 ^d	7.0
		G4	52.7	56.1	3.4 ^d	6.4

a Percent Bias = Bias/Calculated Value X 100
b Bias values in pH units
c Percent bias in microequivalents per liter
d Bias values in uS/cm

Table 4. Summary of results from the European Monitoring and Evaluation Program (EMEP).

STUDY NUMBER NINE - 1986

Constituent	Units	Sample No.	Calculated Value	ISWS Value	Bias, mg/L ISWS - Calc.	Bias, % ^a
SO ₄	mg S/L	G1	1.59	1.65	0.06	3.8
		G2	2.93	2.98	0.05	1.7
		G3	1.51	1.58	0.07	4.6
		G4	3.15	3.22	0.07	2.2
NO ₃	mg N/L	G1	1.23	1.25	0.02	1.6
		G2	0.19	0.21	0.02	10.5
		G3	1.33	1.36	0.03	2.2
		G4	0.23	0.25	0.02	8.7
NH ₄	mg N/L	G1	0.21	0.17	-0.04	-19.0
		G2	0.24	0.19	-0.05	-20.8
		G3	1.20	1.15	-0.05	-4.2
		G4	1.08	1.01	-0.07	-6.5
pH	pH units	G1	4.05	4.04	-0.01 ^b	2.3 ^c
		G2	4.66	4.52	-0.14 ^b	38.0 ^c
		G3	4.07	4.05	-0.02 ^b	4.7 ^c
		G4	4.59	4.45	-0.14 ^b	38.0 ^c
Mg	mg/L	G1	0.48	0.468	-0.012	-2.5
		G2	0.41	0.402	-0.008	-2.0
		G3	0.06	0.056	-0.004	-6.7
		G4	0.07	0.069	-0.001	-1.4

^a Percent Bias = Bias/Calculated Value X 100
^b Bias values in pH units
^c Percent bias in microequivalents per liter
^d Bias values in uS/cm

Table 4. (Continued)

STUDY NUMBER NINE - 1986

Constituent	Units	Sample No.	Calculated Value	ISWS Value	Bias, mg/L ISWS - Calc.	Bias, %
Na	mg/L	G1	2.02	1.99	-0.03	-1.5
		G2	3.02	2.98	-0.04	-1.3
		G3	2.18	2.14	-0.04	-1.8
		G4	3.37	3.34	-0.03	-0.9
Cl	mg/L	G1	2.27	2.26	-0.01	-0.4
		G2	2.09	2.08	-0.01	-0.5
		G3	3.32	3.24	-0.08	-2.4
		G4	3.08	3.10	0.02	0.6
Ca	mg/L	G1	0.19	0.189	-0.001	-0.5
		G2	0.86	0.851	-0.009	-1.0
		G3	0.16	0.159	-0.001	-0.6
		G4	0.80	0.801	0.001	0.1
K	mg/L	G1	0.36	0.394	0.034	9.4
		G2	0.30	0.303	0.003	1.0
		G3	0.12	0.126	0.006	5.0
		G4	0.15	0.158	0.008	5.3
Conductivity	uS/cm	G1	58.5	61.2	2.7 ^d	4.6
		G2	40.2	43.3	3.1 ^{d, a}	7.7
		G3	62.6	65.4	2.8 ^{d, a}	4.5
		G4	48.1	51.6	3.5 ^d	7.3

^a Percent Bias = Bias/Calculated Value X 100

^b Bias values in pH units

^c Percent bias in microequivalents per liter

^d Bias values in uS/cm

Continued participation in interlaboratory comparisons such as these is an overall part of our analytical laboratory's quality assurance program. The reputation of our laboratory facility is based in part on its performance on interlaboratory cooperative efforts such as this. In addition to providing an independent assessment of the accuracy of our laboratory measurements, the methods documentation supplied with the analytical results forms a data base that can be used by all participants to compare their methodologies to those used by other laboratories.

REFERENCE

- Lampe, R. L., and J. C. Puzak, 1981: Fourth Analysis of Reference Precipitation Samples by the Participating World Meteorological Organization Laboratories. World Meteorological Organization, Geneva, Switzerland.
- Aspila, K. I., and S. Todd, 1985: LRTAP Intercomparison Study L-8: Major Ions, Nutrients, and Physical Properties in Water. National Water Research Institute, Burlington, Ontario, Canada.
- Aspila, K. I., G. Dookhran, P. Leishman, and S. Todd, 1985: LRTAP Intercomparison Study L-9: Major Ions, Nutrients, and Physical Properties in Water. National Water Research Institute, Burlington, Ontario, Canada.

CHAPTER 8

QUALITY ASSURANCE OF PRECIPITATION CHEMISTRY ANALYSES USING ION BALANCE CALCULATIONS

Jacqueline M. Lockard

INTRODUCTION

The National Atmospheric Deposition Program (NADP) was initiated in 1978 to assess spatial and temporal trends in precipitation chemistry within the United States. Organized under the auspices of the State Agricultural Experiment Stations, this network was designed to assess both the deleterious and beneficial effects of atmospheric deposition on a national scale (Stensland, et al., 1980). From the beginning of the program, the Illinois State Water Survey (ISWS) has been responsible for the chemical analyses of precipitation and dry deposition samples generated from the monitoring network. Over 50,000 wet deposition samples representing 200 sites have already been processed by the ISWS Laboratory.

A rigorous internal quality assurance program has been developed to ensure that the laboratory measurements are of the highest quality. As a part of this program, each sample analysis is verified by the use of an ion balance calculation. The ion balance data have been used in part to develop objective criteria for the reanalysis of samples on a routine basis. A closer examination of these data has revealed patterns in the ion ratios that are a function of sample pH, site location, and collection season. These patterns are discussed in terms of how to most effectively utilize ion balance data to verify the accuracy of laboratory measurements.

ION BALANCE CALCULATION

Ion balance calculations are a valuable component of the laboratory quality assurance program. A large imbalance can be indicative of an error in analysis. It may also be an indication that additional ionic species are present in the sample and that further analyses are necessary to completely characterize the sample. By selecting a maximum allowable imbalance and reanalyzing all samples with an imbalance greater than this maximum, an imbalance that resulted from analytical error can be detected.

An ion balance may be calculated using one of several different methods. Figure 1 presents four commonly employed methods and demonstrates how the results obtained from each can be compared to those derived from the other methods. The calculation may vary from a simple ion ratio as utilized by the NADP in its annual data summaries (NADP/NTN, 1985) to the more complex calculations recommended by the US Environmental Protection Agency (USEPA) (Topol, et al., 1985). Although similar to the

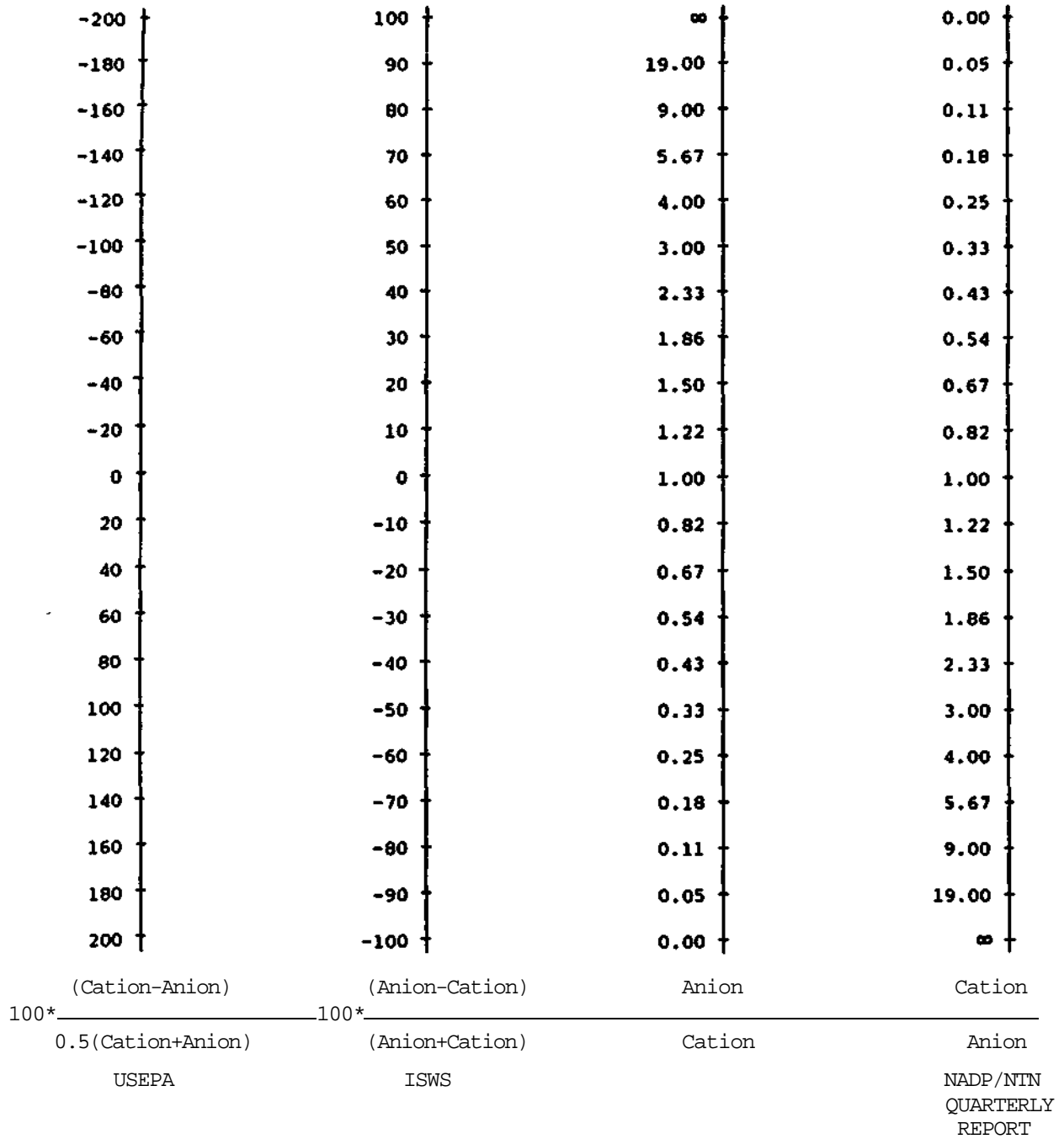


Figure 1. Comparison of ion balance calculation methods.

calculation method employed by the ISWS, the formula for the calculation recommended by the American Society for Testing and Materials (ASTM) (ASTM, 1983) presents still another method. The ASTM method employs the formula:

$$\text{Percentage Error} = \frac{\text{Cations} - \text{Anions}}{\text{Cations} + \text{Anions}} \times 100$$

It is important to know which method a laboratory employs, not only for purposes of data comparisons, but also for data interpretations, particularly when this information will be used to evaluate laboratory performance.

The calculation method employed by the ISWS is more completely described as follows:

$$\text{Ion Percent Difference (IPD)} = \frac{[\text{Anion} - \text{Cation}]}{[\text{Anion} + \text{Cation}]} \times 100, \text{ where}$$

$$\text{Anion} = [\text{SO}_4^{-2}] + [\text{NO}_3^-] + [\text{Cl}^-] +$$
$$[\text{PO}_4^{-3}] + [\text{OH}^-] + [\text{HCO}_3^-], \text{ and}$$

$$\text{Cation} = [\text{Ca}^{+2}] + [\text{Mg}^{+2}] + [\text{Na}^+] +$$
$$[\text{K}^+] + [\text{NH}_4^+] + [\text{H}^+], \text{ with}$$

all analyte concentrations expressed in microequivalents/liter.

The hydrogen ion concentration and hydroxide ion concentrations are both calculated from the measured sample pH. The bicarbonate ion concentration is also a calculated value, which assumes the sample to be in equilibrium with atmospheric carbon dioxide (Lockard, 1987). The concentration of all other analytes used in the calculation are measured in the laboratory.

The computer program that calculates an ion balance for each sample also determines the ion sum or total ionic strength of the sample. The analyte concentrations have already been converted to microequivalents per liter as part of this ion balance calculation. To obtain the ion sum, the total anion concentration expressed in microequivalents per liter is added to the total cation concentration, also in microequivalents. The formula is:

$$\text{Ion Sum (IS)} = [\text{Anion} + \text{Cation}] \text{ ueq/L}$$

Both the ion sum (IS) and the ion percent difference (IPD) are used to select samples for reanalysis. Those criteria are.

when IS < 50 ueq/L, reanalyze if IPD > ± 60%;

when 50 ueq/L IS < 100 ueq/L, reanalyze if IPD > ± 30%;

and, when IS 100 ueq/L, reanalyze if IPD > ± 15%

The original goal set by the ISWS quality assurance coordinator was to select approximately six percent of the network samples for routine reanalysis. The above criteria have proven to be adequate in obtaining that desired goal (Lockard, 1987). In 1985, with analytical data from over 30,000 samples available, a reassessment of the ion balance criteria was conducted to answer the following questions:

1. Can the ion balance data be utilized to develop a better set of criteria for the reanalysis of samples?
2. Are there regional and/or seasonal patterns in the ion balance data?
3. Are there site specific ion balance characteristics that can be used to more efficiently select samples for reanalysis?

REGIONAL AND SEASONAL PATTERNS

In order to gain a better understanding of the factors affecting ion imbalances, the distribution of the ion percent difference data was examined. Figure 2 is the histogram of ion percent difference values calculated for the network precipitation samples collected in 1984. The population includes only wet side samples with volumes greater than 35 mLs. A 35 mL sample is necessary to ensure sufficient sample for the complete analyses of the eleven parameters routinely determined in precipitation samples. In the 1984 data set there were 5442 complete sample analyses with the median ion percent difference equal to 0.9%. The mean ion percent difference for this population was 0.7% with a standard deviation of 7.6%.

The plot in Figure 2 approximates a normally distributed population with a mean difference near 0%. It indicates that 95% of the samples fall within + 15%, or within twice the standard deviation (s) of the population mean. The 5% of the data set that lie outside of the + 2s are currently being reanalyzed if the ionic strength is greater than or equal to 100 microequivalents per liter. Of those samples reanalyzed, however, only 0.1-0.2% of the concentration data is changed from that originally reported. A more rigorous examination of ion balance data was conducted to determine the feasibility of alternate reanalysis criteria using site specific information.

Regional Patterns

The 1984 network ion balance data were subsequently used to generate an isopleth map of median ion percent difference values. This map is presented in Figure 3. The 0% difference line falls in the middle of the country with the eastern half showing a positive ion percent difference and the western half, a negative difference, indicating regional differences do exist.

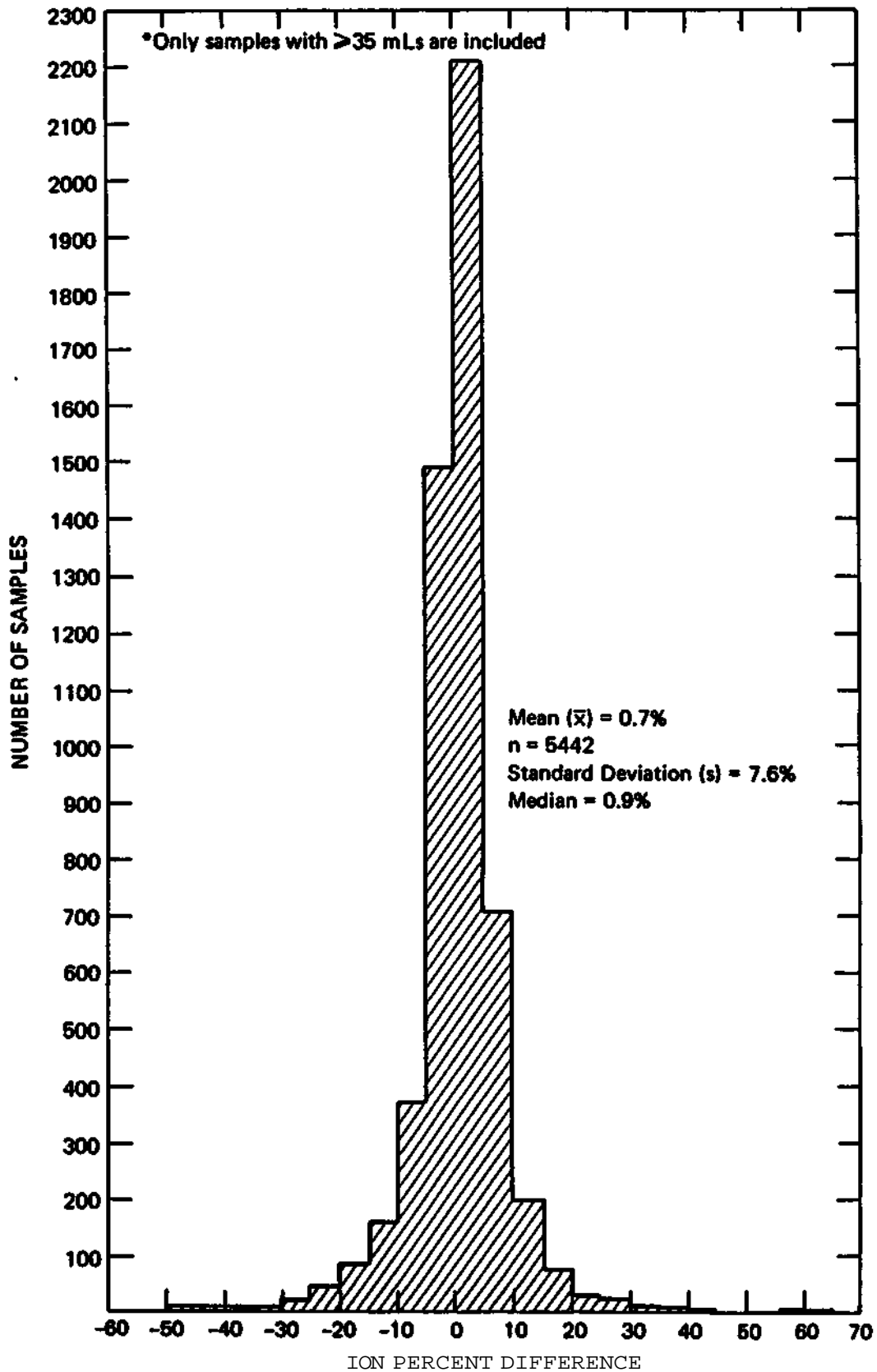


Figure 2. Ion Percent Difference histogram for 1984 NADP/NTN network data.

A positive ion percent difference results when the total measured anion concentration is greater than the total measured cation concentration. This positive difference may be the result of the presence of unmeasured cations, such as trace metal ions, in the precipitation samples collected at eastern sites. Conversely, a negative percent difference results when the total cation concentration is greater than the anion concentration. These negative differences may be due to unmeasured organic acid anions that could be present in western precipitation samples. These regional trends present a general criterion that can be used to assess data quality. Based solely on the information provided by the isopleth map in Figure 3, possible criteria would be to reanalyze the sample, or at least be concerned about the quality of the sample analysis, when:

1. the precipitation sample is from a site in the eastern half of the U.S. and the ion percent difference is negative,
2. the precipitation sample is from a site in the central part of the U.S. and the ion percent difference is not close to 0%,
3. the precipitation sample is from a site in the western half of the U.S. and the ion percent difference is positive.

These broad criteria can be further refined by examining seasonal patterns and, if they are present, by reformulating the regional criteria to include the seasonal trends.

Seasonal Patterns

In Figure 4, the 1984 data are divided into four equal seasonal units with the resultant isopleth maps showing the seasonal pattern that exists. The maps are again plots of the median ion percent difference values. The 0% difference line remains in the middle of the country, except in the winter plot. During the winter sampling period, the 0% difference line shifts well into the west and most of the network data exhibit positive ion percent differences. The data from samples collected from sites to the east of the 0% difference line are always positive and those west of the line, almost always negative. The positive differences to the east and negative differences to the west of the 0% difference contour is a pattern that remains consistent for all seasons, including winter.

Adding this seasonal trend to the regional pattern would result in only a minor modification to the broad criteria described above. That modification would be the addition of a fourth criterion that would indicate sample reanalysis when:

4. the precipitation sample is collected during the winter and the ion percent difference is negative.

Even with the addition of this criterion that includes both regional and seasonal patterns, the resultant set of reanalysis criteria is still very general and the number of samples that would be suspect would be very large. Knowing that there were patterns for the network as a whole led to

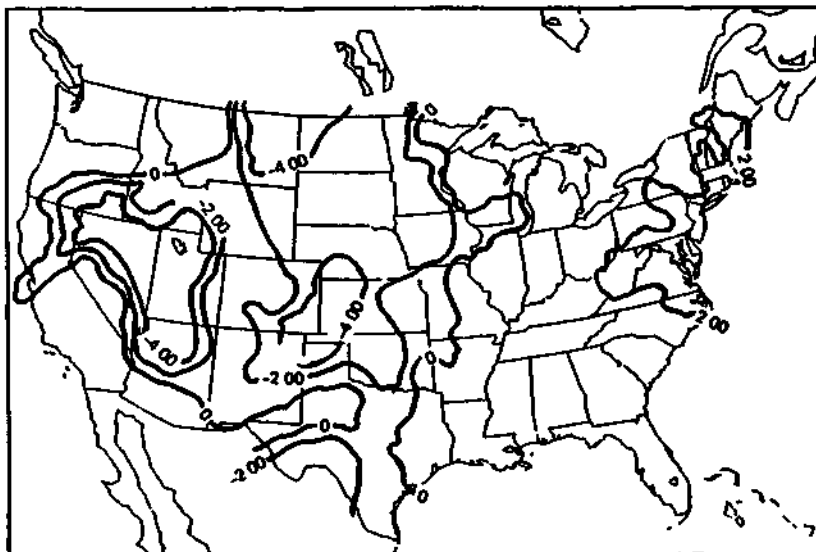


Figure 3. Isopleth map of median ion percent difference values for 1984 NADP/NTN data.

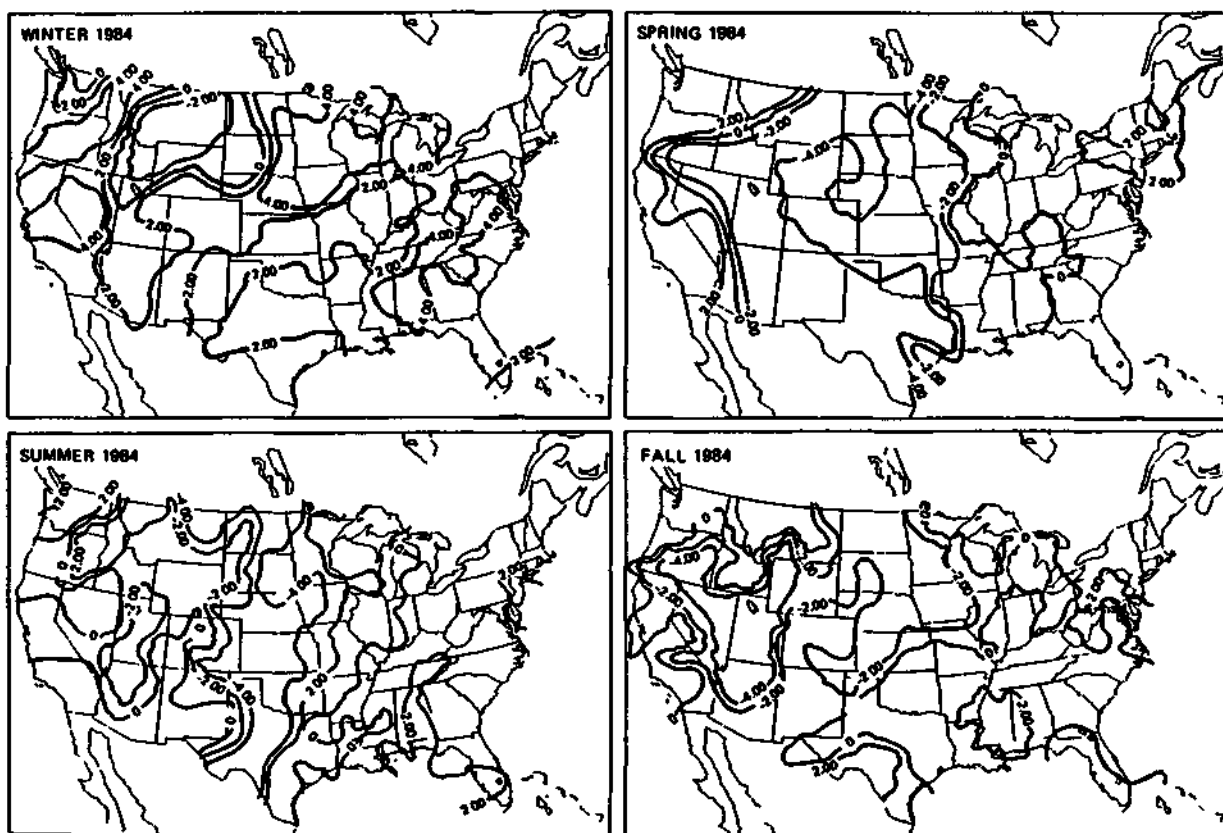


Figure 4. Isopleth maps of seasonal differences in median ion percent difference values for 1984 NADP/NTN data.

the examination of the data from individual sites to see if these overall patterns were consistent, and to explore the possibility of there being site specific patterns to use in refining the reanalysis criteria.

SITE SPECIFIC PATTERNS

Ten percent of the sites that had participated in the network throughout 1984 were selected for closer study. In addition to the ion percent difference data, precipitation amounts and pH values were used in the search for site specific patterns. Correlations between these three variables were first examined. The mean rainfall did not show any correlation to either of the other two variables and will not be discussed. There were, however, significant correlations found between the ion balance data and the sample pH values.

Site Selection

In selecting the sites to be studied in more detail, an attempt was made to select a variety of location types, i.e., coastal, agricultural, forest, prairie, etc. and to include all regions of the continental U.S. Only sites with more than 10 precipitation samples in 1984 were considered. This group was further screened by requiring that a candidate site must have been operating successfully for at least two years. From the list of those sites that remained, 15 were selected. Table 1 provides siting information as well as the annual mean precipitation for each site. Figure 5 is a map of the location of each of the sites. It should be noted that 4 (MN16, NC25, NH02, and PA29) of these 15 were among the first 7 sites with which the network started and 3 others (CA45, IL11, and OR02) have been part of the network and collecting samples since 1979.

Ion Percent Difference Data

A comparison of the percentage of times within the 1984 sampling period each site showed a positive ion percent difference and a negative ion percent difference was made. The results of this comparison are presented in Figure 6. The regional trends of predominantly positive ion percent differences in the east and negative differences in the west with the 0% difference characterizing the central U.S. is again evident. The variability of the data, however, emphasizes the inappropriateness of using only the broad criteria that resulted from the regional and seasonal analysis of the data and illustrates the need for developing more specific guidelines for data assessment. Sites such as NC25 and FL11 follow the pattern of positive median ion percent differences in the east, but have nearly as many samples with a negative difference. If only the regional/seasonal criteria were used, approximately half of the samples from these two sites would be selected for reanalysis. The likelihood that the original analyses of that many samples would be in error, is remote. The regional/seasonal criteria, while providing useful guidelines, are

Table 1. Siting Summary for Fifteen Sites Selected for the Ion Percent Difference Study.

Site ID	Site Name	Location City, State	Site Description	1984 Mean Precipitation \pm Std. Deviation
CA45	Hopland	Hopland, California	Mountain	1.06 \pm 1.11
CO19	Rocky Mountain National Park	Estes Park, Colorado	Mountain	0.42 \pm 0.39
FL11	Everglades National Park	Homestead, Florida	Coastal	1.20 \pm 1.49
IL11	Bondville	Bondville, Illinois	Agricultural	0.73 \pm 0.62
KS31	Konza Prairie	Manhattan, Kansas	Prairie	0.93 \pm 1.09
MA01	North Atlantic Coastal Lab	South Well Fleet, Massachussettes	Coastal	1.17 \pm 1.00
MN16	Marcell Experimental Forest	Grand Rapids, Minnesota	Forest	0.79 \pm 1.02
NC25	Coweeta	Otto, North Carolina	Forest	2.00 \pm 1.66
NH02	Hubbard Brook	West Thornton, New Hampshire	Mountain/Forest	1.06 \pm 0.90
OH49	Caldwell	Wooster, Ohio	Agricultural	0.80 \pm 0.62
OK25	Clayton Lake	Clayton, Oklahoma	Prairie	1.65 \pm 0.62
OR02	Alsea Guard Ranger Station	Corvallis, Oregon	Forest	1.85 \pm 1.73
PA29	Kane Experimental Forest	Milford, Pennsylvania	Forest	1.14 \pm 0.81
TN00	Walker Branch Watershed	Oak Ridge, Tennessee	Mountain/Forest	1.16 \pm 1.36
TX53	Victoria	Victoria, Texas	Coastal	0.80 \pm 0.86

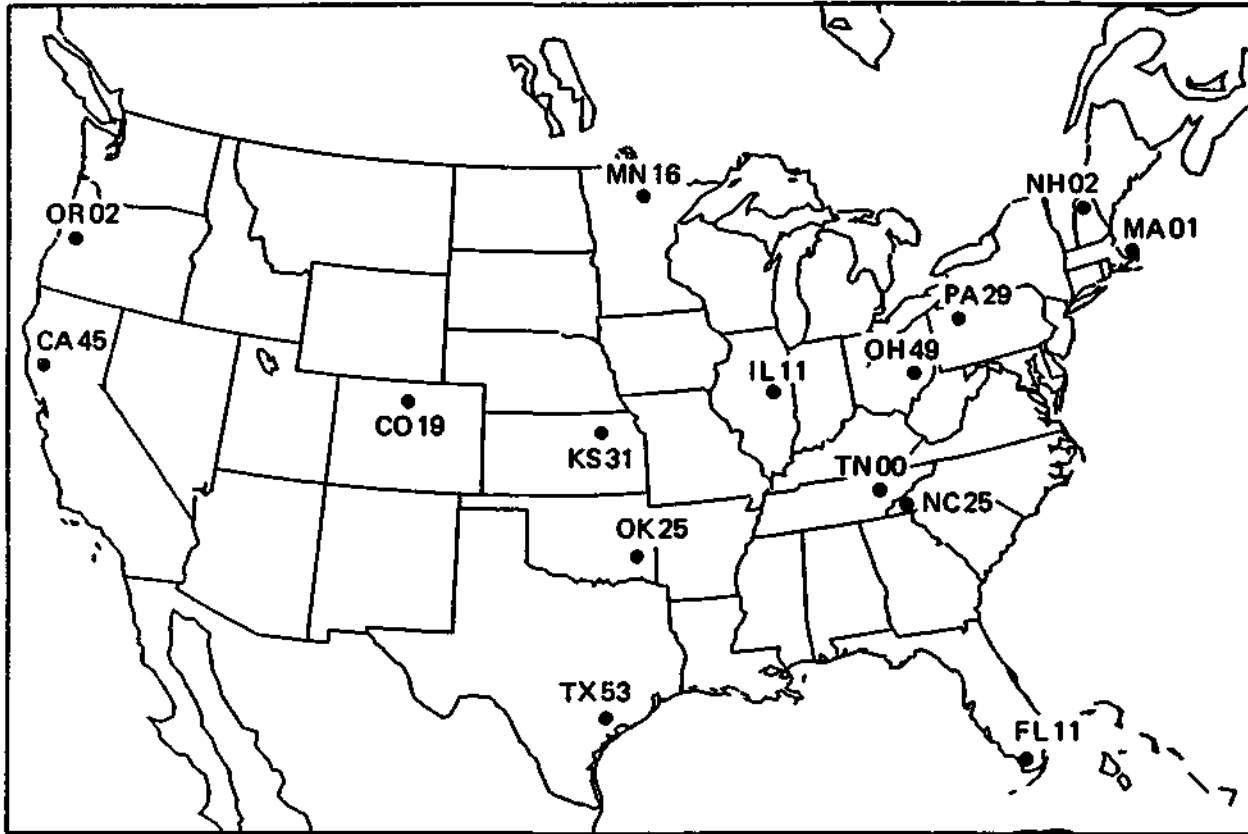


Figure 5. The location of the fifteen sites selected for the study of ion percent difference.

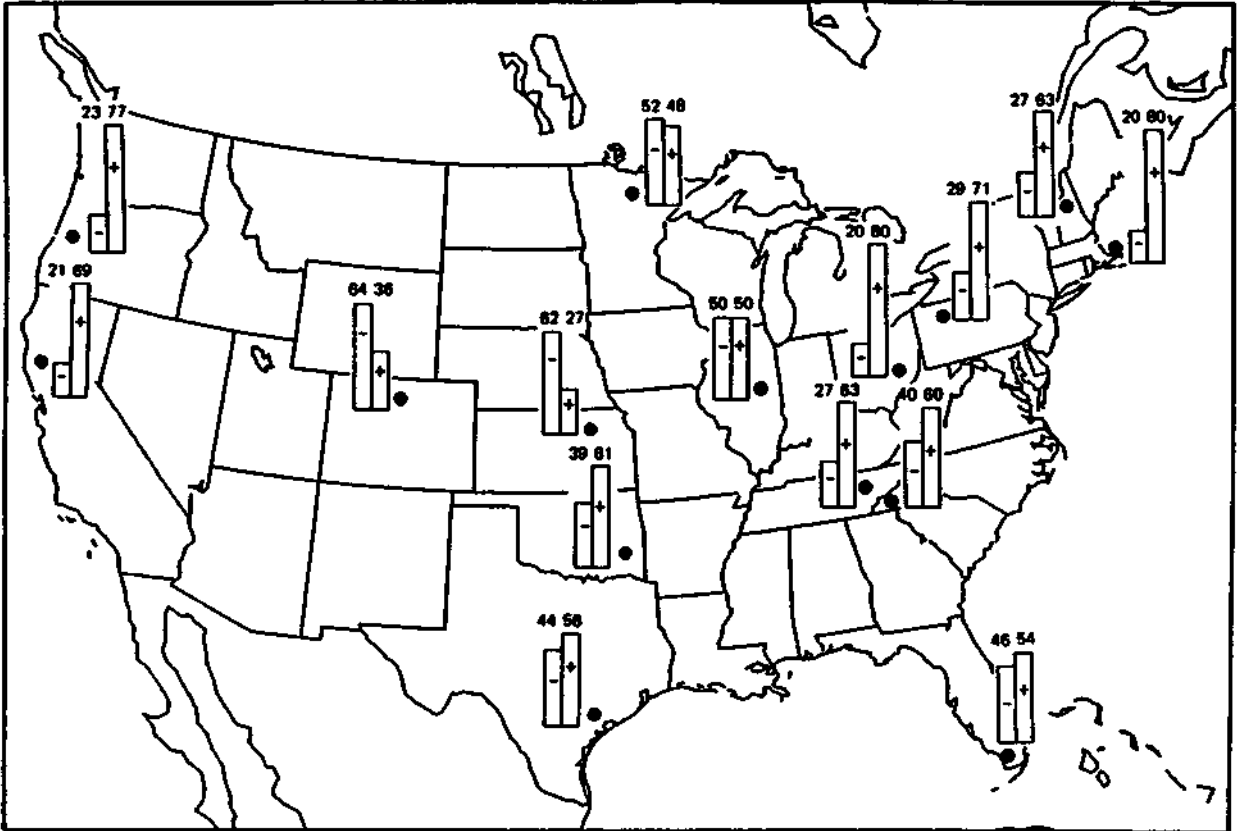


Figure 6. The percentage of negative and positive ion percent difference values in 1984 for each study site.

obviously too broad and are far less selective than the criteria in current use.

A statistical summary of the ion percent difference data and the median pH values for the 15 study sites is given in Table 2. Included in this table are the number of precipitation samples, the median ion percent difference, the mean ion percent difference and standard deviation, and the median pH for each site. The mean and standard deviation values were used in a Student's t-test to determine if the mean was statistically different from 0 at the 95th confidence interval. For 5 of the 15 study sites, the mean percent difference values were significantly different from 0. All results from this t-test are included in Table 2.

The information in Table 2 is arranged according to increasing mean ion percent different values. A comparison of the median and mean ion percent difference values for the sites indicates that these two values are typically very similar for each of the sites. This also suggests that site specific data contain few, if any, outliers. Most ion percent different values for a site will be found within a certain range that can be determined and is specific for each site. For the 15 sites in this study, the CA45 site had the largest difference between the two values, that of 1.34%, which was actually very small. These data also suggest that the closer the ion percent different is to zero, the smaller the standard deviation about the mean, conversely, the further away, the larger the standard deviation.

Ion Percent Difference Versus pH

Included in Table 2 are the median pH values for the 15 study sites. Comparing the median and mean differences with the median pH values, another pattern emerges. Those sites whose median pH values are greater than pH 5.0 are also the sites showing mean differences that deviate most from zero. These sites also typically have the largest variation in ion percent difference values. The ion percent difference data and the pH data were plotted for all fifteen sites. Eight of these plots are presented as Figures 7 through 10. These are temporal plots of all data points for 1984 from the eight selected sites. These plots show one of the correlations that can be made between ion percent difference and pH.

The plots in Figure 7 compare two northeastern sites. The pH values are all less than pH 5.0 with very little variability. The ion percent difference (IPD) plot shows the expected positive differences and the same relative lack of variability as does the plot of pH values. Figure 8 presents a plot for another northeastern site but compares the data from that site to that from a site in the northwest. The Hubbard Brook (NH02) site shows more variability in sample pH values than that found in the other two northeastern sites and has corresponding increased variability in the IPD values. The median pH for NH02 is still below pH 5.0 and the IPD values are predominately positive, as expected. The Corvallis (OR02) site shows similar variation in pH values, but has a median pH greater than pH 5.0. The IPD line on the OR02 plot shows a large degree of variation which could have been predicted from the high pH values found at the site.

Table 2. Statistical Summary of 1984 Ion Balance Data for Fifteen Study Sites.

Site	n	Median Ion % Difference	Mean Ion % Difference	Standard Deviation	Significantly Different From 0 (95th)	Median pH
C019	36	-2.63	-2.21	9.79	NO	5.46
KS31	37	-1.04	-1.88	4.45	YES	4.97
MN16	34	-0.37	-1.20	9.92	NO	5.21
TX53	39	0.21	-0.76	5.81	NO	5.25
IL11	40	-0.05	0.13	3.11	NO	4.34
OK25	38	1.43	0.31	5.95	NO	4.88
FLU	35	0.46	0.84	4.79	NO	5.13
NH02	46	1.35	1.35	5.76	NO	4.38
TN00	43	0.59	1.76	3.79	YES	4.39
NC25	30	1.45	1.82	5.05	NO	4.67
MA01	40	1.62	2.04	5.05	YES	4.15
PA29	35	1.73	2.41	4.69	YES	4.15
OR02	37	2.38	2.91	9.96	NO	5.54
OH49	41	2.42	3.14	3.97	YES	4.15
CA45	26	3.51	4.85	14.37	NO	5.56

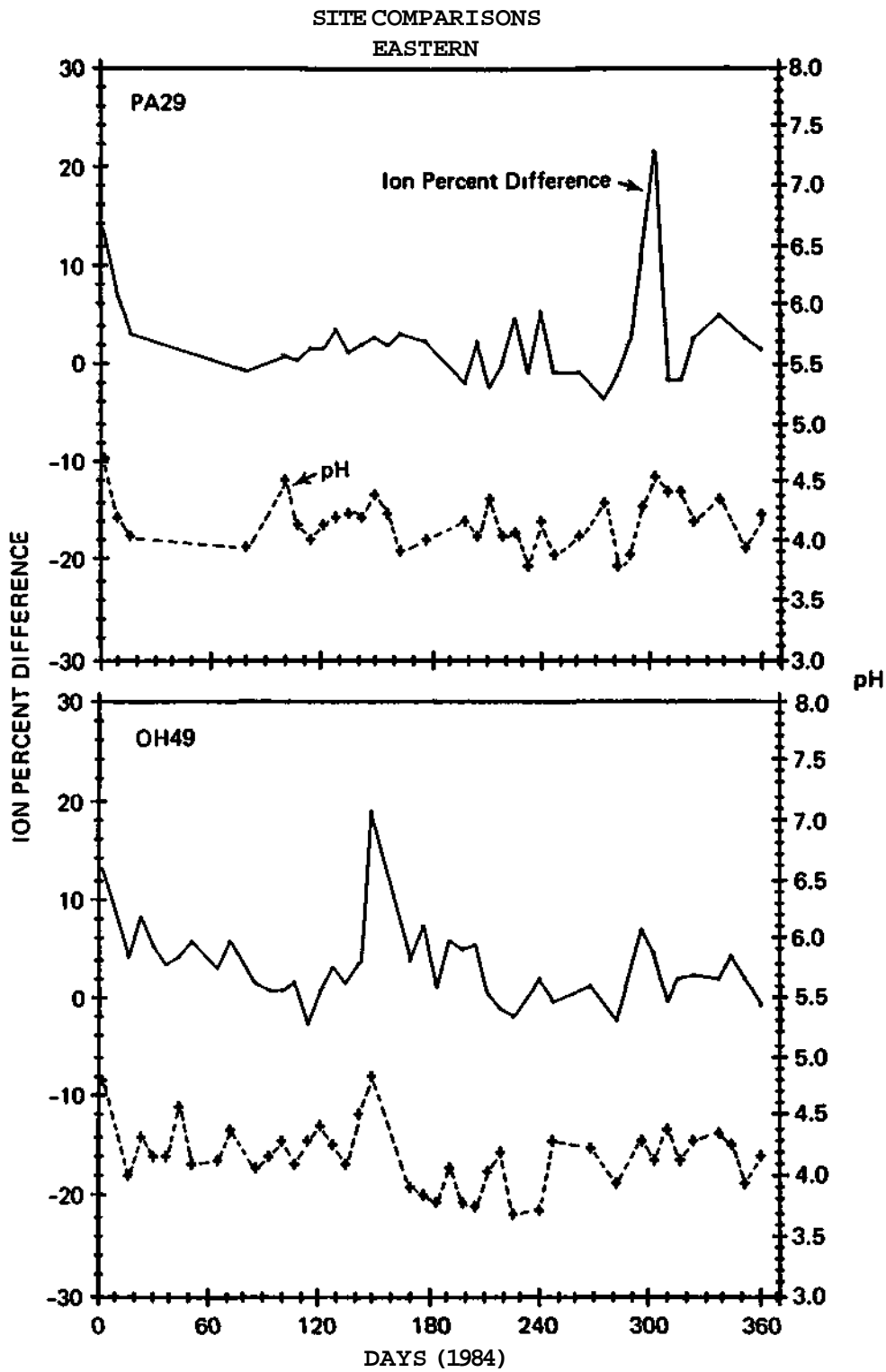


Figure 7. Temporal plots of annual pH and ion percent difference values for two eastern sites with positive differences.

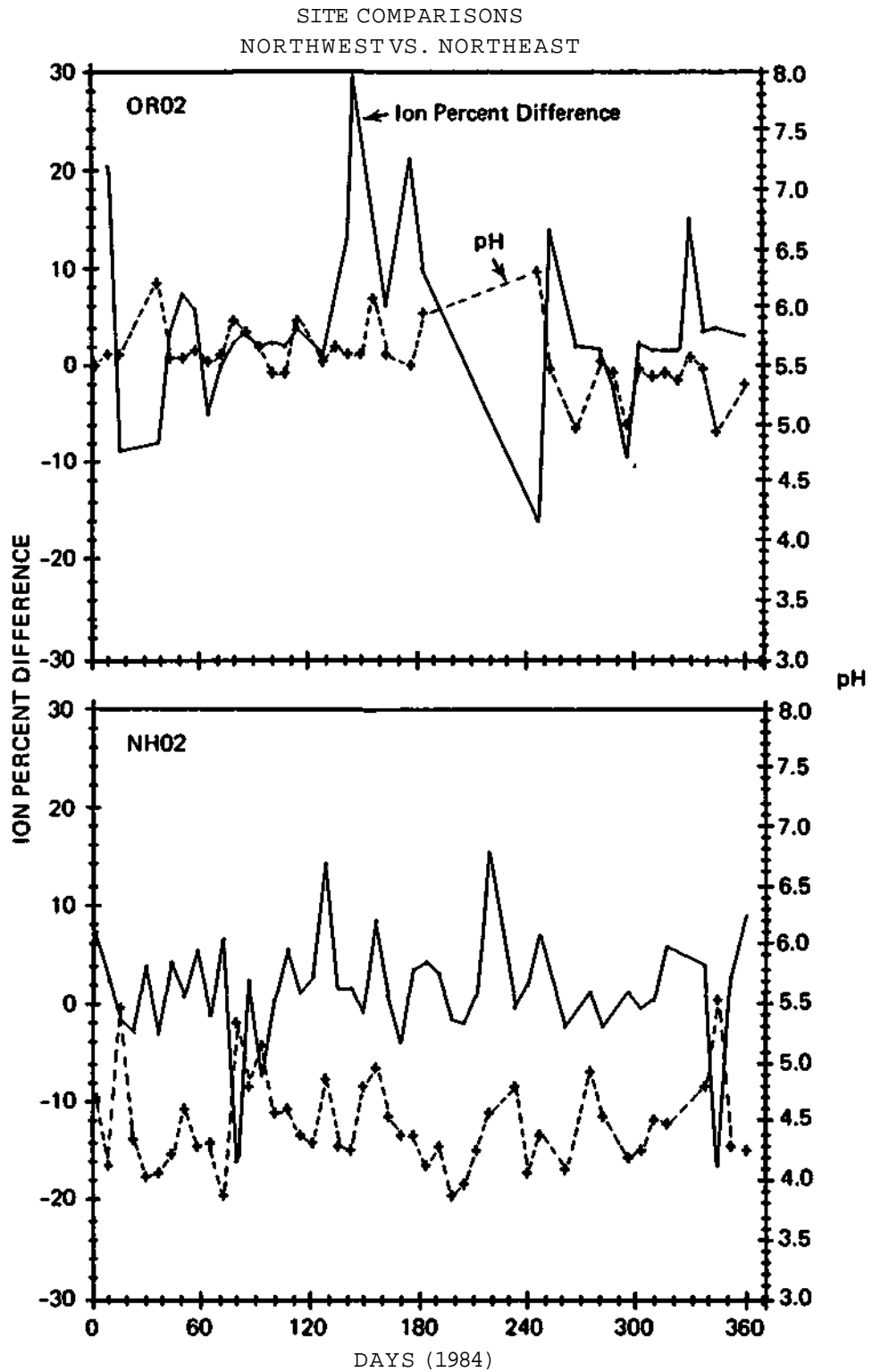


Figure 8. Temporal plots of annual pH and ion percent difference values that compare two northern sites. The eastern site median difference is positive and the western site, zero.

The plots in Figure 9 are for two sites that are near the 0% difference contour. The median IPD value is close to zero in both plots but the variability is quite different for each site. The Bondville (IL11) site has typically low pH values with little variation and the Victoria (TX53) site higher pH values with large variations. The relative IPD variability for both sites is similar to the variability seen in pH values.

The final two plots (Figure 10) are for mountain sites. These plots again compare an eastern site to one in the west. All of the patterns that have been discussed previously are evident on these plots. The Oak Ridge (TN00) site has a positive IPD, a median pH less than pH 5.0, and exhibits small variations in both the pH values and the IDP lines. The data from the Rocky Mountain (C019) site show all of the opposite characteristics. The IPD has a negative bias, the median pH is greater than pH 5.0, and the variations in both pH values and IDP are quite large.

These plots have shown that there can be useful comparisons made on a site by site basis as well as for the network as a whole. The regional and seasonal patterns discussed earlier remain consistent. More importantly, each site exhibits unique patterns that can be utilized to select reanalysis criteria that take these differences into account. By presenting the IPD data in a slightly different manner, this becomes even more evident.

Control Charts

Control charts have been used to assess analytical bias and precision for many years. To generate these charts, a true or target value must first be selected. For charts that plot analytical data, this true or target value may be a calculated concentration value, a median concentration value or a mean concentration value for the ion being charted. The difference of a measured value from this true value is the bias for that measurement. After several analytical measurements have been made, a mean and standard deviation can be calculated. This standard deviation (s) is an indication of the precision of the analytical measurements and is used to set both warning and control limits on the control chart (ASTM, 1976).

For the 1984 ion balance data set, a mean ion percent difference and standard deviation were calculated. Control charts using this statistical information, were prepared for the same eight sites for which the pH versus IPD plots were made. These charts are temporal plots of the ion percent difference for each site. The target value for each site is the mean IPD. This appears as a solid line on the charts. A warning limit of plus or minus two times the standard deviation and the control limit of $\pm 3s$ are also plotted. The control charts are presented in the same order as were the previous site plots, and are contained in Figures 11 through 14.

Presentation of the data in this manner again shows the regional pattern already discussed. The small expected variation about the mean for eastern sites with median pH values less than pH 5.0 is clearly evident in the plots in Figure 11. The large degree of variability that

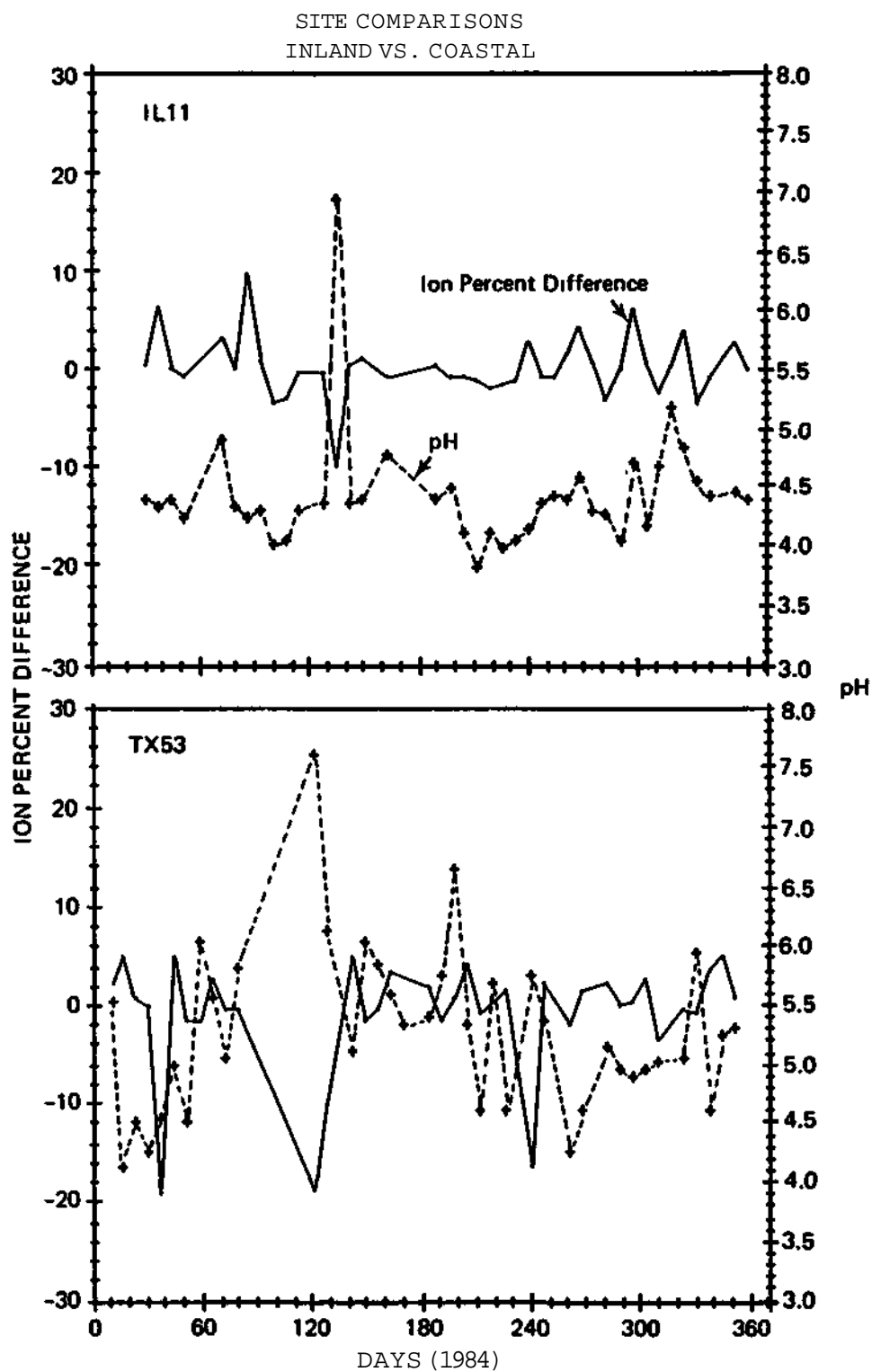


Figure 9. Temporal plots of annual pH and ion percent difference values for two sites with zero median differences.

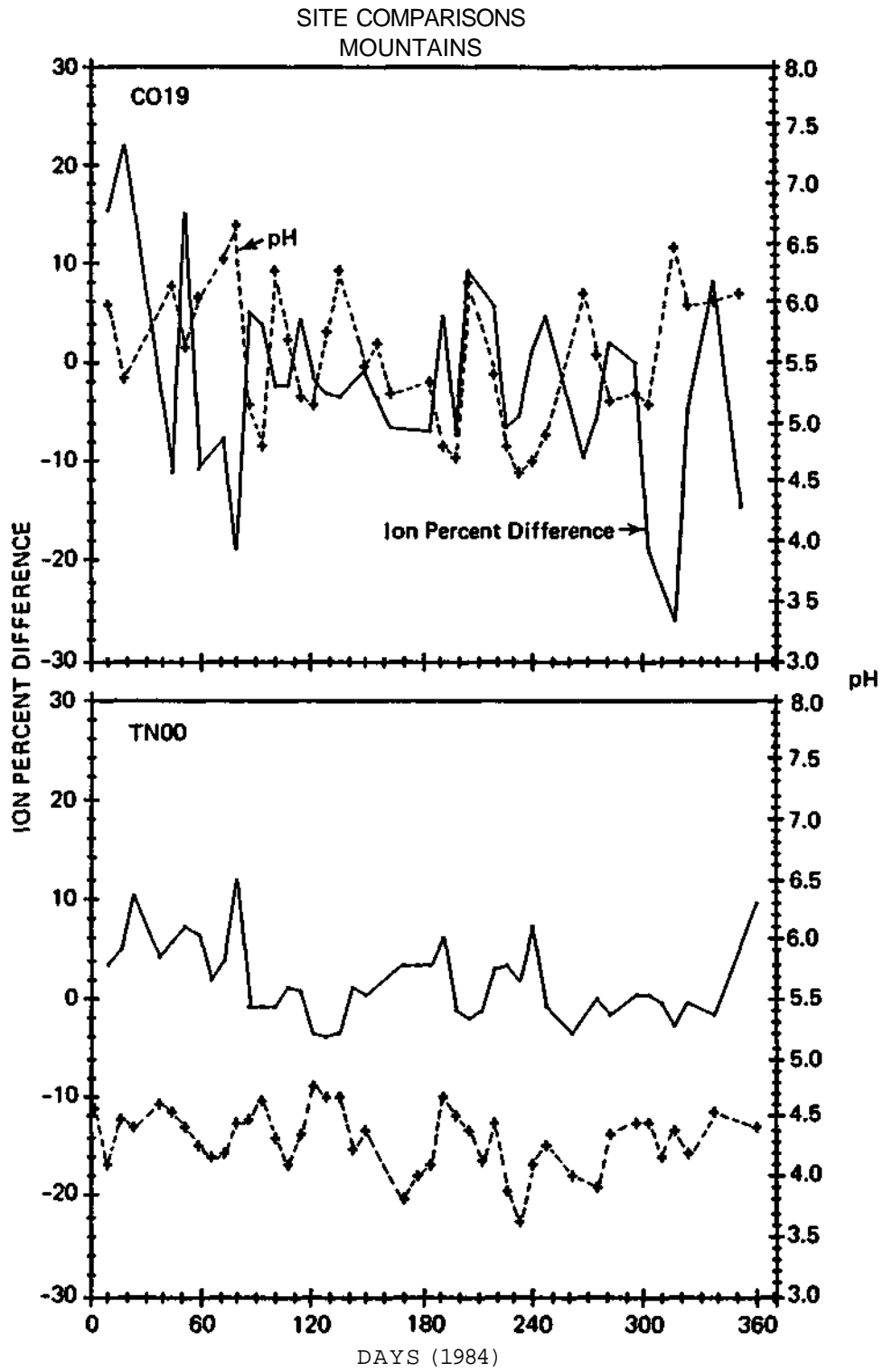


Figure 10. Temporal plots of annual pH and ion percent difference values for two mountain sites. The eastern site showing the positive median difference and the western, negative.

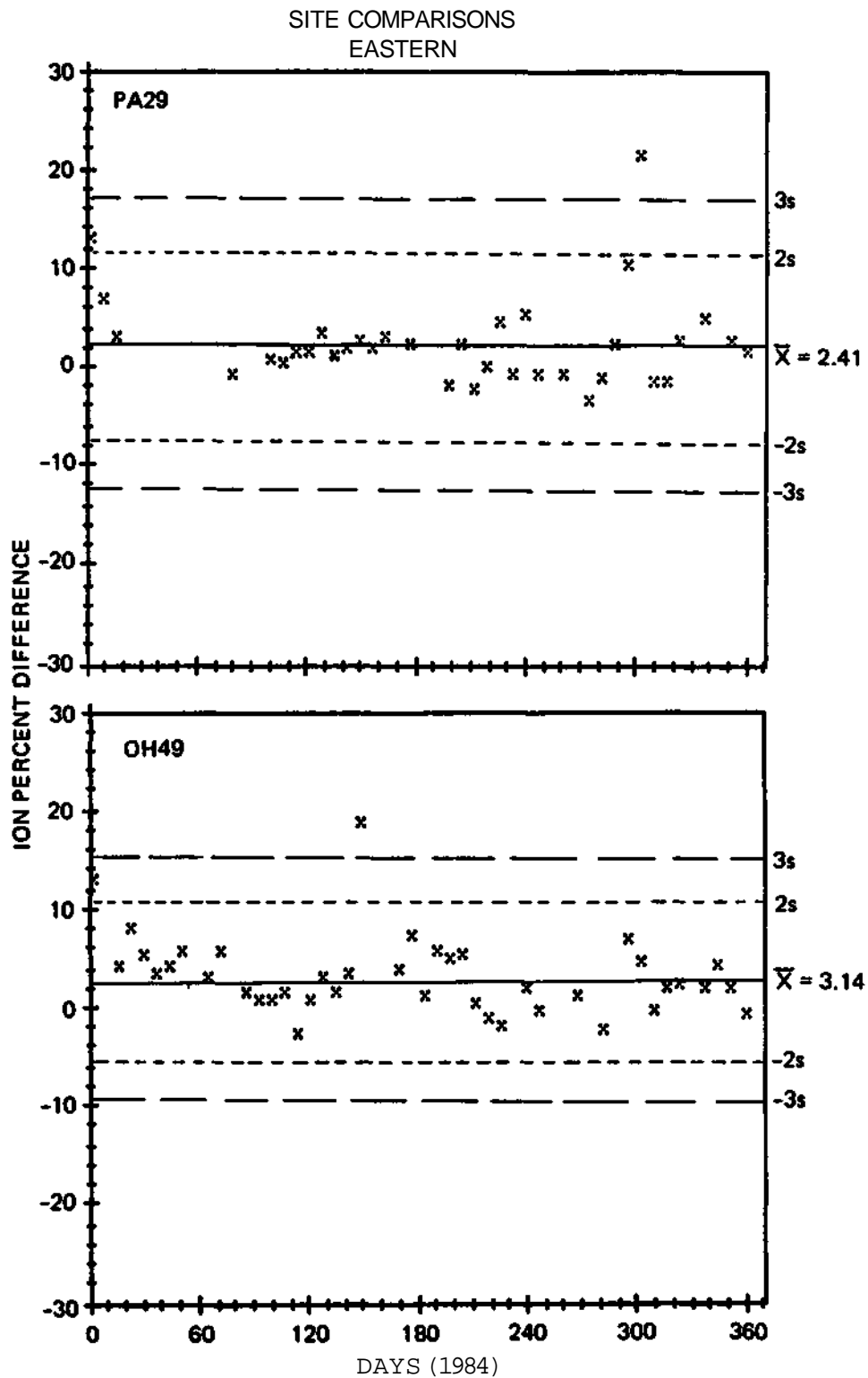


Figure 11. Control chart of ion percent difference data for two eastern sites each showing a data point outside of the control limits.

characterizes the differences between eastern and western sites is apparent in the plots in Figures 12 and 14. The variation in IPD values that are possible between sites with similar mean IPD values are presented in Figure 13. Closer examination of these plots reveals specific patterns for the IPD data from each site. This site specific information can also be used in the selection of samples for reanalysis.

Both charts in Figure 11 reveal points outside of the control limits. Each also has a point between the warning and the control limits. These data points are candidates for reanalysis. Examination of the charts in Figures 12 through 14 shows there are data beyond the warning and/or control limits for all eight sites. Reanalysis of these samples falling beyond the + 2s limit would be another way of detecting analytical errors when they occur. Additionally, when reanalysis and original values are the same and no analytical error is apparent, the fact that these IPD data points were outside of the preset limits for the site may indicate an anomalous sample that warrants further examination. Even when the cause of the deviation of one particular sample from the site norm cannot be found, the fact that it is very different from the typical precipitation sample from that site is evident and can be utilized in the interpretation of the data from the site. Using the data from each site to calculate a mean IPD and to set warning and control limits would be a possible alternative for the reanalysis selection criteria in current use by the laboratory.

CONCLUSIONS

The information obtained from the ion balance calculation provides a wealth of information to use to verify the correctness of the analytical data. The ISWS has used the ion percent difference and ion sum to develop criteria used to select samples for reanalysis. These same IPD data have been plotted to show regional and seasonal patterns that occur in network precipitation samples. Comparisons of these data with the pH values for individual sites indicate that there are consistent patterns in the correlation between these two variables. Those patterns are: as pH values increase, the variability in the IPD values typically increases, and that the variability in the pH values for each site is mirrored by the variability in the IPD values for that site. Finally, these IPD data, when plotted in the form of a control chart, provide clearly visible site specific patterns that can be utilized to detect both analytical and possible sampling errors when they occur.

REFERENCES

American Society for Testing and Materials: "Standard Method of Reporting Results of Analysis of Water"; Method D596; 1983 Annual Book of ASTM Standards; p. 43.

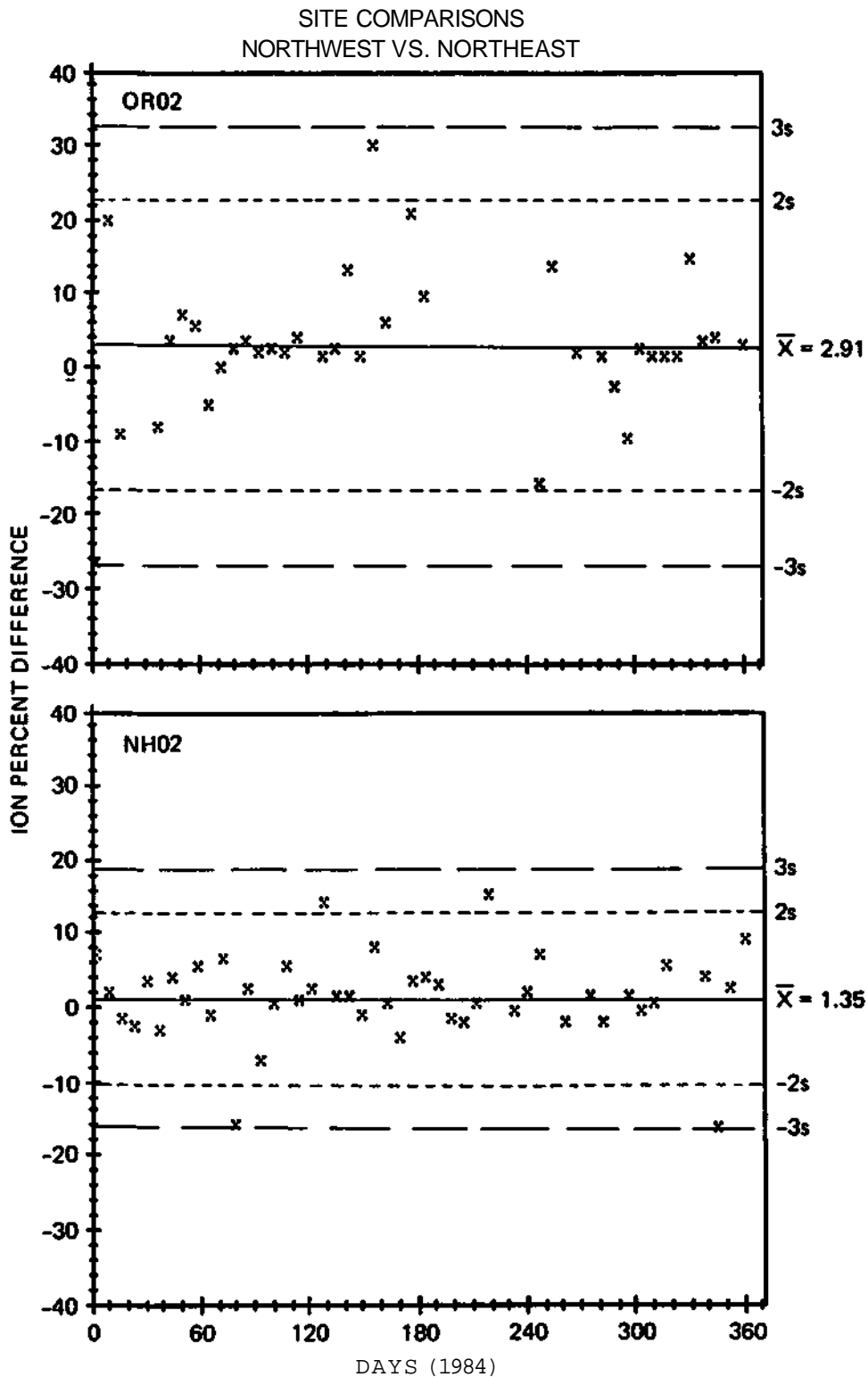


Figure 12. Control chart of ion percent difference data for two northern sites showing the variation in control limits that may exist between sites.

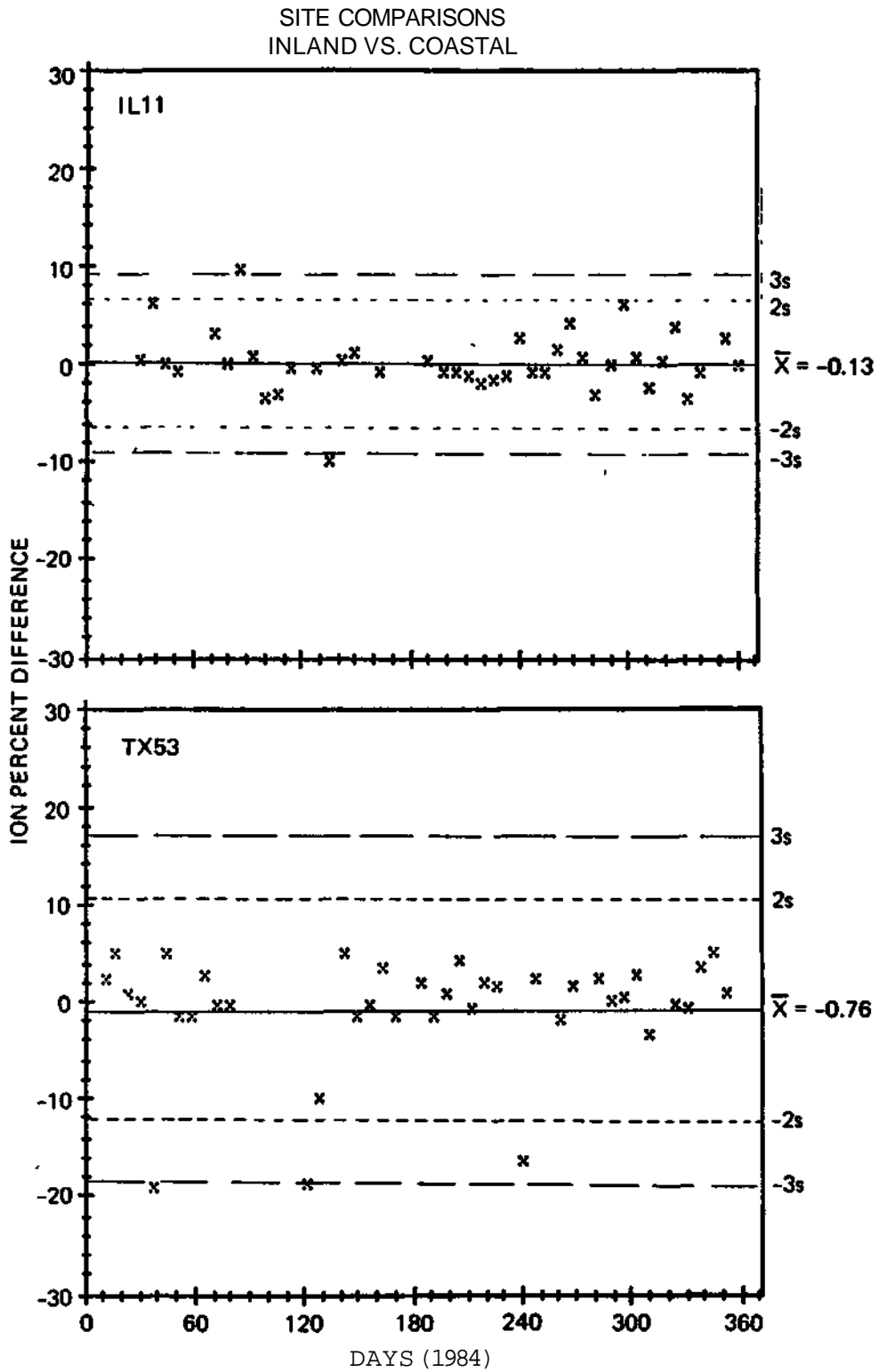


Figure 13. Control chart of ion percent difference data for two middle U.S. sites each showing data points outside of the control limits.

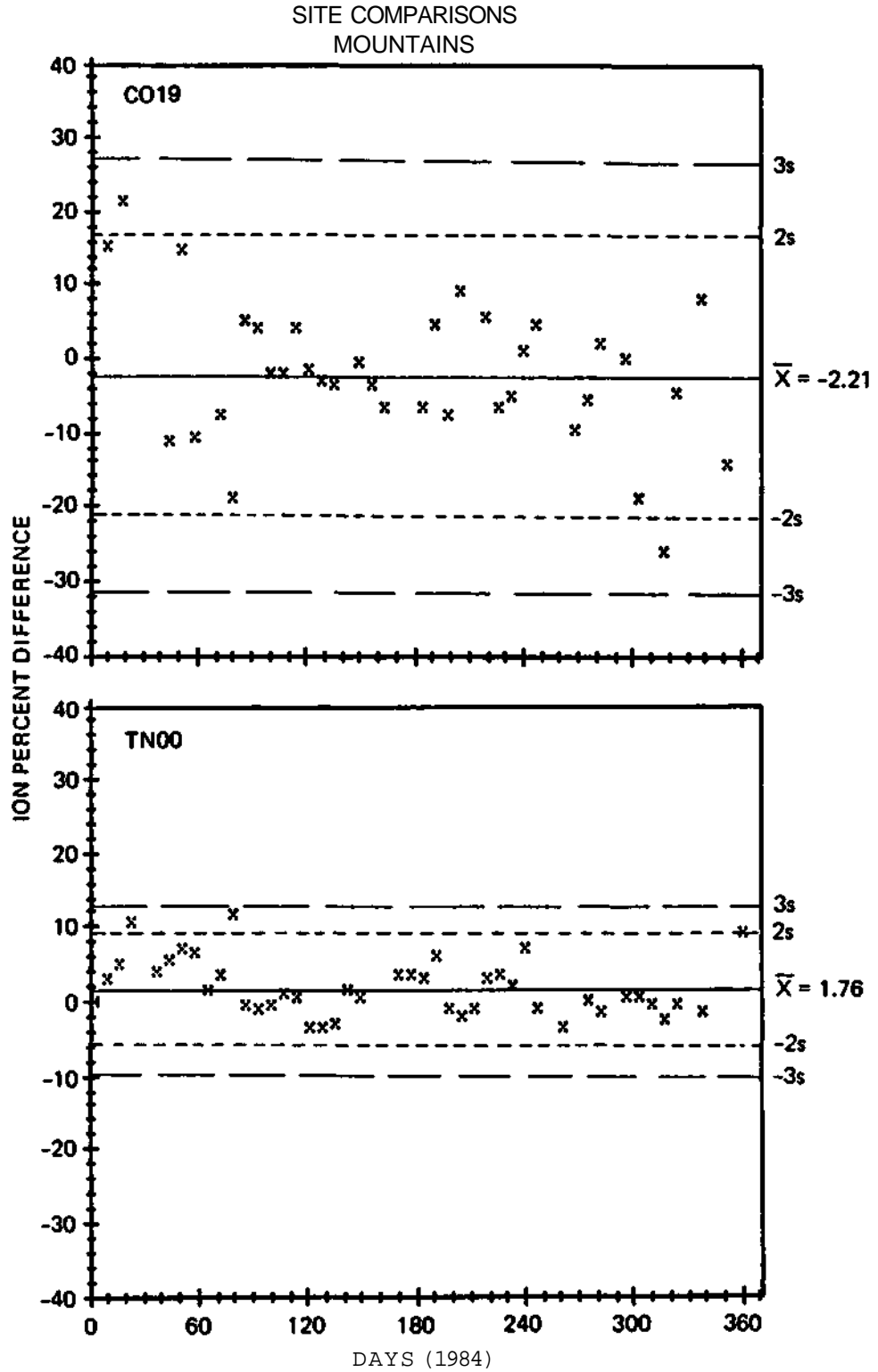


Figure 14. Control chart of ion percent difference data for two mountain sites showing the variation in control limits that may exist between eastern and western sites.

ASTM Manual on Presentation of Data and Control Chart Analysis: American Society for Testing and Materials; STP 15D; 1976.

Lockard, J.M.: Quality Assurance Report - NADP/NTN Deposition Monitoring - Laboratory Operations - Central Analytical Laboratory - July 1978 through December 1983: NADP/NTN Coordinator's Office; Natural Resource Ecology Laboratory; Colorado State University; Ft. Collins, CO 80523; May 1987.

NADP/NTN Annual Data Summary. Precipitation Chemistry in the United States. 1983: NADP/NTN Coordinator's Office; Natural Resource Ecology Laboratory; Colorado State University; Ft. Collins, CO 80523; June 1985.

Stensland, G.J., R.G. Semonin, M.E. Peden, V.C. Bowersox, F.F. McGurk, L.M. Skowron, M.J. Slater, and R.K. Stahlhut: NADP Quality Assurance Report - Central Analytical Laboratory. Jan. 1979-Dec. 1979: 1980; Champaign, IL 61820.

Topol, L.E., M. Lev-On, J. Flanagan, R.J. Schwall, A.E. Jackson. Quality Assurance Manual for Precipitation Measurement Systems: U S. Environmental Protection Agency; Environmental Monitoring Systems Laboratory; Research Triangle Park, NC 27711; 1985.

CHAPTER 9

A COMPARISON OF ION CHROMATOGRAPHY AND AUTOMATED COLORIMETRY FOR THE DETERMINATION OF MAJOR ANIONS IN PRECIPITATION

Susan R. Bachman

INTRODUCTION

Precipitation monitoring is a means by which an adequate description of deposition chemistry is obtained. The chemical quality of precipitation is being measured by several sampling networks nationwide in an effort to assess the relative contribution of inorganic constituents to the overall precipitation acidification process. According to the National Acid Precipitation Assessment Program's Annual Report to Congress (NAPAP, 1985), over 190 sites in the National Atmospheric Deposition Program/National Trends Network (NADP/NTN) are monitoring wet deposition for chemical analysis. In this network, weekly precipitation samples are analyzed for Ca, Mg, Na, K, Cl, NO₃, PO₄, SO₄, conductivity and pH. If we are to understand the full impact of acid deposition on man and his surroundings, then as many chemical constituents as possible should be included in any monitoring and research effort. A composite of these analyses forms a valuable data set for use by varied scientific organizations, governmental authorities, and environmental research groups. Credibility and accuracy of these data are crucial to the understanding of spatial and temporal trends in wet deposition. Analytical methods validation within a sampling network is a valuable and necessary component of the overall monitoring design.

Two prime considerations should be addressed when analyzing precipitation samples. The first concern is the volume of sample available for analysis. Quite often, weekly sample volumes from semi-arid collection sites or from a dry sampling period are very small, thus limiting the number of analyses that can be performed. Secondly, the constituents of interest in precipitation are typically at low levels of concentration. These limitations demand the use of analytical methods with high sensitivity, low sample volume requirements, and freedom from significant chemical interferences (Small, 1975). The two most common methods utilized and referenced for the determination of the anions Cl, NO₃, and SO₄ in atmospheric samples are automated colorimetry and ion chromatography (Fung, et al., 1979). These two methods, and their associated instrumentation, were selected for an analytical comparability study because of their widespread use. Limited work by others in this field have demonstrated the comparability of these techniques for precipitation analyses (Pyen, 1986). For this study, 200 randomly selected precipitation samples were chosen from the NADP/NTN network and analyzed by the Illinois State Water Survey laboratory. Samples collected during a late summer, early fall period included varied climatic and geographic regions. Statistical comparisons of data obtained from each of the methods were the major emphases of this study. Detection limits, precision, method bias, and analyte concentration values were compared.

EXPERIMENTAL METHODS

The two analytical techniques compared were chemically suppressed ion chromatography (IC) and segmented flow automated wet chemistry (AWC). The ion chromatography instrumentation used was the Dionex Model QIC Automated wet chemical instrumentation included Technicon AutoAnalyzer (AA) II and Scientific Instruments Corporation components.

Automated Wet Chemical Procedures

The Technicon Model AA II was employed for the analyses of Cl and NO₃, whereas the Scientific Instruments Model AC 200 colorimeter was used for the SO₄ analyses. The Cl and NO₃/NO₂ analyses were conducted using a dual channel colorimeter. Each channel was fitted with a 15 mm path length glass flow cell that was preceded by a 480 nm wavelength filter for Cl and a 520 nm wavelength filter for NO₃/NO₂. Sample and reagent flows (mL/min) were regulated by employing flow-rated polyvinylchloride tubing with a peristaltic pumping system. Prior to analysis, each sample was filtered through a 0.45 um Millipore filter, then stored in a deionized water (DI) rinsed 60 mL high density polyethylene (HDPE) bottle. An automated sampler with a 1:4 sample to rinse ratio was used to aspirate a sample aliquot from the sample cup and introduce it into the analytical stream of each of the two respective systems.

The AWC chloride analyses were performed using the ferric thiocyanate method, where liberated thiocyanate is measured from mercuric thiocyanate in the presence of ferric ions. The nitrate-nitrite analyses utilized the cadmium reduction method whereby measurement of nitrite is made after complexation with sulfanilamide. The sulfate analyses employed the methylthymol blue method in which a barium thymol blue complex is formed and measured at a wavelength of 460 nm (Peden, et al., 1986).

Ion Chromatographic Procedures

The ion chromatographic analyses were performed on a Dionex Model QIC fitted with a single high pressure valve, a LDC/Milton Roy variable speed pump and corresponding pressure gauge, and a 6 uL constant volume conductivity cell with a digital readout. The individual ions within a precipitation sample are separated by each ion's affinity for the exchange sites within the separation column. Exchange columns used were the Dionex HPIC-AG3 guard column (4 x 50 mm), the HPIC-AS3 separation column (4 x 250 mm) and the anion fiber suppressor (AFS). The standard eluent concentration of 2.8 mM NaHCO₃ and 2.2 mM Na₂CO₃ was used with the continual regenerant concentration of 0.025N H₂SO₄ passing through the AFS. Gravity regenerant flow through the AFS was regulated at 3.2 mL/min. A 100 uL sample loop was used to regulate the volume of standards and samples directed onto the separator column. The conductivity detector was set at 10 uS/cm full scale. The eluent pump flow was set at 2.8 mL/min. Each of the anions in the chromatograms was identified by its characteristic retention times. At the described elution rate, six samples could be analyzed per hour.

At the time this study was conducted, the IC was not interfaced to an autosampler and integrator, therefore all samples were manually injected. Sample loop and solution transmission lines were rinsed with ten times the volume of the sample loop before the sample was injected into the analytical columns. A dual-channel strip chart recorder was used to record all chromatograms at two sensitivity levels, 10 mV and 1 V full scale. Figure 1 illustrates a typical sample chromatogram employing eluent matching to eliminate a negative conductance reading (the water dip).

Selection of Working Ranges and Calibration Standards

The working range chosen for each of the analytical methods was determined from the percentile concentration values calculated from over 5000 precipitation samples collected from the NADP/NTN sampling network. A working range of 0.10-2.00 mg/L was set for Cl with three additional calibration standards equally distributed throughout the concentration range. Nitrate-nitrite analyses had a working range of 0.10-5.00 mg/L, again with three other evenly distributed standards. The sulfate analysis had a working range of 0.10-8.00 mg/L. A cumulative frequency plot (Figure 2) shows the precipitation concentration values that were used to select the appropriate calibration standards and working ranges. Note the large percentage of samples at the lower concentration ranges.

Standard reagent grade salts and chemicals were used to prepare standard solutions, eluents, and color reagents for the two methods. For this comparison study, peak height measurements from X-Y strip chart recorders were used for recording results, both for the AWC and the IC analyses. Each channel of the recorder was adjusted to read full scale using the maximum standard concentration for each of the analytes. Each analyte calibration curve was established at the beginning of the day's analysis by performing a least squares regression of the standard concentration values against their measured peak heights. Calibration curves were reestablished after every 36 samples to correct for column degradation (AWC analysis of NO₃/NO₂) or system fluctuation due to instrumental baseline drift.

RESULTS AND DISCUSSION

To properly compare the two analytical methods, as many identical analytical conditions as possible were maintained throughout the analyses of all 200 samples. An evenly distributed range of five standard concentrations was used in the development of each of the calibration curves for both methods. Table 1 lists these standards, which were prepared immediately before the comparison study from 1000 mg/L stock solutions. Standards, as well as samples, were refrigerated at 4°C throughout the study, and were brought to thermal equilibrium shortly before the time of analysis.

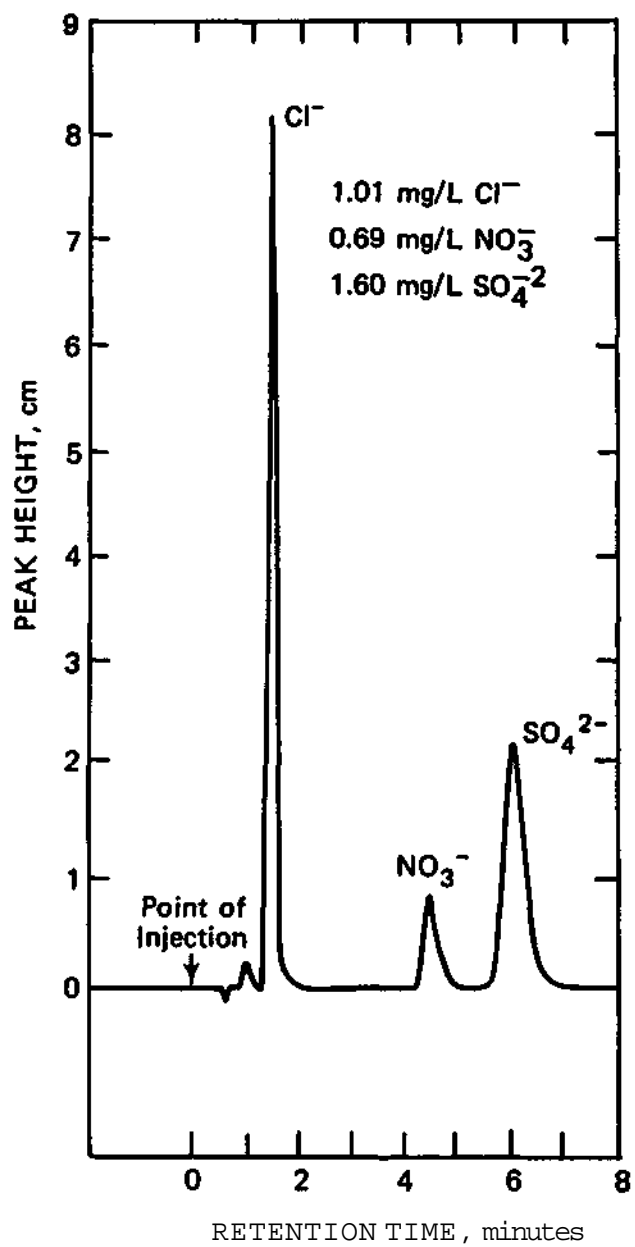


Figure 1. Chromatogram of anions in a precipitation sample analyzed by IC under conditions described in text.

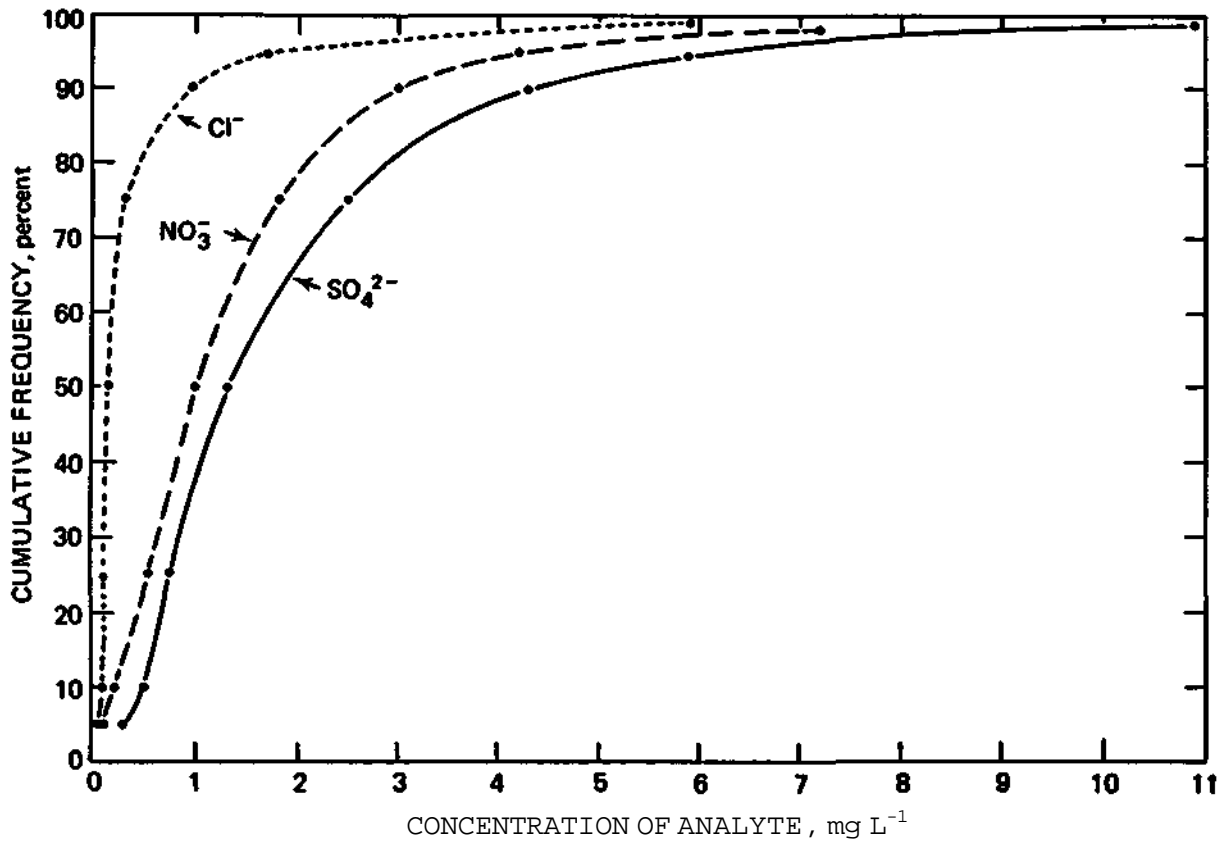


Figure 2. Cumulative frequency concentrations of Cl, NO₃, and SO₄ at various percentile levels. Data compiled from over 5000 precipitation samples analyzed in the NADP/NTN network, 1984.

Table 1. Calibration standards and quality control check solutions used in methods comparison study.

Calibration Standards (mg L ⁻¹)			
	Cl	NO ₃	SO ₄
Standard 1	0.10	0.10	0.10
Standard 2	0.25	0.25	0.25
Standard 3	0.50	1.00	1.50
Standard 4	1.00	3.00	5.00
Standard 5	2.00	5.00	8.00

Quality Control Check Solutions (mg L ⁻¹)			
	Cl	NO ₃	SO ₄
Concentration 1	0.18	0.62	0.94
Concentration 2	0.43	2.36	3.60

Table 2. Comparison of method detection limits (MDL) for automated colorimetry and ion chromatography.

Analyte	Automated Colorimetry			Ion Chromatography		
	MDL	s	n	MDL	s	n
Cl, mg/L	0.05	0.017	10	0.024	0.008	10
NO ₃ , mg/L	0.02	0.009	10	0.021	0.007	10
SO ₄ , mg/L	0.10	0.034	10	0.024	0.008	10

s = standard deviation

n = number of samples

Before the 200 precipitation samples were analyzed, each of the method's detection limits (MDL) were determined under the described operating conditions. The MDL for each analyte was calculated from replicate analyses of the 0.10 mg/L calibration standard using three times the standard deviation of the measured mean concentration. Resultant MDLs are listed in Table 2.

A method bias for each of the three analytes was also determined. Ten randomly selected samples were spiked at two concentration levels and the percent recovery data were calculated. Table 3 shows the comparability of the two systems in terms of method bias at approximately the 25% and 75% percentile concentration levels for each of the methods. The mean percent recovery for the colorimetric method was 101.4% compared to 100.6% for the ion chromatographic method. Also compared are the quality control check sample (QCS) results obtained from internally prepared USEPA reference standards of known concentrations. Mean recoveries were 100.0% for the colorimetric method and 102.6% for the ion chromatographic method. QCS data were collected daily throughout this comparison study.

The analytical data compiled for each of the methods are plotted in Figure 3. The plots and the resulting statistics were derived from three sets of paired data. An important feature of a methods comparison can be detected from a visual examination of these raw data plots. Possible concentration differences at varying concentrations can be observed. Least squares regression was used to fit each set of data to a straight line. The 1:1 fit line is also shown. The correlation coefficient (r), y-intercept (b), and slope (m) are also indicated for each analyte comparison. The agreement between the two methods for all three analytes is excellent throughout the entire concentration range.

Table 4 summarizes the mean and median concentration differences that were calculated from the 209 data pairs shown in Figure 3. The differences were determined by subtracting individual IC from paired AWC results. Both the mean and median concentration differences for all three anions were near or below the reported method detection limits. The calculated means for each method are also presented in Table 4. A Student's t-test performed using the means of each analyte population revealed no significant differences between IC and AWC results at the 95% confidence level.

A paired t-test performed using the mean concentration differences and the associated standard deviation of the differences revealed a small but significant difference (95% confidence level) for sulfate and nitrate determinations between AWC and IC results. A possible factor contributing to this observed statistical difference for nitrate is the influence of nitrite concentrations on the AWC results. The AWC technique measures both nitrite and nitrate in solution. The IC procedure measures nitrite and nitrate as separate peaks on the chromatogram. Although no quantitative analyses were performed to measure the concentration of nitrite present in these samples, a review of the IC chromatograms indicated that approximately 15% of the precipitation samples that were analyzed contained nitrite at levels near the method detection limit. No explanation for the significance of the sulfate differences is apparent at this time.

Table 3. Method bias determined from percent recoveries of spiked and quality control check solutions (QCS)

Analyte	Concentr. Level	Automated Colorimetry		Ion Chromatography	
		Spiked	QCS	Spiked	QCS
Cl	a	101.9	100.0	101.7	105.6
	b	106.5	103.5	100.9	102.4
NO ₃	a	97.0	101.6	100.6	101.3
	b	98.2	98.1	97.3	102.8
SO ₄	a	99.3	95.7	102.4	97.9
	b	105.4	101.1	100.9	102.5

a = approximate 25% concentration level

b = approximate 75% concentration level

Table 4. Statistical data summarized for methods comparison study.

Analyte	n	Mean AWC	Mean IC	Median Difference	Mean Difference	Standard Deviation
Cl, mg/L	209	0.38	0.37	0.00	0.01	0.06
NO ₃ , mg/L	209	1.31	1.27	0.01	0.04	0.09
SO ₄ , mg/L	209	1.98	2.02	-0.03	-0.04	0.11

n = number of samples

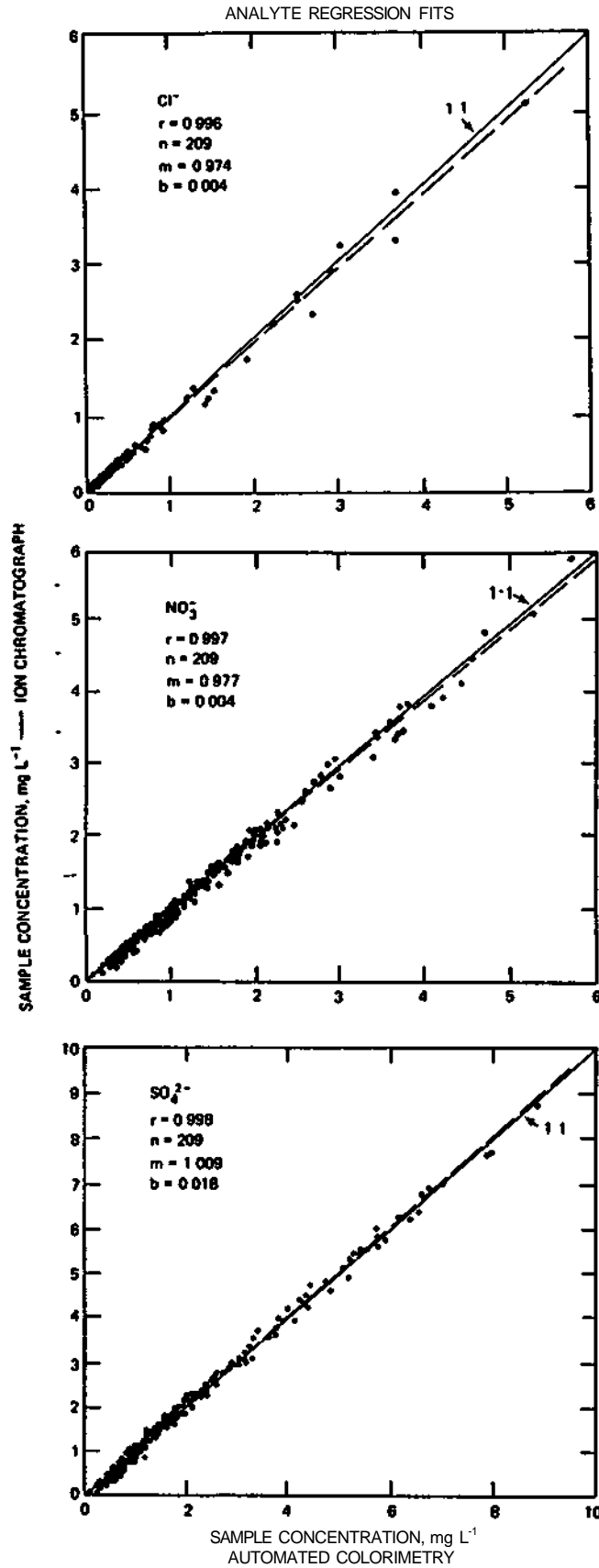


Figure 3. Automated wet chemical results versus ion chromatographic results for Cl, NO₃, and SO₄ (r = correlation coefficient, n = number of samples, m = slope, b = y-intercept).

Two factors other than statistics must be considered when making comparisons between these two methods of analysis. The speed of analysis by the automated colorimetric method is 5-10 times faster than the ion chromatographic method but the end result is quantification of only one analyte. The volume of sample needed for analysis is also twice as great (in this study) for the colorimetric method. These factors, along with the required larger number of reagents, some of which include hazardous compounds, are detracting aspects of automated colorimetry. Anion analysis by IC requires two simple reagents that can be made in large volumes at less frequency. The overall instrumental start-up and preparation time is minimal for IC analysis. Interferences from other sample components are reduced while a detailed profile of the anionic species in the precipitation sample are chromatographed.

CONCLUSION

The two analytical methods of automated colorimetry and ion chromatography have been compared with respect to comparability of analytical results and physical features. Detection limits are somewhat improved with the ion chromatograph. A bias for one method over the other was not detected with regard to sample concentrations. A wide range of analyte values was examined and correlations between the two methods were excellent. Instrumental features, reagents, and consumable products are other factors that should be considered when selecting between these two analytical methods.

REFERENCES

- Fung, K. K., et al., 1979: Comparison of Ion Chromatography and Automated Wet Chemical Methods for Analysis of Sulfate and Nitrate in Ambient Particulate Filter Samples, Ion Chromatographic Analysis of Environmental Pollutants, 2, Ann Arbor Science, Ann Arbor, Michigan, pp. 203-209.
- National Acid Precipitation Assessment Program, Annual Report to the President and Congress, 1985: Washington, D.C., p. 57.
- Peden, M. E., et al., 1986: Methods for the Collection and Analysis of Precipitation, United States Environmental Protection Agency, EMSL, Cincinnati, OH, #CR810780-01.
- Pyen, G. S., M. R. Brown, and D. E. Erdman, 1986: Automated Chromatographic Determination of Anions in Precipitation Samples, American Laboratory. 180, #5, pp. 22-32.
- Small, H., T. S. Stevens, and W. C. Bauman, 1975: Anal. Chem., 47, p. 1801.

CHAPTER 10

LONG-TERM IONIC STABILITY OF PRECIPITATION SAMPLES

Mark E. Peden and Loretta M. Skowron

INTRODUCTION

Previous work by Peden and Skowron (1978, 1979) has examined the variables affecting the ionic stability of major inorganic components in wet deposition. This research has shown the importance of utilizing wet-only collectors for the study of wet deposition chemistry and has provided data on the chemical changes that can take place in samples after the time of collection. Filtration of samples to remove particulates and refrigeration at 4°C were the two preservation methods they recommended to maintain sample integrity until all desired chemical analyses could be completed. Data from this early work on precipitation stability have led to the widespread use of these two techniques in many precipitation monitoring programs. The long-term stability of precipitation samples has not, however, previously been examined.

Most ion stability studies, including the work performed in this laboratory, have focused on short-term chemical changes that occur in precipitation samples. The time scale involved in these studies has varied from hours to six weeks after collection. The long-term stability of ions in solutions is an area of interest that is important if archived samples are ever used for purposes other than their original intent. An example of this instance would include the measurement of trace metals in archived wet deposition samples that were originally collected only for major ion determinations. By investigating the long-term stability of the major ion species, inferential deductions may be made about the suitability of these types of samples for varied study purposes.

EXPERIMENTAL

The Central Analytical Laboratory (CAL) of the National Atmospheric Deposition Program/National Trends Network (NADP/NTN) is required to archive 60 mL aliquots, stored at 4°C, of each precipitation sample collected from the national network. These aliquots are prepared at the time of sample receipt and are filtered through a 0.45 micrometer membrane filter. These aliquots are handled in an identical manner to the samples that are analyzed by the laboratory for the major inorganic ions. Sample storage bottles are manufactured from the same material and obtained from the same vendor as the bottles used in routine analyses. An archival sample aliquot is not prepared if the sample volume is insufficient.

The CAL protocols require that these samples be maintained for a period of five years before they are discarded. In 1985, the CAL had accumulated refrigerated aliquots from the start of network operations in 1978 and was beginning to discard samples from the 1978-1979 period. A subset of these early samples was selected for reanalysis to obtain the first known data set on long-term stability of precipitation samples.

In order to obtain as much information as possible from the study results, samples were selected from twelve sites that encompassed different geographic regions of the NADP/NTN network. Samples were also selected to equally represent both warm and cold season sampling periods to determine if seasonal collection differences in long-term stability were apparent. The sites selected included:

CA 88 - Davis, CA	NC 41 - Raleigh, NC
CO 21 - Manitou, CO	NE 15 - Mead, NE
FL 03 - Bradford Forest, FL	NH 02 - Hubbard Brook, NH
GA 41 - Experiment, GA	NY 20 - Huntington Wildlife, NY
IL 11 - Bondville, IL	OH 17 - Delaware, OH
MN 16 - Marcell Experimental Forest, MN	WV 18 - Parsons, WV

Eight samples from each site were selected from the sampling period of November 28, 1978 to November 6, 1979. The analyses were made in September, 1985 and the chemical data were compared with the results obtained six years earlier. Two of the 96 sample pairs were eliminated from further statistical evaluations using the Grubbs t-test for identification of outliers. An examination of the raw concentration data for these two sample pairs indicated that one had been contaminated and the second appeared to have been misnumbered at the time of aliquot preparation in 1979.

Of the eleven constituents that were originally measured in these samples, only eight parameters were examined in the refrigerated aliquots. Orthophosphate concentrations were not determined because more than 95 percent of the original values were at or below the method detection limit. Sodium and potassium were also not determined since previous work by Peden and Skowron (1978, 1979) has shown these two constituents to be the most conservative of the species in wet deposition. The remaining constituents that were measured in the six year old aliquots are pH, conductivity, Ca, Mg, Cl, SO₄, NO₃, and NH₄.

The analytical procedures that were used for the reanalyses were identical to those that were used previously, with the exception of Cl, NO₃, and SO₄. In 1985, the determination of these three anions were performed by chemically suppressed ion chromatography. Previous analyses in 1978-1979 had been conducted using segmented-flow automated wet chemical techniques. An extensive comparison of these two techniques has shown them to be equivalent, so that any concentration differences found between original and reanalysis values are attributable to sample degradation and not analytical biases.

RESULTS

Plots of the original versus reanalysis results for each of the eight constituents are shown in Figures 1-8. These figures also contain a linear least squares fit of the concentration data and the 1:1 correspondence line for reference. The agreement between original and reanalysis values for SO_4 , NO_3 , Cl, Ca, and Mg is excellent, which is consistent with earlier work on short-term stability. Conductivity, pH, and NH_4 results show much poorer correlations, with pH generally decreasing and conductivity increasing from their original values. NH_4 results are highly variable but with low level concentrations slightly elevated from their original values.

Table 1 summarizes these results for each constituents and provides the range and mean values tabulated for both data sets. Examination of the mean differences reported in Table 1 reveals relatively small differences between the two data sets, with the exception of the conductivity and pH measurements. Table 2 summarizes the results from the regression analyses applied to the concentration data as well as the results of a paired t-test on the original versus reanalysis values. The t-test results for Ca, NH_4 , and Cl indicate no significant differences between the two data sets after six years. These results show that evaporative losses from the high density polyethylene bottles are not a factor in long-term sample stability and that Ca and Cl are among the most conservative of the ions that were measured. The statistical equivalency of the two NH_4 data sets is a function of the variability of the concentration differences more than an indication of sample stability.

Figure 9 displays a plot of the ratios (expressed as a % recovery) of the reanalysis mean values to the original mean values for each of the eight constituents under study. Data used for this graphical representation of the results were extracted from Table 1. Figure 9 indicates that, on average, Ca, Mg, SO_4 , NO_3 , and Cl data are within 10% of their original concentrations after six years of refrigerated storage. Only NH_4 , pH, and conductivity values have increased by greater than 10%.

In order to detect any site specific patterns in the stability of these constituents, the paired t-test previously used on the data set as a whole was performed on the data from each of the twelve sites. A summary of the significance of these test results is presented in Table 3. No clear pattern of site specific stability characteristics is apparent from this table, which is not surprising given the limited data set. There is, however, a range of significant differences from one site to another. The Colorado and Minnesota sites each had only one ion that showed significant differences upon reanalysis. The North Carolina site revealed apparent instability in six of the eight constituents examined. The only consistent trend that is seen in this table is that when both sulfate and ammonium show significant differences for a given site, the pH values also show significant differences. A similar examination of the data by separating samples into warm and cold season collection periods did not reveal any significant differences between the two data sets.

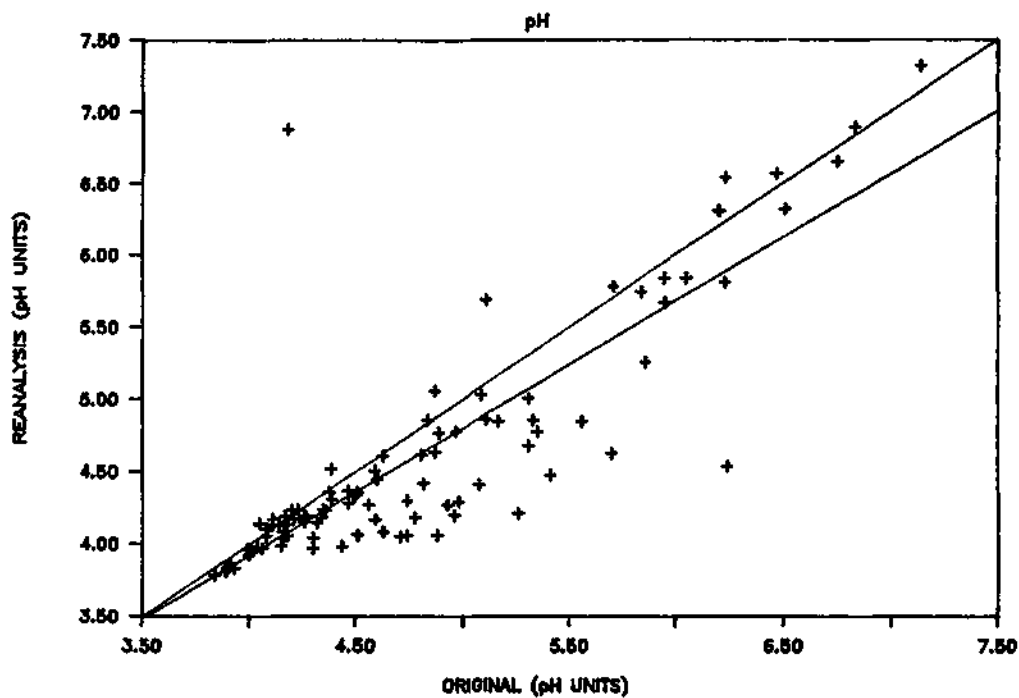


Figure 1. Original versus reanalysis results for pH.

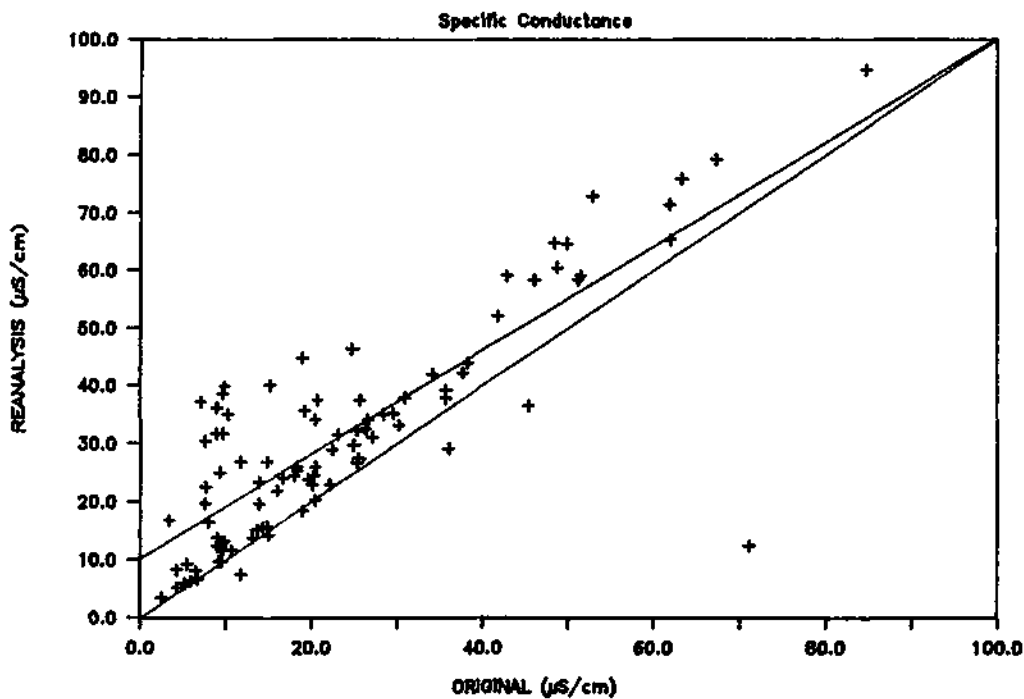


Figure 2. Original versus reanalysis results for specific conductance.

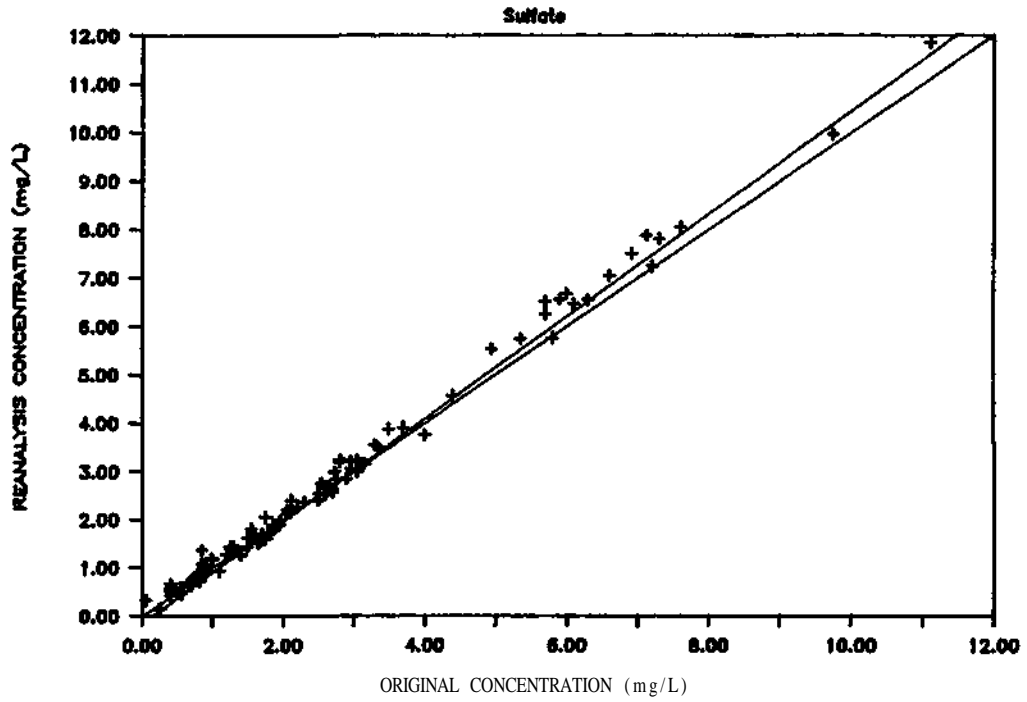


Figure 3. Original versus reanalysis results for sulfate.

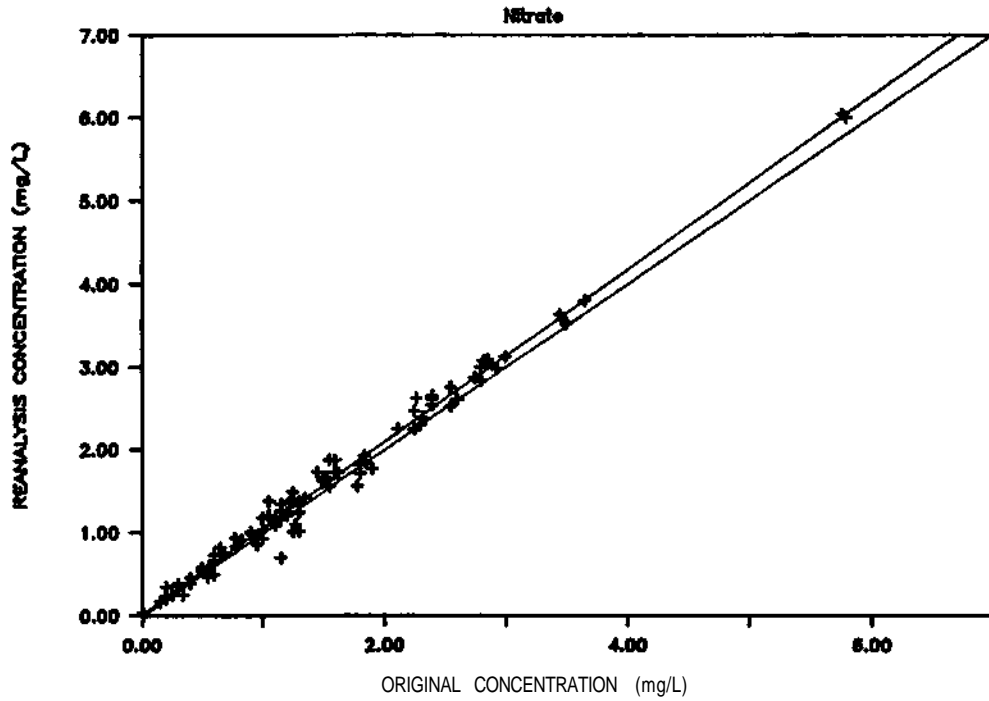


Figure 4. Original versus reanalysis results for nitrate.

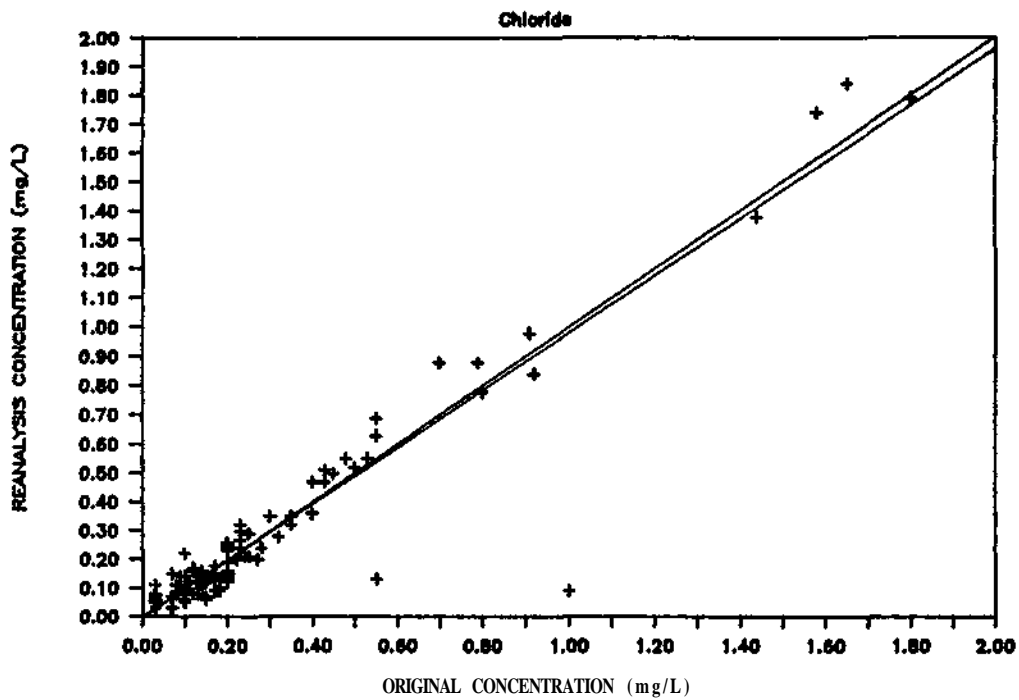


Figure 5. Original versus reanalysis results for chloride.

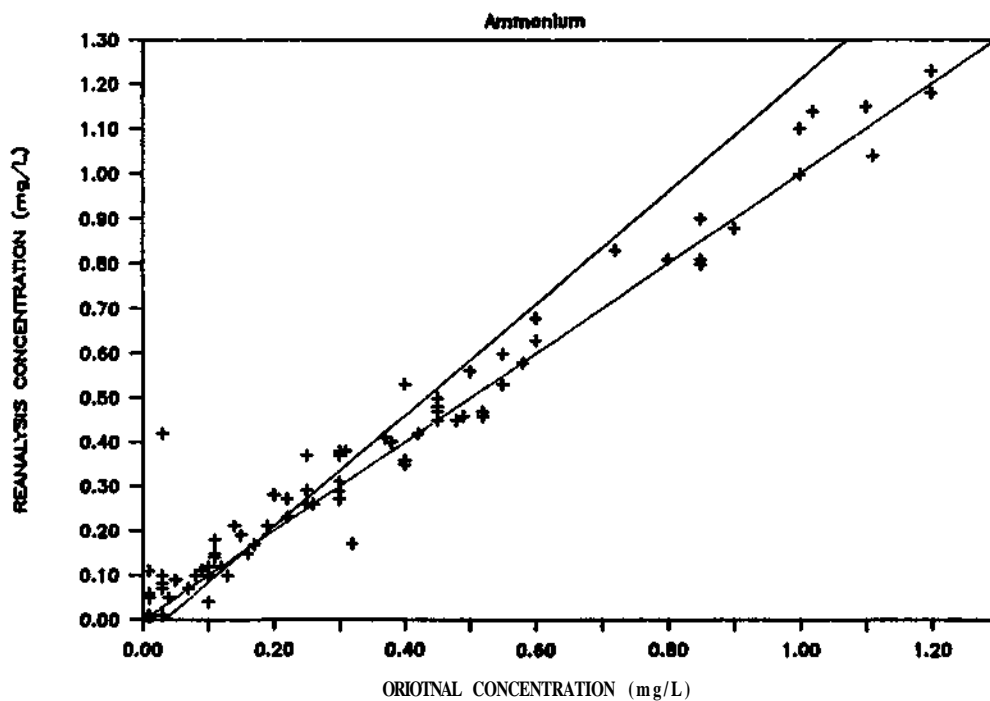


Figure 6. Original versus reanalysis results for ammonium.

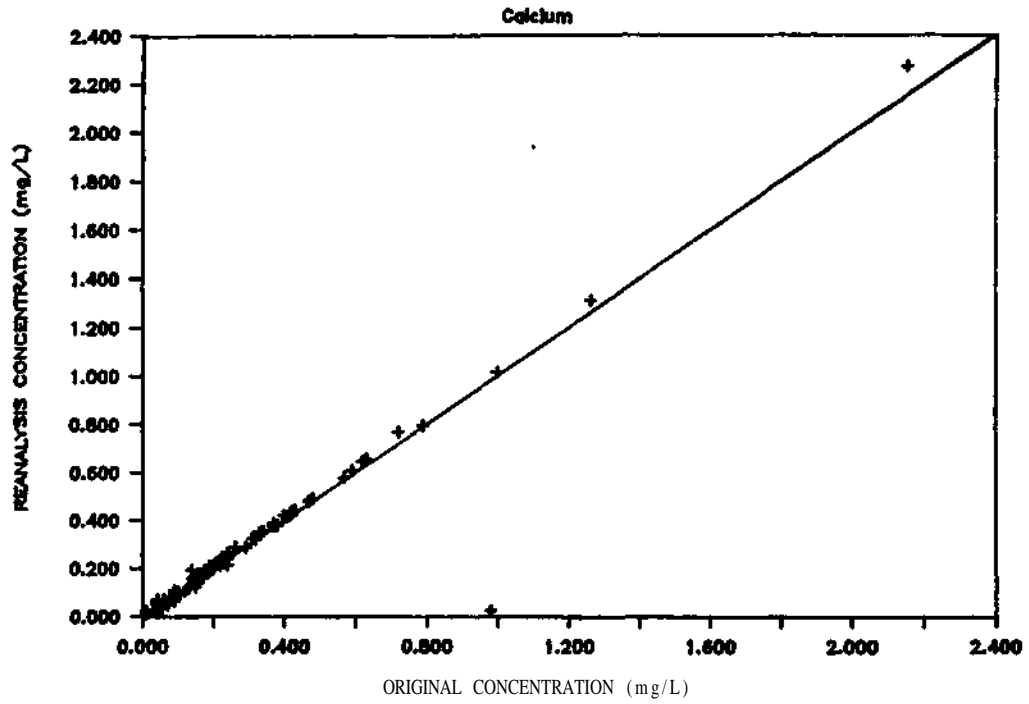


Figure 7. Original versus reanalysis results for calcium.

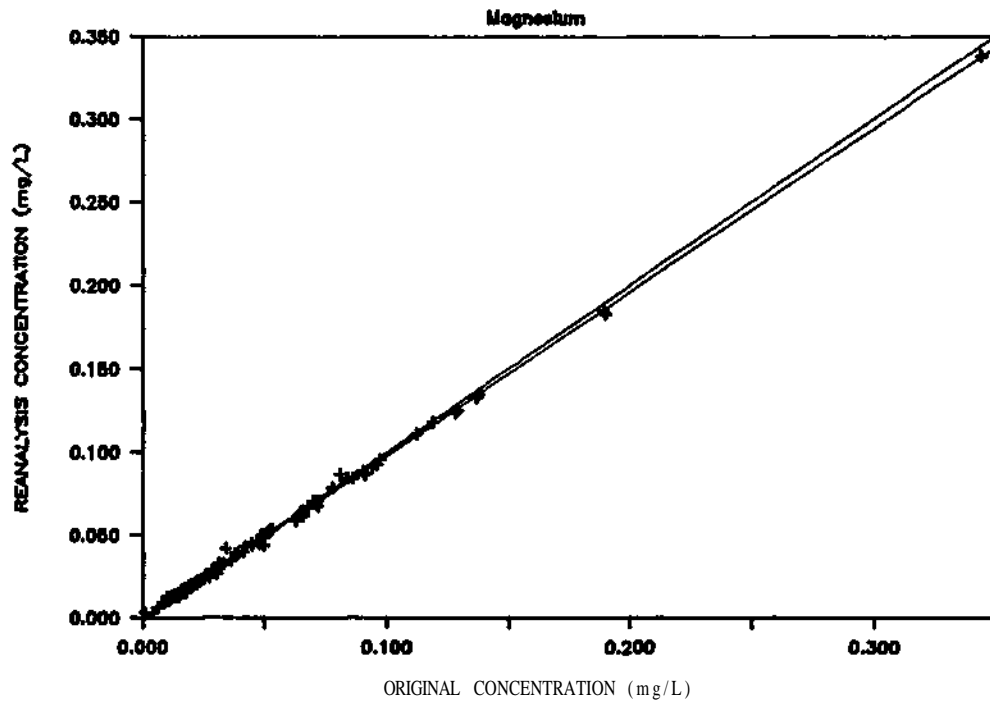


Figure 8. Original versus reanalysis results for magnesium.

Table 1. Summary of results from five year reanalyses of precipitation samples^a

Constituent	Original Values			Reanalysis Values			Mean Diff. ^b
	Min.	Max.	Mean	Mm.	Max.	Mean	
SO ₄ , mg/L	0.05	11.10	2.70	0.14	11.86	2.85	-0.15
NO ₃ , mg/L	0.01	5.80	1.57	0.01	6.04	1.64	-0.07
NH ₄ , mg/L	0.01	1.80	0.32	0.01	3.90	0.37	-0.04
Cl, mg/L	0.03	1.80	0.31	0.03	1.84	0.30	0.01
Ca, mg/L	0.010	4.830	0.303	0.013	4.930	0.302	0.001
Mg, mg/L	0.001	1.038	0.060	0.003	1.020	0.059	0.001
pH, units	3.84	7.14	4.43	3.78	7.32	4.28	0.15
Conduct., uS/cm	2.5	84.7	23.4	3.4	94.8	31.0	-7.6

a. n = 94

b. Mean difference = Original Mean - Reanalysis Mean

Table 2. Summary of least squares regression analyses and paired t-test results from five year reanalysis data.

Constituent	Regression Results			Paired t-test Results Significant at 95% Confidence Level? ^a
	r ²	slope	y-intercept	
SO ₄ , mg/L	0.99	1.06	-0.02	Yes
NO ₃ , mg/L	0.99	1.04	0.02	Yes
NH ₄ , mg/L	0.83	1.25	-0.04	No
Cl, mg/L	0.89	0.98	0.00	No
Ca, mg/L	0.968	1.005	-0.002	No
Mg, mg/L	1.000	0.981	0.000	Yes
pH, units	0.71	0.88	NA	Yes
Conduct., uS/cm	0.7	0.9	10.2	Yes

a. "Yes" response indicates that reanalysis values and original values are significantly different at the 95% confidence level.

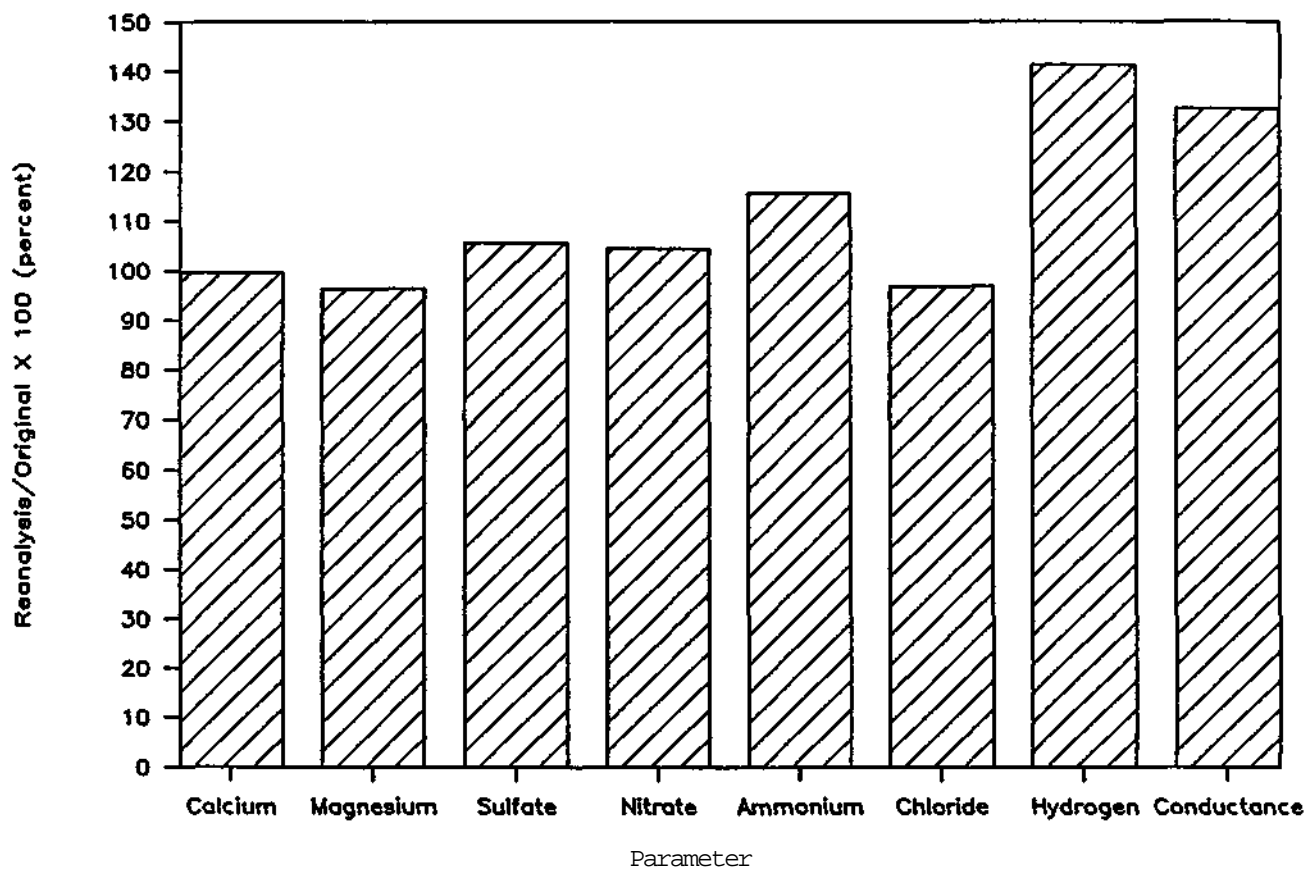


Figure 9. Percentage recovery results after six years of refrigerated storage.

Table 3. Significance of differences between reanalysis and original results on a site specific basis.^a

Constituent	Site Identification											
	CASS	CO21	FLO3	GA41	IL11	MN16	NC41	NE15	NHO2	NY20	OH17	WV18
SO ₄ , mg/L	No	No	No	No	No	No	Yes	No	No	No	Yes	Yes
NO ₃ , mg/L	No	No	No	Yes	Yes	No	Yes	Yes	Yes	No	No	No
NH ₄ , mg/L	No	Yes	No	Yes	No	No	Yes	No	Yes	No	Yes	Yes
Cl, mg/L	Yes	No	Yes	No	No							
Ca, mg/L	No	No	Yes	No	No	Yes	No	Yes	No	No	No	No
Mg, mg/L	No	No	No	Yes	Yes	No	Yes	No	No	Yes	No	No
pH, units	Yes	No	Yes	No	No	No	Yes	No	No	Yes	Yes	Yes
Conduct., uS/cm	Yes	No	Yes	Yes	No	No	Yes	No	Yes	Yes	Yes	Yes

a. "Yes" response indicates that reanalysis values and original values are significantly different at the 95% confidence level.

CONCLUSIONS

The long-term stability of precipitation samples has been investigated by measurement of samples stored in a refrigerator for six years. Of the eight constituents measured, Ca, Mg, Cl, SO₄, and NO₃ revealed reanalysis results within 10% of their original values. Evaporative losses during storage were not evident. Hydrogen ion concentrations increased by nearly 40%, on average, with a concomitant increase in solution conductivity. Ammonium results did not reveal a significant change in mean concentration, although the data were highly variable compared to the other analyte differences that were measured. No distinct patterns of long-term stability related to geographic regions or collection seasons were evident in this limited study. The suggested linkage between SO₄, NH₄, and pH changes during six years of storage can only be verified through additional research.

REFERENCES

- Peden, M. E., and L. M. Skowron, 1978: Ionic stability of precipitation samples. Atmospheric Environment, 12, 2343-2349 pp.
- Semonin, R. G., J. Bartlett, D. F. Gatz, M. E. Peden, L. M. Skowron, and G. J. Stensland, 1979: Study of Atmospheric Pollution Scavenging. Seventeenth Progress Report to the U.S. Department of Energy, Pollutant Characterization and Safety Research Division, Contract EY-76-S-02-1199, 118 pp.

CHAPTER 11

SYNTHETIC RAINWATER REFERENCE SAMPLES

Loretta M. Skowron and Mark E. Peden

INTRODUCTION

Wet deposition is collected and analyzed for chemical composition as a part of many monitoring networks. Data are used for spatial and temporal trend analyses and to assess the effects of "acid rain". In order to compare data from different laboratories and/or obtained with different instrumentation and techniques, the quality of the analytical determinations must be documented. One component of a quality assurance program makes use of reference materials. Reference materials have known and stable concentrations of the analyte of interest, and are used to establish the accuracy of chemical measurements. The National Bureau of Standards (NBS) provides Standard Reference Materials (SRM's) with certified chemical properties. Since 1986, SRM 2694 (I and II), Simulated Rainwater, has been available from the NBS. The Illinois State Water Survey (ISWS) has made extensive use of these solutions for verification of the accuracy of analytical methods, performance assessments of new instrumentation, and as quality control check samples during routine sample analysis. A complete description of SRM 2694 is available from the NBS (Koch, 1986).

When SRM 2694 is used for quality assurance purposes during the analysis of precipitation samples, several limitations become apparent. SRM's are relatively expensive, so that the cost of using them becomes prohibitive when they are used for several parameters by several chemists on a daily basis. Another drawback is that the certified concentrations of the parameters in SRM 2694 do not adequately reflect those actually found in wet-only deposition. There are also problems associated with the long-term stability of ammonium ion and pH in low ionic strength solutions (Koch, 1986). Nitrate, chloride, and ammonium concentrations are not certified by the NBS.

Our goal was to formulate and prepare a reference material that could be used as a quality control check sample with the following characteristics:

1. NBS traceable bias and precision
2. Available at low cost
3. Ionic concentrations approximating natural rainwater
4. Long-term stability

NBS traceability was accomplished by comparing our results with the certified NBS values. Multiple measurements performed over a five month period were used to assess long-term stability.

FORMULATION

Our initial goal was to formulate solutions containing the major inorganic ions that are routinely measured in precipitation. The target concentrations were chosen to represent values of weekly wet-only deposition samples from throughout the United States. The 25th and 75th percentile concentration values of samples collected during 1985 for the National Atmospheric Deposition Program (NADP)/National Trends Network (NTN) were used as these target values. These data represent 6089 samples obtained from over 200 sites located throughout the United States. These concentrations were compared with those found in NBS SRM 2694 in order to assess needed changes in formulation.

Ions of interest were calcium, magnesium, potassium, sodium, ammonium, nitrate, chloride, sulfate, and hydrogen (as pH). The specific conductance was not a major concern because reference solutions for this measurement are already available. However, the specific conductances were calculated for the synthetic solutions and found to be in an appropriate range for natural precipitation samples. Whenever possible, salts consisting of combinations of the ions of interest were used in the formulations. Nitric and sulfuric acids were the source of hydrogen ion.

The initial target values were slightly modified due to the restrictions imposed by the ratios of ions existing in the selected salts. For example, calcium chloride, $\text{CaCl}_2 \cdot 2\text{H}_2\text{O}$, is the source chemical for both calcium and chloride. If one calculates the amount needed to obtain the target calcium concentrations, the concomitant chloride concentrations are too high. Our synthetic reference solutions representing the 25th and 75th percentile concentration levels are referred to as ISWS-A and ISWS-B, respectively. Table 1 lists the NBS SRM target values, ISWS calculated target values, and the 25th and 75th percentile NADP/NTN wet deposition concentrations.

One liter of a stock solution was prepared containing all the ions of interest. This stock solution was then diluted 800:1 and 200:1 with deionized water to obtain the working solutions, ISWS A and ISWS B, respectively. Deionized water was filtered through a 0.2 μm point of use cartridge filter to prevent the introduction of bacteria into both the stock and diluted solutions. ACS-reagent grade salts were weighed to 0.1 mg with a Sauter RE1614 top-loading electronic balance. ACS-reagent grade acids were diluted with deionized water using a volume adjustable air-displacement Eppendorf pipet. The concentrations of ions in the stock solution, with their sources, are listed in Table 2. Salts were not dried and acids were not standardized because absolute accuracy was not necessary for the preliminary feasibility study. The true values would be verified using NBS certified solutions and ion balance calculations.

All solutions were stored in Nalge high density polyethylene bottles that were rinsed five times with deionized water, soaked one week with deionized water, emptied, and air-dried under a laminar flow clean air workstation. Synthetic solution ISWS-A was prepared by pipetting 1.25 mL of the stock solution into a one liter Class A volumetric flask partially filled with deionized water. The flask was then filled to volume with

Table 1. Target values for SRM 2694-I, SRM 2694-II, ISWS A, ISWS B, compared with NADP/NTN wet deposition data.

Ion	SRM 2694-I, mg/L ^a	SRM 2694-II, mg/L ^a	ISWS-A, mg/L	ISWS-B, mg/L	25th percentile, mg/L ^b	75th percentile, mg/L ^b
Ca	0.01	0.05	0.076	0.303	0.06	0.29
Mg	0.025	0.05	0.018	0.070	0.021	0.071
K	0.05	0.1	0.013	0.051	0.012	0.049
Na	0.2	0.4	0.047	0.190	0.036	0.185
NH ₄	0.1	1.0	0.092	0.370	<0.02	0.37
NO ₃	0.5	7	0.485	1.942	0.48	1.84
Cl	0.25	1.0	0.134	0.536	0.09	0.36
SO ₄	2.7	11	0.642	2.567	0.71	2.55
pH ^c	4.3	3.6	5.89	4.37	5.91	4.31
Specific conduc- tance, uS/cm	25	130	7.0	27.5	8.1	26.6

a from Koch, 1986

b from NADP/NTN data base, 1985

c pH units

Table 2. Chemical sources and calculated ionic concentrations in the synthetic rain stock solution.

Ion	Calculated Stock Concentration (mg/L)	Source
Ca	60.60	222.3 mg CaCl ₂ 2H ₂ O
Mg	14.06	142.5 mg MgSO ₄ 7H ₂ O
K	10.28	22.9 mg K ₂ SO ₄
Na	37.91	140.1 mg NaNO ₃
NH ₄	73.68	269.9 mg (NH ₄) ₂ SO ₄
Cl	107.22	222.3 mg CaCl ₂ 2H ₂ O
SO ₄	55.53	142.5 mg MgSO ₄ 7H ₂ O
	12.62	22.9 mg K ₂ SO ₄
	196.22	269.9 mg (NH ₄) ₂ SO ₄
	<u>248.96</u>	254.2 mg H ₂ SO ₄
Total	513.33	
NO ₃	103.19	140.1 mg NaNO ₃
	<u>285.73</u>	290.4 mg HNO ₃
Total	387.92	
H	5.24	254.2 mg H ₂ SO ₄
	<u>4.65</u>	290.4 mg HNO ₃
Total	9.89	

deionized water and mixed thoroughly. The solution was poured directly into four 250 mL bottles and distributed for analysis. Solution ISWS-B was prepared in the same manner using 5.00 mL of stock solution per liter volume.

SAMPLE ANALYSIS AND RESULTS

The solutions were analyzed using U.S. Environmental Protection Agency methods (Peden, et al., 1986). Calcium, magnesium, potassium, and sodium were measured by flame atomic absorption spectroscopy using an Instrumentation Laboratory Model 951 spectrophotometer, Method 200.6. Ammonium was measured using Method 350.7, an automated colorimetric determination with phenate. Nitrate, chloride, and sulfate were measured using chemically suppressed ion chromatography, Method 300.6, with a Dionex Model QIC system. The pH was measured with a Beckman Futura combination glass electrode, Model 39835, and an Orion 811 pH meter using Method 150 6. Specific conductance was measured using Method 120.6 utilizing a Yellow Springs Instrument (YSI) Model 32 meter and a YSI Model 3403 specific conductance cell with a cell constant of 1.0.

The samples were analyzed 3-4 times per week for five months, or until insufficient sample volume remained. Plots of the data, as concentration versus time, are depicted in Figures 1-10. The mean concentrations for samples measured over time are summarized and compared to the target concentrations in Table 3. The ratios of ISWS-B/ISWS-A are also given.

Since one stock solution was diluted to make both synthetic solutions, the ratios of these solution measurements can be used to assess the accuracy of the dilutions and to verify our calculated concentration values. The target value of B/A for all parameters is 4.0, except pH and specific conductance. Their calculated target value are 3.98 and 3.93, respectively. Dissolved atmospheric carbon dioxide, as carbonic acid, is present at a significant level in unbuffered solutions with a pH greater than 4.5, and must be taken into account for solution ISWS-A. There were no significant differences between the measured concentration ratios and the calculated target ratios for all parameters.

NBS SRM 2694-I and 2694-II samples were analyzed by ISWS staff in order to establish NBS traceability, and to verify the precision and bias of our measurements. Table 4 summarizes these data. There were no significant differences between our values and the certified values for all parameters.

The stability of the synthetic solutions over time was assessed with statistical analyses. All data points were used; there were no outliers. A linear least squares regression was applied to the data to obtain the slope of the measured concentrations versus time. None of the measured parameters for ISWS-A, ISWS-B, and the concentration ratio (B/A) had a slope significantly different from zero at the 95% confidence level.

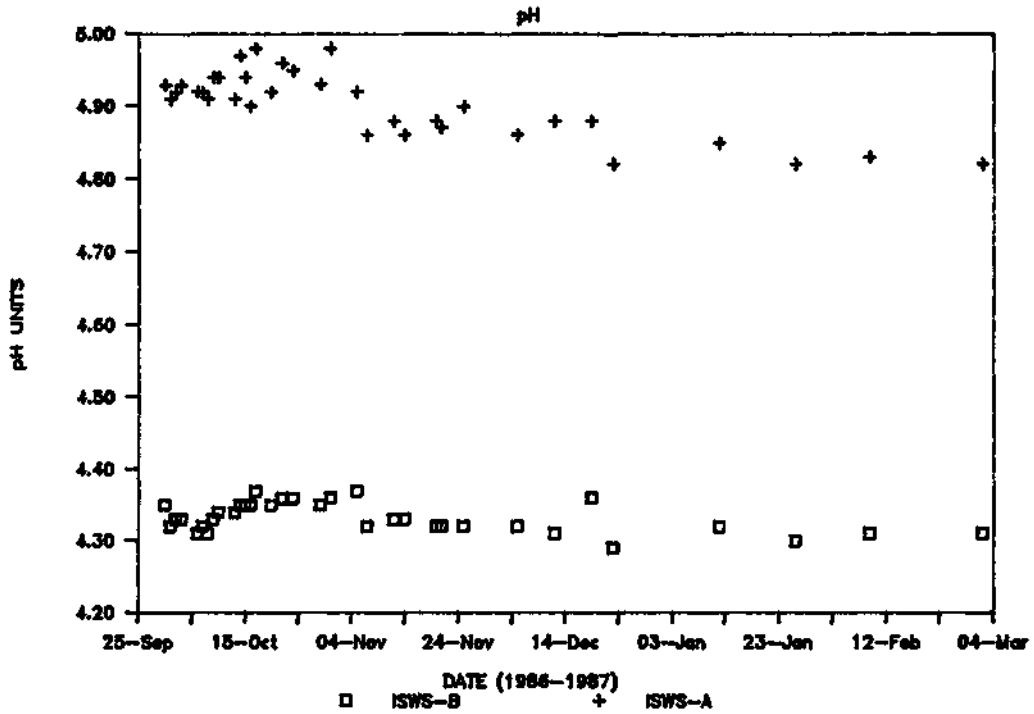


Figure 1. pH values versus time for ISWS-A and ISWS-B synthetic precipitation samples.

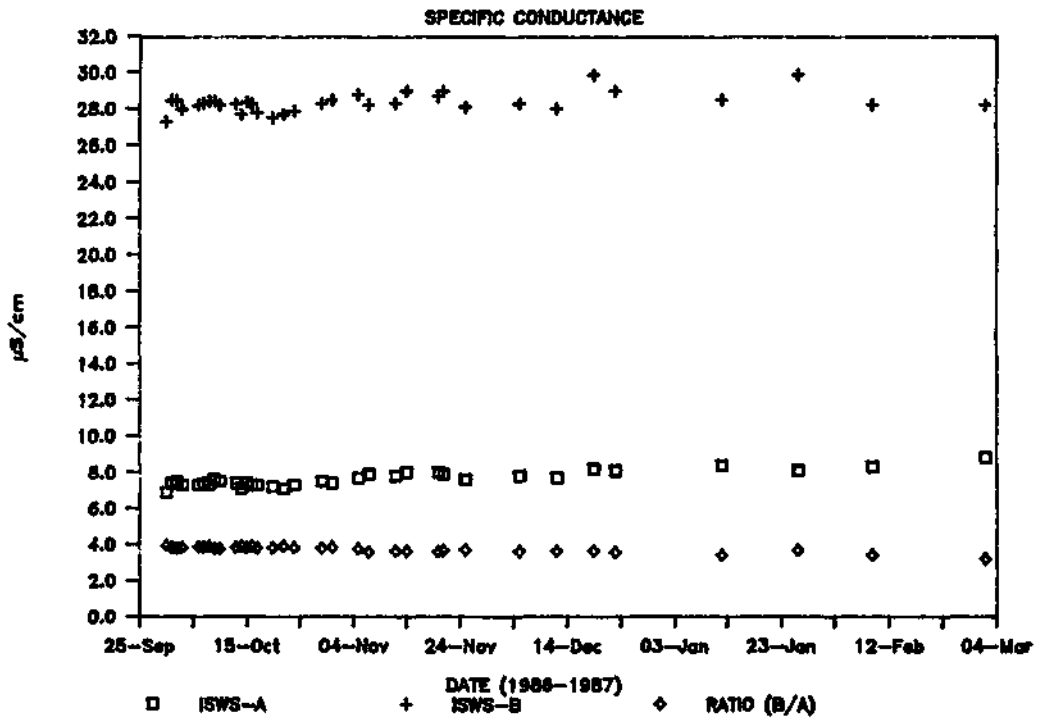


Figure 2. Specific conductance versus time for ISWS-A and ISWS-B synthetic precipitation samples.

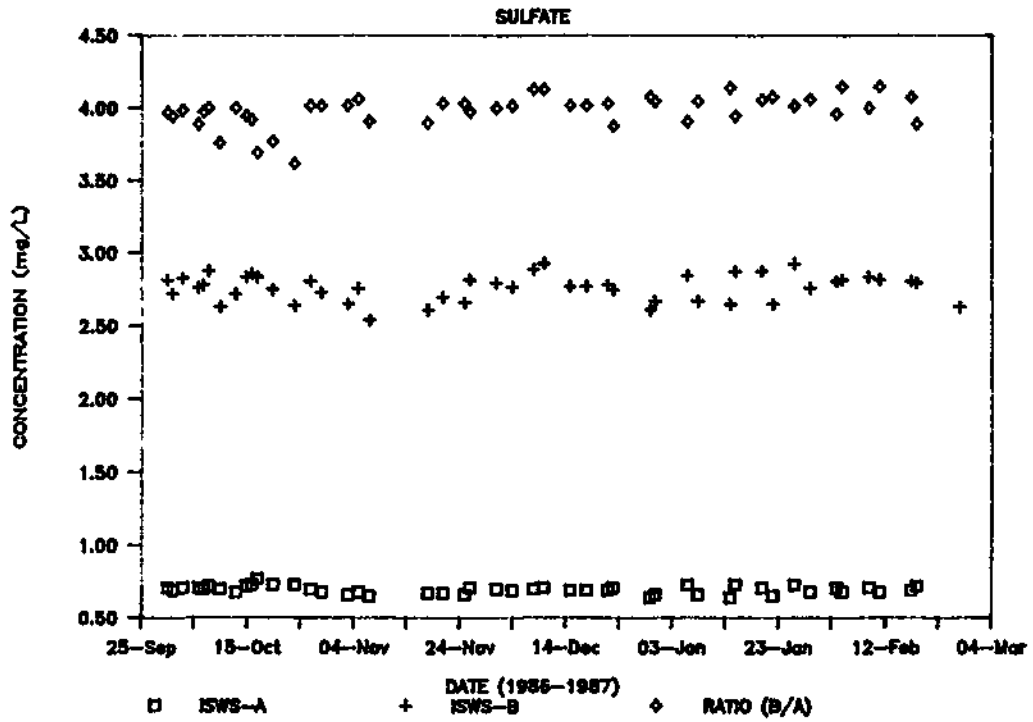


Figure 3. Sulfate concentrations versus time for ISWS-A and ISWS-B synthetic samples.

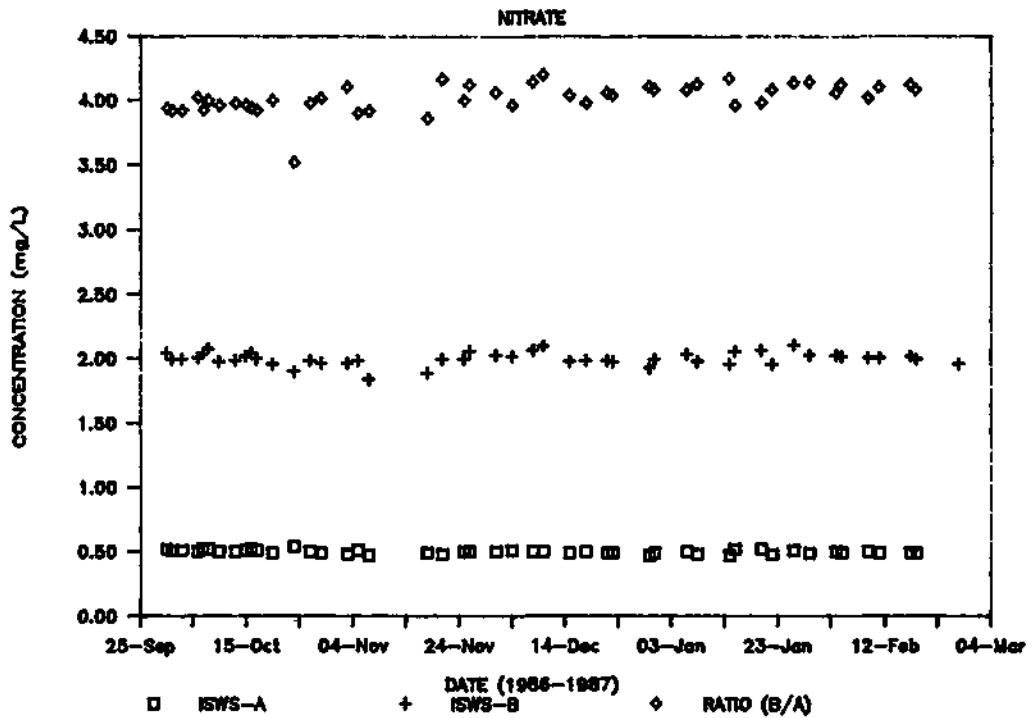


Figure 4. Nitrate concentrations versus time for ISWS-A and ISWS-B synthetic samples.

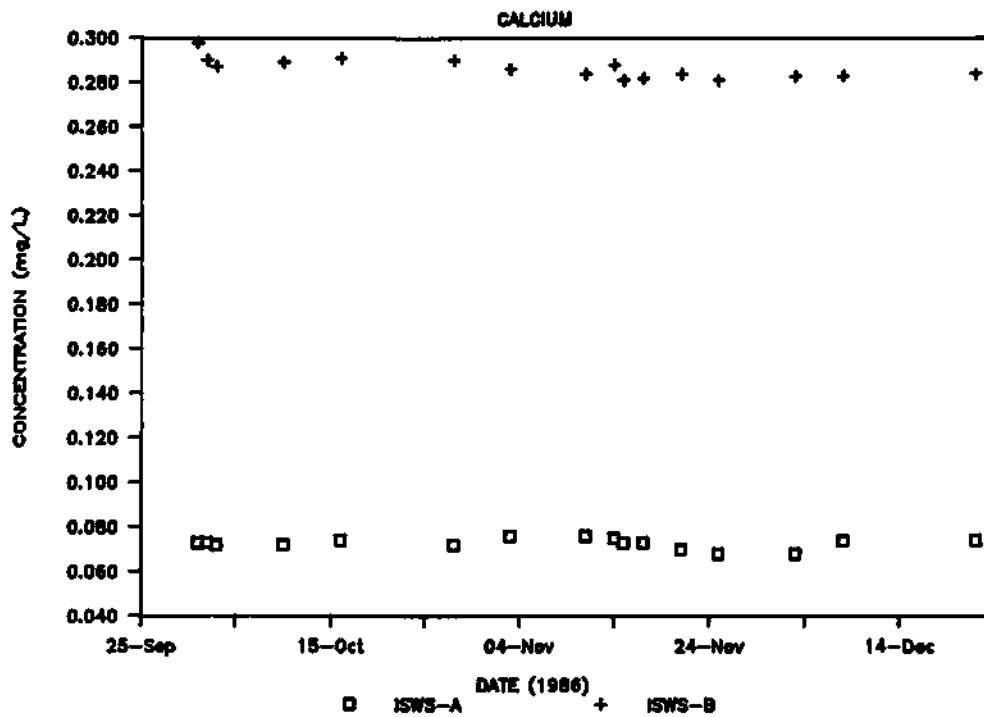


Figure 5. Calcium concentrations versus time for ISWS-A and ISWS-B synthetic samples.

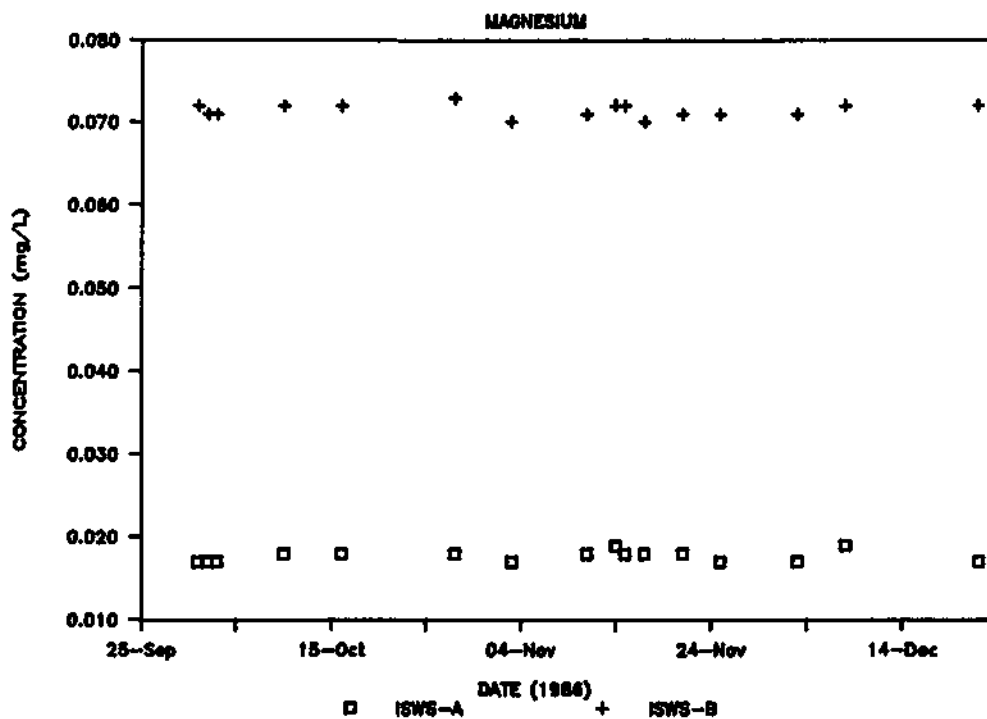


Figure 6. Magnesium concentrations versus time for ISWS-A and ISWS-B synthetic samples.

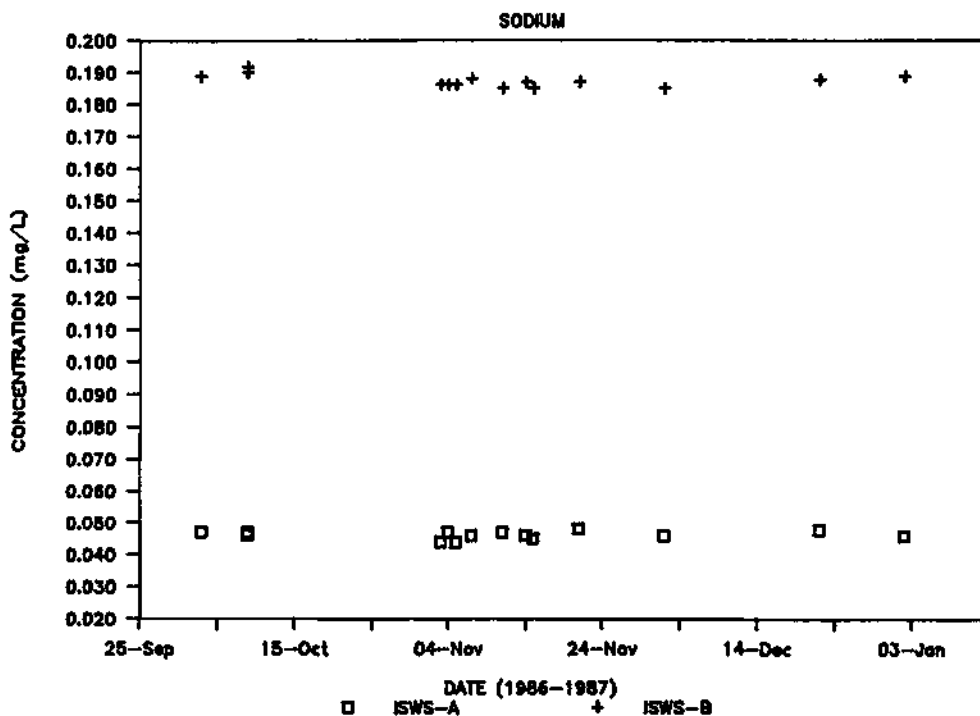


Figure 7. Sodium concentrations versus time for ISWS-A and ISWS-B synthetic samples.

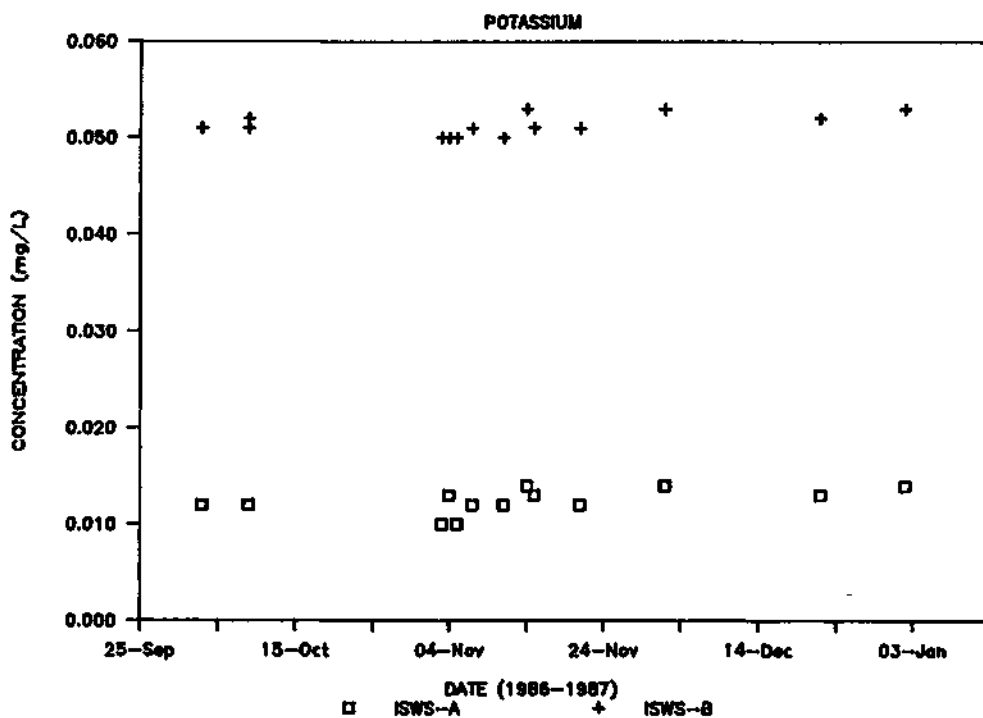


Figure 8. Potassium concentrations versus time for ISWS-A and ISWS-B synthetic samples.

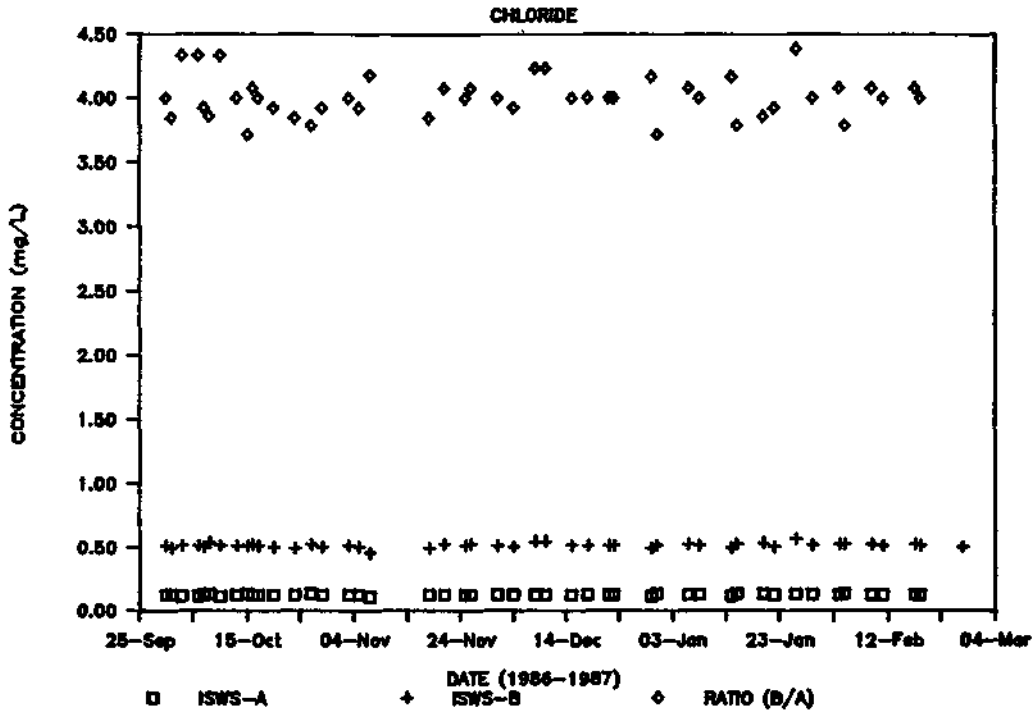


Figure 9. Chloride concentrations versus time for ISWS-A and ISWS-B synthetic samples.

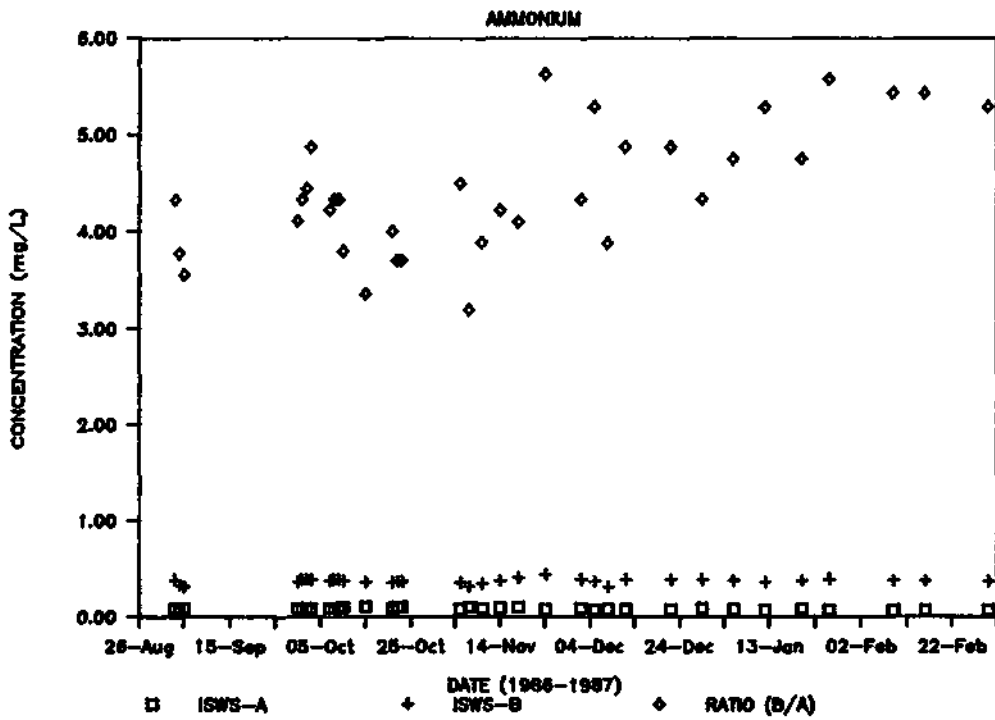


Figure 10. Ammonium concentrations versus time for ISWS-A and ISWS-B synthetic samples.

Table 3. Mean concentrations for samples measured over time.

Ion	ISWS Sample	Target Conc., mg/L	Mean, mg/L	Standard Dev., mg/L	n	Minimum, mg/L	Maximum, mg/L
Ca	A	0.076	0.073	0.002	16	0.068	0.076
	B	0.304	0.286	0.004	16	0.281	0.298
	B/A ^a	4.0	3.918	0.127	16	3.737	4.162
Mg	A	0.018	0.018	0.001	16	0.017	0.019
	B	0.070	0.071	0.001	16	0.070	0.073
	B/A ^a	4.0	3.944	0.143	16	3.789	4.235
K	A	0.013	0.012	0.001	14	0.010	0.014
	B	0.051	0.051	0.001	14	0.050	0.053
	B/A ^a	4.0	4.250	0.384	14	3.786	5.000
Na	A	0.047	0.046	0.001	14	0.044	0.048
	B	0.190	0.187	0.002	14	0.185	0.192
	B/A ^a	4.0	4.065	0.104	14	3.896	4.227
NH ₄	A	0.092	0.09	0.01	34	0.07	0.11
	B	0.370	0.38	0.03	34	0.31	0.45
	B/A ^a	4.0	4.36	0.65	34	3.20	5.63
NO ₃	A	0.485	0.50	0.01	46	0.47	0.54
	B	1.942	2.00	0.05	46	1.84	2.11
	B/A ^a	4.0	4.02	0.22	46	3.96	4.08
Cl	A	0.134	0.13	0.01	46	0.11	0.14
	B	0.536	0.52	0.02	46	0.46	0.57
	B/A ^a	4.0	4.00	0.16	46	3.71	4.38
SO ₄	A	0.642	0.70	0.03	46	0.64	0.77
	B	2.567	2.76	0.09	46	2.54	2.93
	B/A ^a	4.0	3.94	0.11	46	3.62	4.15
pH	A	4.91 ^b	4.90	0.04	34	4.82	4.98
	B	4.31	4.33	0.02	34	4.29	4.37
	B/A ^{ac}	3.98 ^b	3.72	0.28	34	3.24	4.17
Spec. Cond., uS/cm	A	7.0 ^b	7.6	0.4	34	6.9	8.8
	B	27.5	28.4	0.5	34	27.3	29.9
	B/A ^a	3.82 ^b	3.74	0.2	34	3.2	4.0

a There are no units associated with this ratio.

b Calculation assumes solution equilibrium with atmospheric CO₂.

c Units used for calculation are microequivalents per liter.

Table 4. NBS SRM 2694, Simulated Rainwater, certified concentrations compared with ISWS values.

Constituent	Certified		ISWS Values ^d	
	2694-I	2694-II	2694-I	2694-II
Calcium, mg/L	0.014±0.003	0.049±0.011	0.015±0.004	0.046±0.006
Magnesium, mg/L	0.024±0.002	0.051±0.003	0.024±0.002	0.050±0.003
Potassium, mg/L	0.052±0.007	0.106±0.008	0.050±0.004	0.105±0.003
Sodium, mg/L	0.205±0.009	0.419±0.015	0.200±0.010	0.422±0.023
Ammonium, mg/L	_____ ^a	(1.0) ^b	_____	1.03±0.02
Nitrate, mg/L	_____ ^a	7.06 ±0.15	_____	7.23 ±0.08
Chloride, mg/L	(0.24) ^b	(1.0) ^b	0.25 ±0.02	1.04 ±0.03
Sulfate, mg/L	2.75 ±0.05	10.9 ±0.2	2.86 ±0.12	11.19 ±0.18
pH @ 25 °C	4.27 ±0.03	3.59 ±0.02	4.28 ±0.03	3.59 ±0.02
Specific Cond., uS/cm @ 25.0 °C	26 ±2	130 ±2	26.0 ±1.2	130 ±2

a Values are not certified.

b Values are not certified, but are included for information only.

c Estimated uncertainties are two standard deviations of the certified values based on proven reliable methods of analysis, except for the uncertainties associated with SO₄, pH, and specific conductance. These are based on scientific judgement and are roughly equivalent to two standard of the certified value.

d Estimated uncertainties are two standard deviations of the means of nine replicate analyses of 2694-I and six replicate analyses of 2694-II.

(Student's t-test). This indicates that the concentrations of all ions for both high and low range samples did not change with time.

The first half and the second half (chronological order of analysis) measurements were also compared to examine solution stability. Table 5 shows the mean concentrations of each half, as well as the mean concentrations for all analyses. A Student's t-test (95% confidence level) was also performed on these data. Several small but significant differences between the first and second groups of analyses were found. These were for calcium in the high concentration sample, ammonium, nitrate, and pH in the low concentration sample, and specific conductance in both. Strict interpretation of these data is impractical because the absolute concentration differences are very small. There was a shift of approximately 0.05 pH units on November 10 for both ISWS-A and ISWS-B measurements. This was probably due to the replacement of an old pH electrode with a new one in the laboratory. If this discrepancy is factored out, there is no significant difference between the first half and the second half pH values. The remaining differences may be real, but there is the possibility that they, too, are a result of routine variability introduced by new calibration standards or slight modifications to instrument control settings.

Ion balances (Lockard, 1987) were calculated for the measured concentration of the synthetic solutions, ISWS-A and ISWS-B. The measurements were also divided chronologically into first and second halves. Calculated ion percent differences and conductivity percent differences were well within the laboratory control limits. Table 6 summarizes these data. The only significant difference between the first and second halves of analyses was for the specific conductance. Once again, the absolute numbers are very small, so that a conservative interpretation of the data is recommended.

CONCLUSIONS

Our original objective at the beginning of this study was to develop internally formulated reference materials that could be used in conjunction with NBS Standard Reference Materials. The purpose of the NBS reference material program is to provide source materials that can be used to ensure NBS traceability. The high cost of certified standards provided through this program, however, precludes their use on a routine basis to monitor laboratory performance. A review of the certified analytes contained in the NBS SRM for rainwater indicated that many laboratories could benefit from using internally formulated solutions that more closely approximated the concentration levels characteristic of wet deposition. In addition, solutions that contained all of the major ions of interest in precipitation were needed.

Results that have been presented indicate that a concentrated stock solution containing all of the major constituents in wet deposition can be easily prepared using commonly available salts and mineral acids. Dilutions of this single stock solution to the concentration levels

Table 5. Stability test comparing the mean concentrations of the first half of analyses with the second half.

Ion	ISWS Sample	Mean Conc.,	Mean Conc.,	Mean Conc.,	Pooled Std. Dev.	Significant Difference
		All Samples mg/L	First Half, mg/L	Second Half, mg/L		
Ca	A	0.073	0.074	0.072	0.003	no
	B	0.286	0.289	0.283	0.003	yes
Mg	A	0.018	0.018	0.018	0.001	no
	B	0.071	0.072	0.071	0.001	no
K	A	0.012	0.012	0.013	0.001	no
	B	0.051	0.051	0.052	0.001	no
Na	A	0.046	0.046	0.047	0.001	no
	B	0.187	0.188	0.187	0.002	no
NH ₄	A	0.09	0.09	0.08	0.01	yes
	B	0.38	0.37	0.38	0.03	no
NO ₃	A	0.50	0.50	0.49	0.01	yes
	B	2.00	1.99	2.01	0.05	no
Cl	A	0.13	0.13	0.13	0.01	no
	B	0.52	0.52	0.53	0.02	no
SO ₄	A	0.70	0.70	0.69	0.03	no
	B	2.76	2.75	2.78	0.09	no
pH ^a	A	4.90	4.93	4.87	0.03	yes
	B	4.33	4.34	4.33	0.02	no
Spec. _b Cond.	A	7.6	7.3	8.0	0.3	yes
	B	28.4	28.1	28.6	0.5	yes

a Microequivalents/liter used for calculations.

b Units are microSiemens/cm.

Table 6. Ion balance data for synthetic precipitation sample measurements.

Parameter	ISWS-A All Data	ISWS-B All Data	ISWS-A 1st Half	ISWS-A 2nd Half	ISWS-B 1st Half	ISWS-B 2nd Half
Anions ^a	26.7	104.5	26.8	26.3	104.2	105.4
Cations ^a	25.0	97.4	24.2	25.4	96.0	97.3
Ion % Diff. ^b	4.97	1.84	4.05	4.01	3.31	3.53
Cond. % Diff. ^c	-6.67	-4.71	-6.82	-8.24	-5.21	-5.18
Calculated pH	4.85	4.27	4.85	4.84	4.26	4.26
Calculated Conductance	7.1	27.1	6.8	7.3	26.6	27.1

a Units are microequivalents/liter.

$$b \text{ Ion \% difference} = \frac{(\text{Anions} - \text{Cations})}{(\text{Anions} + \text{Cations})} \times 100$$

$$c \text{ Conductivity \% Difference} = \frac{(\text{Calculated Conductance} - \text{Measured Conductance})}{\text{Measured Conductance}} \times 100$$

characteristic of wet deposition have resulted in stable formulations that can be used for routine quality control checks as well as internal blind audit samples.

The long term stability of these solutions is still under investigation, although five months of data indicate that sample integrity is maintained without the addition of any chemical preservatives or refrigerated storage. Ongoing studies are focusing on the long term stability of both the stock concentrate as well as the dilutions. Included in this work will be the development of statistical guidelines for using data obtained from these solution analyses to ensure traceability to the NBS Standard Reference Material.

REFERENCES

- Koch, W. F. , editor, 1986: Methods and Procedures Used at the National Bureau of Standards to Prepare, Analyze and Certify SRM 2694. Simulated Rainwater, and Recommendations for Use. NBS Special Publications 260-106, Center for Analytical Chemistry, National Bureau of Standards. Gaithersburg, MD 20899, 67 pp.
- Peden, M. E. , et al., 1986: Methods for Collection and Analysis of Precipitation. Illinois State Water Survey, 2204 Griffith Dr., Champaign, IL 61820, 276 pp. Contract Report 381.
- Lockard, J. M., 1987: Quality Assurance Report-NADP/NTN Deposition Monitoring: Laboratory Operations - Central Analytical Laboratory- July 1978 through December 1983. NREL, Ft. Collins, CO 80523, 180 PP.

CHAPTER 12

PRELIMINARY DATA FOR DAILY AMBIENT AEROSOL MEASUREMENTS
AT THE BONDVILLE RESEARCH SITE

Gary J. Stensland

INTRODUCTION

The Illinois State Water Survey (ISWS) has been involved in a major research program to investigate the precipitation scavenging of trace constituents in the atmosphere. One part of this study, the routine collection and analysis of event precipitation samples, was begun in June 1979 at the Bondville Research Site, 13 kilometers southwest of Champaign, Illinois. Previous research had shown the usefulness of simultaneously measuring the chemical concentrations in both air and precipitation. Therefore a routine ambient air sampling program was included with the precipitation chemistry collection project. The field methods and laboratory procedures for the ambient aerosol sampling were chosen to be consistent with the goals and procedures for the precipitation chemistry sampling. The unique features of the Bondville daily aerosol data set are that a) it is a rather long daily record (starting in May 1977); b) it includes data for Ca^{2+} , Mg^{2+} , Na^+ , and K^+ which are often neglected in other studies; and c) the method includes an extraction step designed to simulate dissolution of particles in raindrops (i.e., a "soluble" extraction rather than a total extraction).

A chapter in the Seventeenth Progress Report presented a description and a rather thorough evaluation of our sampling procedure (Stensland and Bartlett, 1979). A major emphasis of the chapter was to determine precision with triplicate sampling with polycarbonate filters and to describe differences when various filter media (polycarbonate and cellulose), filter set-ups (single and stacked), and pore sizes (0.4 and 0.8 μm) were used for determining ambient aerosol levels of the following soluble ions: NO_3^- , NH_4^+ , SO_4^{2-} , and Ca^{2+} . A chapter in the Eighteenth Progress Report discussed our original soluble extractions procedure (using deionized water and 20 minutes shaking) versus the modified extraction procedure which was used for our ambient aerosol filter extractions after June 1979 (pH = 3 HCl and 24-48 hours shaking) (Bartlett and Stensland, 1980). Another 1980 chapter included a comparison of cellulose versus polycarbonate filters for 73 daily samples, a comparison of polycarbonate versus teflon (Fluoropore) filters for six samples, and results for one year of daily aerosol sampling at the first collection site at Willard Airport, 10 kilometers south of Champaign (Stensland and Bartlett, 1980). A chapter in the Nineteenth Progress Report presented a comparison of total (x-ray fluorescence) analysis versus our soluble (DI water and 20 minutes shaking) type of analysis for 24 pairs of daily aerosol samples collected at the Bondville site in summer, 1978 (Stensland and Gatz, 1981).

The purpose of this chapter is to present additional methodological and ambient data results. The ambient data results are called preliminary since additional work is needed to develop the best procedure to correct for blanks and for flow calibration. Another chapter in this report will compare these preliminary aerosol results to precipitation chemistry data by calculating scavenging ratios.

EXPERIMENTAL PROCEDURES

The field site is located 13 kilometers southwest of Champaign-Urbana in east-central Illinois and is called the Bondville site. The surrounding area is rural farmland. The low-volume aerosol sampling system consists of Gast piston-type vacuum pumps with inverted polyethylene funnels serving as weather shields housing the filter holders. Daily at 10 AM, a mechanical timer activates one of four identical systems so that the aerosol sampling system requires servicing only twice per week. The filter unit consists of a 37 mm polycarbonate filter (Nuclepore™ before February 1983), or a 37 mm teflon filter (Zefluor supported PTFE with support pads, used after February 1983) with a pore size of 0.8 μm diameter for polycarbonate or 1.0 μm for teflon, mounted in Millipore Field Monitor plastic filter holders. The units are mounted face down under the inverted funnel with the filter surface 2 cm above the funnel's rim and 2 meters above the ground.

The volume drawn through the daily filter samples by the vacuum pumps was determined by manual reading of the pressure and rotameter gauges on the pumps, and calculating the volume for each sample. The readings are made after the pumps have warmed up by running for at least two minutes. The volumes are presented for an ambient pressure of one atmosphere; no temperature correction is made. The mean of the corrected initial and final flow values are used to calculate the total air volume sampled. Air is drawn through the filters for 30 minutes out of each hour for 24 hours, with about 20 cubic meters of air being sampled per day. The pumps were calibrated with a dry test meter (an intermediate standard which is periodically tested by sending it to USEPA). In recent years a dry gas meter has been attached to each vacuum pump to provide a second independent daily sample volume determination. The dry gas meters are calibrated with the dry test meter. Further checks of this pump/calibration system are in progress and may produce some changes in our daily sample volume values. This is the main reason that we presently refer to our aerosol data as preliminary data subject to revision. The revisions are unlikely to alter the major features of the results presented in this report.

After the collection period, the filters are stored in sterilized petri dishes at room temperature. Storage time before chemical analysis was typically 2 months but ranged from several days to 5 months.

In the extraction procedure, each filter is placed in a pre-washed 50 ml Nalgene linear polyethylene (LPE) bottle with 25 ml of pH 3 hydrochloric acid solution and agitated for at least 24 hours on a shaker at

room temperature. This solution is then filtered through a Millipore HA 0.45 μm filter and collected in another 50 ml Nalgene LPE bottle.

The extraction solutions are stored at room temperature until the ion concentrations are measured.

The analytical method for the SO_4 was methylthymol blue automated on the Technicon Autoanalyzer II. (Note that for the remainder of this chapter, the charge symbols will not be shown for the ions.) Ca, K, Mg and Na ions were determined by flame atomic absorption. In 1977-78 NO_3 and NH_4 were also measured but subsequently we learned that the simple system was inadequate for determining representative ambient air concentrations of these nitrogen species. In 1977-78 we also measured Cl but this also was discontinued when we began using the pH 3.0 HCl extraction solution in June 1979

RESULTS AND DISCUSSION

Comparison of Teflon and Polycarbonate Filters

This section compares the aerosol concentration results for two filter media (polycarbonate and teflon) for a summer month in 1982 and a winter month in 1984. A previous report (Dolske and Stensland, 1983) showed that the two filter media produced very different results for sulfate for the summer month.

Results from pairs of polycarbonate and teflon filters sampling simultaneously during 24 hours at the field sites are shown in Tables 1-8. The 1984 data in Tables 1-4 were mostly from days in February from sampling equipment located at the main field site, seven kilometers south of Bondville, IL. The 1982 data in Tables 5-8 were from days in June from sampling equipment located at the Monticello Road field site, about 5 kilometers southeast of the Bondville field site.

The second column in each table gives the ion concentration for the polycarbonate filters; the third column is the value for the corresponding teflon filter. The fourth column gives the differences and the fifth column presents the ratio of the two values. Table 9 consolidates the ratio values for the two sampling periods.

By examining all the ion values for the filters for each day we note the following. On 23 February 1984, for all four constituents (SO_4 , Ca, Mg, and K), the values for the teflon filters are much less than the corresponding values from the polycarbonate filters. On 4 June 1982, the values for SO_4 , Mg, and K are all much less from the polycarbonate filter than for the teflon filter. The feature is less extreme for Ca but has the same tendency. We feel these data indicate that an air leak probably existed (most likely in the plastic filter holder system) on these two days and therefore the data for 23 February 1984 and 4 June 1982 will be eliminated for further analysis.

Table 1. Winter 1984 comparison of daily aerosol sampling of sulfate at the Bondville, IL field research site with polycarbonate (N) and teflon (T) filters. Aerosol concentrations are in $\mu\text{g}/\text{m}^3$.

Date On	$(\text{SO}_4)_N$	$(\text{SO}_4)_T$	$-(\text{SO}_4)_N - (\text{SO}_4)_T$	$(\text{SO}_4)_N / (\text{SO}_4)_T$
13184	1.606	2.209	-.603	.727
20184	1.365	3.177	-1.812	.430
20384	1.652	2.462	-.810	.671
20684	1.180	1.626	-.446	.726
20784	2.408	2.850	-.442	.845
20884	2.265	4.694	-2.429	.483
20984	5.596	5.214	.382	1.073
21084	.525	1.256	-.731	.418
21384	1.188	1.040	.148	1.142
21484	1.757	1.297	.460	1.355
21584	2.858	5.451	-2.593	.524
21684	2.403	4.208	-1.805	.571
21784	5.590	9.714	-4.124	.575
22084	2.503	1.680	.823	1.490
22184	1.673	2.070	-.397	.808
22284	1.455	2.336	-.881	.623
22384	3.619	.136	3.483	26.610*
30184	2.716	5.493	-2.777	.494
Median	2.08	2.40	-.67	.671
Mean	2.35	3.16	-.81	.762
Std. Dev.	1.39	2.30	1.68	.323

*Not used to calculate summary statistics on this table.

Table 2. Winter 1984 comparison of daily aerosol sampling of calcium at the Bondville, IL field research site with polycarbonate (N) and teflon (T) filters. Aerosol concentrations are in $\mu\text{g}/\text{m}^3$.

<u>Date On</u>	<u>(Ca)_N</u>	<u>(Ca)_T</u>	<u>(Ca)_N-(Ca)_T</u>	<u>(Ca)_N/(Ca)_T</u>
13184	.237	.302	-.065	.785
20184	.252	.301	-.049	.837
20384	.144	.150	-.006	.960
20684	.346	.403	-.057	.859
20784	.356	.257	.099	1.385
20884	.202	.213	-.011	.948
20984	.330	.264	.066	1.250
21084	.012	.026	-.014	.462
21384	.204	.032	.172	6.375*
21484	.369	.277	.092	1.332
21584	.272	.442	-.170	.615
21684	.069	.112	-.043	.616
21784	.049	.060	-.011	.817
22084	.270	.242	.028	1.116
22184	.472	.523	-.051	.902
22284	.434	.504	-.070	.861
22384	.480	.014	.466	34.286*
30183	.510	.690	-.180	.739
Median	.271	.260	-.012	.848
Mean	.278	.267	.011	.905
Std. Dev.	.149	.190	.143	.259

*Not used to calculate summary statistics on this table.

Table 3. Winter 1984 comparison of daily aerosol sampling of magnesium at the Bondville, IL field research site with polycarbonate (N) and teflon (T) filters. Aerosol concentrations are in $\mu\text{g}/\text{m}^3$.

Date On	(Mg) _N	(Mg) _T	(Mg) _N - (Mg) _T	(Mg) _N / (Mg) _T
13184	.017	.031	-.014	.548
20184	.022	.030	-.008	.733
20384	.017	.020	-.003	.850
20684	.066	.076	-.010	.868
20784	.073	.056	.017	1.304
20884	.027	.031	-.004	.871
20984	.050	.034	.016	1.471
21084	.001	.005	-.004	.200
21384	.024	.003	.021	8.000*
21484	.040	.029	.011	1.379
21584	.040	.062	-.022	.645
21684	.017	.013	.004	1.308
21784	.021	.015	.006	1.400
22084	.023	.020	.003	1.150
22184	.056	.064	-.008	.875
22284	.039	.048	-.009	.812
22384	.047	.001	.046	47.000*
30184	.047	.067	-.020	.701
Median	.033	.030	-.004	.870
Mean	.035	.034	.001	.945
Std. Dev.	.019	.023	.017	.358

*Not used to calculate summary statistics on this table.

Table 4. Winter 1984 comparison of daily aerosol sampling of potassium at the Bondville, IL field research site with polycarbonate and teflon (T) filters. Aerosol concentrations are in ug/m³.

Date On	(K) _N	(K) _T	(K) _H - (K) _T	(K) _N / (K) _T
13184	.034	.052	-.018	.654
20184	.039	.075	-.036	.520
20384	.016	.025	-.009	.640
20684	.035	.051	-.016	.686
20784	.042	.048	-.006	.875
20884	.063	.086	-.023	.733
20984	.135	.113	.022	1.195
21084	.002	.031	-.029	.064
21384	.028	.013	.015	2.154*
21484	.034	.024	.010	1.417
21584	.045	.080	-.035	.562
21684	.029	.048	-.019	.604
21784	.031	.051	-.020	.608
22084	.039	.027	.012	1.444
22184	.043	.049	-.006	.878
22284	.048	.056	-.008	.857
22384	.047	.001	.046	47.000*
30184	.039	.062	-.023	.629
Median	.039	.050	-.012	.670
Mean	.042	.050	-.008	.773
Std. Dev.	.027	.028	.022	.346

*Not used to calculate summary statistics for this table.

Table 5. Summer 1982 comparison of daily aerosol sampling of sulfate at the Bondville, IL field research site with polycarbonate (N) and teflon (T) filters. Aerosol concentrations are in $\mu\text{g}/\text{m}^3$.

Date On	$(\text{SO}_4)_\text{N}$	$(\text{SO}_4)_\text{T}$	$(\text{SO}_4)_\text{T}$	$(\text{SO}_4)_\text{N} - (\text{SO}_4)_\text{T}$	$(\text{SO}_4)_\text{N} / (\text{SO}_4)_\text{T}$
60482	.165	6.407	7.8	-6.242	.026
60582	7.361	13.010	12.5	-5.649	.566
60682	7.371	17.525	17.0	-10.154	.421
60782	4.130	9.001	8.2	-4.871	.459
60882	2.247	7.557	4.8	-5.310	.297
60982	4.139	6.894	6.1	-2.755	.600
61082	1.296	.750	1.6	.546	1.728
61182	1.745	1.793	4.0	-.048	.973
61282	4.200	6.870	8.1	-2.670	.611
61382	.606	1.340	1.5	-.734	.452
61482	5.420	4.065	7.5	1.355	1.333
61582	4.048	6.629	6.3	-2.581	.611
61682	2.275	1.738	3.3	.537	1.309
61782	.178	14.182	14.0	-14.004	.013
61882	6.694	9.827	7.8	-3.133	.681
61982	4.006	3.209	3.5	.797	1.248
62082	1.014	.941	2.1	.073	1.078
62182	.595	.893	1.6	-.298	.666
62282	.988	1.099	2.2	-.111	.899
62382	1.339	1.100	2.4	.239	1.217
62482	2.057	4.806	5.1	-2.749	.428
62582	10.283	21.298	22.4	-11.015	.483
62682	10.565	22.965	21.3	-12.400	.460
62782	6.027	10.635	11.6	-4.608	.567
62882	2.090	9.183	9.4	-7.093	.228
Median	2.275	6.624		-2.749	.600
Mean	3.634	7.349		-3.715	.694
Std. Dev .	3.019	6.460		4.407	.428

Table 6. Summer 1982 comparison of daily aerosol sampling of calcium at Che Bondville, IL field research site with polycarbonate (N) and teflon (T) filters. Aerosol concentrations are in ug/m³.

<u>Date On</u>	<u>(Ca)_N</u>	<u>(Ca)_T</u>	<u>(Ca)_N-(Ca)_T</u>	<u>(Ca)_N/(Ca)_T</u>
60482	.149	.661	-.512	.225
60582	.756	.790	-.034	.957
60682	.608	.653	-.045	.931
60782	.296	.281	.015	1.053
60882	.626	.643	-.017	.974
60982	.442	.500	-.058	.884
61082	1.966	1.118	.848	1.758
61182	1.126	.934	.192	1.206
61282	.307	.298	.009	1.030
61382	1.906	2.914	-1.008	.654
61482	.795	.483	.312	1.646
61582	.216	.154	.062	1.403
61682	.439	.234	.205	1.876
61782	.427	.325	.102	1.314
61882	.397	.248	.149	1.601
61982	.402	.215	.187	1.870
62082	.572	.454	.118	1.260
62182	1.387	1.642	-.255	.845
62282	.673	.821	-.148	.820
62382	.690	.648	.042	1.065
62482	.980	1.399	-.419	.700
62582	.762	1.122	-.360	.679
62682	.823	1.249	-.426	.659
62782	.317	.443	-.126	.716
62882	.013	.086	-.073	.151
Median	.61	.64	-.02	.974
Mean	.68	.73	-.05	1.051
Std. Dev.	.49	.61	.34	.461

Table 7. Summer 1982 comparison of daily aerosol sampling of magnesium at the Bondville, IL field research site with polycarbonate (N) and teflon (T) filters. Aerosol concentrations are in ug/m³.

Date On	(Mg) _N	(Mg) _T	(Mg) _N - (Mg) _T	(Mg) _N / (Mg) _T
60482	.007	.162	-.155	.043
60582	.153	.184	-.031	.832
60682	.089	.122	-.033	.730
60782	.044	.073	-.029	.603
60882	.130	.156	-.026	.833
60982	.050	.074	-.024	.676
61082	.319	.188	.131	1.697
61182	.163	.154	.009	1.058
61282	.034	.047	-.013	.723
61382	.094	.151	-.057	.622
61482	.094	.072	.022	1.306
61582	.022	.031	-.009	.710
61682	.075	.055	.020	1.364
61782	.036	.041	-.005	.878
61882	.023	.025	-.002	.920
61982	.033	.026	.007	1.269
62082	.064	.052	.012	1.231
62182	.063	.072	-.009	.875
62282	.104	.122	-.018	.852
62382	.104	.098	.006	1.061
62482	.139	.206	-.067	.675
62582	.085	.147	-.062	.578
62682	.096	.160	-.064	.600
62782	.035	.053	-.018	.660
62882	.007	.017	-.010	.412
Median	.08	.07	-.01	.832
Mean	.08	.10	-.02	.848
Std. Dev.	.07	.06	.05	.344

Table 8. Summer 1982 comparison of daily aerosol sampling of potassium at the Bondville, IL field research site with polycarbonate (N) and teflon (T) filters. Aerosol concentrations are in $\mu\text{g}/\text{m}^3$.

<u>Date On</u>	<u>(K)_N</u>	<u>(K)_T</u>	<u>(K)_N-(K)_T</u>	<u>(K)_N/(K)_T</u>
60482	.018	.203	-.185	.089
60582	.099	.140	-.041	.707
60682	.061	.088	-.027	.693
60782	.055	.092	-.037	.598
60882	.104	.126	-.022	.825
60982	.074	.108	-.034	.685
61082	.083	.044	.039	1.886
61182	.061	.051	.010	1.196
61282	.059	.084	-.025	.702
61382	.048	.065	-.017	.738
61482	.099	.070	.029	1.414
61582	.111	.190	-.079	.584
61682	.042	.035	.007	1.200
61782	.050	.072	-.022	.694
61882	.064	.070	-.006	.914
61982	.059	.042	.017	1.405
62082	.069	.052	.017	1.327
62182	.029	.030	-.001	.967
62282	.033	.035	-.002	.943
62382	.044	.041	.003	1.073
62482	.051	.080	-.029	.638
62582	.135	.250	-.115	.540
62682	.157	.307	-.150	.511
62782	.072	.119	-.047	.605
62882	.015	.053	-.038	.283
Median	.06	.07	-.02	.707
Mean	.07	.10	-.03	.849
Std. Dev.	.03	.07	.05	.394

Table 9. Summary tabulation of the ratios of (Ion)_N + (Ion)_T from Tables 1-8.

<u>Date</u>	<u>SO₄</u>	<u>K</u>	<u>Mg</u>	<u>Ca</u>
13184	.73	.65	.55	.78
20184	.43	.52	.73	.84
20384	.67	.64	.85	.96
20684	.73	.69	.87	.86
20784	.84	.88	1.30	1.38
20884	.70	.73	.87	.95
20984	1.26	1.20	1.47	1.25
21084	.42	.06	.20	.46
21384	1.14	2.12	7.00	6.38
21484	1.36	1.42	1.38	.33
21584	.52	.56	.64	.62
21684	.57	.60	1.31	.62
21784	.58	.61	1.40	.82
22084	1.49	1.44	1.15	1.12
22184	.81	.88	.88	.90
22284	.62	.86	.81	.86
30184	.49	.63	.70	.74
60582	.57	.71	.83	.96
60682	.42	.69	.73	.93
60782	.46	.60	.60	1.05
60882	.30	.82	.83	.97
60982	.60	.68	.68	.88
61082	1.73	1.89	1.70	1.76
61182	.97	1.20	1.06	1.21
61282	.61	.70	.72	1.03
61382	.45	.74	.62	.65
61482	1.33	1.41	1.31	1.65
61582	.61	.58	.71	1.40
61682	1.31	1.20	1.36	1.88
61782	.01*	.69	.88	1.31
61882	.68	.91	.92	1.60
61982	1.25	1.40	1.27	1.87
62082	1.08	1.33	1.23	1.26
62182	.67	.97	.88	.84
62282	.90	.94	.85	.82
62382	1.22	1.07	1.06	1.06
62482	.43	.64	.68	.70
62582	.48	.54	.58	.68
62682	.46	.51	.60	.66
62782	.57	.60	.66	.72
62882	.23	.28	.41	.15

*June 17 SO₄ data are not used in further analysis.

By examining the rows in Table 9, we observe rather consistent ratio values for each ion in the row. A day like 10 February 1984 is an exception in that the ion ratios differ markedly. The ambient concentrations for this day in Tables 1-4 indicate that this was a rather clean day, on which the low levels being measured would be relatively imprecise. We considered but then decided against a screening procedure which would have flagged or eliminated the rather clean days.

The SO_4 ratio in Table 9 for 17 June 1982 is very different from the other ion ratios for this day. We are eliminating the SO_4 (but not the other ions) data for this day from further analysis even though we do not have a causal explanation for the difference.

We see in Tables 1 and 5 that the teflon sulfate values are generally larger than the polycarbonate values (in 13 out of 18 cases in Table 1 and in 19 out of 25 cases in Table 5). Laboratory comparison studies of polycarbonate and teflon filters with various submicron sizes of monodisperse test aerosols indicated that the $0.8 \mu\text{m}$ polycarbonate filters would capture only a fraction of the submicron aerosols while the $1.0 \mu\text{m}$ teflon filters would capture greater than 99.99% of all particles in the size range $0.03\text{-}1.0 \mu\text{m}$ (Liu and Lee, 1976). Most of the ambient aerosol sulfate mass is reported to be in submicron particle sizes.

The calcium and magnesium values in Table 9 are closer to 1.00 than those for SO_4 as is to be expected for these generally supermicron sized particles. Somewhat surprisingly, the potassium values in Table 9 are often similar to the values for sulfate.

It is known that handling can result in some fraction of the larger particles being dislodged from the filter surfaces on which they were deposited. If this were a more severe problem for one filter media than for the other filter media, then this would produce average ratios which are different than 1.00.

When the polycarbonate sulfate values were greater than the teflon sulfate values (see Table 9), then the same was generally true for potassium, calcium, and magnesium. Thus we do not think ion measurement precision nor handling loss of larger particles are good explanations for the cases where polycarbonate values exceeded teflon values. A filter holder air leak could be the explanation and we intend to evaluate this in a future test.

A statistical summary of the ion concentration ratios for polycarbonate ($.8 \mu\text{m}$) versus teflon filters is shown in Table 10. The results are presented for the two separate sampling periods and for the combined data set. The statistical test results for the paired t-test and the Wilcoxon paired sample test are shown. The SO_4 ratios are always statistically different than 1.00. The same is generally true for K (note the result for the combined set and the fact that the median K ratio values are quite low). The Ca and Mg ratios are not statistically different from 1.00 (although Mg is for the summer data). These data will be used in the future to adjust the 1978-1983 ambient aerosol data record for polycarbonate filters at Bondville such that it can be compared to the teflon filter record collected since 1983. We will likely use the median ratios

Table 10. Statistical summary for polycarbonate (0.8 μm) and teflon (1.0 μm) filters concentration ratios.

Ratios: (Conc.)N + (Conc.)x

<u>Winter:</u>	<u>SO₄</u>	<u>Ca</u>	<u>Mg</u>	<u>K</u>
Median	.671	.861	.871	.686
Mean	.762	1.227	1.360	.854
Std. Dev.	.3229	1.3500	1.7459	.4740
Std. Error	.078	.327	.423	.115
N	17	17	17	17
t-test*	Yes (.008)	No	No	No
Wilcoxon	Yes (.014)	No	No	No

Summer:

Median	.611	1.002	.832	.723
Mean	.753	1.085	.882	.880
Std. Dev.	.3939	.4368	.3070	.3687
Std. Error	.082	.089	.063	.075
N	23	24	24	24
t-test	Yes (.006)	No	Yes (.07)	No
Wilcoxon	Yes (.006)	No	Yes (.04)	Yes (.10)

Combined:

Median	.617	.948	.852	.707
Mean	.757	1.144	1.080	.870
Std. Dev.	.3610	.9186	1.1534	.4101
Std. Error	.057	.143	.180	.064
N	40	41	41	41
t-test	Yes (.0001)	No	No	Yes (.05)
Wilcoxon	Yes (.0002)	No	No	Yes (.03)

* Paired t-test; No means the ratios are not statistically different than 1.00 at level .01. Yes means statistically different at level .10 and the level is listed.

* Wilcoxon paired sample test; Refer to above explanation for levels listed.

in Table 10 to make the correction. Additional analyses are required to examine the effect of outliers and to establish an uncertainty estimate for the median ratio values.

Blank Levels

Our quality assurance program includes the use of two types of blanks and these QA data are summarized in Table 11.

As filters are loaded in the laboratory in the plastic filter holders, every tenth filter is identified as a laboratory blank. These blanks are not loaded into the filter holder but instead are stored in sterilized petri dishes at room temperature in the laboratory until the associated group of nine filters have returned to the laboratory after exposure in the field. The laboratory blank is then placed with the other nine filters and all undergo identical handling as the filters are extracted and the extraction solutions measured for cations and anions. Thus the laboratory blanks are handled like daily aerosol filters except that the steps of loading the filter into the filter holder, transport to the field, exposure in the field, and handling in the field by the site operator are not included in the process. Field blanks are like the laboratory blanks except that the four steps listed above are included. To simulate field exposure, on each Tuesday one field blank filter is loaded under an inverted plastic funnel at the Bondville field site and then removed on the following Friday. This three-day exposure procedure is reasonable since daily filters also remain under the inverted funnels for three or four days, one of these days being the actual sampling day for the filter.

As usual, there are a few relatively high values for the individual filter blanks so the mean values in Table 11 are usually much higher than the medians. The blank data are presented in terms of concentration in the filter extraction solution (mg/L) so that the levels can be easily compared to the typical analytical detection limits which are shown in the third line in Table 11. For example, the median laboratory blank values for SO_4 , Mg, and K are all approximately detection limit values. The means and medians for 83-86 laboratory blanks are generally somewhat lower than the values for 79-83, especially for SO_4 , Ca, and Na, the ions with blank levels that are measurably above the detection limits. This same feature is not evident for the field blanks. The field blank levels are generally somewhat higher than the corresponding laboratory blanks, as is to be expected. The greatest difference between field and laboratory blanks occurs for calcium which should be the best indicator of ambient dust accumulation on the field blanks.

The most important data in Table 11 are the last two lines where the median and mean field blanks are compared to the median and mean ambient aerosol levels for the Bondville site. The values can be considered to represent bias values which could be used to correct individual or average ambient aerosol concentrations. We see that the mean ratios are somewhat larger than the median ratios. The bias for SO_4 , Ca, and Mg is less than 10%; the bias for K is about 15%; and the Na bias is about 35%. The Na bias is unacceptably large and limits the usefulness of the Na data.

Table 11. Comparison of blanks to ambient aerosol levels for the Bondville site.

Laboratory Blanks (mg/L)						
	<u>n</u>	<u>SO₄</u>	<u>Ca</u>	<u>Mg</u>	<u>Na</u>	<u>K</u>
Median, 6/79-5/83	121	.10	.015	.002	.030	.004
Mean, 6/79-5/83	121	.232	.024	.002	.044	.005
Typical D.L.*		-.10*	-.01	-.003	-.003	-.003
Median, 2/83-6/86	105	.05	.005	.002	.014	.003
Mean, 2/83-6/86	105	.189	.013	.002	.025	.006
Field Blanks (mg/L)						
Median, 8/79-6/83	125	.05	.020	.002	.038	.006
Mean, 8/79-6/83	125	.275	.040	.004	.068	.007
Median, 2/83-6/86	156	.05	.020	.003	.018	.007
Mean, 2/83-6/86	156	.192	.043	.0049	.035	.011
(Field Blank ÷ Ambient Aerosol) x 100%						
2/83-6/86 (Medians)	2.1%	7.4%	6.8%	33.3%	13.5%	
2/83-6/86 (Means)	6.4%	11.4%	8.2%	38.5%	17.1%	

*Negative signs are used to identify detection limit values.

As of now we have not subtracted the bias values from the ambient aerosol data. An examination of the individual field and laboratory blanks values indicates that there are specific periods when the blank values are unusually high. This suggests that it may be best for some applications to incorporate this time variation of the blanks into the scheme to correct the ambient aerosol data. Further work is necessary before deciding on the sample by sample correction scheme.

Seasonal Summary of Bondville Aerosol Data

The ambient aerosol data have been carefully screened to remove samples which may have been collected with malfunctioning equipment and therefore would be unrepresentative samples. The valid daily samples, resulting from this screening process, are statistically summarized by season in Table 12. The seasons have meteorological definitions, i.e., summer is June-August and winter is December-February.

The June 1979-May 1983 period represents data collected mainly with polycarbonate filters (through February 6, 1983) although teflon filter data from February 7, 1983 through May 1983 are included to provide a complete three-year period. The second data summary period, February 1983-June 1986, represents entirely teflon filter data. These particular summary periods were chosen because of the precipitation chemistry data available (summarized in another chapter). If one adjusts the polycarbonate data with the median ratios for the combined data set in Table 10, then one would find that 1983-1986 period in Table 12 has concentrations about 10-20% lower than those for the 1979-1983 period.

The major points concerning seasonality to be discussed with these preliminary data are most clearly illustrated in Table 13:

- a) Na has the highest median for the winter season. Road salting probably accounts for the feature but higher winter levels due to increased wave action on the oceans needs to be considered also.
- b) The Na minimum differs for the two time periods being in summer for 1983-1986 and in fall for 1979-1983.
- c) For the other ions (SO_4 , Ca, Mg, and K) the two periods are about the same in that the minimum aerosol concentration is usually in the winter and the maximum is usually in summer (except the K maximum is in the fall). The K pattern is clearly different than that for Ca and Mg, probably because of different sources. Both unpaved roads and soil dust are sources for Ca and Mg whereas the high fall K values would suggest a third important source for K, namely the organic dust related to crop harvesting.

Much more detailed analyses and interpretation will be carried out after these preliminary data have been finalized.

Table 12. Ambient aerosol concentrations for the Bondville Research Site by season and by ion for two time periods. S.E. is the standard error.

February 1983 - June 1986

	W		Sp		Su		F		All	
	Mean ±S.E.	Median Number								
(SO ₄) _A	3.54 ±.15	2.91 n=273	4.05 ±.17	3.22 n=322	7.68 ±.39	5.98 n=281	4.83 ±.31	3.29 n=228	5.01 ±.14	3.56 n=1104
(Ca) _A	.26 ±.02	.19 n=273	.48 ±.03	.35 n=322	.76 ±.04	.61 n=281	.64 ±.06	.45 n=228	.533 ±.018	.368 n=1104
(Mg) _A	.040 ±.002	.031 n=273	.080 ±.004	.058 n=322	.118 ±.005	.093 n=281	.109 ±.011	.068 n=228	.086 ±.003	.060 n=1104
(K) _A	.064 ±.003	.058 n=273	.076 ±.005	.056 n=322	.101 ±.005	.078 n=281	.113 ±.007	.090 n=228	.087 ±.003	.068 n=1104
(Na) _A	.091 ±.007	.053 n=273	.108 ±.012	.034 n=322	.065 ±.006	.024 n=281	.007 ±.008	.034 n=228	.086 ±.035	.035 n=1104

June 1979 - May 1983

	W		Sp		Su		F		All	
	Mean ±S.E.	Median Number								
(SO ₄) _A	2.84 ±.13	2.32 n=294	4.11 ±.16	3.54 n=301	5.52 ±.24	4.69 n=285	3.29 ±.17	2.59 n=288	3.99 ±.088	3.13 n=1321
(Ca) _A	.34 ±.02	.27 n=294	.55 ±.03	.38 n=301	.69 ±.03	.62 n=285	.90 ±.07	.65 n=288	.614 ±.020	.449 n=1321
(Mg) _A	.057 ±.004	.042 n=294	.091 ±.005	.061 n=301	.101 ±.005	.085 n=285	.117 ±.006	.082 n=288	.092 ±.002	.065 n=1321
(K) _A	.054 ±.002	.048 n=294	.073 ±.005	.052 n=304	.082 ±.004	.066 n=285	.096 ±.007	.071 n=288	.075 ±.002	.059 n=1321
(Na) _A	.142 ±.012	.090 n=294	.145 ±.014	.067 n=301	.148 ±.011	.083 n=285	.081 ±.005	.058 n=288	.119 ±.005	.062 n=1321

Table 13. Concentrations in Table 12 normalized to 1.00 in cleanest season.

	February 1983 - June 1986			
	W	Sp	Su	F
(SO ₄) _A	1.00	1.11	2.05	1.13
(Ca) _A	1.00	1.84	3.21	2.37
(Mg) _A	1.00	1.87	3.00	2.19
(K) _A	1.04	1.00	1.39	1.61
(Na) _A	2.21	1.42	1.00	1.42
	June 1979 - May 1983			
(SO ₄) _A	1.00	1.53	2.02	1.12
(Ca) _A	1.00	1.41	2.30	2.41
(Mg) _A	1.00	1.45	2.02	1.95
(K) _A	1.00	1.08	1.38	1.48
(Na) _A	1.55	1.16	1.43	1.00

CONCLUSIONS

- The teflon filters are significantly more efficient in collecting SO₄ and K particulate matter than are 0.8 μm polycarbonate filters.
- The Na blank levels are unacceptably large for the aerosol data.
- SO₄, Ca, and Mg are maximum in summer and minimum in winter; K is maximum in fall and minimum in winter and spring; and Na is maximum in winter.

REFERENCES

- Bartlett, J. and G. J. Stensland, 1980: Ambient air filter extraction procedures. In Study of Atmospheric Pollution Scavenging, by R. G. Semonin et al., COO-1199-60. 18th Prog. Rept. to the Dept. of Energy, Pollutant Characterization and Safety Research Division, Contract EY-76-S-02-1199, 76-81.
- Dolske, D. A. and G. J. Stensland, 1983: A comparison of ambient airborne sulfate concentrations determined by several different filtration techniques. Proceedings of the 3rd National Symposium on Recent Advances in Pollutant Monitoring of Ambient Air and Stationary Sources, Raleigh, NC, May 6-10, 10 pp.
- Liu, B. Y. and K. W. Lee, 1976: Efficiency of membrane and Nuclepore filters for submicron aerosols. Environ. Sci, and Technol., 10:345-350.
- Stensland, G. J. and J. D. Bartlett, 1979: Measurements of atmospheric nitrate, sulfate, ammonium, and calcium using various filter setups. In Study of Atmospheric Pollution Scavenging, by R. G. Semonin et al., COO-1199-58. 17th Prog. Rept. to the Dept. of Energy, Pollutant Characterization and Safety Research Division, Contract EY-76-S-02-1199, 47-63.
- Stensland, G. J. and J. D. Bartlett, 1980: Ambient aerosol measurements at Champaign, Illinois. In Study of Atmospheric Pollution Scavenging, by R. G. Semonin et al., COO-1199-60. 18th Prog. Rept. to the Dept. of Energy, Pollutant Characterization and Safety Research Division, Contract EY-76-S-02-1199, 1-21.
- Stensland, G. J. and D. F. Gatz, 1981: Comparison of total versus soluble data for ambient aerosol filter samples. In Study of Atmospheric Pollution Scavenging, by R. G. Semonin et al., COO-1199-63. 19th Prog. Rept. to the Dept. of Energy, Pollutant Characterization and Safety Research Division, Contract DE-AC02-76EV01199, 24-29.

CHAPTER 13

RATIOS OF ION CONCENTRATIONS IN PRECIPITATION TO AEROSOLS AT THE BONDVILLE SITE

Gary J. Stensland and Van C. Bowersox

INTRODUCTION

Gases and aerosols are incorporated into precipitation by scavenging processes which occur within and below clouds. In this chapter we present aerosol and precipitation chemistry data for SO_4^- , Ca^{++} , Mg^{++} , K^+ , and Na^+ . (For convenience, the charge symbols will not be shown for the remainder of this chapter.) These data are summarized by season from measurements made at the Bondville Field Site, operated under this contract. Of the five species, only SO_4 has both particle and gaseous species to consider. Only recently has SO_2 , the primary gaseous sulfur component, been measured at the site (as part of a dry deposition project) so for this chapter no SO_2 data are presented.

METHODS

For this chapter we have used the precipitation chemistry data from the NADP/NTN sampler at the Bondville site. The methods for the NADP/NTN program are well known. The analytical measurements (see Peden *et al.*, 1986) are done in the same laboratory that measures the Bondville aerosol samples. The precipitation samples are weekly wet-only samples collected with an Aerochem Metrics sampler. Only valid samples for weeks with a sample volume corresponding to precipitation >0.02 inches were used in the analysis.

The detailed procedures for the Bondville aerosol data were discussed in detail in an earlier chapter in this report.

RESULTS

Since the aerosol data are still preliminary, it is not appropriate to carry out a detailed analysis. The results that follow are intended only to point out some major features in the data.

Tables 1 and 2 present a numerical summary of the data by season for "A," aerosol, and "P," precipitation, for two time periods: 1979-83, and 1983-86. At the bottom of each table are listed the ratios of the precipitation to aerosol concentrations, called the scavenging ratios. The magnitudes of the seasonally averaged ion concentrations relative to one

Table 1. Ambient aerosol concentrations ($\mu\text{g}/\text{m}^3$), precipitation concentrations (mg/L), and ratios of precipitation concentrations to aerosol concentrations.

"A" = aerosol and "P" = precipitation.

June 1979 - May 1983

	W		Sp		Su		F		All	
	Mean \pm S.E.	Median n								
(SO ₄) _A	2.84 \pm .13	2.32 n=294	4.11 \pm .16	3.54 n=301	5.52 \pm .24	4 69 n=285	3.29 \pm .17	2 59 n=288	3.99 \pm .088	3.13 n=1321
(SO ₄) _P	2.76 \pm .22	2.54 n=30	3.32 \pm .20	3.01 n=40	4.64 \pm .38	3.80 n=46	3.67 \pm 46	2 66 n=35	3.69 \pm .18	3.07 n=151
(Ca) _A	.34 \pm .02	.27 n=294	.55 \pm .03	.38 n=301	.69 \pm 03	.62 n=285	.90 \pm .07	.65 n=288	.614 \pm .020	.449 n=1321
(Ca) _P	.31 \pm .06	.15 n=30	.36 \pm .04	.28 n=40	.40 \pm .05	.31 n=46	.58 \pm .16	.22 n=35	413 \pm .043	.269 n=151
(Mg) _A	.057 \pm .004	.042 n=294	.091 \pm .005	.061 n=301	.101 \pm .005	.085 n=285	.117 \pm .006	.082 n=288	.692 \pm .002	.065 n=1321
(Mg) _P	.053 \pm .011	.025 n=30	.051 \pm .006	.041 n=40	.057 \pm .007	.041 n=46	.075 \pm .020	.036 n=35	.059 \pm .006	.07 n=151
(K) _A	.054 \pm .002	.048 n=294	.073 \pm 005	.052 n=304	082 \pm .004	.066 n=285	.096 \pm .007	.071 n=288	.075 \pm .002	.059 n=1321
(K) _P	.028 \pm .005	.018 n=30	.035 \pm .004	.030 n=40	.074 \pm .020	.028 n=46	.050 \pm 011	.029 n=35	.049 \pm .007	.027 n=151
(Na) _A	.142 \pm .012	.090 n=294	.145 \pm .014	.067 n=301	.148 \pm .011	.083 n=285	.081 \pm .005	.058 n=288	.119 \pm .005	.062 n=1321
(Na) _P	.081 \pm .016	.054 n=30	.088 \pm .010	.076 n=40	.110 \pm .012	.093 n=46	.077 \pm .010	.072 n=35	.091 \pm .006	.072 n=151
P/A (SO ₄)	0.97	1.09	0.81	0.85	0.84	0.81	1.12	1.03	.92	.98
P/A {Ca}	0.91	0.56	0.65	0.74	0 58	0.50	0.64	0.34	.67	.60
P/A {Mg}	0.93	0.60	0.56	0.67	0.56	0 48	0.64	0.44	.64	57
P/A {K}	0.52	0.38	0.48	0.58	0.90	0.42	0.52	0.41	.65	.46
P/A {Na}	0.57	0.60	0 61	1.13	0 74	1 12	0.95	1.24	.76	1.16

Table 2. Ambient aerosol concentrations ($\mu\text{g}/\text{m}^3$), precipitation concentrations (mg/L), and ratios of precipitation concentrations to aerosol concentrations.

"A" = aerosol and "P" = precipitation.

February 1983 - June 1986

	W		Sp		Su		F		All	
	Mean \pm S.E.	Median n								
(SO ₄) _A	3.54 \pm .15	2.91 n=273	4.05 \pm .17	3.22 n=322	7.68 \pm .39	5.98 n=281	4.83 \pm .31	3.29 n=228	5.01 \pm .14	3.56 n=1104
(SO ₄) _P	2.33 \pm .22	2.01 n=22	3.20 \pm .27	2.75 n=43	4.08 \pm .31	3.74 n=32	3.03 \pm .41	2.27 n=31	3.23 \pm .17	2.74 n=128
(Ca) _A	.26 \pm .02	.19 n=273	.48 \pm .03	.35 n=322	.76 \pm .04	.61 n=281	.64 \pm .06	.45 n=228	.533 \pm .018	.368 n=1104
(Ca) _P	.23 \pm .09	.09 n=22	.50 \pm .14	.22 n=43	.43 \pm .07	.31 n=32	.41 \pm .13	.18 n=31	.415 \pm .061	.212 n=128
(Mg) _A	.040 \pm .002	.031 n=273	.080 \pm .004	.058 n=322	.118 \pm .005	.093 n=281	.109 \pm .011	.068 n=228	.086 \pm .003	.060 n=1104
(Mg) _P	.029 \pm .007	.016 n=22	.052 \pm .009	.036 n=43	.063 \pm .012	.034 n=32	.059 \pm .014	.033 n=31	.053 \pm .006	.033 n=128
(K) _A	.064 \pm .003	.058 n=273	.076 \pm .005	.056 n=322	.101 \pm .005	.078 n=281	.113 \pm .007	.090 n=228	.087 \pm .003	.068 n=1104
(K) _P	.026 \pm .009	.014 n=22	.036 \pm .006	.028 n=43	.041 \pm .008	.028 n=32	.042 \pm .011	.022 n=31	.037 \pm .004	.023 n=128
(Na) _A	.091 \pm .007	.053 n=273	.108 \pm .012	.034 n=322	.065 \pm .006	.024 n=281	.007 \pm .008	.034 n=228	.086 \pm .035	.035 n=1104
(Na) _P	.079 \pm .016	.057 n=22	.090 \pm .017	.068 n=43	.085 \pm .030	.049 n=32	.098 \pm .019	.063 n=31	.089 \pm .011	.060 n=128
P/A {SO ₄ }	.66	.69	.79	.85	.53	.63	.63	.69	.64	.77
P/A {Ca}	.88	.47	1.04	.63	.57	.51	.64	.40	.78	.58
P/A {Mg}	.72	.52	.65	.62	.53	.42	.54	.49	.62	.55
P/A {K}	.41	.47	.50	.41	.41	.36	.37	.24	.43	.34
P/A {Na}	.87	1.08	.83	2.00	1.31	2.04	1.27	1.85	1.03	1.71

another in aerosols and in precipitation are shown in Table 3. To calculate the values in this table, the median concentrations for each season in Table 2 were normalized by the lowest median concentration for that season. This was done separately for aerosols and precipitation. For ambient aerosols we see that Na has the lowest median concentration, except for winter, with K and Mg generally about 2 times larger, Ca about 10 times larger, and SO_4 about 100 times larger. For precipitation, K is lowest for all seasons, with Mg about 1.4 times larger, Na about 3 times larger, Ca about 9 times larger, and SO_4 about 120 times larger.

Median ion concentrations for precipitation are normalized by season in Table 4. (An analogous table for aerosols was presented in another chapter and is included here as Table 5.) Each row in Tables 4 and 5 was normalized separately, so these tables should be examined by comparing one row to the others. All the precipitation rows in Table 4 are at a minimum in the winter, except for Na in the 83-86 period. This agrees with the winter minimum in the aerosol data in Table 5, except for Na, which has a winter maximum for aerosols. Although this winter maximum may be real, the Na aerosol blank levels were very high; and we need to examine this blank data for evidence of a strong seasonal pattern. We have also recently discovered potential Na blank problems for NADP/NTN precipitation data, which may have produced a step function change in 1981. Overall, one must be very cautious in interpreting the Na aerosol or precipitation data at this time.

The maximum values, by row, in Tables 4 and 5 are always in the summer season for SO_4 . Summer is also the maximum for Ca and Mg, except for the aerosol in 79-83, where the values are similar in summer and fall. The second highest values for Ca and Mg in precipitation are in the spring, while for aerosol they are in the fall. For K in precipitation, the maximum is in the spring or summer, but the fall values are also high. For K in aerosol, the maximum is in the fall for both time periods. Thus for Ca, Mg, and K there is evidence that the highest values for aerosols do not occur in the same seasons as for precipitation. The pattern of aerosols relative to precipitation is different for Ca and Mg than it is for K. For Na, the maximum values for aerosols occur in the winter, while for precipitation they occur in spring or summer; however, the pattern for Na is open to question until further analyses of the blank data for both aerosol and precipitation are completed.

Notice that the scavenging ratios for SO_4 and K are larger for 1979-83 in Table 1 than for 1983-86 in Table 2. This is explained by the change in filter media between the two periods, as discussed elsewhere in the aerosol chapter. One should have greater confidence in the scavenging ratios in Table 2, when teflon filters were used for ambient aerosol collection.

The scavenging ratios for K in Table 2 might be too low, because the solubility of K in precipitation is not the same as for the aerosol extractions. The scavenging ratios for K in Table 2 are lower than those for Ca or Mg. From previous studies we know that Ca and Mg are likely to be >90% soluble in both precipitation samples and in aerosol extraction solutions. For K, the corresponding values are smaller. Only 50% or 60% of the total K is soluble in precipitation. Aerosol extractions at pH 2

Table 3. Median aerosol or precipitation concentrations in Table 2 normalized to 1.00 for the ion with the lowest concentration.

February 1983 - June 1986

	<u>W</u>	<u>Sp</u>	<u>Su</u>	<u>F</u>	<u>All</u>
Normalized Median Aerosol Concentrations					
(SO ₄) _A	93.9	94.7	249.2	96.8	101.7
(Ca) _A	6.1	10.3	25.4	13.2	10.5
(Mg) _A	1.0	1.7	3.9	2.0	1.7
(K) _A	1.9	1.6	3.2	2.6	1.9
(Na) _A	1.7	1.0	1.0	1.0	1.0
Normalized Median Precipitation Concentrations					
(SO ₄) _P	143.6	98.2	133.6	103.5	119.1
(Ca) _P	6.4	7.9	11.1	8.2	9.2
(Mg) _P	1.1	1.3	1.2	1.5	1.4
(K) _P	1.0	1.0	1.0	1.0	1.0
(Na) _P	4.1	2.4	1.8	2.9	2.6

Table 4. Median precipitation concentrations in Tables 1 and 2 normalized to 1.00 in the season with the lowest concentration.

February 1983 - June 1986

	W	Su	Su	F
(SO ₄) _P	1.00	1.37	1.86*	1.13
(Ca) _P	1.00	2.44	3.44*	2.00
(Mg) _P	1.00	2.25	2.44*	2.06
(K) _P	1.00	2.00*	2.00*	1.57
(Na) _P	1.16	1.39*	1.00	1.29

June 1979 - May 1983

(SO ₄) _P	1.00	1.19	1.50*	1.05
(Ca) _P	1.00	1.87	2.07*	1.47
(Mg) _P	1.00	1.64	1.64*	1.44
(K) _P	1.00	1.67*	1.56	1.61
(Na) _P	1.00	1.41	1.72*	1.33

*Maximum values by row.

Table 5 Median aerosol concentrations in Tables 1 and 2 normalized to 1.00 in the season with the lowest concentration.

	February 1983 - June 1986			
	W	Sp	Su	F
(SO ₄) _A	1.00	1.11	2.05*	1.13
(Ca) _A	1.00	1.84	3.21*	2.37
(Mg) _A	1.00	1.87	3.00*	2.19
(K) _A	1.04	1.00	1.39	1.61*
(Na) _A	2.21*	1.42	1.00	1.42
	June 1979 - May 1983			
(SO ₄) _A	1.00	1.53	2.02*	1.12
(Ca) _A	1.00	1.41	2.30	2.41*
(Mg) _A	1.00	1.45	2.02*	1.95
(K) _A	1.00	1.08	1.38	1.48*
(Na) _A	1.55*	1.16	1.43	1.00

*Maximum values by row.

or 3 are more acidic than precipitation, and the greater acidity results in a larger fraction of the K being dissolved. Concentrations of K in aerosol extractions are relatively large compared to precipitation, and thus the scavenging ratios for K are biased low and are unrepresentative. If the scavenging ratios were calculated with total (instead of soluble) concentrations, then these solubility differences would be absent.

In Table 2, the scavenging ratios from median concentrations are similar for Ca and Mg. For all data, the scavenging ratio is .58 for Ca, while for Mg it is .55. Both of these values are much less than the SO₄ value of .77. This may result from the oxidation of SO₂ to SO₄ in precipitation. In the discussion that follows, the scavenging ratios are used to infer the fraction of SO₄ that results from the dissolution and oxidation of SO₂ in precipitation.

Using the previous notation,

$(SO_4)_P / (SO_4)_A$ - the aerosol based scavenging ratio for SO₄, which is its concentration in precipitation divided by its ambient aerosol concentration;

$(SO_4)_{p\text{-part}} / (SO_4)_A$ = the concentration in precipitation from scavenged particles divided by the ambient aerosol concentration;

$(SO_4)_{p\text{-gas}} / (SO_4)_A$ = the concentration in precipitation from scavenged gases divided by the ambient aerosol concentration;

where

$(SO_4)_{p\text{-part}}$ = the concentration in precipitation from scavenged particles; and

$(SO_4)_{p\text{-gas}}$ = the concentration in precipitation from scavenged gases.

From these definitions it follows that

$$\begin{aligned} (SO_4)_P / (SO_4)_A &= [(SO_4)_{p\text{-part}} + (SO_4)_{p\text{-gas}}] / (SO_4)_A \\ &= (SO_4)_{p\text{-part}} / (SO_4)_A + (SO_4)_{p\text{-gas}} / (SO_4)_A. \end{aligned} \quad (1)$$

For Ca,

$$(Ca)_P / (Ca)_A = (Ca)_{p\text{-part}} / (Ca)_A + (Ca)_{p\text{-gas}} / (Ca)_A \quad (2)$$

but

$$(Ca)_{p\text{-gas}} / (Ca)_A = 0,$$

because Ca has no gaseous component in precipitation.

Assume

$$(Ca)_{p\text{-part}} / (Ca)_A = (SO_4)_{p\text{-part}} / (SO_4)_A, \quad (3)$$

i.e., that sulfate and calcium particles have the same scavenging ratio.

Using (1), (2), and (3) and solving for the gaseous component of SO₄ in precipitation,

$$\begin{aligned} (\text{SO}_4)_{\text{P-gas}}/(\text{SO}_4)_{\text{A}} &= (\text{SO}_4)_{\text{P}}/(\text{SO}_4)_{\text{A}} - (\text{SO}_4)_{\text{P-part}}/(\text{SO}_4)_{\text{A}} \\ &= (\text{SO}_4)_{\text{P}}/(\text{SO}_4)_{\text{A}} - (\text{Ca})_{\text{P}}/(\text{Ca})_{\text{A}} \end{aligned} \quad (4)$$

Substituting the scavenging ratios based on median concentrations for all data in Table 2 into equation (4) gives:

$$(\text{SO}_4)_{\text{P-gas}}/(\text{SO}_4)_{\text{A}} = .77 - .58 = .19 \quad (5)$$

From equation (5) it follows that:

$$(\text{SO}_4)_{\text{P-gas}} = .19 (\text{SO}_4)_{\text{A}} \text{ and}$$

$$(\text{SO}_4)_{\text{P-part}} = .58 (\text{SO}_4)_{\text{A}}$$

Finally,

$$\begin{aligned} (\text{SO}_4)_{\text{P-part}}/[(\text{SO}_4)_{\text{P-part}} + (\text{SO}_4)_{\text{P-gas}}] &= .58 (\text{SO}_4)_{\text{A}}/ [.58(\text{SO}_4)_{\text{A}} + .19 (\text{SO}_4)_{\text{A}}] \\ &= \frac{.58}{.77} = .75 \end{aligned}$$

This analysis of the scavenging ratios suggests that 75% of the sulfate in precipitation is from the scavenging of sulfur particles, while 25% results from the scavenging of sulfur gases. Using the data in Table 2, the fractions for summer are 81% particulate and 19% gaseous, and for winter the values are 68% particulate and 32% gaseous. The differences between the two seasons suggest that in winter a greater portion of the ambient air sulfur is in the gaseous form and gaseous scavenging of sulfur is more important than in the summer.

CONCLUSIONS/FUTURE RESEARCH

- From this preliminary report we conclude that scavenging ratios for Na and K may be affected by problems related to sampling, handling, and extraction methods, which make the values unrepresentative. Values cannot be directly compared to those for SO₄, Ca, and Mg.
- Further sensitivity and statistical analyses are required to see if differences in the scavenging ratios for SO₄ and Ca or for SO₄ and Mg can be used to predict the gaseous versus particulate contributions to the total SO₄ in precipitation. The present results indicate that particulate removal is more important than gaseous removal for sulfur, especially in the summer.

CHAPTER 14

A COMPUTER PROGRAM FOR CALCULATING STATE AVERAGES FROM POINT VALUES

Jack Su and Gary J. Stensland

INTRODUCTION

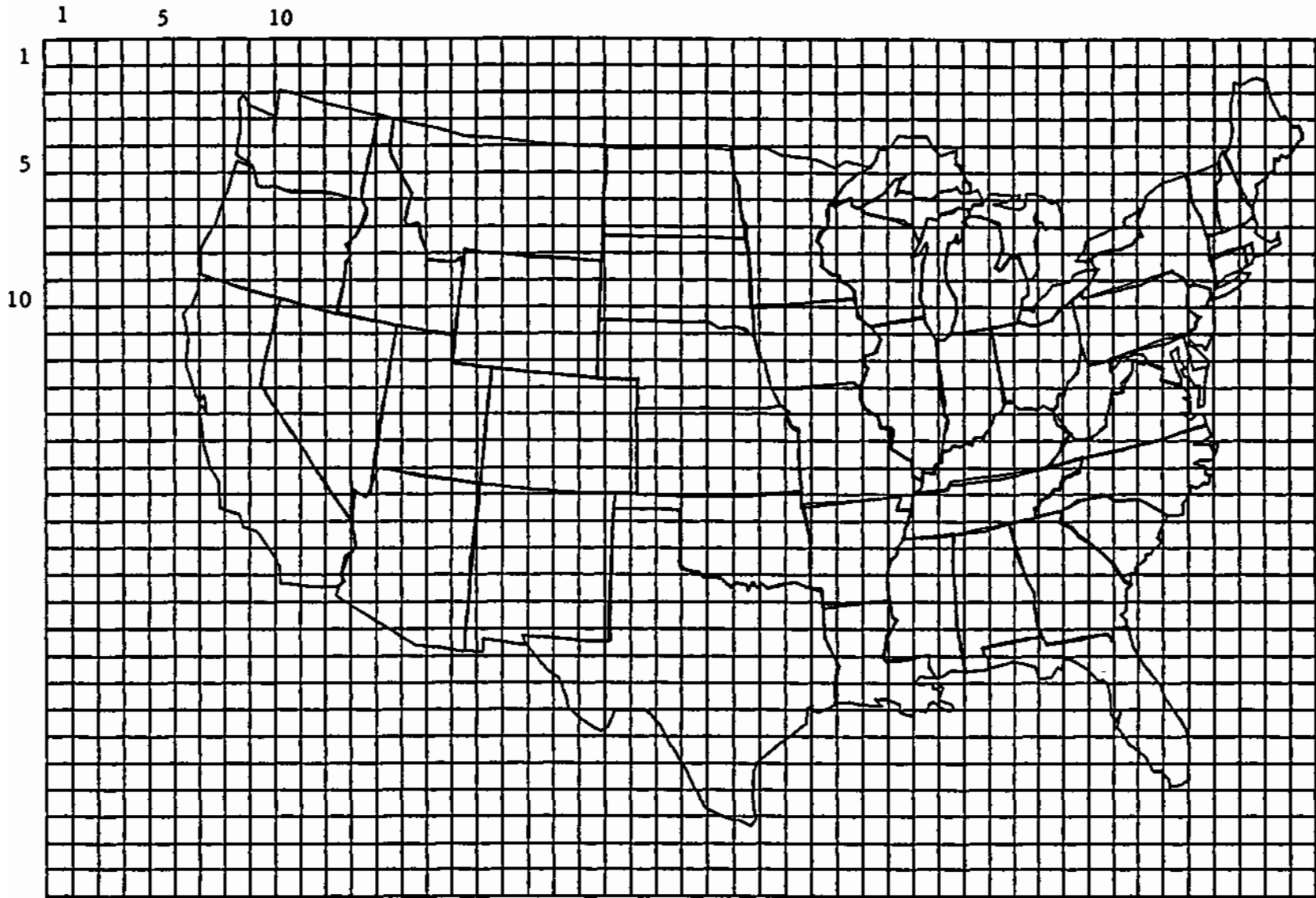
It is often important to estimate environmental variables on a state-by-state basis. Such data are necessary to make informed policy decisions concerning the allocation of limited national and state resources among competing goals, such as pollution control, research, and waste cleanup. For this reason, we have developed a computer program to calculate a single representative statistic for each state, given a variable that is measured at a limited number of sites across the United States. Our program is called AREA for ARea Estimating Algorithm.

METHODS AND PROCEDURES

The AREA program was developed on the VAX 11/750 using standard Fortran 77. An IBM AT version of the program compiled using MS Fortran 4.0 is also available. To improve the performance of the program we first digitized simplified state boundaries for all 48 states using the boundaries found in the graphics package distributed by the National Center for Atmospheric Research (NCAR, 1981). This step was necessary to minimize the computational time required in subsequent steps. In this simplified scheme, each state is defined by an average of 30 points. This is in contrast to the NCAR graphics package which has over 500 points for each state. A very small deviation in area, an average of less than 1 percent, was introduced by using the simplified boundaries. A computer-generated map using the digitized data set is shown in Figure 1.

The program itself consists of two parts, which are summarized in Figures 2 and 3. The first part of the AREA program reads in the data for each site and calculates a descriptive statistic for the environmental variable. Then, based on the size of the grid squares selected, an array is initialized so that it will cover all 48 states. The index of the array corresponds to the location of the center of each grid square (see Figure 1). The calculated descriptive statistics along with the spatial coordinates of the data collection sites are then piped into a spatial analysis routine. The spatial analysis subprogram interpolates the values of the environmental variable at the sites to the corners of each grid square. Any spatial analysis algorithm will suffice; some examples include Laplacian smoothing splines, optimum interpolation, and Kriging. In the current version of the program, we implemented an objective analysis scheme developed by Barnes (Barnes, 1964) and modified by Achtemeier (Achtemeier, et al., 1977).

Figure 1. An overlay of the 100 km by 100 km grid squares on the U.S. map depicted by the simplified state boundaries.



a) in Figure 4

b) in Figure 4

Figure 2 Flow diagram of the program that calculates area-weighted state averages

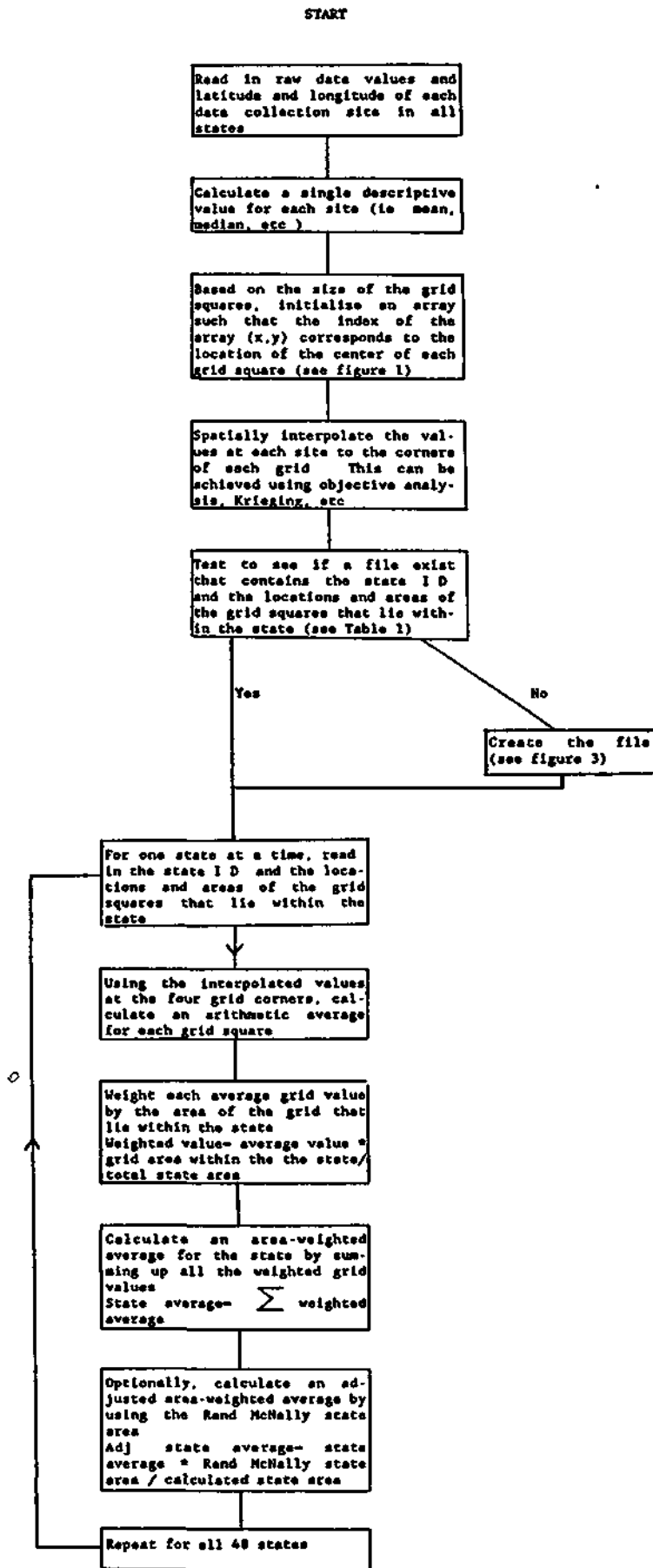
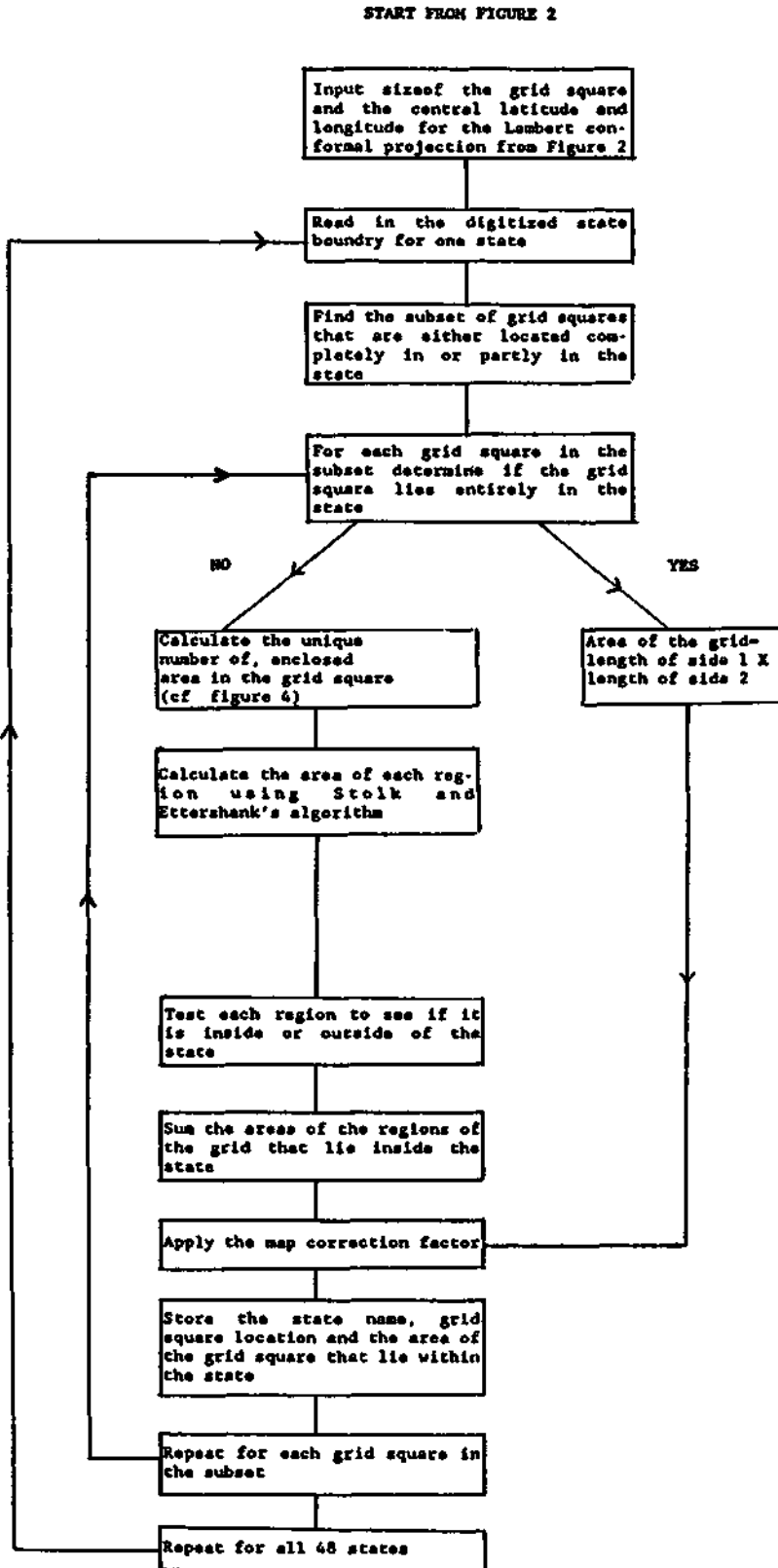


Figure 3 Flow diagram of the subprogram that calculates the area of states by summing enclosed grid square areas.



The two-step modified Barnes objective analysis scheme makes successive corrections to the initial grid corner interpolated values using negative exponential weighting factors. The first step involves interpolating the values from the sites to the grid corners. The second involves interpolating from the grid corners back to the sites and comparing the actual values versus the estimated values. The differences are then again interpolated to the grid corners and added to the original estimates. The initialization process requires specification of parameters which dictate (1) the number of sites nearest to the grid corner (typically we use the nearest 5 to 7 sites to estimate values for a grid corner, depending on network density), (2) the location of the grid corners, and (3) the relative importance of each site used in the interpolation as a function of its distance away from the grid corner. This last parameter called CHNG changes the steepness of the negative exponential function. The weighting factor for each site used in interpolating to a grid corner is defined as

$$WT(k)=EXP(-(DIST(k) / AVGDIS^2)*CHNG),$$

where for site k , $WT(k)$ is the weighting factor, $DIST(k)$ is the distance from site k to the corner of the grid square, $AVGDIS$ is the average distance to the corner of the grid square from all the sites used in the interpolation, and $CHNG$ is the parameter that changes the steepness of the function. $CHNG$ is usually set to +2.3025 so that a weight of .1 is assigned to sites located at the square of the average distance (i.e. $WT(k)=.1$ when $DIST(k)=AVGDIS^2$).

Once the final values for each grid corner are calculated, the program determines if a file exists that contains (1) the state names, (2) the locations of the grid squares in each given state, and (3) the area of each grid square that lies within the state. If this file is not found, the program creates it using the second major part of the program, which will be explained later. For now assume that such a file exists. Table 1 shows an example of what such a file would look like in ASCII code. In real practice, this file is a sequentially indexed binary file, which allows for fast, direct access to the data.

For each state, AREA reads from the file the state name and the location and area of the grid squares that lie within the state. Then an arithmetic average of the environmental variable is calculated for each grid square using the interpolated values at its four corners. This average value for the grid square is then weighted by the actual area of the grid square that lies within the state. Thus, for a grid square with the center at location (x,y) ,

$$WTVAl(x,y) = AVGVAL(x,y) * (GAREA(x,y) / SAREA)$$

where $WTVAl$ is the weighted value, $AVGVAL$ is the average value of the environmental variable. $GAREA$ is the area of the grid square that lies within the state, and $SAREA$ is the total calculated area for that state.

Once all the weighted grid values are calculated, it is a simple matter to solve for an area-weighted average for the whole state by summing up all the weighted grid values. In certain cases, because of the

TABLE 1. Example of grid areas included in one state, Alabama, using a grid square size of 100 km by 100 km (see Figure 1). The area of each grid square that is located within the state is the adjusted area using the map correction factor.

STATE CODE	NUMBER OF GRID SQUARES THAT OVERLAP THIS STATE		
AL		24	
	36	19	2619.1
	36	20	4667.2
	36	21	3928.7
	36	22	3350.6
	36	23	2068.7
	36	24	278.6
	37	19	7060.3
	37	20	10299.8
	37	21	10236.3
	37	22	10169.1
	37	23	9268.1
	37	24	5038.0
	38	19	8211.3
	38	20	10289.5
	38	21	10225.5
	38	22	10157.8
	38	23	5655.7
	39	19	141.0
	39	20	2615.5
	39	21	6855.4
	39	22	9088.4
	39	23	3984.2
	40	22	65.1
	40	23	307.3
			AREA INSIDE THE STATE (sq. km)

- Note 1) Some grid squares are entirely within the state boundaries while others are partially within the state boundaries. (x,y) are the rectangular coordinates of the center of the grid squares.
- 2) The six grid squares entirely within the state of Alabama (cf. Figure. 1) have different areas because of the map correction factor.

possible errors resulting from the digitizing of the state boundaries and from the number of significant digits used in the calculations, this area-weighted average is adjusted to the "actual" state area. The state areas found in Rand McNally's 1986 road atlas were used as the actual areas. A 1986 edition was used because the digitizing was done on a map produced by the NCAR graphics package, which used state boundaries created by Hershey in 1963 (Hersey, 1963). This adjustment should bring the values in line with the currently established state areas. It is interesting to note that state areas have changed in the past 25 years (see Table 2). For some states, the state area listed in Rand McNally's 1986 road atlas is significantly different from the 1963 atlas. Florida, for example, has an area approximately 8 percent larger in the 1986 edition as compared to the 1963 edition.

The above procedure is repeated to calculate an area-weighted value for all 48 states.

The second major part of the AREA program is shown in Figure 3. This part of AREA calculates the file used above (see Table 1). First, initial parameters must be entered for the Lambert conformal projection with two standard parallels, which converts latitude and longitude into x, y distance coordinates. This projection is used because it conserves angles and produces minimal distortions. We used a 30 degree and a 60 degree standard parallel with a center of projection at 38 degrees latitude and 100 degrees longitude. This part of AREA uses the same grid size and the same grid locations defined previously in the spatial analysis.

For each state, AREA first reads in the digitized state boundary. For reasons of efficiency it then calculates the subset of grid squares which lie either completely or partly inside this particular state. This initial culling from the total number of grid squares shown in Figure 1 reduces the number of iterations required in subsequent calculations. For each grid square in the subset, the program tests to see if the grid square lies entirely within the state. If it does, then calculating the area of that grid square is trivial. If the state boundary crosses the grid square, then a sophisticated procedure is used to calculate the area of the grid square that is within the state. First, the procedure determines the maximum number of unique enclosed regions within a grid square. A unique enclosed region is defined by the combination of the four sides of the grid square and the state boundary. For example, in Figure 4a, there are three unique enclosed regions, two of which are part of the Atlantic Ocean (shaded area) and one of which is part of North Carolina. If there are N number of unique regions, then the area of each N-1 unique region is calculated using Stolk and Ettershank's algorithm (Stolk and Ettershank, 1977). The area of the last (Nth) unique region can be calculated much faster by subtracting the sum of the areas of the N-1 unique regions from the total area of the grid square.

The Stolk and Ettershank algorithm is a simple application of Stokes' theorem to a standard line integral. Basically, a unique enclosed area can be defined by a sequence of n points, with each point determined by an x and y value. Then the enclosed area is

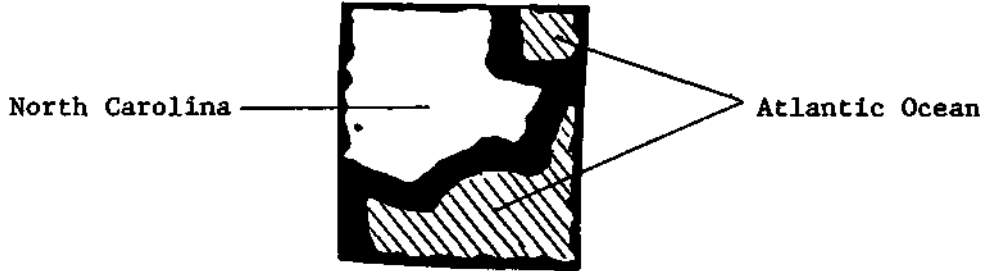
$$\text{AREA} = 1/2 * \text{ABS} \left(\sum_k^{n-1} (X_k Y_{k+1} - X_{k+1} Y_k) \right).$$

Table 2. Comparing the state area printed in 1986 versus 1963. The 1963 values are from The World Almanac and Book of Facts for 1963. and the 1986 values are from Rand McNally 1986 Road Atlas.

STATE NAME	STATE AREA (sq. miles)	
	1986	1963
Alabama	50708.0	51609.0
Alaska	566432.0	586400.0
Arizona	113417.0	113909.0
Arkansas	51945.0	53104.0
California	156361.0	158693.0
Colorado	103766.0	104247.0
Connecticut	4862.0	5009.0
Delaware	1982.0	2057.0
Florida	54157.0	58560.0
Georgia	58073.0	58876.0
Idaho	82677.0	83557.0
Illinois	55748.0	56400.0
Indiana	36097.0	36291.0
Iowa	55941.0	56290.0
Kansas	81787.0	82264.0
Kentucky	39650.0	40395.0
Louisiana	44930.0	48523.0
Maine	30920.0	33215.0
Maryland	9891.0	10577.0
Massachusetts	7826.0	8257.0
Michigan	56817.0	58216.0
Minnesota	79289.0	84068.0
Mississippi	47296.0	47716.0
Missouri	68995.0	69686.0
Montana	145587.0	147138.0
Nebraska	76483.0	77227.0
Nevada	109889.0	110540.0
New Hampshire	9027.0	9304.0
New Jersey	7521.0	7836.0
New Mexico	121412.0	121666.0
New York	47831.0	49576.0
North Carolina	48798.0	52712.0
North Dakota	69273.0	70665.0
Ohio	40975.0	41222.0
Oklahoma	68782.0	69919.0
Oregon	96184.0	96981.0
Pennsylvania	44966.0	45333.0
Rhode Island	1054.0	1214.0
South Carolina	30225.0	31055.0
South Dakota	75955.0	77047.0
Tennessee	41328.0	42244.0
Texas	262134.0	267339.0
Utah	82096.0	84916.0
Vermont	9267.0	9609.0
Virginia	39780.0	40815.0
Washington	66570.0	68192.0
West Virginia	24070.0	24181.0
Wisconsin	54464.0	56154.0
Wyoming	97203.0	97914.0

Figure 4. Two enlarged grid squares from Figure 1.
The hatched areas are outside of the state.

- a) An example of three unique, enclosed areas in a grid square.
This grid square is located at $x=46$ and $y=14$ in Figure 1.



- b) An example of two unique enclosed areas in a grid square.
This grid square is located at $x=43$ and $y=13$ in Figure 1.



Once the areas of all the unique regions are known, each unique region is tested to see if it lies within or outside the state. This step is absolutely crucial because some state boundaries fold back on themselves, making generalizations impossible. The test (for an example of this, see Figure 5) is made by creating a line between a point within the state to a point inside of the unique region to be tested, and then calculating the number of times the state boundary intersects this line. If there are no intersections or if there is an even number of intersections, then the unique region lies within the state. If there is an odd number of intersections, then it lies outside of the state. All of the unique regions that lie within the state for each grid square are summed.

After the area within the state for each grid square is calculated, a map correction factor is applied to each area. The map correction factor is necessary because there is a slight distortion involved in projecting a three-dimensional surface on to a two-dimensional plane. For a Lambert conformal projection with a 30 and a 60 degree standard parallel, the map correction factor (Saucier, 1955) is

$$\text{MCF} = (\text{SIN}(30) / \text{SIN}(\text{LATX})) * (\text{TAN}(\text{LATX}/2.0) / \text{TAN}(15))^{*n},$$

where MCF is the map correction factor, LATX is the colatitude of the point to which one wants to apply the map correction factor (note: colatitude = 90 - latitude), and n is the cone constant. The cone constant is defined as.

$$n = \frac{\log(\cos(\text{thetal})) - \log(\cos(\text{theta2}))}{\log(\tan(45 - (\text{thetal} / 2))) - \log(\tan(45 - \text{theta2} / 2))}$$

where thetal and theta2 are the two standard parallels (in this case, 30 and 60).

This map correction factor applies to distances. To implement the above equation for a particular grid area, one simply calculates the map correction factor for each side of the grid square. The total corrected area of the grid square is then calculated as the product of the length of the corrected base and the corrected height of the grid square. The corrected value for the area within the state for each grid square is then,

$$\text{CAREAWS} = (\text{CTOTAREA} / \text{TOTAREA}) * \text{AREAWS},$$

where CAREAWS is the corrected area within a state, CTOTAREA is the corrected total area for the grid square, TOTAREA is the uncorrected total area for a grid square, and AREAWS is the uncorrected area of the portion of the grid square that lies within the state.

The map correction factor is applied to each grid square in the subset. Then the state name, the location of the center of each grid square in the subset, and the map factor corrected area that lies within the state for each grid square are stored in a file. This entire procedure is repeated for each of the 48 states.

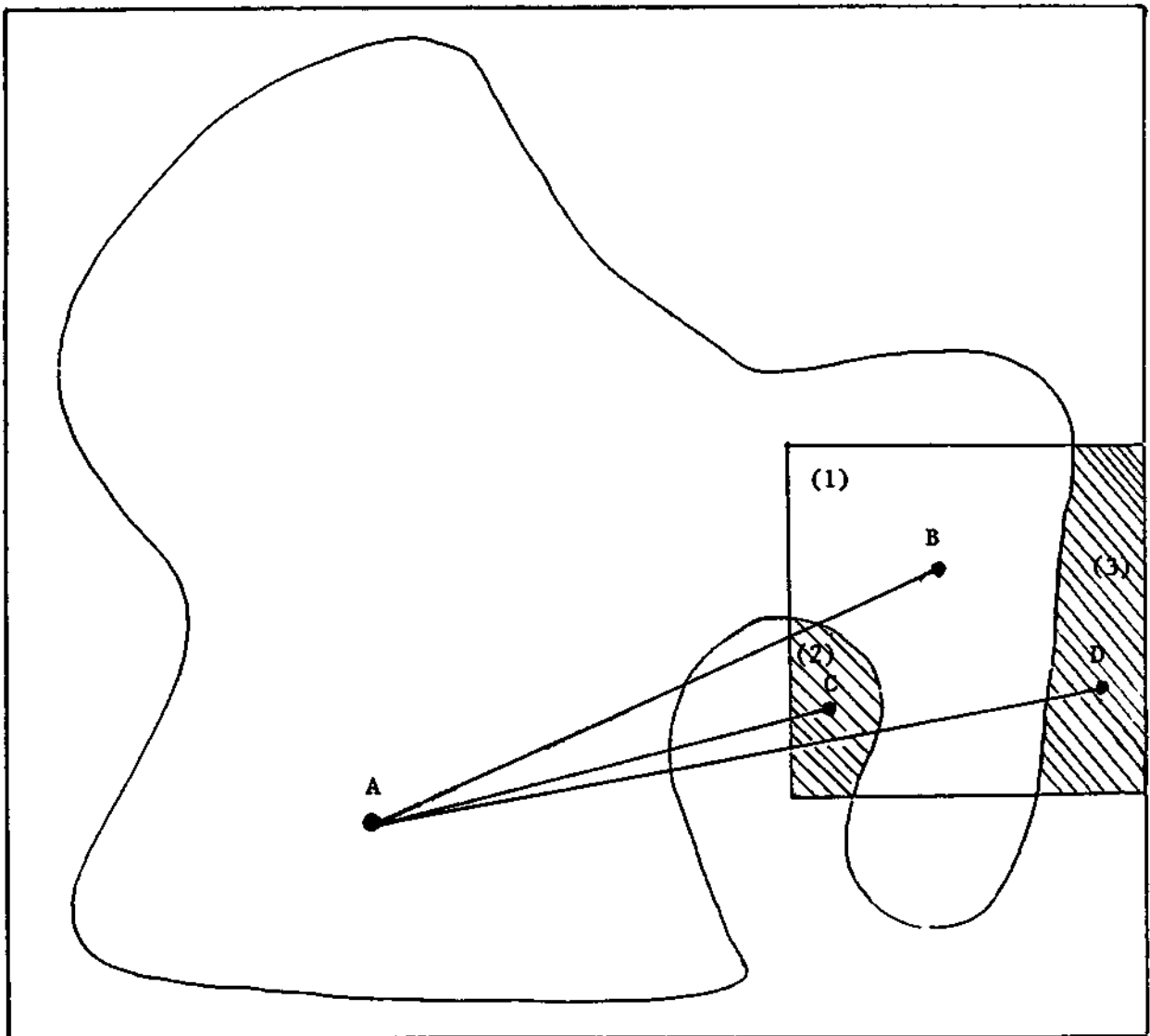
Figure 5. An hypothetical example demonstrating how to determine if a region is inside or outside of the state (for further explanation refer to the text).

Line A-B intersects the state boundary twice, so region (1) is in the state.

Line A-C intersects the state boundary once so region (2) is outside the state.

Line A-D intersects the state boundary three times so region (3) is in the state.

State Boundary



At every step of this program, care was taken to minimize the computation time required without sacrificing precision. Copies of the source code may be obtained from the authors.

RESULTS AND DISCUSSION

To demonstrate how the AREA program will work, we have used the NADP/NTN precipitation chemistry data set as an example. In this example we calculate the area-weighted average deposition of Ca, Mg, K, Na, NH_4 , NO_3 , Cl, SO_4 , and H^+ for all 48 states. Validated wet deposition samples since the inception of the NADP/NTN network up to and including December 1986 are used. These data are processed through two check programs, which produce a list of summary statistics for each site. In this example we chose the median deposition at each site as the input environmental variable for use in calculating area-weighted state averages.

The grid size used in the modified Barnes scheme was 100 km by 100 km. Figure 1 depicts how this size grid square appears over a digitized map of the United States. Table 3 summarizes how the calculated state areas using this grid size compare to the state areas published in Rand McNally's 1986 road atlas. Note that for the majority of states, the differences between the calculated state areas and the actual state areas are quite small. All of the states except Florida, Massachusetts, and New Jersey have absolute differences of less than 4 percent. Even these differences may not be "real" when one considers how state area estimates have changed over the years (see Table 2). For example, if we were to use the 1963 atlas values, Florida would have a difference of only -1.22 percent.

Table 4 shows the calculated area-weighted deposition of different ions for the 48 states. The values presented are not adjusted to the actual state areas as given by Rand McNally's 1986 road atlas. The reason for this is because the unit of the result is kg per hectare per week. If the results were presented in kg per state per week, then the adjustment to the actual state area should be applied. The area-weighted state depositions for each ion are sorted from lowest to the highest in Table 4.

A comparison of running AREA on the VAX 11/750 and on the IBM AT (8 MHz version with an 80287 math co-processor chip) shows that it takes much longer to run on the IBM AT. In running the above example with the 100 km by 100 km grid squares, the VAX 11/750 took 4 minutes and 39 seconds of CPU (central processor unit) time. On the AT, it took 10 minutes and 43 seconds. It is important to note that because the VAX is a multi-user system, the actual time required to run the AREA program can be significantly longer than the CPU time. This is not true of a single user IBM AT. The IBM AT version of AREA was compiled using Microsoft's Fortran 4.0, which is an optimizing compiler. The optimization procedure improved the performance of the AREA program significantly when compared to using a non-optimizing compiler such as the Professional Fortran. The major cause of the difference in CPU time between the VAX and the AT is the time consumed reading and writing to the mass storage device. The disk pack on

Table 3. Comparison of calculated area vs. actual area. Area is calculated using 100 km X 100 km grid squares. Actual area is taken from Rand and McNally 1986 Road Atlas.

STATE NAME	ACTUAL AREA (hectares)	CALCULATED AREA (hectares)	% DIFF.
Alabama	13133311.00	13658094.00	3.98
Arizona	29374866.00	29363004.00	-0.04
Arkansas	13453692.00	13033058.00	-3.13
California	40497312.00	40823880.00	0.81
Colorado	26875268.00	27189678.00	1.17
Connecticut	1259252.13	1290077.88	2.45
Delaware	513335.66	496318.31	-3.32
Florida	14026598.00	14981809.32	6.81
Georgia	15040838.00	15365595.00	2.16
Idaho	21413244.00	21523378.00	0.51
Illinois	14438666.00	14472945.00	0.24
Indiana	9349080.00	9687815.00	3.62
Iowa	14488652.00	14050881.00	-3.02
Kansas	21182734.00	21422952.00	1.13
Kentucky	10269302.00	10669804.78	3.90
Louisiana	11636816.00	12040114.00	3.47
Maine	8008243.00	8321365.30	3.91
Maryland	2561757.00	2495746.75	-2.58
Massachusetts	2026924.63	2151720.25	6.16
Michigan	14715534.00	14425816.00	-1.97
Minnesota	20535756.00	21351366.00	3.97
Mississippi	12249607.00	12650596.00	3.27
Missouri	17869622.00	17628104.00	-1.35
Montana	37706860.00	36489836.00	-3.23
Nebraska	19809004.00	20280854.00	2.38
Nevada	28461118.00	29521104.00	3.72
New Hampshire	2337982.25	2414882.75	3.29
New Jersey	1947929.88	2044981.50	4.98
New Mexico	31445562.00	32140862.00	2.21
New York	12388172.00	12671734.00	2.29
North Carolina	12638623.00	12734916.00	0.76
North Dakota	17941624.00	18343144.00	2.24
Ohio	10612476.00	10729698.00	1.10
Oklahoma	17814454.00	18189032.00	2.10
Oregon	24911540.00	24321082.00	-2.37
Pennsylvania	11646140.00	11993646.00	2.98
Rhode Island	272984.75	277317.75	1.59
South Carolina	7828239.00	7710498.50	-1.50
South Dakota	19672254.00	20103840.00	2.19
Tennessee	10703902.00	10782805.00	0.74
Texas	67892392.00	69428528.00	2.26
Utah	21262766.00	21989440.00	3.42
Virginia	10302972.00	10320740.00	0.17
Vermont	2400141.75	2454892.75	2.28
Washington	17241550.00	17699364.00	2.66
West Virginia	6234101.00	6128044.00	-1.70
Wisconsin	14106111.00	14538467.00	3.07
Wyoming	25175460.00	25354918.00	0.71

Table 4. Deposition of major ions measured by NADP/NTN network.

DEPOSITION IN KILOGRAMS PER HECTARE PER WEEK

Calcium		Magnesium		Potassium		Sodium		Ammonium	
NV	0.0045	NV	0.0010	NV	0.0005	MT	0.0022	ME	0.0003
ID	0.0049	WY	0.0011	WY	0.0005	WY	0.0022	MT	0.0003
WY	0.0051	ID	0.0013	UT	0.0007	NV	0.0026	ID	0.0005
CA	0.0051	CO	0.0013	MT	0.0007	CO	0.0030	WA	0.0005
OR	0.0052	MT	0.0014	CO	0.0008	WI	0.0030	WY	0.0005
MT	0.0056	CA	0.0016	CA	0.0009	SD	0.0030	NV	0.0007
VT	0.0056	VT	0.0016	ID	0.0009	ND	0.0031	FL	0.0007
ME	0.0058	NE	0.0017	AZ	0.0009	MN	0.0031	NM	0.0009
WA	0.0059	UT	0.0017	VT	0.0010	NE	0.0033	AZ	0.0011
NH	0.0062	NM	0.0017	NH	0.0010	VT	0.0033	OR	0.0014
CO	0.0072	KS	0.0018	ME	0.0011	ID	0.0034	CO	0.0033
MA	0.0078	NH	0.0020	SD	0.0012	MI	0.0036	UT	0.0037
RI	0.0079	ME	0.0020	NM	0.0012	IA	0.0039	CA	0.0039
SC	0.0079	OR	0.0021	CT	0.0013	NM	0.0040	NH	0.0042
CT	0.0082	WI	0.0022	ND	0.0013	UT	0.0041	VT	0.0044
NJ	0.0093	SD	0.0023	WI	0.0013	IL	0.0041	ND	0.0047
NE	0.0095	AZ	0.0023	MI	0.0013	KS	0.0042	TX	0.0055
GA	0.0095	MN	0.0025	NE	0.0014	NH	0.0046	AL	0.0066
ND	0.0095	ND	0.0025	MA	0.0014	AZ	0.0046	MS	0.0066
NM	0.0095	TN	0.0026	RI	0.0014	IN	0.0048	GA	0.0066
SD	0.0097	KY	0.0026	OH	0.0015	OH	0.0050	MA	0.0067
AZ	0.0099	MO	0.0026	MN	0.0015	MO	0.0050	SD	0.0067
DE	0.0100	OK	0.0027	WA	0.0015	CA	0.0052	CT	0.0069
NC	0.0101	WA	0.0027	IL	0.0016	PA	0.0053	SC	0.0072
UT	0.0101	VA	0.0028	IN	0.0016	ME	0.0053	RI	0.0076
WI	0.0101	PA	0.0028	KS	0.0016	KY	0.0054	MN	0.0089
MS	0.0102	MI	0.0028	KY	0.0016	NY	0.0054	NJ	0.0090
AL	0.0105	SC	0.0028	OR	0.0017	WV	0.0055	TN	0.0091
MI	0.0106	CT	0.0029	PA	0.0017	CT	0.0063	NC	0.0093
MD	0.0107	AR	0.0029	TN	0.0018	VA	0.0064	VA	0.0101
NY	0.0109	NY	0.0029	NJ	0.0018	TN	0.0066	LA	0.0103
PA	0.0111	TX	0.0030	NY	0.0018	MD	0.0073	WI	0.0105
MN	0.0112	NC	0.0031	MD	0.0018	OK	0.0075	DE	0.0118
TN	0.0114	MA	0.0031	DE	0.0020	RI	0.0079	KS	0.0119
VA	0.0117	WV	0.0031	NC	0.0020	NJ	0.0079	NE	0.0120
FL	0.0120	MD	0.0031	WV	0.0020	AR	0.0084	MD	0.0121
AR	0.0123	OH	0.0032	VA	0.0020	MA	0.0086	AR	0.0129
KY	0.0126	IL	0.0032	MO	0.0021	OR	0.0089	OK	0.0131
LA	0.0129	RI	0.0033	IA	0.0022	NC	0.0090	MI	0.0131
KS	0.0131	AL	0.0033	SC	0.0022	WA	0.0093	KY	0.0135
IN	0.0141	GA	0.0033	TX	0.0023	DE	0.0100	WV	0.0151
OH	0.0143	NJ	0.0034	GA	0.0023	SC	0.0100	PA	0.0153
IL	0.0152	IN	0.0034	OK	0.0024	TX	0.0106	MO	0.0157
WV	0.0157	IA	0.0035	AR	0.0025	GA	0.0113	NY	0.0164
MO	0.0167	MS	0.0035	AL	0.0028	AL	0.0123	IL	0.0183
TX	0.0173	DE	0.0039	MS	0.0031	MS	0.0132	IN	0.0192
OK	0.0190	LA	0.0046	LA	0.0035	LA	0.0194	OH	0.0197
IA	0.0209	FL	0.0058	FL	0.0035	FL	0.0328	IA	0.0205

Table 4. continued

DEPOSITION IN KILOGRAMS PER HECTARE PER WEEK							
Nitrate		Chloride		Sulfate		Hydrogen (from pH)	
NV	0.0111	MT	0.0027	NV	0.0134	NE	0.0000
MT	0.0137	WY	0.0029	MT	0.0181	NV	0.0000
WY	0.0152	CO	0.0030	ID	0.0188	SD	0.0000
ID	0.0171	ND	0.0032	WY	0.0191	ND	0.0000
OR	0.0193	NV	0.0034	CA	0.0228	UT	0.0000
UT	0.0245	SD	0.0034	UT	0.0275	CA	0.0001
ND	0.0250	NE	0.0042	CO	0.0291	IA	0.0001
AZ	0.0258	MN	0.0042	OR	0.0302	CO	0.0001
NM	0.0267	ID	0.0046	ND	0.0339	MN	0.0001
CO	0.0291	WI	0.0050	SD	0.0359	ID	0.0001
CA	0.0301	NM	0.0050	AZ	0.0420	NM	0.0001
WA	0.0310	VT	0.0057	NE	0.0445	MT	0.0001
SD	0.0334	KS	0.0059	WA	0.0453	KS	0.0001
NE	0.0438	IA	0.0061	NM	0.0462	WY	0.0001
MN	0.0521	UT	0.0063	MN	0.0532	AZ	0.0001
FL	0.0540	AZ	0.0067	KS	0.0612	OK	0.0002
TX	0.0558	MI	0.0069	WI	0.0697	OR	0.0003
ME	0.0559	CA	0.0075	ME	0.0808	WI	0.0003
KS	0.0611	NH	0.0082	IA	0.0818	TX	0.0003
WI	0.0667	ME	0.0082	TX	0.0833	WA	0.0006
SC	0.0779	IL	0.0087	OK	0.0927	MO	0.0008
MS	0.0805	MO	0.0088	VT	0.0997	FL	0.0011
IA	0.0813	IN	0.0108	FL	0.1103	LA	0.0012
GA	0.0824	OK	0.0114	MI	0.1122	AR	0.0013
OK	0.0829	OH	0.0114	NH	0.1136	IL	0.0013
NC	0.0854	KY	0.0119	MS	0.1187	MS	0.0014
AL	0.0857	NY	0.0127	MO	0.1273	MI	0.0015
MO	0.0933	CT	0.0129	AR	0.1297	ME	0.0015
LA	0.0946	TN	0.0134	LA	0.1389	NC	0.0021
AR	0.0959	OR	0.0139	NC	0.1523	GA	0.0022
TN	0.0974	PA	0.0140	SC	0.1533	AL	0.0022
VT	0.0994	VA	0.0141	GA	0.1538	IN	0.0023
NH	0.1057	WV	0.0141	MA	0.1562	SC	0.0023
MI	0.1060	AR	0.0142	AL	0.1580	TN	0.0026
IL	0.1062	WA	0.0154	IL	0.1580	VT	0.0026
KY	0.1179	NC	0.0163	CT	0.1589	NH	0.0028
DE	0.1207	TX	0.0172	TN	0.1697	OH	0.0031
VA	0.1220	SC	0.0185	IN	0.1808	VA	0.0033
IN	0.1234	MD	0.0185	NY	0.1821	KY	0.0034
MA	0.1243	MA	0.0188	RI	0.1842	DE	0.0036
RI	0.1307	NJ	0.0189	VA	0.1899	MA	0.0036
CT	0.1335	GA	0.0206	DE	0.1917	CT	0.0036
OH	0.1434	AL	0.0216	MD	0.1965	MD	0.0039
NJ	0.1463	RI	0.0217	PA	0.2059	NY	0.0040
MD	0.1467	MS	0.0220	KY	0.2061	PA	0.0041
PA	0.1557	DE	0.0233	OH	0.2066	RI	0.0043
WV	0.1601	LA	0.0330	NJ	0.2073	WV	0.0044
NY	0.1608	FL	0.0554	WV	0.2441	NJ	0.0047

the VAX handles input and output much faster than the hard disk on the AT. This means that the differences in CPU time noted above would increase if one increased the number of grid squares, that is, decreased the grid square size. Another limitation of the IBM AT is that there is only 640 KB of addressable memory. This means that after loading the program, only 512 KB of memory is left for data manipulation, assuming that one started with the full 640 KB of memory. This translates to an approximate minimum grid square size of 30 km by 30 km.

CONCLUSION

The AREA program is a useful program that will calculate area-weighted statistics on a state-by-state basis for variables that change with geographical locations. The current implementation of AREA can be easily altered to suit the user's needs. For example, if a user requires a standard error of estimates for his or her summary statistics, he or she can substitute a Krieking routine in place of the modified Barnes' scheme (note, Krieking takes much longer to run than the modified Barnes' scheme). The AREA program is general enough that a user, with only a few minor changes, can incorporate AREA as a subroutine into his or her own program.

Future changes to the AREA program might include: (1) re-digitizing the state boundaries using a more current map of the United States, (2) incorporating different spatial analysis routines into the program so that the users will have an option as to how they wish to do the interpolation procedure, and (3) grouping key areas of the United States so that area-weighted statistics can be calculated on a regional basis (for example, solving for the sulfate deposition in the Northeastern United States). These future changes could make the AREA program even more generally applicable.

REFERENCES

- Achtemeier, G.L., P.H. Hildebrand, P.T. Schickedanz, B. Ackerman, S.A. Changnon, R.G. Semonin, "Illinois precipitation enhancement program design and evaluation techniques for high plains cooperative program," Ill. State Water Survey Final Report on Contract 14-06-D-7197, Appendix B (1977).
- Barnes, S.L., "A technique for maximizing details in numerical weather map analysis," J. Appl. Meteorol., 3, 396-409 (1964).
- Hersey, A.V., "The plotting of maps on a CRT printer," NWL Report NO. 1844 (1963).
- Rand McNally 1986 Road Atlas. Rand McNally and Comp., New York, New York, (1986).

"The SCD Graphics Utilities," NCAR technical Note, NCAR-TN/166+1A, (1981).

Stolk, R. , G. Ettershank, "Calculating the area of an irregular shape,"
BYTE. 12:2, 135-136, (1986).

The World Almanac and Book of Facts for 1963. New York World-Telegram
Corp., New York, New York, (1963).

CHAPTER 15

THE DESCRIPTION AND COMPARISON OF A PROTOTYPE TRAJECTORY MODEL WITH THE ARL-ATAD MODEL

Kevin G. Doty

INTRODUCTION

Concerns surrounding air and precipitation quality have led to frequent use of trajectory models in the past decade in an attempt to relate natural and anthropogenic sources of various constituents to those observed in the media in question. These trajectory models range in complexity from efforts such as using the output of a prognostic, mesoscale, numerical weather prediction model (such as Anthes and Warner (1978)), to those using observed rawinsonde data in a relatively simple diagnostic model. An example of the latter is the Air Resources Laboratories Atmospheric Transport and Dispersion (ARL-ATAD) Model of Heffter (1980) (hereafter referred to as the ATAD model). The ATAD model was designed to calculate large numbers of boundary layer trajectories from several origins in an economical manner. Chapter 6 in this report gives the results of trajectory analyses for five years of "event" precipitation chemistry data for a site in central Illinois. The goal of the analyses and the type of data led to the development of a new trajectory model (hereafter referred to as the ISWS model). Discussion in this chapter will include: 1) an overview of some recent work with the ATAD model; 2) a description of the ATAD model; 3) sources of error in trajectory calculations; 4) a description of the ISWS model; 5) comparison of the ATAD and ISWS models; and 6) conclusions.

SOME RESULTS OF THE ATAD MODEL

The ATAD model has been used widely in the meteorological research community. No attempt will be made here to provide a thorough review of applications. Rather a few results, mostly recent, will be reviewed in light of the purposes of this chapter.

Much effort has been expended in examining possible source regions of SO_x and NO_x which are thought to be primarily responsible for contributing to the observed strong acidity in precipitation in much of eastern North America. Stunder *et al.* (1986) gave a comparison between the ATAD model and the Branching Atmospheric Trajectory (BAT) model (Heffter, 1983) when applied to event precipitation chemistry data at the Whiteface Mountain site in upstate New York (which is part of the Multi-State Atmospheric Power Production Pollution Study (MAP3S) network). In examining the predominant direction of 48 hour back trajectories in relation to sulfate deposition, it was concluded that knowing the time of precipitation on the scale of six hours or less was more important than the choice of trajectory models. Wilson *et al.* (1982) performed trajectory analyses for MAP3S sites at Illinois and Whiteface Mountain for 1978 precipitation chemistry data using the ATAD model. One finding, based on 48

hour back trajectories grouped in 30° sectors, was that precipitation and the deposition of sulfate, nitrate, and hydrogen ions was highest for the southwest sector relative to each site. Henderson and Weingartner (1982) used the ATAD model in analyzing the MAP3S data at Ithaca, New York for the period October 1977 to October 1979. No significant correlations were found when SO_x and NO_x emissions were summed along 48 hour back trajectories and compared with observed sulfate and nitrate depositions. The authors hypothesized that time spent over a specified emission area, intervening precipitation events between the emission area and arrival at the site, and precipitation intensity at the site all contributed to the lack of a relationship. When additional variables were introduced to measure the three latter factors, significant correlations were observed.

A study with a different inclination was performed by Raynor and Hayes (1983). Pollen samples during 1977-1979 in wet and dry conditions of one or two days in length at Albany, New York were examined taxonomically for types with a distant origin from New York. A modified version of the ATAD model produced back trajectories which identified source areas which consistently agreed with known source regions of specific pollens. In addition, transport as indicated by the trajectories was often in warm sectors of low pressure centers and even across warm fronts.

Based on these few studies one can say that the ATAD model shows considerable skill in defining source regions relatively large in size. The model's ability for any given data set (e.g., one year of precipitation chemistry data), is likely a function of the number of applications, the time scale of the sampling period being modeled, and the regime of synoptic types encountered. The limitations of the ATAD or of any other diagnostic trajectory model are likely dominated by the nature of the input wind data.

SOURCES OF ERROR IN TRAJECTORY CALCULATIONS

Two recent studies have investigated the possible error in calculating trajectories based on standard upper-air data, which are taken at stations with an approximate average separation distance of 400 km at 12 hour intervals. Kuo et al. (1985) gave the results of a set of observing system simulation experiments (OSSE), which used a mesoscale model (Anthes and Warner, 1978) to develop a three-dimensional wind field on a fine spatial and temporal scale that was considered the "real" atmosphere. This data set was then degraded in time and space in various combinations to investigate the effects on trajectory calculations. Trajectories calculated from these various combinations were then compared against those calculated with the "real" atmosphere. Their results, based on one cyclonic system, indicated that increasing the temporal resolution of the wind data would provide a more efficient way of decreasing trajectory error than increasing the spatial density of stations. For the mode of comparison where trajectories were calculated at a constant level above the surface within the boundary layer (similar to the ATAD model), the average horizontal transport error after 25 and 50 hours of travel was 200 and 400 km, respectively, for 88 trajectories started from a grid across the United States. Kuo et al. (1985) did not discuss how the errors varied in relation to the

relative position of the trajectories with respect to the cyclonic system.

Kahl and Samson (1986) used the additional upper-air wind data that was part of the Cross-Appalachian Tracer Experiment (CAPTEX) to investigate the role of various factors in producing error in trajectory calculations. In contrast to Kuo *et al.* (1985), their results indicated that increasing the spatial density of stations reduced errors more than increasing the temporal resolution of the wind data. Whereas the limitation of the OSSE experiment was only one cyclonic storm, CAPTEX by design investigated only periods of relatively persistent flow over the Midwest and northeastern United States. How these limitations might affect the conclusions is not clear. Kahl and Samson (1986) estimated there was a 50% probability of exceeding an error of 150 and 220 km after 24 and 48 hours of trajectory travel, respectively, as based on the CAPTEX data and their analytical techniques. Kahl and Samson (1986) also concluded that linear temporal resolution between the 12 hour observing times was the best choice given the fact that higher order schemes did not produce better results.

Another major source of error in trajectory calculations is the issue of vertical motion. Atmospheric flow under adiabatic and frictionless conditions conserves its potential temperature (Dutton, 1976). Therefore, isentropic trajectory models use this fact to determine the vertical displacements of air parcels. However, isentropic models have the following disadvantages: their expense to run, their possible nonapplicability in diabatic conditions, and their difficulties within the boundary layer when potential temperature surfaces become nearly vertical. A model such as the ATAD model assumes transport parallel to earth's surface and may be in serious error when sufficient vertical motion is coupled with vertical wind shear. Martin *et al.* (1987) compared isobaric trajectories versus those with vertical velocities derived from the data set of the European Center of Meteorological Weather Forecasts (ECMWF) and found that for transport under 48 hours the two groups were similar. While it is clear that vertical motion can have profound effects on a given trajectory, its effect remains unclear when large numbers of trajectories are calculated and the ensemble patterns investigated.

DESCRIPTION OF THE ATAD MODEL

The ATAD model uses the North American wind-temperature data set (NAMER-WINDTEMP) provided by the National Climatic Center (NCC) of the National Oceanic and Atmospheric Administration (NOAA). While primarily consisting of rawinsonde station observations at 00 and 12 Greenwich Mean Time (GMT), there are also some pilot balloon (PIBAL) observations at the intermediate times of 06 and 18 GMT. The maximum height of the data is 500 mb.

One has the option of allowing the program to determine the transport layer automatically or manually prescribing it to be a certain fixed layer above the terrain. In the automatic method the model searches for a significant potential temperature inversion at the top of the planetary boundary layer which is used to define the top of the transport layer. Starting at 300 m above the surface, the model searches upward through the data

levels at one station until one or more consecutive layers are found with a lapse rate of -5° C/km or less which results in a temperature increase from the base of the inversion of at least 2° C. The top of the transport layer is defined at the altitude within the critical inversion that produces exactly a 2° C increase from the bottom of the inversion. The top of the transport layer determined in this way will subsequently be referred to as H_c . If no such critical inversion is found, then the top of the transport layer is set to the value of 3000 m above the surface. The transport wind for a station is then based on all wind data between 150 m above the surface and the top of the transport layer. The transport wind is a layer-weighted average, where each layer is defined by half the distance between adjacent observations. The transport wind at a station is then calculated by summing the products of each observed wind component and its respective layer depth and then dividing by the total transport layer depth. This process is done for each of the stations within a selected radius of the current trajectory position.

The transport wind components are multiplied by a time step of 3 hours to get north-south and west-east displacements based on each station's transport wind components. The new displacement from the current trajectory position is calculated by summing the products of each station displacement and a weighting factor, and then dividing the weighted sum by the sum of the weighting factors. The calculations for a trajectory are terminated if a minimum number of specified stations with defined transport winds are not within the selected radius of the current trajectory position.

The weighting factors are described by (1)-(3).

$$W_1 = 1/D^2 \tag{1}$$

$$W_2 = 1 - .50 * |(\sin(\theta))| \tag{2}$$

$$W = W_1 * W_2 \tag{3}$$

In (1), D is the distance from the rawinsonde station in question to the point which is halfway on the trajectory displacement produced by using the transport wind of the station in question alone, and therefore weights nearby data more heavily. W_2 weights those wind observations more heavily which are upwind and downwind of the current trajectory position. In (2), θ is the angle between the distance from the current trajectory location and a given station, and the displacement produced by the same station's transport wind. The final weighting factor is then the product of W_1 and W_2 .

The ATAD model allows the user to calculate forward or backward trajectories starting at 00, 06, 12, and 18 GMT. The procedure described above to determine the transport layer depth is used all the time for backward trajectories and for those forward trajectories starting at 12 or 18 GMT. For the first 12 hours of forward trajectories started at 00 GMT and for the first 6 hours of trajectories started at 06 GMT, the transport layer depth is chosen as the minimum of two alternatives. The first is the transport depth as described above, whereas the second is given by (4).

$$D = 2(2 * k * t)^{1/2} \tag{4}$$

In (4), K is an eddy diffusivity set at $1.0 \text{ m}^2/\text{sec}$, t is the time in seconds from the beginning of the trajectory start, and D is the estimated transport layer depth in m resulting from small scale turbulent motions. After 12 GMT all forward trajectories are treated by the first alternative.

If data are not available at a given station for a certain time, then winds 6 hours either side of the needed time are averaged for the needed time. The winds at a given time are used 3 hours either side of that time. For example, 12 GMT winds would be used from 09 to 15 GMT for a given trajectory parcel.

DESCRIPTION OF THE ISWS MODEL

Introduction

The development of the ISWS model was the result of the need to investigate possible source regions affecting the event precipitation chemistry data collected at Bondville, Illinois. The goal was to refine the basic structure of the ATAD model without an overwhelming demand on computer resources. Significant changes were made in the following areas input data structure, calculation of transport layer depth, horizontal and temporal interpolation, and parcel advection technique.

Input Data Structure

The standard ATAD model reads the NAMER-WINDTEMP data set which consists of sequential records. Finding data at the needed synoptic time and for the specified spatial domain can use substantial computer input/output (I/O) time. One option to resolve this issue is to perform horizontal and vertical interpolation on the rawinsonde data profiles to a uniform grid system. This is certainly a viable option, but two main reasons arose for not pursuing it at this time. One is that the ATAD model uses the vertical potential temperature profile to determine the transport layer depth, and this feature was desired in the new model as well. It was uncertain how much of the vertical temperature structure would be lost in vertically gridded data and therefore make the latter feature less applicable. The other reason is that most interpolation schemes require consideration of terrain elevations and the surface pressure/temperature fields to determine the lower boundary conditions. Given the large number of cases to be considered, the latter requirement made gridding of the wind data unfeasible at this time.

The option chosen was to transform the formatted, sequential data of the NAMER-WINDTEMP data set onto unformatted, sequential indexed files as defined on the VAX-750 computer at the Illinois State Water Survey. An index key consisting of a Julian day, the GMT time, rawinsonde station identification number, and a wind/temperature flag then enables one to access data at a given station and time without sequentially reading through unneeded data as with sequential files. The disadvantage is that such a file structure is system dependent and makes the trajectory model less portable for outside users.

Determination of Transport Layer Depth

Inspection of potential temperature profiles during January and July of 1985 at Peoria, Illinois and Dayton, Ohio demonstrated that the search for a potential temperature inversion as used in the ATAD model was a good technique for 00 GMT soundings in July and to a lesser extent for 00 GMT soundings in January. This was probably an indication of the dominant role of convective motions within the summer boundary layer. The technique was less consistent for 12 GMT soundings when such a feature is typically not present. Since turbulence within the boundary layer can be produced by convective and/or mechanical (i.e., wind shear) mechanisms, it was decided to pursue a method to estimate the depth of the mechanically mixed layer for strong wind conditions. The ATAD method of finding a critical potential temperature inversion seemed to handle the convective cases very well.

The depth of the neutral Ekman layer is a function of the surface layer friction velocity, u^* (Tennekes, 1973). Monin-Obukhov similarity theory (Monin and Obukhov, 1954) was used to derive u^* from rawinsonde data. Similarity theory is applicable only in the approximate lower 10% of the boundary layer, so given the rather coarse vertical resolution of rawinsonde data it was realized that the requirements of the theory would not be fully met. However, the main application of determining the neutral depth was for strong wind situations, during which the depth of the mixed layer will be relatively large and most of the needed data would be within the requirements of similarity theory. For a complete discussion of the theory and a reference for the equations discussed below, the reader is referred to Panofsky and Dutton (1984). The major variables and constants used in the equations (5)-(25) are the following: u and w , mean horizontal and vertical wind speeds; u' and w' , deviations from the mean values of u and w ; θ and θ' , mean and deviation from the mean of potential temperature; z , vertical distance; g , acceleration of gravity; k , von Karmen constant; T , absolute temperature; and K_h and K_m , eddy diffusivities for heat and momentum, respectively. The goal of the following derivation is to demonstrate how u^* was obtained from rawinsonde data within the model.

The equation describing the balance of turbulent kinetic energy in the boundary layer for homogeneous mean flow has two production terms, P_m and P_t as given by (5) and (6). P_m describes the action of vertical eddies on the mean wind profile, while P_t describes the production of kinetic energy through the motions resulting from instability. The flux Richardson number, R_f , in (7) is the ratio of these two production terms (except for a sign change) and is a stability parameter describing the relative effects of convective and mechanical sources of turbulence. Given the difficulty of measuring the eddy

$$P_m = -\overline{u'w'} \frac{\partial u}{\partial z} \quad (5)$$

$$P_t = \frac{g}{T} \overline{w'\theta'} \quad (6)$$

$$R_f = \frac{P_t}{-P_m} \quad (7)$$

fluxes of momentum and heat, the fluxes can be related to the vertical gradient of the mean variables as given in (8) and (9). Substituting into (7), a new form of R_f is given by (10). If one can assume that the ratio of the eddy

$$\overline{u'w'} = -K_m \frac{\partial u}{\partial z} \quad (8)$$

$$\overline{w'\theta'} = -K_h \frac{\partial \theta}{\partial z} \quad (9)$$

$$R_f = \frac{\frac{g}{T} K_h \frac{\partial \theta}{\partial z}}{K_m \left(\frac{\partial u}{\partial z}\right)^2} \quad (10)$$

diffusivities is on the order of one, then the so-called gradient Richardson number R_i is obtained in (11). In determining R_i , the main source of error is measuring the vertical wind shear accurately. Given this hindrance, a further simplification can be made to yield the bulk Richardson number R_b as given by (12). R_b depends on only one vertical gradient - that of temperature which

$$R_i = \frac{\frac{g}{T} \frac{\partial \theta}{\partial z}}{\left(\frac{\partial u}{\partial z}\right)^2} \quad (11)$$

$$R_b = \frac{\frac{g}{T} \frac{\partial \theta}{\partial z} z^2}{u^2} \quad (12)$$

is measured more accurately than wind shear. Surface values (i.e., at a height of 10 meters) from the rawinsonde data were used for T and u to calculate R_b . The lowest two temperature values of a sounding were used to calculate the vertical potential temperature gradient.

If the equation describing the balance of turbulent kinetic energy is made nondimensional, the normalized wind shear function ϕ_m arises as given by (13). In making the equation nondimensional, use is made of the Monin-Obukhov length scale L as defined in (14). At heights above L , convection is the dominant

$$\phi_m = \frac{kz}{u_*} \frac{\partial u}{\partial z} \quad (13)$$

$$L = - \frac{u_*^3 T}{kg \overline{w'\theta'}} \quad (14)$$

$$R_f = \phi_m^{-1} \frac{z}{L} \quad (15)$$

producer of turbulence, whereas, at heights below approximately $L/10$, wind shear is the main mechanism, with a transition zone in between. Substituting (13) and (14) into (10) defines R_f in terms of ϕ_m as given by (15). Experimental results have determined functional forms for ϕ_m and its vertically integrated counterpart, ψ_m , as given by (16) and (17) for stable conditions

$$\phi_m = 1 + \beta \frac{z}{L} \quad (16)$$

$$\psi_m = -\beta \frac{z}{L} \quad (17)$$

$$u = \frac{u_*}{k} \left[\ln \frac{z}{z_0} - \psi_m \right] \quad (18)$$

($L > 0$). The constant β is given as 4.7 (Businger, 1973), but for model simplicity this value was rounded to 5.0. If (13) is integrated vertically, one receives (18) describing the diabatic wind profile within the surface layer where Z_0 is the roughness length. For neutral conditions $\psi_m=0$ and (18) becomes the log-linear wind profile equation. One can also describe the vertical wind profile in the surface layer in terms of a power law as in (19), where u_1 is

$$\frac{u}{u_1} = \left(\frac{z}{z_1} \right)^p \quad (19)$$

$$p = \frac{\phi_m}{\ln \frac{z}{z_0} - \psi_m} \quad (20)$$

the wind speed at a fixed height z_1 and u is the wind speed at any height z . Logarithmic differentiation of (19) and substitution from (13) and (18) define p as given by (20), where it is seen that the wind exponent p is a function of the roughness length and the nondimensional similarity functions ψ_m and ϕ_m .

Combining (11)-(13) and (20) results in (21), which gives the gradient Richardson number as a function of the wind exponent p and the bulk Richardson number. Substituting from (16) and (17) into (20) and then squaring the resulting equation results in (23) for p^2 for stable conditions. The final step in the derivation is to assume $K_n = K_m$, whereby R_i has the same equation as R_f in (15). Combining the latter form of (15) and (21) and (23) gives equation (24), which relates R_b and the function E implicitly to the nondimensional height z/L .

$$R_i = R_b \frac{\frac{u^2}{z^2}}{\left(\frac{\partial u}{\partial z} \right)^2} = \frac{R_b}{p^2} \quad (21)$$

$$\alpha = \frac{z}{L} \quad (22)$$

$$p^2 = \frac{1 + 10\alpha + 25\alpha^2}{\ln\left(\frac{z}{z_0}\right)^2 + 10\alpha\left[\ln\left(\frac{z}{z_0}\right)\right] + 25\alpha^2} = E(\alpha) \quad (23)$$

$$\alpha E(\alpha) - R_b(5\alpha + 1) = 0 \quad (24)$$

To solve (24) for L, it is necessary to know Z_0 and R_b . The calculation of R_b was discussed above. If the neutral form of (18) is applied to two different levels, Z_0 can be solved as a function of the wind speed at two heights within the surface layer. The latter technique was applied to 00 GMT wind profiles for January-March for 1981-1985 for rawinsonde stations in the eastern half of the United States. Given the fact that the neutral form of (18) was used and the character of the rawinsonde data, there was considerable scatter in the individual Z_0 values. After removing exceptionally large values, anywhere from 200-300 values were averaged at a station to obtain an estimate of the roughness length. These values were compared to a map of roughness lengths by Walcek et al. (1986) who used regional landuse data to derive their values. Those values derived from rawinsonde data which seemed aberrant were adjusted accordingly.

Given Z_0 and R_b , (24) was solved iteratively by the method of false position (Kreyszig, 1972) to obtain the Monin-Obukhov length L. Knowing L, (18) was solved for the friction velocity u^* . Since (16) and (17) only apply to stable conditions, a simplified approach was used when the potential temperature gradient used to calculate R_b was less than .50 °K/km. In these cases, u^* was solved directly from the neutral form of (18) without determining L. The unstable regime forms of (16) and (17) could be used, but this was not done because of the increased complexity and the emphasis on strong wind conditions under stable and neutral stratification.

The depth of the Ekman neutral layer (H_n) is given by (25), which involves the constant C_1 , the surface layer friction velocity u^* , and the Coriolis parameter f . A large range of values exist in the literature for C_1 , so

$$H_n = C_1 \frac{u^*}{f} \quad (25)$$

a conservative value of $C_1=.185$ used by Benkley and Schulman (1979) and derived by Plate (1971) was utilized in the model.

Another estimate of the mixed layer plays a minor role in the ISWS model. Nieuwstadt (1984) recommended the use of (26) in estimating the depth of the

$$H_s = (\sqrt{3} k R_f)^{1/2} \left(\frac{u_* L}{f} \right)^{1/2} \quad (26)$$

turbulent stable layer (H_s) for nocturnal conditions. As used in the model, R_f was actually replaced by R_i values. Equation (26) was originally derived by Zilitinkevich (1972). H_s was then one factor used in the process of determining the transport layer depth of 12 GMT soundings.

With H_c , H_n , and H_s defined, the next step in the model was to derive the top of the transport layer (T_t) from these parameters. The basic decision process is given in Table 1. Rather than discuss each possibility, only a few comments will be given. The potential temperature profile is examined to determine H_c as described earlier for the ATAD model. In the ISWS model, the temperature profile is scanned vertically to determine the location of any temperature inversions, with the bottom and top of the lowest inversion in the profile denoted by I_b and I_t , respectively. This leads to four general categories in Table 1 between 00 and 12 GMT soundings and situations where temperature inversions are and are not present. For 12 GMT soundings with no inversions, a choice is made between H_c and an average of H_n and H_c (denoted by H_b), while for situations with I_b below 100 m above the surface the maximum of H_s and 100 m is chosen. If a 12 GMT sounding has an inversion base above 100 m it is treated as a 00 GMT sounding. For 00 GMT soundings with no inversions, again a choice is made between H_n and H_c but with the emphasis on maximizing the depth of transport layer. In the case of 00 GMT soundings with inversion data, H_c is chosen as long as it is bracketed by the temperature inversion. If T_t is set to H_n , it must not exceed I_b if $H_n > I_b$.

Once T_t has been determined for a 12 GMT sounding, it is compared with the T_t value at the same station 12 hours previously. The final T_t value for the 12 GMT sounding is the maximum of the two values. The basis for this technique is that pollutants mixed throughout a relatively large depth at 00 GMT continue to be transported throughout that layer even though the mixed layer may be quite small 12 hours later.

Although no statistics were calculated, examination of several test runs of the ISWS model showed that H_c played the dominant role in determining T_t with the criteria in Table 1. Given that H_n is the largest for strong wind conditions, its role is the largest for winter situations when intense synoptic scale systems exist. Unfortunately, after the model comparisons in this chapter and the runs for chapter 6 had been completed, a mistake was found in the model code regarding equation (23), which would affect the eventual determination of H_n . This error should not affect results for spring and summer, but may play some role in the cool season results.

With T_t determined, the transport wind at a station was calculated by a layer-weighted average using data from 150 m above the surface up to T_t in the same manner as in the ATAD model.

Table 1. Decision table used by ISWS trajectory model to determine top of transport layer depth using the model estimates of H_c , H_n , and H_s . Decision flow is downward in each category. Once T_t has been determined, no further consideration of conditions is considered.

Variable Description

H_c	Top of transport layer as defined by ATAD model
H_n	Neutral Ekman layer depth
H_b	Average of H_c and H_n
H_s	Depth of turbulent stable layer by equation (XX)
I_b	Base of temperature inversion
I_t	Top of temperature inversion
T_t	Top of transport layer to be used by ISWS model
XMISS	Variable missing or undefined
OTHER	Conditions other than described in a category
MAX	Maximum of two values

GMT Time	I_b, I_t Undefined		I_b, I_t Defined	
12	Condition	Choice	Condition	Choice
	$H_n = \text{XMISS}$	$T_t = H_c$	$I_b > 100 \text{ m}$	Treat as 0000 GMT
	$H_n < H_c$	$T_t = H_n$	$H_s = \text{XMISS}$	$T_t = 100 \text{ m}$
	$H_n > H_c$	$T_t = H_b$	OTHER	$T_t = \text{MAX}(H_s, 100)$
00	Condition	Choice	Condition	Choice
	$H_n = \text{XMISS}$	$T_t = H_c$	$H_c = \text{XMISS}$	$T_t = 3000 \text{ m}$
	$H_n < H_c$	$T_t = H_c$	$I_b < H_c < I_t$	$T_t = H_c$
	$H_n > H_c$	$T_t = H_b$	$I_b < 100$ and	
			$H_n < H_c$	$T_t = H_c$
			$H_n > H_c$	$T_t = H_b$
			$H_n < H_c < I_b$	$T_t = H_c$
			$H_n > I_b$	$T_t = I_b$
			OTHER	$T_t = H_b$

HORIZONTAL AND TEMPORAL INTERPOLATION AND PARCEL ADVECTION

Horizontal Interpolation

Achtemeier (1986) developed a two-pass objective analysis scheme which was a modified form of a procedure of Barnes (1964, 1973). Since gridded data were not being used in this analysis, a one-pass form of Achtemeier's (1986) technique was used. It essentially is an exponential weighting procedure for data which are within a specified radius, D^* , of the current trajectory position. The horizontal interpolation procedure used in the model is described by (27)-(29).

$$D_b = \frac{\sum_{i=1}^n D_i}{n} \quad \text{for } D_i \leq D^* \quad (27)$$

$$N_i = (D_i/D_b)^2 \quad (28)$$

$$W_i = \exp(-2.3026 N_i) \quad (29)$$

In (27) and (28), D_i is the distance from a specified rawinsonde station to the current trajectory position, while D_b is the average of all these values which are less than or equal to D^* , which was set at 500 km. The interpolated horizontal transport wind components (U and V) at the current trajectory position are then the weighted averages described by (30) and (31), where U_i and V_i are the station transport wind components.

$$U = \frac{\sum U_i W_i}{\sum W_i} \quad (30)$$

$$V = \frac{\sum V_i W_i}{\sum W_i} \quad (30)$$

Temporal Interpolation

Once U and V at the current trajectory position are obtained at the 00 and 12 GMT times which bracket the current trajectory time, they are linearly interpolated to the current trajectory time. Thus, the needed wind components are updated at every time step. This also allows the trajectory to be started at any time and not just the 00, 06, 12, and 18 GMT times as in the ATAD model.

Parcel Advection

A two-step advection process called the predictor-corrector method was used as described by Scott and Achtemeier (1986) which was a modification of a scheme developed by Achtemeier (1979). Using the interpolated wind components at time t (U_t and V_t) derived as described above, the parcel is advected from the position with cartesian coordinates (X_t, Y_t) using a time step of three hours to time $t+3$ and a new tentative position (X_{t+3}, Y_{t+3}) . A new set of transport wind components is then determined for (X_{t+3}, Y_{t+3}) , which will be denoted by U_{t+3} and V_{t+3} . The final displacement from the position (X_t, Y_t) is then accomplished by using the average of the wind components (U_t, V_t) and (U_{t+3}, V_{t+3}) . Although details will not be given here, a Lambert-Conformal map projection was used in the model to assist in the process of handling (u, v) wind components and displacements on a (x, y) coordinate system. The Lambert-Conformal map projection has the least amount of distortion for latitudes between 30° and 60° North as compared to other common forms of map projections (Anthes and Warner, 1978).

COMPARISON BETWEEN THE ATAD AND ISWS MODELS

Methods and Data Set

To compare the two models, it was decided to choose two months in both the cool and warm seasons. The periods chosen were December 1984 through January 1985 and June through July of 1985. The cool and warm seasons were chosen a priori without considering the synoptic conditions characteristic of each period. Back trajectories 72 hours in duration were calculated each day with starting times of 00, 06, 12, and 18 GMT with Bondville, Illinois as the origin. The local climatological data for the Morrow Plots site near the Illinois State Water Survey indicated that December 1984 was mild and warm while January 1985 was extremely cold, the average temperature being 7.4° F below normal. Above normal precipitation and below normal temperatures were the pattern for both June and July of 1985. Because of its structure, the ATAD model was run on a slightly fewer number of cases than the ISWS model. A grid consisting of 100 km squares as shown in Figure 1 was used in the comparison. At each three hour interval of a trajectory, its location was stored in the appropriate grid square. The count in each grid square was then expressed as a percentage of the total number of points within the grid square domain. This technique is similar to that used by Ashbaugh (1983). With these percentages assigned to their respective grid square centers, they were then contoured using the CONREC routine in the National Center for Atmospheric Research (NCAR) graphics system. These plots for the 24 and 48 hour periods for the cool and warm test periods comprise Figures 2-5 and 8-11.

To give an indication of the model comparison with time, the horizontal difference between the ATAD and ISWS models for each three hour trajectory location for the starting times of 00, 06, 12, and 18 GMT was calculated. The maximum and the average of these absolute differences in km are plotted against time in hours along the back trajectory routes for each starting time. These results are given in Figures 6-7 and 12-13.

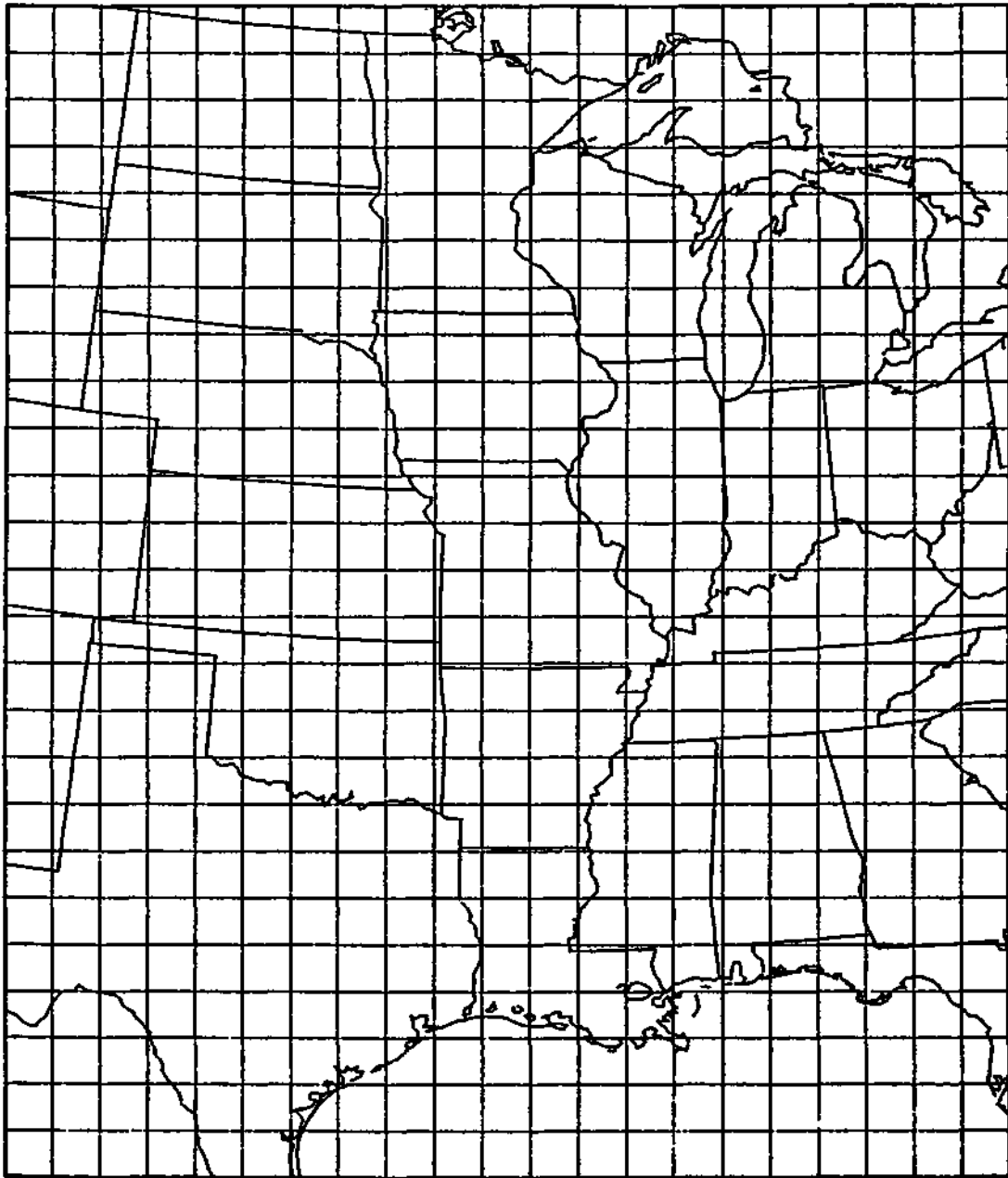


Figure 1. Grid of 100 km squares used to tally locations of trajectories at a specified time.

Comparison for December 1984-January 1985

Figures 2 and 3 give the spatial patterns for all trajectories 24, hours back in time from the origin for the ATAD and ISWS models, respectively. The general patterns for both models are very similar, with two broad areal maxima. One was over Minnesota, while the other was from the southern tip of Lake Michigan southwestward over Illinois to Missouri. The Minnesota maximum is likely a reflection of the frequent arctic invasions which occurred in January 1985 across the Midwest. The main difference between the two plots is that the ISWS model dispersed the Minnesota maximum over a larger area, which is evident by the tight contour gradient over southwestern Minnesota for the ATAD model and the relatively weak gradient over the same area for the ISWS model. The comparison at 24 hours consisted of approximately 200 points for both models. While the ATAD model had fewer start times, more of the ISWS trajectories had exited the domain by 24 hours so that the ATAD model had more trajectory endpoints within the domain.

Figures 4 and 5 give the same comparison for all trajectories 48 hours back in time. Many trajectories have left the plotting domain by this time so only about 140 trajectories are involved. The main feature in both models at this time is an areal maximum from Minnesota southward to northern Missouri. Again the ISWS model has spread the maximum over a larger area with less intense contour gradients than the ATAD model.

The average absolute difference between the trajectory locations of the two models with time is shown in Figure 6. The minimum number of locations available for each of the starting times ranged from 50 at 3 hours to 21 at 72 hours. The four time groups of trajectories demonstrated similar behavior up to 48 hours of travel, after which those starting at 18 GMT have larger differences. The average differences between the two models are quite small, being around 50 km after 24 hours of travel and around 100 km after 48 hours of travel. The maximum differences in Figure 7 show some interesting patterns which are not explainable at this time. All the groups are similar until the 36 hour time, when the 00 and 18 GMT trajectory groups follow similar paths whereas the 06 and 12 GMT each show different behavior. The 00 and 18 GMT trajectories show a steep increase in the maximum differences from 36 hours and beyond, while the 12 GMT trajectories first exhibit a peak in the maximum differences around 48 hours followed by a gradual decline. The 06 GMT trajectories have a similar peak but at about 42 hours, which is followed by a decline and then a rapid increase bringing its maximum difference at 72 hours very close to those of the 00 and 18 GMT group. The maximum differences at 24 hours are all clustered around 200 km, which is about four times as great as the average difference at that time. The maximum differences at 48 hours for most of the groups is around 600 km, which is about six times as great as the average difference at the same time.

Comparison for June-July 1985

Figures 8 and 9 show the spatial comparisons for the two models for the warm test period for all trajectories at the 24 hour time period. As in the winter case, both models exhibit very similar patterns. Basically three areal maxima exist. one in the Minnesota-Wisconsin region, one from the southern tip

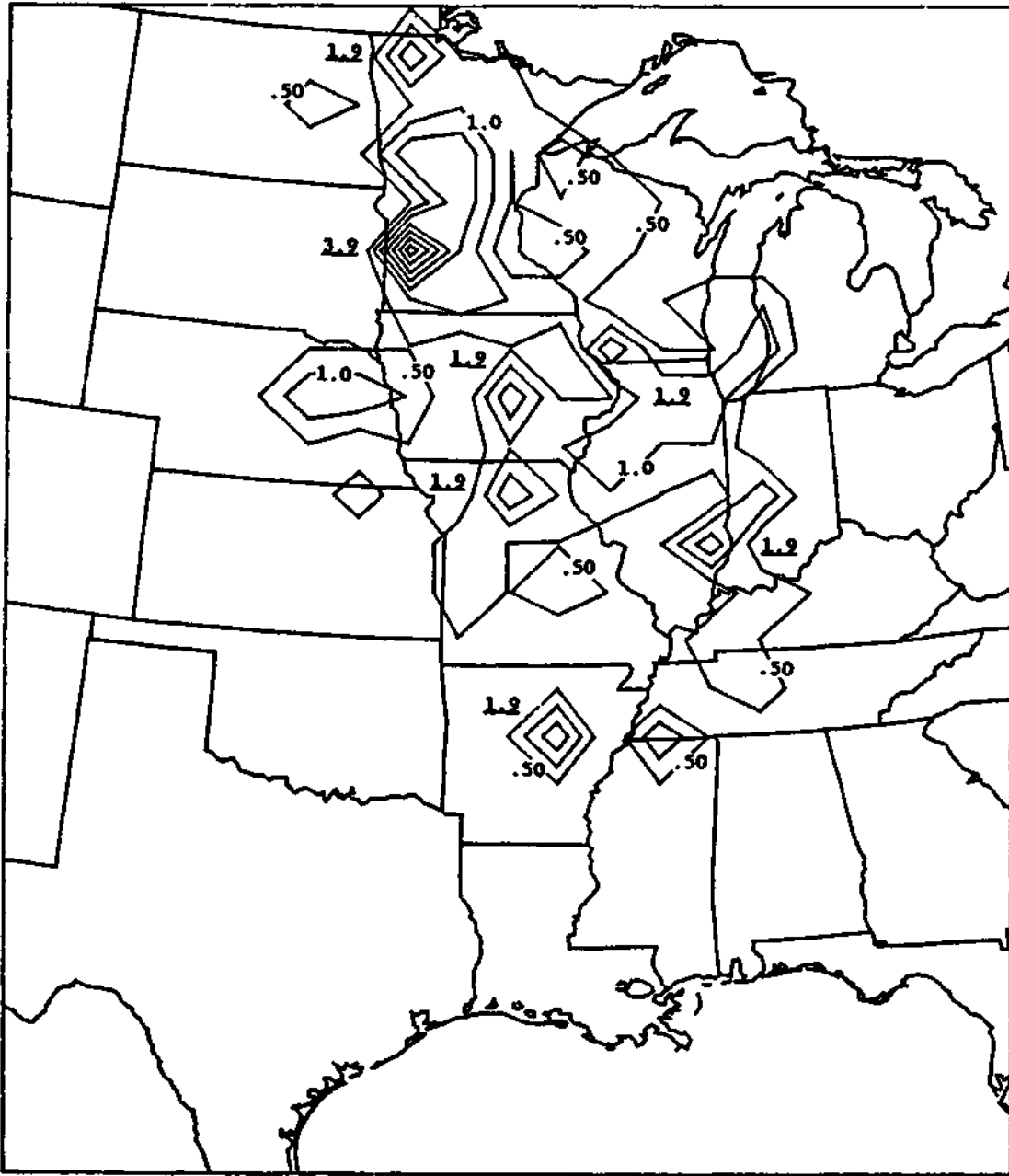


Figure 2. Percentage contours of back trajectory locations for ARL-ATAD model 24 hours back in time for period of December 1984-January 1985. Contour interval is 0.50% with grid square maxima underlined. Total number of trajectories in domain is 208.

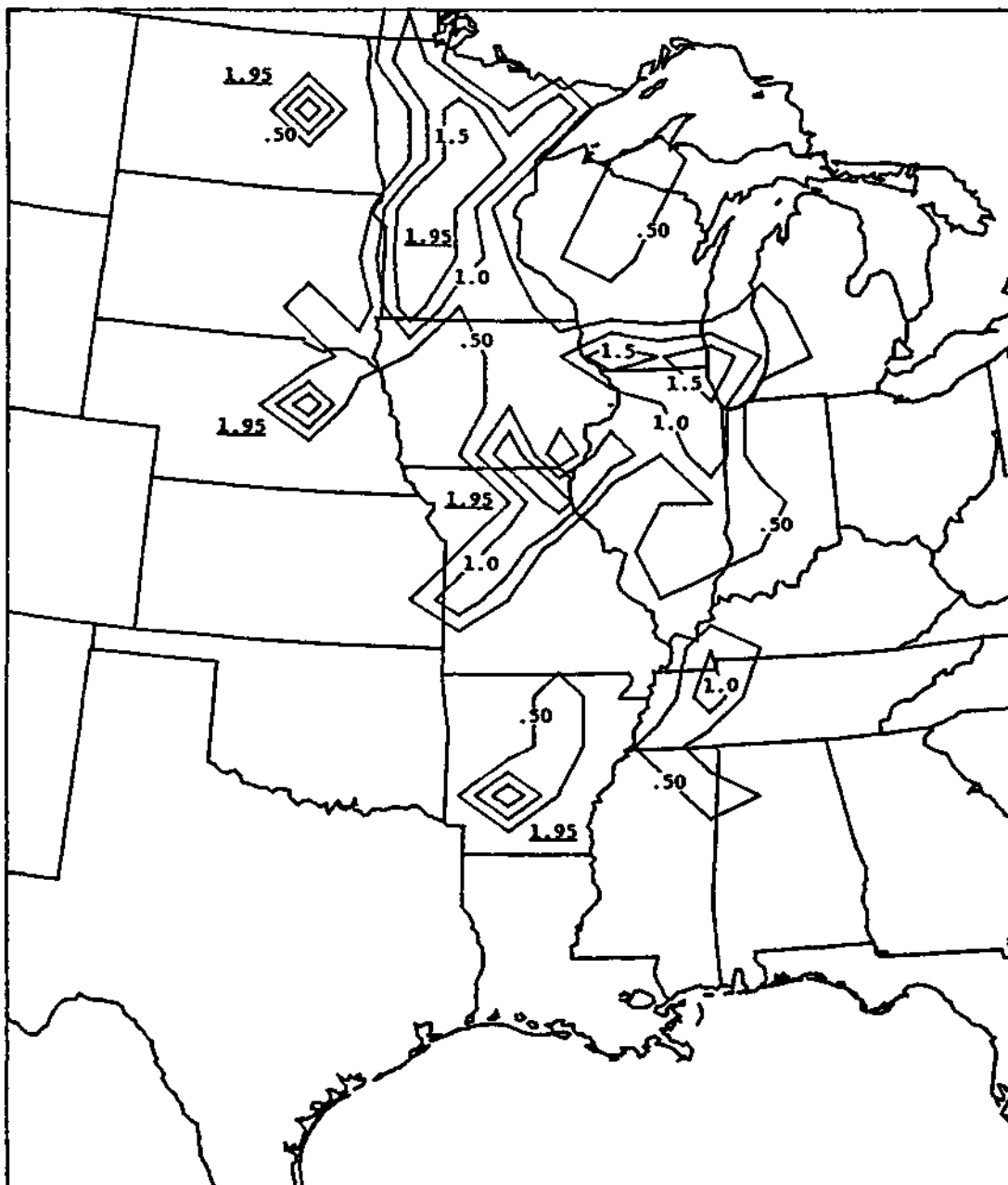


Figure 3. Percentage contours of back trajectory locations for ISWS model 24 hours back in time for period of December 1984-January 1985. Contour interval is 0.50% with grid square maxima underlined. Total number of trajectories in domain is 205.

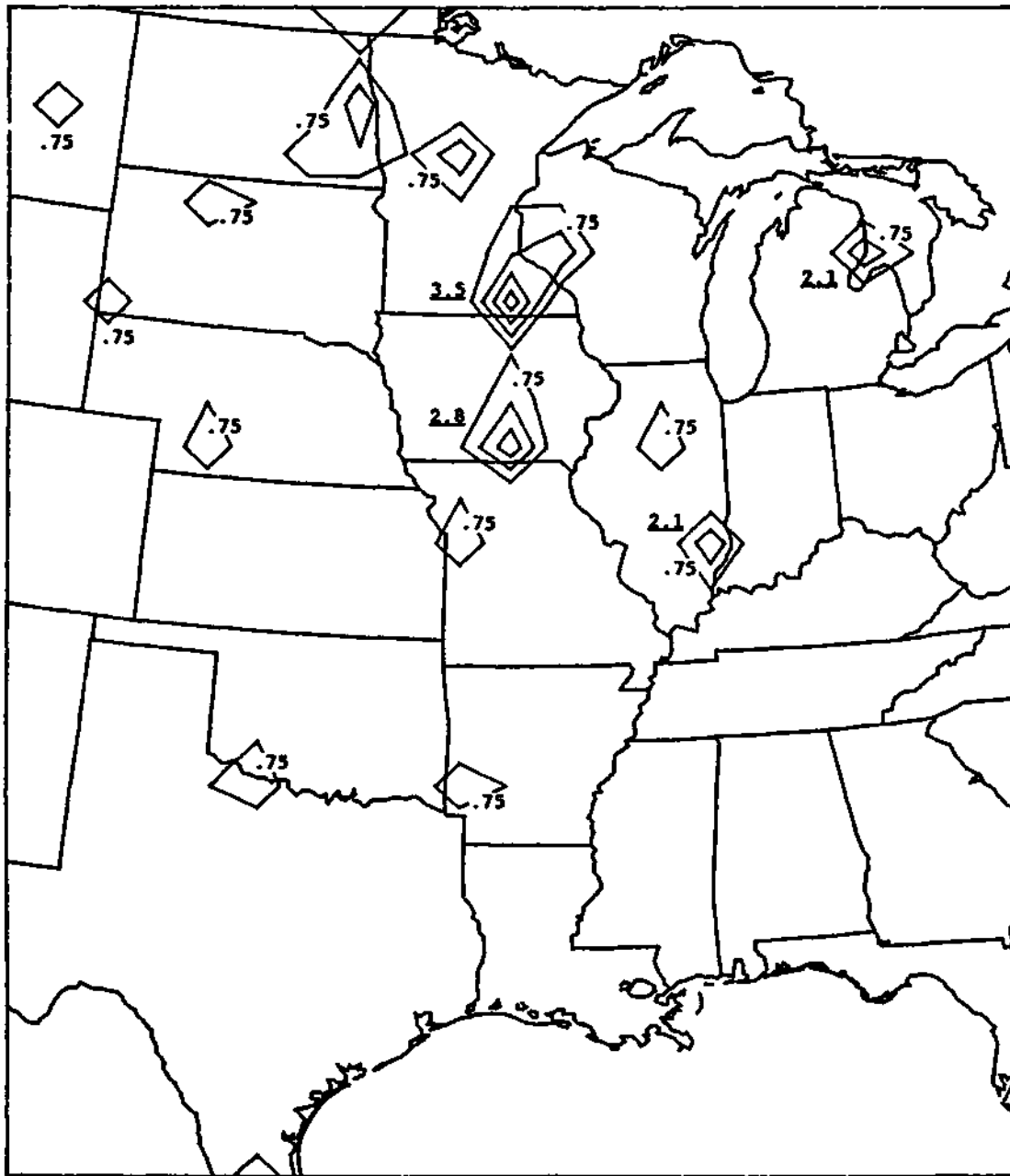


Figure 4. Percentage contours of back trajectory locations for ARL-ATAD model 48 hours back in time for period of December 1984-January 1985. Contour interval is 0.75% with grid square maxima underlined. Total number of trajectories in domain is 143.

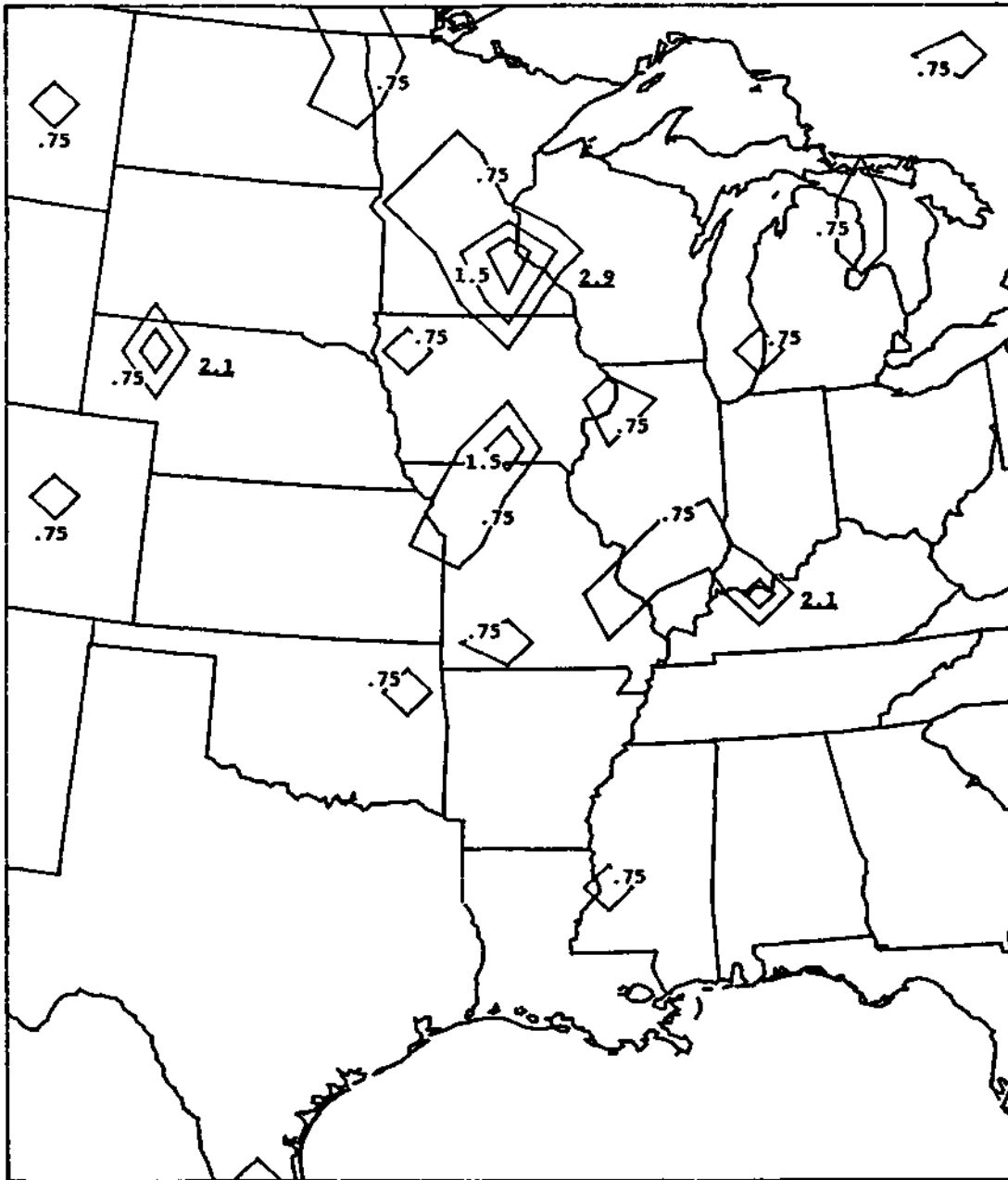


Figure 5. Percentage contours of back trajectory locations for ISWS model 48 hours back in time for period of December 1984-January 1985. Contour interval is 0.75% with grid square maxima underlined. Total number of trajectories in domain is 140.

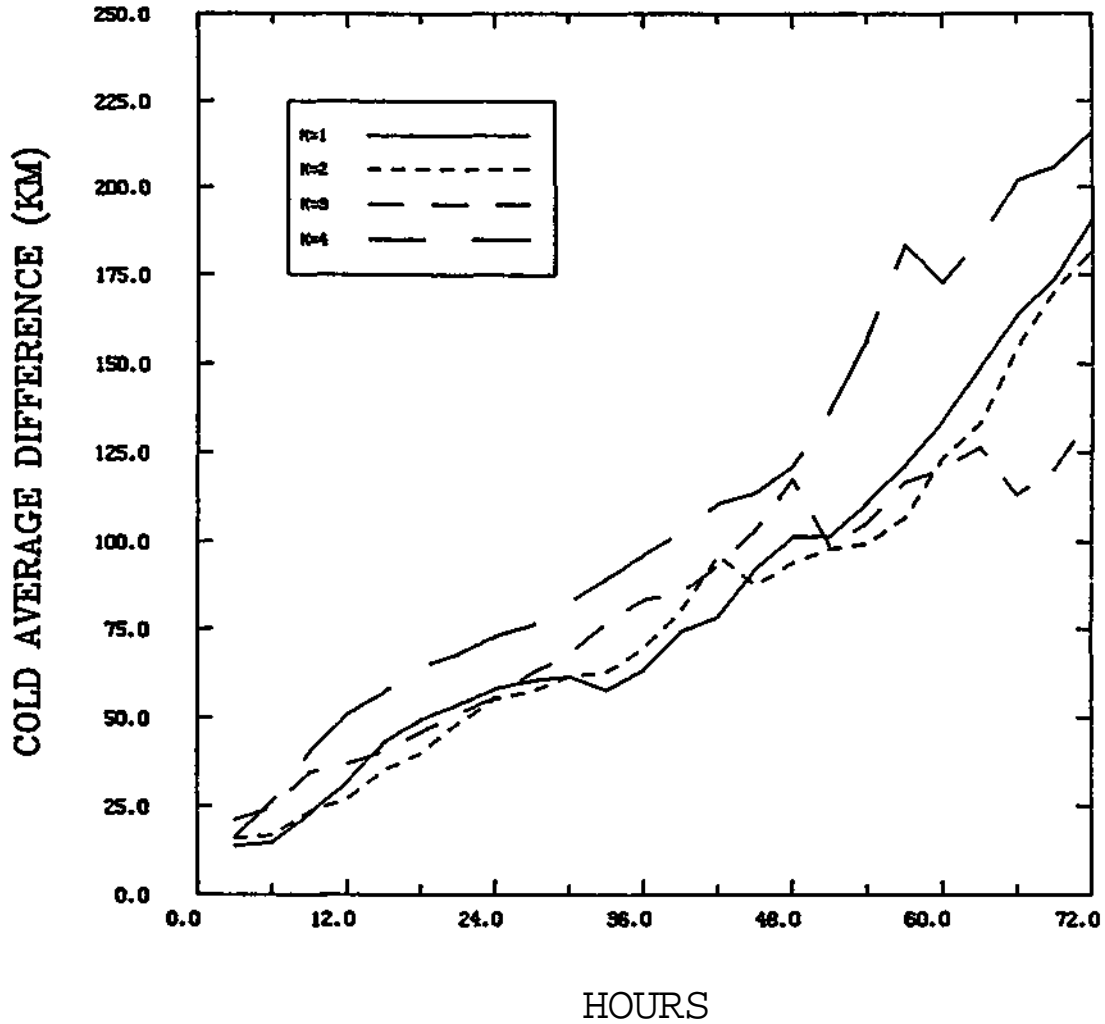


Figure 6. Plot of average absolute difference between ARL-ATAD and ISWS models in km (ordinate) versus back trajectory time in hours (abscissa) for period of December 1984-January 1985. Values of K=1,2,3,4 correspond to back trajectory starting times of 00, 06, 12, and 18 GMT, respectively.

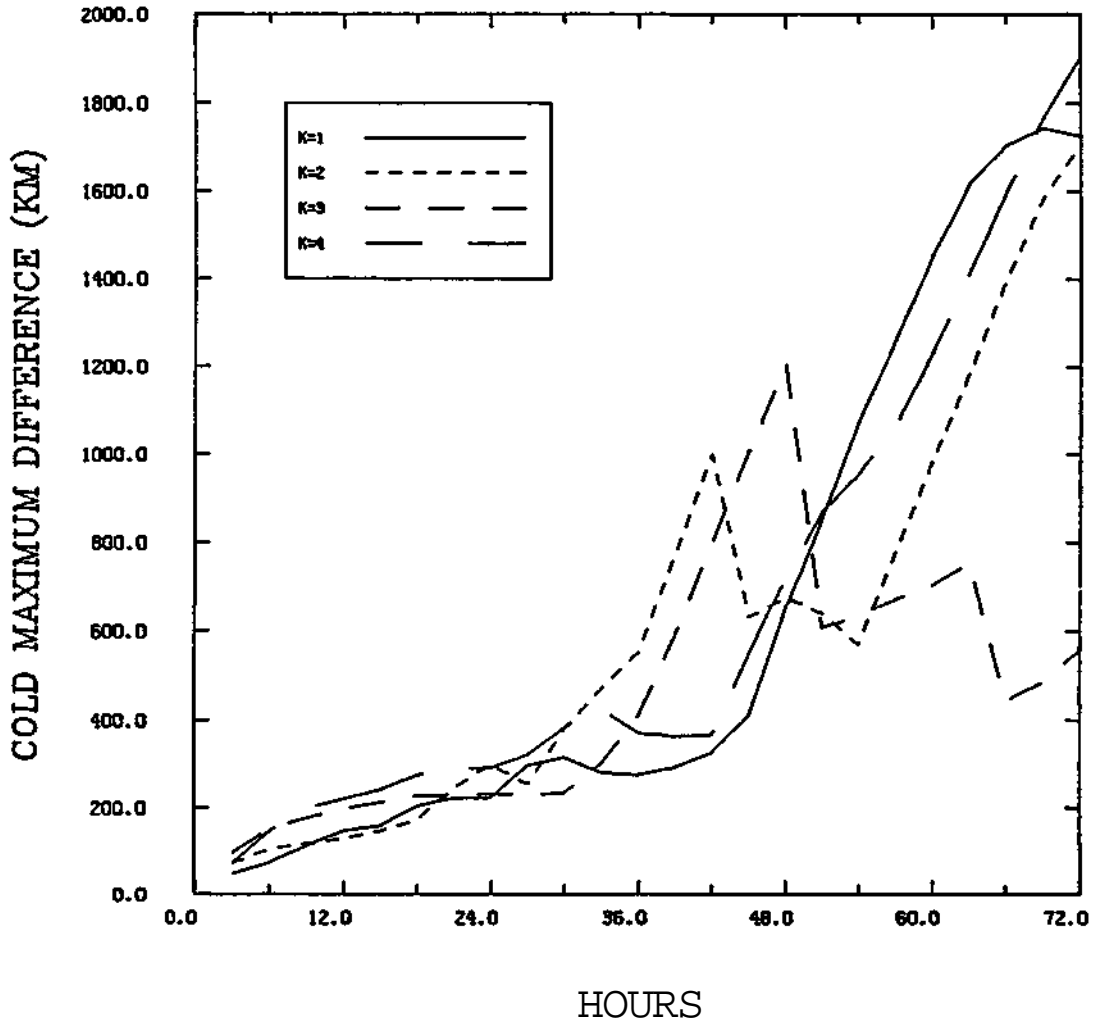


Figure 7. Plot of maximum absolute difference between ARL-ATAD and ISWS models in km (ordinate) versus back trajectory time in hours (abscissa) for period of December 1984-January 1985. Values of K=1,2,3,4 correspond to back trajectory starting times of 00, 06, 12, and 18 GMT, respectively.

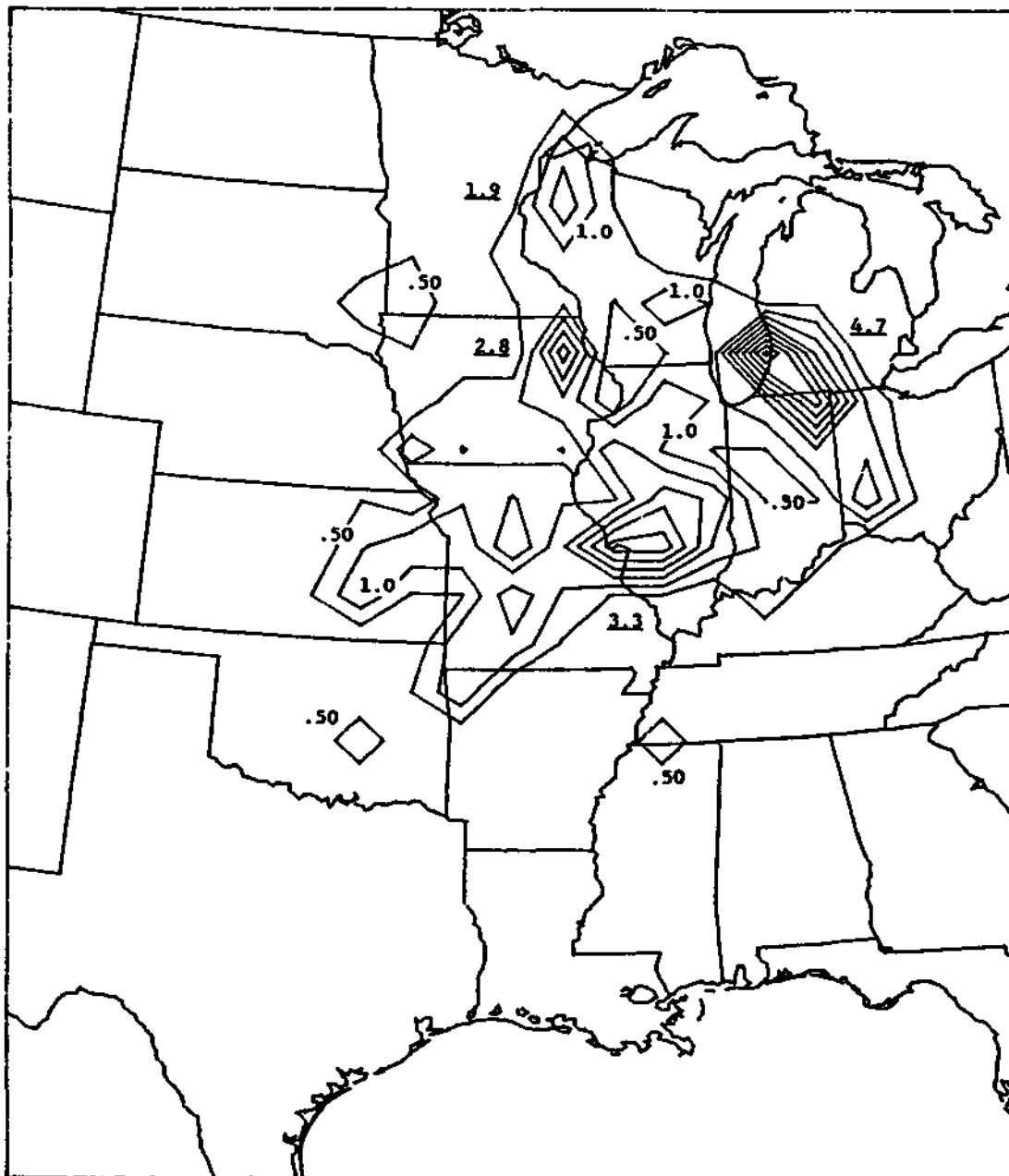


Figure 8. Percentage contours of back trajectory locations for ARL-ATAD model 24 hours back in time for period of June-July 1985. Contour interval is 0.50% with grid square maxima underlined. Total number of trajectories in domain is 213.

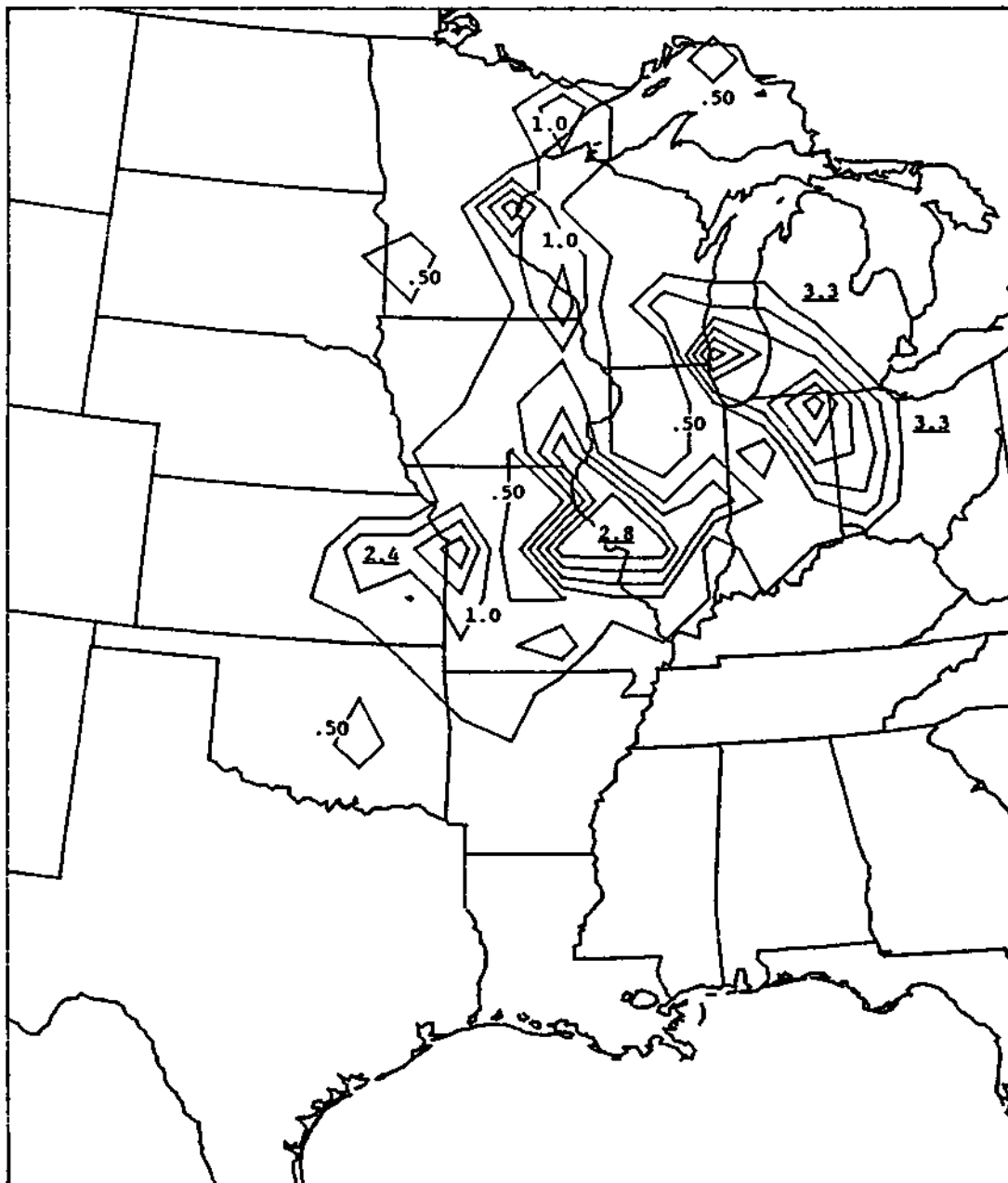


Figure 9. Percentage contours of back trajectory locations for ISWS model 24 hours back in time for period of June-July 1985. Contour interval is 0.50% with grid square maxima underlined. Total number of trajectories in domain is 212.

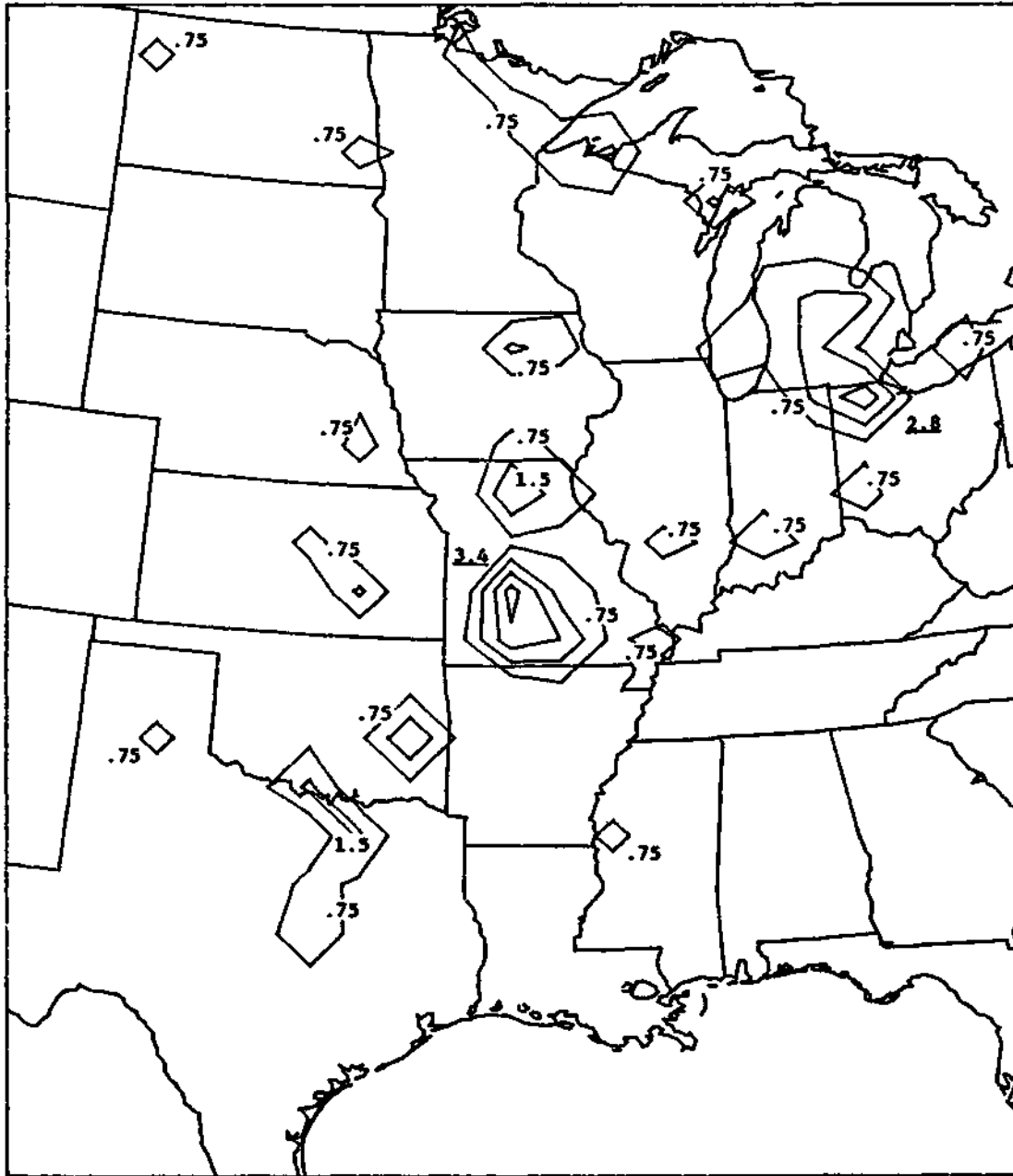


Figure 10. Percentage contours of back trajectory locations for ARL-ATAD model 48 hours back in time for period of June-July 1985. Contour interval is 0.75% with grid square maxima underlined. Total number of trajectories in domain is 179.

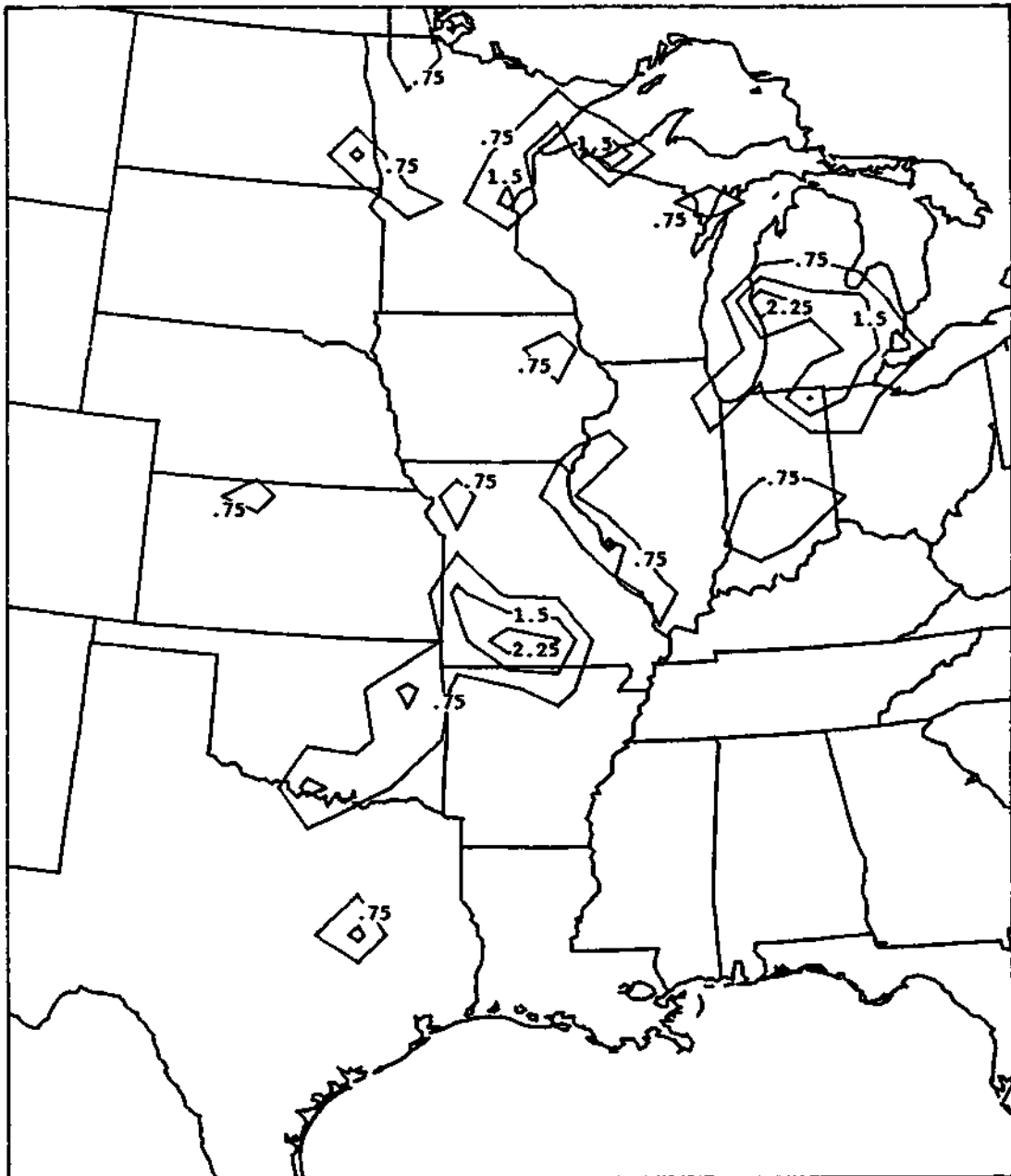


Figure 11. Percentage contours of back trajectory locations for ISWS model 48 hours back in time for period of June-July 1985. Contour interval is 0.75% with grid square maxima underlined. Total number of trajectories in domain is 175.

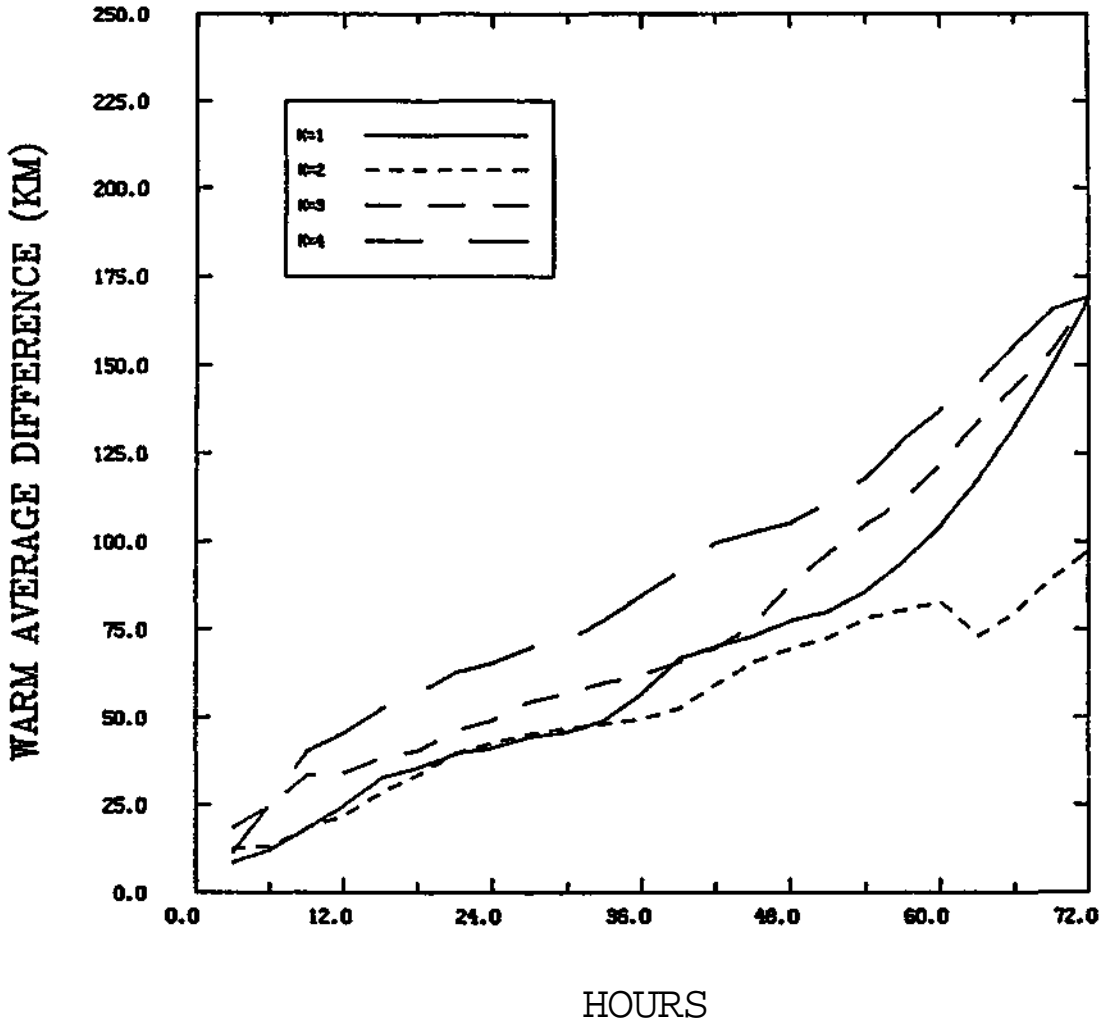


Figure 12. Plot of average absolute difference between ARL-ATAD and ISWS models in km (ordinate) versus back trajectory time in hours (abscissa) for period of June-July 1985. Values of K=1,2,3,4 correspond to back trajectory starting times of 00, 06, 12, and 18 GMT, respectively.

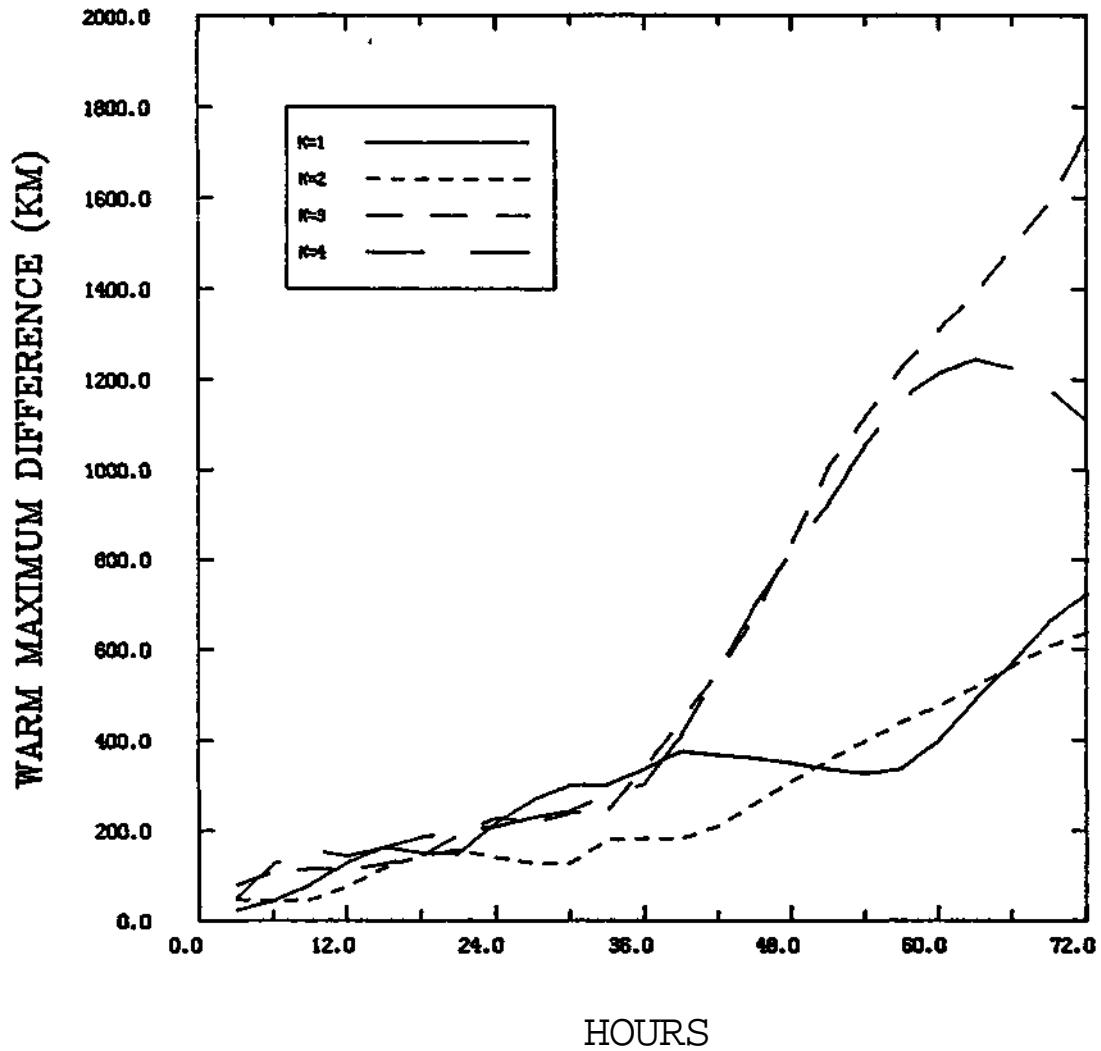


Figure 13. Plot of maximum absolute difference between ARL-ATAD and ISWS models in km (ordinate) versus back trajectory time in hours (abscissa) for period of June-July 1985. Values of K=1,2,3,4 correspond to back trajectory starting times of 00, 06, 12, and 18 GMT, respectively.

of Lake Michigan southeastward across Indiana and Ohio, and one from central Illinois southwestward across Missouri. Although not to the same degree as in the winter case, there is the tendency for the ISWS model to disperse maxima as compared to the ATAD model. This is most clearly seen in the second areal maximum described above, where the ATAD model has a very intense gradient across southern Michigan and adjacent parts of Indiana and Ohio, whereas the ISWS model has much weaker gradients in the same area. For both models, the 24 hour comparison was based on about 200 trajectory locations.

Figures 10 and 11 give the comparison for the 48 hour period. The main difference is that the disjointed maxima over Missouri, Arkansas, and Oklahoma for the ATAD model are merged into basically one area for the ISWS model. Other major patterns between the two are very similar.

Figure 12 shows that the average difference for all starting times at the 24 hour mark ranged from 30-60 km, and 60-100 km at the 48 hour mark. All the starting times exhibited similar patterns in essentially linear growth with time, with the exception that the 18 GMT group had larger errors for much of the 72 hour period. The minimum number of trajectories contributing to Figures 12 and 13 ranged from 49 at the 3 hour mark to 37 at 72 hours. The maximum differences in Figure 13 show similar behavior for the 00 and 06 GMT groups and the 12 and 18 GMT groups. At the 24 hour mark, all groups had maximum differences at around 200 km, and at 48 hours around 300 km for the 00 and 06 GMT group and around 800 km for the 12 and 18 GMT group. In general the average and maximum differences for the warm test period were smaller than the cool test period, as would be expected given the stronger winds in the cool period.

CONCLUSIONS

A modified version of the ATAD model was compared with the ATAD model for the periods December 1984-January 1985 and June-July 1985. Both models exhibited very similar behavior in both the warm and cool test periods. One difference consistently noted between the two models was the characteristic of the ISWS model to disperse maxima over a wider area as compared to the ATAD model. This was probably due to the combination of the time interpolation at each time step and the predictor-corrector advection method, which should allow more influence of winds changing with time. If a comparison was done between the two models for times with precipitation only, larger differences might be expected given the larger wind shears generally present in such situations. The ISWS model takes a factor of about 3.6 times more CPU time on the VAX-750 than does the ATAD model. To the extent this comparison was typical of both model's performances, it seems the extra time needed to run the ISWS model may not be warranted given its similarity to the ATAD results.

ACKNOWLEDGEMENTS

This research has been funded as part of the National Acid Precipitation

Assessment Program by the Department of Energy under Contract DE-AC02-76EV01199.

REFERENCES

- Achtemeier, G. L., 1986: On the notion of varying successive corrections objective analyses Mon. Wea. Rev., 114, 40-49.
- Achtemeier, G. L., 1979: Evaluation of operational objective streamline methods. Mon. Wea. Rev., 107, 198-206.
- Anthes, R. A. and T. T. Warner, 1978: Development of hydrodynamic models suitable for air pollution and other mesometeorological studies. Mon. Wea. Rev., 106, 1045-1078.
- Ashbaugh, L. L., 1983: A statistical trajectory technique for determining air pollution source regions. J. Air Pollut. Control Assoc, 33, 1096-1098.
- Barnes, S. L., 1964: A technique for maximizing details in numerical weather map analysis. J. Appl. Meteor., 3, 396-409.
- _____, 1973: Mesoscale objective analysis using weighted time-series observations. NOAA Tech Memo. ERLNSSL-62, 60pp. [NTIS COM-73-10781].
- Benkley, C. W. and L. L. Schulman, 1979: Estimating hourly mixing depths from historical meteorological data. J. Appl. Meteor., 18, 772-780.
- Businger, J. A. "Turbulent transfer in the atmospheric surface layer." In Workshop on Micrometeorology, ed. D. A. Haugen. Boston: American Meteorological Society, 1973.
- Dutton, J. A., 1976: The Ceaseless Wind. McGraw-Hill, New York, 579 pp.
- Heffter, J. L., 1980: Air Resources Laboratories Atmospheric Transport and Dispersion Model (ARL-ATAD). NOAA Tech. Memo. ERL ARL-81, Air Resources Laboratories; Silver Springs, Maryland.
- Heffter, J. L., 1983: Branching Atmospheric Trajectory (BAT) Model. NOAA Tech. Memo. ERL ARL-121; Air Resources Laboratories; Rockville, Maryland.
- Henderson, R. G. and K. Weingartner, 1982: Trajectory analysis of MAP3S precipitation chemistry data at Ithaca, NY. Atmos. Environ., 16, 1657-1665.
- Kahl, J. D. and P. J. Samson, 1986: Uncertainty in trajectory calculations due to low resolution meteorological data. J. Climate Appl. Meteor., 25, 1816-1831.
- Kreyszig, E., 1972: Advanced Engineering Mathematics. Wiley, New York, 866 pp.

- Kuo, Y. H. , M Skumanich, P. L. Haagenson and J. S. Chang, 1985 The accuracy of trajectory models as revealed by the Observing System Simulation Experiments. Mon. Wea. Rev., 113, 1852-1867.
- Martin, D. , C. Mithieux and B. Strauss, 1987: On the use of the synoptic vertical wind component in a transport trajectory model. Atmos. Environ, 21, 45-52.
- Monin, A. S. and A. M. Obukhov, 1954: Basic laws of turbulent mixing in the atmosphere near the ground. Tr. Akad. Nauk SSSR Geofiz Inst, 24, 163-187.
- Nieuwstadt, F. T. M., 1984: Some aspects of the turbulent stable boundary layer. Bound. Layer Meteor., 30, 31-55.
- Panofsky, H. A. and J. A. Dutton, 1984: Atmospheric Turbulence. Wiley, New York, 397 pp.
- Plate, E. J., 1971: Aerodynamic Characteristics of Atmospheric Boundary Layers. U.S. Atomic Energy Commission, 190 pp. [NTIS TID-25465].
- Raynor, G. S. and J V. Hayes, 1983: Testing of the Air Resources Laboratories trajectory model on cases of pollen wet deposition after long-distance transport from known source regions. Atmos. Environ, 17, 213-220.
- Scott, R. W. and G. L. Achtemeier, 1986: Identification of long range pest flight patterns via wind transport modeling, Illinois State Water Contract Report 379, Illinois State Water Survey, 48 pp.
- Stunder, B. J. B. , J. L. Heffter and U. Dayan, 1986: Trajectory analysis of wet deposition at Whiteface Mountain: A sensitivity study. Atmos. Environ., 20, 1691-1695.
- Tennekes, H. " Similarity laws and scale relations in planetary boundary layers. " In Workshop on Micrometeorology. ed. D. A. Haugen. Boston: American Meteorological Society, 1973.
- Walcek, C. J., R. A. Brost and J. S. Chang, 1986: SO₂, Sulfate, and HNO₃ deposition velocities computed using regional landuse and meteorological data. Atmos Environ., 20, 949-964.
- Wilson, J W., V. A. Mohnen and J. A. Kadlecck, 1982: Wet deposition variability as observed by MAP3S. Atmos. Environ., 16, 1667-1676
- Zilitinkevich, S. S., 1972: On the determination of the height of the Ekman boundary layer. Bound. Layer Meteor., 3, 141-145.

CHAPTER 16

SCREENING CRITERIA FOR NADP DRY BUCKET DATA

Donald F. Gatz, Van C. Bowersox, and Jack Su

INTRODUCTION

Dry bucket samples were collected at all National Atmospheric Deposition Program (NADP) sites from the network's inception in mid-1978 until June 1984, when the collection of the dry samples became optional. At the dry network's peak in June 1984, 151 sites collected dry bucket samples; as of January 1987, the dry bucket sampling network numbered 46 sites. To March 1987, 3968 dry bucket samples had been analyzed by the NADP Central Analytical Laboratory at the Illinois State Water Survey. A portion of the data have been analyzed previously by Semonin (1984).

A one-month intercomparison of dry deposition monitoring and measurement methods at an Illinois grassland site included a detailed comparison of results for sulfur dry deposition to buckets and other surrogate surfaces, as well as fluxes measured by micrometeorological techniques (Dolske and Gatz, 1984). Sulfur dry deposition fluxes measured by the bucket collectors were consistently the highest of those measured by the various surrogate surfaces.

Indeed, evaluations of dry deposition monitoring methods for atmospheric particles (e.g., Hicks et al., 1980, Hicks et al., 1986) usually raise a number of objections to the use of bucket collectors for monitoring dry deposition. One is that the collectors are subject to contamination by insects, bird droppings, and other foreign matter during their often lengthy exposures. Another is that the shape, surface characteristics, and exposure conditions of the collector are so dissimilar from those involved in the natural processes of dry deposition that dry bucket collections cannot be used to predict dry deposition to natural surfaces. This latter objection applies primarily to the deposition of small (approximately 1 μm and smaller) particles, such as sulfate particles. For "large particles," surrogate surfaces, particularly those designed with suitable aerodynamic flow characteristics, are acknowledged as potentially valuable monitoring devices for the measurement of the sedimentation flux (Hicks et al., 1986).

Although buckets are not in the class of aerodynamically-designed collectors described by Hicks et al., a considerable effort has already been devoted to the collection and analysis of several thousand NADP dry bucket samples from sites in many regions of the U.S. Thus it is prudent to find out whether the data set might be effectively screened to remove contaminated samples, so as to yield a data set useful for estimating (at least) large particle dry fluxes.

A previous examination of the frequency of contaminated NADP dry bucket samples (Hicks, 1985), based on an unstated number of samples, found many

sites with high frequencies of contamination by bird droppings, and noted that essentially all sites experienced "contamination" by soil particles. The degree of bird droppings contamination was assessed using the ratio of dissolved phosphate to sulfate concentrations, on an arbitrary scale. Soil particle contamination was characterized by the ratio of dissolved calcium to sulfate, again using an arbitrary scale as an index of the degree of contamination.

There is little question that bird droppings should be considered contaminants of atmospheric dry deposition samples, or that phosphate can serve as an effective indicator of their presence, although other ions, such as K and NH_4 , are probably no less effective. On the other hand, one may question why soil or other surficial particles should be considered to be contaminants (provided that collectors are sited such that locally resuspended materials are not their major source), since they are true atmospheric constituents and are deposited as a result of atmospheric processes. Further, they have the potential to neutralize acids in precipitation or fog water that later impacts on surfaces where they may deposit. Thus they may mediate certain effects of precipitation acidity. The choice of the Ca/SO_4 ratio appears to be more appropriate as an index of unpaved road contaminants (Gatz *et al.*, 1985) than soils

It is clear that there is not a consensus on the question of whether soil particles should be considered to be contaminants in dry deposition samples. However, if the frequency of the more obvious contamination of the NADP dry bucket samples is so high as to preclude analyses of the data for useful purposes, then there is no reason to devote additional time and resources to the collection of additional samples or to sample or data analysis. It would be useful, therefore, to conduct an independent examination of the data to see whether effective methods for screening contaminated samples from the data set can be identified. Another benefit might be to identify types of sample contamination that preclude any meaningful uses of the analytical data. Samples thus contaminated could be discarded without analyses.

Thus, the purpose of this work was to analyze a portion of the existing dry bucket data set to determine the effect of various screening criteria on the frequency distribution of measured dry fluxes of each measured ion.

METHODS

Field and Laboratory Methods

Dry deposition samples are collected in white linear polyethylene buckets that have been cleaned at the NADP Central Analytical Laboratory (CAL) and shipped to sites in sealed polyethylene bags and packed in protective rigid shipping containers. Until May 1982 the buckets were scrubbed by hand, using a natural sponge to remove particles, followed by repeated rinsings with deionized water until the specific conductance of the rinse water was less than 2 $\mu\text{S}/\text{cm}$. In May 1982 the procedure was changed. Since that time, the buckets have been emptied of sample, wiped

free of particulate matter, and then washed in a commercial dishwasher. For the period when the samples analyzed in this paper were collected, the dishwasher used tap water from the city supply for the wash cycle and deionized water for the three successive rinse cycles that follow. No detergent has ever been used in any of the washing operations.

When the network began operations, the sampling period for the dry bucket samples was two months, beginning and ending on the first Tuesday of even-numbered months (February, April, etc.). Beginning on December 2, 1980, the collection period was changed to eight weeks, with bucket changes again made on Tuesdays. The sample bucket is removed from the sampler with care to avoid contamination, a polyethylene lid is pounded securely into place with a rubber mallet, and the bucket is shipped back to the CAL in the same manner as it was shipped to the site.

Laboratory procedures for handling and analyzing the dry samples at the CAL, including quality control procedures, have been published (Stensland *et al.*, 1980; Lockard, 1987). Briefly, 250 mL of deionized water are added to the samples, the water is swirled to insure contact with the walls, and the samples are allowed to equilibrate for 24 hr or overnight. Then they are filtered through a 0.45 μ m pore diameter Millipore type HA filter, and the filtrates are handled and analyzed in the same way as precipitation samples (Peden *et al.*, 1986).

Ion concentrations reported as "less than detection limit" were assumed to have a value of one-half of the detection limit in subsequent dry flux calculations.

STATISTICAL AND GRAPHICAL METHODS OF COMPARISON

Statistical Tests

Both parametric and non-parametric tests of the significance between means of the unscreened and screened data sets were performed using the SAS GLM procedure (SAS, 1982). The parametric test was the main-effects analysis of variance model (Neter *et al.*, 1985). The significance testing assumes that the error variance is normally distributed. This assumption may not be met for many of the ions. The non-parametric test was the Kruskal-Wallis k-sample test (Kruskal and Wallis, 1952). In both cases, when significant differences between means were indicated, the Fischer least-significant-difference test (Sokal and Rohlf, 1981) and the Tukey-Kramer significant difference test (Dunnett, 1980) were applied to identify the data sets that were significantly different from each other.

Percentile Comparisons

A graphical method described by Cleveland (1985) was used to compare the frequency distributions of dry fluxes of certain measured ions computed from the unscreened data set to those computed from data sets satisfying a series of successively more stringent screening criteria. The

method involves plotting dry flux values corresponding to the same percentiles in the unscreened data set against those in the screened data set. The percentiles chosen were the 1st, 5th, 10th, 25th, 50th, 75th, 90th, 95th, and 99th. The ordinates are the values in the screened data sets, and the abscissas are the values in the unscreened. The scales along the top and right of the graph are actual fluxes on a log scale, and those at the bottom and left are log base 10 values of the fluxes. Perfect agreement between the distributions of the respective fluxes in the respective data sets would result in straight lines, and differences from perfect agreement appear as departures, either positive or negative, of the plotted points from a straight line.

To illustrate the differences between distributions in more detail, Tukey sum-difference plots (Cleveland, 1985) are provided. These show the differences between the fluxes at each percentile value of the respective distributions, plotted against their corresponding sum. The purpose of these additional plots is to show how the differences between distributions vary over the combined distribution of values. Again, log values are shown on the left and bottom scales. The top scales show actual values of the sum of the fluxes, plotted on a log scale. Because a difference of logs is equivalent to the log of a quotient, the scales on the right edges of the sum-difference graphs show values of the ratio: screened flux/unscreened flux. In other words, the values on the right ordinate show the number of times the flux from the screened data set exceeded that in the unscreened at each percentile.

RESULTS

For each measured ion (H, Na, Mg, Cl, K, Ca, NH_4 , NO_3 , PO_4 , and SO_4), the means, standard errors, and the percentile values listed earlier were computed for six separate data sets. The data sets included: (A) the unscreened data set, and (B through F) subsets of set A satisfying successively more stringent screening criteria, as detailed in Table 1. Note that application of the screening criteria caused the deletion of only 21 samples between data sets A and B, an additional 517 samples between B and C, 137 samples between C and D, 270 samples between D and E, and 16 samples between E and F.

Main Effects

Plots of the mean dry deposition fluxes for ten ions measured in the dry bucket samples are shown in Figures 1-5 for the unscreened and the various screened data sets. The error bars shown are the 95% confidence limits for the mean values. The results of parametric tests of significance between means of the several data sets and non-parametric tests of the significance of differences between sampled populations are given in Table 2. The assumption of a normal distribution of sample values is implicit both in the figures and the parametric test results. Thus, these respective results are expected to be consistent with each other. The following discussion of the effects of screening level on the mean dry fluxes of the various ions will refer to both the table and the appropriate figures.

Table 1. Screening criteria for dry bucket data.

Data set	Screening level	Number of samples	Screening criteria
A	(unscreened)	1269	None
B	1	1248	Gross handling error or contamination (e.g., bucket blew out of sampler)
C	2	731	Set B criterion, plus water in the bucket when opened at the CAL
D	3	594	Sets B and C criteria, plus observed water marks, indicating water was in the bucket, but evaporated before reaching the laboratory
E	4	324	Sets B - D criteria, plus one or more contaminants observed (e.g., plant parts or pieces, bird droppings, insects, handling contamination, or other contamination)
F	5	308	Sets B - E criteria, plus bucket covered part of the time during dry weather

Figure 1 shows results for H and Na. For H the mean dry flux decreased by a factor of about 10 as samples containing water were eliminated at the second screening level. Further screening to remove water-spotted (screening level 3), visually contaminated (screening level 4), and incomplete samples (screening level 5) produced no further significant changes in the mean dry flux. Results of both parametric and non-parametric tests in Table 2 confirm what is quite apparent in Figure 1, namely that the means of data sets A and B were both significantly (5%) different from those of data sets C, D, E, and F.

For Na (Figure 1), the mean fluxes tended to increase as the screening level increased, but the 95% confidence limits widened accordingly, so the statistical tests (Table 2) found no significant differences between means.

Figure 2 shows results for Mg and Cl. For both ions, elimination of wet and water-spotted samples (levels 2 and 3) caused increases in the mean dry fluxes, and elimination of contaminated samples (level 4) caused subsequent small decreases, but none of the differences was significant at the 5% level (Table 2).

Figure 3 shows contrasting results for K and Ca. For K, there was a slight, non-significant increase in the mean flux as wet and water-spotted samples were removed, and then a sharp decrease in the mean as contaminated samples were removed. The statistical results in Table 2 agree that there are significant differences between means, but give somewhat conflicting indications of which means are different. The various tests agreed that data sets C and D were different from E and F, but didn't agree on whether A and B were different from E and F, which appears rather likely from Figure 3. The parametric tests indicated significance between AB and EF. The non-parametric tests did not, but on the other

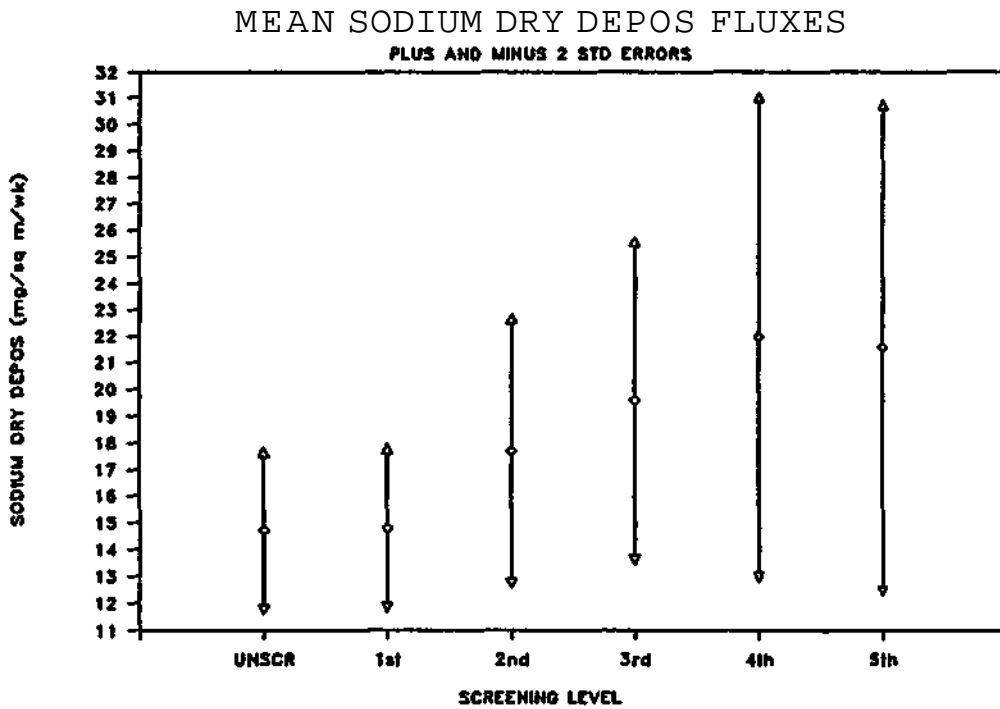
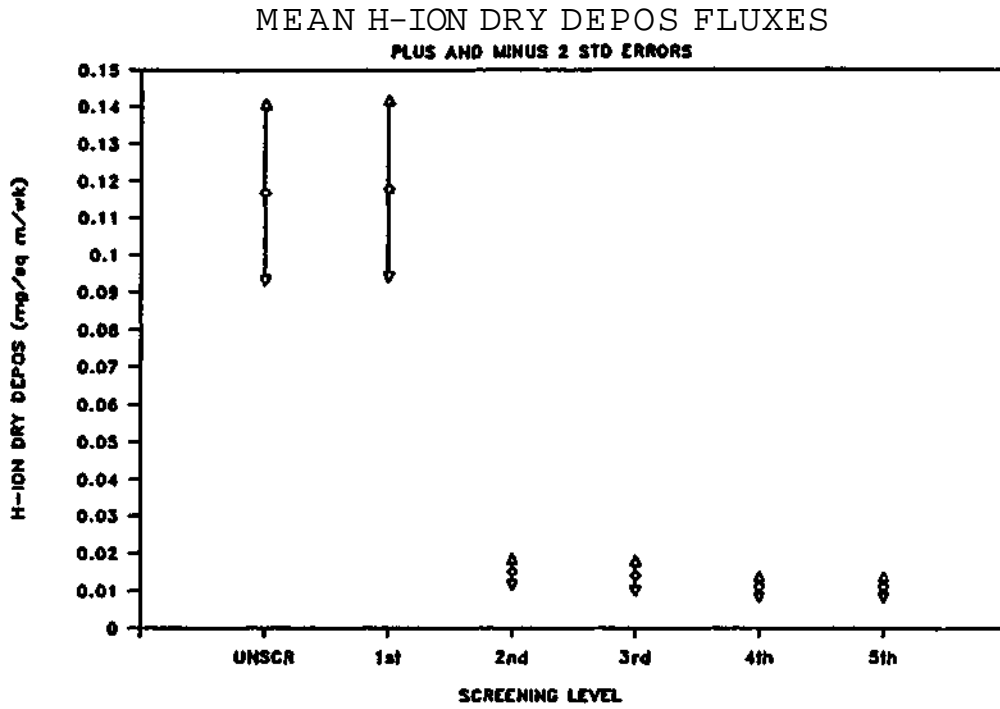


Figure 1. Mean dry deposition fluxes and their 95% confidence limits for hydrogen and sodium as a function of screening level.

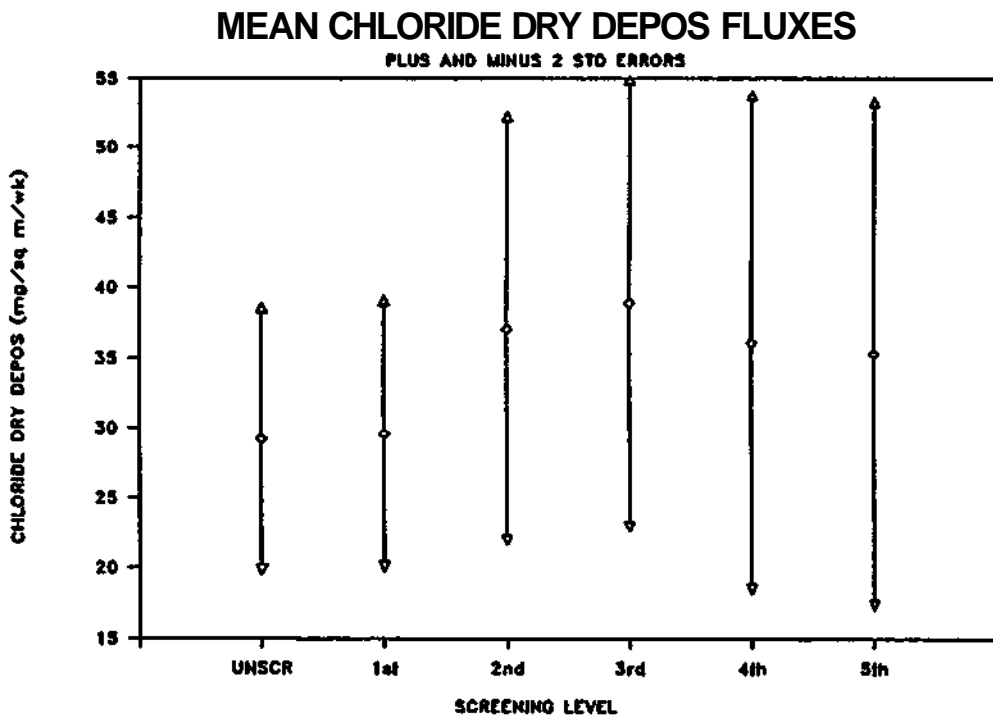
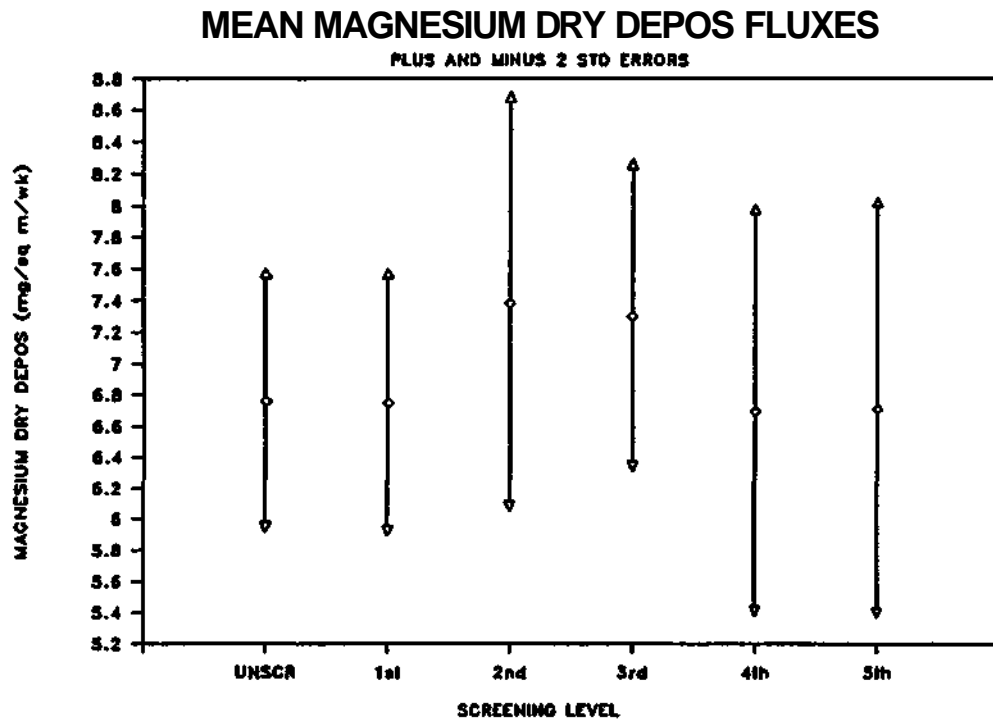


Figure 2. Mean dry deposition fluxes and their 95% confidence limits for magnesium and chloride as a function of screening level.

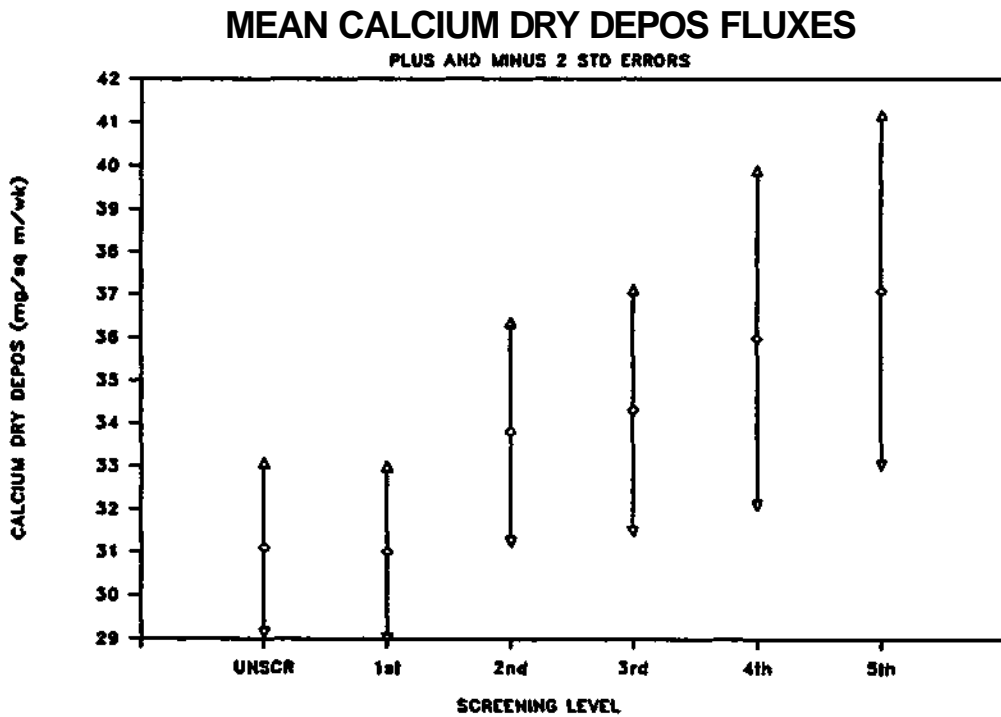
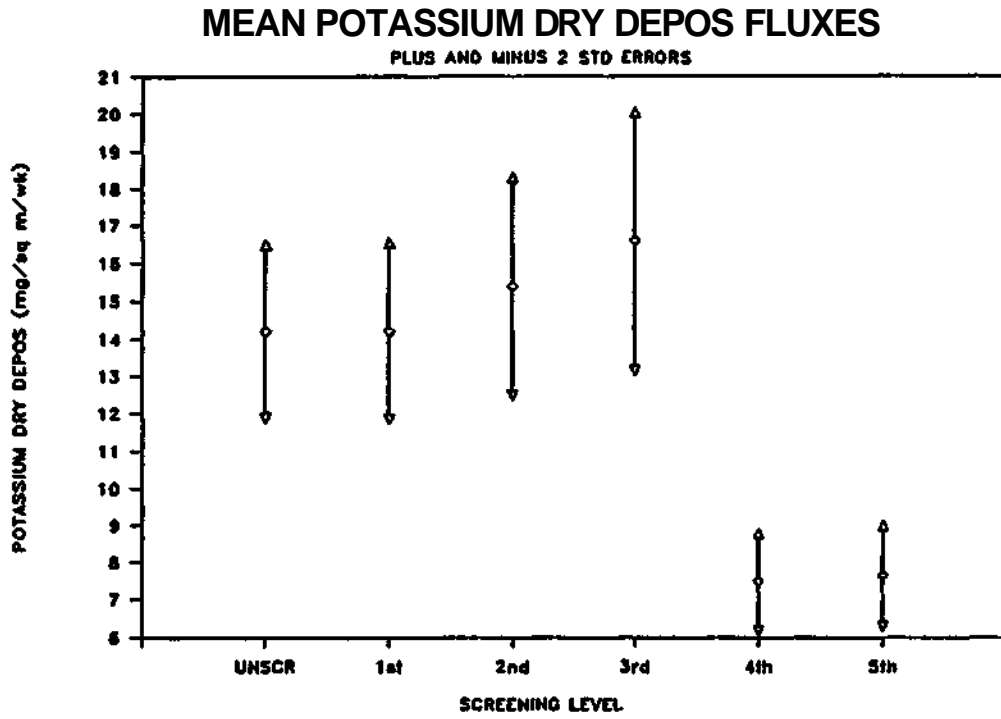


Figure 3. Mean dry deposition fluxes and their 95% confidence limits for potassium and calcium as a function of screening level.

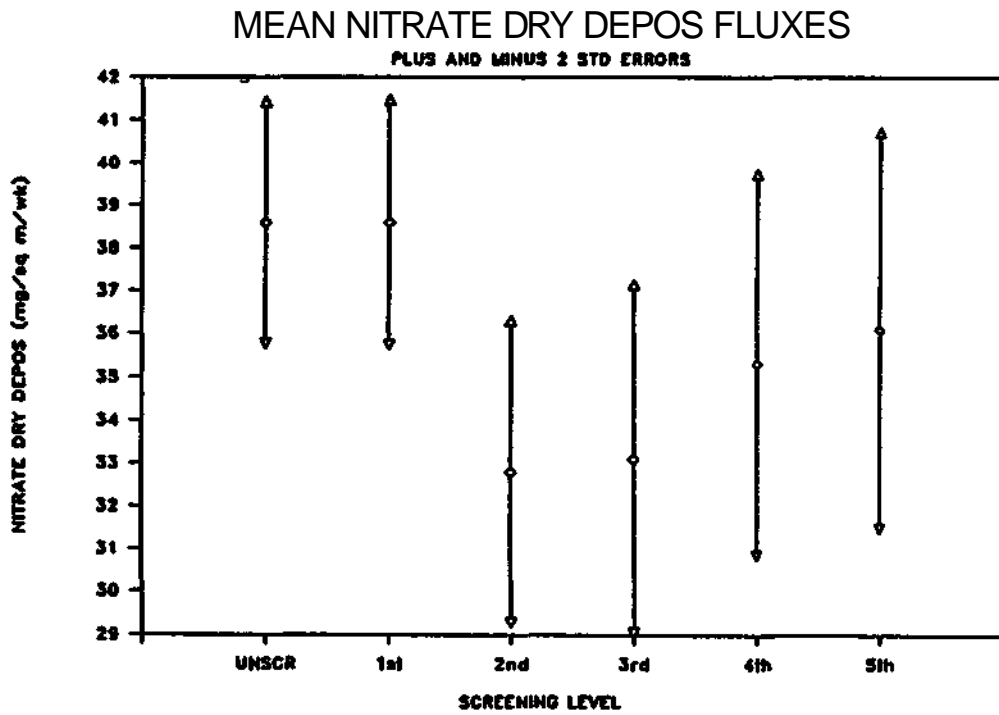
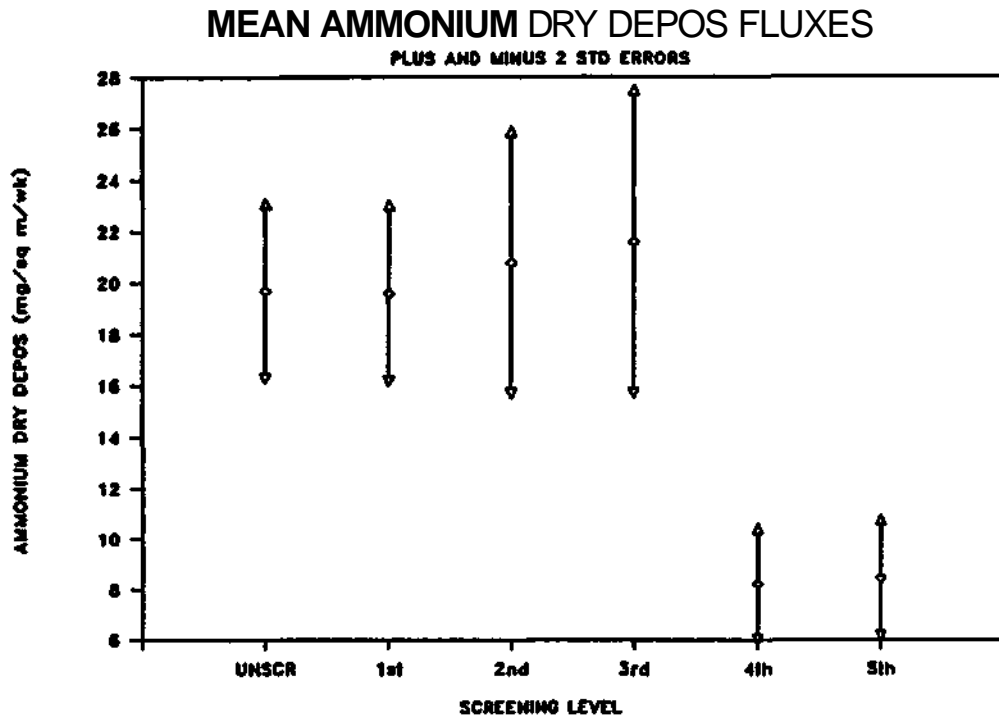


Figure A. Mean dry deposition fluxes and their 95% confidence limits for ammonium and nitrate as a function of screening level.

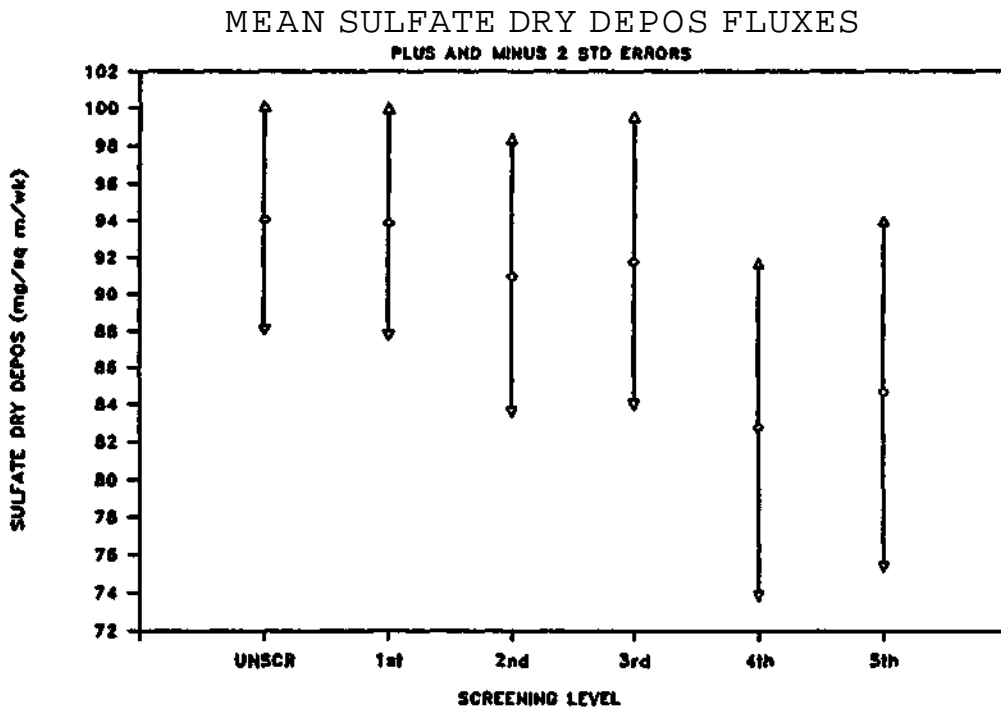
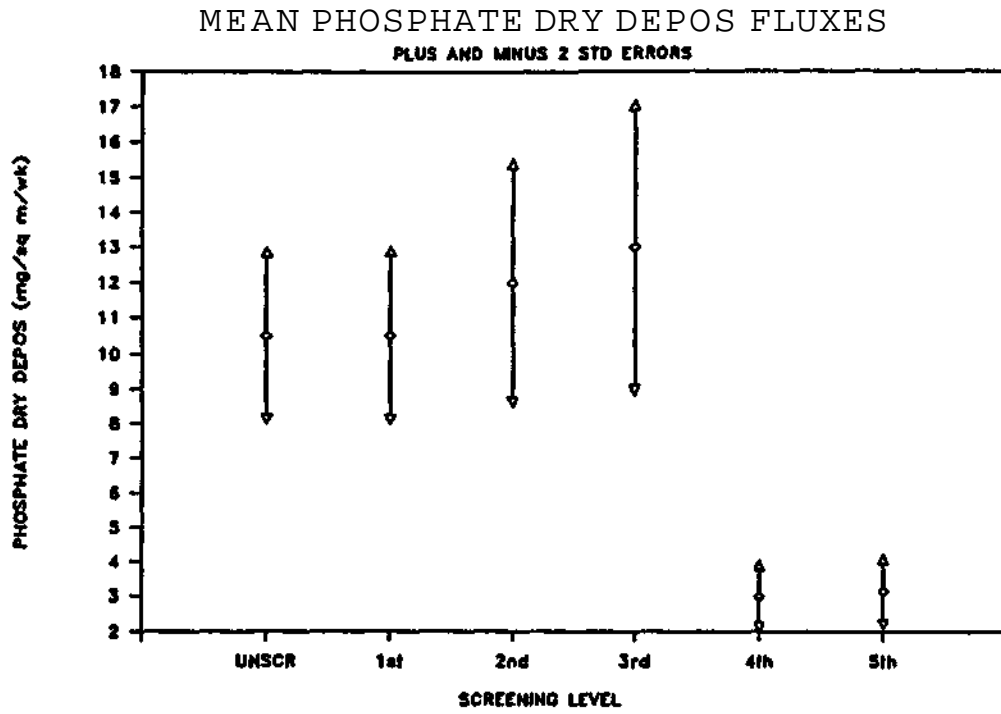


Figure 5. Mean dry deposition fluxes and their 95% confidence limits for phosphate and sulfate as a function of screening level.

Table 2. Results of statistical tests for differences between means of unscreened and screened dry bucket flux measurements. A 5% significance level was used. The code used to indicate the data sets that are significantly different from each other is interpreted as follows: AB vs CD means that A is not different from B, nor C from D, but both A and B are different from both C and D.

	Parametric tests			Nonparametric tests		
	Significant differences?	Fischer	Tukey	Significant differences?	Fischer	Tukey
H	Yes	AB vs CDEF	AB vs CDEF	Yes	AB vs CDEF	AB vs CDEF
Na	No	—	—	No	—	—
Mg	No	—	—	No	—	—
Cl	No	—	—	No	—	—
K	Yes	ABCD vs EF	CD vs EF	Yes	ABEF vs CD	ABEF vs CD
Ca	Yes	AB vs EF	none	Yes	AB vs CDEF	AB vs EF, and B vs D
NH ₄	Yes	ABCD vs EF	ABCD vs EF	Yes	ABD vs EF, AB vs C, and CD vs EF	ABCD vs EF
NO ₃	Yes	AB vs CD	none	No	—	—
PO ₄	Yes	ABCD vs EF	ABCD vs E, and CD vs F	Yes	AB vs CD vs EF	AB vs CD vs EF
SO ₄	No	—	—	No	—	—

hand, found that A and B were significantly different from C and D, which appears very questionable in Figure 3.

A careful check of the data and methods used for the non-parametric tests on K found no errors, however. It appears that the differences in results between the parametric and non-parametric tests resulted from somewhat unusual distributions of samples values in the various data sets, i.e., departures of the frequency distributions from the normal distribution, which is assumed by the parametric tests.

In contrast to the decrease in the mean K dry flux at the highest screening levels, Ca dry fluxes increased from each screening level to the next. The results of the tests in Table 2 agreed for the most part that data sets A and B were different from E and F, but disagreed on the significance of the differences between AB and CD.

Figure 4 shows results for NH_4 and NO_3 . For NH_4 the mean dry fluxes remained quite similar as wet samples were eliminated (levels 2 and 3), but dropped sharply upon elimination of the visually contaminated samples (level 4). For the most part the results in Table 2 agreed that data sets A, B, C, and D were different from E and F, but one of the non-parametric tests found a difference between AB and C, which appears to be anomalous.

For NO_3 , only the parametric tests found any significant differences, but they were ones one might suspect from Figure 4, namely between data sets AB and CD.

Figure 5 shows results for PO_4 and SO_4 . The PO_4 plot looks very similar to that of NH_4 , with a tendency for increasing means through screening level 3, and then a sharp drop as the visually contaminated samples were removed. The statistical tests agreed for the most part that data sets A and B were different from E and F, but the non-parametric tests also found differences between data sets AB and CD that one would not suspect from examination of Figure 5.

For SO_4 , the plot in Figure 5 shows a trend of decreasing mean dry flux as screening level increases, but the error bars are wide relative to these changes, and none of the differences was found to be significant by the statistical test in Table 2.

A summary of the examination of differences in mean dry deposition fluxes as a function of screening level may be stated as follows. For four ions--Na, Mg, Cl, and SO_4 --there were no significant differences between the means of the unscreened data sets and any of the respective screened data sets. For NO_3 , the parametric test indicated that elimination of wet samples produced a significant reduction in the mean dry flux, but the non-parametric test found no significant differences.

For five ions--H, K, Ca, NH_4 , and PC_4 --both parametric and non-parametric tests agreed that there were significant differences between means, although they did not always agree on which data sets were different. For one of these five ions--Ca--increasing the stringency of the screening criteria increased the mean dry deposition flux. For the other four, mean values decreased significantly as the screening level

increased, although not always at the same level. For H, elimination of the wet samples caused the significant decrease in mean dry flux. Finally, for K, NH_4 , and PO_4 , it was elimination of the visually contaminated samples that made the difference.

Up to now we have been concentrating on differences between means of the respective data sets. In the following paragraphs, we examine in somewhat more detail the differences between data sets in terms of their overall frequency distributions.

Graphical Comparisons

We will look in detail at Mg, K, and Ca, three generally large-particle elements for which bucket measurements of dry deposition flux may be best suited, and elements representing three different behaviors with respect to the trends of their mean values with increasing screening level. Mg showed no significant differences between means as screening level increased. K showed a marked drop in mean dry flux when visually contaminated samples were removed. Finally, mean Ca dry fluxes increased with screening level.

Figures 6, 7, and 8 show percentile comparison and sum-difference plots comparing screened and unscreened data sets for Mg, K, and Ca, respectively. In the percentile comparison plots (upper panels), the straight lines represent perfect agreement between percentile values computed from the unscreened data set and the various screened data sets. In Figures 6-8, screening levels 1-5 represent data sets B-F, respectively, as defined in Table 1.

For Mg (Figure 6) the percentile comparison plot (upper panel) shows that the lines for the various screened data sets are all quite close to the 1:1 line. This indicates that the frequency distributions of the screened data sets, some of which had only about 25% of the samples in the unscreened data set, are very similar to that of the unscreened data. Note that some of the lines representing the various screened distributions fall above the 1:1 line, and some fall below; the same line might be above the 1:1 line in one portion of the distribution, and below in another. This indicates that differences between the unscreened and screened data sets may be either positive or negative.

The differences between unscreened and screened Mg distributions are shown in more detail in the lower panel of Figure 6. These differences are labeled $\log_{10}(\text{all}) - \log_{10}(\text{level})$ (i.e. unscreened minus screened) on the left ordinate, and the equivalent ratio (i.e., unscreened/screened) on the right ordinate. We see that, except for the lowest (1st) percentile value, most of the unscreened/screened ratios are close to, but less than, 1. This means that Mg flux values at the respective percentiles are higher in the screened data set than the unscreened. The lowest unscreened/screened ratios occurred at the highest (99th) percentile. In order for the 99th percentile value of a screened data set to be greater than that of the unscreened data set, the values removed in the screening steps must have been intermediate values, rather than the highest values. Thus, at least for Mg, the highest observed dry fluxes were not eliminated by

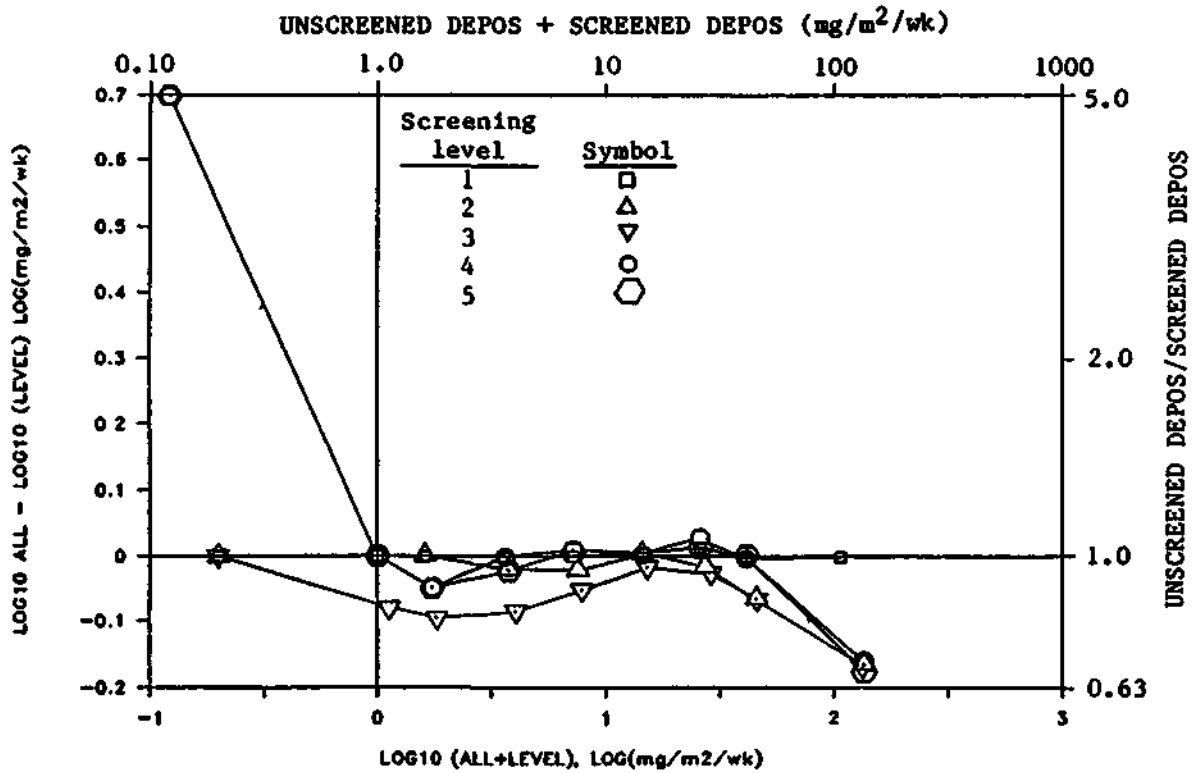
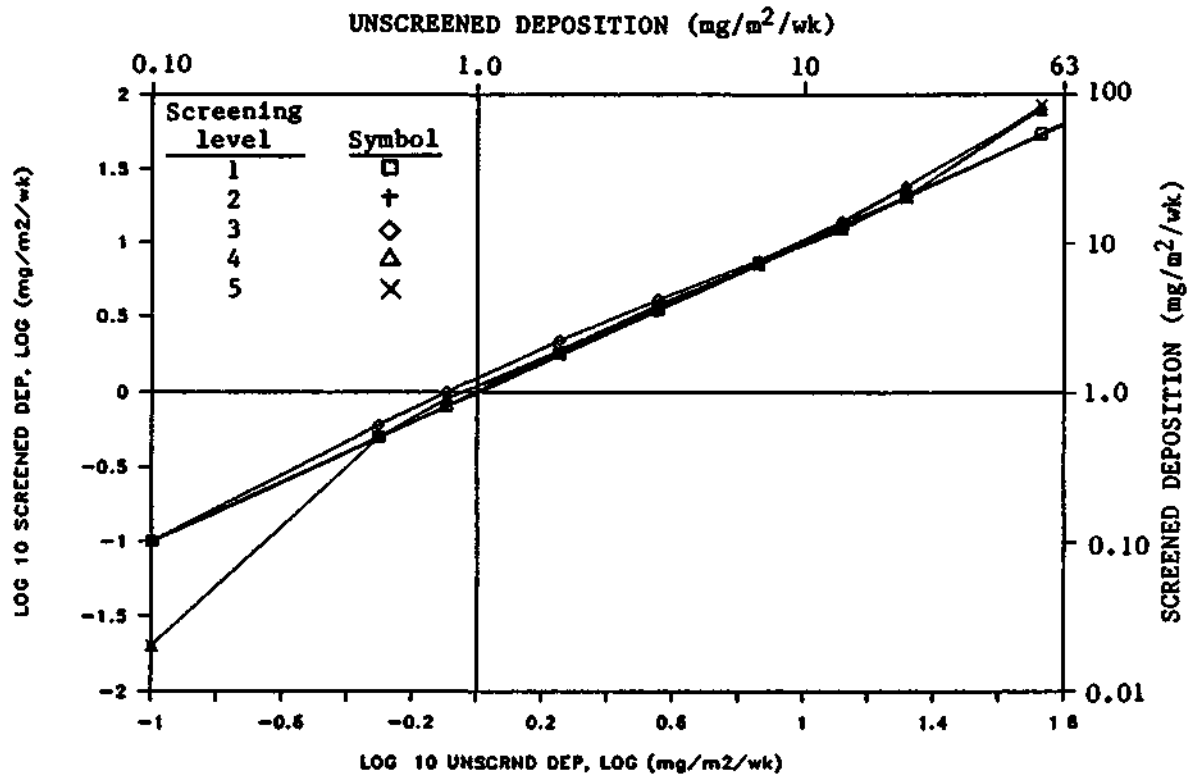


Figure 6. Magnesium percentile comparison (top) and sum-difference (bottom) plots for NADP dry bucket screening.

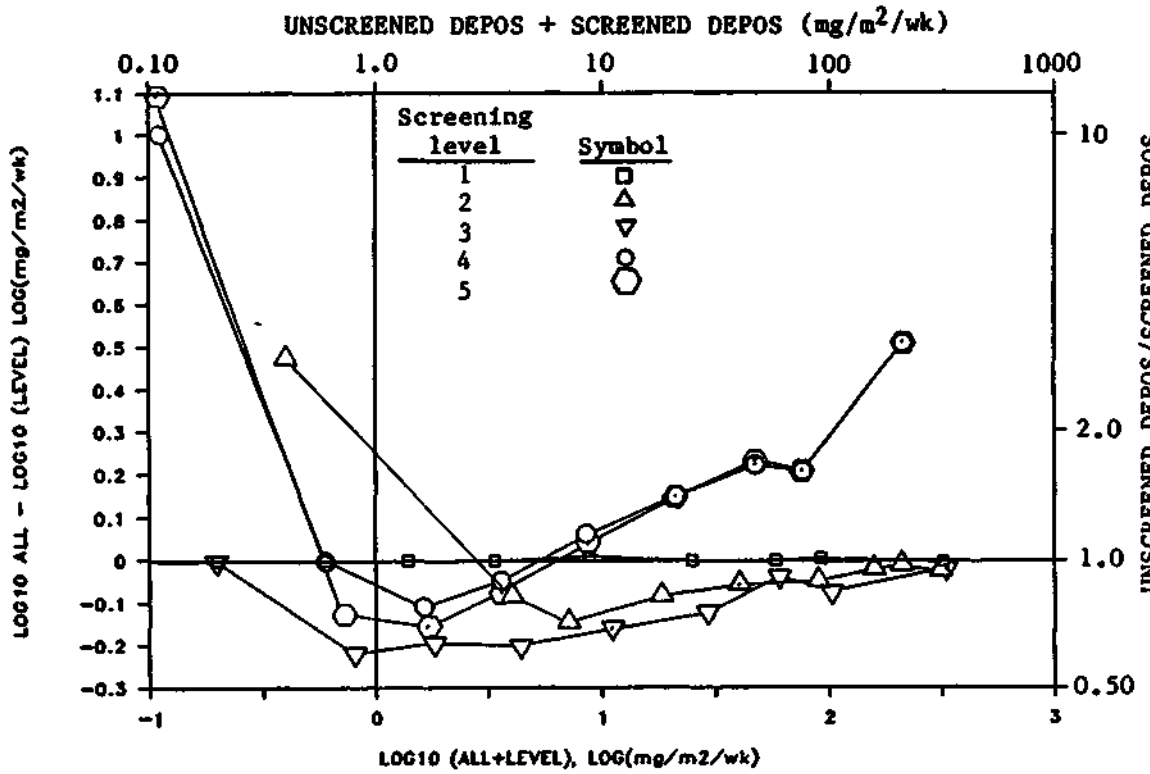
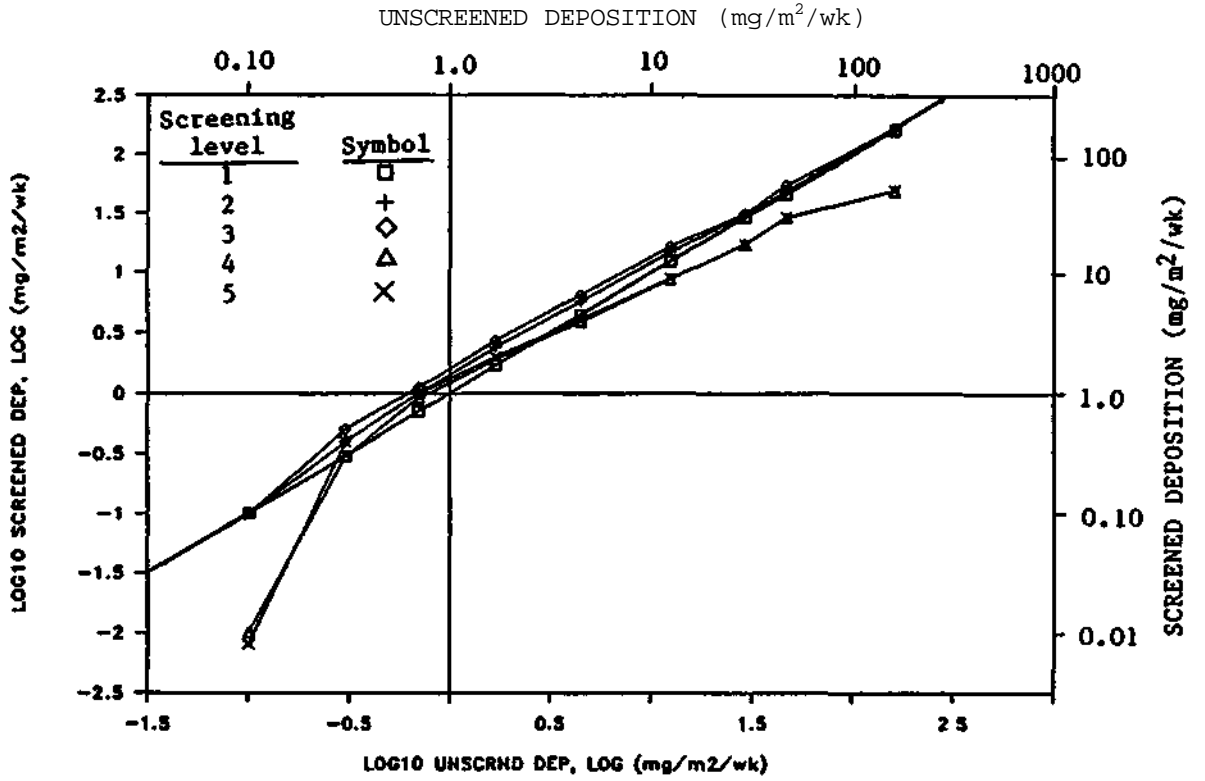


Figure 7. Potassium percentile comparison (top) and sum-difference (bottom) plots for NADP dry bucket screening.

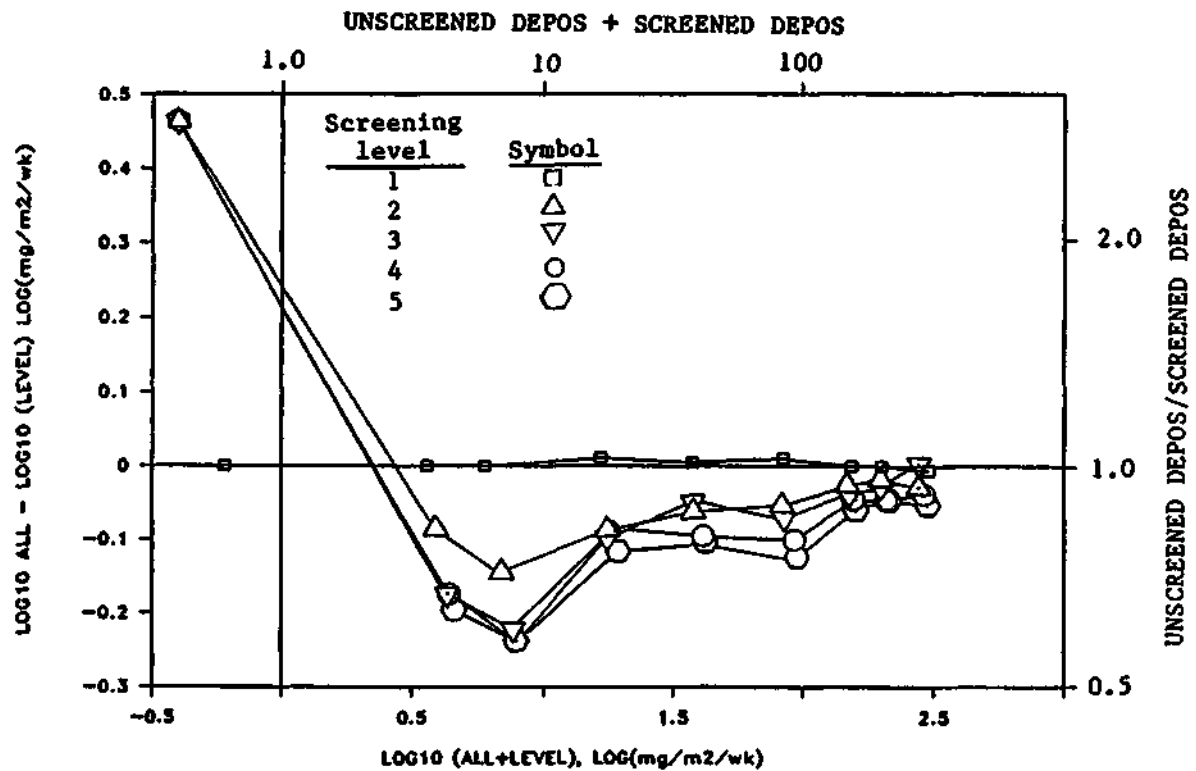
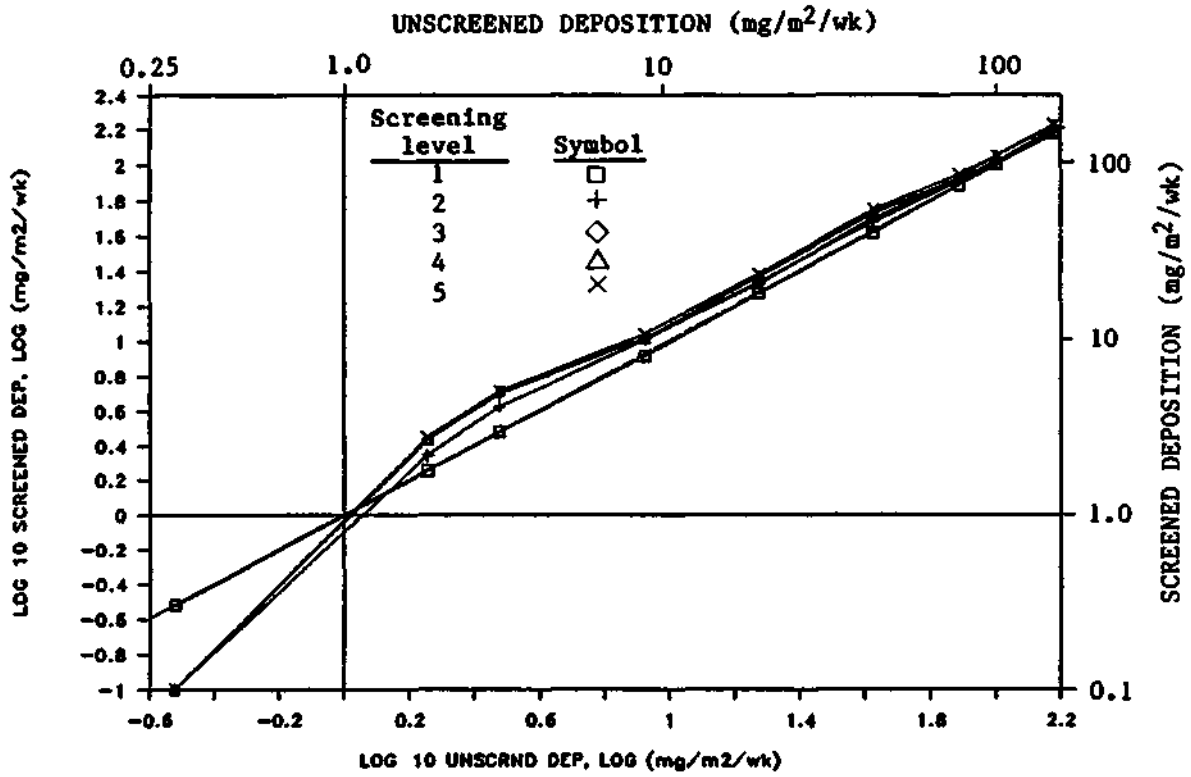


Figure 8. Calcium percentile comparison (top) and sum-difference (bottom) plots for NADP dry bucket screening.

removing wet or contaminated samples from the data set. These results are consistent with the earlier findings that mean Mg dry flux did not change significantly as a function of screening level, and that the highest observed fluxes were likely to have occurred in samples other than wet or water-spotted ones, or ones with visually observable contamination.

Results for K are shown in Figure 7. Overall, the percentile comparison plot (upper panel) shows somewhat less bunching of the lines near the 1:1 line than was the case for Mg, and in particular the lines representing the 4th and 5th screening levels show substantial departures below the 1:1 line. This indicates that removal of samples with visual contamination resulted in substantial changes in the frequency distribution.

As indicated in the top panel, and confirmed in more detail in the sum-difference plot (lower panel), the K fluxes at the respective percentiles are lower in the screened than the unscreened data sets. This is particularly true at the upper end of the combined distribution. Thus, in contrast to the situation for Mg, removal of visually contaminated samples removed many high flux values from the original data set. Note that this did not occur at the lower screening levels (i.e., 1-3), where, as in the case of Mg, the unscreened/ screened ratios were close to, but less than, 1 over most of the combined distribution. Note also that removal of the few samples that were grossly mishandled or presumed grossly contaminated (level 1) had almost no effect on the distribution--the box symbols are almost exactly on the zero line of the sum-difference plot. The same is true for Mg (Figure 6), but the box symbols are difficult to distinguish among the other overlapping symbols. These results are again consistent with those based on comparison of mean dry fluxes, presented earlier.

Results for Ca are shown in Figure 8. Again, consistent with the earlier results, it is quite clear in the upper panel that the respective percentile values of the dry fluxes are higher in the screened data sets than the unscreened, since the lines representing the various screening levels are predominantly above the 1:1 line. The lower panel confirms that the unscreened/ screened ratios were almost all less than 1 at screening levels 2-5, except for the 1st percentile. Thus, for Ca, as for Mg, removal of wet and visually-contaminated samples resulted in increased dry flux values at all percentiles above the 1st. Again, removal of the few samples in screening level 1 had very little effect on the distribution.

DISCUSSION AND CONCLUSIONS

It is quite clear from the results presented that "dry" fluxes of H ion are substantially decreased if samples containing water are eliminated from the data set, and some evidence that the same may be true for nitrate. Similarly, the dry fluxes of K, NH_4 , and PO_4 , while relatively insensitive to elimination of samples containing water, are much reduced when samples having one or more types of visual contamination are eliminated. However, identification of the specific contaminants has been left for the future. The dry flux of Ca actually increased significantly as the screening level increased. The dry fluxes of the remaining ions

examined--Na, Mg, Cl, and SO₄--showed no significant differences between screening levels, although the Na mean values also increased with screening level.

If all users of the dry bucket data set require complete data on each sample (i.e., valid analyses of each ion), these results suggest that samples containing water, or those with certain contaminants (yet to be identified) need not be analyzed. This would eliminate 65-75% of the current dry bucket analyses. On the other hand, if users of the data on dry fluxes of Na, Mg, Cl, SO₄, and perhaps NO₃, do not require valid analyses of the other ions, then useful information can be obtained by analyzing all samples for this limited set of ions.

It is probably prudent to discard the grossly mishandled samples without analysis. Individual sample "dry depositions" would, of course, be highly suspect. However, this analysis of the current data set, which included only 21 such samples out of a total of more than 1200, did not indicate that any substantial error in the population mean would occur if they were included. Further, our analyses did not bring to light any strong evidence to support elimination of either water-spotted or incomplete samples.

Finally, the present analyses suggest that additional future work on the current data set should include quantification of the individual effects of each potential difficulty (e.g., water in the sample, or visual contamination), and particularly, each different form of contamination. In addition, the samples might be grouped regionally (at least east vs west) to see whether there are regional differences in the way that potential contaminants affect the measurement of dry fluxes using buckets.

REFERENCES

- Cleveland, W.S., 1985: The Elements of Graphing Data, Wadsworth Advanced Books and Software, Monterey, CA 93940, 323 pp.
- Dolske, D.A., and D. F. Gatz, 1984: A field intercomparison of methods for the measurement of particle and gas dry deposition. J. Geophys Res., 90(D1), 2076-2084.
- Dunnett, C W., 1980: Pairwise multiple comparisons in the homogeneous variance, unequal sample size case. J Amer Statist. Assoc., 75, 789-795.
- Gatz, D.F., W.R. Barnard, and G.J. Stensland, 1985. Dust from unpaved roads as a source of cations in precipitation, Paper 85-6B.6, Annual Meeting of the Air Pollution Control Association, Pittsburgh; Illinois State Water Survey, Champaign, RS-672

- Hicks, B.B., 1985: Network monitoring of dry deposition of trace gases and submicron particles, In: Special Environmental Report No. 16, Lectures presented at the WMO Technical Conference on observation and measurement of atmospheric contaminants, TECOMAC, Vienna, 17-21 October 1983, WMO - No. 647.
- Hicks, B.B., M.L. Wesely, and J.L. Durham, 1980: Critique of methods to measure dry deposition. Workshop Summary. EPA-600/9-80-050, and available as NTIS PB81-126443.
- Hicks, B.B., M.L. Wesely, S.E. Lindberg, and S.M. Bromberg, Editors, 1986: Proceedings of the NAPAP workshop on dry deposition, March 25-27, 1986, Harpers Ferry, West Virginia. Available from: The Librarian, NOAA/ATDD, P.O. Box 2456, Oak Ridge, TN 37831.
- Kruskal, W.H., and W.A. Wallis, 1952: Use of ranks in one-criterion analysis of variance. J. Amer. Statist. Assoc., 47. 583-621.
- Lockard, J.M., 1987: Quality assurance report, NADP/NTN deposition monitoring, laboratory operations, Central Analytical Laboratory, July 1978 through December 1983. Available from Coordinator's Office, Natural Resource Ecology Laboratory, Colorado State University, Fort Collins, CO 80523
- Neter, J., W. Wasserman, and M.H. Kutner, 1985: Applied Linear Statistical Models. 2nd Edition, Richard D. Irwin, Inc., Homewood, Illinois 60430.
- Peden, M.E., S.R. Bachman, C.J. Brennan, B. Demir, K.O. James, B.W. Kaiser, J.M. Lockard, J.E. Rothert, J. Sauer, L.M. Skowron, and M.J. Slater, 1986: Development of standard methods for the collection and analysis of precipitation. Final Report, Contract CR810780-01, U.S. EPA/EMSL, Cincinnati, Ohio; Illinois State Water Survey, Champaign 61820, CR-381.
- SAS Institute, Inc., 1982: SAS User's Guide: Statistics. 1982 Edition, Cary, North Carolina.
- Semonin, R.G., 1984: Dry bucket analysis of the NADP network. In: Semonin, R.G., et al., Study of Atmospheric Pollution Scavenging, 20th Progress Report, Contract DE-AC02-76EV01199, U.S. Dept. of Energy, Illinois State Water Survey, Champaign, CR347, pp 137-150.
- Sokal, R.R., and F.J. Rohlf, 1981: Biometry. 2nd Edition, Freeman and Co., New York, 859 pp.
- Stensland, G.J., R.G. Semonin, M.E. Peden, V.C. Bowersox, F.F. McGurk, L.M. Skowron, M.J. Slater, and R.K. Stahlhut, 1980: NADP Quality Assurance Report -- Central Analytical Laboratory, January, 1979-December, 1979. Illinois State Water Survey, Champaign, Illinois.

CHAPTER 17

AN ANNOTATED DESCRIPTION OF THE ATMOSPHERIC CHEMISTRY
SAMPLING STATION AT BONDVILLE, ILLINOIS

Scotty R. Dossett

INTRODUCTION

The Illinois State Water Survey (ISWS) Atmospheric Chemistry Section has carried out studies involving the chemical and physical components of wet and dry deposition and aerosol materials at the field site since February 1978. These studies have included elaborate collection and analysis procedures and substantial research in the areas of sampling development and monitoring. The changing requirements of resource decision makers require information that can only be gained at sites which contain historical records regarding all of these activities. The following paper will briefly detail the physical and climatological characteristics and the history of the site development.

Location of the Field Site

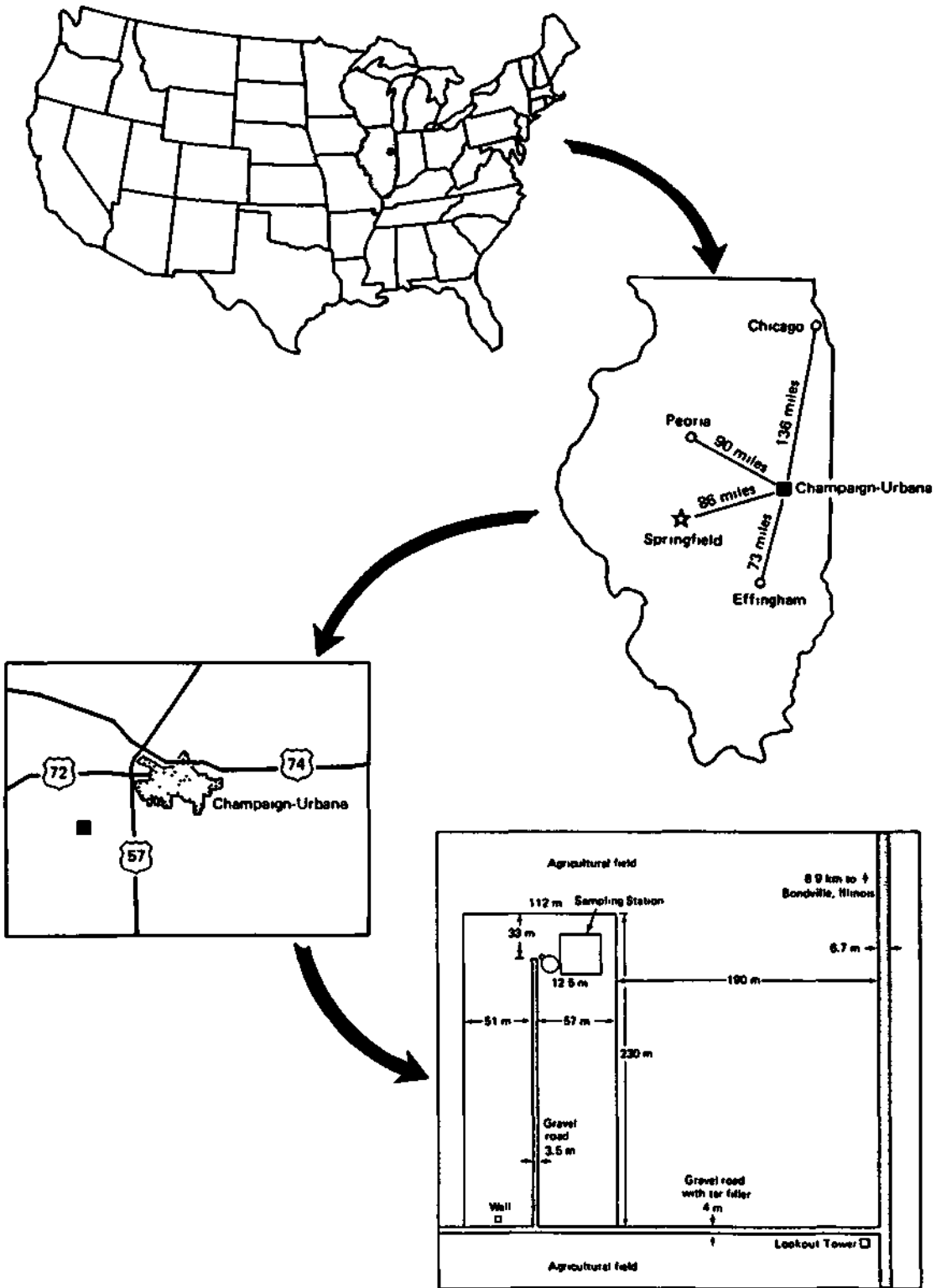
The sampling plot is located 12.8 km west-southwest of Champaign, IL. By conventional road map it is 10.8 km west of central Champaign on Illinois Route 10 and 6.9 km south of Bondville, IL (the town for which the site is named) on County Highway 19. The site is located at latitude 40° 03' 12" and longitude 88° 22' 19" (see Map 1). This puts the area in Township 18 North, Range 7 East, in Champaign County Illinois.

The site can be found on the Bondville, IL 7 5 minute topographic map, standard USGS quadrangle. This map was revised in 1975 and is USGS number N4000-W8815/7.5. One predominant feature of the immediate area, labeled LOOKOUT TOWER, is 300 meters southwest of the station. The field site is owned by the University of Illinois Board of Trustees and is part of a 101.7 ha farm.

AREA PHYSIOGRAPHY AND SOILS

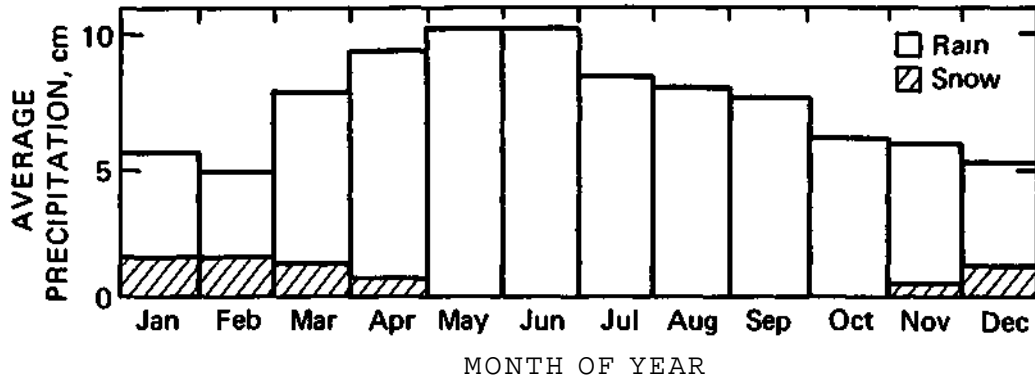
The portion of the U.S. which surrounds the field site was greatly affected by glaciation during the Pleistocene epoch. It is characterized by low, broad terminal and lateral moraines with interspersed flat or gently rolling morainal and outwash areas. Glaciation deposited approximately 70 meters of heterogeneous drift over which was lain up to 2 meters of windblown silt or loess during the period following the retreat of the ice. Six major watersheds drain the area in a broad dendritic pattern which exits the area toward the southwest and southeast. The soils surrounding the sampling plot are largely derived of the windborne loess deposits. In addition, large amounts of clay sized material deposited as outwash caused natural vegetation to secede into wet, marshy lowlands. During the agricultural revolution the land was substantially drained and modern agronomic practices began. The soils surrounding the site are somewhat poorly drained to poorly drained, friable and hold tremendous capacity as cropland.

Map 1



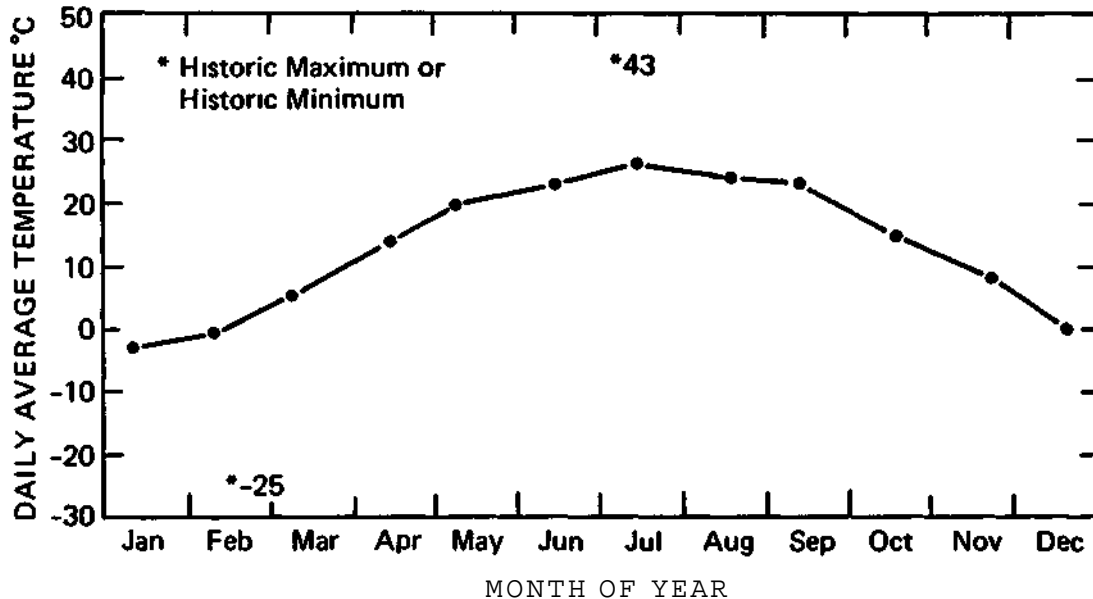
AREA CLIMATOLOGICAL CHARACTERISTICS

Located in the center of the North American continent, the field station experiences typical continental temperate climate. In general, rainfall is distributed evenly throughout the seasons with maximum values occurring in April, May and June, and minimum amounts during the winter months of December, January, and February.

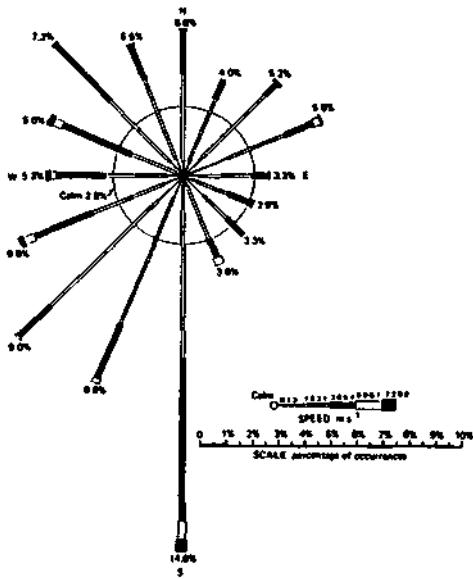


Average Annual Precipitation Total - 91.1 cm.
Historic Monthly Value Range - 29.4 cm - Trace
(Maximum value June 1902 - minimum November 1904)
Percent of Precipitation during growing season - 63

Temperatures at the site range from record lows near -30°C to highs near $+40^{\circ}\text{C}$. The combination of high summer temperatures and high summer rainfall results in hot, muggy weather during the months of July and August.



Winds at the field station are plotted below in the form of a conventional wind rose.



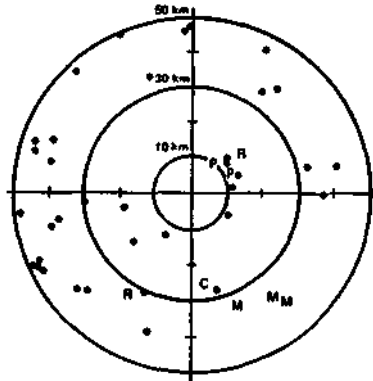
For this period the prevailing wind direction varies from the south to southwest in every month except February (in which the prevailing direction is northwest).

(from Changnon)

AIR QUALITY SOURCE CHARACTERISTICS

The anthropogenic sources of atmospheric constituents are shown in Figure 1 below. This plot of known emitters represents those polluters within 10 km, 30 km, and 50 km radii. The crosshair of the map represents the field station. Larger emitters are classified by an initial in this scheme: M - mines or oil wells (note the cluster of 3 in the southeastern quadrant); R - refinery; P - power plant (note 2 such plants in 10 km range in the northeast quadrant); F - foundry or metal refining facility; and C - chemical plant.

Figure 1. Point Sources of Emission Within 50 km of Site



(Robertson, 1987)

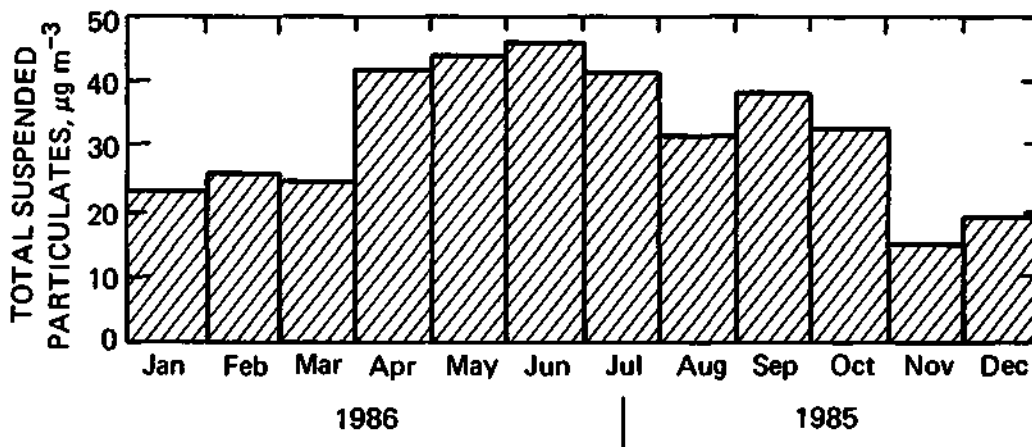
The large cluster of sources in the 10 to 15 km range in the NE quadrant represent the Champaign-Urbana metropolitan area.

The annual emissions for the 50 km surrounding area from point sources are as follows, (from Robertson, 1987).

Combined Annual Emissions (metric tons)

SO ₂	23,189.4
Hydrocarbons	4,247.6
NO _x	7,457.8
Total particulates	37,952.6

The land use practices immediately surrounding the site are typical of the "corn belt" region of the country. Agricultural cultivation as a result can provide significant inputs into the air quality regime at the site. The table below shows monthly values for total suspended particulates throughout one year (Hopke, 1986).



Site Description

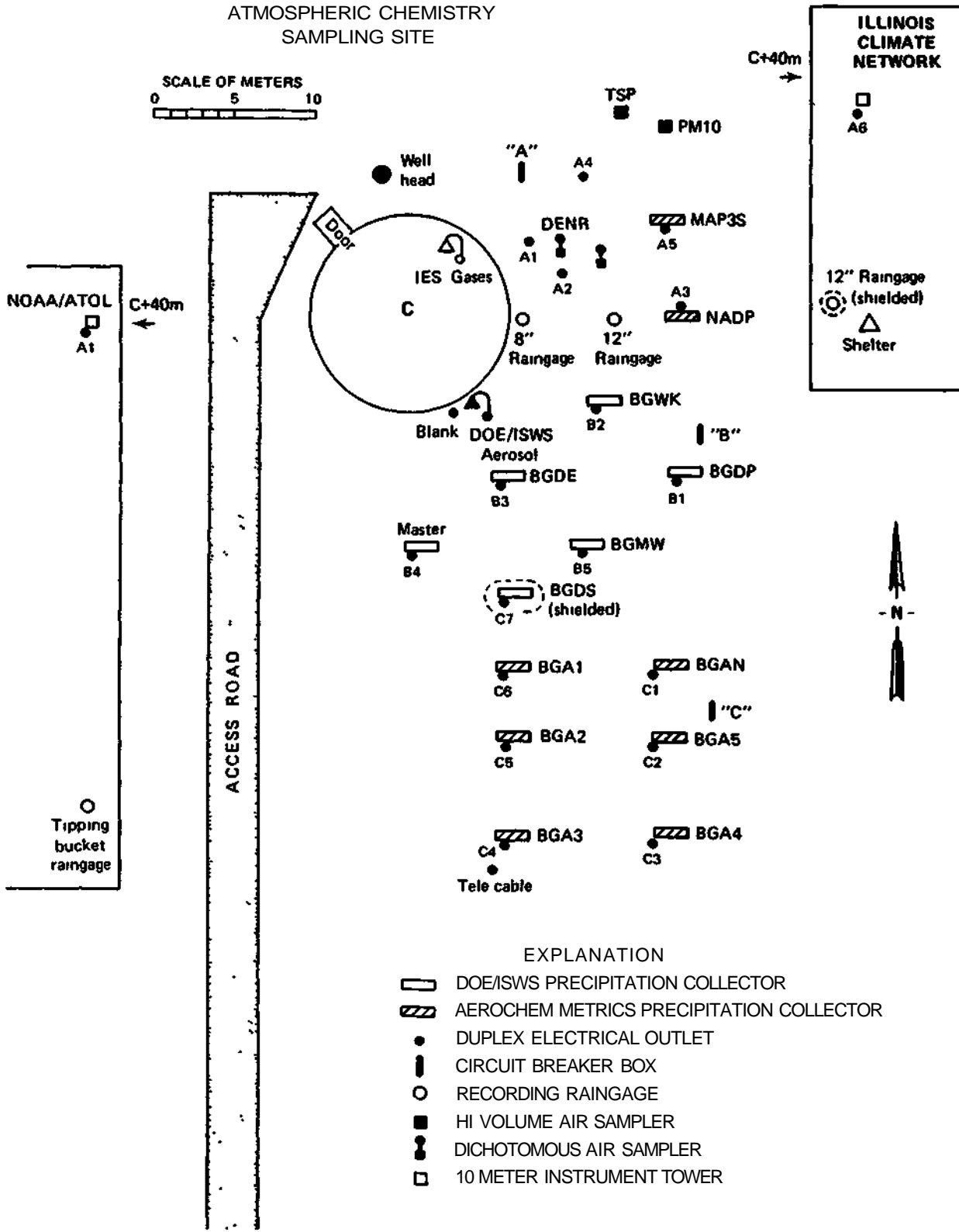
The area surrounding the field site is generally flat with approximately 5 m of relief within the surrounding 300 m diameter area. All sampling devices are located within a 30 x 30 m square inside a 2.5 ha grass covered plot (see Map 1 and 2).

The grass field surrounding the site has a homogeneous cover of fescue grasses with a few patches of weeds due to recent disturbances. The area immediately surrounding the collecting devices is mowed once annually in order to reduce the amount of standing plant material and to help prevent the spread of weeds.

Agricultural activities in the immediate area are composed exclusively of annual rotations of corn and soybeans.

Map 2

BONDVILLE
ATMOSPHERIC CHEMISTRY
SAMPLING SITE



EXPLANATION

-  DOE/ISWS PRECIPITATION COLLECTOR
-  AEROCHEM METRICS PRECIPITATION COLLECTOR
-  DUPLEX ELECTRICAL OUTLET
-  CIRCUIT BREAKER BOX
-  RECORDING RAINGAGE
-  HI VOLUME AIR SAMPLER
-  DICHOTOMOUS AIR SAMPLER
-  10 METER INSTRUMENT TOWER

RESEARCH AT THE SITE

The major research efforts at the field site include:

PRECIPITATION CHEMISTRY

MAP3S Network

Since November 1979 the site has served as station no. 5 in the 10-station MAP3S network. MAP3S is an event based precipitation chemistry sampling project. Because of its event sampling protocol MAP3S is meant to provide data for those interested in developing and verifying long-range transport models as well as to provide data on the regional deposition of major inorganic cations and anions. MAP3S site selection criteria include: nominal local sources such as air, ground, or water traffic, storage of fuels or agricultural materials and current continuous sources (point sources) of pollution within 50 km. In addition to regional selection requirements the location of instruments within the MAP3S site are carefully defined.

NADP/NTN Network

The field station serves as the IL11 (Bondville) monitoring station for this network. Since February of 1979 weekly samples (ending Tuesday) have been collected from the same point. NADP/NTN analyzes wet deposition samples for the major inorganic anions and cations, pH and conductance. In addition, a dryfall bucket collector is removed every 8 weeks and the same analysis is performed. NADP consists of a network of over 200 sampling locations evenly distributed throughout the North American continent (as opposed to the eastern bias of the MAP3S sampling network). The protocol for site selection and operation for NADP/NTN are documented in the following publications:

- Instruction Manual - NADP/NTN Site Selection and Installation, NADP/NTN Coordinator's Office, July 1984;
- NADP Instruction Manual - Site Operation, NADP/NTN Coordinator's Office, 1987.

DOE/ISWS

A series of DOE/ISWS wet/dry samplers are "slaved" together in a daily vs weekly vs monthly wet-only sampling protocol experiment. In addition system blank and sampling precision activities are carried out within this system. Analysis is done on major inorganic cations and anions, pH and conductance.

Two elements of interest by earth scientists, Beryllium⁷ and ¹⁰, have inputs almost exclusively from the upper atmosphere. The ISWS and the Carnegie-Mellon Institute cooperate in this project. Two wet/dry collectors are used to collect the relatively large amount of sample needed for this analysis.

Other

In addition to those efforts listed above, the field site has been used at varying intervals for projects relating to DA loading (system blank samples by the NADP/NTN network), precipitation collector response to hanging baffle shielding and other projects related to individual researcher needs.

AIR CHEMISTRY

U.S. DOE/ISWS

One 37 mm teflon filter is collected each day with a medium volume pump and analysis is performed for SO₄, chloride, and extractable Ca, Mg, Na, and K. The filters are extracted using a deionized water solution.

NOAA/ATDL

Bondville serves as a CORE satellite site for the National Oceanic and Atmospheric Administration dry deposition sampling network. This project which began sampling during the summer of 1985 uses a staged filterpack device and a low volume air pump and data logger system to collect air quality data. The analysis are performed at the Atmospheric Turbulence and Diffusion Department, a portion of the Oak Ridge National Laboratory in Tennessee. The meteorological instrumentation associated with the filterpack allows the calculation of the deposition velocities of aerosol components.

Illinois Department of Energy and Natural Resources (DENR)

The University of Illinois Institute for Environmental Studies (IES), in conjunction with DENR, samples total suspended particulates (TSP), the inhalable fraction (PM-10), SO_x and NO_x. These efforts are to characterize background levels in order to ascertain the effects of the Abbott Power Plant conversion at the University of Illinois on ambient air quality.

In cooperation with the Hazardous Waste Research and Information Center dichotomous sampling for airborne hazardous substances is carried out. Bondville serves as a background site due to its location far from any major industrial or urban sources.

METEOROLOGICAL INSTRUMENTATION

Illinois Climate Center (ICN)

The Bondville station serves as 1 of 9 ICN stations throughout the State. These stations continuously monitor wind speed and direction, temperature and relative humidity, hemispherical direct and diffuse radiation (by pyronometer), soil temperature and moisture and precipitation. These climatological data are used by interested scientists in many aspects of the on-going research at the field station.

At present the list of collecting devices in use at the site is as follows.

<u>Item</u>	<u>Quantity</u>
<u>WEATHER INSTRUMENTS</u>	
Cup Anemometer	1
Propeller Anemometer	2
Wind vane (direction)	3
U.S. Standard 8" Raingage (weighing)	1
Tipping Bucket Raingage	1
U.S. Standard 12" Raingage	2
Radiometer	2
Hygrothermograph	1
Soil Moisture Probe (Neutron)	1
Relative Humidity Sensor	1
Surface Wetness Sensor	1
Max-Min Thermometer	1
Aspirated Temperature Probe	1
<u>AIR QUALITY INSTRUMENTS</u>	
Ambient Gas Monitors	2 (SO _x , NO _x)
Medium Volume Aerosol Pumps w/Filterpack	4
Low Volume Aerosol Pumps w/Filterpack	1
High Volume TSP Sampler	1
High Volume PM10 Sampler	1
<u>PRECIPITATION QUALITY INSTRUMENTS</u>	
HASL Type Wet/Dry Precipitation Collector	14

History

As mentioned previously, the field site was initially constructed as part of a large U.S. DOE effort. The Electrical Engineering Department at the University of Illinois was the contractor for that work. The field site was turned over to the Atmospheric Sciences Section of the ISWS during the Fall of 1977. The first field project began soon afterwards.

Figure 2

Timeline of the major research activities at the Field Site.

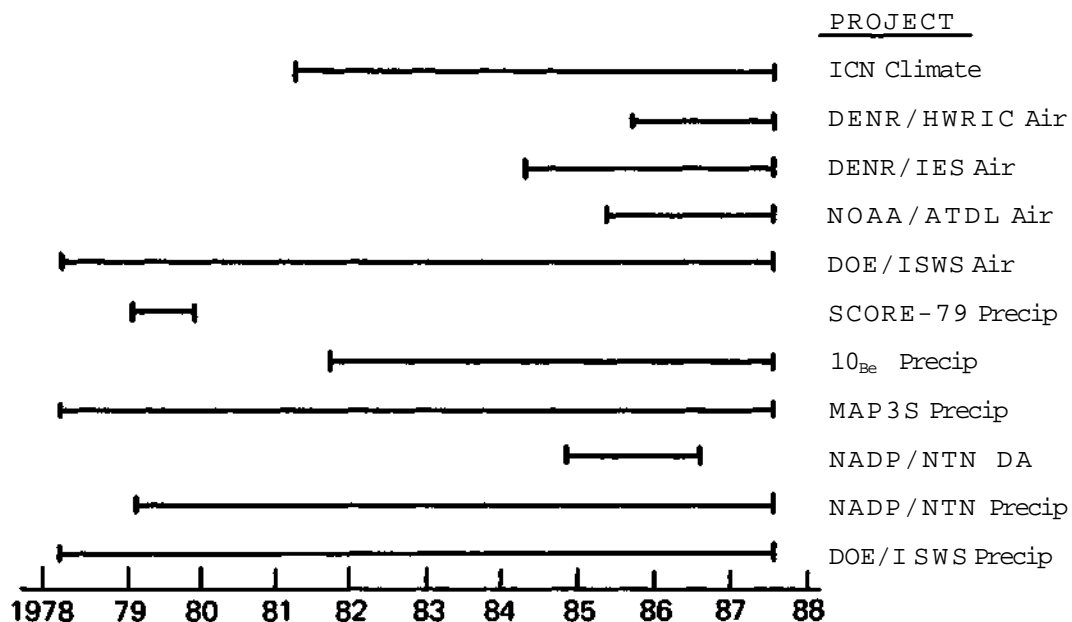
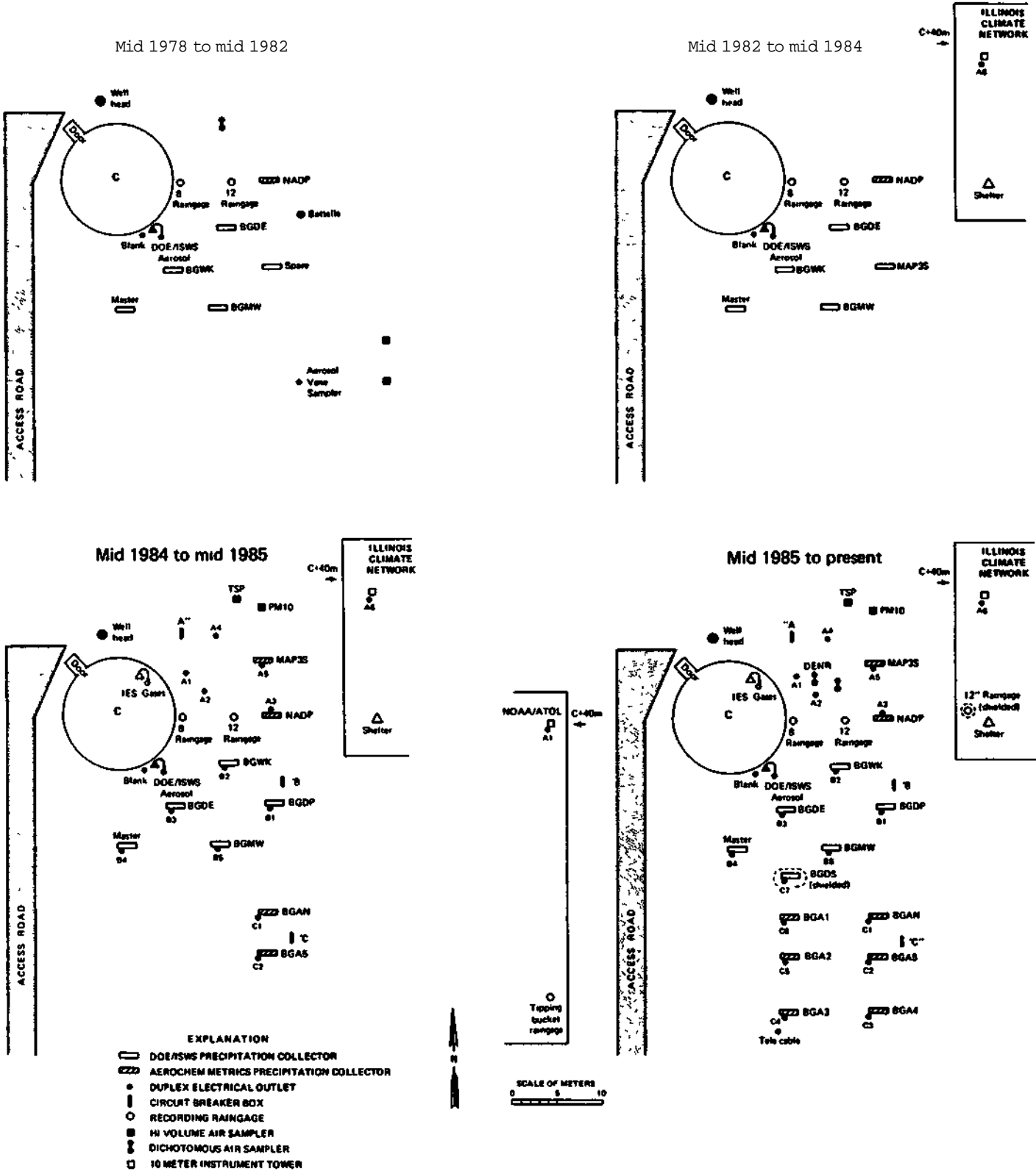


Figure 2 illustrates the consistent growth in the number of major research projects at the field station. Note that some of the projects (the DOE/ISWS wet deposition system) are nearing the tenth year of operation.

The following map series shows benchmark dates and the amount and position of sampling instruments associated with the research activities listed in Figure 2.

Map 3

Bondville Atmospheric Chemistry Sampling Site



Future

The field station has been selected as one of the first sites for a new EPA dry deposition monitoring network. The National Dry Deposition Network (NDDN) will begin operations during the summer of 1987. NDDN will eventually expand to a planned number of 100 sites throughout the U.S. The sampling protocol for NDDN includes air quality, meteorological and precipitation chemistry measurements. After its installation the field site will include its first ozone monitor and have duplicate filter monitors for the nitrogen and sulfur species.

No other specific projects are expected to commence in the near future at this time. The large undisturbed area of the grass plot, the ample electrical power source and a generally accessible nature combine to make the site an ideal environment for future field research.

SUMMARY

The maps, figures and text included have described the area surrounding the Bondville Field station, detailed the history of the research activities and briefly described the research currently supported at the site. DOE contract funds make up a considerable portion of the budget upon which the Bondville site depends. Data collected at the Bondville site offer a mix of precipitation and air chemistry information with meteorological measurements. As such the site offers a good opportunity for the research community to study in detail the interrelated nature of the climatology, wet deposition, dry deposition, and aerosol components of the atmosphere.

REFERENCES

Changnon, S. A., 1959: Summary of Weather Conditions at Champaign-Urbana, Illinois. Illinois State Water Survey Bulletin No. 47.

Hopke, P. K.: Ambient Air Monitoring to Assess the Impact of the Abbot Power Plant Reconversion Project. Annual Report for September 85 to August 86, Illinois Department of Energy and Natural Resources, ENR Contract No. ER-3, (undated).

Illinois Agricultural Experiment Station, 1974: Soil Report 114, University of Illinois at Urbana-Champaign Agricultural Experiment Station.

NOAA, Environmental Data and Information Service, National Climatic Center, 1982: Climatology of the United States. No. 20.

NOAA, Environmental Data and Information Service, National Climatic Center, 1982: Climatology of the United States. No. 81, September.

Robertson, J.- NADP/NTN Site Directory, (unpublished).